ANNUAL REVIEW

INSTITUTE
FOR
MOLECULAR
SCIENCE

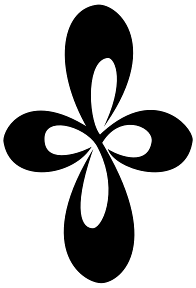

2000

Published by
Institute for Molecular Science
Okazaki National Research Institutes
Myodaiji, Okazaki 444-8585, Japan
Phone: +81-564-55-7418 (Secretary Room)
Facsimile: +81-564-54-2254 (Secretary Room)
URL: http://www.ims.ac.jp/

Editorial Committee 2000

IMS 2000

It is only two months before we celebrate forthcoming 21st century. During the past 20th century, molecular science has made conspicuous development and as a result, many important facts in the neighboring research fields such as biology and environmental science have been unveiled at the molecular level.

This year, IMS determined three basic research items as main fundamental objects of research. They are, (1) design and synthesis of novel materials, (2) basis of photo-physics and photo-chemistry, and (3) reaction dynamics, respectively. Bio-molecular science which is one of the important targets of IMS belongs to the category of science composed of above three basic items.

In this annual review, a reader may find the new aspects of molecular science conducted at IMS in the fiscal year 2,000 which extends from basic reaction dynamics in gas phase to complex biological problems such as protein folding.

November, 2000

Koji Kaya

KAYA, Koji
Director General

CONTENTS

Department of Theoretical Studies

I-A Development of New Numerical Techniques in the Study of Molecular Structure

I-B Electron-Hydrogen Bond in Water Clusters and Their Complexes with Atomic Ions

I-C Computational Chemistry of Atomic and Molecular Processes in Atmospheric Environment

I-D Prediction of Protein Tertiary Structures from the First Principles

I-E Development of Simulation Algorithms for Complex Systems

I-F Theory of Nonadiabatic Transition

I-G Theoretical Studies of Chemical Reaction Dynamics

I-H New Way of Controlling Molelular Processes

I-I New Methods to Treat Scattering Problems

I-J Theoretical Study of Multi-Dimensional Tunneling

I-K Theoretical Studies of Ultrafast Nonlinear Optical Spectroscopy of Molecules in Condensed Phases

I-L Quantum dynamics in the condensed phases

I-M Soft Matter Physics in Biomimetic Systems

I-N Liquid-Liquid Phase Transition of Water and Its Potential Surface

I-O Development of Techniques for Prediction of Conformations and Applications to Proteins and Organic Compounds

I-P Microscopic Solvation of Alkali Atom and Aggregates in Polar Solvent Clusters

I-Q Theoretical Analyses on Nonlinear Behavior of Complex Systems

I-R Electronic Structure of a Molecule in Solution

I-S Solvation Thermodynamics of Protein and Related Molecules

I-T Collective Density Fluctuations in Polar Liquids and Their Response to Ion Dynamics

I-U Liquid-Solid Interface

I-V Dimensional Crossovers and Excitation Spectra in Quasi-One-Dimensional Organic Conductors

I-W Optical Excitations in Charge-Lattice-Ordered Phases of One-Dimensional Materials

I-X Magnetic and Optical Properties of Two-Dimensional Metal-Complex and Organic Conductors

I-Y Multi-Phase Stability and Nonlinear Dynamics near Phase Boundary

Department of Molecular Structure

II-A Laser Cooling and Trapping of Metastable Helium Atoms

II-B Spectroscopic Studies on Atoms and Ions in Liquid Helium

II-C Endohedral Metallofullerenes: New Fullerene Molecules with Novel Properties

II-D Structure and Function of Respiratory Terminal Oxidases

II-E Structure and Function of Transmembrane Electron Transfer System in Neuroendocrine Secretory Vesicles

II-F Structure and Function of Steroidogenic Cytochrome P450 System

II-G Biomolecular Science

II-H Fast Dynamics of Photoproducts in Solution Phases

II-I Molecular and Electronic Structures of Metallofullerenes and the Fullerene Radical Anions

II-J State Correlated Raman Spectroscopy

Department of Electronic Structure

III-A Photochemical Synthesis of Exotic Atomic-Molecular Binary Clusters in Solution: π Radical -Transition Metal Alternatively Stacking $(\pi–d)_n$ Clusters

III-B States of Neutral and Ionic Molecular Associates in Solutions

III-C Ultrafast Dynamics and Structural Changes of Excited Cation Radicals in Solution

III-D Spectroscopic and Dynamical Studies on Charge Delocalization and Charge Transfer in Aromatic Molecular Cluster Ions

III-E Structures and Reactivities of Metal Clusters

III-F Spectroscopy and Dynamics of Vibrationally Excited Molecules and Clusters

III-G Time-Resolved Photoelectron Imaging on Ultrafast Chemical Dynamics

III-H Crossed Beam Studies on Bimolecular Reaction Dynamics

III-I Non-Adiabatic Molecular Photodissociation Dynamics Studied by Polarization Spectroscopy

III-J Photochemistry on Well-Defined Surfaces

III-K Structure and Properties of Polyoxometalates with a Magnetic, Electronic, or Biological Significance

RESEARCH ACTIVITIES IV --------81

Department of Molecular Assemblies

IV-A Spectroscopic Study of Organic Conductors

IV-B Solid State Properties of Organic Conductors with p-d Interaction

IV-C Microscopic Investigation of Molecular-Based Conductors

IV-D Development of Magnetic Organic Superconductors

IV-E Structural and Electrical Properties of Molecular Crystals at Low Temperature and/or High Pressure

IV-F Development of New Functional Molecular Materials

IV-G Electrical Properties of Organic Semiconductors in Ultrahigh Vacuum

IV-H Preparation and Characterization of Highly Oriented Organic Films

IV-I Properties of Gas Adsorption on Single-Walled Carbon Nanotube Aggregates

IV-J Electronic Properties of Pristine and Doped Snigle-walled Carbon Nanotubes aggregates

IV-K Structural and Electronic Properties of Fullerene-based Compounds

IV-L Development of Pulsed Field Gradient NMR Spectroscopy

IV-M Phase Transition Mechanism of Reentrant Liquid Crystal

IV-N Systematic Study of Organic Conductors

IV-O Photoelectron Spectroscopy of Organic Solids in Vacuum Ultraviolet Region

Department of Applied Molecular Science

V-A Molecular Mechanisms of Oxygen Activation by Heme Enzymes

V-B Model Studies of Non-Heme Proteins

V-C Aqueous Organometallic Chemistry

V-D Magnetic Structure of Oligo-Nitroxide-Transition Metal Complexes

V-E Synthesis of Chiral Molecule-Based Magnets

V-F Synthesis and Characterization of Quantum-Spin Systems

V-G Pressure Effects on Molecular Magnetism

V-H Desorption Induced by Electronic Transitions at the Surface of Van der Waals Condensates

V-I Bioinorganic Studies on Structures and Functions of Non-Heme Metalloenzymes Using Model Complexes

V-J Synthesis and Physical Properties of Novel Molecular Metals

V-K Fast Bimolecular Reaction Kinetics in Solution

V-L Development of Model Core Potentials and Post Hartree-Fock Calculations to Atoms and Molecules

V-M Theoretical Study of the Electronic Structures of Weakly Bound Molecules

V-N Theory for Quantum Liquids and Molecular Dynamics Study Using Potentials by *ab initio* Molecular Orbital Calculations

V-O Determination of Structures of Neutral Clusters

V-P Reaction Dynamics in the Gas Phase and on Surface

V-Q Millimeter-Wave Spectroscopy Combined with Pulsed-Jet Expansion Technique for the Detection of the Novel Unstable Species and the van der Waals Mode Transitions of Molecular Clusters

V-R Ion-Molecule Reactions in the Troposphere

V-S Monte Carlo Simulation of Molecular Clusters

V-T Development of Shaped Pulse Solid-State NMR Spectroscopy

V-U Development of ^{13}C High-Resolution NMR Spectroscopy for Nematic and Cholesteric Liquid Crystals

Department of Vacuum UV Photoscience

VI-A Electronic Structure and Decay Mechanism of Inner-Shell Excited Molecules

VI-B Soft X-ray Photoelectron-Photoabsorption Spectroscopy and Electronic Structure of Transition Metal Compounds

VI-C Observation of Vibrational Coherence (Wavepacket Motion) in Solution-Phase Molecules Using Ultrashort Pulses

VI-D Studies of Primary Photochemical/physical Processes Using Femtosecond Electronic Spectroscopy

VI-E Studies of Photochemical Reactions Using Picosecond Time-Resolved Vibrational Spectroscopy

VI-F Synchrotron Radiation Stimulated Surface Reaction and Application to Nanoscience

VI-G Photoionization Dynamics Studied by Electron Spectroscopy Combined with a Continuous Synchrotron Radiation Source

VI-H Development of a Laser-Synchrotron Radiation Combination Technique to Study Photoionization of Polarized Atoms

VI-I Vacuum UV Spectroscopy Making Use of a Combination of Synchrotron Radiation and a Mode-Locked or Pulsed UV Laser

VI-J Monochromator Newly Developed on the Beam Line BL2B2 in UVSOR

VI-K Thin Film Preparation with Chemical Vapor Deposition Using Vacuum Ultraviolet Radiation

VI-L Ultraviolet, Visible and Infrared Spectroscopy of Solids

VI-M Dynamics and Relaxation of Atoms and Molecules Following Core-Level Excitation

VI-N Study on RF-Photocathode for Compact X-Ray Sources

Coordination Chemistry Laboratories

VII-A New Insight into Mechanism of Oxygen Activation in Biological Oxygenases

VII-B Electronic Structure and Reactivity of Metal Cluster Complexes

VII-C Research on the Relationship between Structure of Vanadyl Complex and Insulin-Mimetic Activity

VII-D Syntheses of Transition Metal-Sulfur Clusters and Development of Their Catalysis

VII-E Reductive Activation of Carbon Monoxide derived from Carbon Dioxide and Oxidative Activation of Hydroxy- and Oxo-Groups Derived from Water

VII-F Synthesis of Transition-Metal Chalcogenido Complexes and Their Cluster-Forming Reactions

VII-G Artificial Photoreaction systems on a Protein Surface

VIII-E Molecular Mechanism of Heme Degradation and Oxygen Activation by Heme Oxygenase

VIII-F Designing Artificial Photosynthesis at Molecular Dimensions

VIII-G Development of New Metal Complexes as Redox Catalysts

VIII-H Development of Organic n-Type Semiconductors for Molecular Thin-Film Devices

VIII-I The Effects of the 2D Spin-Echo NMR Experiment on a Solid-State Homonuclear Sipn-1/2 Pair

VIII-J The Applications of Double-Rotation NMR Method

Equipment Development Center

VIII-K Development of "IMS Machines"

VIII-L Development of New Laser Materials

Ultraviolet Synchrotron Orbital Radiation Facility

VIII-M Development of the UVSOR Light Source

VIII-N Researches by the USE of UVSOR

Computer Center

VIII-O Theoretical Studies on Electronic Structure and Dynamics of Electronically Excited States in Polyatomic Molecules

(a) Chemical Reaction Dynamics

(b) Molecular Photophysics and Science

(c) Novel Material Science

(1) Special Projects
(2) Research Symposia
(3) Cooperative Research
(4) Use of Facility
(5) UVSOR

Abbrevations

IMS: Institute for Molecular Science
GUAS: The Graduate University for Advanced Studies

ORGANIZATION AND STAFF

Organization

The Institute for Molecular Science comprises twenty two research laboratories — each staffed by a professor, an associate professor, two research associates and several technical associates —, two research laboratories with foreign visiting professors, and five research facilities.

The laboratories are grouped into six departments and one facility for coordination chemistry:

Department of Theoretical Studies	Theoretical Studies I Theoretical Studies II Theoretical Studies III[1] Theoretical Studies IV
Department of Molecular Structure	Molecular Structure I Molecular Structure II[1] Molecular Dynamics
Department of Electronic Structure	Excited State Chemistry Excited State Dynamics Electronic Structure[1] Molecular Energy Conversion[2]
Department of Molecular Assemblies	Solid State Chemistry Molecular Assemblies Dynamics Molecular Assemblies[1]
Department of Applied Molecular Science	Applied Molecular Science I Applied Molecular Science II[1] Molecular Clusters[3]
Department of Vacuum UV Photoscience	Photochemistry Chemical Dynamics Interface Molecular Science[3] Synchrotron Radiation Research[2]
Coordination Chemistry Laboratories	Synthetic Coordination Chemistry[3] (–March ’00) Complex Catalysis Functional Coordination Chemistry Coordination Bond[1]

The research facilities are:

• Laser Research Center for Molecular Science	Advanced Lasers for Chemical Reaction Studies Advanced Lasers for Synchrotron Radiation Applications Advanced UV and IR Tunable Lasers
• Research Center for Molecular Materials	Organic Materials Section Hybrid Materials Section Materials Characterization Section Structure Control Section
• Equipment Development Center	
• UVSOR (Ultraviolet Synchrotron Orbital Radiation) Facility	

- Computer Center

1) Professors and associate professors are visiting professors from other universities.
2) Research laboratories with foreign visiting professors.
3) Professors, associate professors, and research associates, along with their positions, are transferred from other universities.

Scientific Staff

KAYA, Koji	**Professor, Director-General**

Emeritus Professors

NAGAKURA, Saburo	President, The Kanagawa Academy of Science and Technology
HIROTA, Eizi	President, The Graduate University for Advanced Studies
KIMURA, Katsumi	Senior Researcher, Molecular Photonics & Photoelectron Group, Communications Research Laboratory
MOROKUMA, Keiji	Professor, Emory University, U. S. A.
INOKUCHI, Hiroo	Chief Scientist of Space Utilization Research Program, National Space Development Agency of Japan
MARUYAMA, Yusei	Professor, Hosei University
YOSHIHARA, Keitaro	Professor, Japan Advanced Institute of Science and Technology
HANAZAKI, Ichiro	
IWAMURA, Hiizu	Professor, University of the Air
SAITO, Shuji	Professor, Fukui University
IWATA, Suehiro	Professor, Hiroshima University

Department of Theoretical Studies

Theoretical Studies I

IWATA, Suehiro	Professor (–March ’00)[1)]
OKAMOTO, Yuko	Associate Professor
IKEGAMI, Tsutomu	Research Associate
SUGITA, Yuji	Research Associate
TSURUSAWA, Takeshi	Technical Associate
NAGASHIMA, Takehiro	Technical Associate (April ’00–)
YODA, Takao	IMS Fellow (April ’00–)
KOVALENKO, Andriy F.	Research Associate of Research for the Future Program (–November ’00)
NISHIKAWA, Takeshi	Research Associate of Research for the Future Program
ITOH, Masakatsu	Research Associate of Research for the Future Program
MITSUTAKE, Ayori	Graduate Student (–September ’99), JSPS Post-Doctoral Fellow (October ’99–March ’00), Research Associate of Research for the Future Program (April ’00–)
LEE, Sang Yeon	Visiting Scientist (from Kyungpook National University, Korea); MONBUSHO Invited Fellow (December ’99–February ’00)[2)]
ISHIKAWA, Yasuyuki	Visiting Scientist (from University of Puerto Rico, U. S. A.); MONBUSHO Invited Fellow (May–August ’00)[3)]
SATOH, Katsuhiko	JSPS Post-Doctoral Fellow (–March ’00)[4)]
CHEN, Feiwu	Research Fellow (–April ’00)[5)]
HASHIMOTO, Tomohiro	Research Fellow (–March’00)[1)]
SALAI, Cheettu Ammal	Visiting Scientist
OHTSUKA, Hiroshi	Graduate Student (–September ’99)
OKADA, Kazutoshi	Graduate Student (–March ’00)

Theoretical Studies II

NAKAMURA, Hiroki	Professor
OSHEROV, Vladimir	Visiting Professor (–December ’99)[6)]
TANIMURA, Yoshitaka	Associate Professor
ZHU, Chaoyuan	Research Associate
OKUMURA, Ko	Research Associate
TAKAMI, Toshiya	Research Associate
SUZUKI, Yoko	Technical Associate
MIYAZAKI, Kunimasa	IMS Fellow (–March ’00)[7)]
MISHIMA, Kenji	IMS Fellow
KATO, Tsuyoshi	IMS Fellow (May ’00–)
MIL’NIKOV, Gennady V.	Visiting Scientist; JSPS Post-Doctoral Fellow (–December ’99), Visiting Scientist (February–March, May–July ’00)

BIAN, Wensheng	Visiting Scientist; JSPS Post-Doctoral Fellow (February ’00–)
IMAMURA, Yutaka	JSPS Post-Doctoral Fellow (–March ’00)8)
PICHL, Lukas	Graduate Student
NAGAYA, Kuninobu	Graduate Student
KAMISAKA, Hideyuki	Graduate Student
HINO, Osamu	Graduate Student
FUKAMI, Hiroshi	Graduate Student (from Kyoto University)* (August ’00–)

Theoretical Studies III

TANAKA, Hideki	Visiting Professor (from Okayama University) (–March ’00)
KIKUCHI, Takeshi	Visiting Professor (from Kurashiki University of Science and the Arts) (April ’00–)
HASHIMOTO, Kenro	Visiting Associate Professor (from Tokyo Metropolitan University) (–March ’00)
KINOSHITA, Masahiro	Visiting Associate Professor (from Kyoto University) (April ’00–)
KOVALENKO, Andriy F.	Research Associate (May ’00–)

Theoretical Studies IV

HIRATA, Fumio	Professor
YONEMITSU, Kenji	Associate Professor
SATO, Hirofumi	Research Associate
KISHINE, Jun-ichiro	Research Associate
SETHIA , Ashok	IMS Fellow
KUWABARA, Makoto	IMS Fellow
IMAI, Takashi	Graduate Student (–March ’00), Research Associate of Research for the Future Program (April ’00–)
AKIYAMA, Ryo	JSPS Post-Doctoral Fellow (–March ’00), Research Fellow (April–August ’00)9)
MORI, Michiyasu	JSPS Post-Doctoral Fellow
SUMI, Tomonari	JSPS Post-Doctoral Fellow (April ’00–)
IMAMURA, Chikara	Visiting Scientist (from Yamaguchi Prefectural University) (April ’00–)
HARANO, Yuichi	Graduate Student (from Kobe University)*
YAMAZAKI, Takeshi	Graduate Student
MIYASHITA, Naoyuki	Graduate Student

Department of Molecular Structure

Molecular Structure I

MORITA, Norio	Associate Professor
MORIWAKI, Yoshiki	Research Associate
KUMAKURA, Mitsutaka	Technical Associate (–March ’00)10)

Molecular Structure II

AKASAKA, Takeshi	Visiting Professor (from Niigata University)
TSUBAKI, Motonari	Visiting Associate Professor (from Himeji Institute of Technology) (–March ’00)11)
SASADA, Hiroyuki	Visiting Associate Professor (from Keio University) (April ’00–)

Molecular Dynamics

KITAGAWA, Teizo	Professor
KATO, Tatsuhisa	Associate Professor
MATSUSHITA, Michio	Research Associate (–March ’00)12)
MIZUTANI, Yasuhisa	Research Associate
HAYASHI, Naoki	Technical Associate
NAGATOMO, Shigenori	Technical Associate
IWASE, Tadashi	Research Fellow (December ’99), IMS Fellow (January–March ’00), Research Fellow (April ’00–)
KIM, Younkyoo	Visiting Scientist; MONBUSHO Invited Fellow (from Hankuk University of Foreign Studies, Korea) (June–August ’00)13)

MO, Yu-jun	Visiting Scientist; MONBUSHO Invited Fellow (from Henan University, China) (May ’00–)
LI, Zheng-qiang	Visiting Scientist; MONBUSHO Invited Fellow (from Jilin University Changchun, China) (May ’00–)
HUDECEK, Jirika	Visiting Scientist; JSPS Invited Fellow (from Charles University, Czech Republic) (July–August ’00)14)
VERMA, Alan L.	Visiting Scientist; JSPS Invited Fellow (from North-Eastern Hill University, India) (July ’00–)
NAKUL, Chandra M.	Visiting Scientist; JSPS Post-Doctral Fellow (from Tata Institute of Fundamental Research, India) (–March ’00)15)
HU, Ying	Visiting Scientist; JSPS Post-Doctral Fellow (from Fudan University, China)
UCHIDA, Takeshi	JSPS Post-Doctral Fellow
KANEMOTO, Katsuichi	JSPS Post-Doctral Fellow (April ’00–)
AKI, Michihiko	Graduate Student
YAMAMOTO, Kohji	Graduate Student (–March ’00)16)
HARUTA, Nami	Graduate Student
OKUNO, Daichi	Graduate Student
OKUBO, Shingo	Graduate Student
SATO, Akira	Graduate Student (April ’00–)

Department of Electronic Structure

Excited State Chemistry

NISHI, Nobuyuki	Professor
TSUKUDA, Tatsuya	Associate Professor (January ’00–)
NAKABAYASHI, Takakazu	Research Associate
NEGISHI, Yuichi	Research Associate (July ’00–)
KOSUGI, Kentaroh	Graduate Student
HINO, Kazuyuki	Graduate Student (from Kyushu University)* (April ’00–)
KAMO, Satoshi	Graduate Student (from Tsukuba University)* (April ’00–)

Excited State Dynamics

FUJII, Masaaki	Professor
SUZUKI, Toshinori	Associate Professor
KOHGUCHI, Hiroshi	Research Associate
SAKAI, Makoto	Research Associate
KATAYANAGI, Hideki	Technical Associate
SAEKI, Morihisa	IMS Fellow
WHITAKER, Benjamin J.	Visiting Scientist; MONBUSHO Invited Fellow (from University of Leeds, UK) (June ’00–)
WATANABE, Takeshi	JSPS Post-Doctoral Fellow (April ’00–)
ISHIUCHI, Shun-ichi	Graduate Student
HOSSAIN, Delwar	Graduate Student
TSUBOUCHI, Masaaki	Graduate Student

Electronic Structure

MATSUMOTO, Yoshiyasu	Visiting Professor (from GUAS) (–March ’00)17)
YAMASE, Toshihiro	Visiting Professor (from Tokyo Institute of Technology) (April ’00–)
TAMAI, Naoto	Visiting Associate Professor (from Kwansei Gakuin University) (–March ’00)18)
OHSHIMA, Yasuhiro	Visiting Associate Professor (from Kyoto University) (July ’00–)
INOKUCHI, Yoshiya	Research Associate

Molecular Energy Conversion

MARKOSYAN, Ashot Surenovich	Visiting Professor (from M. V. Lomonossov Moscow State University, Russia) (–March ’00)
MO, Yu-Jun	Visiting Professor (from Honan University, China) (May ’00–)
WHITHAM, Christopher J.	Visiting Associate Professor (from Oxford University, UK) (–June ’00)
GRITSENKO, Victor V.	Visiting Associate Professor (from Institute for Chemical Physics Research Russian Academy of Sciences, Russia)

(June ’00–)

Department of Molecular Assemblies

Solid State Chemistry

YAKUSHl, Kyuya	Professor
NAKAMURA, Toshikazu	Associate Professor
NAKAZAWA, Yasuhiro	Research Associate (–March ’00)[19]
YAMAMOTO, Kaoru	Research Associate
URUICHI, Mikio	Technical Associate
MAKSIMUK, Mikhail	IMS Fellow
TSUKADA, Hiroshi	IMS Fellow
DROZDOVA, Olga	Visiting Scientist; MONBUSHO Invited Fellow (from Ioffe Physical Technical Institute) (April ’00–)
SIMONYAN, Mkhitar	Visiting Scientist (from Armenian Academy of Science) (May ’00–)
NAKANO, Chikako	Research Fellow
OUYANG, Jianyong	Graduate Student (–March ’00)[20]
DING, Yuqin	Graduate Student

Molecular Assemblies Dynamics

KOBAYASHI, Hayao	Professor
TADA, Hirokazu	Associate Professor (April ’00–)
OGATA, Hironori	Research Associate
FUJIWARA, Hideki	Research Associate
OISHl, Osamu	Technical Associate
OKANO, Yoshinori	Technical Associate (April ’00–)
TAMURA, Itaru	IMS Fellow (October ’00–)
NARYMBETOV, Bakhyt	Visiting Scientist; JSPS Post-Doctoral Fellow (–March ’00)[21]
TANAKA, Hisashi	JSPS Post-Doctoral Fellow
ADACHI, Takafumi	Research Fellow (–March ’00)[22]
FUJIWARA, Emiko	Graduate Student (–March ’00), Research Fellow (April ’00–)

Molecular Assemblies

TOKUMOTO, Madoka	Visiting Professor (from Electrotechnical Laboratory)
MORI, Takehiko	Visiting Associate Professor (from TokyoInstitute of Technology)
HASEGAWA, Shinji	Research Associate

Department of Applied Molecular Science

Applied Molecular Science I

WATANABE, Yoshihito	Professor
INOUE, Katsuya	Associate Professor
HOSOKOSHI, Yuko	Research Associate
UENO, Takafumi	Research Associate (March ’00–)
AHN, Kwang-Hyun	Visiting Scientist (from Kyung Hee University, Korea); MONBUSHO Invited Fellow (February–July ’00)[23]
KIM, Cheal	Visiting Scientist (from Seoul National Polytechnic University, Korea); MONBUSHO Invited Fellow (July–August ’00)[24]
ROACH, Mark P.	Visiting Scientist; JSPS Post-Doctoral Fellow (–November ’99)[25]
KUMAGAI, Hitoshi	JSPS Post-Doctoral Fellow[26]
MATSUI, Toshitaka	JSPS Post-Doctoral Fellow (–March ’00)[27]
YAMAHARA, Ryo	Visiting Scientist (from Nagoya Institute of Technology)
KISHIDA, Mitsumi	Visiting Scientist (from Nagoya Institute of Technology)
NAKAI, Hidetaka	Research Fellow (from Kinki University)
SUZUKI, Kazuharu	Research Fellow (from Graduate University)
IWAHORI, Fumiyasu	Graduate Student (–March ‘00)[28]
MAKIHARA, Nobuyuki	Graduate Student
HARA, Isao	Graduate Student
YANG, Huijun	Graduate Student
SUZUKI, Kentaro	Graduate Student

KATO, Shigeru	Graduate Student
OHASHI, Masataka	Graduate Student
ABURA, Tsutomu	Graduate Student
KATOH, Keiichi	Graduate Student

Applied Molecular Science II

ARAKAWA, Ichiro	Visiting Professor (from Gakushuin University) (–March ’00)[29]
MASUDA, Hideki	Visiting Professor (from Nagoya Institute of Technology) (April ’00–)
MISAKI, Yohji	Visiting Associate Professor (from Kyoto University) (–March ’00)[30]
IWATA, Koichi	Visiting Associate Professor (from The University of Tokyo) (April ’00–)
OGO, Seiji	Research Associate

Molecular Clusters

MIYOSHI, Eisaku	Professor (–March ’00)[31]
KASAI, Toshio	Professor (from Osaka University)
TANAKA, Keiichi	Associate Professor (–March ’00)[32]
NAGATO, Kenkichi	Associate Professor (–March ’00)[33]
TAKASU, Masako	Associate Professor (from Kanazawa University)
HARADA, Kensuke	Research Associate (–March ’00)[34]
KUBO, Atsushi	Research Associate (from Kyoto University)
CHE, Dock-Chil	Research Associate (from Osaka University)
HASHIMOTO, Masahito	IMS Fellow (from Kanazawa University)
GHOSH, Tapas K.	IMS Fellow (–March ’00)[35]
MIZOGUCHI, Asao	IMS Fellow (–October ’99)[36]
SUMI, Tomonari	JSPS Post-Doctoral Fellow (–March ’00)[37]
NOGUCHI, Hiroshi	JSPS Post-Doctoral Fellow (from Kyoto University)
HASHINOKUCHI, Michihiro	Research Fellow (from Osaka University)
NOSAKA, Makoto	Research Fellow (from Kanazawa University)
ICHIKAWA, Shinji	Research Fellow (from Kyoto University)
NISHIYAMA, Yusuke	Research Fellow (from Kyoto University)

Department of Vacuum UV Photoscience

Photochemistry

KOSUGI, Nobuhiro	Professor
TAHARA, Tahei	Associate Professor
TAKATA, Yasutaka	Research Associate (–April ’00)[38]
TAKEUCHI, Satoshi	Research Associate
HATSUI, Takaki	Research Associate (August ’00–)
ADACHI, Jun-ichi	Technical Associate (–September ’99)[39]
MIZUNO, Misao	Technical Associate
OJI, Hiroshi	IMS Fellow (April ’00–)
ARZHANTSEV, Sergei Yur’evich	Visiting Scientist; JSPS Post-Doctoral Fellow
FUJINO, Tatsuya	JSPS Post-Doctoral Fellow
NAGASONO, Mitsuru	JSPS Post-Doctoral Fellow (April ’00–)
FUJIYOSHI, Satoru	Graduate Student

Chemical Dynamics

URISU, Tsuneo	Professor
MITSUKE, Koichiro	Associate Professor
MIZUTANI, Masakazu	Research Associate
NONOGAKI, Youichi	Research Associate (April ’00–)
MEKARU, Harutaka	IMS Fellow (–February ’00)[40]
ONO, Masaki	IMS Fellow
IWASAKI, Kota	JSPS Post-Doctoral Fellow
AZUMA, Yasushi	JSPS Post-Doctoral Fellow (April ’00–)
YOSHIMURA, Daisuke	Research Fellow (April ’00–)
NIIKURA, Hiromichi	Graduate Student (–March ’00)[41]
NODA, Hideyuki	Graduate Student
WANG, Zhihong	Graduate Student (October ’99–)
YOKOYAMA, Takahiro	Graduate Student (from Nagoya University)

Interface Molecular Sicence

KUROSAWA, Kou	Professor
NAGAOKA, Shin-ichi	Associate Professor
FUKUI, Kazutoshi	Associate Professor
TAKASHIMA, Yoshifumi	Research Associate
TAKEZOE, Noritaka	IMS Fellow (–May ’00)42)
MIURA, Hiroshi	Graduate Student (–September ’99)43)
YANAGITA, Hideaki	Graduate Student
SAKAKIBARA, Tsutomu	Graduate Student
KIHARA, Takayoshi	Graduate Student (October ’99–)
DOI, Youichirou	Graduate Student (October ’99–)
KAWASAKI, Yasuhiro	Graduate Student (April ’00–)
TANAKA, Takashi	Graduate Student (April ’00–)

Synchrotron Radiation Research

PAVLOV, Lubomir Iordanov	Visiting Professor (from Bulgarian Academy of Science, Bulgaria) (September ’99–March ’00)44)
SEIJO, Luis	Visiting Associate Professor (from University Autonoma de Madrid, Spain) (–December ’99)45)
AHN, Kwang Hyun	Visiting Associate Professor (from Kyung-Hee University, Korea) (February–July ’00)46)
MIL’NIKOV, Gennady V.	Visiting Associate Professor (from Russian Academy of Science, Russia) (August ’00–)47)

Coordination Chemistry Laboratories

TANAKA, Koji	Director

Synthetic Coordination Chemistry

NISHIDA, Yuzo	Professor (–March ’00)48)
EBIHARA, Masahiro	Associate Professor (–March ’00)49)
OZAWA, Tomohiro	Research Associate (–March ’00)50)
KUMITA, Hideyuki	Graduate Student (from Nagoya Institute of Technology)* (–March ’00)
KOBAYASHI, Teruyuki	Graduate Student (from Yamagata University)* (–March ’00)48)
OKUTSU, Wataru	Graduate Student (from Yamagata University)* (–March ’00)48)
TAKAHASHI, Yasuyuki	Graduate Student (from Yamagata University)* (–March ’00)48)
NISHINO, Satoshi	Graduate Student (from Yamagata University)* (–March ’00)48)
KUNITA, Mami	Graduate Student (from Yamagata University)* (–March ’00)48)

Complex Catalysis

UOZUMI, Yasuhiro	Professor (April ’00–)
TANIGUCHI, ISAO	Visiting Professor (from Kumamoto University) (April ’00–)
SAKURAI, Hiromu	Visiting Professor (from Kyoto Pharmaceutical University) (–March ’00)
TANAKA, Yasutaka	Visiting Associate Professor (from Shizuoka University) (April ’00–)
MIZOBE, Yuji	Visiting Associate Professor (from the Unicersity of Tokyo) (–March ’00)
DANJO, Hiroshi	JSPS Post-Doctral Fellow (April ’00–)
SHIBATOMI, Kazutaka	Graduate Student (from Nagoya City University)* (April ’00–)
YASOSHIMA, Kayo	Graduate Student (from Nagoya City University)* (April ’00–)
NAKAZONO, Maki	Graduate Student (from Nagoya City University)* (April ’00–)
TANAKA, Hirotaka	Graduate Student (from Nagoya City University)* (April ’00–)
NAKAO, Ryu	Graduate Student (from Nagoya City University)* (April

’00–)

Functional Coordination Chemistry

TANAKA, Koji	Professor
HIROYUKI, Kawaguchi	Associate Professor (May ’00–)
TSUGE, Kiyoshi	Research Associate (–March ’00)[51]
MIZUKAWA, Tetsunori	Technical Associate
SHIREN, Kazushi	IMS Fellow (April ’00–)
WADA, Hiroaki	Visiting Scientist (from the Institute of Physical and Chemical Research) (Octover ’99–)
WADA, Toru	Graduate Student
TOMON, Takashi	Graduate Student
KOBAYASHI, Katsuaki	Graduate Student
KOMURO, Takashi	Graduate Student (May ’00–)

Coordinatiom Bond

AIDA, Takuzo	Visiting Professor (from the University of Tokyo)
HAMACHI, Itaru	Visiting Professor (from Kyusyu University)

Research Facilities

Laser Research Center for Molecular Science

FUJII, Masaaki	Director

Advanced Lasers for Chemical Reaction Studies

SATO, Shin-ichiro	Associate Professor (–April ’00)
WATANABE, Kazuo	Research Associate (–June ’00)

Advanced Lasers for Synchrotron Radiation Applications

SARUKURA, Nobuhiko	Associate Professor
OHTAKE, Hideyuki	Research Associate
MURAKAMI, Hidetoshi	IMS Fellow (October ’99–)
LIU, Zhenlin	Graduate Student
KAWAHATA, Eiji	Graduate Student
KOZEKI, Toshimasa	Graduate Student
ONO, Shingo	Graduate Student
SUZUKI, Yuji	Graduate Student (April ’00–)

Advanced UV and IR Tunable Lasers

TAIRA, Takunori	Associate Professor
KURIMURA, Sunao	Research Associate
CHA, Myoungsik	Visiting Associate Professor; MONBUSHO Invited Fellow (June ’00–)
SHOJI, Ichiro	IMS Fellow
PAVEL, Nicolaie	Visiting Scientist; JSPS Post-Doctoral Fellow
SAIKAWA, Jiro	Graduate Student
SATO, Yoichi	Graduate Student

Research Center for Molecular Materials

WATANABE, Yoshihito	Director
KUWAHARA, Daisuke	Research Associate

Organic Materials Section

YAMASHITA, Yoshiro	Associate Professor (–March ’00)[52]
TANAKA, Shoji	Research Associate
TOMURA, Masaaki	Technical Associate
ZAMAN, Mohammed Badruz	IMS Fellow
SUZUKI, Kazuharu	Graduate Student (–March ’00)
AKHTARUZZAMAN, Mohammed	Graduate Student (April ’00–)

Hybrid Materials Section

FUJII, Hiroshi	Associate Professor
FUNAHASHI, Yasuhiro	Research Associate

MIZUTANI, Mamoru	IMS Fellow (–March ’00)
IKEUE, Takahisa	JSPS Post-Doctoral Fellow (April ’00–)

Materials Characterization Section

NAGATA, Toshi	Associate Professor
ITO, Hajime	Research Associate
KIKUZAWA, Yoshihiro	Graduate Student
ITO, Kaname	Graduate Student (April ’00–)

Structure Control Section

SUZUKI, Toshiyasu	Associate Professor
SAKAMOTO, Youichi	Research Associate
HEIDENHAIN, Sophie	Visiting Scientist
KOMATSU, Shingo	Graduate Student (from Kyushu University) (April ’00–)

Equipment Development Center

YAKUSHI, Kyuya	Director
WATANABE, Michio	Associate Professor
ASAKA, Shuji	Research Associate (–May ’00)

Ultraviolet Synchrotron Orbital Radiation Facility

KOSUGI, Nobuhiro	Director
KAMADA, Masao	Associate Professor
HAMA, Hiroyuki	Associate Professor (–March ’00)[53]
KATOH, Masahiro	Associate Professor (March ’00–)
SHIGEMASA, Eiji	Associate Professor
KIMURA, Shin-ichi	Visiting Associate Professor (from Kobe University)
TANAKA, Shin-ichiro	Research Associate (–October ’99)[54]
HOSAKA, Masahito	Research Associate
GEJO, Tatsuo	Research Associate
KOUDA, Shigeru	Research Associate
TAKAHASHI, Kazutoshi	Research Associate (April ’00–)
MORÉ, Sam Dylan	Visiting Scientist; JSPS Post-Doctral Fellow
TANAKA, Senku	Graduate Student (April ’00–)

Computer Center

IWATA, Suehiro	Director (–March ’00)
HIRATA, Fumio	Director (April ’00–)
AOYAGI, Mutsumi	Associate Professor
NANBU, Shinkoh	Research Associate
MINAMINO, Satoshi	Technical Associate
OKADA, Kazutoshi	Research Fellow (April ’00–)
CHOE, Jong-In	Visiting Scientist (from Chung-Ang University, Korea) (August ’00–)
CHUNG, Gyusung	Visiting Scientist (from Konyang University, Korea) (–January ’00)
KINOSHITA, Tomoko	Graduate Student

* Carries out graduate research of IMS on Cooperative Education Program of IMS with other graduate schools.

Technical Staff

SAKAI, Kusuo	Technical Division Head
MATSUDO, Osamu	Technical Section Chief
KATO, Kiyonori	Technical Section Chief
NISHIMOTO, Fumio	Technical Section Chief
YAMANAKA, Takaya	Technical Section Chief
KINOSHITA, Toshio	Electronic Structure (Unit Chief)
UEDA, Tadashi	Laser Research Center for Molecular Science (March ’00–)
NAGATA, Masaaki	Research Center for Molecular Materials (Unit Chief)
YOSHIDA, Hisashi	Research Center for Molecular Materials (Unit Chief)
NOMURA, Sachiyo	Research Center for Molecular Materials (–May ’00)
SAKAI, Masahiro	Research Center for Molecular Materials
TAKAYAMA, Takashi	Research Center for Molecular Materials; Unit Chief (June ’00–)
MAKITA, Seiji	Research Center for Molecular Materials (February ’00–)
MIZUTANI, Nobuo	Equipment Development Center (Unit Chief)
SUZUI, Mitsukazu	Equipment Development Center (Unit Chief)
UCHIYAMA, Kouichi	Equipment Development Center
TOYODA, Tomonori	Equipment Development Center
YANO, Takayuki	Equipment Development Center (–September ’99)
KONDOU, Takuhiko	Equipment Development Center
KOBAYASHI, Kazuhiro	Equipment Development Center
HAYASHI, Kenji	Equipment Development Center
HASUMOTO, Masami	UVSOR Facility (Unit Chief)
YAMAZAKI, Jun-ichiro	UVSOR Facility; Unit Chief (June ’00–)
NAKAMURA, Eiken	UVSOR Facility
KONDO, Naonori	UVSOR Facility
MIZUTANI, Fumiyasu	Computer Center (Unit Chief)
TESHIMA, Fumitsuna	Computer Center
NAITO, Shigeki	Computer Center

List of Present Addresses

1) Department of Chemistry, Faculty of Science, Hiroshima University, 1-3-1 Kagamiyama, Higashi-Hiroshima, 739-8526
2) Department of Industrial Chemistry, Kyungpook National University, 1370 Sankyuk-dong, Puk-ku, Taegu, 702-701 S. Korea
3) Department of Chemistry, University of Puerto Rico, P. O. Box 23346 San Juan, PR 00931-3346, U.S.A
4) Department of Chemistry, University of Southampton, Highfield, Southampton SO17 1BJ, United Kingdom
5) Chemistry department, Indiana University, 800 East Kirkwood Ave. Bloomington, Indiana, 47405-7102, USA
6) Institute of Chemical Physics, Russian Academy of Science, Chernogolovka, Moscow, Russia
7) IRI, Technische Universiteit Delft, Mekelweg 15, 2629JB Delft, Nederland (the Netherlands)
8) Department of Physics, University of Illinois, 1110 West Green Street, Urbana, IL, 61801, USA
9) Department of Chemistry and Chemical Biology, Baker Laboratory, Cornell University, Ithaca, NY 14853, USA
10) Department of Physics, Faculty of Science, Kyoto University, Kyoto 606-8502
11) Department of Life Science, Fuculty of Science, Himeji Institute of Technology, 3-2-1 Koto, Kamigoricho, Akogun, Hyogo 678-1297
12) Center for the Study of Excited States of Molecules, Huygens Laboratory, Leiden University, P.O. Box 9594, 2300RA Leiden, The Netherlands.
13) Department of Chemistry, Hankuk University of Foreign Studies, Yongin, Kyungki Do, 449-791, Korea.
14) Department of Biochemistry, Faculty of Science, Charles University, Albertov 812030, 12840 Praha 2, Cech Republic.
15) School of Biological Sciences, University of Missouri-Kansas City, 103 Biological Sciences Building, 5007 Rockhill Road, Kansas City, Missouri 64110, U.S.A.
16) Department of Chemistry, Faculty of Science, Kobe University, Nada, Kobe, 657-8501
17) The Graduate University for Advanced Studies, Hayama-cho 240-0193
18) Department of Chemistry, School of Science, Kwansei Gakuin University, 1-1-155 Uegahara, Nishinomiya 662-8501
19) Microcalorimetry Research Center, Faculty of Science. Osaka University. Toyonaka. Osaka 560-853 l
20) Japan Advanced Institute of Science and Technology, Asahidai 1-1, Tatsukuchi, Nomi-gun, Ishikawa 923-1292

21) Complex Institute of National Science, Karakalpak branch of Uzbek Academy of Science, Nukus 742000, Uzbekistan
22) Midorigaoka, Asahikawa 078-8302
23) Department of Chemistry, Kyung Hee University, Yongin, 449-701, Korea
24) Department of Fine Chemistry, Seoul National Polytechnic University, Seoul 139-743, Korea
25) Department of Molecular Biology, MB8, The Scripps Research Institute, 10550 N. Torrey Pines Rd.La Jolla, CA, USA 92037
26) Institut de Physique et Chimie des Materiaux de Strasbourg 23 Rue du Loess, 67037 Strasbourg Cedex, France
27) Laboratory of Bioreaction Design, Institute for Chemical Reaction Science, Tohoku University, 2-1-1, Katahira, Aobaku-ku, Sendai, 980-8577
28) Laboratoire de chemie du solide et Inorganique moleculaire, UMR6511, Universite de Rennes1 Campus de Beaulieu 35042 Rennes Cedex, France
29) Department of Physics, Gakushuin University, 1-5-1, Mejiro, Toshima, Tokyo 171-8588
30) Department of Molecular Engineering, Graduate School of Engineering, Kyoto University, Yoshida, Sakyo-ku, Kyoto 606-8501
31) Graduate School of Engineering Sciences, Kyushu University, 6-1 Kasuga Park, Fukuoka 816-8580
32) Department of Chemistry, Faculty of Sciences, Kyushu University, 6-10-1 Hakozaki, Higashiku, Fukuoka 812-8581
33) Department of Mechanical Engineering, Kochi National College of Technology, 200-1 Monobe, Nankoku 783-8508
34) Department of Chemistry, Faculty of Sciences, Kyushu University, 6-10-1 Hakozaki, Higashiku, Fukuoka 812-8581
35) Department of Chemistry, Faculty of Science and Technology, Tokyo Institute of Technology, 3-14-1 Hiyoshi, Kouhokuku, Yokohama, Kanagawa 223-8522
36) Department of Physics, Faculty of Science, Tokyo Institute of Technology, 2-12-1 Ohokayama, Meguro-ku, Tokyo 152-8551
37) Department of Theoretical Studies, IMS, Okazaki 444-8585
38) Soft X-ray Spectroscopy Laboratory, RIKEN Harima Institute, 1-1-1, Kouto, Mikazuki, Sayo, Hyogo 679-5148
39) Institute of Materials Structure Science, Tsukuba 305-0801
40) Laboratory of Advanced Science and Technology for Industry, Himeji Institute of Technology, 1479-6 Kanaji, Kamigori, Ako, Hyogo 678-1201
41) Femtosecond Science Program Steacie Institute for Molecular Sciences, National Research Council of Canada (NRC), 100 Sussex Dr., Ottawa, Ontario, Canada K1A0R6
42) Usio Inc., 1194, Sazuchi, Bessho-cho, Himeji, Hyogo 671-0224
43) Department of Electronics, Electronic Engineering, Fukui University, Fukui 910-8507
44) Institute of Electronics, Bulgarian Academy of Sciences, 72 Tzarigradsko chaussee, 1784 Sofia, Bulgaria
45) Department of Chemistry, University Automona de Madrid, 28049 Madrid, Spain
46) Department of Chemistry, Kyung-Hee University, Yongin-Kun, Kyung-Ki Do, 449-701, Korea
47) Institute of Structural Macrokinetics, Chernogolovka Russian Academy of Science, 142432, Chernogolovka
48) Faculty of Science, Yamagata University, 1-4-12 Koshirakawa-cho, Yamagata 990-0021
49) Faculty of Engineering, Gifu University, 1-1 Yanagido, Gifu 501-1193
50) Department of Chemistry, Nagoya Institute of Technology, Gokisyo-cho, Showa-ku, Nagoya 460-0061
51) Faculty of Science, Hokkaido University, Kita 8 Nishi 5, Kita-ku, Sapporo 060-0808
52) Department of Electronic Chemistry, Interdisciplinary Graduate School of Science and Engineering, Tokyo Institute of Technology, 4259 Nagatsuta-cho, Midori-ku, Yokohama 226-8502.
53) Laboratory of Nuclear Science,Tohoku University, 1-2-1 Mikamimine, Taihaku-ku, Sendai, Miyagi 982-0826
54) Department of Physics, Graduate school of Science, Nagoya University, Furo-cho, Chikusa, Nagoya 464-8602

COUNCIL

KAYA, Koji **Director-General**

Councillors

Chairperson	HOSOYA, Haruo	Professor, Ochanomizu University
Vice-Chairperson	HIROTA, Noboru	Professor Emeritus, Kyoto University
	OHTSUKA, Eiko	Professor Emeritus, Hokkaido University
	OGINO, Hiroshi	Professor, Tohoku University
	KIHARA, Motohiro	Director, Accelerator Laboratory, High Energy Accelerator Research Organization
	KYOGOKU, Yoshimasa	Professor, Fukui University of Technology
	GOTO, Keishi	President, Toyohashi University of Technology
	KONDOW, Tamotsu	Invited Professor, Toyota Technological Institute
	SAHARA, Makoto	Director-General, National Museum of Japanese History
	SHIMIZU, Ryoichi	Director, The Institute of Statistical Mathematics
	TAKAHASHI, Riichi	President and Chief Operating Officer, TOYOTA Central Research & Development Laboratories, Inc.
	TSUCHIYA, Soji	Professor, Japan Women’s University
	NAKANISHI, Atsuo	Executive Director, Japan Academic Association for Copyright Clearance
	FUKUYAMA, Hidetoshi	Director, Institute for Solid State Physics, The University of Tokyo
	HONDA, Kenichi	President, Tokyo Institute of Polytechnics
	MATSUO, Minoru	President, Nagoya University
	YAMAZAKI, Toshimitsu	Visiting Scientist, RI Beam Science Laboratory, RIKEN
	YAMAMURA, Shosuke	Professor Emeritus, Keio University
	KIEFER, Wolfgang*	Professor, Wuerzburg University
	ZARE, Richard N.*	Professor, Stanford University

The Council is the advisory board for the Director-General.
* Two of the councillors are selected among distinguished foreign scientists.

Distinguished Research Consultants

BABA, Hiroaki	Professor Emeritus, Hokkaido University
NAGAKURA, Saburo	President, The Kanagawa Academy of Science and Technology
TANAKA, Ikuzo	Chancellor, Nezu Scholarship Association, Educational Foundation
INOKUCHI, Hiroo	Chief Scientist of Space Utilization Research Program, National Space Development Agency of Japan
TSUCHIYA, Soji	Professor, Japan Women’s University

Administration Bureau

TERAO, Shigemi	Director-General, Administration Bureau
OKADA, Kazuhiko	Director, General Affairs Department (–March ’00)
SUNADA, Hitoshi	Director, General Affairs Department (April ’00–)
KAWANO, Masatoshi	Director, Finance and Facilities Department
NARUSE, Hakaru	Head, General Affairs Division (–March ’00)
OYAMA, Takuya	Head, General Affairs Division (April ’00–)
INDEN, Toshio	Head, Personnel Division
TAIMA, Hitoshi	Head, Research Cooperation Division (–March ’00)
HAYASHI, Masanori	Head, Research Cooperation Division (April ’00–)
ONO, Yukitsugu	Head, International Affairs Division
IWAKAMI, Nobuyoshi	Head, Budget Division
WATABE, Hidemasa	Head, Accounts Division (–March ’00)
YUUKI, Masanori	Head, Accounts Division (April ’00–)
FUNATO, Hideaki	Head, Construction Division
SATO, Hisashi	Head, Equipment Division

BUILDINGS AND CAMPUS

The IMS campus covering 62,343 m^2 is located on a low hill in the middle of Okazaki city. The inequality in the surface of the hill and growing trees are preserved as much as possible, and low-storied buildings are adopted for conservation of the environment. The buildings of IMS are separated according to their functions as shown in the map. The Research Office Building and all Research Facilities except for the Computer Center are linked organically to the Main Laboratory Buildings by corridors. Computer Center, Library and Administration Buildings are situated between IMS and neighboring National Institute for Basic Biology and National Institute for Physiological Sciences, because the latter two facilities are common to these three institutes.

The lodging facility of IMS called Yamate Lodge, located within ten minutes' walk, has sleeping accommodations for 15 guests and two families. Mishima Lodge, located within four minutes' walk east of IMS can accommodate 74 guests and 20 families. Scientists who visit IMS as well as the two other institutes can make use of these facilities. Foreign visiting scientists can also live at these lodgings with their families during their stays. The Okazaki Conference Center was built in April, 1997 in Mishima area, which has four conference rooms capable of between 50 and 250 attendance.

1. Research Office Building
2 Main Laboratory Building
3. Equipment Development Center
4. Laser Research Center for Molecular Science
5. Research Center for Molecular Materials
6. Low-Temperature Facilities Building
7. Computer Center
8. Library
9. Central Administration
10. UVSOR Facility
11. Power Station
12. Waste-Water Disposition Facilities
13. Faculty Club
14. South Laboratory Building
15. Okazaki Conference Center

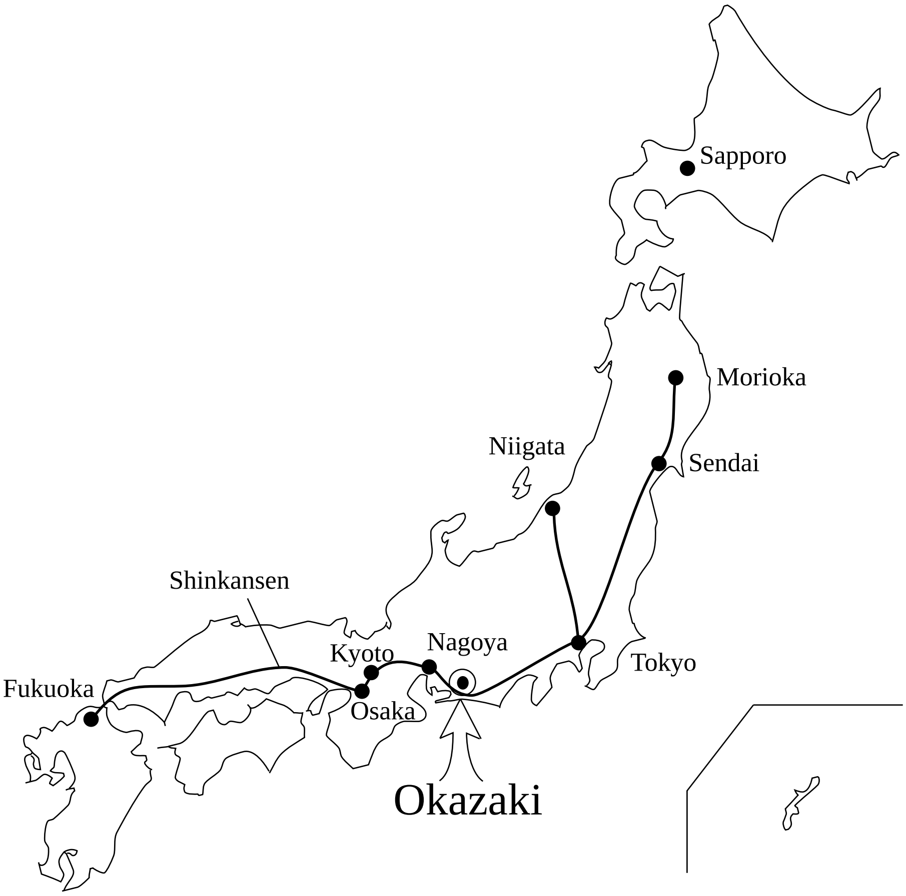

Okazaki (population 330,000) is 260 km west of Tokyo, and can be reached by train in about 3 hours from Tokyo via Shinkansen and Meitetsu Line.

The nearest large city is Nagoya, about 40 km northwest of Okazaki.

RESEARCH ACTIVITIES I
Department of Theoretical Studies

I-A Development of New Numerical Techniques in the Study of Molecular Structure

Although theories of the electronic structure of molecules have been extensively developed for last decades, almost always new methods and techniques have to be developed to meet new experimental advances.

I-A-1 Spectral Density Calculation by Using the Chebyshev Expansion

IKEGAMI, Tsutomu; IWATA, Suehiro

A method to calculate the spectral density of any state vectors with respect to a set of eigenstates of a Hamiltonian is proposed. An expectation value of a spectral density operator, $\delta(H\text{-}E)$, gives the spectral density of the state vector. The operator is evaluated by using the Chebyshev expansion method without the diagonalization procedure for the Hamiltonian. Two expansion schemes are examined. The one is the direct expansion, where the delta function is expanded in the Chebyshev polynomials. This scheme is simple and efficient, though it is difficult to guarantee the convergence of the expansion, especially for a bound system. The other is the indirect expansion, where the expansion is performed in the Fourier space. Here, the convergence is guaranteed, independently of the energy spectrum of the Hamiltonian. This scheme is identical in the spirit to Heller's autocorrelation function method, though the explicit time propagation of the wavepacket is avoided. Because of this, a spectral transformation function is naturally introduced to improve resolution at the low energy region.

I-A-2 Calculation of the ZEKE Spectrum of CO

IKEGAMI, Tsutomu; IWATA, Suehiro

The ZEKE spectrum of CO is calculated by using the spectral density method. The ab initio potential energy curves of the excited states of CO^+, calculated by Okada and Iwata, are fitted to the two states model (2×2 matrix). The diagonal part is fitted well with the Morse functions and the off-diagonal is assumed to constant. The centrifugal part (Hund's case a) is added to obtain the rot-electronic potential curves. The Gaussian wavepacket, corresponding to the vibrational wavefunction of the ground state of CO, is placed on the coupled potential energy curves, and its spectral density is calculated. A series of the vibrational predissociation spectra of CO^+ is thus obtained for several rotational states. They are superimposed to obtain the rot-vibrational spectrum. The rotational line strengths for the photoionization process are calculated based on the BOS model,1) borrowing the coefficients from the experimental result by Shiell *et al.*2) The results are shown in Figure 1. The line widths for $v = 3$ and 4, whose levels are above the avoided crossing, are broad due to the short lifetime of the states. However, the line width for $v = 5$ becomes narrow again. By using Zhu-Nakamura's theory, it was found that the perfect reflection condition at the avoided crossing is met for the energy level of $v = 5$, which results in the long lifetime of the state.

References
1) A. D. Buckingham, B. J. Orr and J. M. Sichel, *Philos. Trans. R. Soc. London*, Ser. A 268, 147 (1970).
2) R. C. Shiell, M. Evans, S. Stimson, C.-W. Hsu, C. Y. Ng and J. W. Hepburn, *Chem. Phys. Lett.* **315**, 390 (1999).

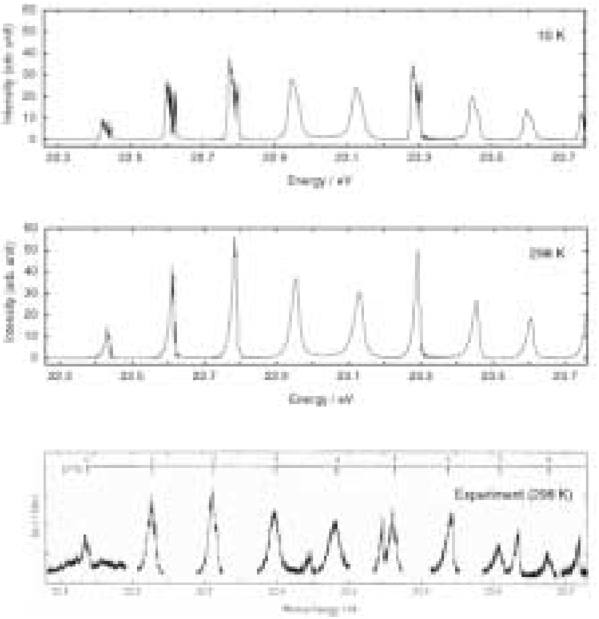

Figure 1. Calculated and experimental ZEKE spectra of CO.

I-A-3 Nonadiabatic Relaxation Through a Conical Intersection

IKEGAMI, Tsutomu; IWATA, Suehiro

Nonadiabatic relaxation process is studied on two dimensions-two levels system with a conical intersection. The upper potential energy surface is concave around the conical intersection, while the nonadiabatic coupling is increased to infinity at the intersection. From a classical point of view, the trajectory running on the upper surface with less kinetic energy is more attracted to the conical intersection, and hence the nonadiabatic transition to the lower surface is expected to occur more frequently. This dependence of the transition probability is qualitatively different from the one-dimension system, where all the trajectories pass the same line independent of the kinetic energy. The above classical picture is examined quantum mechanically by using the wavepacket propagation method. The Gaussian wavepacket is placed behind the conical intersection, and is injected toward the intersection with several kinetic energies. The parameters of the model are tuned to simulate typical photochemical processes. As expected, the more fractions of the wavepacket stay on the upper surface with the increase of the injection energy. The destructive interference can also be observed on the upper surface, which is due to the Berry's phase, if the system setup is taken to be symmetric.

I-B Electron-Hydrogen Bond in Water Clusters and Their Complexes with Atomic Ions

While we have been studying water cluster anions $(H_2O)_n^-$, we have found a unique structural unit in which the OH bonds surround an excess electron. We call it OH{e}HO structure. This structure is also found in the water cluster complexes with a group 1 metal atom. The correlation between the HO bond lengthening and the downward shift of HO stretching harmonic frequency in the OH{e}HO structure is almost identical with that in the ordinal hydrogen bond. Because of that, we call the interaction electron-hydrogen bond. In addition to the vibrational spectroscopy, we theoretically examine the electronic absorption spectra, which hopefully help to identify the isomers of the clusters.

I-B-1 Theoretical Studies of the Water-Cluster Anions Containing the OH{e}HO Structure: Energies and Harmonic Frequencies

TSURUSAWA, Takeshi; IWATA, Suehiro

[*Chem. Phys. Lett.* **315**, 433 (2000)]

In addition to isomers having a dipole-bound electron, the internal bound isomers of trimer, tetramer and hexamer water anions are found using ab initio MO calculations. The internal bound isomers have a characteristic OH{e}HO structure. The interaction between the excess electron {e} and the surrounding OH bonds holds the structure stable. The calculated vibrational infrafed spectrum for a hexamer anion with two double proton-acceptor water molecules shows a qualitatively similar vibrational spectrum with the one observed by Johnson and his coworkers. A strong correlation between the vertical detachment energy and the distribution of the excess electron is also found.

I-B-2 Electron-Hydrogen Bonds and OH Harmonic Frequency Shifts in Water Cluster Complexes with a Group 1 Metal Atom, $M(H_2O)_n$ (M = Li and Na)

TSURUSAWA, Takeshi; IWATA, Suehiro

[*J. Chem. Phys.* **112**, 5705 (2000)]

The harmonic vibrational frequencies for $M(H_2O)_n$ (M = Li and Na) are calculated with ab initio MO methods. Three types of isomers, surface, quasi-valence and semi-internal, exhibit the characteristic frequency shifts $\Delta\nu_{OH}$. The calculated spectral patterns are related to the geometric conformations around the localized electron {e} in the cluster. The downward shifts of OH frequencies are strongly correlated with the lengthening of OH bond distances, as is well known in the hydrogen bonds. The magnitude of the downward shift is as large as that for the hydrogen bond. The correlation of the shifts with the distance between the center of the electron {e} and the hydrogen atom reveals two types of interaction schemes. The characteristics of the structural unit OH{e}HO in $M(H_2O)_n$ and its OH modes are common with those found in water anion clusters. The interaction between the localized electron and OH bonds can be called electron-hydrogen bond.

I-B-3 Theoretical Study of Photoabsorption Cross Sections of Water Cluster Anions

CHEN, Fei-Wu[1]; TSURUSAWA, Takeshi; IWATA, Suehiro
([1]JST)

Photoabsorption cross sections of water dimer and trimer anions are calculated with an ab initio molecular orbital method. Because the electron detachment energy of these small water cluster anions is less than 0.3 eV, all of the photoabsorption spectra in the near infrared and visible region are due to the bound-free transitions. To construct the bound-free continuum spectrum, the L^2 integrable method is used with the single reference polarization configuration interaction (POL CI) method. The convergence on the basis set is examined by adding diffuse functions. Two isomers of dimer anion and three isomers of trimer anion are studied. The calculated photoabsorption spectra of three trimer anions are shown in Figure. The spectra was drawn from the vertical ionization energy IE_{th}, which is given in the figure along with SEM; SEM is the volume of the excess electron distribution containing a half of the electron. The spectrum of isomer of dipole bound electron (c) is different from those of the isomers of internally trapped electron.

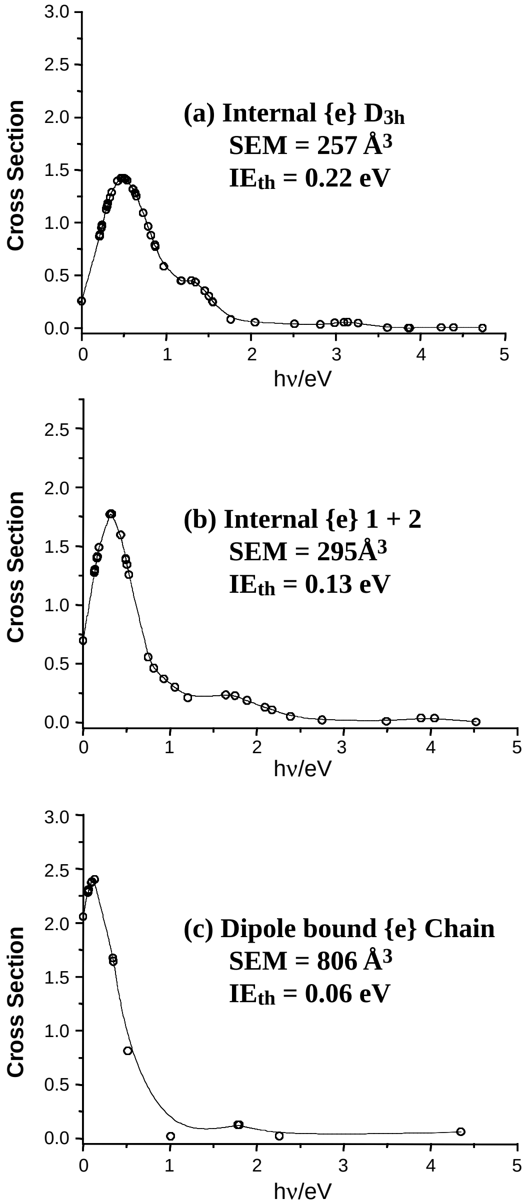

I-B-4 Theoretical Study of Photoabsorption Spectra of $M(H_2O)_n$ (M = Li and Na)

IWATA, Suehiro[1]; CHEN, Fei-Wu[2]; TSURUSAWA, Takeshi
([1]IMS and Hiroshima Univ.; [2]JST)

By examining the electron distribution of the singly occupied orbital (SOMO) of $M(H_2O)_n$ (M = Li and Na) of several isomers, we have shown that most of isomers of $n = 3$ and 4 and all of isomers of $n > 4$ are the ion pair complexes $M^+(H_2O)_n^-$ (*J. Phys. Chem. A* **103**, 6134 (1999)). To characterize the electronic structure of the complexes, the photoabsorption spectrum is theoretically constructed with ab initio MO calculations of single-excitation level of approximation (SCI). In n = 1 and 2, the lowest transitions are the intra-valent $s \rightarrow p$ transitions, while in the ion-pair complexes, the lowest transitions are of back-charge transfer to the metal's *s* and *p* orbitals from the trapped electron in the OH{e}HO structure. Notably, below the ionization threshold, which is about 3.5 eV, many but weak Rydberg type transitions are predicted.

I-C Computational Chemistry of Atomic and Molecular Processes in Atmospheric Environment

In 1998 we launched a new research project, "Computational Chemistry for Atmospheric Environmental Molecule" under Research and Development Applying Advance Computational Science and Technology administrated by Japan Science and Technology Corporation (ACT-JST). The atmospheres on the earth as well as on the sun and on planets consist of simple molecules, for which we can now perform the state-of-art calculations from the first principle of quantum mechanics. The calculated molecular physical properties such as spectroscopic constants are accurate enough to be used as "the experimental data." Moreover, physical and chemical phenomena in the atmosphere sometimes involve a sequence of complex processes. To explore the processes, development of new theoretical methods might be required, based both on classical and quantum theories.

I-C-1 Accurate Potential Energy and Transition Dipole Moment Curves for Several Electronic States of CO^+

OKADA, Kazutoshi[1]; IWATA, Suehiro
([1]GUAS)

[*J. Chem. Phys.* **112**, 1804 (2000)]

Accurate calculations were performed for several doublet and quartet states of CO^+ using the multi-reference configuration interaction method. With a single set of molecular orbitals the accurate transition dipole moments were evaluated. The calculated lifetimes of the vibronic states of the $A^2\Pi$ and $B^2\Sigma^+$ states were in excellent agreement with the available experimental data. The calculated vibrational level spacings and rotational constants up to v = 40 of the $^2\Sigma^+$ state were compared with the latest experimental data, and quantitative agreement was attained.

I-C-2 Ab initio MO Study of the *A*, *D* and Third $^2\Pi$ States of CO^+

OKADA, Kazutoshi[1]; IWATA, Suehiro
([1]GUAS)

[*J. Electron. Spectrosc. Relat. Phenom.* **108**, 225 (2000)]

Ab initio MO calculations were performed for three $^2\Pi$ states of CO^+ with the multi-reference configuration interaction method. Spectroscopic constants were evaluated also for other low-lying states. For the $^2\Sigma^+$ state, $A^2\Pi$, and $B^2\Sigma^+$ states, the calculated spectroscopic constants are in very good agreement with experimental data within the limit of experimental accuracy. In the photoelectron spectra, a series of the vibrational progression assigned to the $D^2\Pi$ state persists up to v = 9, whereas the calculated adiabatic potential energy holds only three vibrational levels below a barrier at R = 1.44 Å, which results from an avoided crossing with the upper state, third $^2\Pi$. The observed progression was analyzed in terms of the resonant states obtained from the coupling of two strongly interacting diabatic states, second and third $^2\Pi$.

I-C-3 Theoretical Studies of Einstein's *A* and *B* Coefficients of Rovibrational Transitions for Carbon Monoxide: Simulation of Temperature Distribution of CO in the Solar Atmosphere

OKADA, Kazutoshi[1]; AOYAGI, Mutsumi; IWATA, Suehiro
([1]GUAS and JST)

Accurate calculations of potential energy and dipole moment curves were performed for the ground state of CO with the multi-reference configuration interaction method. Vibrational and spectroscopic constants were evaluated. Rovibrational levels on the potential energy curve were obtained. Transition intensities between rovibrational levels were obtained by accurately evaluating Einstein's *A* and *B* coefficients under an assumption of the thermal distribution among the rovibronic levels. We successfully simulated the infrared absorption spectra observed on a satellite of NASA in the atmosphere of the Sun. The comparison of the simulated spectrum for the Δv = 2 transitions with the observed spectrum indicates that carbon monoxide molecules in the sun atmosphere are distributed in the temperature range of 5000–5500 K.

I-C-4 Theoretical Study on the Hydrogen Abstraction from Saturated Hydrocarbons by OH Radical

HASHIMOTO, Tomohiro[1]; IWATA, Suehiro
([1]JST)

Weakly-bound reactant and product complexes in the hydrogen abstraction by OH radical from CH_4, C_2H_6, and C_3H_8 are investigated using ab initio molecular orbital methods. Calculated binding energies of CH4 and OH reactant complex at CCSD(T)/aug-cc-pVTZ (aug-cc-pVDZ) levels are 0.54 (0.74) kcal/mol. Including zero-point vibrational energy corrections at MP2 level with the corresponding basis sets reduce the binding energies to 0.16 (0.08) kcal/mol which are much smaller than the experimental estimation (about 0.60 kcal/mol). Product complex for the CH_4 + OH system, which is more stable than the reactant complex, has the binding energies of 0.77 (0.79) kcal/mol at CCSD(T)/aug-cc-pVTZ (aug-cc-pVDZ) levels with MP2 zero-point energy corrections. The reactant and product complexes are also found for C_2H_6 + OH and C_3H_8 + OH systems at CCSD(T)/aug-cc-pVDZ level of theory. These binding energies have a tendency to get larger as the number of carbon atom increases.

I-C-5 Theoretical Study on the Reaction Mechanism for Oxidation of Isoprene

AMMAL, S. Salai Cheettu[1]; HASHIMOTO, Tomohiro[1]; IWATA, Suehiro
([1]JST)

The reaction of OH radical with isoprene molecule followed by the addition of O_2 molecule to form the peoxy radicals were studied by ab initio molecular orbital methods. The equilibrium geometries and vibrational frequencies were determined for all reactants, products, and transition states, as well as activation and reaction energies. Geometries were obtained at the UHF and UMP2/cc-pVDZ levels while energies were computed at UMP4, PMP2, and PMP4 levels. The addition of OH radical to the terminal carbon atoms of isoprene molecule are found to be more favorable in the first step of the reaction, whereas the radicals obtained by the addition of OH at the two inner carbon atoms are found to have lower activation barriers for the addition of O_2 molecule in the second step of the reaction. The six peroxy radicals obtained are much closer in stability and among them the radicals possessing the OH and OO· groups at the neighboring carbon atoms are found to be more stable.

I-D Prediction of Protein Tertiary Structures from the First Principles

Prediction of the three-dimensional structures of protein molecules by computer simulations is a very challenging problem in theoretical molecular science. The difficulty of the problem lies in two facts: (1) the inclusion of accurate solvent effects is non-trivial and time-consuming (2) there exist huge number of local minima in the energy function, forcing conventional simulations to get trapped in states of energy local minima. We have been exploring the strategies that allow us to overcome these difficulties.

I-D-1 Helix-Coil Transitions of Amino-Acid Homo-Oligomers in Aqueous Solution Studied by Multicanonical Simulations

MITSUTAKE, Ayori; OKAMOTO, Yuko

[*J. Chem. Phys.* **112**, 10638 (2000)]

Helix-coil transitions of homo-oligomers in aqueous solution are studied by multicanonical Monte Carlo simulations. The solvation effects are represented by the sum of the terms that are proportional to the solvent-accessible surface area of the atomic groups. Homo-oligomers of length 10 are considered for three characteristic amino acids, alanine, valine, and glycine, which are helix former, helix indifferent, and helix breaker, respectively. We calculated as a function of temperature the distributions of the backbone dihedral angles, the average values of total energy, and its component terms of the homo-oligomers. It is shown that for homo-alanine the helix-coil transition exists and that the transition temperature in water is considerably lower than in gas phase, which implies that the effects of solvation tend to reduce helical content. Moreover, the helix propagation parameter s and nucleation parameter σ of the Zimm-Bragg model were calculated. The s values that were obtained from the simulations in aqueous solution are in remarkable agreement with the experimental results.

I-D-2 Multidimensional Replica-Exchange Method for Free Energy Calculations

SUGITA, Yuji; KITAO, Akio[1]; OKAMOTO, Yuko
([1]Kyoto Univ.)

[*J. Chem. Phys.* **113**, 6042 (2000)]

We have developed a new simulation algorithm for free energy calculations. The method is a multidimensional extension of the replica-exchange method. While pairs of replicas with different temperatures are exchanged during the simulation in the originalreplica-exchange method, pairs of replicas with different temperatures and/ or different parameters of the potential energy are exchanged in the new algorithm. This greatly enhances the sampling of the conformational space and allows accurate calculations of free energy in a wide temperature range from a single simulation run, using theweighted histogram analysis method.

I-D-3 Replica-Exchange Multicanonical Algorithm and Multicanonical Replica-Exchange Method for Simulating Systems with Rough Energy Landscape

SUGITA, Yuji; OKAMOTO, Yuko

[*Chem. Phys. Lett.* **329**, 261 (2000)]

We propose two efficient algorithms for configurational sampling of systems with rough energy landscape. The first one is a new method for the determination of the multicanonical weight factor. In this method a short replica-exchange simulation is performed and the multicanonical weight factor is obtained by the multiple-histogram reweighting techniques. The second one is a further extension of the first in which a replica-exchange multicanonical simulation is performed with a small number of replicas. These new algorithms are particularly useful for studying the protein folding problem.

I-D-4 Multicanonical Algorithm Combined with the RISM Theory for Simulating Peptides in Aqueous Solution

MITSUTAKE, Ayori; KINOSHITA, Masahiro[1]; OKAMOTO, Yuko; HIRATA, Fumio
([1]Kyoto Univ.)

[*Chem. Phys. Lett.* **329**, 295 (2000)]

This letter contributes to the development of the first-principles prediction methods for peptide and protein conformations in aqueous solution. We report results of the first attempt to combine the multicanonical algorithm for extensive sampling of the phase space and the reference interaction site model theory for incorporating solvent effects. Met-enkephalin in aqueous solution is chosen as an example system. Averages of the energy functions, end-to-end distance, and dihedral-angle distributions are calculated as functions of temperature.

I-D-5 A pH-dependent Variation in α-Helix Structure of the S-peptide of Ribonuclease A Studied by Monte Carlo Simulated Annealing

NAKAZAWA, Takashi[1]; BAN, Sumiko[1]; OKUDA, Yuka[1]; MASUYA, Masato[2]; MITSUTAKE, Ayori; OKAMOTO, Yuko
([1]Nara Women's Univ.; [2]Kagoshima Univ.)

[submitted for publication]

Low-energy conformations of the S-peptide fragment (20 amino-acid residues long) of ribonuclease A were studied by Monte Carlo simulated annealing. The obtained lowest-energy structures have a-helices with different size and location, depending distinctively on the energy functions that allow for protonation and deprotonation of acidic amino-acid residues. The simulation started from completely random initial conformation and was performed without any bias towards a particular structure. The most conspicuous a-helices arose from the simulation when both Glu 9 and Asp 14 were assumed to be electrically neutral, whereas the resulting conformations became much less helical when Asp 14 rather than Glu 9 was allowed to have a negative charge. Together with experimental evidence that the a-helix in the S-peptide is most stable at pH 3.8, we consider the carboxyl group of Asp 14 should be protonated at this weakly acidic condition to facilitate the helix formation. In contrast, a negative charge at Asp 14 appears to function in support of a view that this residue is crucial to helix termination owing to its possibility to form a salt bridge with His 12. These results indicate that the conformation of the S-peptide depends considerably on the ionizing state of Asp 14.

I-E Development of Simulation Algorithms for Complex Systems

Developing a powerful simulation algorithm that can alleviate the multiple-minima problem is important in many complex systems. We have been advocating the uses of the so-called generalized-ensemble algorithms such as multicanonical algorithm and replica-exchange method.

I-E-1 Replica-Exchange Monte Carlo Methods for the Isobaric-Isothermal Ensemble

OKABE, Tsuneyasu[1]; KAWATA, Masaaki[2]; OKAMOTO, Yuko; MIKAMI, Masuhiro[3]
([1]JST; [2]Natl. Inst. Adv. Interdisc. Res.; [3]Natl. Inst. Mater. Chem. Res.)

[submitted for publication]

We propose an extension of Replica-Exchange Monte Carlo (REMC) method for canonical ensembles to isothermal-isobaric ensemble as an effective method to search for stable states quickly and widely in complex configuration space. We investigated the efficiency of the new method on a benchmark testing system which consists of 256 Lennard-Jones particles. The new method enables one to shorten dramatically the relaxation time of phase change from liquid structure to crystal structure in comparison with the conventional Monte Calro method.

I-E-2 Ab Initio Replica-Exchange Monte Carlo Method for Cluster Studies

ISHIKAWA, Yasuyuki[1]; SUGITA, Yuji; NISHIKAWA, Takeshi; OKAMOTO, Yuko
([1]Univ. Puerto Rico)

[*Chem. Phys. Lett.* **333**, 199 (2001)]

We have developed and implemented an algorithm for ab initio replica-exchange Monte Carlo simulations based on an ab initio correlated electronic structure theory. The many-body interactions in metal, semiconductor and molecular clusters are described by ab initio correlated method at the level of second-order Moller-Plesset perturbation theory. The replica-exchange Monte Carlo procedure allows for an efficient sampling of the global and low-lying local minima in a single simulation run, and thus, is ideally suited for locating energy minima of complex systems which possess a number of local minima. We have successfully applied the replica-exchange Monte Carlo method to the geometry optimization of the Li_6 cluster.

I-F Theory of Nonadiabatic Transition

I-F-1 Non-Adiabatic Transitions in a Two-State Exponential Potential Model

PICHL, Lukas[1]; OSHEROV, Vladimir I.[2]; NAKAMURA, Hiroki
([1]GUAS; [2]IMS and Inst. Chem. Phys., Russia)

[*J. Phys. A: Math. Gen.* **33**, 3361 (2000)]

A general two-state exponential potential model is investigated and the corresponding two-channel scattering problem is solved by means of semiclassical theory. The analytical expression for the non-adiabatic transition matrix yields a unified expression in the repulsive and previously studied attractive case. The final formulae are expressed in terms of model-independent quantities, *i.e.* the contour integrals of adiabatic local momenta. Oscillations of the overall transition probability below the crossing of diabatic potentials are observed in the case of strong coupling. The theory is demonstrated to work very well even at energies lower than the diabatic crossing region. Based on our results the unified theory of non-adiabatic transitions, covering the Landau-Zener-Stueckelberg and Rozen-Zener-Demkov models in such an energy range, is possible.

I-F-2 Complete Solutions of the Landau-Zener-Stueckelberg Curve Crossing Problems, and Their Generalizations and Applications

NAKAMURA, Hiroki

[*The Physics of Electronic and Atomic Collisions*, Y. Itikawa *et al.* Eds., Am. Inst. Phys., 495 (2000)]

The compact analytical complete solutions recently obtained for the two-state Landau-Zener-Stueckelberg problems are reviewed and explained. The theory covers both Landau-Zener (LZ) type in which the two diabatic potential curves cross with the same sign of slopes and the nonadiabatic tunneling (NT) type in which the potentials cross with different signs of slopes. The theory is applicable virtually in the whole range of energy and coupling strength and is convenient for practical use. The new theory for time-dependent nonadiabatic transition can be formulated from the time-independent theory of the LZ-type. The utilizability of the theory to various multi-channel problems and also to multi-dimesional problems is demonstrated and explained. The intriguing phenomenon of complete reflection which appears in the NT-case is explicitly utilized to propose a new type of molecular switching and to control molecular processes such as molecular photodissociation. Also proposed is a new way of controlling molecular processes by using time-dependent external fields. Finally, a trial to formulate a unified analytical theory to cover both Landau-Zener-Stueckelberg and Rosen-Zener-Demkov types of nonadiabatic transitions is briefly touched upon.

I-F-3 Complete Reflection in Two-State Crossing and Noncrossing Potential Systems

PICHL, Lukas[1]; NAKAMURA, Hiroki; HORACEK, Jiri[2]
([1]GUAS; [2]IMS and Charles Univ.)

[*J. Chem. Phys.* **113**, 906 (2000)]

A semiclassical study is made for the complete transmission and the complete reflection phenomena in two coupled molecular potential systems. The conditions for these phenomena to occur are expressed analytically in terms of nonadiabatic transition probabilities and phase integrals, which can be provided by the semiclassical theory. We also introduce an exactly solvable analytical model of diabatically avoided crossing, in which two diabatic potentials coupled by a constant coupling are close together in a certain spatial region. These models and phenomena may be useful in controlling various molecular processes in laser fields, since in the dressed or Floquet state formalism molecular potentials can be shifted up and down and are made to cross or avoid crossing with other potentials.

I-F-4 Nonadiabatic Transitions due to Curve Crossings: Complete Solutions of the Landau-Zener-Stueckelberg Problems and Their Applications

ZHU, Chaoyuan; TERANISHI, Yoshiaki[1]; NAKAMURA, Hiroki
([1]IMS and Inst. Phys. Chem. Res.)

[*Adv. Chem. Phys.* in press]

- A. Basic Theory
- B. Control by Laser Field
  - (1) Landau-Zener Type of Nonadiabatic Transition
  - (2) Rosen-Zener Type of Nonadiabatic Transition
  - (3) Exponential Type of Nonadiabatic Transition

VIII. Future Perspectives

I-F-5 New Type of Nonadiabatic Dynamics: Transitions between Asymptotically Degenerate States

OSHEROV, Vladimir I.[1]**; NAKAMURA, Hiroki**
([1]IMS and Inst. Chem. Phys., Russia)

Nonadiabatic transitions between asymptotically degenerate potential curves are discussed. Both crossing and non-crossing two-coupled-Morse-potential systems are studied semiclassically as well as quantum mechanically. Conditions for the appearance of the new type of nonadiabatic transition are clarified. The case of inverse power potentials at infinity is also analyzed. New expressions of nonadiabatic transition probability are obtained.

I-G Theoretical Studies of Chemical Reaction Dynamics

I-G-1 Electronically Adiabatic Chemical Reactions Analyzed by the Semiclassical Theory of Nonadiabatic Transition

ZHU, Chaoyuan; NAKAMURA, Hiroki; NOBUSADA, Katsuyuki[1]
([1]Hokkaido Univ.)

[*Phys. Chem. Phys.* **2**, 557 (2000)]

The previously proposed qualitative conceptualization of heavy-light-heavy (HLH) chemical reactions on a single potential energy surface (PES) as vibrationally nonadiabatic transitions at avoided crossings along the potential ridge lines is confirmed and further extended. An analytical as well as quantitative analysis of three-dimensional HLH reactions is carried out by applying the new semiclassical theory of nonadiabatic transition established by Zhu and Nakamura. About one thousand avoided crossings which appear in the sea of adiabatic potential curves obtained in the hyperspherical coordinate approach are classified into relevant and irrelevant ones for reactive transitions by introducing a certain diabatic decoupling procedure based on the dimensionless parameter of the new semiclassical theory. Thus about one hundred of three kinds of avoided crossings relevant for reactive transitions are specified and treated analytically. The cumulative reaction probabilities can be quite nicely reproduced quantitatively. This indicates that the clarification and conceptualization of reaction mechanisms can be done even analytically. State-to-state reaction processes can be qualitatively nicely comprehended as before, but cannot be quantitatively well reproduced, simply because inelastic transitions are not necessarily localized and cannot be well comprehended in terms of nonadiabatic transitions due to avoided crossings. An interesting series of avoided crossings responsible for rotationally inelastic transitions are found at energy lower than the threshold of reaction in the case of exo- or endoergic reaction.

I-G-2 Quantum Reaction Dynamics of O(^{3}P) + HCl on a New Ab Initio Potential Energy Surface

NOBUSADA, Katsuyuki[1]**; NAKAMURA, Hiroki; LIN, Yongjing**[2]**; RAMACHANDRAN, B.**[2]
([1]Hokkaido Univ.; [2]Louisiana Tech. Univ.)

[*J. Chem. Phys.* **113**, 1018 (2000)]

Quantum reaction dynamics of O(^{3}P) + HCl $\leftrightarrow$ OH + Cl is studied by using a new *ab initio* potential energy surface calculated by Ramachandran et al. [*J. Chem. Phys.* **111**, 3862 (1999)]. The hyperspherical *elliptic* coordinate approach is applied with an emphasis on elucidating reaction dynamics for J (total angular momentum quantum number) = 0. In terms of the previously established concept that reactive transitions are nothing but vibrationally nonadiabatic transitions at important avoided crossings, clear interpretations are given for the following dynamical features: (i) reactivity depending on potential energy surface topography, (ii) final rotational state distributions for specified initial rovibrational states, and (iii) resonance structures appearing in some reactions. Thermal rate constants are approximately estimated from the present $J = 0$ results by using the *J-shift* approximation. The present results are compared with our previous ones based on the different potential energy surface calculated by Koizumi-Schatz-Cordon (KSG). The calculated adiabatic potential energy curves of the present new surface have deep wells in the OH + Cl channel in contrast to the KSG potential energy surface. Consequently, the new surface leads to quite different dynamics from those on the KSG surface. Comparisons with the results obtained by quasiclassical trajectory calculations are also made.

I-G-3 Quantum-Classical Correspondence in the O(^{3}P) + HCl and Cl(^{2}P) + OH Reactions for Total Angular Momentum $J = 0$

LIN, Yongjing[1]**; RAMACHANDRAN, B.**[1]**; NOBUSADA, Katsuyuki**[2]**; NAKAMURA, Hiroki**
([1]Lousiana Tech. Univ.; [2]Hokkaido Univ.)

A method for carrying out quasiclassical trajectory (QCT) calculations of A + BC (v,j) reactive collisions for the special case of the total angular momentum $J = 0$

is described. Since quantum reactive scattering calculations involving heavier atoms are not straightforward for the $J > 0$ case, this method is useful to establish the extent to which classical mechanics is applicable to a particular reaction. The method is tested by comparing the results of trajectory calculations for the $J = 0$ case with analogous quantum mechanical (QM) calculations for the $O(^3P)$ + HCl reaction and the reverse reaction $Cl(^2P)$ + OH. The S4 potential surface, which is based on MRCI+Q/cc-pVTZ energies scaled by the Scaled External Correlation method [B. Ramachandran, E. A. Schrader III, J. Senekowitsch and R. E. Wyatt, *J. Chem. Phys.* **111**, 3862 (1999)], is used for these calculations. The QCT and QM cumulative reaction probabilities are found to be in good agreement, especially for the Cl + OH reaction. The agreement between the two types of state-resolved reaction probabilities is less striking but improves considerably as the initial diatomic rotational quantum number j increases. A comparison is also made between the exact and J-shifted QCT thermal rate coefficients. These are found to be in excellent agreement, which is in keeping with similar agreement observed in the case of the quantum mechanical exact and J-shifted thermal rate coefficients.

I-G-4 New Implementation of the Trajectory Surface Hopping Method with Use of the Zhu-Nakamura Theory

ZHU, Chaoyuan; NAKAMURA, Hiroki; NOBUSADA, Katsuyuki[1]
([1]Hokkaido Univ.)

The Zhu-Nakamura theory, the complete set of analytical solutions of the Landau-Zener-Stueckelberg curve crossing problems, can be applied to multi-dimensional reaction dynamics involving electronically nonadiabatic transitions due to potential energy surface crossings. The theory can be incorporated into various types of semiclassical propagation methods such as the trajectory surface hopping method, the semiclassical method with use of the initial value representation and the cellular frozen Gaussian propagation method. Even the phases due to nonadiabatic transition are provided by the Zhu-Nakamura theory and can be taken into account. The simplest application of the theory is the usage of nonadiabatic transition probability in the trajectory surface hopping method. Even the classically forbidden transitions can be properly treated. First application is made to the collinear H_3^+ reaction system and shows very encouraging good agreement with the quantum mechanical results.

I-G-5 Diabatic Slow Variable Discretization Approach in Time-Independent Reactive Scattering Calculations

MIL'NIKOV, Gennady V.[1]; NAKAMURA, Hiroki
([1]IMS and Inst. Struct. macrokinetics, Russia)

We propose a new recipe for the R matrix propagation which combines advantages of the slow Variable Discretization (SVD) and the diabatic-by-sector approach. Within the framework of the hyperspherical coordinate approach this novel scheme allows us to avoid calculations of surface functions for most of the DVR (discrete variable representation) radial points, which significantly reduces the computational time and required memory with the simplicity and the accuracy of the SVD preserved. The properties of the R-matrix propagation as a variational procedure are discussed to justify a proper choice of numerical parameters. This is checked by a test calculation of the reaction $O(^3P) + HCl \rightarrow OH + Cl$ using a LEPS potential energy surface (PES). The applicability of the method is further demonstrated by accurate quantum calculations of the endoergic reaction $H(^2S) + O_2(^3\Sigma_g^-) \rightarrow OH(^2\Pi) + O(^3P)$.

I-G-6 Quantum Dynamics in the DH_2^+ Reaction System

KAMISAKA, Hideyuki[1]; NAKAMURA, Hiroki; NOBUSADA, Katsuyuki[2]
([1]GUAS; [2]Hokkaido Univ.)

As one of the typical electronically nonadiabatic chemical reactions, we have carried out quantum mechanically accurate calculations of the title system. The potential energy surface used is an analytical fit of the new ab initio calculations done by Ichihara *et al*. For the quantum dynamics the hyperspherical elliptic coordinate system is employed. At low energies where only the electronically adiabatic processes occur, the overall feature can be explained by the statistics basically because of the deep potential well in the ground electronic potential surface. There appears, however, an interesting deviation from the statistics in the case of electronically nonadiabatic reactions.

I-H New Way of Controlling Molelular Processes

I-H-1 Laser Control of Molecular Photodissociation with Use of the Complete Reflection Phenomenon

NAGAYA, Kuninobu[1]; TERANISHI, Yoshiaki[2]; NAKAMURA, Hiroki
([1]GUAS; [2]Inst. Phys. Chem. Res.)

[*J. Chem. Phys.* in press]

A new idea of controlling molecular photodissociation branching by a stationary laser field is proposed by utilizing the unusual intriguing quantum mechanical phenomenon of complete reflection. By introducing the Floquet (or dressed) state formalism, we can artificially create potential curve crossings, which can be used to control molecular processes. Our control scheme presented here is summarized as follows. First, we prepare an appropriate vibrationally excited state in the ground electronic state, and at the same time by applying a stationary laser field of the frequency ω we create two nonadiabatic tunneling (NT) type curve crossings between the ground electronic bound state shifted up by one photon energy $\hbar\omega$ and the excited electronic state with two dissociative channels. In the NT-type of curve crossing where the two diabatic potential curves cross with opposite signs of slopes, it is known that the complete reflection phenomenon occurs at certain discrete energies. By adjusting the laser frequency to satisfy the complete reflection condition at the NT type curve crossing in one channel, the complete dissociation into the other channel can be realized. By taking one-and two-dimensional models which mimic the HOD molecule and using a wave packet propagation method, it is numerically demonstrated that a molecule can be dissociated into any desired channel selectively. Selective dissociation can be realized even into such a channel that cannot be achieved in the ordinary photodissociation because of a potential barrier in the excited electronic state.

I-H-2 New Way of Controlling Molecular Processes by Lasers

TERANISHI, Yoshiaki[1]**; NAGAYA, Kuninobu**[2]**; NAKAMURA, Hiroki**
([1]Inst. Phys. Chem. Res.; [2]GUAS)

[*Quantum Control of Molecular Reaction Dynamics*, R. J. Gordon and Y. Fujimura Ed., World Scientific, in press]

Control of molecular processes by lasers has attracted much attention recently, and several schemes have been proposed such as coherent control, pump-dump method, pulse-shape driven method, adiabatic rapid passage with linear chirp, and π-pulse. Considering the importance of nonadiabatic transitions due to curve crossing not only in ordinary molecular processes but also in molecular processes induced by lasers, we have proposed a new way of controlling nonadiabatic transitions by sweeping laser frequency and/or intensity at curve crossings among the dressed (or Floquet) states. By using the newly developed time-dependent theory of nonadiabatic transitions, we can analytically formulate appropriate control conditions. On the other hand, the intriguing phenomenon of complete reflection in the nonadiabatic tunneling (NT) type transition in the time-independent framework has been utilized to propose a new mechanism of molecular switching and a new possibility of controlling molecular photodissociation. These new ideas are briefly reviewed in this report.

I-I New Methods to Treat Scattering Problems

I-I-1 Analytical Treatment of Singular Equations in Dissociative Recombination

PICHL, Lukas[1]**; NAKAMURA, Hiroki; HORACEK, Jiri**[2]
([1]GUAS; [2]Charles Univ.)

[*Comput. Phys. Commun.* **124**, 1 (2000)]

The Lippmann-Schwinger type singular integral equation, which arises in the multi-channel quantum defect theory of dissociative recombination process, is investigated. The singularity of its kernel is treated analytically by introducing an energy dependent quadrature. In many cases of physical interest the energy-dependent coupling potential, which gives the integral kernel of the equation, is quasi-separable in a way that allows to write down an analytical solution. The analytical treatment as well as the new solution are illustrated by taking the H_2^+ as an example. Our method is demonstrated to be much better than the conventional ones, such as the first order perturbation theory and the grid method.

I-I-2 Stable and Efficient Evaluation of Green's Function in Scattering Problem

MIL'NIKOV, Gennady V.[1]**; NAKAMURA, Hiroki; HORACEK, Jiri**[2]
([1]IMS and Inst. Struct. macrokinetics, Russia; [2]IMS and Charles Univ.)

A new methodology similar to the R-matrix propagation technique is invoked to propose the practical recipe for efficiently calculating the Green's function in scattering problem. High accuracy of the proposed approach is demonstrated by taking examples of very deep tunneling and complex-valued nonlocal potential which describes low-energy dissociative attachment process between electron and molecules.

I-J Theoretical Study of Multi-Dimensional Tunneling

I-J-1 Theoretical Study of Multidimensional Proton Tunneling in the Excited State of Tropolone

WOJCIK, Marek J.[1]**; NAKAMURA, Hiroki; IWATA, Suehiro; TATARA, Wiktor**[1]
([1]Jagiellonian Univ.)

[*J. Chem. Phys.* **112**, 6322 (2000)]

Ab initio CIS/6-3lG** and CIS/6-3l ++G** calculations have been carried out in the Ã-state of tropolone for the stable and saddle point structures. The calculated energies and geometries have been compared with the previous results of Vener *et al.* The energy barrier for the proton tunneling amounts to 12.0 kcal/mol from the CIS/6-31G** calculations, and l3.0 kcal/mol from the CIS/6-31++G** calculations. The normal mode frequencies have been computed including modes coupled to the proton tunneling mode. Two-dimensional and three-dimensional model potentials, formed from symmetric mode coupling potential and squeezed double well potential, have been fitted to the calculated energy barrier, geometries, and frequencies, and used to analyze proton dynamics. The calculated energy splittings for different vibrationally excited states have been compared with the available experimental data. The CIS/6-3l ++G** calculation gives good estimation of the tunneling energy splitting in the vibrationally ground state of tropolone. The model PES explain monotonic decrease in tunneling splittings with the excitation of the out-of-plane modes, however underestimate the actual splittings. The increase of the tunneling splitting with the excitation of the v_{13} and v_{14} modes is qualitatively correct.

I-K Theoretical Studies of Ultrafast Nonlinear Optical Spectroscopy of Molecules in Condensed Phases

Nonlinear optical interactions of laser fields with matter provide powerful spectroscopic tools for the understanding of microscopic interactions and dynamics processes. We attempt to provide theoretical basis for a wide class of nonlinear spectroscopic techniques, focusing on the underlying physical processes in the condensed phases.

I-K-1 Two-Dimensional Line Shape Analysis of Photon Echo Signal

OKUMURA, Ko; TOKMAKOFF, Andrei[1]; TANIMURA, Yoshitaka
(*[1]MIT)*

[*Chem. Phys. Lett.* **314**, 488(1999)]

We analyze the two-dimensional (2D) line shape obtained by 2D Fourier transforming the time-domain response of a photon echo signal as a function of the two coherence periods, t_1 and t_3. The line shape obtained for a two level system with homogeneous and inhomogeneous broadening is shown to be sensitive to the magnitude of both of these line-broadening mechanisms. It is shown that the ellipticity of the 2D line shape can be related to the ratio of homogeneous to inhomogeneous broadening.

I-K-2 Cage Dynamics in the Third-Order Off-Resonant Response of Liquid Molecules: A Theoretical Realization

OKUMURA, Ko; BAGCHI, Biman[1]; TANIMURA, Yoshitaka
(*[1]Indian Inst. Sci.)*

[*Bull. Chem. Soc. Jpn.* **73**, 873 (2000)]

It is generally believed that the ultrafast initial spectroscopic response from the molecules in the condensed phase originates from small amplitude inertial motions within the cage formed by the nearest-neighbor solvent molecules surrounding the probe, or the cage effect. However, no quantitative estimate of this dynamics has been available for the currently popular experiments which measure the third-order off-resonant response. In this work, we fill this gap by a microscopic approach and demonstrate that the cage dynamics alone can produce the initial rise in the subpicosecond (200[fs]) range in the third-order response. A simple analytical expression for the initial Gaussian time constant relevant to various kinds of the third-order off-resonant experiments is presented, which is found to be rather strongly dependent on the temperature. Connection with the non-polar solvation dynamics is also discussed.

I-K-3 Two-Dimensional Spectroscopy for Harmonic Vibrational Modes with Nonlinear System-Bath Interactions: Gaussian-Markovian Case

TANIMURA, Yoshitaka; STEFFEN, Thomas[1]
(*[1]Univ. Groningen)*

[*J. Phys. Soc. Jpn.* **69**, 4095 (2000)]

The relaxation processes in a quantum system nonlinearly coupled to a harmonic Gaussian-Markovian heat bath are investigated by the quantum Fokker-Planck equation in the hierarchy form. This model describes frequency fluctuations in the quantum system with an arbitrary correlation time and thus bridges the gap between the Brownian oscillator model and the stochastic model by Anderson and Kubo. The effects of the finite correlation time and the system-bath coupling strength are studied for a harmonic model system by numerically integrating the equation of motion. The one-time correlation function of the system coordinate, which is measured in conventional Raman and infrared absorption experiments, already reflects the inhomogeneous character of the relaxation process. The finite correlation time of the frequency fluctuations, however, is directly evident only in the two- and three-time correlation function as probed by multidimensional spectroscopic techniques such as the Raman echo and the fifth-order 2D Raman experiment.

I-K-4 Two-Dimensional Spectroscopy and the Harmonically Coupled Anharmonic Oscillators

OKUMURA, Ko; JONAS, M. David[1]; TANIMURA, Yoshitaka
(*[1]Univ. Colorado)*

Experimentally it is established that the 4th-order anharmonicity plays significant roles in many molecules; based on the local (anharmonic) modes picture with couplings between them, the Darling-Dennison coupling manifests itself, which has been confirmed experimentally. It has been shown that this order of anharmonicity can be selectively studied via the 7th order off-resonant optical processes (Okumura and Tanimura, *J. Chem. Phys.* **106**, 1687 (1997)). We obtained fairly compact analytical result for the 7th-order signal and numerically present the signal from CH stretch vibrations in methylene chloride as two dimensional contour maps. By virtue of the two-dimensionality the results demonstrate the possibility of giving further insight into such mechanism that is not available in the one-dimensional high resolution spectroscopy.

I-K-5 Two-Dimensional Raman and Infrared Signals Measured from Different Phase-Matching Conditions

KATO, Tsuyoshi; TANIMURA, Yoshitaka

We developed a theoretical method that can explicitly treat the phase-matching condition of two-dimensional optical measurements. This method might be a rational tool for the analysis of observed signals under non-impulsive excitation. We use this method to separate the contribution of the signal from different Liouville pathways associated with the different phase-matched condition. It is expected that the effects of mode coupling, anharmonicity of the system potential and nonlinearity of the polarizability will be pronounced by the spatial discrimination of the signal, which can be achived experimentally.

I-L Quantum dynamics in the condensed phases

We investigate quantum dynamics of molecules in the condensed phases by means of various statistical physics approaches involving the path integral and Fokker-Planck equation approaches for a reduced density matrix. Effects of dissipation on a quantum rotator, proton tunneling and electron transfer processes are investigated and compared with the classical dynamics.

I-L-1 Path-Integral Approach to Rotational Relaxation Processes of a Molecule in Solvation

SUZUKI, Yoko; TANIMURA, Yoshitaka

A two-dimensional rotator coupled to a Brownian oscillators bath is considered to study rotational relaxation processes in a dissipative environment. Nonequilibrium generating functional of the rotator is evaluated by transforming the Hamiltonian in diagonal form and by carrying out the functional integrals of the bath coordinates and the rotator angel. The difference between the free particle and the rotator arises from the cyclic boundary condition supplied for the rotator angel. Using the generating functional, we obtain the analytical expression of optical response function, which is defined by the two-time correlation function of dipole moment or polarizability of the rotator, is obtained from the generating functional. The qunatal dynamics of rotator under the influence of the heat-bath is investigated by calculating Raman spectrum for various temperatures and the coupling strength between the rotator and the bath.

I-L-2 Proton Tunneling in a Dissipative Environment: Raman Response and Reaction Rate

TANIMURA, Yoshitaka

A double well potential system coupled to a colored Brownian oscillators bath is considered to study tunneling dynamics in a dissipative environment. The quantum Fokker-Planck equation for a colored nose bath in a low temperature is reduced in a multi-dimensional hierarchy form. A chemical reaction rate and Raman response spectrum are calculated for various coupling strength and temperature. Compared with the classical results, which are obtained by solving classical Fokker-Planck equation, we investigate the effects of tunneling processes on the reaction rate and spectrum. In the quantal case, the low frequency peak is observed in the Raman spectrum, which is due to the level splitting of vibrational levels induced by tunneling.

I-M Soft Matter Physics in Biomimetic Systems

Various efforts have been undertaken to make smart things useful in daily life by mimicking biomaterials. Such field has been propelled mainly from technological and practical viewpoint. However, this field has a great potential to give new ideas, concepts, and problems to soft matter physics as pure science. We have been studied two such examples, *i.e.*, nacre, which typically constitutes seashells, and a certain kind of artificial muscle, which can be driven by a small electric field.

I-M-1 On the Toughness of Biocomposites

DE GENNES, Pierre-Gilles[1]; OKUMURA, Ko
([1]Collège de France)

[*C. R. Acad. Sci. Paris* **IV**, 257 (2000)]

The fracture energy G of nacre (a stacking of aragonite/organic layers) is much larger than the corresponding energy G_0 for pure aragonite (although the organic cement thickness d_0 is very small: nanometers). We present here a qualitative explanation for this difference. The basic idea is that a weak cement reduces drastically the stress concentration near the fracture tip.

I-M-2 Why is Nacre Strong?: Elastic Theory and Fracture Mechanics for Biocomposites with Stratified Structures

OKUMURA, Ko; DE GENNES, Pierre-Gilles[1]
([1]Collège de France)

[*Eur. Phys. J. E.* submitted]

Nacre, stratified ceramic layers surrounded by organic matrix, is a tough material found inside certain seashells. We construct a coarse grained elastic energy for such an anisotropic system and present an analytic solution for a notch crack normal to the stratified sheets. This analysis proves the reduction in stress concentration which was announced in our earlier work (P. G. de Gennes and K. Okumura, *C. R. Acad. Sci. Paris* t.1, Serie IV, 257 (2000)) and the related increase in toughness.

I-M-3 Mechanoelectric Effects in Ionic Gels

DE GENNES, Pierre-Gilles[1]**; OKUMURA, Ko; SHAHINPOOR, Mohsen**[2]**; KIM, Kwang J.**[2]
([1]Collège de France; [2]Univ. New Mexico Albuquerque, U. S. A.)

[*Europhys. Lett.* **50**, 513 (2000)]

Certain fluorinated ion-exchange membranes, when swollen and suitably plated by conducting electrodes, display a spontaneous curvature increasing with the applied electric field E. There is also an inverse effect, where an imposed curvature induces an electric field (in open circuit conditions). We present here a compact description of these effects in the linear regime, and in static conditions: this is based on linear irreversible thermodynamics, with two driving forces (E and a water pressure gradient Δp) and two fluxes (electric current and water current). We also give some qualitative estimates of the three Onsager coefficients, which come into play.

I-N Liquid-Liquid Phase Transition of Water and Its Potential Surface

Water in supercooled state exhibits many anomalous properties such as divergence of the thermodynamic response functions, liquid-liquid (amorphous-amorphous) transition. Recent computer simulation and theoretical model predict this kind of transition. In view of experimental aspect, it is hard to follow this transition since the area that the transition is expected to be observed in temperature-pressure diagram is inaccessible by experiment, called 'no man's land.' Careful examination of the supercooled water show various kind of unique properties, in particular in configuration space.

I-N-1 The Melting Temperature of Proton-Disordered Hexagonal Ice: A Computer Simulation of TIP4P Model of Water

GAO, Guangtu[1]; ZENG, Xiao C.[1]; TANAKA, Hideki
([1]Univ. Nebraska)

[*J. Chem. Phys.* **112**, 8534 (2000).]

We report computer simulation results of free energies of proton-disordered hexagonal ice and liquid water at atmospheric pressure with TIP4P model of water. A new reference system is used to calculate the free energy of the ice phase. The melting point of proton-disordered hexagonal ice at atmospheric pressure is found to be T_m = 238 K. This result is consistent with a previous estimation, 230 K < T_m < 250 K, from molecular dynamic simulation of the surface melting of the proton-disordered hexagonal ice [G.-J. Kroes, *Surf. Sci.* **275**, 365 (1992)].

I-N-2 Hydrogen Bonds between Water Molecules: Thermal Expansivity of Ice and Water

TANAKA, Hideki

[*Phys. Chem. Chem. Phys.* **2**, 1595 (2000)]

The free energy components of two low pressure crystalline ices and an amorphous form of water are calculated over a wide range of temperatures. The Gibbs free energy at a given temperature is minimized with respect to volume of a system. This enables us to evaluate a thermal expansivity at fixed temperature and pressure from only intermolecular interaction potential. The negative thermal expansivity in low temperature is obtained for both crystalline ices and an amorphous form, which arises from the bending motion of hydrogen bonded molecules.

I-N-3 Potential Energy Surfaces of Supercooled Water: Intrabasin and Interbasin Structures Explored by Quenching, Normal Mode Excitation, and Basin Hopping

TANAKA, Hideki

[*J. Chem. Phys.* **113**, 11202 (2000)]

We investigate the potential energy surfaces of supercooled water; both intrabasin structures and distributions of the potential energy basins in configuration space by the steepest descent quenching and the normal mode excitation. The paths from liquid configurations to the corresponding local energy minima and the root mean square distance exhibit different characters below and above the temperature 213 K where the thermodynamics and structural properties change abruptly. The root mean square distance in the temperature range (298 K to 173 K) is larger than the corresponding harmonic oscillator system and it drastically increases above 223 K. Also increases the complexity along the steepest descent path by increasing the number of inflection points. In order to investigate the other potential energy basins distributed in the vicinity of the (central) basin that the molecular dynamics trajectory visits, the distributions of these basins are examined by the normal mode excitation. The number of distinct basins increases with increasing temperature in the same volume of configuration space. The minimum potential energy of the adjacent basin at low temperature is almost always higher than the minimum potential energy of the central basin while that of the adjacent basin at high temperature is comparable to the central basin. The locations of the other basin centers are mostly orthogonal to the normal mode excitation. The potential energy surfaces are also examined by the basin hopping technique to seek for lower energy configurations started with a random and high-energy molecular arrangement. It is found that energetically more stable molecules aggregate rather heterogeneously in the intermediate energy levels which are hardly observed in the simulation while the stable molecules distribute homogeneously in the lowest energy levels.

I-N-4 Molecular Dynamics Study of the Connectivity of Water Molecules in Supercooled States

TANAKA, Hideki

[*Mol. Liq.* in press]

We examine distributions of four-coordinated supercooled water molecules in two state points where the densities are considerably different from each other. It is found, although the coordination numbers are all four in local energy minimum structures free from thermal excitation, the magnitude of the connectivity of tetrahedrally coordinated molecules differs significantly between two supercooled states. We also investigate thermodynamic properties for liquids composed of two kinds of deformed water molecules having wider bond angles in order to compare the properties of those liquids with those of a realistic water model.

I-N-5 Ice Nanotube: What Does the Unit Cell Look Like?

KOGA, Kenichiro[1]; PARRA, R. D.[2]; TANAKA, Hideki; ZENG, Xiao C.[2]
([1]Fukuoka Univ. Edu.; [2]Univ. Nebraska)

[*J. Chem. Phys.* **113**, 5037 (2000)]

It is discovered that for an n-gonal ice nanotube built from stacking a single n-gonal ring of water, the unit cell consists of two stacked n-gonal rings. In one ring the O-H arms of water molecules line up clockwise whereas in the other ring the O-H arms line up counterclockwise. Among the n-gonal ice nanotubes examined, the pentagonal or hexagonal ice nanotube appears to be the most stable.

I-N-6 First-Order Transition in Confined Water between High Density Liquid and Low Density Amorphous Phases

KOGA, Kenichiro[1]; TANAKA, Hideki; ZENG, Xiao C.[2]
([1]Fukuoka Univ. Edu.; [2]Univ. Nebraska)

[*Nature* **406**, 564 (2000)]

Department of Chemistry and Center for Materials Analysis, University of Nebraska, Lincoln, Nebraska 68588, USA Supercooled water and amorphous ice continuously intrigue us withtheir rich metastable phase behaviour. In eighties, a high density amorphous to low density amorphous (HDA-LDA) solid-to-solid phase transition below 140 K was uncovered by Mishima and coworkers. In mid-nineties, a high density liquid to low density liquid (HDL-LDL) liquid-to-liquid phase transition was reported from computer simulations of supercooled water. Recently, a fragile-to-strong liquid transition was also proposed in supercooled water near 228 K, and was observed experimentally in supercooled bilayer water confined in-between hydrophilic slit pores. Here, we report molecular dynamics evidence suggesting a new type of first-order phase transition above the freezing temperature of bulk ice Ih at 0.1 MPa—a liquid-to-bilayer amorphous transition. This metastable phase transition appears uniquely when a two-layer water is confined in a hydrophobic slit pore at a width of less than one nanometer, that is, in a quasi-two-dimensional water. Some characteristics of this first-order transition resemble those found in tetrahedral substances such as liquid silicon, liquid carbon and liquid phosphorus.

I-O Development of Techniques for Prediction of Conformations and Applications to Proteins and Organic Compounds

Various techniques of Prediction of Conformations have been developed in this decades including proteins and organic compounds. However, a prediction of protein 3D strcutures is still unsolved and difficult problem in the area of molecular biophysics. Therefore, the elucidation of the basic mechanism of protein folding is significant to develop a prediction method of protein 3D strcuture. Currently, we are treating simple spin model of the behabior of a protein and trying to understand the basic physics of protein folding. On the other hand, development of a modeling technique of organic compounds in terms of the interactions with a protein is also important especially in the field of drug design. We have developed a new method of QSAR (quantitative structure activity relationship) analysis which can be applied to modeling of drugs. Furthermore, we have applied our modeling techniques to the actual protein, human serum transferrin, and a organic photobase compounds.

I-O-1 Kinetics of a Finite One-Dimensional Spin System as a Model for Protein Folding

KIKUCHI, Takeshi
(IMS and Kurashiki Univ. Sci. Arts)

[*Biophys. Chem.* **85**, 93 (2000)]

Simple spin models were used to analyze the kinetic nature of lowest energy state formation of the spin systems as models of protein folding kinetics in the this work. The models employed in this work were based on the spin systems as models of biopolymers previously proposed for the analysis of the equilibrium nature of transition.[1)] In particular, the effect of frustrations on the kinetics was investigated with the Monte Calro simulations. The results showed that the kinetics of the present systems are characterized by the ratio of foldables (pathways on the energy landscape that leads to the lowest energy state) and the temperature dependence of the mean first passage time of fodables. These properties of the present spin model are corresponding to kinetic behavior of actural proteins. The important thing of the kinetics ofa zero frustration system is the passage from the Levinthal phase at higher temperature to the Arrhenius phase at lower temperature.

Reference

1) T. Kikuchi, *Biophys. Chem.* **65**, 109 (1997).

I-O-2 Molecular Modeling of Human Serum Transferrin for Rationalizing the Changes in Its Physicochemical Properties Induced by Iron Binding. Implication of the Mechanism of Binding to Its Receptor

YAJIMA, Hirofumi[1]; SAKAJIRI, Tetsuya[1]; KIKUCHI, Takeshi[2]; ISHII, Tadahiro[1]
([1]Sci. Univ. Tokyo; [2]IMS and Kurashiki Univ. Sci. Arts)

[*J. Protein Chem.* **19**, 215 (2000)]

In order to rationalize the resulting physicochemical properties of human serum-transferrin (Stf) and the Stf-receptor (TfR) recognition process, we have tried to predict the 3D structures of apo- and iron-loaded Stf using a homology modeling technique to study the changes in the structural characteristics that would take place upon the uptake of iron by Stf in solution. Therein, the crystal structures of both forms for ovotransferrin were used as templates for the Stf modeling. The modeled structure of Stf brought about a satisfactory interpretation for the tyoical physico-chemical properties such that (1) Stf has a negative electrophoretic mobility and its value increases with iron uptake, and (2) the radius of gyration (Rg) of Tf decreases with iron uptake. Moreover, in view of the findings from our capillary electrophoresis experiments, it is inferred that the connecting (bridge) and its neighboring region associated with a surface exposure of negative charge plays an important role in the Stf-receptor recognition process.

I-O-3 A CoMFA Analysis with Conformational Propensity: An Attempt to Analyze the SAR of a Set of Moleculas with Different Conformational Flexibility Using a 3D-QSAR Method

GOHDA, Keigo[1]; MORI, Ichiro[2]; OHTA, Daisaku[3]; KIKUCHI, Takeshi[4]
([1]Novartis Pharma; [2]GlaxoWelcome; [3]Osaka Pref. Univ; [4]IMS and Kurashiki Univ. Sci. Arts)

[*J. Comput. Aided Mol. Des.* **14**, 265 (2000)]

CoMFA analysis, a widely used 3D-QSAR method, has limitations to handle a set of SAR data containing diverse conformarional flexibility since it does not explicitly include the conforamtional entropic effects into the analysis. We presented in thi work an attempt to incorporate the confromational entropy effects of a molecule into a 3D-QSAR analysis. Our attempt is based on the assumption that the conformational entropic loss of a ligand upon making a ligand-receptor complex is small if the ligand in an unbound state has a conformational propensity to adopt an active conformation in a complex state. The conformational propensity is defined as the population ratio of active conformations to stable conformations. The active conformation is defined from the structure of a compound with a rigid structure with high activity. We applied the present method to 20 imidazoleglycerol phosphatase inhibitors with various conformational flexibility. The results show that our method improved the predictability compared with the stadard CoMFA method.

I-O-4 Study on Photobase Generation from α-Aminoketones: Photocrosslinking of Epoxides with Carboxlic Acids

KURA, Hideaki[1]; OKA, Hidetaka[1]; BIRBAUM, Jean-Luvc[1]; KIKUCHI, Takeshi[2]
([1]Ciba Specialty Chem.; [2]IMS and Kurashiki Univ. Sci. Arts)

[*J. Photopolym. Sci. Technol.* **13**, 145 (2000)]

It was demonstrated that α-Aminoketones work effectively as photobase generators in epoxy-based compositions in this work. After irradiation they accelerate the thermal crosslinking reaction of phenol novolac epoxy resin with polyacrylate having carboxylic acid groups despite of their high latency before irradiated. The accelaration effect depends on the structure of the photogenerated amines. Conformational population of the α-aminoketones and the related compounds was also calculated based on the molecular mechanics. The results suggest that folded conformations contribute to the latency of the amine moiety. In the conformations, the bulky benzoyl group of the aminoketone sheilds the amino nitrogen from acidic species present in the composition. By irradiation, the benzoyl part is cleaved and the active tertiary amine base with small substituents is eventually liberated. The investigation using model amines supported the explanation. The compositions used for this study can be utilized in the base-catalyzed imaging application.

I-P Microscopic Solvation of Alkali Atom and Aggregates in Polar Solvent Clusters

The understanding of the structure and dynamics of solvated electron is of fundamental importance in the wide areas of chemistry, physics and biology. Clusters containing polar solvent molecules and a single alkali atom and/or aggregates can be regarded as a prototype for studying this intriguing subject. They are expected to give size dependent information on the spontaneous ionization of the alkali metal and the formation of the solvated electron. To elucidate the electronic nature of the clusters at the molecular level, we have carried out ab initio study in collaboration with the spectroscopic experiments.

I-P-1 Solvation Process of Na_m in Small Ammonia Clusters: Photoelectron Spectroscopy of $Na_m^-(NH_3)_n$ ($m \leq 3$)

TAKASU, Ryozo[1]; ITO, Hideki[1]; NISHIKAWA, Kaori[1]; HASHIMOTO, Kenro[2,3]; OKUDA, Rei[2]; FUKE, Kiyokazu[1]
([1]Kobe Univ.; [2]Tokyo Metropolitan Univ.; [3]IMS)

[*J. Electron. Spectrosc. Relat. Phenom.* **106**, 127 (2000)]

Photoelectron spectra (PESs) of $Na_m^-(NH_3)_n$ ($m \leq 3$) are investigated to explore the solvation of sodium atom and its aggregates in small ammonia clusters. For $Na^-(NH_3)_n$, we examine the PESs with an improved resolution and confirm the spontaneous ionization of Na atom in small clusters. As for $Na_2^-(NH_3)_n$ ($n \leq 8$), vertical detachment energy (VDE) of the transition from the anion to the neutral ground state is found to shift to the red with respect to that of $Na_2(X^1\Sigma_g^+)$, while that of the first excited state derived from $Na_2(a^3\Sigma_u^+)$ increases gradually for $n \geq 4$. In addition, the transitions to the higher-excited states derived from those correlated to the $3^2S + 3^2P$ asymptote are found to be shifted rapidly to the red and become almost degenerate with the $a^3\Sigma_u^+$–type transition. The extensive spectral change is ascribed to the asymmetrical ammoniation and spontaneous ionization of Na_2 in small clusters. We also find the drastic change in the PESs of $Na_3^-(NH_3)_n$; the neutral ground ($^2\Sigma_u^+$–type) and first excited ($^2\Sigma_g^+$–type) states of these clusters become degenerate with each other as the number of NH_3 molecules increases. With the aide of the theoretical calculations, this spectral change is ascribed to the dissociation of Na_3^- core in clusters. This may be the first observation of the dissolution of metal aggregates in small clusters.

I-P-2 Theoretical Study of $[Na(H_2O)_n]^-$ (n = 1–4) Clusters: Geometries, Vertical Detachment Energies and IR Spectra

HASHIMOTO, Kenro[1,2]; KAMIMOTO, Tetsuya[2]; DAIGOKU, Kota[2]
([1]IMS; [2]Tokyo Metropolitan Univ.)

[*J. Phys. Chem. A* **104**, 3299 (2000)]

Geometries, vertical detachment energies (VDEs) and IR spectra of $[Na(H_2O)_n]^-$ (n = 1–4) have been investigated by ab initio MO method at correlated level. Water molecules are bound to Na^- via Na–H as well as hydrogen bond interactions. The calculated VDEs are in good agreement with the recent photoelectron spectroscopy and all observed bands are assignable to the $3^2S(Na)–3^1S(Na^-)$ and $3^2P(Na)–3^1S(Na^-)$ type transitions perturbed by hydration. They are shifted to higher energy with increasing n by keeping their separation almost unchanged, which reflects the hydration structure of Na^-. We also report the calculated IR spectra that are informative about the ionic Na–H bonds and the hydrogen-bond network among water molecules in the clusters.

I-P-3 Theoretical Study of $[Na(NH_3)_n]^-$ (n = 1–4)

HASHIMOTO, Kenro[1,2]; KAMIMOTO, Tetsuya[2]; MIURA, Nobuaki[3]; OKUDA, Rei[2]; DAIGOKU, Kota[2]
([1]IMS; [2]Tokyo Metropolitan Univ.; [3]JST)

[*J. Chem. Phys.* **113**, 9540 (2000)]

In connection with the recent photoelectron spectroscopy of negatively charged Na atom in ammonia clusters, the geometries, electronic state, vertical detachment energies, and harmonic frequencies of $[Na(NH_3)_n]^-$ (n = 1–4) have been studied by *ab initio* MO method. Structure having as many Na–N bonds as possible becomes more stable than other isomers as n grows. The Na 3s electrons are widely spread and delocalized in space outside the $[Na(NH_3)_n]^+$ core for $n \geq 2$. The dramatic red-shifts of the photoelectron band for the 3^2P-type transition with increasing n reflect the electronic change from an atomic state to one-center Rydberg-like states in the neutrals. The frequencies of the combined vibrations of the NH_3 ν_1 mode are nearly degenerate and are expected to coalesce into only one strong IR band in the NH stretch region irrespective of n.

I-Q Theoretical Analyses on Nonlinear Behavior of Complex Systems

When material A and material B form a complex system, for example, an interface (or an interface region) newly appears between the two materials. Structure and properties of the interface are often totally different from those of the bulk materials, with the result that the complex system exhibits highly nonlinear behavior that can never be understood by superposition of the behaviors of the individual materials. We deal with a complex system in which liquid solvent or aqueous solution is one of the constituents. The integral equation theories are applied to the liquid solvent and combined with theoretical methods or computer simulation techniques for the other constituents. Some of the complex systems considered are biomolecules in aqueous solution, molecular assemblies formed by self-organization of surfactant molecules in solvent, metal-liquid interface, solvent-mediated interaction between colloidal particles, liquids at surfaces, and surface-induced phenomena.

I-Q-1 Peptide Conformations in Alcohol and Water: Analyses by the Reference Interaction Site Model Theory

KINOSHITA, Masahiro[1]**; OKAMOTO, Yuko; HIRATA, Fumio**
([1]Kyoto Univ. and IMS)

[*J. Am. Chem. Soc.* **122**, 2773 (2000)]

It is experimentally known that alcohol induces peptides to form α-helix structures much more than water. Though the α-helix structure formed is independent of the alcohol species, degree of the induction increases as bulkiness of the hydrocarbon group in an alcohol molecule increases. In this article we investigate conformations of peptides (Met-enkephalin and the C-peptide fragment of ribonuclease A) in methanol, ethanol, and water using the reference interaction site model theory. Molecular models are employed for the solvents. Our theoretical results show the following. Alcohol indeed facilitates peptide molecules to form the secondary structures with intramolecular hydrogen bonds such as the α-helix. In alcohol a solvophobic atom of a peptide is *less solvophobic* than in water while a solvophilic atom is *less solvophilic*. The solvation free energy in alcohol thus becomes considerably less variable against conformational changes than in water, with the result that the conformational stability in alcohol is governed by the conformational energy. The peptide molecule tends to take a conformation with the lowest conformational energy such as the α-helix, which is independent of the alcohol species. Moreover, these trends are enhanced as bulkiness of the hydrocarbon group in an alcohol molecule increases. In the text, the microscopic origin of the differences between alcohol and water in solvation of peptide molecules, which cannot be obtained by analyses treating the solvent as a dielectric continuum, is discussed in detail.

I-Q-2 Binary Fluid Mixture Confined between Macroparticles: Surface-Induced Phase Transition and Long-Range Surface Forces

KINOSHITA, Masahiro
(Kyoto Univ. and IMS)

[*Chem. Phys. Lett.* **325**, 281 (2000)]

A binary fluid mixture of components 1 and 2, which is confined between two macroparticles separated by distance L, is analyzed by the RISM theory. Particles of component 1 interact through attractive potential, and those of component 2 and those of different components interact through hard-sphere potential. The macroparticle-fluid particle potential is the hard-sphere one. Component 2, the minor component, is enriched near each macroparticle. When the concentration of component 2 in the bulk Y_2 is sufficiently high, the following is observed. As L decreases component 2 is even more enriched in the confined domain, and at the threshold value L_T the theory exhibits a signal of the surface-induced phase transition, appearance of the second phase of component 2 in the confined domain. This phenomenon can occur even when the bulk mixture is stable as a single phase. As Y_2 increases L_T becomes larger. (L_T-d_M) can be far longer than the molecular scale, and the attractive interaction induced between macroparticles becomes correspondingly long range.

I-Q-3 Solvent Effects on Conformational Stability of Peptides: RISM Analyses

KINOSHITA, Masahiro[1]**; OKAMOTO, Yuko; HIRATA, Fumio**
([1]Kyoto Univ. and IMS)

[*J. Mol. Liq.* in press]

We describe features of our methodology for predicting tertiary structures (*i.e.*, conformations) of proteins in solvent just from the amino-acid sequences and molecular models for the solvent. The methodology, which is a combination of the Monte Carlo simulated annealing technique and the reference interaction site model theory, is illustrated for the small peptides, Met-enkephalin and C-peptide. Important roles played by water are discussed, and the alcohol effects on peptide conformations are newly analyzed.

I-Q-4 Effects of a Trace Amount of Hydrophobic Molecules on Phase Transition for Water Confined between Hydrophobic Surfaces: Theoretical Results for Simple Models

KINOSHITA, Masahiro
(Kyoto Univ. and IMS)

[*Chem. Phys. Lett.* **326**, 551 (2000)]

The author has analyzed the phase transition phenomenon for a hydrophilic fluid containing a hydrophobic component at low concentration, which is confined between hydrophobic surfaces, using the RISM-HNC theory with a simple model. Among various hydrophilic fluids, water is doubtlessly the most important one. Water molecules interact through strongly attractive potential, and apolar particles or hydrophobic molecules are soluble only at extremely low concentrations. However, presence of even a trace amount of those molecules affects the phase transition behavior to a drastic extent. Even when the surface separation is far larger than the molecular scale, the wetting of the hydrophobic molecules and the drying of water can occur in the domain confined. The attractive interaction induced between the surfaces become correspondingly long range. As the concentration of the hydrophobic component becomes higher, the wetting/drying transition occurs at a larger surface separation and the induced interaction becomes longer range. The hydrophobic molecules, which are contained in water within biological systems at very low concentrations, have caught little attention so far but should play essential roles in a variety of surface-induced phenomena.

I-Q-5 Methodology for Predicting Approximate Shape and Size Distribution of Micelles

KINOSHITA, Masahiro[1]; SUGAI, Yoshiki[2]
([1]Kyoto Univ. and IMS; [2]Kyoto Univ.)

[*Stud. Surf. Sci. Catal.* in press]

We propose a methodology for predicting the approximate shape and size distribution of micelles with all-atom potentials. A thermodynamic theory is combined with the Monte Carlo simulated annealing technique and the reference interaction site model theory. Though the methodology can be applied to realistic models of surfactant and solvent molecules with current computational capabilities, it is illustrated for simplified models as a preliminary step.

I-R Electronic Structure of a Molecule in Solution

Chemical reaction is undoubtedly the most important issue in the theoretical chemistry, and the electronic structure is a key to solve the problem. As long as molecules in the gas phase are concerned, the theory for the electronic structure has been enjoying its great success. However, when it comes to molecules in solution, the stage of theory is still an infant. We have recently proposed a new method refereed to as RISM-SCF based on the integral equation theory of molecular liquids (RISM) and the ab initio electronic structure theory (SCF).[1)] The integral equation approach replaces the reaction field in the continuum models by a microscopic expression in terms of the site-site radial distribution functions between solute and solvent.

$$V_\lambda = \sum_j \int 4\pi r^2 \frac{q_j}{r} g_{j\lambda}(r) dr$$

where j and λ specify solvent and solute sites, respectively, and r denotes the solvent density. The site-site radial distribution functions $g_{\lambda j}(r)$ can be calculated from the extended RISM equation. Using V_λ the solvated Fock operator is defined as,

$$F^s = F^g - \sum_\lambda V_\lambda b_\lambda$$

where b_λ is a population operator of solute atoms. The statistical solvent distribution around solute is determined by the electronic structure or the partial charges of solute, while the electronic structure of solute is influenced by the solvent distribution. Therefore, the Hartree-Fock equation and the RISM equation should be solved in a self-consistent manner. It is this self-consistent determination of the solute electronic structure and the solvent distribution around the solute that features the RISM-SCF procedure.

The same Fock operator can be derived from a variation principle.[2)] Defining the Helmholtz free energy A as following;

$$A = E_{solute} + \Delta u$$

where E_{solute} is the energy of solute under solvent influence, and $\Delta\mu$ is the solvation free energy represented in terms of the Singer-Chandler formula. The Fock operator for a solute molecule in solvent as well as the RISM-HNC equations can be obtained as the first order variations with respect to the wave functions and the pair correlation functions under the constraint of the orthonormality to the molecular orbitals. The latest development along this line are reported below.

References

1) S. Ten-no, F. Hirata and S. Kato, *Chem. Phys. Lett.* **214**, 391 (1993); *J. Chem. Phys.* **100**, 7443 (1994)
2) H. Sato, F. Hirata and S. Kato, *J. Chem. Phys.* **105**, 1546 (1996).

I-R-1 Ab initio Study of Water: Liquid Structure, Electronic and Thermodynamic Properties over a Wide Range of Temperature and Density

SATO, Hirofumi; HIRATA, Fumio

[*J. Chem. Phys.* **111**, 8545 (1999)]

The electronic and liquid structures of water and its thermodynamic properties are studied over a wide range of temperature (0°–600 °C) and density (0.6–1.4 g/cm^3) based on the ab initio molecular orbital theory combined with the integral equation method of liquid. Unlike standard treatments of water by means of the classical statistical mechanics including molecular simulations, the effective charges on oxygen and hydrogen atoms in water molecules are not "input parameters," but naturally predicted from the theory in the course of self-consistent determination of the electronic structure and the density pair correlation functions in liquids. It is found that the molecular dipole moments and electronic polarization energies decrease with increasing temperature and/or density. The theoretical results for dipole moments are in quantitative accord with the experimental data, which has been determined based on the NMR chemical shift coupled with the molecular dynamics simulation. The state dependence of the electronic structure is discussed in terms of the thermal activation of molecules and intermolecular interactions including the hydrogen bonds. The liquid structure of water is discussed in the wide range of thermodynamic states in terms of $S(r)$, an average response of the pair correlation functions to temperature change which is introduced in the present study in order to make structural characteristics of water more distinctive. It is concluded from the behavior of the function that the short range structure of water retains the characteristics to ice, or the tetrahedral configuration, over relatively wide range of temperature in the normal density (1.0 g/cm^3). The ice-like characteristics of water disappear to large extent both at high (1.4 g/cm^3) and low (0.6 g/cm^3) densities for different reasons: in the high density due to the packing effect, while in the low density due to essentially entropic cause, or increased configuration space available to a molecule. The distance between the nearest-neighbor molecules in water are insensitive to the density change compared with those corresponding to the Lennard-Jones fluid. The difference in the behaviors between the two fluids is explained in terms of the intermolecular interactions and liquid structures. The number of hydrogen bonds is calculated from the oxygen–hydrogen pair correlation function using a new definition based on $S(r)$, which enables us to distinguish the hydrogen-bonded OH pairs from those just in contact due to packing effect. The temperature and density dependence of the quantity is discussed in terms of the liquid structure of water.

I-R-2 Solvent Effects on a Diels-Alder Reaction in Supercritical Water: RISM-SCF Study

HARANO, Yuichi[1]; SATO, Hirofumi; HIRATA, Fumio
([1]Kobe Univ.)

[*J. Am. Chem. Soc.* **122**, 2289 (2000)]

A Diels-Alder reaction in supercritical water is studied by means of combined electronic structure and liquid state theories. The target system is the cycloaddition of cyclopentadiene with methyl vinyl ketone. The rate and the yield of the reaction in supercritical water are calculated and compared with those in ambient water. The activation free energies of the two isomers, cis and trans, are compared. The results are in agreement with the experimentally observed increase of the rate and the yield. The solvation effect for the rate constant is decreased in supercritical water, but the rate is increased because of the thermal excitation rather than the solvation effect. The trans-conformer has shown less activation energy in ambient water and supercritical water compared to the cis-conformer. The estimated yield in supercritical water is more than 600 times higher than in ambient water. The high yield in supercritical water is due to the high solubility of the reactants to supercritical water.

I-R-3 A Theoretical Study on a Diels-Alder Reaction in Ambient and Supercritical Water: Viewing Solvent Effects through Frontier Orbitals

HARANO, Yuichi[1]; SATO, Hirofumi; HIRATA, Fumio
([1]Kobe Univ.)

[*Chem. Phys.* **258**, 151 (2000)]

Solvent effects on the *endo/exo* selectivity of an asymmetric Diels-Alder reaction in ambient and supercritical water are studied by means of a combined electronic structure and liquid state theory. The target system is the cycloaddition of cyclopentadiene with methyl vinyl ketone. The rate constant and the equilibrium constant are obtained from the activation free energies and the free energy change of reaction for the two isomers. The results for the equilibrium constant are in qualitative agreement with the experimentally observed *endo/exo* selectivity. The relative rate constants show that the *endo* reaction occurs preferentially in wide range of thermodynamic conditions. Difference of the solvation free energy shows that *endo/exo* selectivity is enlarged in ambient water by hydrophobic effect and that it disappears completely in supercritical water.

The theoretical results are analyzed in the light of the frontier orbital theory in order to aquire physical insight of solvent effects on the stereo-selectivity.

I-R-4 Self-Consistent Field, *Ab initio* Molecular Orbital and Three-Dimensional Reference Interaction Site Model Study for Solvation Effect on Carbon Monoxide in Aqueous Solution

SATO, Hirofumi; KOVALENKO, Andriy; HIRATA, Fumio

[*J. Chem. Phys.* **112**, 9463 (2000)]

We have developed a three-dimensional (3D) extension of the reference interaction site model-self-consistent field (RISM-SCF) method to treat the electronic structure of a solvated molecule. The site–site treatment of the solute–solvent correlations involving the approximation of radial averaging constitutes a bottleneck of the RISM-SCF method, and thus lacks a 3D picture of the solvation structure for complex solutes. To resolve this problem, we devised out a 3D generalization of the RISM integral equations which yields the 3D correlation functions of interaction sites of solvent molecules around a solute of arbitrary shape. In the present article, we propose a SCF combination of the ab initio molecular orbital (MO) methods and 3D-RISM approach. A benchmark result for carbon monoxide in ambient water is also presented.

I-R-5 Which Carbon Oxide is More Soluble? Ab initio Study on Carbon Monoxide and Dioxide in Aqueous Solution

SATO, Hirofumi; MATUBAYASI, Nobuyuki[1]; NAKAHARA, Masaru[1]; HIRATA, Fumio
([1]Kyoto Univ.)

[*Chem. Phys. Lett.* **323**, 257 (2000)]

In disagreement with an intuitive prediction on the basis of the molecular size and dipole moment, it is observed empirically that the solubility of carbon dioxide (CO_2) in water is larger than that of carbon monoxide (CO). In order to shed light on this puzzling behavior, the solvation free energy of CO and CO_2 in aqueous solution is studied by means of the RISM-SCF/MCSCF method, a combined ab initio molecular orbital theory and statistical mechanics theory of molecular liquids. It is shown that the specific hydrogen bonding between oxygen atoms in CO_2 and water molecules makes CO_2 more soluble.

I-R-6 NMR Chemical Shifts in Solution: A RISM-SCF Approach

YAMAZAKI, Takeshi[1]; SATO, Hirofumi; HIRATA, Fumio
([1]GUAS)

[*Chem. Phys. Lett.* **325**, 668 (2000)]

The NMR chemical shift induced by solvation is formulated based on the ab initio electronic structure theory coupled with the integral equation method of molecular liquids. In order to examine the validity of the theory, the chemical shift of the atoms in a water molecule in water is calculated. The preliminary result with respect to hydrogen gives a reasonable account for the solvation shift, and for its temperature and density dependence.

I-R-7 ElectronL Self-Trapping in Two Dimensional Fluid

SETHIA, Ashok; SINGH, Yashwant; HIRATA, Fumio

[*Chem. Phys. Lett.* **326**, 199 (2000)]

The behavior of an excess electron in two dimensional classical liquid has been studied with the aid of Chandler, Singh and Richardson (CSR) theory [*J. Chem. Phys.* **81**, 1975 (1984)]. The size or dispersion of the wavepacket of a solvated electron is very sensitive to the interaction between the electron and fluid atoms, and exhibits complicated behavior in its density dependence. The behavior is interpreted in terms of an interplay among three causes: The excluded volume effect due to solvent, the pair attractive interaction between the electron and a solvent atom, and a balance of the attractive interactions from different solvent atoms.

I-S Solvation Thermodynamics of Protein and Related Molecules

Concerning biomolecules such as protein, it is a final goal for the biochemistry and biophysics to explore the relation between conformations and biological functions. The first important step toward the goal would be to explain the conformational stability of biomolecules in terms of the microscopic structure of the molecules in solvent. It is an extremely difficult problem by any means due to the overwhelmingly large degrees of freedom to be handled, including protein and solvent. As long as the small and/or short-time fluctuations of protein around the native structure is concerned, a variety of molecular simulation techniques provides a quite powerful tool to explore the microscopic structure of protein and solvent. However, the techniques are not so effective to characterize stability of the macromolecules in solution, to which the thermodynamic limit ($V \to \infty$, $N \to \infty$, with $V/N = const.$) is concerned. In such a case, methods based on the statistical mechanics of liquids should be natural choice for sampling configurations of solvent interacting biomolecules. The extended RISM theory is the most promising candidate of such methods, which provides not only solvation thermodynamics but also microscopic description at the level of the pair correlation functions.1) Obvious technical difficulties which one may face in applying the theory to such a large system are not only the computation time but also the stability of the numerical solution.2)

Here, we present our recent effort to tackle the problem using the two theoretical tools based on the statistical mechanics of liquids: The extended RISM and the scaled particle theories (SPT).3) The studies for the solvation thermodynamics of small molecules such as ions are also included because it is regarded as elementary processes for the solvation of biomolecules, and because it is prerequisite for studying the more complicated molecules.

References

1) M. Kinoshita, Y. Okamoto and F. Hirata, *J. Am. Chem. Soc.* **120**, 1855 (1998).
2) A. Kitao, F. Hirata and N. Go, *J. Phys. Chem.* **97**, 10231 (1993).
3) M. Irisa, K. Nagayama and F. Hirata, *Chem. Phys. Lett.* **207**, 430 (1993).

I-S-1 Salt Effect on Stability and Solvation Structure of Peptide: An Integral Equation Study

IMAI, Takashi[1]; KINOSHITA, Masahiro[2]; HIRATA, Fumio
([1]GUAS; [2]Kyoto Univ.)

[*Bull. Chem. Soc. Jpn.* **73**, 1113 (2000)]

Salt effects on the stability and on the solvation structure of a peptide in a variety of aqueous solutions of the alkali-halide ions are studied by means of the reference interaction site model (RISM) theory. The order of salt effect on the peptide stability is consistent with the experimental results; the order follows the Hofmeister series. The results are further analyzed in order to clarify the nature of the salt effect which determines the Hofmeister series and to find the reason why the Hofmeister series applies so generally to a variety of solutes in aqueous solutions. A heuristic model for explaining salt effects on the solvation structure of the peptide is proposed based on changes in the peptide-water pair correlation functions due to the ion perturbation.

I-S-2 Theoretical Study for Partial Molar Volume of Amino Acids in Aqueous Solution: Implication of Ideal Fluctuation Volume

IMAI, Takashi[1]; KINOSHITA, Masahiro[2]; HIRATA, Fumio
([1]GUAS; [2]Kyoto Univ.)

[*J. Chem. Phys.* **112**, 9469 (2000)]

A Kirkwood-Buff equation for the partial molar volumes of polyatomic molecules in solutions are derived based on the reference interaction site model (RISM) theory of molecular liquids. The partial molar volume of the twenty amino acids in aqueous solution at infinite dilution are calculated using the equation, and the results are discussed in comparison with the experimental data. The results indicate that ionizations of the C– and N–terminus groups give negative contributions to the volume ranging from –3.2 cm^3/mol to –9.7 cm^3/mol depending on the amino acid. Ionization of the dissociable residues also give negative contribution which ranges from –3.0 cm^3/mol to –6.0 cm^3/mol. On the other hand, contribution of the fractional charges on atoms to the volume is not necessarily negative, but rather slightly positive with few exceptions. It is clarified that contribution from an atom group to the volume is largely dependent on the situation where the group is placed. Therefore, it is concluded that the conventional way of determining the partial molar volume from group contributions is not reliable. The theoretical results for the partial molar volume exhibit a systematic deviation from corresponding experimental data, which increases nearly proportionally with increasing temperature and with the number of atoms in the amino acids. In order to account for the deviation, a concept of the "ideal fluctuation volume" is proposed, which is the ideal gas contribution to the volume, originating from the intra-molecular fluctuation of solute.

I-T Collective Density Fluctuations in Polar Liquids and Their Response to Ion Dynamics

As to the model for molecular diffusion in polar liquids, there are two quite different points of view. One is the conventional rot-translation model, and the other the interaction-site description which sees the diffusion of a molecule as a correlated motion of each atom (site).1) It is clearly advantageous to use the interaction-site description compared to the rot-translation model to account for chemical characteristics of solvent as well as solute dynamics. However, the interaction-site description has its own disadvantage in interpreting physical meaning of the results, since it does not give an explicit picture for the rotational relaxation of molecules, which can be directly probed by many experimental means including the dielectric and NMR relaxation. We have solved the problem by extracting collective modes of the density fluctuation from the site-site density correlation functions. In our recent study for dynamics of molecular liquids based on the interaction-site model, we have succeeded to abstract the collective excitations in liquids, which can be identified as optical and acoustic modes, by diagonalizing the collective frequency matrix appearing in the generalized Langevin equation. The two modes arise essentially from the rotational and translational motions of molecules.2) We applied the method to the ion dynamics in a dipolar liquid, and could have explained successfully the peculiar size dependence of friction of alkali and halide ions in terms of response of the collective excitations in solvent to the solute displacement.3)

In the past year, we have elaborated the memory kernel in our generalized Langevin equation base on the mode coupling theory. We have also extended our treatment to dynamics of water and hydrated ions. Those studies as well as other related topics are reviewed below.

References
1) F. Hirata, *J. Chem. Phys.* **96**, 4619 (1992).
2) S. Chong and F. Hirata, *Phys. Rev. E* **57**, 1691 (1998).
3) S. Chong and F. Hirata, *J. Chem. Phys.* **108**, 7339 (1998).

I-T-1 Relaxation of Average Energy and Rearrangement of Solvent Shells in Various Polar Solvents in Connection with Solvation Dynamics: Studied by RISM Theory

NISHIYAMA, Katsura[1]; **HIRATA, Fumio**; **OKADA, Tadashi**[1]
([1]Osaka Univ.)

[*Chem. Phys. Lett.* in press]

We employ a reference interaction-site model (RISM) theory to estimate the relaxation dynamics of average energy of solute-solvent systems as well as time-dependent radial distribution functions of solvents viewed from the solute. The theoretical results indicate that the rearrangement of the second solvent shell is about an order of magnitude slower compared with that of the first shell. We suggest that the slower relaxation of further solvent shells can play a significant role for the dynamic relaxation of the inhomogeneous spectral width, which has been observed in our previous experiments of the time-resolved hole-burning and fluorescence spectroscopy.

I-T-2 Importance of Acoustic Solvent Mode and Solute-Solvent Radial Distribution Functions in Solvation Dynamics: Studied by RISM Theory

NISHIYAMA, Katsura[1]; **HIRATA, Fumio**; **OKADA, Tadashi**[1]
([1]Osaka Univ.)

[*J. Chin. Chem.* in press]

We have applied the reference interaction-site model (RISM) theory to explain our experiments on solvation dynamics of laser dyes in polar organic solvents by means of the transient hole-burning and time-resolved fluorescence spectroscopy [K. Nishiyama and T. Okada, *J. Phys. Chem. A* **101**, 5729 (1997); **102**, 9729 (1998)]. The experiments show that the dynamic response function of the relaxation derived from the inhomogeneous spectral band-width of the solute–solvent system relaxes about an order of magnitude slower than that of average energy of the system. On the basis of our present theoretical prediction, we suggest that the relaxation dynamics of the spectral width might be mainly characterized by the solvent acoustic mode (translational motion) as well as the rearrangement of second plus further solvent shells.

I-U Liquid-Solid Interface

Due to recent progress in experimental techniques in the in situ measurements, the electrochemistry seems making a new epoch in understanding the chemical processes at electrode-solution interfaces. For examples, the scanning tunneling microscope (STM) applied to the interface has been revealing detailed atomic structure of the interface.1) The surface enhanced infrared absorption spectroscopy has provided detailed picture regarding the orientation of water molecules at the surface.2) The information in atomic level have been combined with the traditional techniques in the electrochemistry such as the cyclic voltammogram to provide more complete picture of electrode-solution interfaces. Obviously, the traditional descriptions using electric double layer models, which are based on the continuum models of solvent, mismatch the level of detailness attained by the recent experimental techniques.

Theoretical understanding of the interface has also made great progress in the last two decades, especially, in terms of solvent configuration near electrode surfaces.3) The progress has been mainly driven by two theoretical methods in the statistical mechanics of liquids: the molecular simulation and the integral equation methods. The two methods have reached consistent molecular pictures regarding reorganization of the water structure in the vicinity of the flat electrode surface. Latest topics in those approaches concern the electronic structure of electrode. The method features a self-consistent treatment of the liquid state and the electronic structure of the metal surface. Significance of such treatments will become more and more clear as the methods are extended to chemical reactions at the interface, which are primary motivation for the electrochemistry.

Although the integral equation methods have great advantage in the overall description of the electrode-solution interface both at phenomenological and molecular levels, the models which have been employed for the metal surface seems oversimplified considering the resolution attained by latest development in the experimental techniques stated above. Here, we propose a new approach for the electrode-solution interface based on the reference interaction site method (RISM) of liquids, which can handle both the structured metal surface and water in atomic level.

References

1) K. Itaya and E. Tomita, *J. Surf. Sci.* **201**, L507 (1988).
2) K. Ataka, T. Yotsuyanagi and M. Osawa, *J. Phys. Chem.* **100**, 10664 (1996).
3) L. Blum, *Adv. Chem. Phys.* **78**, 171 (1990).

I-U-1 Potentials of Mean Force of Simple Ions in Ambient Aqueous Solution. I. Three-Dimensional Reference Interaction Site Model Approach

KOVALENKO, Andriy; HIRATA, Fumio

[*J. Chem. Phys.* **112**, 10391 (2000)]

We adapt the three-dimensional reference interaction site model (3D-RISM) to calculate the potentials of mean force for ion–molecular solution as a difference between the chemical potential of solvation of a cluster of solutes and of individual ones. The method yields the solvation structure around the cluster of solutes in detail. The solvation chemical potential is obtained for the three-dimensional hypernetted chain (3D-HNC) closure as well as for its partial linearization (3D-PLHNC approximation). The solvation chemical potential is obtained in a closed analytical form for both the 3D-HNC and 3D-PLHNC closures. The 3D-RISM integral equations are solved by using the supercell technique. A straightforward supercell treatment of ionic solute in polar molecular solvent leads to a big error in the potential of mean force as well as the solvation chemical potential, which for simple ions in water amounts to about 35 kcal/mol. We elaborated corrections to the 3D-RISM integral equations, alleviating the artifact of the supercell periodicity with an accuracy of 0.05 kcal/mol or better and restoring the long-range asymptotics of the solute–solvent correlation functions. The dielectrically consistent siteˆsite RISM/HNC theory (DRISM/HNC) is employed for the solvent correlations to provide a proper description of the dielectric properties of solution. This allowed us to extend the description to solution at a finite salt concentration. We converge both the 3D-RISM and site–site DRISM integral equations by using the method of modified direct inversion in the iterative subspace.

Owing to the proper initial guess of the correlation functions, iteration begins at once for a given temperature and full molecular charge, avoiding a gradual decrease of the temperature and increase of the site charges, which greatly reduces the computation time. We calculate and discuss the potentials of mean force for sodium chloride in ambient water at infinite dilution as well as at a finite concentration.

I-U-2 Potentials of Mean Force of Simple Ions in Ambient Aqueous Solution. II. Solvation Structure from the Three-Dimensional Reference Interaction Site Model Approach, and Comparison with Simulations

KOVALENKO, Andriy; HIRATA, Fumio

[*J. Chem. Phys.* **112**, 10403 (2000)]

We applied the three-dimensional reference interaction site model (3D-RISM) integral equation theory with the 3D hypernetted chain (3D-HNC) closure or its partial linearization (3D-PLHNC) to obtain the potentials of mean force (PMFs) and the solvation structure of sodium chloride in ambient water. The bulk solvent correlations are treated by the dielectrically consistent site–site RISM/HNC theory (DRISM/HNC) to provide a proper description of the dielectric properties of solution and to include the case of a finite salt concentration. The PMF is calculated as a difference in the solvation free energy of an ion pair and of individual ions. We obtained and analyzed in detail the PMFs and solvation structure for ion pairs of NaCl at infinite dilution and a concentration of 1 M. The results are in reasonably good agreement with molecular dynamics simulations for the same model of the solution species. Positions and orientations of water molecules in the first solvation shell around the ion pair are deduced. The short-range hydration structure of the ion pairs at infinite dilution and at moderate concentration is very similar. Ionic ordering and clustering is found in 1 M solution.

I-U-3 Hydration Free Energy of Hydrophobic Solutes Studied by a Reference Interaction Site Model with a Repulsive Bridge Correction and a Thermodynamic Perturbation Method

KOVALENKO, Andriy; HIRATA, Fumio

[*J. Chem. Phys.* **113**, 2793 (2000)]

We modify the site–site as well as three-dimensional (3D) versions of the reference interaction site model (RISM) integral equations with the hypernetted chain (HNC) closures by adding a repulsive bridge correction (RBC). The RBC treats the overestimation of water ordering around a hydrophobic solute in the RISM/HNC approximation, and thus refines the entropic component in the hydration free energy. We build up the bridge functions on r^{-12} repulsive core potentials, and propose RBC expressions for both the site–site and 3D-RISM approaches. To provide fast calculation, we obtain the excess chemical potential of hydration by using the thermodynamic perturbation theory (TPT). The site–site RISM/HNC+RBC as well as 3D-RISM/HNC+RBC approaches are applied to calculate the structure and thermodynamics of hydration of rare gases and alkanes in ambient water. For both approaches, the RBC drastically improves the agreement of the hydration chemical potential with simulation data and provides its correct dependence on the solute size. For solutes of a nonspherical form, the 3D treatment yields the hydration structure in detail and better fits simulation results, whereas the site–site approach is essentially faster. The TPT approximation gives the hydration thermodynamics in good qualitative agreement with the exact results of the thermodynamic integration, and substantially reduces computational burden. The RBC-TPT approximation can improve the predictive capability of the hybrid algorithm of a generalized-ensemble Monte Carlo simulation combined with the site–site RISM theory, used to describe protein folding with due account for the water effect at the microscopic level. The RBC can be optimized for better fit to reference simulation data, and can be generalized for solute molecules with charged groups.

I-U-4 Liquid Structure at Metal Oxide-Water Interface: Accuracy of a Three-Dimensional RISM Methodology

SHAPOVALOV, Vladimir[1]; TRUONG, Thanh N.[1]; KOVALENKO, Andriy; HIRATA, Fumio
([1]Univ. Utah)

[*Chem. Phys. Lett.* **320**, 186 (2000)]

We calculated the structure of water in contact with the MgO 100 surface by using the three-dimensional reference interaction site model 3D-RISM integral equation theory. The spatial distributions of water oxygen and hydrogen over the surface unit cell are calculated and discussed. The water density profiles and the orientations obtained are in good agreement with computer simulations for the same model of the interface. The 3D-RISM approach shows considerable promise as a constituent of a self-consistent description of chemical processes at a metal oxide–water interface.

I-U-5 Self-Consistent, Kohn-Sham DFT and Three-Dimensional RISM Description of a Metal –Molecular Liquid Interface

KOVALENKO, Andriy; HIRATA, Fumio

[*J. Mol. Liq.* in press]

We have developed a self-consistent description of a metal–molecular liquid interface by combination of the Kohn-Sham density functional theory (KS DFT) for the electronic density, and the three-dimensional reference interaction site model (3D RISM) integral equation theory for the classical site distribution profiles of molecular liquid. The electron and classical subsystems are coupled in the mean field approximation. The classical potentials of the metal acting on species of the liquid are taken in the linear response regime. Many-body effects of dense liquid on metal valence electrons are allowed for by averaging pseudopotentials of liquid molecules over the site distributions of liquid. The coupled KS DFT and 3D RISM equations are solved simultaneously by using the procedure of dynamic relaxation. The proposed approach is substantially less time-consuming as compared to a Car-Parrinello type simulation. A partial linearization of the hypernetted chain (PLHNC) closure to the RISM equation is proposed. The calculation is performed in the supercell technique for water at normal conditions in contact with the (100) FCC slab of a metal roughly modeled after copper. The results are in good agreement with the Car-Parrinello simulation for the same model. Further applications of the method proposed are discussed.

I-V Dimensional Crossovers and Excitation Spectra in Quasi-One-Dimensional Organic Conductors

In molecular materials including organic conductors and metal complexes, physical properties sensitively depend on electronic dimensionality, which is controlled by applying external or chemical pressure. Dimensional crossovers are classified according to whether one- or two-particle coherence in directions perpendicular to the highest conductivity is first restored by increasing dimensionality. The restoration of coherence depends on the asymptotic property of the corresponding one-dimensional system. For a one-dimensional gapless phase, interchain hopping easily restores the transverse one-particle coherence. If any excitation spectrum has a gap owing to electron correlation, the transverse one-particle process is so strongly suppressed that the transverse two-particle coherence is relatively easily restored. In quasi-one-dimensional organic conductors $(TMTTF)_2X$, the charge gap suppresses the transverse one-particle coherence and the antiferromagnetic transition takes place from a charge-localized phase. Even in the gapless phase of $(TMTSF)_2X$, effective dimensionality of the optical property is lowered by increasing energy scale. In mixed crystals $(DI\text{-}DCNQI)_2Ag_{1-x}Cu_x$ and $(DMe\text{-}DCNQI)_2Li_{1-x}Cu_x$, random potential scattering causes complex competition among the Mott-insulator, Anderson-insulator, and Fermi-liquid phases.

I-V-1 Quantum Phase Transitions and Collapse of the Mott Gap in the $d = 1 + \varepsilon$ Dimensional Hubbard Model with $2k_F$ Umklapp Scattering

KISHINE, Jun-ichiro

[*Phys. Rev. B* **62**, 2377 (2000)]

We study the low-energy asymptotics of the $d = 1 + \varepsilon$ dimensional Hubbard model with a circular Fermi surface where there is $2k_F$ umklapp scattering present *a priori*. Peculiarity of the $d = 1 + \varepsilon$ dimensions is incorporated through the imbalance between the elementary particle-particle and particle-hole (PH) loops: infrared logarithmic singularity of the PH loop is smeared for $\varepsilon > 0$. The one-loop renormalization-group flows indicate that a quantum phase transition from a metallic phase to the Mott insulator phase occurs at a finite on-site Coulomb repulsion U for $\varepsilon > 0$. We also discussed effects of randomness and obtained phase diagrams in terms of d, U, and strength of random backward scattering.

I-V-2 One– and Two–Band Hubbard Models in $d = 1 + \varepsilon$ Dimensions: Dimensionality Effects on the Charge and Spin Gap Phases

KISHINE, Jun-ichiro

[*J. Phys. Chem. Solids* in press]

To examine dimensionality effects on the charge/spin gap phases in quasi-one-dimensional, strongly correlated chain/ladder systems, we perform the one-loop renormalization-group analysis of the one- and two-band Hubbard models with circular Fermi surfaces in $d = 1 + \varepsilon$ dimensions. The renormalization-group flows indicate that raising dimensionality suppresses the charge and spin gap in the one and two-band cases, respectively. This result gives a clue to understand experimental indication: both the charge gap in the quasi-one-dimensional organic conductor $(TMTTF)_2Br$ and the spin gap in the doped ladder system $(Sr_2Ca_{12}Cu_{24}O_{41})$ are suppressed upon increasing pressure.

I-V-3 Interplay of Randomness, Electron Correlation, and Dimensionality Effects in Quasi-One-Dimensional Conductors

KISHINE, Jun-ichiro; YONEMITSU, Kenji

[*Phys. Rev. B* **62**, in press (2000)]

We study the interplay of randomness, electron correlation, and dimensionality effects in weakly coupled half-filled Hubbard chains with weak quenched random potentials, based on the renormalization-group (RG) approach. We perform a two-loop RG analysis of an effective action derived by using the replica trick, and examine the following crossovers and phase transitions from an incoherent metal regime: (1) a crossover to the Anderson localization regime, (2) an antiferromagnetic phase transition, and (3) a crossover to the quasi-one-dimensional weak-localization regime. The case of $d = 1 + \varepsilon$ $(\varepsilon \ll 1)$ dimensions is also mentioned. Based on the result, we tried a simple simulation of the experimentally suggested successive crossovers [antiferromagnetic, Anderson localization to metallic phases] upon doping in $(DI\text{–}DCNQI)_2Ag_{1-x}Cu_x$.

I-V-4 Charge Gap and Dimensional Crossovers in Quasi-One-Dimensional Organic Conductors

YONEMITSU, Kenji; KISHINE, Jun-ichiro

[*J. Phys. Chem. Solids* in press]

Quasi-one-dimensional quarter-filled organic conductors, $(TMTTF)_2X$ and $(TMTSF)_2X$, show a dimensional crossover, and their electronic properties change accordingly. We describe this using the two-loop perturbative and density-matrix renormalization-group methods, the ε expansion around one dimension, and the random phase approximation. The effect of dimerization on the charge gap and interchain one-particle coherence is clarified. The effect of random potentials is also studied to describe Mott insulator, Anderson localization, and metallic phases of $(DCNQI)_2Ag_{1-x}Cu_x$ mixed crystals.

I-V-5 Dimensionality Effects on the Charge Gap in the Dimerized Hubbard Model at Quarter Filling: the Density-Matrix and Perturbative Renormalization-Group Approaches

YONEMITSU, Kenji; KISHINE, Jun-ichiro

[*J. Phys. Soc. Jpn.* **69**, 2107 (2000)]

We study dimensionality effects on the charge gap in the dimerized Hubbard model at quarter filling, with two approaches. First, we examine three chains coupled via the interchain one-particle hopping integral t_b, by the density-matrix renormalization-group (DMRG) method. Next, we consider the $d = 1 + \varepsilon$ dimensional model, using the perturbative renormalization-group (PRG) method. The dimensionality is controlled through t_b and ε, respectively. Both approaches lead to the conclusion that, for a finite dimerization ratio, the charge gap decreases as the dimensionality increases.

I-V-6 Intra- and Inter-Chain Dynamic Response Functions in Quasi-One-Dimensional Conductors

YONEMITSU, Kenji

[*Synth. Met.* in press]

Intra- and inter-chain excitation spectra are studied in a spinless fermion model on a two-leg ladder at half filling. Numerical results are obtained by application of the density-matrix renormalization-group technique to the quantum transfer matrix for infinite systems. Near the metal-insulator transition, the intra-chain Coulomb repulsion is found to affect local current correlations more sensitively in the rung direction than in the leg direction.

I-W Optical Excitations in Charge-Lattice-Ordered Phases of One-Dimensional Materials

Halogen-bridged binuclear metal complexes, which are often called MMX chains, have strong electron-lattice coupling and electron-electron interaction. Various charge and lattice ordering phases are found and depend on the ligand, the halogen ion and the counter ion. An alternate-charge-polarization phase is observed as well as a metallic phase for the ligand dta. Meanwhile, for the ligand pop, an averaged-valence Mott-insulator phase and a charge-polarization phase are observed as well as a well-known charge-density-wave phase. The competition among these electronic phases is qualitatively understood in a model with strong on-site repulsion, two types of electron-lattice couplings, and two types of elastic couplings. However, the optical properties sensitively depend on the long-range part of the electron-electron interaction. To explain both static and dynamical properties, we add nearest- and next-nearest-neighbor repulsion terms to the model in order to discuss the stability of each phase from the strong-coupling viewpoint and clarify the origin of each peak in the optical conductivity spectrum.

I-W-1 Charge Ordering and Lattice Modulation in Quasi-One-Dimensional Halogen-Bridged Binuclear Metal Complexes

KUWABARA, Makoto; YONEMITSU, Kenji

[*Mol. Cryst. Liq. Cryst.* **343**, 47 (2000)]

We have investigated ground state phase diagrams of the MMX chains in a one-dimensional dimerized 3/4-filled model by exactly diagonalizing 12-site clusters. In charged chains where counter ions are present, competition occurs among a uniform state, a charge-density-wave (CDW) state and a charge-polarization (CP) state. Experimentally observed phases are understood by strengths of a site-diagonal electron-lattice coupling β, the interdimer transfer integral t_{MXM}, and an elastic constant, whose variation is roughly estimated from the inter-atomic spacing, the species of the halogen ion. The CP state is relatively stable for small t_{MXM} and the CDW state for large β. In neutral chains where counter ions are absent, the dimer units can move almost freely. Dimers are alternately shifted to form tetramers because of a strong off-diagonal electron-lattice coupling, thus stabilizing an alternate-charge-polarization (ACP) state.

I-W-2 Charge Ordering and Lattice Modulation in MMX Chains

KUWABARA, Makoto; YONEMITSU, Kenji

[*J. Phys. Chem. Solids* in press]

Ground state phase diagrams for the MMX chains are studied in a one-dimensional two-band model by exactly diagonalizing 18-site clusters. Qualitative behavior of the phase diagrams is explained by the strong-coupling expansion. The relative stability between the charge-density-wave (CDW) and charge-polarization (CP) states observed in charged chains is determined by the kinetic energy gain through second-order processes with respect to intra-dimer charge transfer. Thus the relative stability is ascribed to competition between on-site Coulomb repulsion U and a diagonal electron-lattice coupling (β). The CP state is relatively stable for strong U and the CDW for strong β. In neutral chains, an alternate-charge-polarization (ACP) state is always more stable than the CP state by the energy gain through fourth-order processes with respect to interdimer transfer.

I-W-3 Charge Ordering and Optical Conductivity of MMX Chains

KUWABARA, Makoto; YONEMITSU, Kenji

[*Proc. LLD2K* submitted]

We study the optical conductivity of the halogen-bridged binuclear metal complexes, using a one-dimensional dimerized 3/4-filled-band model and the Lanczos method. The spectra are quite sensitive to the charge ordering pattern and the long-range Coulomb interaction. For instance, in a charge-polarization (CP) state two peaks are generally expected and ascribed to intra-dimer and interdimer charge excitations when long-range interactions are taken into account. However, when the interdimer Coulomb repulsion is weaker than the intra-dimer repulsion, only a single peak may be observed because the oscillator strength of the interdimer charge excitation is much weaker than that of the intra-dimer one. We clarify relations between the various ordering states and their optical conductivity spectra and compare them with experimental results.

I-W-4 Charge Excitations in an Alternate Charge Polarization Phase of a One-Dimensional Two-Band Extended Peierls-Hubbard Model for MMX Chains

KUWABARA, Makoto; YONEMITSU, Kenji

[*Synth. Met.* in press]

We investigate the optical conductivity of a halogen-bridged binuclear metal complex in an alternate-charge-polarization phase observed in $Pt_2(dta)_4I$ below 80 K, using a one-dimensional two-band extended Peierls-Hubbard model and the Lanczos technique, to study the dependence of three main peaks ascribed to intra-dimer, interdimer and halogen(X)-to-metal(M) charge excitations on model parameters. We show that effective energy difference between the M(Pt)-d_{z^2} and X(I)-p_z orbitals (Δ_{eff}) must be small in order to reproduce the optical conductivity spectra observed experimentally. Here Δ_{eff} is defined as $\Delta + U_M - U_X + 2V_{MM} - 2V_{MX}$, where Δ is the bare level difference, U_M (U_X) the on-site Coulomb repulsion at M (X) site, and V_{MM} (V_{MX}) the nearest-neighbor repulsion within a dimer (between M and X sites).

I-W-5 Highly Doped Nondegenerate Conjugated Polymers—A Theory Using the DMRG Method

SHIMOI, Yukihiro[1]; KUWABARA, Makoto; ABE, Shuji[1]
([1]Electron. Tech. Lab.)

[*Synth. Met.* in press]

Highly doped conjugated polymers with a non-degenerate ground state are investigated theoretically by using the density-matrix renormalization-group method. We pointed out a crossover between polaron- and bipolaron-lattice via formation of polaron-pairs. We also indicate that, at high doping concentration, the gaps in charge and spin excitations become negligibly small, while the bond alternation still survives.

I-X Magnetic and Optical Properties of Two-Dimensional Metal-Complex and Organic Conductors

Assembled metal complexes $Et_nMe_{4-n}Z[Pd(dmit)_2]_2$ are two-dimensional electronic materials and show rich phases including paramagnetic-insulator, antiferromagnetic–insulator, superconductor and metallic phases in different temperature and pressure regions and with different cations. The variety comes from the presence of HOMO and LUMO bands near the chemical potential and from strong dimerization of $Pd(dmit)_2$ molecules. The dependence of the ground state on the cation $Et_nMe_{4-n}Z$ was roughly interpreted on the Hückel basis and is now understood from the strong-coupling viewpoint, which enables us to show the correlation between the transport and magnetic properties and the stability criterion of the antiferromagnetic phase. On the other hand, two-dimensional organic conductors θ-(BEDT-TTF)$_2$X have no or very weak dimerization, so that the long-range part of the electron-electron interaction causes charge ordering and consequently insulator phases with different magnetic properties. The charge-ordering and magnetic-coupling patterns are understood on the basis of the anion-dependent anisotropy of Coulomb repulsion strengths and transfer integrals. Some of the optical properties may indicate importance of electron-phonon interaction as well, so that both static and dynamical properties are studied in a consistent manner.

I-X-1 Collective Excitations around Charge Ordered States and Coexistent States with Different Orders

MORI, Michiyasu; YONEMITSU, Kenji

[*Mol. Cryst. Liq. Cryst.* **343**, 221 (2000)]

Some novel ground states have recently been studied in molecular conductors. One is the coexistence of a spin density wave (SDW) and a charge density wave (CDW) in (TMTSF)$_2$PF$_6$, which is quasi-one-dimensional and is basically a quarter-filled system with dimerization. Seo and Fukuyama1) and Kobayashi *et al.*2) have used the Hartree approximation for one-dimensional extended Hubbard models and found coexistence of a $2k_F$ SDW with a $4k_F$ CDW and that with a $2k_F$ CDW, respectively. They claim that not only the on-site but also the nearest neighbor and the next-nearest-neighbor repulsive interactions are important, respectively. We study collective excitation spectra of such states with different orders. The excited states are calculated in the random phase approximation for the one-dimensional extended Hubbard model at quarter filling. In the charge ordered state, a dominant excitation in the current-current correlation function has no charge density modulation. A dominant excitation in the charge uniform state originates from crossing the dimerization gap and modulates the charge density.

References

1) H. Seo and H. Fukuyama, *J. Phys. Soc. Jpn.* **66**, 1249 (1997).

2) N. Kobayashi, M. Ogata and K. Yonemitsu, *J. Phys. Soc. Jpn.* **67**, 1098 (1998).

I-X-2 Anisotropic Collective Excitations around Various Charge Ordering States

MORI, Michiyasu; YONEMITSU, Kenji

[*J. Phys. Chem. Solids* in press]

Among the family of (ET)$_2$X (ET = BEDT-TTF), the θ-type salts have no evident dimeric structure and no antiferromagnetic insulating phase near the superconducting phase in contrast to the κ-type salts. In the paramagnetic insulating phase, charge ordering (CO) states are observed by the X-ray studies.[1] We notice that the various CO states are indeed possible and the intersite repulsive interactions are important in the θ-type salts. It is still hard to distinguish the ground states among many CO candidates in the actual salts. We calculate absorption spectra for various charge ordering (CO) states in the two-dimensional extended Hubbard model at quarter filling with the random phase approximation. Each CO state has its own characteristic and anisotropic excitations. In principle, these features should be observed in the optical measurements and tell which CO state is realized in the θ-(ET)$_2$X salts.

Reference

1) M. Watanabe, Y. Nogami, K. Oshima, H. Mori and S. Tanaka, *J. Phys. Soc. Jpn.* **68**, 2654 (1999).

I-X-3 Stability and Cation Dependence of Magnetic Orders in (Et$_n$Me$_{4-n}$Z)[Pd(dmit)$_2$]$_2$

MORI, Michiyasu; YONEMITSU, Kenji

[*Synth. Met.* in press]

Electronic states of (Et$_n$Me$_{4-n}$Z)[Pd(dmit)$_2$]$_2$ (Z = P, As, Sb) depend on the cations, although they are isostructural and have little differences in the lattice parameters. The experimentally observed Néel temperature is about 30 K for Me$_4$P and 18 K for Me$_4$Sb and Et$_2$Me$_2$P. For Et$_2$Me$_2$Sb, the antiferromagnetic (AF) phase transition is not observed above 5 K by the ESR measurement.[1] The cation dependence of the magnetic phase transitions in the Pd(dmit)$_2$ salts is studied by calculating effective exchange interactions between spins on dimers in a two-band Hubbard model. The effective Hamiltonian in the low-energy region is reduced to a spin-1/2 AF Heisenberg model on the anisotropic triangular lattice. The existence/absence of the magnetic order is understood from the sublattice magnetization calculated within the linear spin wave theory, as shown in Figure 1. For Et$_2$Me$_2$Sb, the AF order is destroyed by magnetic frustration.

Reference

1) T. Nakamura, H. Tsukada, T. Takahashi, S. Aonuma and R. Kato, *Mol. Cryst. Liq. Cryst.* **343**, 187 (2000).

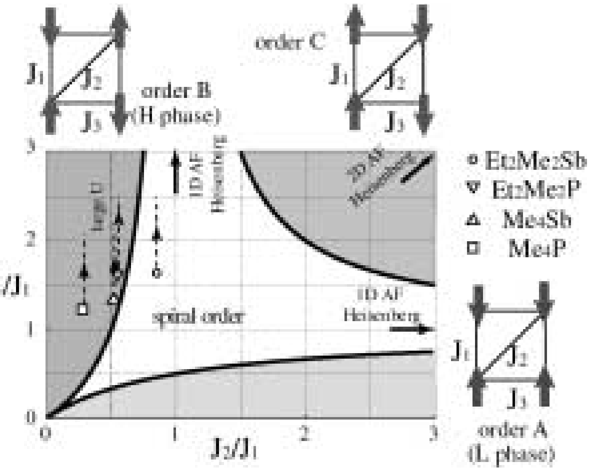

Figure 1. Magnetic phase diagram in the linear spin wave theory for the orders A, B and C. In each shaded region, the displayed magnetic order is stable. The salts with different cations are roughly located on the dashed lines. The position moves upward along the J_3/J_1 axis, as the on-site repulsive interaction is strengthened.

I-Y Multi-Phase Stability and Nonlinear Dynamics near Phase Boundary

In organic donor-acceptor compounds showing a neutral-ionic structural phase transition, each phase is locally stable and separated by a potential barrier from the other phase. To study photoinduced cooperative phenomena and dynamical processes, the high-energy part of the many-body potential is studied as well as the local minima. Techniques developed in molecular dynamics may be useful for such evolution of many-electron states. In conducting polymers possessing a non-degenerate bond-ordered ground state, electroluminescence involves recombination of excitons or polarons, which are produced by nonlinear processes of coupling between many electrons and phonons. Linear excitation analysis around such quasiparticles is useful to compare with experimental data.

I-Y-1 Influence of Short-Range Interference on Ionization Threshold Law

MIYASHITA, Naoyuki[1]; WATANABE, Shinichi[2]; MATSUZAWA, Michio[2]; MACEK, Joseph H.[3]
([1]GUAS; [2]Univ. Electro-Commun.; [3]Univ. Tennessee)

[*Phys. Rev. A* **61**, 14901 (2000)]

Electron-impact ionization of the collinear $Z = 1/4$ model atom is investigated in order to examine a nonclassical behavior of the ionization cross sections. Slightly above the ionization threshold, ab initio calculations reveal a distinctive dip due to short-range dynamics. The dip is a strongly energy-dependent feature in the usually smooth and structureless ionization cross section and is foreign to treatments based on classical, as well as semiclassical mechanics. The $Z = 1/4$ model thus serves as a counterexample to the standard Wannier treatment of near-threshold ionization. The hyperspherical hidden-crossing theory is applied to identify the origin of the dip.

I-Y-2 Potential Analysis for Neutral-Ionic Phase Transition

MIYASHITA, Naoyuki[1]; YONEMITSU, Kenji
([1]GUAS)

Adiabatic potentials around neutral and ionic phases are studied in two-site and four-site extended-Hubbard models with varying energy difference between donor and acceptor sites. Mean-field solutions are searched under the constraints that the spin-density alternation amplitude and the degree of charge transfer take some fixed values. Unstable regions are numerically hard to access, so that we develop several iteration schemes.

I-Y-3 Localized Vibrational Modes of Excitations in Electroluminescent Polymers

JIANG, Hao[1]; XU, Xiao-hua[1]; SUN, Xin[1,2]; YONEMITSU, Kenji
([1]Fudan Univ.; [2]Natl. Lab. Infrared Phys.)

[*Chin. Phys. Lett.* **16**, 836 (1999)]

The localized vibrational modes of an exciton and a polaron are investigated, and the results show that the frequencies of the three even parity modes of the exciton are very different from those of the polaron. For the exciton, three modes are distinctly separated, but, for the polaron, two modes with higher frequencies are close to each other. Then, it is possible to distinguish an exciton from a polaron by watching their Raman spectra. Therefore, the localized modes may be used to specify the exciton and the polaron in electroluminescent polymers.

I-Y-4 Photoinduced Polarization Inversion in a Polymeric Molecule

SUN, Xin[1,2]; FU, Rouli[2]; YONEMITSU, Kenji; NASU, Keiichiro[3]
([1]Fudan Univ.; [2]Natl. Lab. Infrared Phys.; [3]Inst. Mater. Struct. Sci.)

[*Phys. Rev. Lett.* **84**, 2830 (2000)]

The polymeric molecule can exhibit a new photoinduced phenomenon where the electric dipole of the molecule with a bipolaron is reversed by absorbing one photon. This photoinduced polarization inversion occurring in a single molecule is an ultrafast process with a relaxation time of 200 fs.

RESEARCH ACTIVITIES II
Department of Molecular Structure

II-A Laser Cooling and Trapping of Metastable Helium Atoms

In the past two decades, extensive developments have occurred in the laser cooling and trapping of neutral atoms, with many workers reporting the application of these techniques to such diverse atomic species as alkali atoms, alkali earth atoms, and rare gas atoms. Among these, the helium atom is unique on account of its small mass, simple energy level structure, and easy availability in two isotopic forms (^{3}He and ^{4}He) of differing quantum statistics. For this reason, we have been studying the laser cooling and trapping of helium atoms.

II-A-1 Magneto-Optical Trap of Metastable Helium-3 Atoms

KUMAKURA, Mitsutaka; MORITA, Norio

[*Appl. Phys. B: Lasers Opt.* **70**, 555 (2000)]

A magneto-optical trap (MOT) of metastable ^{3}He atoms has been demonstrated for the first time. Some 10^5 atoms have successfully been confined in a region with a diameter of ~0.4 mm at a temperature of ~0.5 mK; the atomic number density is estimated to be ~10^9 /cm^3 at the trap center. These characteristics of the ^{3}He MOT are almost comparable to those of the ^{4}He MOT so far demonstrated by many workers. Monitoring the fluorescence from the MOT, the trap loss rate has also been measured and discussed. Since ^{3}He is a unique fermionic atom on account of its small mass and simple energy level structure, we can expect that such a ^{3}He MOT will be useful as a fundamental tool for future studies on the physics of fermions at ultralow temperatures.

II-B Spectroscopic Studies on Atoms and Ions in Liquid Helium

Atoms and ions in liquid helium are known to reside in bubble-like cavities due to the Pauli repulsive force between electrons. Physical properties of these exotic surroundings are determined by the potential energy of the impurity-He$_n$ system, the surface tension energy of the liquid helium, and the pressure-volume work. Spectroscopic studies of such impurity atoms and ions in liquid helium are expected not only to give information on the structure and dynamics of the bubbles but also to contribute to the study on the property of superfluid liquid helium.

II-B-1 Theoretical Studies on the Spectra of Yb$^+$ Ions in Liquid Helium

MORIWAKI, Yoshiki; MORITA, Norio

[*Eur. Phys. J. D* **13**, 11 (2001)]

In our previous experimental studies on Yb$^+$ in liquid helium, we found that its spectra have two characteristic properties: (1) The $4f^{14}6s\,^2S_{1/2}$–$6p\,^2P_{1/2}$ (D1) excitation spectrum is much broadened and blue-shifted compared with the spectrum of free Yb$^+$ ions, while the emission spectrum of the same transition has relatively small spectral width and shift compared with the excitation spectrum. (2) The excitation spectrum of the $4f^{14}6s\,^2S_{1/2}$–$6p\,^2P_{3/2}$ (D2) transition is doubly peaked. To explain these properties, we have carried out theoretical calculations on the basis of a vibrating bubble model, in which the bubble surface is assumed to vibrate in the spherical (breathing), dipolar and quadrupolar modes. These calculations are essentially based on adiabatic potential curves of an Yb$^+$–He pair, which have been obtained from our complete-active-space self-consistent field (CASSCF) and multi-reference configuration-interaction (MRCI) calculations. Consequently, it has been found that the blue shifts are well understood with this bubble model, and also that the dynamic Jahn-Teller effect due to the quadrupole vibration of the bubble plays an important role for the double-peaked profile of the D2 excitation spectrum.

II-B-2 Measurements of Fine Structure Changing Cross Sections of Ca$^+$ and Sr$^+$ in Collisions with He Atoms

MORIWAKI, Yoshiki; MATSUO, Yukari[1]; MORITA, Norio
([1]RIKEN)

In our previous spectroscopic study of Yb$^+$ in liquid helium, we observed an emission from its $4f^{14}6p\ ^2P_{1/2}$ fine structure level not only when this level was directly excited but also when another fine structure level ($4f^{14}6p\ ^2P_{3/2}$) was excited. This suggested the presence of a fast inter-multiplet transition from $^2P_{3/2}$ to $^2P_{1/2}$ due to the interaction between Yb$^+$ and He atoms. From our estimation, which was based on the comparison between the emission intensities measured when the $^2P_{1/2}$ and $^2P_{3/2}$ levels were excited, we found that the $^2P_{3/2} \rightarrow {}^2P_{1/2}$ transition should be extremely faster than expected for two-body collisions of other atoms and ions with He. This enhancement of the transition may have arisen from some many-body effect, such as the quadrupole vibration of the helium bubble surface. However we could not discuss it any more, because there were no data on the fine structure changing rate in two-body collisions, which was necessary to exactly estimate the many-body effect. This fact motivated us to study fine structure changing rates of alkali-earth ions in two-body collisions with He.

We have started with measurements on Ca^+ and Sr^+ to test our experimental apparatus. These ions have been produced by laser ablation of pure metal samples. Detecting laser induced fluorescence, we have measured cross sections of collision induced transitions between fine structure levels in the $4p^2P_J$ state of Ca^+ and the $5p^2P_J$ state of Sr^+ due to collisions with He atoms at room temperature (298 K). The cross sections obtained are $\sigma(Ca^+: 4p^2P_{3/2} \rightarrow 4p^2P_{1/2}) = 1.17 \pm 0.05$ Å^2, $\sigma(Ca^+: 4p^2P_{1/2} \rightarrow 4p^2P_{3/2}) = (7.92 \pm 0.44) \times 10^{-1}$ Å^2, and $\sigma(Sr^+: 5p^2P_{3/2} \rightarrow 5p^2P_{1/2}) = (1.44 \pm 0.10) \times 10^{-2}$ Å^2. These cross sections are much smaller than those of neutral K and Rb atoms, which have the same electron configurations as Ca^+ and Sr^+, respectively. This may probably be because stronger spin-orbit couplings in the $2P_J$ states of Ca^+ and Sr^+ prevent their electron spins from flip-flopping all the more. On the other hand, it is known that the cross sections of alkali atoms are roughly proportional to $e^{-C\Delta E}$ (where ΔE is the fine structure splitting and C is a constant). This is seen from the fact that the cross sections for alkali atoms are almost on a straight line in Figure 1. However, the present cross sections for Ca^+ and Sr^+ significantly deviate upward from this line, as seen in Figure 1; that is, these cross sections are much larger than expected from only the sizes of the fine structure splittings. This may probably be due to a difference between the interactions in ion-He and atom-He pairs.

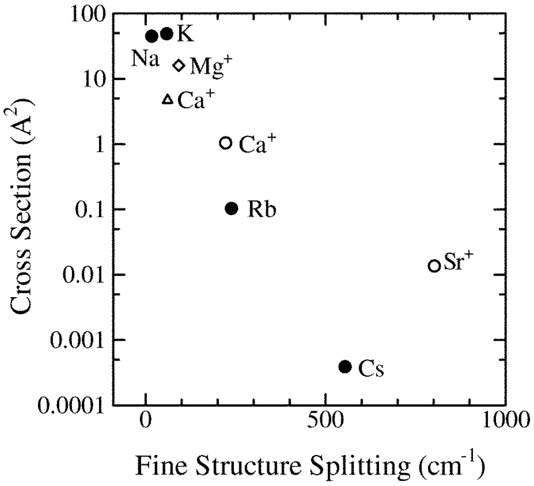

Figure 1. Fine structure changing cross sections so far measured for various alkali atoms and alkali earth ions in collisions with He atoms, as a function of their fine structure splittings; ● shows the one for the $np^2P_{3/2} \rightarrow np^2P_{1/2}$ transition of each alkali atom (for Na, K, Rb and Cs, n = 3, 4, 5 and 6, respectively, and the collision temperature T = 397, 368, 340 and 311 K, respectively) (by Krause), ◇ Mg^+ $3p^2P_{3/2} \rightarrow 3p^2P_{1/2}$ at 1600 K (by Brust), △ Ca^+ $3d^2D_{5/2} \rightarrow 3d^2D_{3/2}$ at 10000 K (by Knoop *et al.*), and ○ the present data.

II-C Endohedral Metallofullerenes: New Fullerene Molecules with Novel Properties

Encapsulation of one or more metal atoms inside hollow fullerene cages (endohedral metallofullerenes) has long attracted special attention because it could lead to new sperical molecules with novel properties unexpected for empty fullerenes. Great efforts have been made for the production and characterization of endohedral metallofullerenes. Up to now it has been demonstrated that group 2 and 3 metals and most lanthanide metals can be trapped inside the higher fullerenes to form soluble and relatively stable endohedral metallofullerenes. Because of the difficulty in producing pure samples in large quantities, the experimental characterization of endohedral metallofullerenes has been hindered. Recent important progress is marked by the successful isolation and purification of metallofullerenes in macroscopic quantities. This has made it possible to investigate the interesting electronic properties and chemical reactivities.

II-C-1 La@C_{82} Anion. An Usually Stable Metallofullerene

AKASAKA, Takeshi[1]**; WAKAHARA, Takatsugu**[2]**; NAGASE, Shigeru**[3]**; KOBAYASHI, Kaoru**[3]**; WÄLCHLI, Markus**[4]**; YAMAMOTO, Kazunori**[5]**; KONDO, Masahiro**[2]**; SHIRAKURA, Shingo**[2]**; OKUBO, Shingo**[2]**; MAEDA, Yutaka**[2]**; KATO, Tatsuhisa; KAKO, Masahiro**[6]**; NAKADAIRA, Yasuhiro**[6]**; NAGAHATA, Ritsuko**[7]**; GAO, Xiang**[8]**; VAN CAEMELBECKE, Eric**[8]**; KADISH, Karl M.**[8]
([1]IMS and Niigata Univ.; [2]Niigata Univ.; [3]Tokyo Metropolitan Univ.; [4]Bruker Japan; [5]PRN; [6]Univ. Electro-Commun.; [7]NIMCR; [8]Univ. Houston)

[*J. Am. Chem. Soc.* **122**, 9316 (2000)]

The anion of the major isomer of La@C_{82} was electrochemically prepared and isolated. Anionic La@C_{82}(–) is very stable in water, even after exposure to air at room temperature. The high stability of La@C_{82}(–) is essentially due to its closed-shell electronic structure. As evidenced by the ESR analysis, La@C_{82}(–) is diamagnetic. These experimental findings are confirmed by density functional calculations. The cage structure of La@C_{82} was determined for the first time and shown to have C_{2v} symmetry based on the ^{13}C NMR measurements of the compound in its anionic form.

II-C-2 Transient Spectroscopic Properties of Endohedral Metallofullerenes, La@C_{82} and La_2@C_{80}

FUJITSUKA, Mamoru[1]**; ITO, Osamu**[1]**; KOBAYASHI, Kaoru**[2]**; NAGASE, Shigeru**[2]**; YAMAMOTO, Kazunori**[3]**; KATO, Tatsuhisa; WAKAHARA, Takatsugu**[4]**; AKASAKA, Takeshi**[5]
([1]Tohoku Univ.; [2]Tokyo Metropolitan Univ.; [3]PRN; [4]Niigata Univ.; [5]IMS and Niigata Univ.)

[*Chem. Lett.* 902 (2000)]

Properties of the excited states of endohedral metallofullerenes (La@C_{82} and La_2@C_{80}) have been investigated by time-resolved absorption spectroscopy. Transient absorption bands of La@C_{82} showed two decay-components, which were attributed to excited states of different spin multiplicity. The properties of photoexcited states of La_2@C_{80} are also reported.

II-C-3 Vibrational Spectroscopy of Endohedral Dimetallofullerene, La_2@C_{80}

MORIYAMA, Masaya[1]**; SATO, Tadatake**[1]**; YABE, Akira**[1]**; YAMAMOTO, Kazunori**[2]**; KOBAYASHI, Kaoru**[3]**; NAGASE, Shigeru**[3]**; WAKAHARA, Takatsugu**[4]**; AKASAKA, Takeshi**[5]
([1]NIMCR.; [2]PRN; [3]Tokyo Metropolitan Univ.; [4]Niigata Univ.; [5]IMS and Niigata Univ.)

[*Chem. Lett.* 524 (2000)]

The first FT-IR spectra of La_2@C_{80} are observed at temperatures from 353 to 83 K by dispersing the sample into the KBr pellet, which confirm that the C_{80} cage has I_h symmetry, as supported from theoretical calculations. Also discussed is the rotational motion of the C_{80} cage.

II-D Structure and Function of Respiratory Terminal Oxidases

In the aerobic respiratory chain of *Escherichia coli*, there are structurally unrelated two terminal oxidases. A heme-copper oxidase, cytochrome *bo* is predominantly expressed under highly aerated growth conditions while an alternative oxidase, a putative heme-heme oxidase, cytochrome *bd*, is predominant under microaerobic conditions. Both oxidases catalyze the two-electron reduction of ubiquinol-8 and the four-electron reduction of dioxygen, whereas only cytochrome *bo* exhibits vectorial proton transport. However, only a little structural information has been given for these ubiquinol oxidases. To clarify the molecular mechanism of electron transfer, chemical reaction of dioxygen, and proton pumping in the two respiratory terminal oxidases, we utilize various molecular spectroscopic techniques (*e.g.*, resonance Raman, EPR, FTIR) in conjunction with methods of molecular biology and biochemistry.

II-D-1 Probing Molecular Structure of Dioxygen Reduction Site of Bacterial Quinol Oxidases through Ligand Binding to the Redox Metal Centers

TSUBAKI, Motonari[1,2]**; HORI, Hiroshi**[2]**; MOGI, Tatsushi**[3]
([1]Himeji Inst. Tech.; [2]Osaka Univ.; [3]Univ. Tokyo)

[*J. Inorg. Biochem.* **82**, 19 (2000)]

Cytochromes *bo* and *bd* are structurally unrelated terminal ubiquinol oxidases in the aerobic respiratory chain of *Escherichia coli*. The high-spin heme-Cu$_B$ binuclear center serves as the dioxygen reduction site for cytochrome *bo*, and the heme b_{595}-heme *d* binuclear center for cytochrome *bd*. Cu$_B$ coordinates three histidine ligands and serves as a transient ligand binding site en route to high-spin heme, one-electron donor to the oxy intermediate, and a binding site for bridging ligands like cyanide. In addition, it can protect the dioxygen reduction site through binding of a peroxide ion in the resting state, and connects directly or indirectly Tyr288 and Glu286 to carry out redox-driven proton pumping in the catalytic cycle. Contrary, heme b_{595} of cytochrome *bd* participate a similar role to Cu$_B$ in ligand binding and dioxygen reduction but cannot perform such versatile roles because of its rigid structure.

II-D-2 Active Site Structure of SoxB-Type Cytochrome *bo*$_3$ Oxidase from Thermophilic *Bacillus*

UCHIDA, Takeshi[1]**; TSUBAKI, Motonari**[1,2,4]**; KUROKAWA, Tatsunori**[3]**; HORI, Hiroshi**[4]**; SAKAMOTO, Junshi**[3]**; KITAGAWA, Teizo**[1]**; SONE, Nobuhito**[3]
([1]IMS; [2]Himeji Inst. Tech.; [3]Kyushu Inst. Tech.; [4]Osaka Univ.)

[*J. Inorg. Biochem.* **82**, 65 (2000)]

Two-subunit SoxB-type cytochrome *c* oxidase in *Bacillus stearothermophilus* was over-produced, purified, and examined for its active site structures by electron paramagnetic resonance (EPR) and resonance Raman (RR) spectroscopies. This is cytochrome *bo*$_3$ oxidase contained heme B at the low-spin heme site and heme O at the high-spin heme site of the binuclear center. EPR spectra of the enzyme in the oxidized form indicated that structures of the high-spin heme O and the low-spin heme B were similar to those of SoxM-type oxidases based on the signals at $g = 6.1$, and $g = 3.04$. However, the EPR signals from the Cu$_A$ center and the integer spin system at the binuclear center showed slight differences. RR spectra of the oxidized form showed that heme O was in a 6-coordinated high-spin ($\nu_3 = 1472$ cm^{-1}), and heme B was in a 6-coordinated low-spin ($\nu_3 = 1500$ cm^{-1}) state. The Fe^{2+}–His stretching mode was observed at 211 cm^{-1}, indicating that the Fe^{2+}–His bond strength is not so much different from those of SoxM-type oxidases. On the contrary, both the Fe^{2+}–CO stretching and Fe^{2+}–C–O bending modes differed distinctly from those of SoxM-type enzymes, suggesting some differences in the coordination geometry and the protein structure in the proximity of bound CO in cytochrome *bo*$_3$ from those of SoxM-type enzymes.

II-E Structure and Function of Transmembrane Electron Transfer System in Neuroendocrine Secretory Vesicles

In neuroendocrine secretory vesicles of animals, intravesiclular ascorbate (AsA$^-$) functions as the electron donor for copper-containing monooxygenases. Upon these monooxygenase reactions, monodehydroascorbate (MDA) radical is produced by oxidation of AsA$^-$. The MDA radical is reduced back to AsA$^-$ by membrane-spanning cytochrome b_{561}. Subsequently, the oxidized cytochrome b_{561} is reduced by cytosolic AsA$^-$. We found previously that purified cytochrome b_{561} from bovine adrenal medulla contains two hemes B per molecule, each exhibiting an independent EPR signal in oxidized state. Radiolytically generated MDA radical oxidized rapidly reduced cytochrome b_{561} to yield the oxidized form. Subsequently, the oxidized form was re-reduced by AsA$^-$ in the medium. At excess MDA radical, only half of the heme was oxidized, indicating that only one of the two heme centers can react with MDA radical.

II-E-1 Reduction of Heme Iron Suppresses the Carbethoxylation of Two Histidyl and One Tyrosyl Residues Indispensable for the Transmembrane Electron Transfer Reaction of Cytochrome b_{561}

TAKEUCHI, Fusako[1]; KOBAYASHI, Kazuo[2]; TAGAWA, Seiichi[2]; TSUBAKI, Motonari[1,3]
([1]Himeji Inst. Tech.; [2]Osaka Univ.; [3]IMS)

We found previously that treatment of oxidized cytochrome b_{561} with diethyl pyrocarbonate (DEPC) caused specific *N*-carbethoxylation of three fully conserved residues (His88, His161, and Lys85) located at the extravesicular side.[1)] The modification lead to a selective loss of the electron accepting ability from AsA$^-$ without affecting the electron-donation to MDA radical. In the present study, we found that the *O*-carbethoxylation of one tyrosyl residue (Tyr218) locating at the extravesicular side was significantly enhanced in an alkaline condition, leading to a very slow reduction process of the oxidized heme with AsA$^-$. Presence of AsA$^-$ during the reaction with DEPC was found to suppress the carbethoxylation of the heme-coordinating histidyl (His88 and His161) and the tyrosyl (Tyr218) residues, whereas the modification level of Lys85 was not affected. Concomitantly, the final reduction level of heme *b* with AsA$^-$ was protected, although the fast reduction process was not fully restored. A similar protective effect was observed in the presence of sodium dithionite or isoascorbate. These results suggest that the modification of the histidine residues were suppressed in the reduced form of heme *b*. On the other hand, Tyr218, together with Lys85, has a role in the recognition/binding process for AsA$^-$ and is indispensable for the fast electron transfer reaction from AsA$^-$.

Reference

1) Tsubaki, M., Kobayashi, K., Ichise, T., Takeuchi, F. and Tagawa, S., *Biochemistry* **39**, 3276 (2000).

II-E-2 Planarian Cytochrome b_{561}: A Transmembrane Electron Transfer Protein Unique to Neuroendocrine Secretory Vesicles

ASADA, Akikazu[1]; KUSAKAWA, Takashi[1]; ORII, Hidefumi[1]; AGATA, Kiyokazu[1]; WATANABE, Kenji[1]; TSUBAKI, Motonari[1,2,3]
([1]Himeji Inst. Tech.; [2]IMS; [3]Osaka Univ.)

Cytochrome b_{561} is a major transmembrane protein of catecholamine and neuropeptide secretory vesicles of central and peripheral nervous system in higher animals. We succeeded in the cloning of a full-length cDNA encoding planarian cytochrome b_{561}. The deduced amino acid sequence showed a very similar transmembrane topology to those of higher vertebrate and contained both putative AsA$^-$- and MDA radical-binding sites.[1)] Among the six totally-conserved His residues in higher vertebrate, one His residue was substituted with Asn residue indicating that His88 and His161 of bovine cytochrome b_{561} play roles as the heme *b* ligands at the extravesicular side. Northern- and Western-blot analyses confirmed the expression of the mRNA and the protein in planarian with the expected sizes, respectively. Distributions of the mRNA and the apoprotein were analyzed with in situ hybridization and immunocytochemical staining, respectively, which showed two morphologically distinct structures, a pair of the ventral nerve cords and the cephalic ganglion cluster in the head region. Present results suggest that the usage of AsA$^-$ for the supply of electron equivalents to the neuroendocrine-specific copper-containing monooxygenases could be originated from organisms having a very simple nervous system.

Reference

1) Okuyama, E., Yamamoto, R., Ichikawa, Y. and Tsubaki, M., *Biochim. Biophys. Acta* **1383**, 269 (1998).

II-F Structure and Function of Steroidogenic Cytochrome P450 System

In adrenal cortex of higher animals, various cytochromes P450 perform steroid hormone biosynthesis. In the mitochondrial inner membranes, cytochromes P450scc and P45011β receive electron equivalents from a 2Fe-2S type ferredoxin, adrenodoxin, to perform the oxygen activation and the site-specific hydroxylations. On the other hand, in the endoplasmic reticulum membranes, there are two microsomal type cytochromes P450; namely P450c21 and P45017α. These cytochromes receive electron equivalents from flavin-containing cytochrome P450 reductase. The former catalyzes the C21 hydroxylation essential for the production of corticosteroid hormones (glucocorticoids and mineralcorticoids). We are currently investigating these steroidogenic cytochrome P450 systems utilizing various biochemical and biophysical techniques.

II-F-1 Direct Heme-Steroid Interaction in Cytochrome P450c21 Studied by FTIR Spectroscopy

TSUBAKI, Motonari[1,2]; TAKEUCHI, Kohji[1]
([1]Himeji Inst. Tech.; [2]IMS)

We showed previously that combination of 20β-hydroxysteroids (17α,20β-dihydroxyprogesterone and 20β-hydroxyprogesterone) with oxidized cytochrome P450c21 purified from bovine adrenocortical microsomes induced a type I difference spectrum and exhibited a concomitant development of a new low-spin signal at g_z = 2.42, g_y = 2.21, and g_x = 1.966 and an increase in intensity of the g8 high-spin signal in EPR spectra.1) Being consistent with these substrate-like properties, we confirmed that cytochrome P450c21 have a 20β-oxidase activity for the 20β-hydroxysteroids in an enzyme-reconstituted system. In the present study, the heme-steroid interaction in reduced state was investigated by analyzing heme-bound C–O stretching vibration with FTIR spectroscopy, to clarify the mechanism of the site- and stereo-selective 20β-oxidase activity. In a substrate-free state, a C–O band was observed at 1949 cm^{-1}. Addition of 17α-hydroxyprogesterone or progesterone caused a peak-shift to 1952 and 1942.5 cm^{-1}, respectively. Additions of 17α,20β-dihydroxyprogesterone and 20β-hydroxyprogesterone caused a shift of main band to 1950 and 1955 cm^{-1}, respectively. Concomitantly, peculiar C–O bands were observed around 1998 cm^{-1} for these 20β-hydroxysteroid complexes. These results suggest a specific interaction between steroid hydroxy group(s) and heme prosthetic group, both in oxidized and reduced states.2)

References

1) Tsubaki, M., Matsumoto, N., Tomita, S., Ichikawa, Y. and Hori, H., *Biochim. Biophys. Acta* **1390**, 197 (1998).
2) Tsubaki, M., in *Molecular Steroidogenesis*, M. Okamaoto, Y. Ishimura and H. Nawata, Eds., Universal Academy Press, Inc.; Tokyo, pp. 69–72 (2000).

II-F-2 Adrenodoxin-Cytochrome P450scc Interaction as Revealed by EPR Spectroscopy: Comparison with Putidaredoxin-Cytochrome P450cam System

TAKEUCHI, Kohji[1]; TSUBAKI, Motonari[1,2,3]; HORI, Hiroshi[3]
([1]Himeji inst. Tech.; [2]IMS; [3]Osaka Univ.)

Cholesterol side-chain cleavage reaction catalyzed by cytochrome P450scc constitutes of three consecutive monooxygenase reactions (22R-hydroxylation, 20S-hydroxylation, and C20-C22 bond scission) to produce pregnenolone.1,2) The electron equivalents necessary for the oxygen activation were supplied from a 2Fe2S-type ferredoxin, adrenodoxin. We found that binding of oxidized adrenodoxin to ferric P450scc complexed with cholesterol or 25-hydroxycholesterol caused a shift of the g = 8 and g = 3.5 high-spin signal of the heme moiety but not for the low-spin signals at 15 K. On the other hand, ligation of CO or NO to the ferrous heme of P450scc complexed with reduced adrenodoxin and various steroid substrates did not show any change in a trough (at 346.8 mT) of the axial EPR spectrum of the reduced adrenodoxin (at 77 K). These results showed a remarkable contrast to those found for the cytochrome P450cam-putidaredoxin-substrate ternary complex suggesting that mode of the cross talk between adrenodoxin and P450scc is different from the *Pseudomonas system*.

References

1) Tsubaki, M., Hiwatashi, A., Ichikawa, Y. and Hori, H., *Biochemistry* **26**, 4527 (1987).
2) Tsubaki, M., Iwamoto, Y., Hiwatashi, A. and Ichikawa, Y., *Biochemistry* **28**, 6899 (1989).

II-G Biomolecular Science

Elucidation of a structure-function relationship of metalloproteins is a current subject of this group and for this purpose we treat proteins and model compounds of their active sites. The primary technique used for this project is the stationary and time-resolved resonance Raman spectroscopy excited by visible and UV lasers. The main themes that we want to explore are (1) mechanism of oxygen activation by enzymes, (2) mechanism of active proton translocation and its coupling with electron transfer, (3) coupling mechanism of proton- and electron transfers by quinones in photosynthetic reaction center, (4) higher order protein structures and their dynamics, and (5) reactions of biological NO. In category (1), we have examined a variety of terminal oxidases, cytochrome P450s, and peroxidases, and also treated their enzymatic reaction intermediates by using the mixed flow transient Raman apparatus and the Raman/absorption simultaneous measurement device. For (2) the third generation UV resonance Raman (UVRR) spectrometer was constructed and we are going to use it to the peroxy and ferryl intermediates of cytochrome *c* oxidase and cytochrome *bo*. In (3) we succeeded in observing RR spectra of quinones A and B in bacterial photosynthetic reaction centers for the first time, but we have focused our attention on detecting tyrosine radical for the P intermediate of terminal oxidases. Some positive evidence was obtained for cytochrome *bo*. For (4) we developed a novel technique for UV resonance Raman measurements based on the combination of the first/second order dispersions of gratings and applied it successfully to 235-nm excited RR spectra of several proteins including mutant hemoglobins and myoglobins. Nowadays we can carry out time-resolved UVRR experiments with nanosecond resolution to discuss protein dynamics. With the newly developed third generation UV Raman spectrometer, we have succeeded in isolating the spectrum of tyrosinate in ferric Hb M Iwate, which was protonated in the ferrous state, and that of the deprotonated state of Tyr244 of bovine cytochrome *c* oxidase. For (5) we purified soluble guanylate cyclase from bovine lung and observed its RR spectra. To further investigate it, we are developing an expression system of this protein.

II-G-1 Resonance Raman Investigation of Fe–N–O Structure of Nitrosylheme in Myoglobin and Its Mutants

TOMITA, Takeshi[1]; HIROTA, Shun[2]; OGURA, Takashi[3]; OLSON, John S.[4]; KITAGAWA, Teizo
([1]Tohoku Univ.; [2]Nagoya Univ.; [3]Univ. Tokyo; [4]Rice Univ.)

[*J. Phys. Chem. B* **103**, 7044 (1999)]

Resonance Raman spectra have been observed for NO adducts of wild-type (WT) sperm whale myoglobin (MbNO) and its H64G, H64L, L29W, V68W, and V68T mutants at neutral and acidic pH. Raman excitation in resonance with the Soret band enabled us to detect the Fe–NO stretching ($\nu_{\text{Fe–NO}}$), N–O stretching (ν_{NO}), and Fe–N–O bending (δ_{FeNO}) bands. The $\nu_{\text{Fe–NO}}$, δ_{FeNO}, and ν_{NO} bands of WT MbNO at neutral pH were observed at 560, 452, and 1613 cm^{-1}, respectively, and substitution of the distal His64 to Gly or Leu caused an upshift of ν_{NO} to 1631–1635 cm^{-1} but no change in $\nu_{\text{Fe–NO}}$. This change in ν_{NO} is considered to be due to the removal of hydrogen bonding between His64 and bound NO. Conversely, substitution of Leu29 with tryptophan (L29W) altered Fe–NO but caused no change in ν_{NO} at neutral pH. This feature resembles that of MbO$_2$ but distinctly differs from that of MbCO, for which the Fe–CO and C–O stretching frequencies have an inverse linear correlation. The change in $\nu_{\text{Fe–NO}}$ for L29W-MbNO is probably caused by tilting of the Fe–N bond from the heme normal on account of steric hindrance from the large indole ring but would not be due to changes in the Fe–N–O bond angle. When pH is lowered to 4, MbNO adopts the five-coordinate structure due to cleavage of the Fe-His bond. Accordingly, the heme maker bands such as ν_3 and ν_{10}, shifted from 1500 and 1636 cm^{-1} at pH 7.4 to 1509 and 1646 cm^{-1} at pH 4 which are in agreement with those of a five-coordinate Fe-protoporphyrin-NO complex in detergent micelles at neutral pH. The $\nu_{\text{Fe–NO}}$ and ν_{NO} bands of acidic MbNO were observed at 520 and 1668 cm^{-1} and exhibited no shift when the distal His was replaced by Gly or Leu. The latter observation supports previous X-ray crystallographic, infrared, and resonance Raman studies which show that the distal histidine becomes protonated at pH 4 and swings out into the solvent away from the bound ligand.

II-G-2 Novel Iron Porphyrin-Alkanethiolate Complex with Intramolecular NH···S Hydrogen Bond: Synthesis, Spectroscopy, and Reactivity

SUZUKI, Noriyuki[1]; HIGUCHI, Tunehiko[1]; URANO, Yasuteru[1]; KIKUCHI, Kazuya[1]; UEKUSA, Hidehiro[2]; OHASHI, Yuji[2]; UCHIDA, Takeshi; KITAGAWA, Teizo; NAGANO, Tetsuo[1]
([1]Univ. Tokyo; [2]Tokyo Inst. Tech.)

[*J. Am. Chem. Soc.* **121**, 11571 (1999)]

Among heme enzymes, cytochrome P450 and NO synthase (NOS) have strong oxidizing ability and unusual structure, in that their heme irons have thiolate coordination. We report here a novel iron porphyrin-alkanethiolate complex with an intramolecular NH···S hydrogen bond that we synthesized in order to examine the influence of the NH···S hydrogen bond on catalytic oxidation. Complex 1 (see Figure 1) was designed to form an NH···S hydrogen bond by introducing amide NH in the vicinity of the thiolate, while complexes 2 and 3 were designed not to form an NH···S hydrogen bond by replacing amide NH with N-methyl or by introducing acetamide in a position apart from the sulfur atom.

Complexes 1-3 were characterized by FAB MS, IR, EPR, electronic absorption spectroscopy, resonance Raman spectroscopy, and X-ray crystal structure analysis. The absorption spectra of the ferrous-CO complexes of 1-3 exhibited typical hyperporphyrin spectra for a thiolate-ligated iron(II) porphyrin-CO complex. The Soret band of the ferrous-CO complex of 1 (456 nm, which arises from a transition between the lone pair p orbital of the thiolate and the e_g orbital of heme) was considerably blue-shifted compared to that of the other complexes, indicating electron deficiency of thiolate in complex 1 arising from the NH···S hydrogen bond.

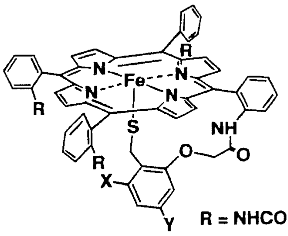

	X	Y
1	-NHCOCH$_3$	H
2	-N(CH$_3$)COCH$_3$	H
3	H	-NHCOCH$_3$
SR	H	H

R = NHCOC(CH$_3$)$_3$

Figure 1. Structures of complexes 1–3 and **SR**.

II-G-3 Mechanism of the Anionic Cyclopolymerization of Bis(dimethylvinylsilyl)methane

SUGA, Yasuhiro[1]**; OKU, Jun-ichi**[1]**; MASUDA, Hideki**[1]**; TAKAKI, Mikio**[1]**; MUKAI, Masahiro**[2]**; KITAGAWA, Teizo**
([1]Nagoya Inst. Tech.; [2]RIKEN)

[*Macromolecules* **32**, 1362 (1999)]

The driving force of the complete cyclization in the anionic cyclopolymerization of bis(dimethylvinylsilyl)-methane with *n*-BuLi/TMEDA in hexane is clarified with resonance Raman and ^{1}H NMR measurements. Vinyl groups coordinating to the lithium cation are detected in both measurements of the polymerization mixture at –70 °C, and they, at least some part of them, are shown to be the vinyl groups in uncyclized end units. Disappearance of these species from the resonance Raman spectrum at –20 °C indicates that the cyclization proceeds fast and is accelerated by the coordination of the second vinyl group in the uncyclized end unit. This is the first case that the interaction between the vinyl group in an uncyclized end unit and the counterion was found in ionic cyclopolymenzation.

II-G-4 Synthesis and Characterization of Novel Alkylperoxo Mononuclear Iron(III) Complexes with a Tripod: Pyridylamine Ligand: A Model for Peroxo Intermediates in Reactions Catalyzed by Non-Heme Iron Enzymes

WADA, Akira[1]**; OGO, Seiji; WATANABE, Yoshihito; MUKAI, Masahiro**[2]**; KITAGAWA, Teizo; JUTSUKAWA, Koichiro**[1]**; MASUDA, Hideki**[1]**; EINAGA, Hisahiko**[1]
([1]Nagoya Inst. Tech.; [2]RIKEN)

[*Inorg. Chem.* **38**, 3592 (1999)]

Previously, by the use of a tripodal pyridylamine ligand, tris-(6-neopentylanaino-2-pyridylmethyl)amine (TNPA), we first succeeded in the preparation of [Fe(tnpa)(OH)(PhCOO)]ClO$_4$ as a model complex for an active form of soybean lipoxygenase-1, in which stable formation of the hydroxo-iron(III) complex was accomplished by intramolecular hydrogen bonds. We also achieved the isolation of [Cu(bppa)(OOH)]ClO$_4$ having Cu(II)-OOH species by employing a similar tripodal pyridylamine ligand, bis(6-pivalamido-2-pyridylmethyl)(2-pyridylmethyl)amine (BP-PA). Here, in order to understand the coordination environment of peroxo intermediates in reactions catalyzed by non-heme iron enzymes, we have tried to synthesize stable alkylperoxo mono-nuclear iron(III) complexes using BPPA ligand and to examaine the physicochemical properties.

The resonance Raman spectra of a MeCN solution containing the complex **2** which were measured at room temperature by using 600 nm laser excitation revealed strong resonance-enhanced Raman features at 873, 838, 629, and 469 cm^{-1}, while that of **3** exhibited the features at 878, 838, 639, 548, and 493 cm^{-1}. The Raman features normally observed at ca. 800 cm^{-1} are in the range characteristic of ν(O–O) vibrations of peroxide species and are insensitive upon the addition of $H_2{}^{18}O$. Since these vibrational data were in agreement with those observed for the terminal η^1-alkylperoxo species obtained from the reaction of Fe(II)–(6–Me$_3$TPA) complexes with alkylperoxides, we deduced that the alkylperoxo moiety is retained on the iron(III) ion in an end-on fashion and the intense absorption bands near 585 and 613 nm for complexes **2** and **3**, respectively, are thus assignable to the alkylperoxo-to-iron(III) charge transfer transition.

II-G-5 Interactions of Phosphatidylinositol 3-Kinase Src Homology 3 Domain with Its Ligand Peptide Studied by Absorption, Circular Dichroism, and UV Resonance Raman Spectroscopies

OKISHIO, Nobuyuki[1]**; NAGAI, Masako**[1]**; FUKUDA, Ryuji**[1]**; NAGATOMO, Shigenori; KITAGAWA, Teizo**
([1]Kanazawa Univ.)

[*Biopolymers (Biospectroscopy)* **57**, 208 (2000)]

Absorption, circular dichroism (CD), and UV resonance Raman (UVRR) spectroscopies were applied to selectively examine the environmental and structural changes of Trp and Tyr residues in the phosphatidylinositol 3-kinase (PI3K) SH3 domain induced by ligand association. Comparison of the spectra of PI3K SH3 in the presence or absence of its ligand peptide RLP1 (RKLPPRPSK) indicated that RLP1 binding changed the environment of Trp55 of the SH3 to be more hydrophilic and its H bonding weaker and that of Tyr residues to be more hydrophobic. The D21N mutant (Asp21 → Asn) of the SH3 yielded a UV CD distinct from that of the wild type, and its spectral changes induced by RLP1 binding were smaller and different from those of the wild type in absorption, CD, and UVRR spectra, suggesting that the mutation of conserved Asp21 affected the conformation of the ligand binding cleft and thus might lead to the decrease in the ligand affinity. These data provide direct evidence for the occurrence of environmental and structural changes of PI3K SH3 by the association of a ligand and the D21N mutation.

II-G-6 Resonance Raman Studies of Oxo Intermediates in the Reaction of Pulsed Cytochrome *bo* with Hydrogen Peroxide

UCHIDA, Takeshi; MOGI, Tatsushi[1]; KITAGAWA, Teizo
([1]Univ. Tokyo)

[*Biochemistry* **39**, 6669 (2000)]

Cytochrome *bo* from *Escherichia coli,* a member of the heme-copper terminal oxidase superfamily, physiologically catalyzes reduction of O_2 by quinols and simultaneously translocates protons across the cytoplasmic membrane. The reaction of its ferric pulsed form with hydrogen peroxide was investigated with steady-state resonance Raman spectroscopy using a home-made microcirculating system. Three oxygen-isotope-sensitive Raman bands were observed at 805/X, 783/753, and (767)/730 cm^{-1} for intermediates derived from $H_2{}^{16}O_2/H_2{}^{18}O_2$. The experiments using $H_2{}^{16}O{}^{18}O$ yielded no new bands, indicating that all the bands arose from the Fe=O stretching ($\nu_{Fe=O}$) mode. Among them, the intensity of the 805/X cm^{-1} pair increased at higher pH and the species giving rise to this band seemed to correspond to the P intermediate of bovine cytochrome *c* oxidase (CcO) on the basis of the reported fact that the P intermediate of cytochrome *bo* appeared prior to the formation of the F species at higher pH. For this intermediate a Raman band assignable to the C–O stretching mode of a tyrosyl radical was deduced at 1489 cm^{-1} from difference spectra. This suggests that the P intermediate of cytochrome *bo* contains an Fe^{IV}=O heme and a tyrosyl radical like compound I of prostaglandin H synthase. The 783/753-cm^{-1} pair, which was dominant at neutral pH and close to the $\nu_{Fe=O}$ frequency of the oxoferryl intermediate of CcO, presumably arises from the F intermediate. On the contrary, the (767)/730-cm^{-1} species has no counterpart in CcO. Its presence may support the branched reaction scheme proposed previously for O_2 reduction by cytochrome *bo*.

II-G-7 A New Measurement System for UV Resonance Raman Spectra of Large Proteins and Its Application to Cytochrome *c* Oxidase

AKI, Michihiko[1]; OGURA, Takashi[2]; SHINZAWA-ITOH, Kyoko[3]; YOSHIKAWA, Shinya[3]; KITAGAWA, Teizo
([1]GUAS; [2]Univ. Tokyo; [3]Himeji Inst. Tech.)

[*J. Phys. Chem. B* **104**, 10765 (2000)]

A new type of ultraviolet resonance Raman (UVRR) measurement system suitable to a limited amount of large protein samples is proposed and the results from its application to bovine cytochrome *c* oxidase (CcO) is presented. To minimize the sample damage caused by high-flux UV laser illumination and to reject visible fluorescence from the sample, frequency-doubling of a mode-locked Ar^+ ion laser and a solar blind multi-channel detector were employed, respectively. A new spinning cell was designed so that the sample solution could be stirred during spinning of the cell. Combination of all these devices resulted in successful observation of high quality UVRR spectra of CcO excited at 244 nm. The RR bands of tryptophan- and tyrosine residues dominated the observed spectra, while an extra band appeared at 1656 cm^{-1}. The frequency of the extra band as well as those of all other bands were unaltered by the redox change of metal centers and ligand binding to heme a_3. Deprotonation of a tyrosine residue(s) with a low pK_a value was detected for the resting state at pH 9.1. Examination of all possible assignments led us to conclude that the extra band arose from the linoleoyl side chain of phospholipids and its intensity suggested the presence of 21 linoleoyl groups per CcO molecule.

II-G-8 An Approach to the O_2 Activating Mononuclear Non-heme Fe Enzymes: Structural Characterization of Fe(II)-Acetato Complex and Formation of Alkylperoxoiron(III) Species with the Highly Hindered Hydrotris(3-tert-butyl-5-isopropyl-1-pyrazolyl)borate

OGIHARA, Tamako[1]; HIKICHI, Shiro[1]; AKITA, Munetaka[1]; UCHIDA, Takeshi; KITAGAWA, Teizo; MORO-OKA, Yoshihiko[1]
([1]Tokyo Inst. Tech.)

[*Inorg. Chim. Acta* **297**, 162 (2000)]

Structural characterization of an F(II)-acetato complex and attempts to synthesize mononuclear Fe(III) dioxygen complexes bearing the highly sterically demanding $Tp^{tBu,iPr}$ (= hydrotris(3-tert-butyl-5-isopropyl-1-pyrazolyl)borate) ligand have been investigated. X-ray crystallography reveals that the acetato complex consists of the distorted square pyramidal Fe(II) center as found for the previously reported O_2-reactive Tp^{iPr2} derivative. In contrast to the less hindered Tp^{iPr2}, (= hydrotris(3,5-diiso-propyl-1-pyrazolyl)borate) complexes, oxidative addition of O_2 to the coordinatively unsaturated Fe(II) centers of the acetato and a hydroxo complexes with $Tp^{tBu,iPr}$ has never been observed in any conditions. Reaction of the ferrous hydroxo complex with ROOH (R = H, alkyl) results in the formation of the thermally unstable intermediates. Especially, the Fe(III)-alkylperoxo complex is characterized by UV-Vis, ESR and resonance Raman spectroscopy. The extremely bulky $Tp^{tBu,iPr}$ ligand hinders the approach of the exogenous O_2 molecule to the Fe(II) centers but stabilizes the unstable Fe(III)alkylperoxo intermediate enough to be detected.

II-G-9 Structures of Reaction Intermediates of Bovine Cytochrome *c* Oxidase Probed by Time-Resolved Vibrational Spectroscopy

KITAGAWA, Teizo

[*J. Inorg. Biochem.* **82**, 9 (2000)]

Structures of reaction intermediates of bovine cytochrome *c* oxidase (CcO) in the reactions of its fully reduced form with O_2 and fully oxidized form with H_2O_2 were investigated with time-resolved resonance Raman (RR) and infrared spectroscopy. Six oxygen-associated RR bands were observed for the reaction of CcO with O_2. The isotope shifts for an asymmetrically labeled dioxygen, $^{16}O^{18}O$, has established that the primary intermediate of cytochrome a_3 is an end-on type dioxygen adduct and the subsequent intermediate (P) is an oxoiron species with Fe=O stretch ($\nu_{Fe=O}$) at 804/764 cm^{-1} for $^{16}O_2/^{18}O_2$ derivatives, although it had been long postulated to be a peroxy species. The P intermediate is converted to the F intermediate with $\nu_{Fe=O}$ at 785/751 cm^{-1} and then to a ferric hydroxy species with $\nu_{Fe\text{–}OH}$ at 450/425 cm^{-1} (443/417 cm^{-1} in D_2O). The rate of reaction from P to F intermediates is significantly slower in D_2O than in H_2O. The reaction of oxidized CcO with H_2O_2 yields the same oxygen isotope-sensitive bands as those of P and F, indicating the identity of intermediates. Time-resolved infrared spectroscopy revealed that deprotonation of carboxylic acid side chain takes place upon deligation of a ligand from heme a_3. UVRR spectrum gave a prominent band due to *cis* C=C stretch of phospholipids tightly bound to purified CcO.

II-G-10 Heme Structure of Hemoglobin M Iwate [α87(F8)His → Tyr]: A UV and Visible Resonance Raman Study

NAGAI, Masako[1]; AKI, Michihiko[2]; LI, Renqiang[1], JIN, Yayoi[1]; SAKAI, Hiroki[3]; NAGATOMO, Shigenori; KITAGAWA, Teizo
(*[1]Kanazawa Univ.; [2]GUAS; [3]Sakai Womens Clinic*)

[*Biochemistry* **39**, 13093 (2000)]

Heme structures of a natural mutant hemoglobin (Hb), Hb M Iwate [α87(F8)His → Tyr], and protonation of its F8-Tyr were examined with the 244-nm excited UV resonance Raman (UVRR) and the 406.7- and 441.6-nm excited visible resonance Raman (RR) spectroscopy. It was clarified from the UVRR bands at 1605 and 1166 cm^{-1} characteristic of tyrosinate that the tyrosine (F8) of the abnormal subunit in Hb M Iwate adopts a deprotonated form. UV Raman bands of other Tyr residues indicated that the protein takes the T quaternary structure even in the *met*-form. Although both hemes of α and β subunits in *met*Hb A takes a six-coordinate (6c) high-spin structure, the 406.7-nm excited RR spectrum of *met*Hb M Iwate indicated that the abnormal α subunit adopts a 5c high-spin structure. The present results and our previous observation of the $\nu_{Fe\text{–}O(tyrosine)}$ Raman band (*Biochemistry* **28**, 2418, (1989)) have proved that F8-tyrosinate is covalently bound to Fe(III)-heme in the α subunit of Hb M Iwate. As a result, peripheral groups of porphyrin ring, especially the vinyl and the propionate side chains, were so strongly influenced that the RR spectrum in the low frequency region excited at 406.7 nm is distinctly changed from the normal pattern. When Hb M Iwate was fully reduced, the characteristic UVRR bands of tyrosinate disappeared and the Raman bands of tyrosine at 1620 (Y8a), 1207 (Y7a), and 1177 cm^{-1} (Y9a) increased in intensity. Coordination of distal His(E7) to the Fe(II)-heme in the reduced α subunit of Hb M Iwate was proved by the observation of the $\nu_{Fe\text{–}His}$ RR band in the 441.6-nm excited RR spectrum at the same frequency as that of its isolated α chain. The effects of the distal-His coordination on the heme appeared as distortion of the peripheral groups of heme. Possible mechanism for the formation of Fe(III)-tyrosinate bond in Hb M Iwate is discussed.

II-G-11 Model Complexes for the Active Form of Galactose Oxidase. Physicochemical Properties of Cu(II)- and Zn(II)-Phenoxyl Radical Complexes

ITOH, Shinobu[1]; TAKI, Masayasu[2]; KUMEI, Hideyuki[2]; TAKAYAMA, Shigehisa[2]; NAGATOMO, Shigenori; KITAGAWA, Teizo; SAKURADA, Norio[3]; ARAKAWA, Ryuichi[3]; FUKUZUMI, Shunichi[2]
(*[1]Osaka City Univ.; [2]Osaka Univ.; [3]Kansai Univ.*)

[*Inorg. Chem.* **39**, 3708 (2000)]

One-electron oxidations of the Cu(II)- and Zn(II)-phenolate complexes of ligand 1H afford relatively stable phenoxyl radical complexes, which exhibit very characteristic UV-NIR features similar to those exhibited by the active forms of the native enzymes. Comparison of the spectroscopic characteristics (UV-vis and ESR) of the Cu(II) and Zn(II) complexes of $1^{\bullet}$ to those of the corresponding complexes of $2^{\bullet}$ indicates that the methylthio group of $1^{\bullet}$ exerts an electron-sharing conjugative effect, thus stabilizing the radical form of the cofactor, as has been demonstrated in model studies of the metal-free radicals. Such an important role for the thioether group (electron-sharing conjugative effect) has also been predicted by ab initio theory and demonstrated by high-frequency ESR studies of model radicals. It should be noted, however, that such an electronic effect of an alkylthio group is not always observed in other model systems, suggesting that the molecular geometry of a complex is also very important to the enhancement of this effect. The smaller ε values for the NIR features of the model complexes as compared to those for the active forms of the native enzymes may indicate a strong contribution from Tyr272$^{\bullet}$ → Tyr495^{-} interligand charge transfer in addition to intramolecular charge transfer from the benzene ring to the alkylthio group in the phenoxyl radical group itself in the enzymatic systems.

II-G-12 Characterization of Imidazolate-Bridged Cu(II)-Zn(II) Heterodinuclear and Cu(II)-Cu(II) Homodinuclear Hydroperoxo Complexes as Reaction Intermediate Models of Cu, Zn-SOD

OHTSU, Hideki[1]; ITOH, Shinobu[2]; NAGATOMO, Shigenori; KITAGAWA, Teizo; OGO, Seiji;

WATANABE, Yoshihito; FUKUZUMI, Shunichi[1]
([1]Osaka Univ.; [2]Osaka City Univ.)

[*Chem. Commun.* 1051 (2000)]

Imidazolate-bridged Cu(II)-Zn(II) heterodinuclear and Cu(II)-Cu(II) homodinuclear hydroperoxo complexes are generated in the reactions between imidazolate-bridged heterodinuclear homodinuclear complexes and H_2O_2 in the presence of triethylamine base and characterized spectroscopically as reaction intermediate models of Cu, Zn-SOD.

II-H Fast Dynamics of Photoproducts in Solution Phases

Picosecond time-resolved resonance Raman (ps-TR^3) spectroscopy is a promising technique to investigate ultrafast structural changes of molecules. However, this technique has not been used as widely as nanosecond TR^3 spectroscopy, mainly due to the lack of light source which has suitable repetition rates of pulses and wavelength tunability. In order to obtain qualified TR^3 spectra, first we need two independently tunable light sources for pump and probe pulses. Second, the repetition rate should be higher than kilohertz to keep a moderate average laser power without making the photon density of probe pulse too high. We succeeded in developing light sources for ps-TR^3 spectroscopy having wide tunability and kHz repetition, and applied them to study fast dynamics of photo-excited molecules. For carbonmonoxy myoglobin (MbCO), vibrational relaxation with the time constant of 1.9 ps was observed for CO-photodissociated heme. For Ni-octaethylporphyrin in benzene, differeces in rise times of population in vibrationally excited levels among various modes were observed in the anti-Stokes spectra for the first time. This technique has been applied to identify the trans ligand of CO in the CO-bound transcriptional factor, Coo A.

On the other hand, we have constructed a nanosecond temperature-jump apparatus using a water absorption in near infrared. The new apparatus based on a Nd:YAG laser was combined with a time-resolved Raman measurement system and applied successfully to explore thermal unfolding of ribonuclease A.

II-H-1 Saturation Raman Spectroscopy as a tool for Studying the Excited States of Complex Organic Molecules: Application to Nickel Octaethylporphyrin

KRUGLIK, Sergei G.[1]; SHVEDKO, A. G.[1]; KITAGAWA, Teizo
([1]B. I. Stepanov Inst. Phys.)

[*Asian J. Phys.* **17**, 365 (1998)]

The nanosecond saturation resonance Raman (RR) technique has been reviewed and its peculiarities have been examined on the basis of a well-known molecular system, nickel octaethylporphyrin [Ni(OEP)] in solution. The results of mathematical treatment of saturation RR spectra of Ni(OEP) in weakly coordinating pyridine solvent suggest that the quantum yield of photogeneration of the six-coordinate Ni(OEP)-(pyridine)$_2$ species is low, with the rate of complexation process being about one tenth of the rate of excitation deactivation within the manifold of four-coordinate species.

II-H-2 Construction of Novel Nanosecond Temperature Jump Apparatuses Applicable to Raman Measurements and Direct Observation of Transient Temperature

YAMAMOTO, Kohji[1]; MIZUTANI, Yasuhisa; KITAGAWA, Teizo
([1]GUAS)

[*Appl. Spectrosc.* in press (2000)]

Two types of nanosecond temperature jump (T-jump) apparatuses applicable to time-resolved Raman measurements were constructed. T-jump was achieved by direct heating of water using near infrared (NIR) pulses at 1.89 μm in one type and at 1.56 μm in the other. The two NIR pulses were generated through stimulated Raman scattering (SRS) of H_2 or D_2 excited by the fundamental line of a Q-switched Nd:YAG laser, in which a single pass configuration with H_2 was sufficient for 1.89-μm pulses but a seeding-amplification configuration with D_2 was necessary for 1.56-μm pulses. The seeding-amplification configuration brought about significant improvements in conversion efficiency, pulse-to-pulse stability, and beam quality. These apparatuses were applied to transient Raman measurements of MoO_4^{2-} solution and transient temperatures of the heated volume were determined from ratios of anti-Stokes to Stokes Raman intensities. Temporal behaviors of the temperature of heated volume upon illumination of nanosecond heat pulses at 1.89-μm or 1.56-μm were explored and its applicability to studies on the primary process of thermal reactions was examined. It became clear that the continuation time of raised temperature is determined only by replacement of sample in the case of thick sample and by both thermal transfer and sample replacement in a case of thin sample, while thermal diffusion is not effective for both samples.

II-H-3 Identification of Histidine 77 as the Axial Heme Ligand of Carbonmonoxy CooA by Picosecond Time-Resolved Resonance Raman Spectroscopy

UCHIDA, Takeshi; ISHIKAWA, Haruto[1]; ISHIMORI, Koichiro[1]; MORISHIMA, Isao[1]; NAKAJIMA, Hiroshi[2]; AONO, Shigetoshi[2]; MIZUTANI, Yasuhisa; KITAGAWA, Teizo
([1]Kyoto Univ.; [2]JIST)

[*Biochemistry* **39**, 12747 (2000)]

The heme proximal ligand of carbonmonoxy CooA, a CO-sensing transcriptional activator, in the CO-bound form was identified to be His77 by using picosecond time-resolved resonance Raman spectroscopy. On the basis of the inverse correlation between Fe–CO and C–O stretching frequencies, we proposed previously that His77 is the axial ligand trans to CO (Uchida *et al.*, *J. Biol. Chem.* **273**, 19988), whereas later a possibility of displacement of His77 by CO with retention of another unidentified axial ligand was reported (Vogel *et al.*, *Biochemistry* **38**, 2679). Although our previous resonance Raman study failed to detect the Fe–His stretching [ν(Fe–His)] mode of CO-photodissociated CooA of the carbonmonoxy adduct due to the rapid recombination, application of picosecond time-resolved resonance Raman technique enabled us to observe a new intense line assignable to ν(Fe–His) at 211 cm^{-1} immediately after photolysis, while it became nondiscernible after 100-ps delay. The low ν(Fe–His) frequency of photodissociated CooA indicates the presence of some strain in the Fe–His bond in CO-bound CooA. This and the rapid recombination of CO characterize the heme-pocket of CooA. The 211 cm^{-1} band was completely absent in the spectrum of the CO-photodissociated form of His77-substituted mutant but the Fe-Im stretching band was observed in the presence of exogenous imidazole (Im). Thus, we conclude that His77 is the axial ligand of CO-bound CooA and CO displaces the axial ligand *trans* to His77 with retention of ligated His77 to activate CooA as the transcriptional activator.

II-H-4 A Role of Solvent in Vibrational Energy Relaxation of Metalloporphyrins

MIZUTANI, Yasuhisa; KITAGAWA, Teizo

[*J. Mol. Liq.* in press (2000)]

The formation of a vibrationally excited photoproduct of metalloporphyrins upon (π,π*) excitation and its subsequent vibrational energy relaxation were monitored by picosecond time-resolved resonance Raman spectroscopy. Stokes Raman bands due to a photoproduct of nickel octaethylporphyrin (NiOEP) instantaneously appeared upon the photoexcitation. Their intensities decayed with a time constant of ~300 ps, which indicates electronic relaxation from the (*d*,*d*) excited state (B_{1g}) to the ground state (A_{1g}), being consistent with the results of transient absorption measurements by Holten and coworkers. Anti-Stokes ν_4 and ν_7 bands for vibrationally excited (*d*,*d*) state of NiOEP decayed with time constants of ~10 and ~300 ps. The former is ascribed to vibrational relaxation, while the latter corresponds to the electronic relaxation from the (d,d) excited state to the electronic ground state. While the rise of anti-Stokes ν_4 intensity was instrument-limited, the rise of anti-Stokes ν_7 intensity was delayed by 2.6 ± 0.5 ps, which indicates that intramolecular vibrational energy redistribution has not been completed in subpicosecond time regime. To study a mechanism of intermolecular energy transfer, solvent dependence of the time constants of anti-Stokes kinetics was investigated using various solvents. No significant solvent dependence of the rise and decay constants was observed for NiOEP. For an iron porphyrin, we observed two phases in intermolecular energy transfer. The fast phase was insensitive to solvent and the slow phase depended on solvents. A model of classical thermal diffusion qualitatively reproduced this behavior. For solute-solvent energy transfer process, low-frequency modes of proteins seem to be less important.

II-I Molecular and Electronic Structures of Metallofullerenes and the Fullerene Radical Anions

The continued interest in radical ions of fullerenes and metallofullerenes has resulted from the discovery of superconductivity in the CT complexes of alkali metals with fullerenes. Spectroscopic information concerning the electronic and spin states of the metallofullerenes has been obtained by cw- and pulsed-EPR measurements.

II-I-1 2D-HYSCORE Measurements of ^{13}C–La@C$_{82}$

OKUBO, Shingo; KATO, Tatsuhisa; AKASAKA, Takeshi[1]; DINSE, K.-P.[2]
([1]Niigata Univ.; [2]TU Darmstadt)

ESEEM (electron spin echo envelope modulation) was detected in the pulsed ESR (Electron Spin Resonance) measurements for two isomers of La@C$_{82}$. Especially the isomer I of La@C$_{82}$ showed the prominent modulation with the frequency of 3 MHz, which was originated from ^{139}La nuclear quadrupole coupling. The origine of the 3 MHz modulation was confirmed by HYSCORE (Hyperfine Sublevel Correlation Spectroscopy) 2D measurements. ^{139}La quadrupole coupling constant of La@C$_{82}$-I was directly determined.

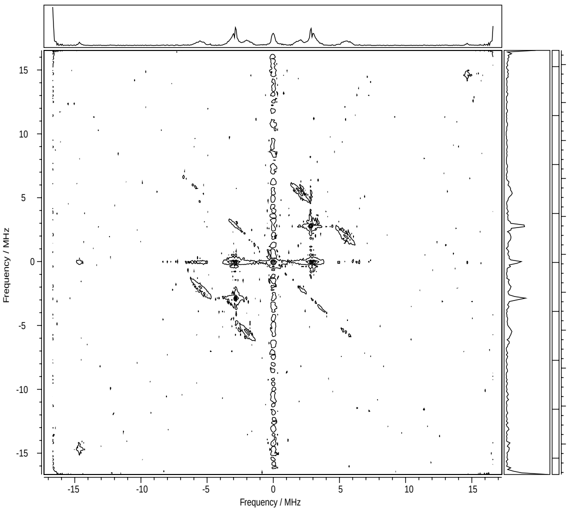

Figure 1. 2D-HYSCORE spectrum of the major isomer of ^{13}C–La@C$_{82}$ obtained at 80 K.

II-I-2 ESR Measurements of La@C$_n$

OKUBO, Shingo; KATO, Tatsuhisa

Full separation of topological isomers of each La@C$_n$ component (n = 76 to 90) was attempted by 2-stage HPLC separation with chlorobenzene eluent, and all species of La@C$_n$ with even number n from 76 to 90 were detected. Among them La@C$_{76}$, La@C$_{80}$-I, II, La@C$_{84}$-I, and II were newly purified, La@C$_{78}$, La@C$_{86}$, and La@C$_{88}$ were partially purified. Their ESR spectra were obtained, as shown in figure, and ESR parameters were determined. Enormous variety of ESR spectra of La@C$_n$s was obtained in terms of g factor, hyperfine coupling constant, and line width. The topological cage structure of La@C$_n$ reflected on the specific values of the ESR parameter. The anisotropic components of g factor, hyperfine coupling constant, and quadrupole coupling constant were estimated from the temperature dependence of the line width of each La@C$_n$.

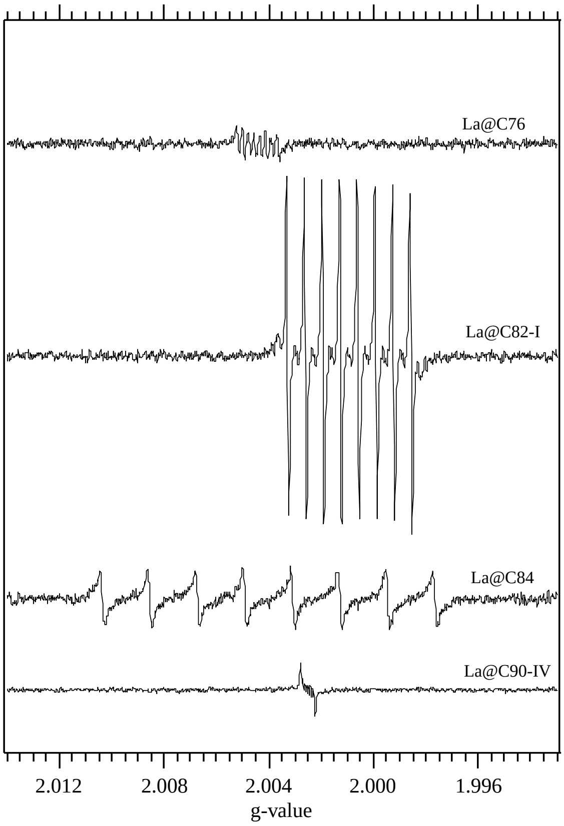

Figure 1. ESR spectra of La@C$_{76}$, La@C$_{82}$-I, La@C$_{84}$, and La@C$_{90}$-IV measured at room temperature in CS$_2$ solution.

II-J State Correlated Raman Spectroscopy

The vibrational Raman polarizability tensor responds to molecular reorientational relaxation process, and the structural environment in condensed media. The measurement of Raman scattering is a powerful technique for the study of molecular motion and of the mechanism of phase transition. We’ve built up the system of multichannel type detection of Raman scattering combined with the temperature controlled cell.

II-J-1 Investigations of Orientational Order for an Antiferroelectric Liquid Crystal by Polarized Raman Scattering Measurements

HAYASHI, Naoki; KATO, Tatsuhisa

The orientational ordering of the antiferroelectric liquid crystal molecules, MHPOBC was investigated in the series of the successive smectic phases by means of polarized Raman scattering measurement without any external field. An improved equation for the analysis of the polarized Raman intensity was derived as a function of an incident laser polarization and the orientational order parameters. Even in the chiral smectic phases, some apparent orientational order parameters could be defined by the proper corrections for the smectic layer structure and an optical disturbance. An unusual change of the orientational order parameters was observed with decrease in temperature. It was concluded that the irregular variation of the order parameter stemmed from the biaxiality of the molecular orientational distribution, which was attributed to the hindrance of molecular rotation around its long axis.

II-J-2 Polarized Raman Scattering Study for Frustoelectric Liquid Crystals

HAYASHI, Naoki; KATO, Tatsuhisa

Orientational ordering for two types of “V-shaped” switching liquid crystals was investigated by polarized Raman scattering measurements. One liquid crystal is based on the ferrielectric phase and the other on the antiferroelectric phase. The apparent orientational order parameters $\langle P_2(\cos\theta)\rangle_{app}$ and $\langle P_4(\cos\theta)\rangle_{app}$ obtained for the ferrielectric based liquid crystal,

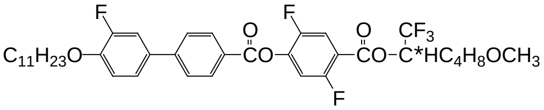

are shown in Figure 1. Square marks show the order parameters obtained with the static electric field of 7 V/μm, circle marks show those without static electric field, and triangle marks show those at the tip of the V-shaped switching. The electric field at the tip of the V-shaped switching is effectively zero, however, the observed order parameters exhibit the similar values of those obtained with the static electric field of 7 V/μm, which are much larger than without static electric field. On the other hand, smaller order parameters were preliminarily obtained at the tip of the V-shaped switching for the other type of antiferroelectric based liquid crystals. The careful comparison of the apparent order parameters for two types of liquid crystal should be necessary for the realistic interpretation of the “V-shaped” switching mechanism.

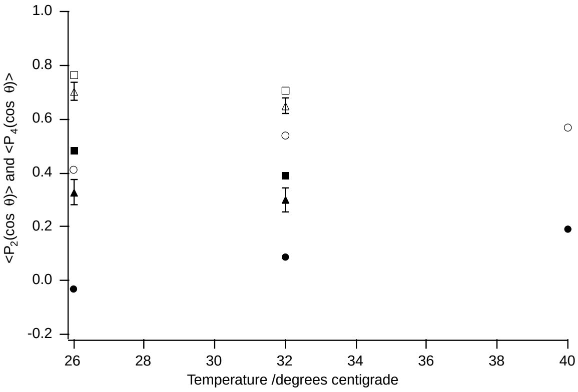

Figure 1. Temperature dependence of apparent orientational order parameters. Open marks show $\langle P_2(\cos\theta)\rangle$ and closed marks show $\langle P_4(\cos\theta)\rangle_{app}$. Square; with the static electric field of 7 V/μm, circle; without static electric field, triangle; at the tip of the V-shaped switching.

RESEARCH ACTIVITIES III
Department of Electronic Structure

III-A Photochemical Synthesis of Exotic Atomic-Molecular Binary Clusters in Solution: π Radical -Transition Metal Alternatively Stacking (π–*d*)$_n$ Clusters

We have started the bulk synthesis of atom-molecule alternatively stacking clusters in solution. Originally, unpaired electrons are located in every atoms and molecules to induce strong interaction among *d* electrons in atoms and π electrons in molecules. Strong coupling of π and *d* electrons is shown by ab initio molecular orbital calculations of $(C_5H_5)V(C_5H_5)V(C_5H_5)V(C_5H_5)$ making inter-atomic and intermolecular distances short. Structural isomers are expected to appear for the clusters expressed by $((C_5H_5)V)_n$ and $((C_5H_5)V)_n(C_5H_5)$. One is cyclic the other is linear. For the analysis of the solid samples soluble in some specific solvents, we have developed a new mass spectrometer with a liquid jet nozzle, a rotating titanium drum for spiral adsorption of the sample on the surface, and a reflectron time-of-flight mass spectrometer situated in a separated high vacuum chamber. Thus we can mass-analyze the synthesized product directly from the solutions.

III-A-1 π Radical-Transition Metal Alternatively Stacking (π–*d*)$_n$–π Clusters: (I) $V_6(C_5H_5)_7$, a Pentagonal Ring $((C_5H_5)V)$ with a Rolling Axis Vanadocene $(C_5H_5)V(C_5H_5)$?

HINO, Kazuyuki[1]; INOKUCHI, Yoshiya; NISHI, Nobuyuki
([1]Kyushu Univ.)

Photochemical treatment of the mixtures of vanadocence (bis(η–cyclopentadienyl) vanadium $((C_5H_5)V(C_5H_5))$ and tetracarbonyl (η–cyclopentadienyl) vanadium $((CO)_4V(C_5H_5))$ in dichloromethane produced the clusters with the compositions of $((C_5H_5)V)_n$ and $((C_5H_5)V)_n(C_5H_5)$ as well as $((C_5H_5)V)_n(C_5H_5)_2$. The product ratio varied with the changes of the ratio of the raw materials and the irradiation time. Addition of tricarbonyl (η–cyclopentadienyl) manganese enhanced the yields of these three kinds of clusters free from contamination of manganese in the clusters. Figure 1 shows the mass spectra of the photoproducts soluble in methanol. Starting from $((CO)_4V(C_5H_5))$, the photolysis produced vanadocene: (m/Z = 181) and $(C_5H_5)_2$: (m/Z = 130). This indicates that C_5H_5 is also dissociated by electronic excitation as well as the CO groups from the carbonyl compound. Addition of vanadocene as a raw material vanishes the signal of vanadocene but produces a new product at m/Z = 503. The main high mass product is found at m/Z = 761. This product is observed in any system with either the carbonyl compound or vanadocene. Therefore we assign this signal to $((C_5H_5)V)_6(C_5H_5)$. This compound must be much more stable than the linear polymer expressed by the same formula, since there is no reason for such a linear cluster to show specific high stability at n = 6. A possible structure for this cluster is shown at the upper right of Figure 1, that has a vanadocene molecule $((C_5H_5)V(C_5H_5))$ vertically inserted in a pentagonal ring $((C_5H_5)V)_5$. The pentagonal ring has 50 electrons (4 × 12 + 2) distributed in the valence orbitals composed of 3*d* and 3*s* atomic orbitals of vanadium and π orbitals of cyclopentadienyl. The ring may act as a wheel rotating around the axle vanadocene. DFT calculation of this compound is now going on to check the stability of this form. The clusters are stable in alcohol solutions or in vacuum but not so stable in air.

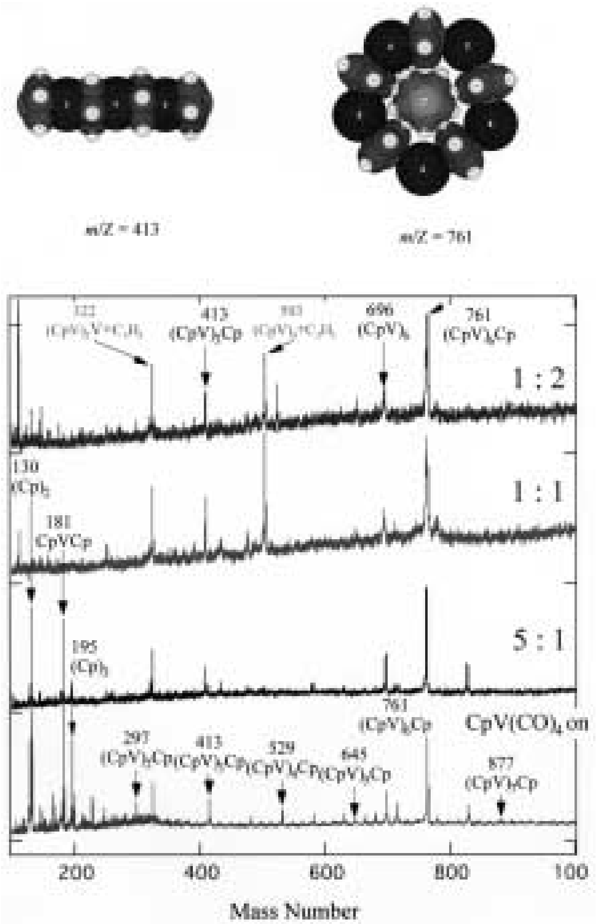

Figure 1. Mass spectra of the photoproducts from the solutions with various mixing ratio of $((CO)_4V(C_5H_5))$ to $(C_5H_5)V(C_5H_5)$.

III-A-2 Development of a New Mass Spectrometer Allowing the Injection of Solution Directly into Vacuum and the Desolvation through the Collision of Liquid Jet with Solvent Gas Flow Rebounded from a Rotating Titanium Drum for Solute Deposition

INOKUCHI, Yoshiya; HINO, Kazuyuki[1]; NISHI, Nobuyuki
([1]Kyushu Univ.)

Mass spectrometry is a very powerful method for determining mass numbers of unknown samples and getting information on molecular structures. We have developed a new mass spectrometer for non-volatile samples. Figure 1(a) shows a schematic diagram of the apparatus. It consists of a liquid beam source, a titanium drum, and a time-of-flight mass spectrometer. Non-volatile samples are dissolved in suitable solvents. Sample solutions are injected through a modified injector needle into the vacuum chamber as a liquid beam. The outer surface of the rotating titanium drum is located at 5 mm away from the exit of the needle. The liquid beam collides with gaseous shock front of the scattered solvent at the drum surface. The solvent is vaporized, and only the solute is fixed as a spiral deposit on the drum. The drum rotates at 1 rpm. The spiral solid deposit line is irradiated by the third harmonics of a Nd:YAG laser (355 nm) introduced through a hole between a sample chamber and a main chamber situated with an ion optics of the mass spectrometer. The produced ions detached from the surface are mass-analyzed by the time-of-flight mass spectrometer with a reflectron. Since the non-volatile samples are directly introduced into the spectrometer as solutions and fixed as a spiral line on the drum, we can measure the mass spectra of the non-volatile samples without exposing them to the air. Figure 1(b) represents mass spectra of polyethylene glycols used for mass calibration. Both spectra show ion signals with uniform interval of m/z = 44. This system is used for the product analysis of the synthesis of $(\pi\text{-}d)_n$ clusters.

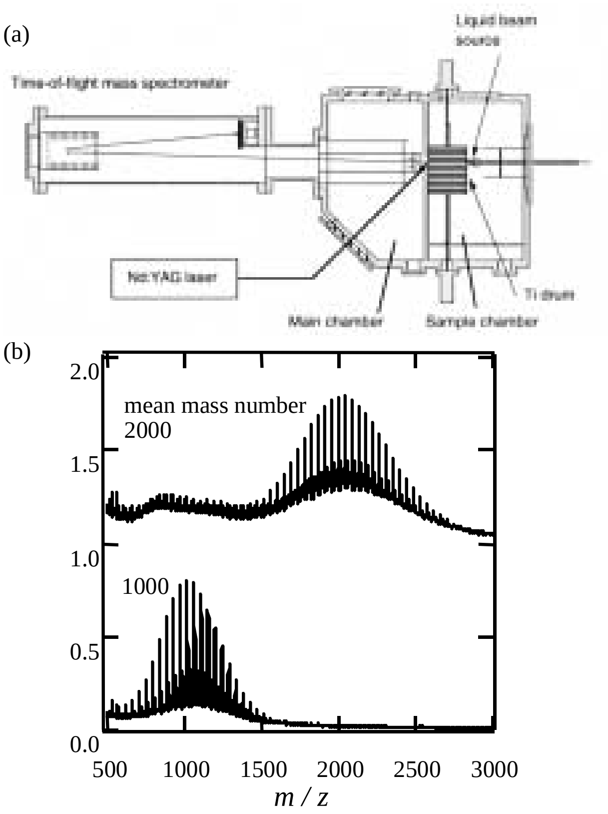

Figure 1. (a) a schematic diagram of the apparatus, (b) mass spectra of polyethylene glycol polymer samples with a mean mass number 2000 (top) and 1000(bottom).

III-B States of Neutral and Ionic Molecular Associates in Solutions

States of molecular associates particularly in aqueous solutions are of great importance in understanding the role of molecules in living organisms. Our recent studies of low frequency Raman spectroscopy of binary aqueous solutions of alcohols and carboxylic acids have shown that these amphiphilic molecules form “microphases” of clusters with the same solute species (*J. Phys Chem.* **102**, 4054 (1998), *J. Phys. Chem. A* **103**, 10851 (1999)). We have extended these studies from both experimental and theoretical point of view.

III-B-1 Monomeric and Cluster States of Acetic Acid Molecules in Solutions: A Raman Spectroscopic Study

NAKABAYASHI, Takakazu; NISHI, Nobuyuki

The purpose of this study is to understand on a microscopic scale about local structures of acetic acid in the liquid and solution states. Since acetic acid has both the hydrogen donor and acceptor sites in a molecule, various kinds of associations of acetic acid molecules can be expected depending on the situation. As shown in Figure 1, acetic acid forms a cyclic dimer in the gas phase, polymer chains in the crystalline state, and the chain clusters as the fragments of the crystalline networks in the liquid state.[1)] In aqueous solution, we have recently suggested that acetic acid preferentially forms microphase aggregates in which the side-on dimer structure is an elementary unit.[2)] In other words, two microphases exist in acetic acid-water binary solutions: one is water rich phase and the other is acetic acid one. What should be discussed next is whether the acetic acid microphases exist in other solvents or not. To examine this point, we have observed Raman spectra of acetic acid in alcohols and aprotic solvents with varying mole fraction of acetic acid (χ_{AA}). Raman spectra of acetic acid in the C=O stretching region are shown in Figure 2. With the addition of water into liquid acetic acid, the C=O band broadens and shifts to a higher wavenumber, which is ascribed to the generation of the side-on dimer microphases.[2)] In alcohols, the C=O band also shifts to a higher wavenumber and the resultant peak position is the same as that observed in water. This result suggests that the side-on dimer microphases also exist in alcohols. Low-frequency Raman spectra also support the above conclusion. In dipolar aprotic solvents such as acetonitrile, however, the spectral shift was apparently different from that in protic solvents: two prominent Raman bands appear on the higher-wavenumber side of the C=O bands observed in protic solvents. Analyses of the temperature and concentration dependencies of the Raman spectra suggest the generation of monomeric acetic acid in dipolar aprotic solvents with dilution. From these results, it is concluded that the acetic acid molecules exist as the microphases in protic solvents and as the monomeric molecules in dipolar aprotic solvents as depicted in Figure 1.

References

1) T. Nakabayashi, K. Kosugi and N. Nishi, *J. Phys. Chem. A* **103**, 8595 (1999).
2) N. Nishi, T. Nakabayashi and K. Kosugi, *J. Phys. Chem. A* **103**, 10851 (1999).

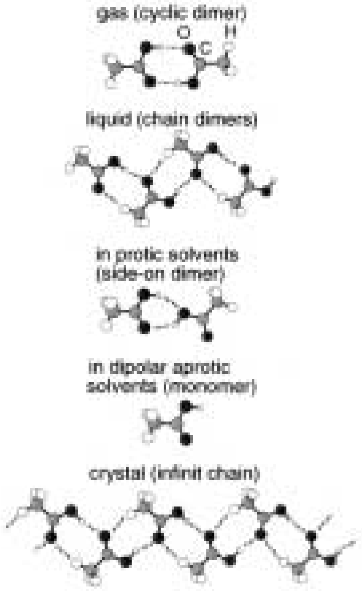

Figure 1. Structures of acetic acid clusters in various situations.

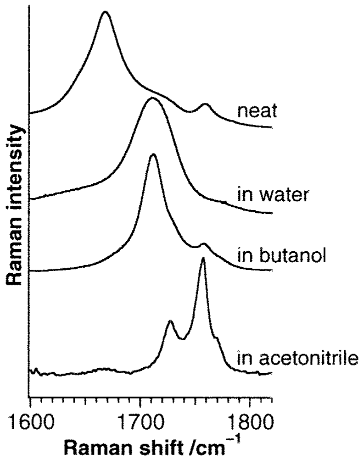

Figure 2. Raman spectra of acetic acid in the C=O stretching region (χ_{AA} = 0.015).

III-B-2 Comparison of the Theoretical Models for Calculating Acetic Acid Clusters in Aqueous Solution

NAKABAYASHI, Takakazu; SATO, Hirofumi; HIRATA, Fumio; NISHI, Nobuyuki

There has been tremendous progress in the theories for calculating molecular properties in solutions. In the present study, we have applied the SCRF and the RISM-SCF methods to clarify the electronic structures of acetic acid clusters in aqueous solution. In the SCRF method, the solute occupies a cavity surrounded by the dielectric continuous solvent. A solute dipole and/or multipole will induce a reaction field, which in turn will act to stabilize the solute. We applied the simplest SCRF model that makes use of a spherical cavity and considers only the solute dipole. The RISM-SCF method is an ab initio self-consistent field method combined with an extended version of the reference interaction site method. The advantage of the RISM-SCF method is to maintain the molecular aspects of solvents and thus to describe local interactions such as hydrogen bonds. Table 1 shows the calculated binding energies of acetic acid dimers (the linear dimer structure is depicted in Figure 1). In the gas phase, the cyclic dimer is the most stable among acetic acid dimers. Force calculations for the cyclic and side-on dimers confirm convergence to the minima on the energy surface, while the linear dimer is optimized to be a saddle point. In aqueous solution, owing to the stabilization in the side-on dimer, the energy difference between the cyclic and side-on dimers is calculated to be reduced by the RISM-SCF method; 3.0 kcal/mol in the solution compared with 8.1 kcal/mol in the gas phase. Decomposition of the solvation energy indicates that the hydration around the free carbonyl oxygen is of great importance for lowering the total energy of the side-on dimer. Marked stabilization is also obtained in the linear dimer. Not only solvation around the free carbonyl oxygen but also the increase in the O–H··O=C hydrogen bond contributes the stabilization in the linear dimer, although the free hydroxyl group has only a minor effect on the solvation energy. From the RISM-SCF results, the cyclic and linear dimer structures as well as the side-on dimer one are suggested in aqueous solution, although force calculations under the RISM-SCF model are needed to discuss whether the linear dimer is at the energy minimum in aqueous solution or not. In the case of the SCRF method, the binding energies in aqueous solution for the cyclic, side-on and linear dimers are calculated to be –12.86, –6.79, and –6.05 kcal/mol, respectively. This result indicates that, within the limits of the electrostatic interactions at the dipole level, the cyclic dimer is fairly stable even in aqueous solution. The SCRF model predicts that the energy difference between the side-on and linear dimers remains almost unchanged on going from the gas phase to aqueous solution, which is also different from the RISM-SCF result.

Figure 1. Chemical structure of the linear dimer.

	Gas	Solution	
		RISM	SCRF
Cyclic	–14.37	–1.32	–12.86
Side-on	–6.25	1.68	–6.79
Linear	–5.55	0.32	–6.05

Table 1. Binding Energies (in kcal/mol) of Acetic Acid Dimers in Gaseous phase and Aqueous Solution at the HF/DZP Level.

III-C Ultrafast Dynamics and Structural Changes of Excited Cation Radicals in Solution

Dynamic behavior and structural change of ion molecules generated in liquid solution, particularly in the presence of electron donor or acceptor species, are of great interest in relation to the formation of complexes as reaction intermediates. As an initiating stage, we have studied photogeneration of aromatic radical cations in polar solvents for understanding ion stabilization and destabilization processes in solution.

III-C-1 First Observation of the Formation Process of a Solvated Aromatic Cation Radical in Polar Solvents: A Two-Photon Pumped Femtosecond Time-Resolved Absorption Study

KAMO, Satoshi[1]; NAKABAYASHI, Takakazu; WATANABE, Kazuo; SAKURAGI, Hirochika[1]; NISHI, Nobuyuki
(*[1]Univ. Tsukuba and IMS)*

Multiple-photoionization of aromatic compounds has been studied extensively in view of its importance in photochemical and photobiological primary processes. Photoionization in condensed phase is considered to be characterized by the production of a solvent-separated electron-cation ion pair. In polar solvents, the resultant charges can be stabilized by the polarization of the solvent and then solvated free cation radicals are produced efficiently. However, direct observations of the formation of the solvated free ion are still lacking. In order to clarify the details of multiple-photoionization process, therefore, we first observed the ultrafast dynamics of the naphthalene cation radical by using two-color two-photon pumped femtosecond time-resolved absorption spectrometer. The neutral naphthalene molecules were excited to the S_1 state by the first pump photon at 267 nm. After 100 ps, the S_1 molecules were excited by the second pump photon at 400 nm through the $S_n \leftarrow S_1$ absorption, producing the naphthalene cation radical. The absorption changes induced by the two-color two-photon pump pulses were probed by a white light continuum with the time resolution of ≈300 fs. Figure 1A shows the transient absorption spectra of naphthalene in ethyl acetate in the delay time of 600 fs–24 ps from the second pump pulse. The transient absorption observed at 600 fs exhibits two broad peaks around 660 and 710 nm. This absorption signal decreases in several picoseconds and the new absorption with peaks around 660 and 690 nm appears at 15 and 24 ps. The spectral profile of the latter absorption changes from a broad one to a sharp one as seen in Figure 1B, indicating that the absorption appeared at 15 and 24 ps arises from the vibrationally hot solvated naphthalene cation radical. The absorption observed at 600 fs is ascribable to its precursor. Almost the same spectral changes are observed in acetonitrile in Figure 2A, although the absorption signal at 600 fs is ≈1.8 times larger in acetonitrile than in ethyl acetate. This suggests that the yield of the solvated cation radical is determined within 600 fs. As shown in Figures 1B and 2B, the peak intensity in acetonitrile rises with a time constant of tens of picoseconds, while that in ethyl acetate remains almost unchanged. This result appears to be consistent with the picosecond Raman study (in the next subsection) suggesting that the Raman intensity change in acetonitrile arises from the fluctuation of the solvation structure due to vibrational relaxation.

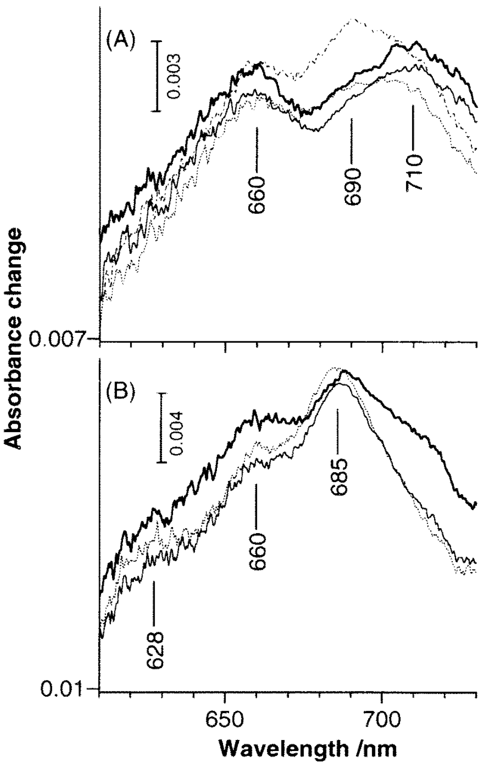

Figure 1. Transient absorption spectra of naphthalene in acetonitrile. (A) Thick-solid line, 600 fs; thin-solid line, 2 ps; dotted line, 15 ps; dash-dotted line, 24 ps. (B) Thick-solid line, 35 ps; thin-solid line, 65 ps; dotted line, 145 ps.

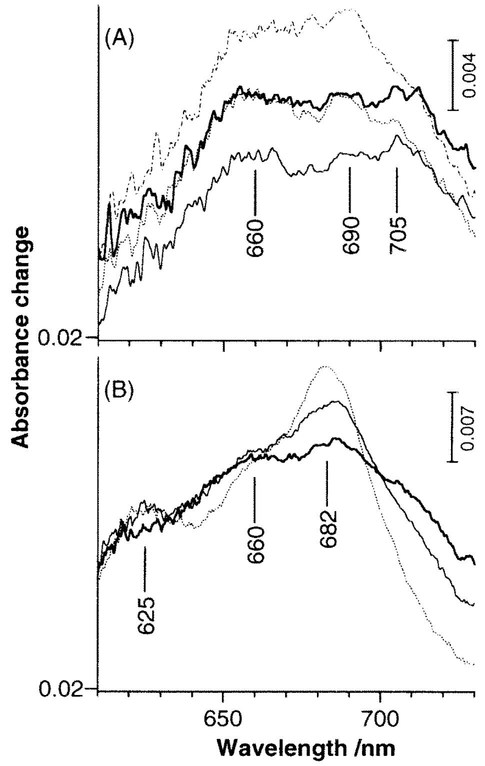

Figure 2. Transient absorption spectra of naphthalene in ethyl acetate. (A) Thick-solid line, 600 fs; thin-solid line, 2 ps; dotted line, 15 ps; dash-dotted line, 24 ps. (B) Thick-solid line, 35 ps; thin-solid line, 65 ps; dotted line, 145 ps.

III-C-2 Vibrational Relaxation Process of Solvated Aromatic Cation Radicals in Polar Solvents: A Two-Photon Pumped Picosecond Time-Resolved Raman Study

NAKABAYASHI, Takakazu; KAMO, Satoshi[1]; SAKURAGI, Hirochika[1]; NISHI, Nobuyuki
([1]Univ. Tsukuba and IMS)

Time-resolved Raman spectroscopy is already well recognized as a powerful technique for studying the structure and dynamics of short lived species in solution. To our knowledge, however, no one has reported picosecond Raman spectra of aromatic cation radicals, primarily because of the difficulty in obtaining two color picosecond pulses with sufficient pulse energies. Recently, we have constructed a two independently tunable Raman spectrometer with the time resolution of 3 ps. By using this system, we have first measured picosecond Raman spectra of aromatic cation radicals (biphenyl, trans-stilbene and naphthalene) in polar solvents. The results for biphenyl in ethyl acetate and acetonitrile are shown in Figure 1. Resonance Raman bands due to the S_1 state and cation radical of biphenyl are observed in this figure. The laser power dependencies confirm that the cation radical is produced through a two photon process. The frequencies of cation bands as well as their bandwidths change with the delay time in both the solvents. Immediately after biphotonic ionization, vibrationally excited cation radicals should be generated because of a large amount of excess vibrational energy. Thus the spectral changes can be ascribed to vibrational relaxation of the cation radical toward a thermal equilibrium with solvents. The time constant of the positional change of the 1610 cm^{-1} cation band is estimated to be 17 ps in acetonitrile and 13 ps in ethyl acetate. The obtained constants are roughly the same as those of other neutral aromatic molecules reported so far, although the interactions between the cation radical and surrounding solvents can be expected to be large. This result therefore supports the very rapid cooling model that the ultrafast energy transfer to the nearest solvent shell first occurs and then the energy flow into the bulk solvent follows in tens of picoseconds. As shown in Figures 1A and 2A, both the Raman intensities arising from the S_1 and cation species show an instrumental-limited rise (< 3 ps) in weak polar solvents such as ethyl acetate. On the other hand, in highly polar solvents such as acetonitrile, the Raman intensities arising from the cation radical rise in tens of picoseconds, and reach their maxima at ≈40 ps (Figures 1B and 2B). Since the picosecond intensity rise only occurs in highly polar solvents forming strong solvent-solute interactions and its time constant is roughly the same as that of vibrational relaxation, it is conceivable that the energy transfer to solvents disturbs the solvation structure, which causes the intensity change in the cation Raman bands.

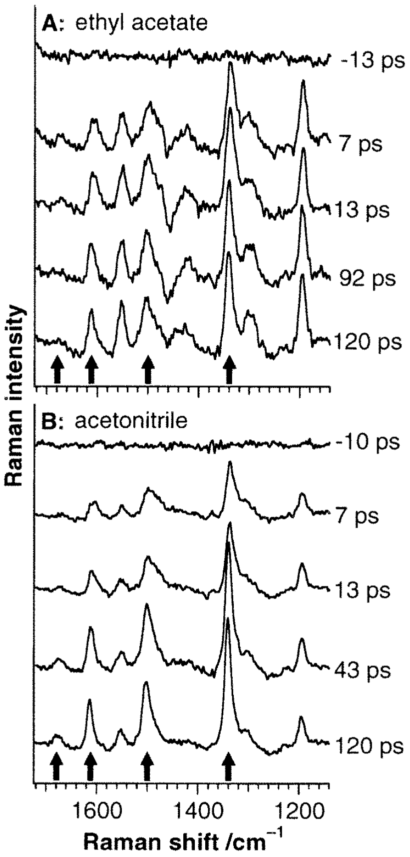

Figure 1. Picosecond time-resolved Raman spectra of biphenyl. Arrows indicates Raman bands due to the cation radical of biphenyl. Pump: 262 nm, probe: 633 nm. The Raman bands of the solvents are subtracted.

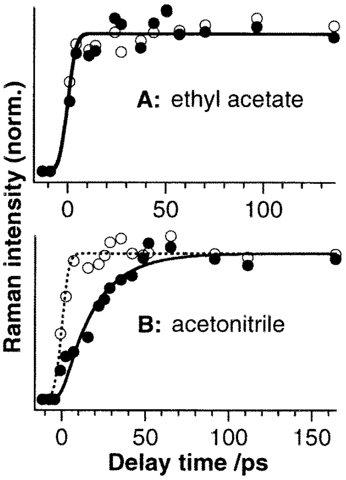

Figure 2. Plot of the transient Raman intensities against the delay time. Blank circles, S_1 (1195 cm^{-1}); filled circles, cation (1340 cm^{-1}).

III-D Spectroscopic and Dynamical Studies on Charge Delocalization and Charge Transfer in Aromatic Molecular Cluster Ions

Electron deficiency of aromatic molecular cations can attract electron rich groups or atoms exhibiting charge resonance(CR) interaction between similar molecules or charge transfer (CT) interaction with electron donor molecules. Here we show intersting cases of benzene cation complexes and clusters.

III-D-1 Photodissociation Spectroscopy of Benzene Cluster Ions in Ultraviolet and Infrared Regions. Static and Dynamic Behavior of Positive Charge in Cluster Ions

INOKUCHI, Yoshiya; NISHI, Nobuyuki

[*J. Chem. Phys.* submitted]

Photodissociation spectroscopy is applied to benzene cluster ions in ultraviolet and infrared regions. In the ultraviolet photodissociation spectrum of $(C_6H_6)_3^+$, a characteristic broad band emerges at 255 nm. This band is assigned to a $\pi^* \leftarrow \pi$ transition of a solvent benzene molecule that exists in the trimer. On the basis of the ultraviolet and the previous near-infrared spectra, we confirm a dimer ion core structure of $(C_6H_6)_3^+$; there are a dimer ion core and the solvent benzene molecule in $(C_6H_6)_3^+$. Figure 1 shows infrared photodissociation spectra of $(C_6H_6)_n^+$ (n = 3–5) (open circles). The spectra clearly show a sharp band at 3066 cm^{-1}. The band is attributed to a C–H stretching vibration of the dimer ion core. The infrared spectra can be reproduced by combining the C–H stretching bands of the dimer ion core and the solvent benzene molecules. The infrared photodissociation spectra of mixed benzene trimer ions with one or two benzene-d_6 molecules demonstrate that there is no correlation between the excited dimer ion core site in the trimer and the photofragment dimer ion species. This implies that a dimer ion core switching, in other words, a charge hopping occurs in photoexcited vibrational states prior to the dissociation. The charge hopping in cluster ions is thought to be a simple example of the charge transportation in condensed phases.

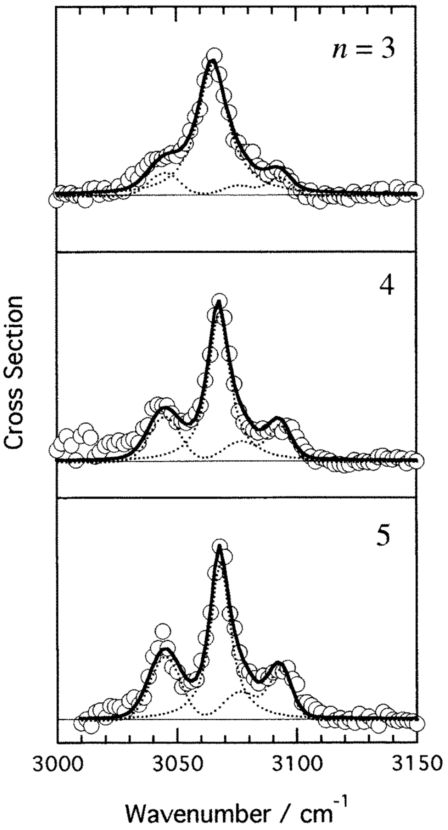

Figure 1. Infrared photodissociation spectra of $(C_6H_6)_n^+$ (n = 3–5).

III-D-2 Charge Transfer Complex of Benzene Cation Vertically Coordinated with Acetic Acid

KOSUGI, Kentaroh; INOKUCHI, Yoshiya; NISHI, Nobuyuki

[*J. Chem. Phys.* in press]

The non-bonding orbital on the oxygen atom of carboxyl group can take a role of strong electron donor for a cationic molecule. Benzene cation is a good electron acceptor molecule as a counter-part of the acetic acid. We have measured vibrational and electronic spectra of acetic acid-benzene cation complexes through ion-trap photodissociation spectroscopy. Ab initio molecular orbital calculation at CASSCF(7,7)/6-31G** level for the analysis of the electronic spectrum and at B3LYP/6-31G** level for the vibrational spectrum demonstrated that there are two or three isomers: charge transfer complex with an acetic acid sitting on a carbon atom of the benzene cation vertically to the ring (vertical isomer V), and in-plane complexes with a cis- or trans- acetic acid hydrogen-bonded to one or two hydrogen atom(s) of the benzene C-H groups (horizontal isomers H). The charge transfer complex shows very broad bands due to charge transfer electronic transitions in near infrared and visible region as seen in Figure 1, where one can see the optimized structure of the vertical complex and the intermolecular bonding and anti-bonding molecular orbitals involved in the electronic transitions. One can see the negative charge in the acetic acid is transferred to the benzene on the electronic transition indicated by V_2.

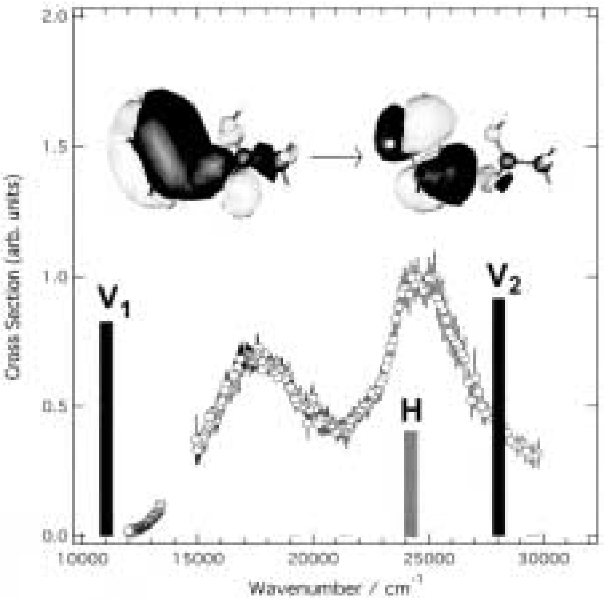

Figure 1. Observed photodissociation spectrum of $(CH_3\text{-}COOH)(C_6H_6)^+$ and the transition energies and oscillator strengths calculated by the MCQDPT method.

III-D-3 Vibrational and Electronic Spectra of (Benzene-Benzyl Alcohol)$^+$; Predominance of Charge Resonance Interaction over Hydrogen-Bonding Interaction

OHASHI, Kazuhiko[1]; IZUTSU, Hironobu[1]; INOKUCHI, Yoshiya; HINO, Kazuyuki[1]; NISHI, Nobuyuki; SEKIYA, Hiroshi[1]
([1]Kyushu Univ.)

[*Chem. Phys. Lett.* **321**, 406 (2000)]

Vibrational and electronic spectra of the benzene-benzyl alcohol hetero-dimer ion are measured by photodissociation spectroscopy. The vibrational spectrum shows a prominent band at 3662 ± 3 cm^{-1}, which is assigned to the stretching vibration of the OH group free from intermolecular perturbations. The electronic spectrum shows a broad band around 950 nm, which arises from a charge resonance interaction between the aromatic rings. These results suggest that the ion has a sandwich-like structure suitable for the resonance interaction, without the hydrogen bond between the OH group of benzyl alcohol and the -electrons of benzene.

III-D-4 Electronic and Vibrational Spectra of Aniline-Benzene Hetero-Dimer and Aniline Homo-Dimer Ions

OHASHI, Kazuhiko[1]; INOKUCHI, Yoshiya; IZUTSU, Hironobu[1]; HINO, Kazuyuki[1]; YAMAMOTO, Norifumi[1]; NISHI, Nobuyuki; SEKIYA, Hiroshi[1]
([1]Kyushu Univ.)

[*Chem. Phys. Lett.* **323**, 43 (2000)]

Structures of (aniline-benzene)$^+$ and (aniline)$_2^+$ are re-investigated by electronic spectroscopy in the near-infrared region and vibrational spectroscopy in the NH stretching region. The spectra of (aniline-benzene)$^+$ indicate a structure including a hydrogen bond between an NH bond of the ionic aniline and the -electrons of the neutral benzene. Two isomers are suggested for (aniline)$_2^+$ in which an NH bond of the ionic aniline forms different types of hydrogen bond with the neutral aniline: one with the -electrons of the aromatic ring and the other with the lone pair of the nitrogen atom.

III-E Structures and Reactivities of Metal Clusters

Clusters of metal atoms constitute a new class of material whose properties deviate significantly from those of isolated atoms and condensed matters. Our research group, started in January 2000, has been developing an experimental setup to study the size and shape dependent catalytic behavior of the metal clusters. The motivation of our research is to understand detailed mechanism of the chemical reactions involving the metal clusters based on the correlation with geometric/electronic structures.

III-E-1 Construction of Apparatus for Mass Analysis of Metal Clusters

NEGISHI, Yuichi; TSUKUDA, Tatsuya

We have designed a plan to exploit a synthetic method of the metal clusters having a well-defined size before studying the chemical reactivities. The metal cluster ions are prepared by reduction of the relevant metal ions in the presence of ionic surfactant molecules which prevent coalescence of the clusters. We have constructed a new apparatus that allows us to monitor mass distributions of the nascent clusters in liquid phase. Figure 1 shows a schematic diagram of the apparatus with 7 stages of differentially pumped vacuum chambers. The apparatus consists of an electrospray ion source and a reflectron time-of-flight (TOF) mass spectrometer. Liquid sample containing the cluster ions is pumped through a fused silica capillary, whose end is supported in a stainless steel needle. Charged aerosol droplets are electrosprayed by means of an electrical potential between the needle tip and a counterelectrode (+3–5 kV). The cluster ions in the droplets are evaporated into the gas phase and further desolvated by collision with an inert gas such as nitrogen. A portion of the ion flow is skimmed and introduced into the acceleration region of the TOF mass spectrometer. In order to increase the detection efficiency for the ions having a mass-to-charge ratio above ~10^4, the ions are accelerated by applying a pulsed output of 30 kV from a homemade pulse generator (rise time ~30 ns, on time ~200 µs). The ions are guided by several sets of ion optics and detected by microchannel plate located at the end of the flight path of 3.1 m. Surface induced dissociation, a powerful diagnostics for structural characterization of large and complex systems, can also be performed with this machine. Cluster ions of interest are mass-selected by pulsed beam deflectors and allowed to collide with a solid surface mounted at the end of the reflectron. Collision energy can be varied by changing the voltage applied to the surface. Secondary ions scattered off the surface are detected by secondary TOF mass spectrometer.

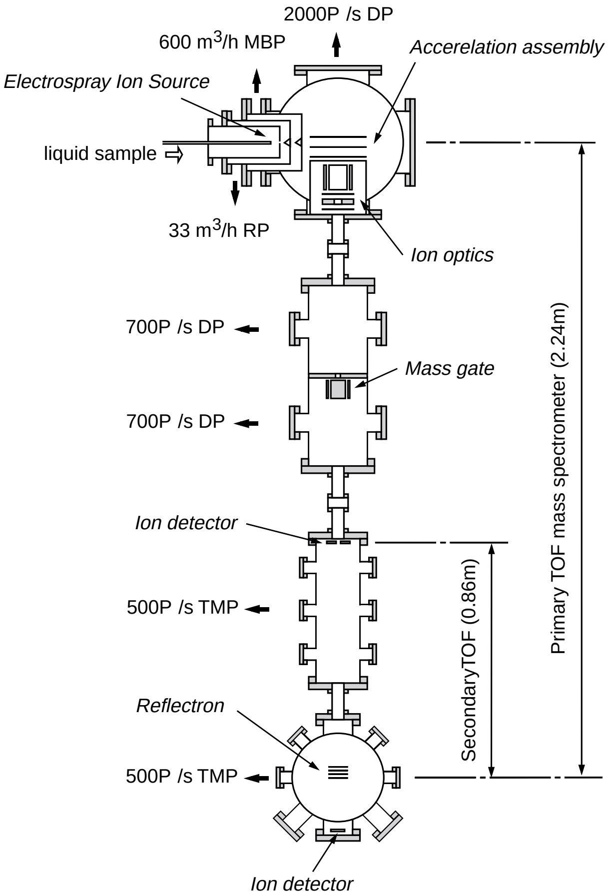

Figure 1. Schematic of experimental apparatus shown in cross section as viewed from above. RP: rotary pump; MBP: mechanical booster pump; DP: oil diffusion pump; TMP: turbo molecular pump.

III-F Spectroscopy and Dynamics of Vibrationally Excited Molecules and Clusters

This research group is studying structure and dynamics of molecules and clusters of in higher vibrational state by two-color double resonance spectroscopy. New spectroscopic methods will also be developed to observe the higher vibrational state under collision-free condition.

III-F-1 IR dip Spectra of Photochemical Reaction Products in a Phenol/Ammonia Cluster—Examination of Intracluster Hydrogen Transfer

ISHIUCHI, Shun-ichi[1]; SAEKI, Morihisa; SAKAI, Makoto; FUJII, Masaaki
([1]GUAS)

[*Chem. Phys. Lett.* **322**, 27 (2000)]

The vibrational transitions of the photochemical reaction products in phenol–$(NH_3)_3$ have been measured by IR dip spectroscopy. Two sharp bands at ~3200 cm^{-1} and a broad band in the region 2700~3100 cm^{-1} are observed. The spectrum is clearly different from that of the cluster in S_0, and also largely different from the IR spectrum of $NH_4^+(NH_3)_2$. This suggests that hydrogen transfer occurs in electronically excited phenol–$(NH_3)_3$. Evidence of hydrogen transfer has also been found in phenol–$(NH_3)_4$ based on the mass spectrum and the IR dip spectrum of the cluster.

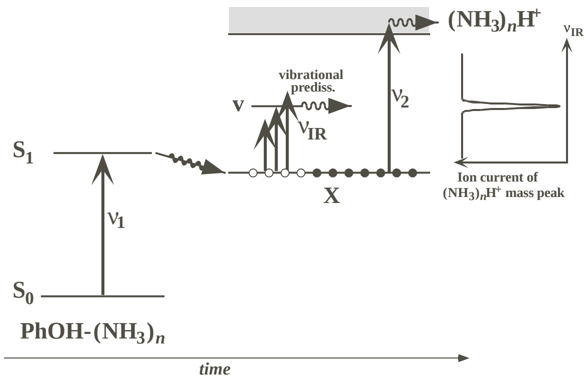

Figure 1. Schematic diagram showing the principle of IR dip spectroscopy which was employed in this work.

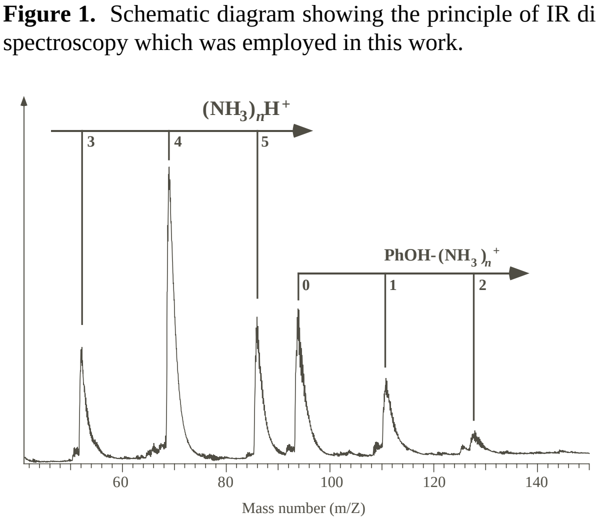

Figure 2. (a) IR dip spectrum of the reaction product which was observed by fixing ν_1 to the lower vibronic band in the S_1 state of PhOH–$(NH_3)_3$ (35498 cm^{-1}) and monitoring $(NH_3)_3H^+$. The third harmonics of the YAG laser was used as the ionization laser ν_2. Here, $(NH_3)_3H$ in the grand state can be ionized by one-photon of 355 nm light (IP = 3.31 eV). The IR laser ν_{IR} was irradiated after 180 ns from the excitation to S_1 due to ν_1. The solid curves and the dotted curves show the spectra obtained by adjusting the laser power of ν_{IR} to 0.2 mJ and 0.4 mJ, respectively. (b) IR dip spectrum of PhOH–$(NH_3)_3$ in S_0. The IR laser ν_{IR} was irradiated before 20 ns from the excitation to S_1 due to ν_1. All other conditions were the same as those for the IR dip spectrum of the reaction product (Figure 2a).

III-F-2 Structural Characterization of the Acridine–$(H_2O)_n$ (n = 1–3) Clusters by Fluorescence Dip Infrared Spectroscopy

MITSUI, Masaaki[1]; OHSHIMA, Yasuhiro[1]; ISHIUCHI, Shun-ichi[2]; SAKAI, Makoto; FUJII, Masaaki
([1]Kyoto Univ.; [2]GUAS)

[*Chem. Phys. Lett.* **317**, 211 (2000)]

Vibrational spectra of supersonically cooled acridine–$(H_2O)_n$ (n = 1–3) clusters in the electronic ground state have been measured by fluorescence dip infrared spectroscopy. The observed O–H stretching fundamentals of the solvents have been analyzed with the aid of density functional calculations, to assign structures of the clusters. In the n = 1 cluster, the water molecule acts as a proton donor which is hydrogen-bonded to the N atom of acridine. The second (third) water in the higher clusters is further hydrogen-bonded to the first (second) one to form a linear "water chain," which surrounds an edge of the acridine molecule approximately in the plane of the aromatic ring.

III-F-3 Internal Methyl Group Rotation in o-Cresol Studied by Pulsed Field Ionization-ZEKE Photoelectron Spectroscopy

SUZUKI, Kazunari[1]; EMURA, Yuji[2]; ISHIUCHI, Shun-ichi[3]; FUJII, Masaaki
([1]YAMAHA; [2]Mitsui Chemical; [3]GUAS)

[*J. Electron. Spectrosc.* in press]

Pulsed field ionization-ZEKE photoelectron spectroscopy and (1+1) R2PI spectroscopy have been applied to cis- and trans-o-cresol. The internal rotational structure in S_1 has been re-assigned for the cis-isomer, and the potential curve for the internal rotation has been determined. In the PFI-ZEKE spectra recorded via different internal rotational levels in the S_1 state, well-resolved low-frequency bands have been observed. The low-frequency bands are assigned to internal rotational motion of the methyl group in the cation. Level energies and relative transition intensities are reproduced well by a one-dimensional rotor model with a three-fold axis potential. Potential curves for the internal rotation have been determined for both cis- and trans-o-cresol cations. The barrier height for the internal rotation is different for the two isomers in the cation, while it becomes similar in S_1. Contributions of steric and electronic factors to the rotational barrier are discussed.

III-F-4 Pulsed Field Ionization-ZEKE Spectroscopy of Cresoles and Their Aqueous Complex: Internal Rotation of Methyl Group and Intermolecular Vibrations

SUZUKI, Kazunari[1]; ISHIUCHI, Shun-ichi[2]; FUJII, Masaaki
([1]YAMAHA; [2]GUAS)

[*Faraday Discuss.* in press]

Pulsed field ionization-ZEKE photoelectron spectroscopy and (1+1) R2PI spectroscopy have been applied to cis- and trans-m-cresol·H_2O clusters. The internal rotational structure in S_1 has been re-assigned, and the potential curve has been determined for the cluster. The PFI-ZEKE spectra of cis- and trans-isomer show low-frequency bands up to 1000 cm^{-1} above the adiabatic ionization potential IP_0. The low-frequency bands are assigned to the internal rotation of the methyl group, the intermolecular stretching and their combination bands in the m-cresol·H_2O cluster cation. Level energies and relative transition intensities are reproduced well by a one-dimensional rotor model with a three-fold axis potential. Potential curves for the internal rotation have been determined for both cis- and trans-isomers of m-cresol·H_2O cations. The effect of the cluster formation upon the internal methyl rotation, and interaction between the methyl rotation and the intermolecular vibration are discussed.

III-F-5 Butterfly Vibration of the Tetrafluorobenzene Cation Studied by Pulsed Field Ionization-ZEKE Photoelectron Spectroscopy

TAKAZAWA, Ken[1]; FUJII, Masaaki
([1]Natl. Res. Inst. Met)

[*J. Electron. Spectrosc.* in press]

The pulsed field ionization-ZEKE photoelectron spectroscopy has been applied to 1,2,4,5-tetrafluorobenzene in a supersonic jet. The spectrum measured by selecting a specific vibronic level of butterfly vibrational mode in S_1 by the first laser shows well-resolved vibrational structure of the cation. A long progression has been assigned to the out-of-plane butterfly vibrational mode 11 with even quantum number in the cation. From the harmonisity and Franck-Condon factor, it has been concluded that the molecular structure of the tetrafluorobenzene cation is flat though that in S_1 is non-planer along the butterfly vibrational mode. The geometrical change upon ionization has been discussed in terms of the electronic structure.

III-G Time-Resolved Photoelectron Imaging on Ultrafast Chemical Dynamics

We have developed a novel experimental technique of time-resolved photoelectron imaging to probe excited state dynamics of isolated molecules and clusters in real time [*J. Chem. Phys.* **111**, 4859 (1999)]. A pump pulse prepares a non-stationary state in the excited electronic state, then a probe pulse projects the wavefunction to the cationic states. With a 1 kHz laser system, one electron image can be recorded for less than a minute, which allows us to map out excited state dynamics quite rapidly.

III-G-1 Femtosecond Time-Resolved Photoelectron Imaging on Ultrafast Dephasing in Pyrazine

TSUBOUCHI, Masaaki[1]**; WHITAKER, Benjamin**[2]**; SUZUKI, Toshinori**
([1]GUAS; [2]Univ. Leeds)

Femtosecond time-resolved photoelectron imaging was applied to ultrafast electronic dephasing in Pyrazine that is the best-known example of an intermediate coupling case in radiationless transition. A tunable pump pulse in 300 nm range prepared Pyrazine molecule in a variety of vibronic levels in $S_1(\pi,\pi^*)$, and the subsequent time-evolution has been probed by either one photon ionization at 197 nm or two-photon ionization at 395 nm. The decay of the optically-prepared S_1 character and the corresponding formation of the T_1 character were clearly observed in both probing schemes. The photoelectron kinetic energy distribution in (1+1') ionization exhibited clear vibrational structure that is essentially determined by Franck-Condon factors between the S_1 and cationic state. For any of the S_1 vibronic levels up to the excess energy of 2000 cm^{-1}, no signature of IVR has been observed in the photoelectron images. On the other hand, (1+2') ionization provided a few sharp lines in the kinetic energy distribution due to the accidental resonance with the 3s and 3p Rydberg states at (1+1') energy. The photoelectron angular distribution in (1+2') ionization exhibited high anisotropy, which proves that the atomic-like electron orbital is involved in the resonant state.

III-H Crossed Beam Studies on Bimolecular Reaction Dynamics

Chemical reactions under thermal conditions occur with various collision energies, internal quantum states, and impact parameters. The experimental data measured under such conditions are highly-averaged quantities, from which detailed feature of reactions can hardly be learned. A crossed molecular beam method allows us to observe chemical reactions of state-selected reagents at well-defined collision energy. Although, this method does not control the impact parameter in reaction, the differential cross section (angular distribution of products) reveals impact-parameter dependence of reaction probability and reaction mechanism. Conventional crossed beam experiments have employed so-called a universal detector (electron bombardment + quadrupole mass analysis + time-of-flight measurements). However, this method provides poor (or no) internal state resolution of products. The internal motions (electronic, vibrational and rotational) of molecules play essential roles in chemical reactions, therefore the measurements of only the scattering distributions are generally insufficient for elucidation of reaction mechanism. We constructed a new crossed beam apparatus with a high-resolution ion imaging detector. The products are state-selectively ionized by resonantly enhanced multiphoton ionization (REMPI) and their scattering distributions are directly visualized by an imaging method. The state-selective detection diminishes the signal intensity, but this is compensated by simultaneous observation of all the scattering angle. A preliminary experiment on the inelastic scattering of NO with Ar achieved the data acquisition more than two orders of magnitude faster than previous methods. A photolytic $O(^1D)$ atomic beam source has also been constructed to study stratospheric chemistry at the state-to-state differential cross section level.

III-H-1 State-Resolved Differential Cross Section Measurements for the Inelastic Scattering of NO + Ar

KOHGUCHI, Hiroshi; SUZUKI, Toshinori

The state-resolved differential cross sections (SR-DCS) of the inelastic scattering NO (j" = 0.5, Ω" = 1/2) + Ar → NO (j', Ω' = 1/2, 3/2) + Ar at 63 meV were measured by a crossed molecular beam ion-imaging method. The dynamics of this system occurs on the two potential energy surfaces that arise from the approach of Ar to NO in the $^2\Pi$ state, and the average and difference potentials of these two determine the spin-orbit changing ($\Delta\Omega = 1$) and conserving transitions ($\Delta\Omega = 0$). Many workers have studied NO + Ar both theoretically and experimentally as a representative system of inelastic scattering of open-shell molecules. In our experiment, twenty final (j', Ω') states in total were observed for both spin-orbit conversing (Ω" = 1/2 → Ω' = 1/2) and changing (Ω" = 1/2 → Ω' = 3/2) processes. The DCSs exhibited complex structures that are sensitive to the final (j', Ω') states; sharp forward scattering for low j' states, broad angular distributions for intermediate *j'* states, and backward scattering for high *j'* states. The results were in excellent agreement with close-coupling calculations on the CCSD(T) surfaces performed by Millard Alexander at Maryland University.

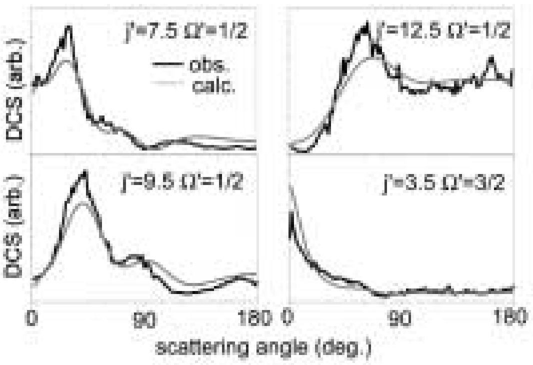

Figure 1. The observed and calculated state-resolved differential cross section of the inelastic scattering of NO + Ar. The final states of scattered NO are denoted as (*j'*, Ω').

III-I Non-Adiabatic Molecular Photodissociation Dynamics Studied by Polarization Spectroscopy

Vector quantities of products provide detailed insights into the stereochemical dynamics of atomic/molecular collisions and molecular photodissociation. As expected from building-up principle of diatomic molecule, the ***orbital alignment*** and ***orientation*** in an atomic fragment carries information on the electronic symmetry of the PES. Furthermore, coherent excitation leading to two different dissociation paths creates characteristic vector correlation.

III-I-1 Atomic Orbital Orientation in Photodissociation of OCS

KATAYANAGI, Hideki; SUZUKI, Toshinori

The orbital orientation of $S(^1D_2)$ was detected in photodissociation of OCS by an ion imaging technique with circularly-polarized probe light. One of the causes for orientation is quantum mechanical interference between the two different dissociation pathways reached by parallel and perpendicular transitions. The magnitude of the orientation is proportional to the asymptotic phase difference between the pathways, making the orientation to be a sensitive probe of the potential energy surfaces. The $S(^1D_2)$ products consist of two components arising from a mixed transition to $2^1A'$, $1^1A''$ and from a pure parallel transition to $2^1A'$. The former appears with high translational energy of 12.7 kcal/mol and the latter 3.8 kcal/mol. As shown in Figure 1, the signal of high energy component showed strong orientation.

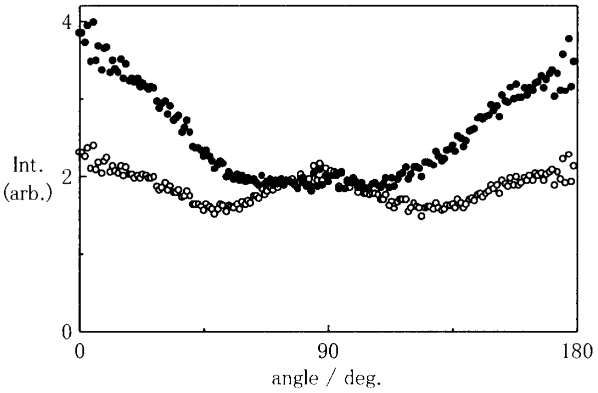

Figure 1. Angular distributions of high and low energy S^+ ions created by linearly polarized 235 nm pump light, and the right (●) left (○) circularly polarized probe light. Definition of θ is illustrated in the figure. ε_{dis} and s_{pr} are polarization vectors of the pump light and a helicity vector of the probe, respectively.

III-J Photochemistry on Well-Defined Surfaces

Upon the irradiation of light in the wavelength range from visible to ultraviolet, a number of adsorbed molecules on metal surfaces reveal variety of photochemical processes, including photo-stimulated desorption, rearrangement of adsorbed states, photodissociation, and photo-initiated reactions with coadsorbates. A central and fundamental question in the surface photochemistry is to clarify how adsorbate-substrate systems are excited by photon irradiation. In addition, since photo-initiated reactions can be induced without any thermal activation of reactants, they may provide good opportunities for studying a new class of surface reactions which may not be induced thermally. We have studied photochemistry of various adsorption systems on well-defined metal and semiconductor surfaces mainly by temperature-programmed desorption (TPD), x-ray photoelectron spectroscopy (XPS), work function measurements, and angular-resolved time-of-flight (TOF) spectroscopy of photodesorbed species associated with pulsed laser irradiation. We have shown that methane weakly adsorbed on Pt(111), Pd(111) and Cu(111) is dissociated or desorbed by irradiation of 6.4-eV photons, which is far below the excitation energy for the first optically allowed transition of methane in the gas phase. We have found that rare gas atoms are also photodesorbed from clean and modified Si(100) surfaces. These are all physisorbed systems where electronic states of adsorbate and substrate are well separated in the ground state. In contrast, we have extended the project to photochemistry of strongly chemisorbed, or compound systems on metal surfaces: AgO chains on an Ag(110) surface.

III-J-1 Excitation Mechanisms and Photochemistry of Adsorbates with Spherical Symmetry

WATANABE, Kazuo; MATSUMOTO, Yoshiyasu

[*Faraday Discuss.* **117**, 207 (2000)]

By comparing the photo-stimulated desorption of Xe from an oxidized Si(100) surface with the photochemistry of methane on metal surfaces, we try to deduce a common concept in the excited state and the excitation mechanism responsible for the photo-induced processes. Xe atoms are desorbed from the oxidized Si(100) surface by the irradiation of photons in the range of 1.16–6.43 eV. The two velocity components with average kinetic energy of 0.85 eV and 0.25 eV are observed in the time-of-fight distributions. The fast component appears only if the photon energy exceeds ~3 eV, but the slow component does in the entire photon energy range. By analogy with the photochemistry of methane on the metal surfaces, the excitation mechanism responsible for the fast component is postulated to be a transition from the 5p state of Xe to the excited state originating in strong hybridization between the 6s-state of Xe and the dangling bond at a surface silicon atom bonded with oxygen inserted in the dimer bond. In this scheme an excited electron is transferred from the adsorbate to the substrate, which is the reverse direction compared with the substrate-mediated excitation frequently assumed in surface photochemistry.

III-J-2 Photo-induced Oxygen Elimination Reaction at an Ag(110)-p(2×1)-O Surface

OTA, Michiharu[1]; WATANABE, Kazuya; MATSUMOTO, Yoshiyasu
([1]GUAS)

When an Ag(110) surface is extensively exposed to oxygen gas, well-ordered AgO chains are formed on the surface. It has been reported that oxygen atoms in the chains are eliminated by UV photon irradiation. However, the excitation mechanism for the photoreaction is completely unknown. Furthermore, there is no information on how oxygen is eliminated and where it goes. We try to uncover these questions by using LEED, XPS, TOF and TPD measurements. After confirming a characteristic LEED pattern of the Ag(110)- p(2×1)-O surface, the surface is irradiated by UV light. The depletion of the oxygen coverage is measured by post-irradiation XPS as a function of the irradiated photon numbers. The most important finding in the photoreaction is that the cross-sections for the photochemical oxygen elimination reaction strongly depend on the coverage of carbon atoms remained at the surface; the cross-section increases with the coverage of carbon atoms. Interestingly, carefully designed experiments show that carbon atoms believed to be at subsurface are more effective than carbon adatoms on the surface. Photodesorbed species are detected by a quadruple mass spectrometer. No oxygen atoms/molecules are detected, but only CO_2 molecules are detected. Therefore, subsurface carbon plays an important role in the reaction. We tentatively assign the subsurface carbon is carbidic and the carbon adatoms is graphitic. Further characterization of the carbon atoms are underway.

Reference

1) Y. Matsumoto, Y. Okawa, K. Suzuki, K. Mukai and K. Tanaka, *J. Am. Chem. Soc.* **118**, 9676 (1996).

III-K Structure and Properties of Polyoxometalates with a Magnetic, Electronic, or Biological Significance

Polyoxometalates constitute model systems for the study of the electron and energy transfer in the infinite metal-oxide lattice and their simplicity allows to treat at the molecular scale the coupling of electronic and nuclear movements, which is an inherent problem for the mixed-valence systems. As is clear from such a variety of both structure and reactivity of polyoxometalates, our current works on polyoxometalates are 1) structure/reactivity relationships with particular regard to the mechanism of electron transfer reactions, 2) magnetic interaction and molecular magnetic device, 3) energy-transfer mechanism and luminescence device (including nonlinear optical device), 4) encapsulation of templates in the photo-induced self-assembly process, 5) template-exchange reaction and topology, and 6) antibacterial effects on MRSA and VRE.

III-K-1 Luminescence and Energy Transfer Phenomena in Tb^{3+}/Eu^{3+}-Mixed Polyoxometallolanthanoates $K_{15}H_3[Tb_{1.4}Eu_{1.6}(H_2O)_3(SbW_9O_{33})(W_5O_{18})_3]\cdot 25.5H_2O$ and $Na_7H_{19}[Tb_{4.3}Eu_{1.7}O_2(OH)_6(H_2O)_6Al_2(Nb_6O_{19})_5]\cdot 47H_2O$

YAMASE, Toshihiro; NARUKE, Haruo
(IMS and Tokyo Inst. Tech.)

[*J. Phys. Chem. B* **103**, 8850 (1999)]

The energy dissipation of Tb^{3+}/Eu^{3+} cations in both heterolanthanide-multinuclear polyoxometalates, $K_{15}H_3[Tb_{1.4}Eu_{1.6}(H_2O)_3(SbW_9O_{33})(W_5O_{18})_3]\cdot 25.5H_2O$ and $Na_7H_{19}[Tb_{4.3}Eu_{1.7}O_2(OH)_6(H_2O)_6Al_2(Nb_6O_{19})_5]\cdot 47H_2O$ is studied by crystal structures, emission and excitation spectra, and emission decay dynamics. The excitation of the Tb^{3+} $^7F_6{}^5 \rightarrow D_4$ transitions produces not only the emission lines of Tb^{3+}, but also those of Eu^{3+}, accompanied by nonexponential rise and decay curves of the emission from Tb^{3+} and Eu^{3+}. There is no significant exchange interaction between the lanthanide ions, as a result of the coordination of aqua and/or hydroxo ligands to the lantahanide ions. The mechanism of the $Tb^{3+} \rightarrow Eu^{3+}$ energy transfer is identified as a Föster-Dexter-type energy transfer from Tb^{3+} (donor) to Eu^{3+} (acceptor). At low temperatures $^5D_4(Tb) + {}^7F_0(Eu) \rightarrow {}^7F_4(Tb) + {}^5D_0(Eu)$ governs the transfer process and at high temperatures it is governed by $^5D_4(Tb) + {}^7F_1(Eu) \rightarrow {}^7F_5(Tb) + {}^5D_1(Eu)$, $^5D_4(Tb) + {}^7F_1(Eu) \rightarrow {}^7F_4(Tb) + {}^5D_0(Eu)$, and $^5D_4(Tb) + {}^7F_2(Eu) \rightarrow {}^7F_5(Tb) + {}^5D_1(Eu)$ interactions which involve the thermally populated $^7F_1$ and $^7F_2$ levels. The nearest-neighbor energy-transfer rates by electric dipole-dipole interactions between a Tb-Eu pair at 4.2 K are estimated to be 4.5×10^4 and 4.7×10^5 s^{-1}, and the critical radii at 4.2 K are 10.3 and 10.0 Å for $K_{15}H_3[Tb_{1.4}Eu_{1.6}(H_2O)_3(SbW_9O_{33})(W_5O_{18})_3]\cdot 25.5H_2O$ (with Tb–Eu separation of 5.05 Å) and $Na_7H_{19}[Tb_{4.3}Eu_{1.7}O_2(OH)_6(H_2O)_6Al_2(Nb_6O_{19})_5]\cdot 47H_2O$ (with 3.76 Å separation), respectively. The low symmetry (C_s for the former and C_1 for the latter) of the LnO_8 (Ln = Tb and Eu) coordination polyhedra allows the nonvanishing electric-dipole transition probability for the $^7F_J \longleftrightarrow {}^5D_0$ (J = 0, 1) transitions which leads to a faster transfer rate at high temperatures.

III-K-2 Mixed-Valence Ammonium Trivanadate with a Tunnel Structure Prepared by Pyrolysis of Polyoxovanadate

NARUKE, Haruo; YAMASE, Toshihiro
(IMS and Tokyo Inst. Tech.)

[*Bull. Chem. Soc. Jpn.* **72**, 2699 (1999)]

The pyrolysis of a polyoxovanadate solid, $(NH_4)_{12}[V_{18}O_{42}(H_2O)]\cdot nH_2O$ ($n \approx 11$), at 300 °C in an Ar + NH_3 atmosphere gave a mixed-valence vanadium oxide, $(NH_4)_xV_3O_7$ ($x \approx 0.6$), isostructural with $Cs_{0.37}V_3O_7$. The crystal structure of $(NH_4)_xV_3O_7$ was refined by the Rietveld method (hexagonal, P63/m, a = 9.8436(6), c = 3.6165(1) Å, V = 303.47(3) Å^3, Z = 2). $(NH_4)_xV_3O_7$ comprises edge- and corner-sharing $V^{IV/V}O_5$ square-pyramids with an approximate ratio of $V^{IV}:V^{V} \approx 0.49:0.51$, to form a columnar cavity along the c-axis, in which ammonium N atoms are hydrogen-bonded to apical O atoms of the $V^{IV/V}O_5$ square-pyramids. A reflux of the $(NH_4)_xV_3O_7$ powder in a 0.6 M LiOH / 2-methoxyethanol solution brought about Li-insertion into the columnar cavity without any structural change in the $\{V_3O_7\}$ framework.

III-K-3 Photoassisted Dehalogenation of Organo-Chlorine Compounds by Paratungstate A in Aqueous Solutions

HU, Changwen; YUE, Bin; YAMASE, Toshihiro
(IMS and Tokyo Inst. Tech.)

[*Appl. Catal., A* **194-195**, 99 (2000)]

Nearly neutral aqueous solutions of 22 organo-chlorine compounds undergo photodegradation ($\lambda > 250$ nm) catalyzed by paratunstate A anion, $[W_7O_{24}]^{6-}$, which was obtained by adjusting pH levels of the Na_2WO_4 solution to 6–7. In each case the organic substrate was decomposed through dehalogenation. The rate of Cl^- formation strongly depends on substrates. The photochemical redox reaction between paratungstate A and substrates proceeds via precomplexation. The Langmuir-type dependence of the reaction rates on the concentration of substrates provides a promising method for the dechlorination of alkyl- and aromatic-chloride compounds such as $ClCH_2CH_2CH_2Cl$, C_3H_7Cl, and $C_6H_5CH_2Cl$.

III-K-4 A Novel-Type Mixed-ligand Polyoxotungstolanthanoate, $[Ln(W_5O_{18})(BW_{11}O_{39})]^{12-}$ (Ln = Ce^{3+} and Eu^{3+})

NARUKE, Haruo; YAMASE, Toshihiro

(IMS and Tokyo Inst. Tech.)

[*Bull. Chem. Soc. Jpn.* **73**, 375 (2000)]

Two isostructural anions, $[Ln(BW_{11}O_{39})(W_5O_{18})]^{12-}$ (Ln = Ce and Eu), were isolated as K^+ salts from aqueous solutions containing tungstate, Ln^{3+}, and BO_3^{3-}, at pH = 7. An X-ray crystallographic analysis showed that the Ln^{3+} center in the anion is chelated by two kinds of tetradentate polyoxotungstate ligands, $[W_5O_{18}]^{6-}$ and α-$[BW_{11}O_{39}]^{9-}$ with a square antiprismatic LnO_8 configuration, which are monovacant derivatives of $[W_6O_{19}]^{2-}$ and α-$[BW_{12}O_{40}]^{5-}$, respectively. The anion is of approximate C_s symmetry, and the observable asymmetry of K–O bonding between two different K^+ cations and the anion causes the two mirror planes within $[(W_5O_{18})Ln]^{3-}$ and $[(BW_{11}O_{39})Ln]^{6-}$ moieties to be canted to each other by 5.2° for Ln = Ce and 4.1° for Ln = Eu.

III-K-5 Photoreduction Processes of α-Dodecamolybdophosphate, α-$[PMo_{12}O_{40}]^{3-}$: ^{31}P-NMR, Electrical Conductivitiy, and Crystallographic Studies

ISHIKAWA, Eri; YAMASE, Toshihiro
(IMS and Tokyo Inst. Tech.)

[*Bull. Chem. Soc. Jpn.* **73**, 641 (2000)]

The photoreduction processes of α-$[PMo_{12}O_{40}]^{3-}$ (α-$PMo_{12}(0)$) in aqueous solutions at pH 2.0 are discussed on the basis of the results of the electrical conductivities and ^{31}P NMR spectra of photolytes, and the crystal structures of α-type two-electron and β-type four-electron reduction species isolated from photolytes as α-$[(^iPr)_2NH_2]_4[HPMo_{12}O_{40}]\cdot 4H_2O$ (**1**) (α-$PMo_{12}(II)$) and β-$[(^iPr)_2NH_2]_3[H_4PMo_{12}O_{40}]\cdot 2H_2O$ (**2**) (β-$PMo_{12}(IV)$): (i) A one-electron reduction species produced by the photoredox reaction of α-$PMo_{12}(0)$ with methanol is degraded to α-B-$[H_3PMo_9O_{31}(OH)_3]^{3-}$ (α-B-$PMo_9(0)$) and Mo^V-containing Mo-triad species (Mo_3). (ii) The formation of the α-type monoprotonated two-electron reduction species, α-$[HPMo_{12}O_{40}]^{4-}$ (α-$PMo_{12}(II)$), results from the isomerization of the β-type two-electron reduction species, β-$[PMo_{12}O_{40}]^{5-}$ (β-$PMo_{12}(II)$), which is produced by coupling between the one-electron reduced α-B-PMo_9 (α-B-$PMo_9(I)$) and Mo_3. (iii) The β-type four-protonated four-electron reduction species, β-$[H_4PMo_{12}O_{40}]^{3-}$ (β-$PMo_{12}(IV)$) as a final product is produced by the disproportionation of α-$PMo_{12}(II)$. The change in the electrical conductivity of the photolytes during photolysis supports the above processes for the photoreduction of α-$[PMo_{12}O_{40}]^{3-}$ to β-$[H_4PMo_{12}O_{40}]^{3-}$ at pH 2.0.

III-K-6 $Na_{10}(glycine)_2[H_2W_{12}O_{42}]\cdot 28H_2O$

NARUKE, Haruo; FUKUDA, Norio; YAMASE, Toshihiro
(IMS and Tokyo Inst. Tech.)

[*Acta Crystallogr., Sect. C: Cryst. Struct. Commun.* **56**, 177 (2000)]

The title compound, decasodium diglycine dihydrogendotetracontaoxododecatungstate(10-) octacosahydrate, consists of a paratungstate $[H_2W_{12}O_{42}]^{10-}$ anion, ten Na^+ cations, two zwitterionoic glycine molecules, and 28 crystallization waters. Two glycine-carboxylate O atoms coordinate three different Na^+ cations and the amino N atom forms hydrogen bonds with both terminal and bridging O atoms, two atoms for each.

III-K-7 Crystal and Electronic Structure and Magnetic Susceptibility of the Photochemically Prepared Layered Vanadyl Phosphate, $Na(VO)_2(PO_4)_2\cdot 4H_2O$

YAMASE, Toshihiro; MAKINO, Haruyo
(IMS and Tokyo Inst. Tech.)

[*J. Chem. Soc., Dalton Trans.* 1143 (2000)]

Prolonged photolysis of the aqueous solutions containing Na_3VO_4, NaH_2PO_4, and MeOH at pH 1.8 adjusted by use of H_3PO_4 led to the formation of a layered vanadyl phosphate, $Na(VO)_2(PO_4)_2\cdot 4H_2O$ (**1**). A single-crystal X-ray structural analysis of dark green crystal of **1** showed that the structure contains layers of vanadium (randomly with 1:1 ratio of V^{4+} and V^{5+}) phosphorus oxide with the water molecules and sodium cations between the layers. The layer is a 4-connected net in which corner-sharing vanadium oxygen octahedra and phosphate tetrahedra alternate. The molecular structure is identical with that of hydrothermally prepared Na^+-compound but reveals the nonzero dihedral angle (2.61°) between the least-square planes (containing equatorial four-oxygen atoms) of the VO_6 octahedra in contrast to the parallel arrangement of the basal least-square planes for the latter. Magnetic susceptibility measurements for **1** show weak ferromagnetic coupling (J/k = 0.87 K) at $T \leq 100$ K and weak antiferromagnetic behavior at $T > 100$ K. The magneto/structural relationship for the retracted-chair-like $V(OPO)_2V$ rings are compared among other layered vanadyl phosphate compounds. The ferromagnetic property of the d_{xy} orbital at one V^{IV} center in the retracted-chaired $V^{IV}(OPO)_2V^{IV}$ ring can be explained in terms of the interaction with the V=O π^* orbital at opposite V^{IV} center, which is possible when both distances of $(O=)V\cdots V(=O)$ and $(O=)V\cdots O(=V)$ are short (~4.55 and ~4.36 Å, respectively). Otherwise, the antiferromagnetic property due to the superexchange interaction between magnetic d_{xy} orbitals at both V^{IV} centers is operative. The results of Extended Hückel (EH) calculations for a fragment model $[V_8P_8O_{40}]^{4-}$ (with $V^{IV}/V^V = 1/1$) support a variety of the magnetic interaction of the unpaired electron at V^{IV} centers in the V–P–O layer consisting of the retracted-chaired $V(OPO)_2V$ rings.

RESEARCH ACTIVITIES IV
Department of Molecular Assemblies

IV-A Spectroscopic Study of Organic Conductors

The reflectivity of an organic conductor provides us with a wealth of information on the electronic structure. For instance, the anisotropy of a band structure, band width, effect of electron-electron correlation, and electron-molecular vibration (*e-mv*) coupling parameters can be extracted from the analysis of the reflectivity or optical conductivity curve. We are investigating the polarized reflection spectra of various organic conductors in the spectral region of 50–33000 cm^{-1} and in the temperature range of 6–300 K. Raman spectroscopy is a complementary method to reflection spectroscopy for understanding molecular vibrations (local phonons). We are investigating the charge ordering (CO) or charge disproportionation phenomena in organic conductors using the technique of vibrational spectroscopy. The charge ordering was found in inorganic narrow-band systems such as copper, manganese, and vanadium oxides. Recently, a charge-ordered ground state has been found in several organic conductors. The Raman and infrared spectra change dramatically at the CO phase transition temperature. Our goal is the complete understanding of the CO phase transition through the interpretation of the vibrational spectra.

IV-A-1 Charge Disproportionation of θ-(BEDT-TTF)$_2$RbZn(SCN)$_4$ Studied by Raman Spectroscopy

YAMAMOTO, Kaoru; YAKUSHI, Kyuya

[*Synth. Met.* in press]

Charge-transfer radical salt θ-(BEDT-TTF)$_2$RbZn(SCN)$_4$ undergoes a metal-to-insulator (MI) transition with a structural change as the temperature is slowly lowered. In the present study, the electronic structure has been investigated by Raman spectroscopy. The observed Raman spectrum around the characteristic frequency of C=C stretching shows noticeable variation accompanying the MI transition. The spectrum of the insulating phase provides multiple C=C stretching modes, though a BEDT-TTF molecule has only two Raman active modes relating to C=C stretching. The multiple peaks can be assigned in a systematic way based on the 2D tetramer model, in which the symmetry of the combination modes and charge disproportionation among four BEDT-TTF molecules are taken into consideration. The resultant assignment indicates the local arrangement of the charge forms a stripe pattern perpendicular to the molecular stacks.

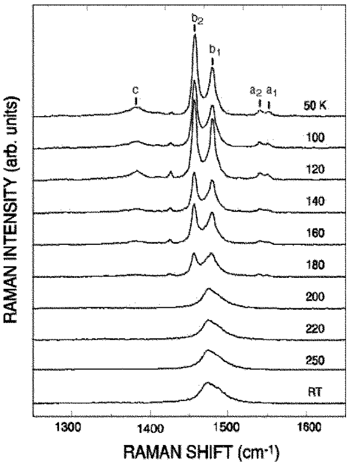

Figure 1. Temperature dependence of the Raman spectrum of θ-(BEDT–TTF)$_2$RbZn(SCN)$_4$ observed on (101) surface.

IV-A-2 Isotope Shift and Charge Susceptibility of C=C Related Normal Modes of BEDT-TTF Molecule

YAMAMOTO, Kaoru; YAKUSHI, Kyuya; MIYAGAWA, Kazuya[1]; KANODA, Kazushi[1]; KAWAMOTO, Atsushi[2]
([1]Univ. Tokyo; [2]Hokkaido Univ.)

We have been developing a method to apply vibrational spectroscopy to the investigation of the spatial charge distribution formed in two-dimensional charge ordering systems. One of the most troublesome problems to the end is in the difficulty in the spectral assignment, owing to the charge-dependent reconstruction of normal modes formed by the combination of vibrations of several chemical bonds. The decisive method to assign the spectrum is the inquiry of the isotope shift. Its interpretation requires thorough knowledge on the relation among the normal mode reconstruction, degree of ionization, and isotope replacement. In the present study, we have investigated the characteristics of the normal modes relating to the C=C bonds of BEDT-TTF by measuring the isotope shift of the Raman and infrared reflectance spectra. It has been recognized as an established argument that the relevant two symmetric C=C modes are constructed from the combinations of two types of C=C bonds, *i.e.*, the ring and central C=C vibrations, in the neutral BEDT-TTF, and the two vibrations are completely separated to form the distinct normal modes in the monocationic state. However, the present study indicates that BEDT-TTF in a nearly monocationic state provides the normal modes based on the combinations of the two C=C stretching modes. It turns out that the replacement of the carbon atoms of the central C=C bond by ^{13}C results in the complete separation of the two types of modes in the relevant normal modes of the nearly monocationic BEDT-TTF.

IV-A-3 Raman-Active C=C Stretching Vibrations of κ-(BEDT-TTF)$_2$Cu[N(CN)$_2$]Br

MAKSIMUK, Mikhail[1]; YAKUSHI, Kyuya;

TANIGUCHI, Hiromi[2]; KANODA, Kazushi[2]; KAWAMOTO, Atsushi[3]
([1]IMS and Inst. Problem Chem. Phys.; [2]Tokyo Univ.; [3]Hokkaido Univ.)

κ-(BEDT-TTF)$_2$X salts are the most extensively investigated charge-transfer salts including Raman and IR spectra. Nevertheless some principal and strong lines in their Raman spectra are not unambiguously assigned yet. We measured the resonant Raman spectra of κ-(BEDT-TTF)$_2$Cu[N(CN)$_2$]Br, κ-(BEDT-TTF)$_2$Cu(CNS)$_2$, and their several isotopic analogues in the region of C=C stretching vibrations with various combinations of polarizations. There exists a big (~50 cm^{-1}) factor group splitting for the ν_3 mode, which is assigned mainly to the stretching of the central C=C bond in a BEDT-TTF molecule. The splitting is ascribed to the inter-dimer *e-mv* interaction inside a conducting layer. The Raman-active *e-mv* coupled ν_3 mode appears in the $b(a,c)b$ spectrum with a broad linewidth, low-frequency shift, and a characteristic temperature dependence. The temperature dependence of the frequency this mode is very different from that of the infrared-active intra-dimer *e-mv* coupled ν_3 mode. An analogous splitting is found for ν_2 of ^{13}C(2) compound (see Figure 1, bottom). However in a ^{12}C(2) crystal, ν_2 and ν_3 provide additional splittings that cannot be explained by a simple factor group analysis. We suppose that a crystal symmetry changes through the C^{12}–C^{13} substitution. These unusual results are still puzzling for us.

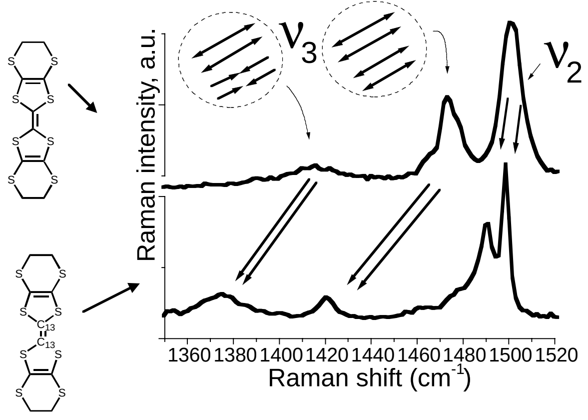

Figure 1. Raman spectra of κ-(BEDT-TTF)$_2$Cu[N(CN)$_2$]Br (top) and κ-(^{13}C(2)-BEDT-TTF)$_2$Cu[N(CN)$_2$]Br (bottom). In the latter, the two central carbon atoms in the BEDT-TTF molecule are replaced by ^{13}C. As a result ν_3 mode is shifted to low-frequency side. Laser polarisation is parallel to the **c**-axis.

IV-A-4 An Influence of the Cooling Rate to the Raman an IR Spectra of Partially Deuterated κ-(BEDT-TTF)$_2$Cu[N(CN)$_2$]Br

MAKSIMUK, Mikhail[1]; YAKUSHI, Kyuya; TANIGUCHI, Hiromi[2]; KANODA, Kazushi[2]; KAWAMOTO, Atsushi[3]
([1]IMS and Inst. Problem Chem. Phys.; [2]Tokyo Univ.; [3]Hokkaido Univ.)

The set of progressively deuterated isotopic analogues of κ-(BEDT-TTF)$_2$Cu[N(CN)$_2$]Br lies on the border between a metal and insulator in the phase diagram of κ-type BEDT-TTF salts. It is known that the cooling rate from 80 K to 50 K influences the volume fraction of the metallic and antiferromagnetic domains in the crystal.

We examined the cooling rate dependence in the Raman and IR spectra of d[0,0], d[2,2], d[3,3], and d[4,4] single crystals, where the numbers denote the deuterium numbers in each ethylene group of BEDT-TTF. In d[0,0], d[4,4] crystals, no cooling rate dependence was found. On the other hand, in d[2,2], d[3,3], we found a cooling rate dependence for (1) factor group splitting of the ν_3 mode, (2) resonance enhancement of the ν_3 intensity, and (3) linewidths of some phonons both in the Raman and infrared spectra. Probably, all these phenomena is associated with the inhomogeneous metal-antiferromagnet domain structure.

Unlike d[3,3], the crystal d[2,2] shows a big sample dependence. The cooling rate was equally important in the 50–150 K range, although the cooling rate in the 50–80 K range was reported to be much more effective to the dc conductivity than that in 80–150 K. For the C=C stretching modes, we found no annealing effect that has been regarded to influence the dc conductivity. Besides, we found no cooling-rate dependence in the optical conductivity at least above 100 cm^{-1}.

IV-A-5 Spectroscopic Evidence for the Charge Disproportionation in a Two-Dimensional Organic Conductor, θ-(BDT-TTP)$_2$Cu(NCS)$_2$

OUYANG, Jianyong[1]; YAKUSHI, Kyuya; MISAKI, Yohji[2]; TANAKA, Kazuyoshi[2]
([1]GUAS; [2]Kyoto Univ.)

[*Phys. Rev. B* in press]

We present spectroscopic evidence for the charge disproportionation in the crystal of θ-(BDT-TTP)$_2$Cu(NCS)$_2$. θ-(BDT-TTP)$_2$Cu(NCS)$_2$ is a highly correlated organic conductor with a quasi-two-dimensional electronic structure. In the electrical resistance of this compound, we found a second-order like phase transition at 250 K. Below this phase transition temperature, the optical absorption in the mid-infrared region exhibits a broadening of the energy gap. The Raman active C=C stretching modes ν_2, ν_3, and ν_4, which are sensitive to the charge on BDT-TTP, split into seven sharp bands and four broad bands. Using the resonance effect, the sharp bands were classified into two groups. At 5 K these groups are reasonably assigned to the charge-poor and charge-rich BDT-TTP molecules. This is direct evidence for the charge disproportionation accompanying the phase transition.

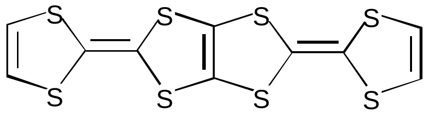

BDT-TTP

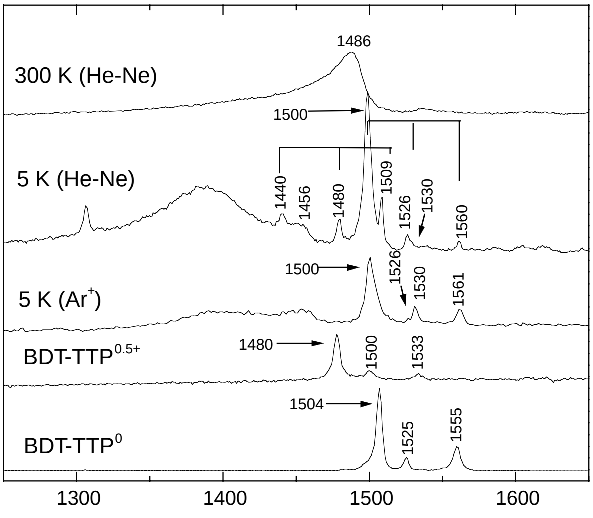

Figure 1. The Raman spectra of the C=C stretching region at 300 K and 5 K in the θ-(BDT-TTP)$_2$Cu(NCS)$_2$ crystal, below which the room-temperature spectra of (BDT-TTP)$_2$AsF$_6$ and BDT-TTP crystals are displayed. The sharp bands at 5 K is classified into two groups as shown in this figure.

IV-A-6 ESR Properties of a Quasi-Two-Dimensional Organic Conductor, θ-(BDT-TTP)$_2$-Cu(NCS)$_2$

SIMONYAN, Mkhitar[1]; YAKUSHI, Kyuya; MISAKI, Yohji[2]; TANAKA, Kazuyoshi[2]
([1]IMS and Inst. Phys. Res. ARAS; [2]Kyoto Univ.)

As shown in IV-A-5, θ-(BDT-TTP)$_2$Cu(CNS)$_2$ undergoes a phase transition accompanying the charge disproportionation. To investigate the magnetic properties, particularly below the phase transition temperature (T_p), we conducted the angular dependence of the g value at 8.5 K around the three crystallographic axes and the temperature dependence of the intensity, g value, and linewidth. The principal axes obtained from the angular dependencies along the a*, c- and b-axes agreed within 11° with those calculated from the principal axes of the molecule. The principal g values are 2.0026, 2.0046, and 2.0130, which requires the principal g values of the molecule as 2.0129, 2.0053, and 2.0022 along the long, short, and normal axes. This means that the hole is located on the both sides of herring bone.

On lowering temperature, the linewidth rapidly decreases from 70 G (300 K) to 10 G (200 K) and levels off below 200 K. We consider that this temperature dependence of the linewidth is associated with the second-order phase transition at 250 K. Below 200 K, the spin susceptibility approximately follows a Bonner-Fisher behavior with J ~ 8 K down to ~5 K. Below 5.2 K a sudden drop is observed for the ESR intensity. We consider this behavior as a magnetic phase transition to a non-magnetic state.

IV-A-7 Infrared Spectroscopic Study of the Band Structure of (EO-TTP)$_2$AsF$_6$

DROZDOVA, Olga[1]; YAKUSHI, Kyuya; MISAKI, Yohji[2]; TANAKA, Kazuyoshi1
([1]IMS and A. F. Ioffe Phys.-Tech. Inst. [2]Kyoto Univ.)

Ethylenedioxy substituted BDT-TTP (EO-TTP) produced a number of organic metals with tetrahedral and octahedral anions.[1)] (EO-TTP)$_2$AsF$_6$ has β-type donor array and shows metallic conductivity down to 1.5 K. Polarized IR reflectance spectra on the conductive (010) plane display well-defined plasma edges along (***E***||***a***) and (***E***||***c***) directions suggesting two-dimensional (2D) while highly anisotropic band structure. We have experimentally estimated intra- (t_a) and inter-stack (t_c) transfer integrals as –0.229 and 0.047 eV, respectively. These transfer integrals yield Fermi surface open in $\mathbf{k}_C$ direction while strongly warped. On the contrary, theoretical calculation (t_{a1} = –0.269, t_{a2} = -0.252, t_c = 0.091 eV) largely over-estimates t_c and gives closed Fermi surface, similar to what was found earlier in (BDT-TTP)$_2$X (X = SbF$_6$, AsF$_6$) compounds.[2)] On lowering temperature down to 13 K, t_a smoothly increases by ~9%.

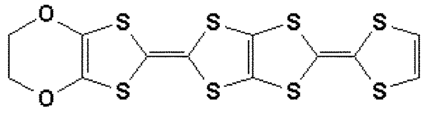

EO-TTP

References

1) Y. Misaki, K. Tanaka, M. Taniguchi, T. Yamabe, T. Kawamoto and T. Mori, *Chem. Lett.* 1249 (1999).
2) J. Ouyang, K. Yakushi, Y. Misaki and K. Tanaka, *J. Phys. Soc. Jpn.* **67**, 3191 (1998).

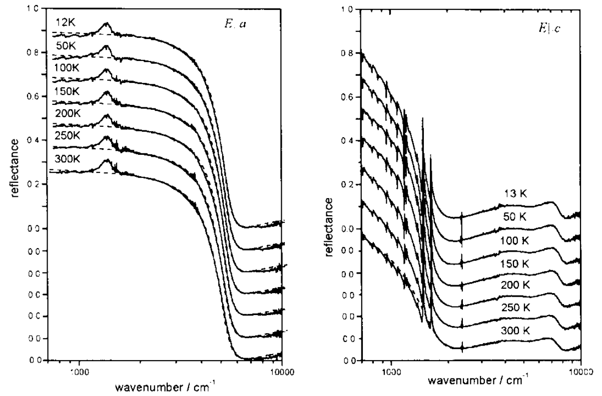

Figure 1. Temperature dependence of IR reflectivity of (EO–TTP)$_2$AsF$_6$ along a- and c-axes. Solid line, experiment; dashed line, Drude-Lorentz model.

IV-A-8 Optical Properties and Metal-Insulator Transitions in Organic Metals (BEDT-ATD)$_2$X-(solvent) (X = PF$_6$, AsF$_6$, BF$_4$; solvent = THF, DHF, DO)

URUICHI, Mikio; YAKUSHI, Kyuya; YAMASHITA, Yoshiro

[*J. Mater. Chem.* **10**, 2716 (2000)]

We present the polarized reflection spectra of (BEDT-ATD)$_2$X(solvent) (X = AsF$_6$, PF$_6$, BF$_4$; solvent = THF, DHF, DO), where THF is tetrahydrofuran, DHF 2,5-dihydrofuran, and DO 1,3-dioxolane. BEDT-ATD$^+$

has an intra-molecular excitation in a very low-energy region (4000–5000 cm^{-1}). These isostructural compounds are characterized as strongly correlated quasi-1D metals. The optical spectra in all these compounds suggest that the screw-axis symmetry is broken below the metal-insulator transition temperature. This broken symmetry is confirmed by the X-ray diffraction experiment in (BEDT-ATD)$_2$BF$_4$(THF) and (BEDT-ATD)$_2$PF$_6$(DHF). The low-temperature structure has the 4k_F-modulated lattice (dimerized structure). The magnetic susceptibility also supports this 4k_F modulation. We present the low-temperature crystal structures of (BEDT-ATD)$_2$BF$_4$(THF) and (BEDT-ATD)$_2$PF$_6$(DHF). BF$_4^-$ and THF are fully ordered in (BEDT-ATD)$_2$BF$_4$(THF) and DHF is almost ordered in (BEDT-ATD)$_2$PF$_6$(DHF). The vibronic modes are observed in the reflection spectra of all these compounds even above the metal-insulator transition temperature, which suggests that the screw-axis symmetry is locally broken.

IV-B Solid State Properties of Organic Conductors with π-d Interaction

Some phthalocyanine molecules contain unpaired d-electrons in the conjugated π-electron system. Due to this nature, the itinerant π-electrons coexist with localized unpaired d-electrons in solid phthalocyanine salts, in which a one-dimensional double-chain system (metal and ligand chain) is formed. Furthermore these chains make up wide (π-band) and narrow (d-band) one-dimensional bands. The energy of the narrow band is close to the Fermi energy of the wide band. The phthalocyanine conductor is thus a two-chain and two-band system. The electronic structure of phthalocyanine conductors is analogous to that of the f-electron system, in which a narrow f-band coexists with a wide s-band and they are hybridized near the Fermi level. To understand the electronic structure of this two-band system, we are investigating the charge-transfer salts of NiPc and CoPc and their mixed crystals.

IV-B-1 Magnetic Exchange Interactions in Quasi-One-Dimensional Organic Alloy of Co$_{0.01}$Ni$_{0.99}$Pc(AsF$_6$)$_{0.5}$

SIMONYAN, Mkhitar[1]**; DING, Yuqin**[2]**; YAKUSHI, Kyuya**
([1]IMS and Inst. Phys. Res. ARAS; [2]GUAS)

[*Phys. Rev. B* in press]

We have continued to study the ESR properties of Co$_x$Ni$_{1-x}$Pc(AsF$_6$)$_{0.5}$ to obtain the magnitude of the magnetic exchange interaction between local spins of Co^{2+} ions and itinerant spins of Pc-ligands. Subsequently to the finding of the hyperfine structure in a insulating phase of Co$_{0.01}$Ni$_{0.99}$Pc(AsF$_6$)$_{0.5}$ below 30 K, we analyzed the temperature dependence of the g value and linewidth in a metallic phase. In this phase, the d- and π-spins are coupled by the exchange interaction. This coupling brings about a bottle-neck state in the spin-relaxation process and yields a single Lorentzian line shape for the ESR signal. We used a molecular field approximation which has been used to interpret the ESR line shape of a dilute alloy. Based on the simulation of the temperature dependence of the g value and line shape, we obtained the exchange interaction as J = 0.013 ± 0.002 eV) and the density of states at Fermi level as D_F = 3.8 ± 0.2 eV^{-1}. From these parameters, we can roughly estimate the Kondo temperature as $T_k \sim 10^{-5}$ K. This means that the exchange interaction between d- and π-spins are extremely small.

IV-B-2 Pressure Dependence of Resistivity in Quasi-One-Dimensional Conductor CoPc-(AsF$_6$)$_{0.5}$

SIMONYAN, Mkhitar[1]**; DING, Yuqin**[2]**; YAKUSHI, Kyuya**
([1]IMS and Inst. Phys. Res. ARAS; [2]GUAS)

At ambient pressure, CoPc(AsF$_6$)$_{0.5}$ shows a broad resistivity minimum at room temperature, which is exceptional among the metallic phthalocyanine conductors. The crystal is so sensitive to temperature that it shows multiple resistivity jumps below 200 K. High pressure suppressed the resistivity jump and allowed us for the first time to conduct the resistance-*vs.*-temperature measurement. As shown in the figure, a metallic phase expands to lower temperature when we increase the pressure. This pressure dependence is different from the analogous compound NiPc(AsF$_6$)$_{0.5}$, in which a metal-insulator transition temperature increased from 40 K to room temperature upon increasing pressure. A hump was found at 75 K at 0.3 GPa, which shifted to high-temperature side upon increasing pressure. Finally, under 0.9 GPa, CoPc-(AsF$_6$)$_{0.5}$ became metallic down to 100 K.

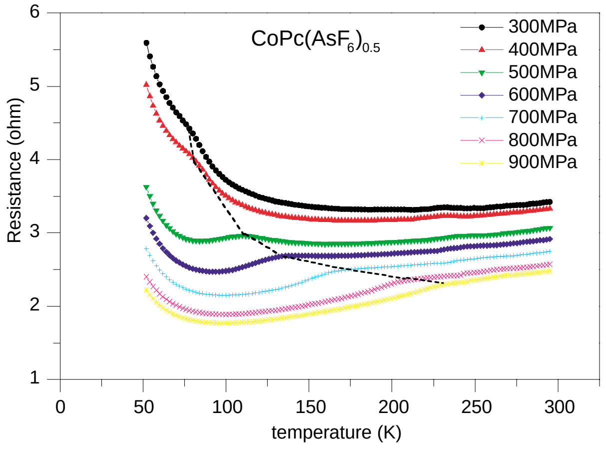

Figure 1. Temperature dependence of the resistance of CoPc-(AsF$_6$)$_{0.5}$

IV-B-3 Antiferromagnetic Phase Transition of DMTSA-$FeCl_4$

NAKANO, Chikako; YAKUSHI, Kyuya; TAKIMIYA, Kazuo[1]; OTSUBO, Tetsuo[1]
([1]Hiroshima Univ.)

We found isostructural charge-transfer salts of DMTSA which involves magnetic and non-magnetic counter anions, (DMTSA)$FeCl_4$ and (DMTSA)$GeCl_4$. Both compounds are semiconductors, room-temperature resistivities being 3×10^1 Ωcm for the $FeCl_4$ salt and 2×10^2 Ωcm for the $GeCl_4$ salt. We found from the magnetic susceptibility of the oriented crystals that the former compound showed an antiferromagnetic phase transition at 12.0 K. DMTSA and $FeCl_4$ forms an mixed stacked structure, which is often found in an ionic crystal. The network of a magnetic interaction seems to be formed by the Se–Se and Se–Cl and Cl–Cl interactions. The heat capacity shows an anomaly near the phase transition temperature. By comparing with the heat capacity of (DMTSA)$GeCl_4$, the contribution of lattice phonons were subtracted. The magnetic heat capacity ranges from 25 K to < 2 K, which suggests a low-dimensional magnetic interaction. The entropy change during this phase transition was close to *Rln6*. This result means that the magnetic moment of Fe^{2+} ($S = 5/2$) mainly contributes to the antiferromagnetic ordering.

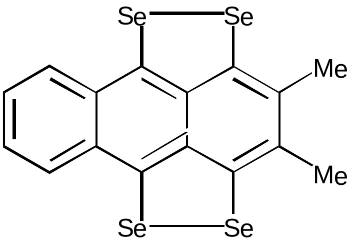

DMTSA

IV-C Microscopic Investigation of Molecular-Based Conductors

Molecular based conductors are one of the most extensively studied materials in the field of solid state physics. Their fundamental properties have been very well clarified: The development of the understanding of the electronic structure enables us systematic investigations of these materials. At the same time, it is true that there still remain several unsolved questions in the molecular based conductors.

To clarify the low temperature electronic states, we performed the static susceptibility, EPR, ^{1}H- and ^{13}C-NMR measurements for molecular based conductors.

IV-C-1 Low-Temperature Electronic States in (EDT-TTF)$_2$AuBr$_2$

NAKAMURA, Toshikazu

[*J. Phys. Chem. Solid* in press]

Magnetic investigation was carried out at low temperatures in a one-dimensional 1/4-filled system, (EDT-TTF)$_2$AuBr$_2$ by performing SQUID, EPR, and ^{1}H-NMR measurements. The electronic phase is discussed for (EDT-TTF)$_2$AuBr$_2$, which undergoes an antiferromagnetic transition at 16 K followed by a resistivity minimum. We observed an anomalous second-peak of the NMR spin-lattice relaxation rate in the magnetic phase, suggesting a stable incommensurate SDW in a 1/4-filled system.

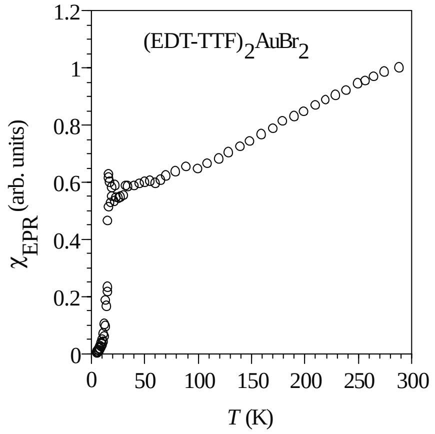

Figure 1. Temperature dependence of the spin susceptibility, χ_{EPR}, of (EDT-TTF)$_2$AuBr$_2$ determined by EPR measurements.

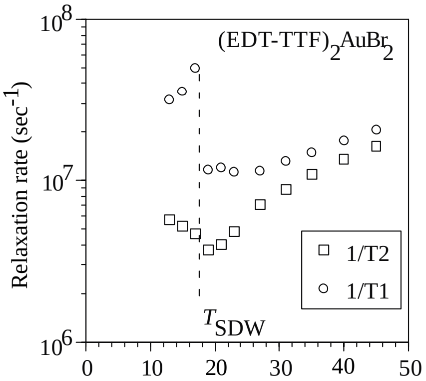

Figure 2. The temperature dependence of the EPR spin-lattice relaxation rate, T_1^{-1}, (circle) and the spin-spin relaxation rate, T_2^{-1}, (square).

IV-C-2 Low Temperature Electronic States of β'-type Pd(dmit)$_2$ Compounds

NAKAMURA, Toshikazu; TSUKADA, Hiroshi; TAKAHASHI, Toshihiro[1]; AONUMA, Shuji[2]; KATO, Reizo[2,3]
([1]Gakushuin Univ.; [2]ISSP; Univ. Tokyo; [3]Inst. Phys. Chem. Res.)

[*Mol. Cryst. Liq. Cryst.* **343**, 187 (2000)]

Research of metal dithiolene complexes *M*(dmit)$_2$ is one of major trend in the development of molecular based conductors with new functions. Although several metallic compounds even at ambient pressure are observed in Ni(dmit)$_2$ compounds, most of Pd(dmit)$_2$ compounds show paramagnetic non-metallic behavior at ambient pressure. In order to clarify the mechanism of the charge localization of β'-type Pd(dmit)$_2$ compounds, we have carried out electron spin resonance measurements for β'-type Pd(dmit)$_2$.

We found that most of them except one compound undergo antiferromagnetic transition. Although they are isostrcural and with little differences in lattice parameters, the EPR linewidth, ΔH_{pp}, and the antiferromagnetic transition temperature, T_N, show a huge sample dependence. We found a close relation between the T_N and inter-stack interaction (Figure.1). Since the crystal structure of the Pd(dmit)$_2$ system is based on the stack of strongly dimerized Pd(dmit)$_2$ molecules, the conduction band is considered to be formed by the two-dimensional half-filled HOMO band. The EPR *g*-values of β'-type Pd(dmit)$_2$ are found to be beyond one radical description which is a good approximation for conventional molecular based conductors; we should consider the wave-function Pd(dmit)$_2$ supermolecules. These experimental facts are evidences from the view point of magnetic investigation that this family is a Mott-Hubbard insulator with dimer as a unit. In order to understand more detailed electronic structure, we synthesized ^{13}C substituted Pd(dmit)$_2$ molecules, and ^{13}C-NMR investigation are performed. The electronic structures of a series of molecular conductors based on Pd(dmit)$_2$ are discussed from microscopic points of view.

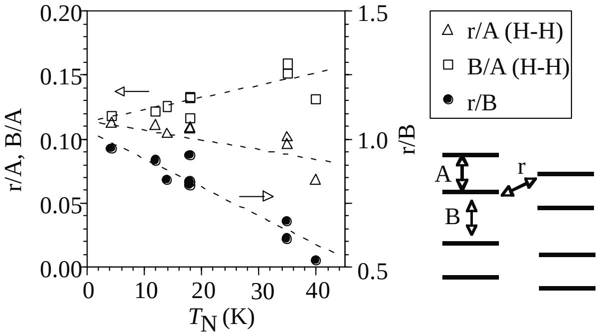

Figure 1. Relationship between the inter-dimer interaction versus the T_N. Previous results determined by ^{1}H-NMR are also included in this figure. The parameters, *A*, *B* and *r*, which are shown in the schematically shown in insets, are same in previous report. The Broken line is a guide to the eye.

IV-C-3 Magnetic Investigation of Organic Conductors Based on TTP Derivatives

TSUKADA, Hiroshi; NAKAMURA, Toshikazu; MISAKI, Yohji[1]; TANAKA, Kazuyoshi[1]
([1]Kyoto Univ.)

Most of TTP based organic conductors possess stable metallic phases. It is widely believed that the extended π orbital reduces on-site Coulomb interaction. To clarify the electronic states of the low-temperature phases, we performed ^{1}H-NMR measurements for (BDT-TTP)$_2$SbF$_6$. Figure 1 show the temperature dependence of the ^{1}H–T_1^{-1} of the (BDT-TTP)$_2$SbF$_6$. The ^{1}H–T_1^{-1} exhibits a characteristic temperature dependence. A large enhancement with a peak around 160 K is well fitted by the BPP type relation, indicating a possible relaxation by molecular motion. But no simple explanation can be offered at present, since the BDT-TTP molecule does not seem to possess internal freedom. Between 20 and 100 K, the ^{1}H–T_1^{-1} shows a T-linear temperature dependence, suggesting Korringa-like relation. The magnitude of the $(T_1T)^{-1}$ of 6.9×10^{-4} (sec^{-1}K^{-1}) is comparable to that of a typical organic superconductor, β-(BEDT-TTF)$_2$I$_3$ (5.8×10^{-4} (sec^{-1}K^{-1})). Below 20 K, the ^{1}H–T_1^{-1} starts to deviate from the Korringa-like behavior and shows a $T^{0.5}$ dependence. To investigate more detail, we carried out measurements operated at 196 MHz. As seen in the inset of Figure 1, low temperature results of the ^{1}H–T_1^{-1} show different behavior between 89.4 MHz and 196 MHz, although those above 20 K agree with each other. The deviation from the Korringa-like behavior seems to be suppressed at high frequency measurements. Moreover estimated ratio, T_1^{-1} (89.4 MHz)/ T_1^{-1} (196 MHz), of 1.39 at 12 K is close to the expected value of 1.48 assuming one-dimensional diffusive propagation of spin-excitation. In conclusion, our NMR measurements for two organic conductors based on TTP derivative tell that 1) the present salts are Q1D electronic system, and that 2) electronic correlation seems to be comparable to those of typical BEDT-TTF salts.

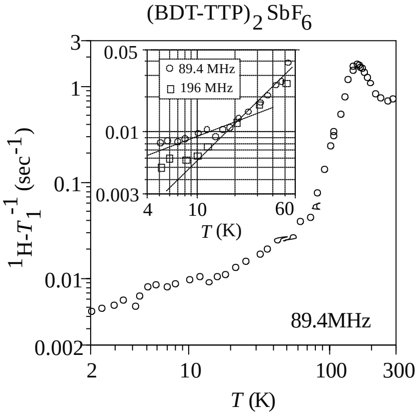

Figure 1. Temperature dependence of the ^{1}H-NMR spin-lattice relaxation rate, ^{1}H–T_1^{-1}, of (BDT-TTP)$_2$SbF$_6$ over the complete range of our investigation. The inset shows the low temperature region of the ^{1}H–T_1^{-1} (a) operated at 89.4 MHz (circle) (b) at 196 MHz (square).

IV-C-4 Possible Charge Disproportionation and New Type Charge Localization in θ-(BEDT-TTF)$_2$CsZn(SCN)$_4$

NAKAMURA, Toshikazu; MINAGAWA, Waka[1]; R. KINAMI, Ryoji[1]; TAKAHASHI, Toshihiro[1]
([1]Gakushuin Univ.)

[*J. Phys. Soc. Jpn.* **69**, 504 (2000)]

We have investigated the magnetic properties of the θ-(BEDT-TTF)$_2$CsZn(SCN)$_4$. A large enhancement of the ^{1}H-NMR-T_1^{-1} and the spin susceptibility was observed below 20 K. The principal axes of the EPR *g*-tensor have been found to change their directions, keeping the principal values constant. The abrupt rotation of the axes has indicated a phase transition at 20 K. We have proposed a possible model of the electronic state of a quarter-filled two-dimensional system, θ-(BEDT-TTF)$_2$CsZn(SCN)$_4$: In the high-temperature metallic region, a charge disproportionation seems to grow as temperature decreases. The low temperature insulating phase is essentially a state of charge localization where most of the sites are local spin-singlet. The low-temperature magnetism is originated from small number of unpaired local moments. To understand the unusual transition in a quarter-filled two-dimensional system, more works are required. We are preparing ^{13}C-NMR lineshape analysis.

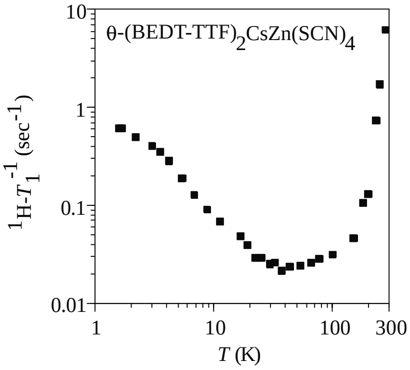

Figure 1. Temperature dependence of the ^{1}H-NMR spin-lattice relaxation, T_1^{-1}.

IV-D Development of Magnetic Organic Superconductors

Since the discovery of the first organic superconductor (Bechgaard salt) $(TMTSF)_2PF_6$ in 1980, a grate progress has been made in the field of molecular conductors. Soon after the discovery of Bechgaard salt having one-dimensional metal nature, we tried to find a way to develop two-dimensional metals without one-dimensional metal instabilities and found the first κ-type organic superconductor with two-dimensional cylindrical Fermi surface in 1987. However, the elevation of T_c of organic superconductors has been stoped since the discovery of κ-$ET_2Cu[N(CN)_2]X$ (X = Cl, Br) in 1990 and the progress of molecular design of organic metals became rather stagnant in the last 10 years.

Until recently, the fields of molecular conductors and molecular magnets have been developed almost independently with each other. But recently increasing attention has been attracted to the interplay of magnetism and conductivity in the molecular system, which began to arouse new streams in these fields. The first paramagnetic organic superconductor was found in 1995. The first antiferromagnetic organic superconductor was discovered in the last year. The recent discoveries of antiferromagnetic organic superconductors, metamagnetic organic metal, field-induced metallic states, superconductor-to-antiferromagnetic insulator transition, etc in BETS (= bis(ethyleneditho)tetraselenafulbalene) conductors seem to suggest the opening of new field of magnetic molecular conductors.

IV-D-1 BETS as a Source of Molecular Magnetic Superconductors (BETS = Bis(ethylenedithio)-tetraselenafulvalene)

KOBAYASHI, Hayao; KOBAYASHI, Akiko[1]**; CASSOUX, Patrick**[2]
([1]Univ. Tokyo; [2]CNRS)

[*Chem. Soc. Rev.* **29**, 325 (2000)]

BETS-based salts incorporating Fe^{3+} ions are most interesting candidate systems for the observation of interplay of conductivity and magnetism. Indeed, in λ- and κ-$(BETS)_2FeCl_4$, conduction electrons in the BETS layers do interact with spins localised on the $FeCl_4^-$ anions. Since the size of non-magnetic GaX_4^- anion (X = Cl, Br) approximatly equal to that of FeX_4^-, $(BETS)_2GaX_4$ system can take the crystal structure almost identical to that of $(BETS)_2FeCl_4$. Furthermore we can prepare a series of BETS conductor with mixed-matal and mixed-halogen atoms. Systematic studies on λ-$(BETS)_2Fe_xGa_{1-x}Cl_{4-y}Br_y$ have provided a number of interesting systems, including conductors with an antiferromagnetic metal state, a metamagnetic organic metal, and an antiferromagnetic organic superconductor. Unprecedented superconductor-to-insulator transitions and superconductor-to-metal transitions have been also observed. In this report the recent our studies on the BETS systems are reviewed.

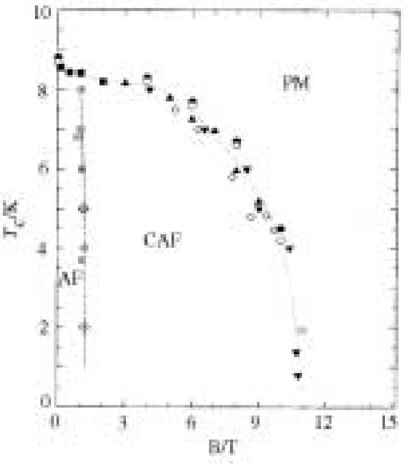

Figure 1. Temperature-magnetic field diagram of λ-$(BETS)_2FeCl_4$.

IV-D-2 Superconductivity, Antiferromagnetism and Phase Diagram of a Series of Organic Conductors, λ-$(BETS)_2Fe_xGa_{1-x}Br_yCl_{4-y}$

TANAKA, Hisashi; KOBAYASHI, Hayao; KOBAYASHI, Akiko[1]**; CASSOUX, Patrick**[2]
([1]Univ. Tokyo; [2]CNRS)

[*Adv. Mater.* **12**, 1685 (2000)]

Recently a series of organic conductors based on BETS molecules and magnetic anions seem to attract an increasing interest because of their many novel properties produced by tuning the composition of the anions. They exhibit not only usual superconducting transitions but also unprecedented superconductor-to-insulator transitions. In this paper we report the electric and magnetic properties of λ-$BETS_2Fe_xGa_{1-x}Br_yCl_{4-y}$, which are strongly modified from those of λ-$BETS_2Fe_xGa_{1-x}Cl_4$ without Br atoms due to the large enhancement of electron correlation effect by Cl → Br exchange. λ-$BETS_2Fe_xGa_{1-x}Br_yCl_{4-y}$ ($x \approx 0.5$, $y = 1.0$) showed a superconducting-to-insulator transition around 2 kbar where the system takes a superconducting state at 2.5–7 K. Furthermore, a superconductor-to-metal transition, which never encountered in other organic conducting systems, was also discovered for $x = 0.1–0.2$ and $y = 1.0$. It is very interesting that the magnetic susceptibility of λ-$BETS_2Fe_xGa_{1-x}BrCl_3$ shows a clear antiferromagnetic behavior even when Fe-content is very small ($x = 0.1–0.2$). The unique electric and magnetic properties reported in this paper will give a clue to clarify the role of the π-d interaction in magnetic organic superconductors.

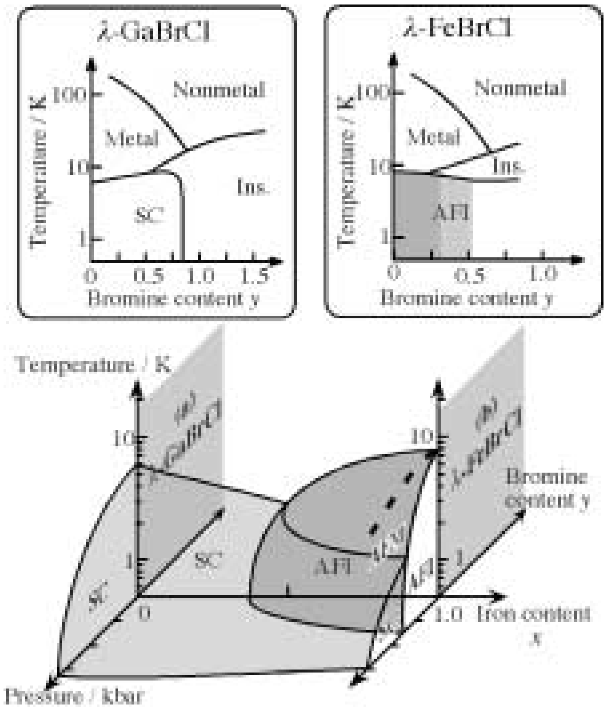

Figure 1. *P-T-x* phase diagrams of λ-BETS$_2$Fe$_x$Ga$_{1-x}$Cl$_4$ and *T-y* phase diagrams of λ-BETS$_2$MBr$_y$Cl$_{4-y}$ (M = Fe, Ga).

IV-D-3 Fermi Surface and Phase Transition in Magnetic Field Parallel to the Conducting Plane in λ-(BETS)$_2$FeCl$_4$

UJI, Shinya[1]; SHINAGAWA, Hideyuki[1]; TANAKA, Hisashi; KOBAYASHI, Hayao; TOKUMOTO, Madoka[2]; KOBAYASHI, Akiko[3]
([1]Natl. Res. Inst. Met.; [2]Electrotech. Lab.; [3]Univ. Tokyo)

λ-(BETS)$_2$FeCl$_4$ is a very unique magnetic organic conductor having antiferromagnetic insulating ground state and exhibiting a field-restored metallic state at ambient pressure and a pressure-induced superconductivity. Shubnikov de-Haas and angular dependent magneto-resistance oscillation (AMRO) experiments were performed to study the Fermi surface. The SdH oscillations were ascribed to the two external cross sectional areas of corrugated two-dimensional Fermi surface. The cross sectional areas are estimated to be 15% and 19% of the first Brillouin zone. These results are consistent with that obtained from the AMRO measurements (17%) and also with the simple extended Hückel tight-binding band calculation reported before (see Figure 1). The resistance gradually decreases above 17 T and then becomes negligible above 19 T under magnetic fields along the direction parallel to the conduction plane. The behavior is associated with change in the magnetic torque. The results show that a phase transition is present around 18 T.

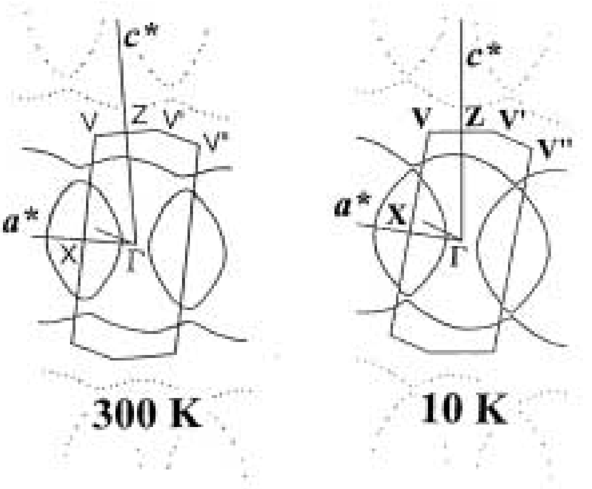

Figure 1. Cross section of calculated two-dimensional Fermi surface of λ-(BETS)$_2$FeCl$_4$.

IV-D-4 Anisotropy of Magnetic Suscepotibilities of λ-(BETS)$_2$FeBr$_x$Cl$_{4-x}$

KOBAYASHI, Hayao; FUJIWARA, Emiko; FUJIWARA, Hideki; TANAKA, Hisashi; KOBAYASHI, Akiko[1]
([1]Univ. Tokyo)

Owing to π-d coupling and strong electron correlation of π electron system, λ-(BETS)$_2$FeCl$_4$ takes many interesting phases such as antiferromagnetic insulating phase and field-induced ferromagnetic metal phase above 11 T. We have previously reported that the easy axis of the π-d coupled antiferromagnetic spin structure is approxomately paralell to the needle axis of the crystal, that is the *c* axis. But recently precise torque measurements by Sasaki and Toyota suggested that the easy axis fairly diviates from the *c* axis. In order to confirm this, we measured magnetization by rotating one single crystal in SQUID magnetometer. As shown in Figure 1, the susceptibilities showed that the easy axis deviates from the needle axis by about 35°. The angular dependence of the magnetization of single crystal was made also on the Br-containing system λ-(BETS)$_2$FeBr$_{0.6}$Cl$_{3.4}$. The rotation of the easy axis by the Cl → Br exchange, which was previousely reported, was confirmed.

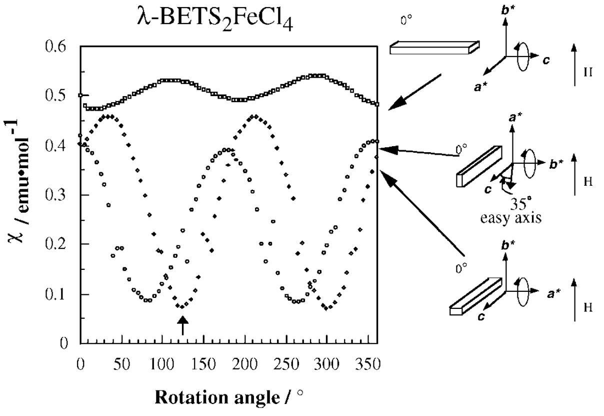

Figure 1. The angular dependence of the susceptibility of λ-(BETS)$_2$FeCl$_4$.

IV-D-5 A Novel Antiferromagnetic Organic Superconductor κ-$(BETS)_2FeBr_4$ [where BETS = Bis(ethylenedithio)tetraselenafulvalene]

FUJIWARA, Hideki; FUJIWARA, Emiko; NAKAZAWA, Yasuhiro; NARYMBETOV, Bakhyt Zh.; KATO, Kiyonori; KOBAYASHI, Hayao; KOBAYASHI, Akiko[1]; TOKUMOTO, Madoka[2]; CASSOUX, Patrick[3]
([1]Univ. Tokyo; [2]IMS and Electrotech. Lab.; [3]CNRS)

The electrical and magnetic properties of κ-$(BETS)_2FeBr_4$ salt showed that this system is the first antiferromagnetic organic metal at ambient pressure (T_N = 2.5 K). The characteristic field dependence of the magnetization at 2.0 K indicates a clear metamagnetic behavior. The small resistivity drop observed at T_N clearly shows the existence of the interaction between π metal electrons and localized magnetic moments of Fe^{3+} ions. In addition, this system underwent a superconducting transition at 1.1 K. The magnetic field dependence of the superconducting critical temperature cleared that the superconductivity in this system is strongly anisotropic also in the conduction plane because of the existence of the metamagnetically induced internal field based on the antiferromagnetic ordering of the Fe^{3+} 3d spins in contrast to the cases of the other conventional organic superconductors. Furthermore, the specific heat measurement exhibited a λ-type large peak corresponding to the three-dimensional antiferromagnetic ordering of high-spin Fe^{3+} ions. The lack of distinct anomaly in the C_p *vs.* T curve at T_c strongly suggests the coexistence of the superconductivity and the antiferromagnetic order below T_c.

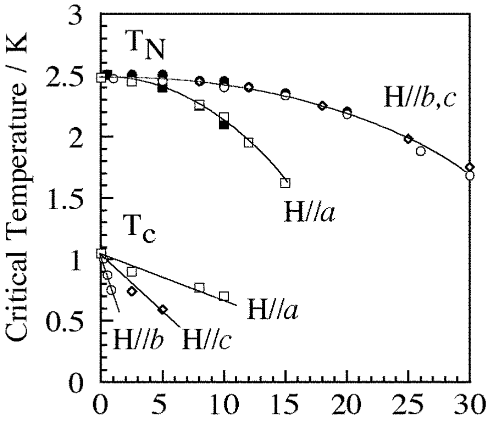

Figure 1. The H-T plots of the Néel temperatures (T_N) and the superconducting transition temperatures (T_c) under the magnetic fields applied along the three axes (squares; *a*-axis, circles; *b*-axis and triangles; *c*-axis) determined by electrical resistivity measurements (opened symbols) and SQUID measurements (closed symbols).

IV-D-6 The *x*-Dependence of Electrical Properties and Antiferromagnetic Ordering between Fe^{3+} Ions in κ-$BETS_2FeCl_xBr_{4-x}$ System

FUJIWARA, Emiko; FUJIWARA, Hideki; KATO, Kiyonori; KOBAYASHI, Hayao; OTSUKA, Takeo[1]; KOBAYASHI, Akiko[1]
(1Univ. Tokyo)

The magnetic and electrical properties of κ-$BETS_2FeCl_xBr_{4-x}$ (x = 0.1, 0.5, 1.2, 2.0, 2.3, 3.0, 3.4 and 4.0) were examined to check the possibility of the antiferromagnetic ordering of Fe^{3+} spins and/or the possibility of superconductivity of π electron system. The temperature dependence of the magnetic susceptibility and the field (H) dependence of the magnetization (M) of κ-$BETS_2FeCl_xBr_{4-x}$ at 2 K revealed that the Néel temperature shifts to lower temperature with the increase of chlorine contents. Moreover, the rotation of easy spin axis from the direction parallel to the crystal plane to the direction approximately perpendicular to the crystal plane was observed. The temperature corresponding to the small resistivity drop, which is in good agreement with the Néel temperature, shifts to lower temperature with the increase of the chlorine contents. On the other hand, the critical temperature of superconductivity shifts to lower temperature quickly with the increase of the chlorine contents (T_c = 0.7 K for x = 0.1).

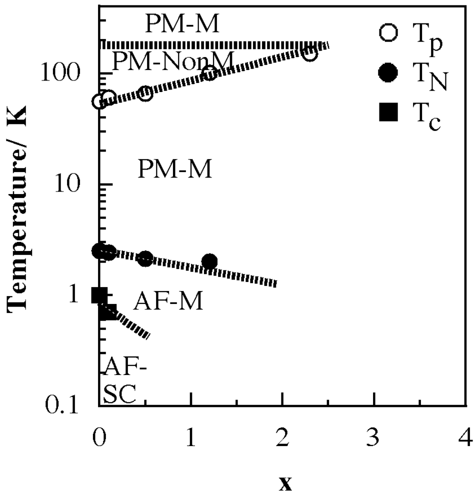

Figure 1. T-x phase diagram of κ-$BETS_2FeCl_xBr_{4-x}$. The temperature of resistivity peak (T_p) are opened circles (○), Néel temperature (T_N) are filled circles (●) and superconducting transition temperature (T_c) are filled squares (■).

IV-D-7 Successive Antiferromagnetic and Superconducting Transition in an Organic Metal, κ-$(BETS)_2FeCl_4$

OTSUKA, Takeo[1]; KOBAYASHI, Akiko[1]; MIYAMOTO, Yasuhisa; WADA, Nobuo; FUJIWARA, Emiko; FUJIWARA, Hideki; KATO, Kiyonori; KOBAYASHI, Hayao
([1]Univ. Tokyo)

[*Chem. Lett.* 732 (2000)]

We have previously reported the crystal structures and electrical properties of κ-$(BETS)_2FeX_4$ (X = Cl, Br) systems. Unlike κ-$(BETS)_2FeBr_4$ exhibiting anomalous resistivity peak around 60 K, κ-$(BETS)_2FeCl_4$ shows a nomal metallic behavior down to 2 K. Recently we have found κ-$(BETS)_2FeBr_4$ to be the first antiferromagnetic organic superconductor, which undergoes an antiferromagnetic transition at 2.5 K (T_N) and a superconducting transition at 1.1 K (T_c). A step-like resistivity anomaly at T_N gave the first direct evidence for π-d interaction between π metal electrons and localized magnetic moments in the anion sites. Since the magnitude of π-d interaction is considered to be strongly dependent on the energy level of p orbitals of halogen atoms of the anion, it may be of interest to examine precisely the susceptibility of κ-$(BETS)_2FeCl_4$. The *ac* magnetic susceptibility of κ-$(BETS)_2FeCl_4$ down to 60 mK revealed the successive phase transitions from paramagnetic metal to metallic antiferromagnet and then to superconductor which correspond to the similar transitions observed in Br-analogue λ-$(BETS)_2FeBr_4$. But the transtion temperatures are significantly lowered (T_N = 0.6 K, T_c = 0.1 K).

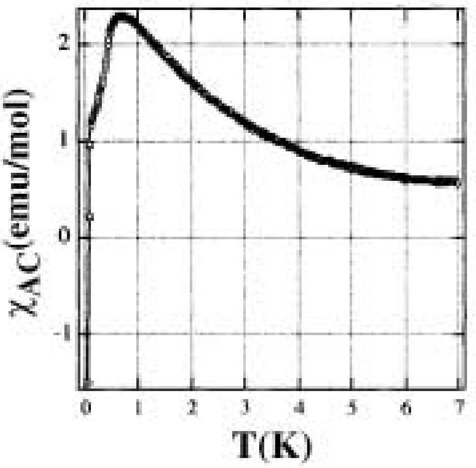

Figure 1. The temperature dependence of *ac*-magnetic susceptibility for κ-$(BETS)_2FeCl_4$ (polycrystalline sample).

IV-E Structural and Electrical Properties of Molecular Crystals at Low Temperature and/or High Pressure

Since the molecular crystal is very soft and rich in the structural freedom, various structural phase transitions are expected at high pressure and/or low temperature. Therefore the precise three-dimensional X-ray structure analyses at high pressure and/or low temperature are very important in the studies of solid state physics and chemistry of molecular crystals. We have examined low-temperature structures of some molecular crystals including C_{60} molecular magnet by using low-temperature imaging plate system equipped with liquid He refrigerator. As for the structural studies at high pressure, we have continued to examine the crystal structure of molecular superconductor α-$[(CH_3)_2(C_2H_5)_2N][Pd(dmit)_2]_2$ exhibiting a superconductivity at 2–6 kbar. We have measured the high-pressure resistivity of $(TMTTF)_2PF_6$, the sulfur-analog of the first organic superconductor $(TMTSF)_2PF_6$ and found the superconducting transition around 52 kbar for the first time. Furthermore, we have recently succeeded to measure the resistivity of organic single crystal up to 150 kbar.

IV-E-1 Origin of Ferromagnetic Exchange Interactions in a Fullerene-Organic Compound

NARYMBETOV, Bakhyt Zh.; OMERZU, Ales[1]; TOKUMOTO, Madoka[2]; KOBAYASHI, Hayao; MIHAILOVIC, Dragan[1]
([1]Jozef Stefan Inst., Slovenia; [2]Electrotech. Lab.)

[*Nature* **407**, 883 (2000)]

Almost a decade ago, the ferromagnetism of TDAE*C_{60} (TDAE = tetrakis(di-methylamino)ethylene, T_c = 16 K) was reported but the origin of ferromagnetic properties of this compound has still remained mysterious. Inspite of serious efforts by many research groups and suggestion that the orientaions of C_{60} molecules may be important, in the absence of structural data at low temperatures there has been little progress in the understanding of the microscopic interactions which lead to this unusual phenomenon. To resolve this problem we have performed a comparative structural study of the two different magnetic forms of TDAE–C_{60} crysyals at low temperature. Identifying the relative orientations of C_{60} molecules as the primary variable controling the ferromagnetic order parameter, we show that both Ferromagnetic and low-temperature spin-glass-like ordering are possible in this materrial, depending on the degree of disorder.

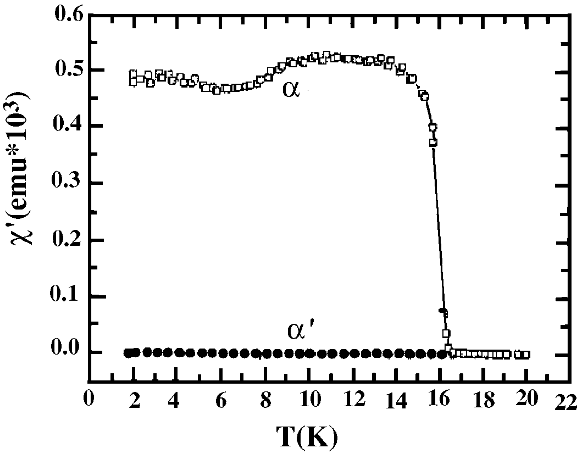

Figure 1. The *ac* susceptibility χ of paramagnetic (α') and ferromagnetic (α) sample of C_{60}*TDAE.

IV-E-2 Low temperature X-ray Crystal Structure Determination of α-(BEDT–TTF)$_2$I$_3$—Stripe-Like Charge Distribution at Low Temperature

TAMURA, Itaru; KOBAYASHI, Hayao; INOKUCHI, Makoto[1]; KOBAYASHI, Akiko[2]
([1]Sci. Univ. Tokyo in Yamaguchi; [2]Univ. Tokyo)

α-(BEDT–TTF)$_2$I$_3$ is a well-known organic conductor, exhibiting a M-I transition around 135 K. Recently, the charge distribution in this compound at low temperature was investigated both theoretically and experimentally. With the aim of determining the charge distribution in this system, we performed X-ray diffraction experiments at various temperature. The reliability factor of the structure analyses (*R*) in the metallic phase was about 3% where the space group P1- was adopted. The structure analyses at 125 K and at 100K (the insulator phase) were also successfully made on the basis of the space group P1- (R ≈ 3%). However, *R*-values of the structure analyses below 75 K were higher than 6%. These results suggest the loss of inversion symmetry, in other words, the change of charge distribution at low temperature. Thus we repeated the structure analyses based on the space group P1. *R*-factor became about 3%. Figure 1 shows the temperature dependence of charges of crystallography-cally independent BEDT-TTF molecules estimated by using the emprical relation between bond lengths and the charge of BEDT-TTF molecule. The charges of molecule A and C were increased below 75 K, indicating the development of stripe-like charge distribution at low temperature.

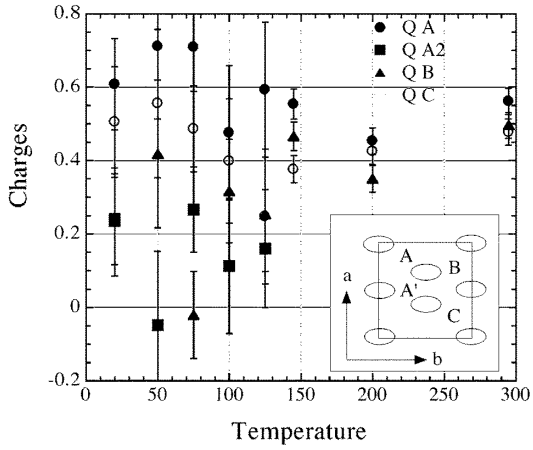

Figure 1. Temperature dependence of charge of BEDT–TTF. The inset is the schematic draw of the molecular arrangement. Molecules A and A' were related to each other by inversion symmetry in the metallic phase.

IV-E-3 Crystal and Band Structure Examinations of High-Pressure Molecular Superconductor [(C$_2$H$_5$)$_2$(CH$_3$)$_2$N][Pd(dmit)$_2$]$_2$ at 10 kbar

ADACHI, Takafumi; NARYMBETOV, Bakhyt Zh.; KOBAYASHI, Hayao; KOBAYASHI, Akiko[1]
([1]Univ. Tokyo)

Based on the X-ray intensity data collected by diamond anvil cell specially designed to reduce the background X-ray diffraction from the high-pressure cell, the crystal structure of [(CH$_3$)$_2$(C$_2$H$_5$)$_2$N]-[Pd(dmit)$_2$]$_2$ was determined at 10 kbar to see the origin of the peculiar *P–T* phase diagram of this molecular superconductor where the insulating phase appears at the high-pressure side of the superconducting phase. We have previousely proposed a pressure-induced HOMO-LUMO "re-inversion" mechanism to explain this *P–T* phase diagram. However, it was revealed that the lattice constants is doubled along the stacking direction of Pd(dmit)$_2$ molecues above 8 kbar. This structure change is associated with the pressure-induced disorder-order transition of (CH$_3$)$_2$(C$_2$H$_5$)$_2$N. The possibility of the pressure-induced HOMO-LUMO re-inversion was ruled out by the simple tight-binding band calculation based on the crystal structure determined at high pressure.

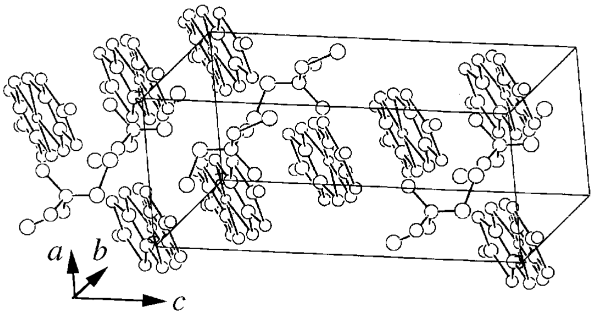

Figure 1. The crystal structure of [(CH$_3$)$_2$(C$_2$H$_5$)$_2$N]-[Pd(dmit)$_2$]$_2$ at 10 kbar.

IV-E-4 Superconducting Transition of (TMTTF)$_2$PF$_6$ above 50 kbar [TMTTF = Tetramethyltetrathiafulvalene]

ADACHI, Takafumi[1]; FUJIWARA, Emiko; KATO, Kiyonori; KOBAYASHI, Hayao; MIYAZAKI, Takafumi[2]; TOKUMOTO, Madoka[3]; KOBAYASHI, Akiko[4]
([1]IMS and Electrotech. Lab.; [2]Ehime Univ.; [3]Eletrotech. Lab.; [4]Univ. Tokyo)

[*J. Am. Chem. Soc.* **122**, 3238 (2000)]

Two decades passed since the discovery of the first organic superconductor (TMTSF)$_2$PF$_6$. However, there are many physicists and chemists who still regard TMTSF superconductor (Bechgaard salt) to be the most attractive organic conductor. Besides the superconductivity, this system exhibits novel transport phenomena related to the spin density wave (SDW) instability originated from one-dimensional nature of the electronic structure. Almost a decade ago, the generalised pressure-temperature (*P–T*) phase diagram was proposed, where all the Bechgaard salts including isostructural sulphur analogues ((TMTTF)$_2$X (X = PF$_6$, AsF$_6$, ClO$_4$...) were located. This diagram tells us that (TMTTF)$_2$Br and (TMTTF)$_2$PF$_6$ become superconductors by applying 25 kbar and 35 kbar, respectively. In fact, the superconductivity of (TMTTF)$_2$Br was discovered in 1994 (T_c = 0.8 K at 26 kbar). However, there have been no "TM$_2$X systems" whose superconductivities were confirmed in both Se- and S-analogues. We have recently succeeded to improve the technique of diamond anvil four-probe resistivity measurements and obtained the resistivity of an organic single crystal up to 150 kbar. In the course of these studies, we have found the superconducting transition of $(TMTTF)_2PF_6$ above 52 kbar.

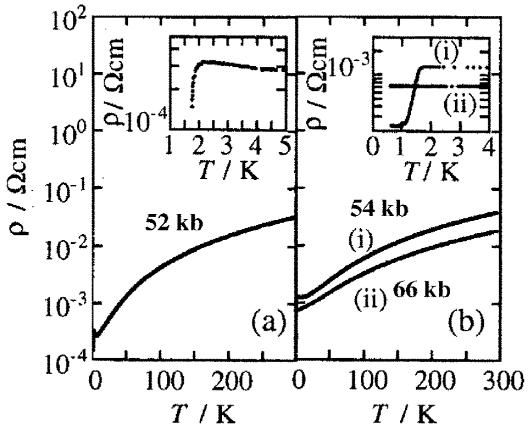

Figure 1. Resistivity of $(TMTTF)_2PF_6$ at high pressure.

IV-E-5 Electrical Resistivity Measurements of Organic Single Crystals by Diamond Anvil Cell up to 15 GPa

ADACHI, Takafumi; TANAKA, Hisashi; KOBAYASHI, Hayao; MIYAZAKI, Takafumi[1]
([1]Ehime Univ.)

At present, diamond anvil is used for very wide purpose in various high pressure experiments including resistivity measurements. In order to obtain reliable resistivity data, we must adopt the four-probe method. Since the first diamond anvil four-probe resistivity measurements by Mao and Bell, many trials have been made. However these methods seem to be inapplicable to soft organic materials. In 1985, Tozer and King reported the four-probe resistivity measurements on organic single crystal under 7.5 GPa. We have recently succeeded to obtain the accurate resistivity data of organic single crystal up to 15 GPa. The diamond anvil cell was the essentially the same to that designed by Takemura more than 20 years ago. The size of the needle-shaped single crystal was about 0.25 mm in length. Inconel T301 was used as a gasket and annealed gold wires were used as leads, which were fixed to the single crystal by gold paints. An example of the pressure dependence of the resistivity is given in Figure 1.

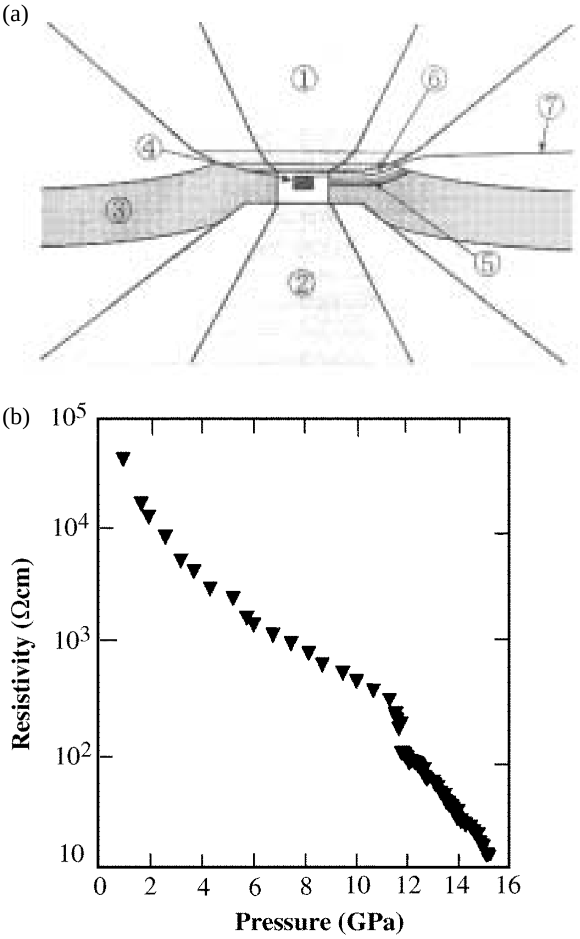

Figure. 1. (a) Schematic drawing of sectional view around the sample. (b) Pressure dependence of the resistivity of the crystal of TMTTeN.

IV-F Development of New Functional Molecular Materials

Molecule can be regarded as the smallest nano-system where various functions can be assembled. The development of new molecules will be the most important driving force for further development of materials chemistry. Although the development of fruitful systems has been still continued in the field of molecular metals, we have to grow out of the conventional molecular conductors. Two main targets of our present stuies are (1) molecular metals and superconductors composed of single-component molecules and (2) pure organic magnetic metals. Very recently, we have succeeded to prepare the first single-component molecular metal. Based on the idea on the construction of metal band by using multi-sulfur planar π molecules developed by us in 1980s, the neutral Ni complex molecules having extended TTF-ligands were synthesized. Very simple crystal structure, closely packed molecular arrangement and metallic behavior of this system show that the boundary between “molecular crystal” and “metallic crystal” was removed by this finding.

IV-F-1 A Three-Dimensional Synthetic Metallic Crystal Composed of Single Component Molecules

TANAKA, Hisashi; OKANO, Yoshinori; KOBAYASHI, Hayao; SUZUKI, Wakako[1]; KOBAYASHI, Akiko[1]

([1]Univ. Tokyo)

[*Science* **291**, 285 (2001)]

Since the discoveries of semiconducting properties of phthalocyanine and condensed aromatic hydrocarbons around 1950 and the discoveries of one-dimensional molecular metals around 1970, many chemists have dreamed to design single-component and/or three-dimensional molecular metals composed of planar molecules. Especially, the design of single component molecular metal had been one of the final goals of the chemists in this field. Although three-dimensional metals and superconductors have been already realized by the discoveries of alkali-metal C_{60} complexes around 1990, the single component molecular metals remained to be developed up to 2000. Preparation, crystal structure analysis and resistivity measurements of the crystal of [Ni(tmdt)$_2$] (tmdt = trimethylenetetrathiafulvalenedithiolate) molecule revealed that the first metallic crystal composed of single component molecules was discovered. [Ni(tmdt)$_2$] crystal retained metallic state down to 0.6 K. The compact three-dimensional molecular arrangement and the tight-binding electronic band structure calculation showed the system to be not only the first single-component molecular metal but also the first three-dimensional synthetic metal composed of planar molecules.

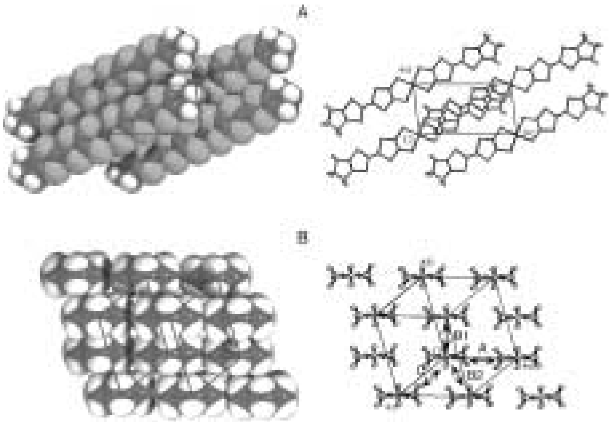

Fugure 1. The crystal structure of [Ni(tmdt)$_2$].

IV-F-2 Development of Single-Component Molecular Metals Based on Transition Metal Complexes with Extended-TTF Dithiolate Ligands

TANAKA, Hisashi; KOBAYASHI, Hayao; KOBAYASHI, Akiko[1]
([1]Univ. Tokyo)

Novel molecular conductors composed of neutral transition metal complex molecules with extended TTF-like ligands, ptdt, dmdt and tmdt were developed (M= Ni, Pd, Pt, Cu, Co, Au; ptdt = propylenedithiotetrathiafulvalenedithiolate, dmdt = dimethyltetrathiafulvalene-dithiolate and tmdt = trimethylenetetrathiafulvalenedithiolate). These molecules have extended π conjugated systems. The synthetic works were made under strictly inert atomsphere because these metal complexes were very sensitive to oxygen. By electrochemical oxidation, black microcrystals of the neutral complexes were obtained, which showed very high conductivities (compaction pellet): [Ni(dmdt)$_2$], 200–400 Scm^{-1}; [Pd(dmdt)$_2$], 100 Scm^{-1}; [Co(dmdt)$_2$], 1–2 Scm^{-1}. The molecular conformations and magnetic properties were revealed to be dependent on the central metal atoms.

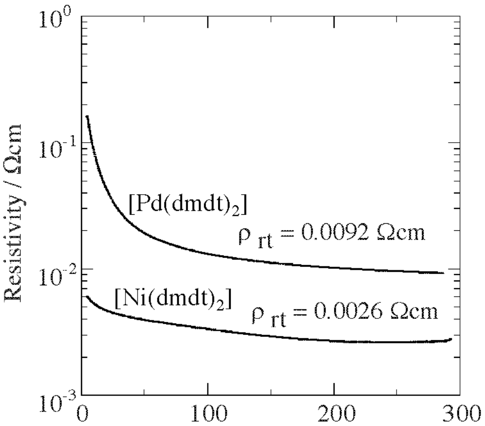

Figure 1. Temperature dependence of the resistivities of [M(dmdt)$_2$] (M = Ni, Pd) (compaction pellet).

IV-F-3 Synthesis and Properties of a New Organic Donor Containing a TEMPO Radical

FUJIWARA, Hideki; FUJIWARA, Emiko; KOBAYASHI, Hayao

In the course of the development of new types of organic conductors, the interests have been focused on the molecular conductors and superconductors containing magnetic transition metal anions for the investigation of the interplay between the conductivity and magnetism. On the other hand, several attempts have been performed using donors containing a stable TEMPO or NN radical to investigate the interaction between conduction electrons of the charge-transfer complex and localized spins of the organic stable radical parts for the development of novel organic conducting-magnetic multifunctional materials and organic ferromagnetic metals. Among them, very recently we have synthesized a new donor containing a TEMPO radical, TEMPOET, and investigated the physical properties of its cation radical salts. Herein we report the synthesis and physical properties of a new TEMPO-containing electron donor **1** in which a TEMPO radical part connects to the EDT–TTF skeleton through a pyrrolidine ring. The ESR spectra of **1** indicated three absorption lines (g =2.0062, aN = 15.5 G) characteristic of TEMPO radical. The donor **1** is paramagnetic and showed antiferromagnetic interaction at low temperature region (θ = –2.4 K). The CV measurement revealed **1** shows two pairs of reversible redox waves (+0.48 and +0.86 V *vs.* Ag/AgCl) and one oxidation wave (+0.83 V).

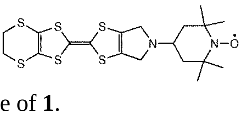

Figure 1. Structure of **1**.

IV-F-4 Synthesis, Structures and Properties of an New TSeF Derivative Containing Pyrazino-Ring and Its Cation Radical Salts

FUJIWARA, Emiko[1]; FUJIWARA, Hideki; KOBAYASHI, Hayao; TOKUMOTO, Madoka[1]; KOBAYASHI, Akiko[2]
([1]IMS and Electrotech. Lab.; [2]Univ. Tokyo)

In the search for new molecular conductors, enhancement of the intermolecular interaction by the condensation of hetero ring and the substitution of chalcogen atoms is considered to be very important to realize two-dimensional metals. From this viewpoint, we had synthesized a novel unsymmetrical donor containing pyrazino-ring: PEDTTSeF and reported the crystal structures and physical properties of its cation radical salts. Several of them showed metallic conducting behavior down to low temperatures due to their interesting zig-zag β”-type two-dimensional donor arrangements and strong side-by-side interaction between the chalcogen atoms and nitrogen atoms. We have also synthesized the other novel TSeF derivative containing pyrazino-ring: pyrazino–TSeF. The donor shows two pairs of reversible redox waves (+0.79 and 1.14 V *vs.* Ag/AgCl in PhCN). The oxidation potentials are slightly positively shifted compared with those of BETS (+0.70 and +0.97 V) under identical conditions. According to the crystal structure analysis, the stoichiometry of the ClO_4^- salt was determined to be 1:1 (D:A) (Figure 1). The cation radical salts were prepared by electrolytic oxidation. The ClO_4^- and PF_6^- salts are semiconductors, due to a 1:1 stoichiometry at least in respect of the ClO_4^- salt.

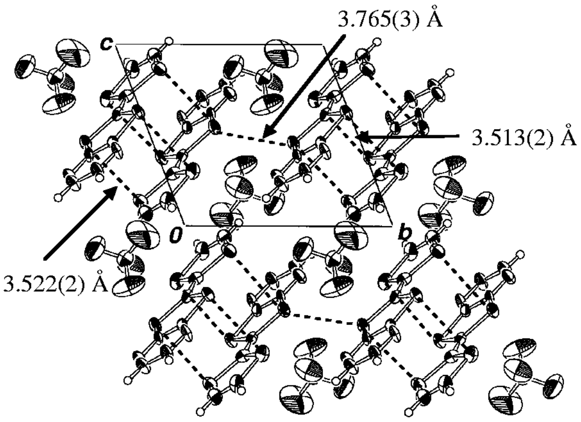

Figure 1. Crystal structure of the ClO_4^- salt of pyrazino–TSeF.

IV-G Electrical Properties of Organic Semiconductors in Ultrahigh Vacuum

The mechanism of carrier transport in organic semiconductors and carrier injection from metal electrodes becomes the most important subject to be elucidated for high performance organic thin film devices. The electrical properties are modified easily by adsorbed gas molecules, which makes it difficult to obtain reliable experimental results. We have studied intrinsic properties under ultrahigh vacuum conditions to strip away the veil of oxygen.

IV-G-1 Quasi-Intrinsic Semiconducting State of Titanyl-phthalocyanine Films Obtained under Ultrahigh Vacuum Conditions

TADA, Hirokazu; TOUDA, Hiroshi[1]; TAKADA, Masaki[1]; MATSUSHIGE, Kazumi[1]
([1]Kyoto Univ.)

[*Appl. Phys. Lett.* **76**, 873 (2000)]

We investigated eectrical properties of titanyl-phthalocyanine (TiOPc) films under ultrahigh vacuum (UHV) conditions to avoid the influence of gas adsorption. The field-effect measurement revealed that TiOPc films exhibited an n-type semiconducting behavior in UHV. The electron mobility at room temperature was 9×10^{-6} $cm^2V^{-1}s^{-1}$ with activation energy of 0.20 eV. The conductivity and carrier density were 9×10^{-8} Scm^{-1} and 6×10^{16} cm^{-3}, respectively. A clear conversion from n-type to p-type behavior was observed when the film was exposed to oxygen. Strict control of atmosphere made it possible to obtain a quasi-intrinsic state where both p- and n-type conductions appeared simultaneously (Figure 1).

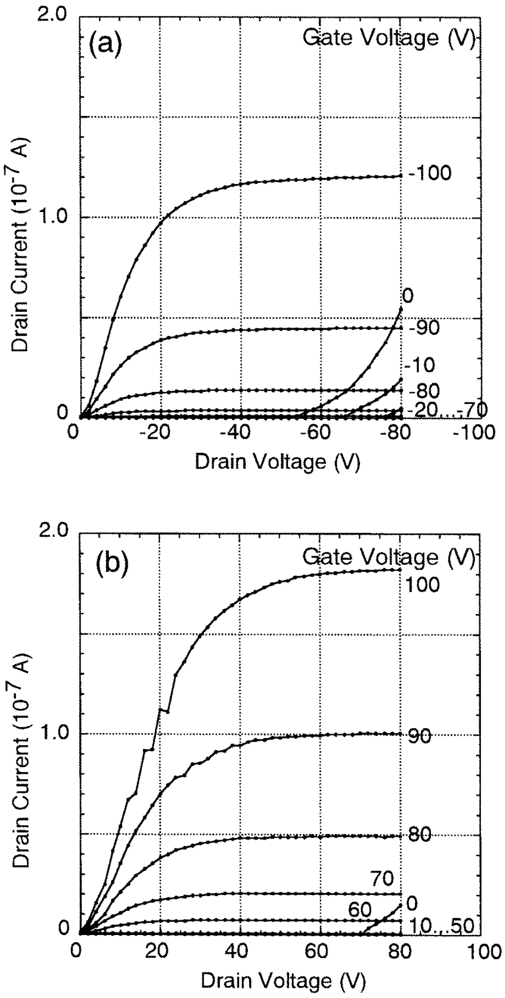

Figure 1. Field-effect transistor characteristics of a TiOPc film measured in a well-controlled atmosphere. Both (a) p-type and (b) n-type conductions appeared simultaneously.

IV-H Preparation and Characterization of Highly Oriented Organic Films

Preparation of ordered and highly-oriented films of organic materials is one of the most promissing way not only to improve the characteristics of organic opto-electronic devices such as light emitting diodes, chemical sensors and field effect transistors, but also to study the mechanism of carrier transport and energy transfer in molecular systems. We have established the method of preparation of highly-oriented films on various substrates and studied the correlation between film strcture and optical and electrical properies.

IV-H-1 Substrate-Induced Order and Multilayer Epitaxial Growth of Substituted Phthalocyanine Thin Films

SCHLETTWEIN, Derck[1]; TADA, Hirokazu; MASHIKO, Shinro[2]
([1]Bremen Univ.; [2]CRL)

[*Langmuir* **2000**, 2872 (2000)]

Thin films of hexadecafluorophthalocyaninatooxovanadium ($F_{16}PcVO$) are vapor-deposited under organic molecular beam epitaxy (OMBE) conditions on the (100) surfaces of NaCl, KCl, and KBr and on quartz glass. Beginning at submonolayer coverages and extending to a film thickness of several tens of nanometers the film structure is determined in situ by reflection high energy electron diffraction (RHEED). Following deposition the film morphology is characterized by tapping mode atomic force microscopy (AFM) and chromophore coupling of the molecules within the films is studied by optical absorption spectroscopy. Highly ordered growth of crystalline domains of $F_{16}PcVO$ with dimensions in the micrometer range leading to films of quite uniform thickness is observed. On KBr a commensurate square lattice is seen in RHEED of the first monolayers with the molecules parallel to the substrate surface which is also preserved at higher film thickness. On KCl a surface lattice of the same size is formed which is, however, understood as a result of point-on-line coincidence. Diffraction of transmitted electrons yield a constant three-dimensional crystal structure of the films on KBr and KCl with a tetragonal unit cell of $a = b = 1.47$ nm and $c = 0.62$ nm. On NaCl with its smaller lattice constant no ordered relative orientation is possible and hence an increased part of the film appears amorphous. On quartz glass on the other hand, ordered films are formed with the molecular plane predominantly oriented cofacially parallel to each other and vertical to the surface. Calculations of molecular mechanics as well as of periodic surface potentials are performed to support the proposed structures and to discuss the crystallization in thin films of phthalocyanines and related materials.

IV-H-2 Ordered Growth of Substituted Phthalocyanine Thin Films: Hexadecafluorophthalocyaninatozinc on Alkali Halide (100) and Microstructured Si Surfaces

SCHLETTWEIN, Derck[1]; HESSE, Karsten[1]; TADA, Hirokazu; MASHIKO, Shinro[2]; STORM, Uwe[1]; BINDER, Joseph[1]
([1]Bremen Univ.; [2]CRL)

[*Chem. Mater.* **2000**, 989 (2000)]

Physical vapor deposition of hexadecafluorophthalocyaninatozinc ($F_{16}PcZn$) is performed under UHV conditions from monolayer coverages to an average thickness of about 20 nm on the (100) surfaces of NaCl, KCl, and KBr and on quartz glass as well as on microstructured interdigitated electrode arrays on amorphous SiO_2. UV-vis absorption spectroscopy indicates stacks of cofacial parallel molecules for thin films on SiO_2 and NaCl, whereas a component typical for a head-to-tail arrangement of molecules is detected on KCl and KBr. Atomic force microscopy shows well-defined crystals oriented in a defined azimuth angle relative to the substrate lattice on KCl and KBr, indicating a growth in molecular square lattices parallel to the substrate surface which is confirmed by molecular mechanics and periodic surface potential calculations. Plateaus of molecules predominantly standing upright on the surface are seen for the films on NaCl and SiO_2 which is confirmed by the relative intensity of optical absorptions and by the electrical conductivity changes observed during growth on SiO_2. The temperature dependence of the electrical conductivity of films on SiO_2 yields an increase of the thermal activation energy around 200 °C corresponding to a loss in spectral fine structure. A clear correlation is seen between film structure and electrical as well as optical properties of molecular semiconductor thin films.

IV-H-3 Energy Transfer in Highly Oriented Permethyl-Dodecasilane and -Octadecasilane Films

TADA, Hirokazu; TOJO, Tomoaki[1]; KAKO, Masahiro[2]; NAKADAIRA, Yasuhiro[2]; MATSUSHIGE, Kazumi[1]
([1]Kyoto Univ.; [2]Univ. Electro-Commun.)

[*J. Organomet. Chem.* **611**, 85 (2000)]

Heterostructured films of permethyl-dodecasilan (DM12) and permethyl-octadecasilane (DM18) were prepared on silicon and fused quartz plates under ultrahigh vacuum conditions and the films were characterized by optical absorption and photoluminescence spectroscopy, and atomic force microscopy. The molecules were found to form highly oriented films in a layer-by-layer growth mode with their molecular chains perpendicular to the substrate surface. Moreover it was found on the basis of optical measurement that the energy transfer progressed effectively from the optically excited state of DM12 generated by the σ-σ^* one-electron transition to that of DM18 through the interface between the layers.

IV-I Properties of Gas Adsorption on Single-Walled Carbon Nanotube Aggregates

The discovery and bulk synthesis of single-walled carbon nanotubes (SWNTs) has stimulated great interest as a material of a novel nano-scale electronic devices owing to their unique structure. On the other hand, another intrigunging property of SWNTs aggregates is gas adsorption due to the nature with particularly high surface to volume ratio and correpondingly high coverage. It is well known that actual SWNT aggregates form crystalline bundles arrenged in triangular lattices with a lattice constant of 1.7 nm. If we assume that the diameter of tube is 1.3 nm, two kinds of cylindrical micropores must be exist: one is the intra-tube pore with the diameter about 0.9 nm, and interstitial pore between the tubes (inter-tube pore) with that about 0.3 nm. However, as grown SWNTs are known to be capped at the ends. Cutting is needed to open the capped ends and to enable gas to adsorb in intra-tube pore. The properties of gas adsorption on micropores in SWNTs were studied in this project. ^{129}Xe-NMR were performed for xenon gas adsorbed SWNTs samples both before and after heat treatment. Several kinds of gas adsorption isotherm measurements were also performed for both end-closed (capped) and end-opened (uncapped) SWNTs.

IV-I-1 Properties of Micropores in Single-Walled Carbon Nanotubes Studied by N_2 Gas Adsorption Isotherm Measurements

OGATA, Hironori; KUNO, Shogo[1]; SAITO, Yahachi[1]
([1]Mie Univ.)

The effects of heat treatments on the property of micropores have been studied on SWNTs by means of the N_2 adsorption isotherm measurements. SWNT samples used in this study were synthesized by the dc arc discharge method using non-ferromagnetic Pt-Rh mixed catalyst. Amorphous carbon and nano-graphite particles contained in the raw soots obtained were removed by modified Tohji's procedure using hydrogen peroxide (H_2O_2), as follows: (1) The raw soots was heated at 100 °C for 10 hours in 20% H_2O_2 solution in a flask with reflux attachment to oxidize only the amorphous carbon uniformly. (2) The residual soots were added distilled water and was sonicated for 3 hours and collect the precipitate after leaveing it for 12 hours to separate SWNTs and nano-graphite particles. Procedures (1)–(2) were repeated several times. The purification procedure was monitered and the purity of SWNTs were checked by both Scanning Electron Microscope and Powder X-ray diffraction measurements. The heat treatments were performed at 420 °C for 20 minutes in the dried air. Figure 1 shows the adsorption isotherms of N_2 on the as-prepared (△), after H_2O_2-treated (●) and heat-treated (○) SWNTs at 77 K. The adsorption isotherms are close to type II, which include features of a type I due to micropore fillings. Most distinguished feature is the large increase of the amount of N_2 gas adsorbed at low p/p_0 region. The high resolution α_s-plot analysis revealed that the heat treatment increases the intensity of two upward swings (*f*- and *c*-swing) below $\alpha_s = 1.0$. This fact suggests that the heat treatment leads to the micropore filling and capillary-like condensation inside the tube space.

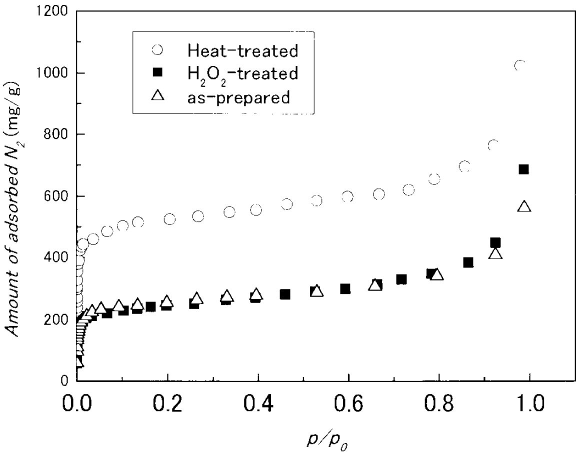

Figure 1. N_2 adsorption isotherms for SWNTs at 77 K.

IV-I-2 Direct Evidence of Xenon Gas Adsorption Inside of Snigle-Walled Carbon Nanotubes Studied by ^{129}Xe-NMR

OGATA, Hironori; KUNO, Shogo[1]; SAITO, Yahachi[1]
([1]Mie Univ.)

It is well known that ^{129}Xe-NMR of xenon gas adsorbed in confined pore is essential way to investigate the pore structure. The most distinctive advantage of this technique is to detect only xenon gas confined in uniform pore and by analyzing the value of ^{129}Xe chemical shift we can get the information about the size of the pore through the value of mean free path of xenon gas. Effects of heat treatments on the micropore structure of SWNTs were studied by ^{129}Xe-NMR for xenon gas adsorbed SWNTs samples. Figure 1 shows the ^{129}Xe-NMR spectra for the xenon gas adsorbed on SWNTs samples before and after treatments. The pressure of xenon gas adsorbed was about 15×10^4 Pa at 296 K for each samples. The reference signal for the chemical shift was set to that of xenon gas extrapolated at zero pressure. One sharp peak at about 1 ppm is contained in raw soots sample (a), which is attributed to be free xenon gas. Weak broad peak is added in soots after H_2O_2 treatment (b). This peak is strongly enhanced after heat treatment (c). Repititive heat treatment, however, decrease this peak intensity ((d): after two times' treatments, (e): after three times' treatments), which is casused by burning down the SWNTs. It was also confirmed by Raman scattering measurements. From the extrapolated value of the ^{129}Xe shift at zero pressure ($\delta(S)$ = 75 ppm) (Figure 2), we can conclude that the broad peak is attribute to the Xe gas confined inside the tube space.

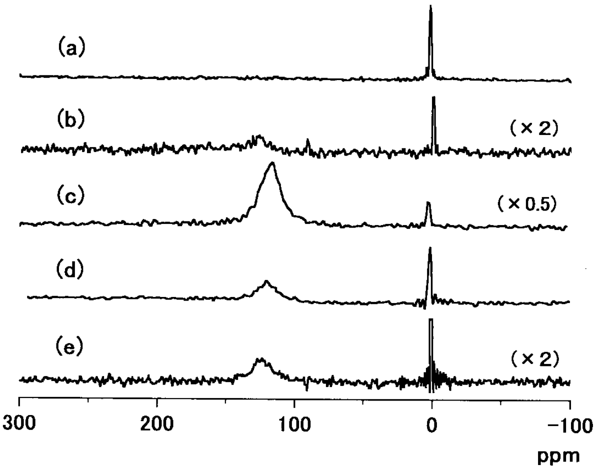

Figure 1. ^{129}Xe-NMR spectra for xenon gas adsorbed SWNTs after various treatments.

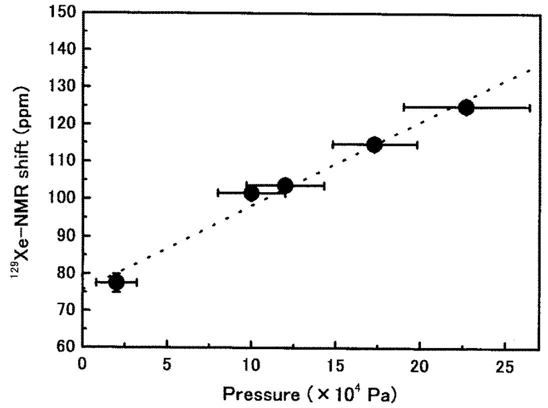

Figure 2. Pressure dependence of the xenon gas on ^{129}Xe-NMR shift for xenon gas adsorbed SWNTs.

IV-J Electronic Properties of Pristine and Doped Snigle-walled Carbon Nanotubes aggregates

^{13}C NMR and Raman scattering measurements were performed for both pristine and doped single-walled carbon nanotubes (SWNTs) aggregates to investigate the electronic structure below 100 K.

IV-J-1 Electronic States of Single-Walled Carbon Nanotube Aggregates Studied by Low Temperature ^{13}C-NMR

OGATA, Hironori; KUNO, Shogo[1]; SAITO, Yahachi[1]
([1]Mie Univ.)

^{13}C-NMR experiments have been carried out for single-walled carbon nanotubes aggregates (SWNTs), which were produced by using non-ferromagnetic Rh-Pt mixed catalysts. Hydrogen peroxide was used to remove amorphous carbon particles in the raw soot almost perfectly. Figure 1 shows the ^{13}C NMR spectrum measured at 10 K. From the line shape analysis, the ^{13}C spectrum is considered to be composed of two components with the shift tensors (δ_{11},δ_{22},δ_{33}) = (194,182,194) ppm and (203,180,52) ppm. To obtain more detailed information about the electronic state of SWNTs, we performed ^{13}C spin lattice relaxation time (T_1) measurement by the saturation-recovery method. The obtained saturation recovery curves could be fit with a double-exponential function: approximately one-third of the ^{13}C-nuclear spins relaxes much faster than the other two-thirds. Temperature dependence of ^{13}C-T_1 found that both components follow a Korringa-like behavior ($T_1 \times T$ = 3100 ± 500 (sec.K) and $T_1 \times T \fallingdotseq$ 12000 (sec.K)) in the temperature region between 4.2 K and 100 K. The fast-relaxing and slow relaxing components are thought to be associated with metallic and semiconducting SWNTs, respectively.

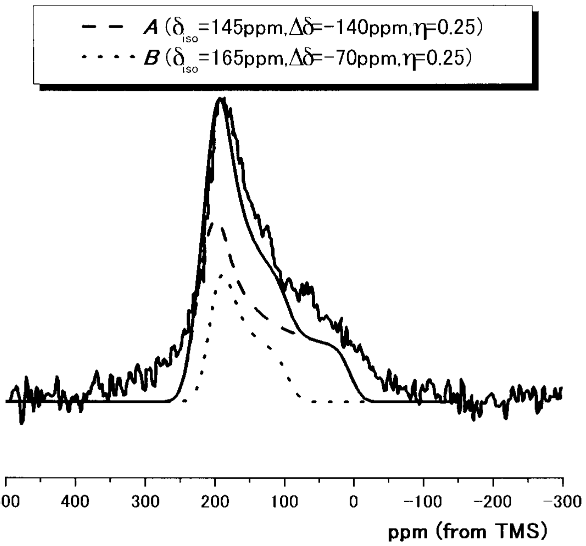

Figure 1. ^{13}C NMR spectrum of SWNTs at 10 K.

IV-J-2 Electronic States of Alkali-Metal Doped Single-Walled Carbon Nanotube Aggregates

OGATA, Hironori; YAKUSHI, Kyuya; KUNO, Shogo[1]; SAITO, Yahachi[1]
(1Mie Univ.)

Electronic states of alkali-metal doped single-walled carbon nanotube aggregates (SWNTs) were studied by both ^{13}C-NMR and Raman spectroscopy. The effects of opening the ends of SWNTs on the intercalation level and the evolution of electronic states were also studied. Dopings of alkali metals were performed for both pristine (capped) and open-ended (uncapped) SWNTs samples by two-bulb method. Raman scattering spectra of the tangentia (E_{2g}) modes of SWNTs showed more downshift by using the SWNTs (uncapped) as a host sample. This result suggests that opening the ends lead to dope inside the tube and achieve higher doping level. Recovery of ^{13}C-magnetization for pristine SWNTs was found to be able to fit with a double-exponential function. On the other hand, single exponential-like curve fitting can be reproduced the data points of ^{13}C-magnetization curve for both K-doped SWNTs samples (Figure 1). Furthermore, The values of spin-lattice relaxation time (T_1) become shorter by K-dopings. Temperature dependence of ^{13}C-T_1 found that both K-doped samples follow a Korringa-like behaviors ($T_1 \times T = 400 \pm 50$ (sec.K) for capped sample and $T_1 \times T = 170 \pm 50$ (sec.K) for uncapped) in the temperature region between 4.2 K and 100 K. This result suggests that cap-opening enables to achieve higher intercalation level. The value of density of states at Fermi level increases three times as much as that of metallic tube for capped sample and four times for uncapped sample by K-doping.

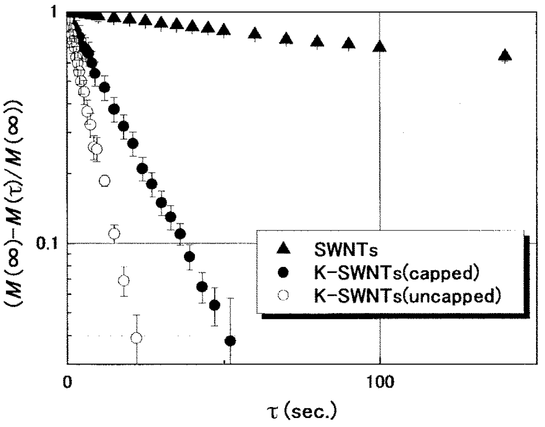

Figure 1. Recovery curve of ^{13}C-NMR for pristine SWNTs (▲), K-doped SWNTs (capped) (●) and K-doped SWNTs (uncapped) (○) measured at 25 K.

IV-J-3 Electronic States of Br_2 Doped Single-Walled Carbon Nanotube Aggregates

OGATA, Hironori; YAKUSHI, Kyuya; KUNO, Shogo[1]; SAITO, Yahachi[1]

([1]Mie Univ.)

Electronic states of Br_2 doped single-walled carbon nanotube aggregates (SWNTs) were studied by both ^{13}C-NMR and Raman spectroscopy. The effects of opening the ends of SWNTs on the intercalation level and the evolution of electronic states were also studied. Doping of Br_2 was performed for both pristine (capped) and open-ended (uncapped) SWNTs samples by measureing the adsorption isotherm of Br_2 *in-situ* in order to controll the doping level and obtain the information on the composition of the doped samples. For both samples, dopings of Br_2 were stopped when the micropore-fillings were completed. The compositions of the samples were evaluated to be (Br/C =) 0.09 for capped sample and 0.2 for uncapped sample. Raman scattering spectra of the tangential (E_{2g}) modes of SWNTs showed more upshift by using the SWNTs (uncapped) as a host sample. This result suggests that opening the ends lead to dope inside the tube and achieve higher doping level. Recovery of ^{13}C-magnetization for both Br_2-doped SWNTs was found to be able to fit with a single exponential-like function (Figure 1). Temperature dependence of ^{13}C-nuclear spins relaxation found that both Br_2-doped samples follow a Korringa-like behaviors ($T_1 \times T = 950 \pm 200$ (sec.K) for capped sample and $T_1 \times T = 1550 \pm 250$ (sec.K) for uncapped) in the temperature region between 4.2 K and 100 K. This result suggests that cap-opening enables to achieve higher intercalation level. The value of density of states at Fermi level increases about 1.8 times as much as that of metallic tube for capped sample and 1.4 times for uncapped sample by Br_2-doping. Decrease in density of states by increase in the doping level is a characteristic nature of the electronic states of SWNTs.

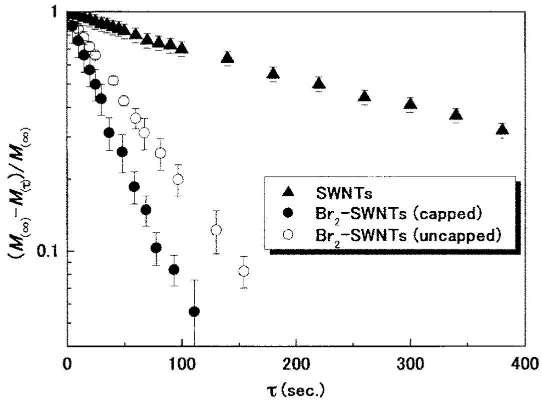

Figure 1. Recovery curve of ^{13}C-NMR for pristine SWNTs (▲), Br_2-doped SWNTs (capped) (●) and Br_2-doped SWNTs (uncapped) (○) measured at 25 K.

IV-K Structural and Electronic Properties of Fullerene-based Compounds

Structural and electronic properties were studied for several types of fullerene-based compounds in this project. Recently, Oszlanyi *et al.* found that Na_4C_{60} forms two-dimensional polymeric phase of body-centered monoclinic (bcm: *I2/m*) at room temperature. The structure and electronic states of Na_4C_{60} polymer phase were investigated by

X-ray powder diffraction, ESR, electric resistivity and solid state ^{13}C-NMR measurements.

IV-K-1 Study on the Physical Properties of Na_4C_{60}

TAKABAYASHI, Yasuhiro[1]; KUBOZONO, Yoshihiro[1]; FUJIKI, Satoshi[1]; KASHINO, Setsuo[1]; ISHII, Kenji[2]; SUEMATSU, Hiroyoshi[2]; OGATA, Hironori
([1]Okayama Univ.; [2]Univ. Tokyo)

The structure and electronic states of Na_4C_{60} polymer phase were investigated by X-ray powder diffraction, ESR, electric resistivity and solid state ^{13}C-NMR measurements. The spin susceptibility determined from ESR showed a rapid increase with a decrease in temperature from 100 to 50 K and a rapid decrease below 50 K. Further, the slope of plots of the peak-to-peak line width, ΔH_{pp}, *versus* temperature changes at 100 K. These results suggest the transformation of a Pauli paramagnetic state around 100 K. The lattice constants, a and b, determined from temperature dependent X-ray powder diffraction showed a discontinuous change around 50 K, while the c shows a continuous variation. The results suggest the structural transition around 50 K which may be associated with the transformation found by ESR. This transition can be attributed to the dimerization due to CDW or Spin-Peierls as in the case of CsC_{60}, because the ESR and the X-ray diffraction suggest the nonmagnetic ground state and the structural transition, respectively. New Bragg diffractions were not found below 100 K as in CsC_{60}. The registivity at 300 K was 6.9×10^3 Ωcm, which is larger than those of K_3C_{60} and Rb_3C_{60}. The temperature dependence of the registivity showed a semiconducting behavior from 300 to 190 K. The band gap energy, E_g, estimated from the registivity was 0.8 eV, which is in agreement with those of K_4C_{60} and Rb_4C_{60}. Figure 1 shows the temperature dependence of ^{13}C-NMR spectrum for Na_4C_{60}. Appearance of a new peak at 70 ppm at low temperature suggests that existence of sp^3-like carbon in this compound. Temperature dependence of ^{13}C-nuclear spin-lattice relaxation time didn't follow a Korringa-like behavior in the temperature region between 300 K and 4.2 K, which suggests a non-metallic behavior for Na_4C_{60} polymer.

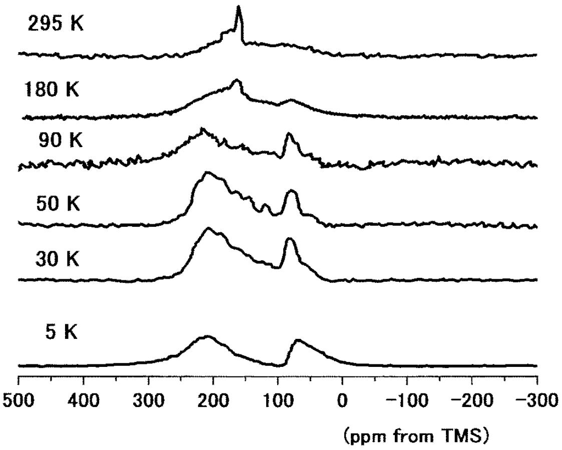

Figure 1. Temperature dependence of ^{13}C-NMR spectrum for Na_4C_{60} polymer.

IV-L Development of Pulsed Field Gradient NMR Spectroscopy

Pulsed field gradient spin echo (PGSE) nuclear magnetic resonance (NMR) is a powerful method for the study of dynamics in condensed matter since it probes translational motion of molecules selectively, without being affected by vibrational or rotational motions. Due to this advantage it has been widely applied to the dynamics of molecules in liquids. However, applications of this technique to strongly dipole-coupled spin systems with short T_2 or to the study of slow and anisotropic self-diffusion are still challenging works because combined techniques of line-narrowing, pulsing of sharp and intense field gradients, and two-dimensional field-gradient generation are necessary.

In the present study we applied the technique to the study of self-diffusion in solid state, with the use of the laboratory-made spectrometer equipped with a rotatable quadrupole coil.

IV-L-1 Direct Measurement of Self-Diffusion Coefficients in Solids: Plastic Crystalline Hexamethylethane

OISHI, Osamu

Direct measurements of self-diffusion coefficients in solids were made possible without resorting to classical indirect methods such as line width or relaxation time measurements. This experiment was made possible with an automatic PGSE apparatus equipped with a quadrupole coil and a high power FG current driver. The diffusion coefficient D as small as 10^{-13} m^2s^{-1} was measured in the plastic crystalline phase of hexamethylethane (HME). The activation energy E_a was found to be 89 kJ mol^{-1}.

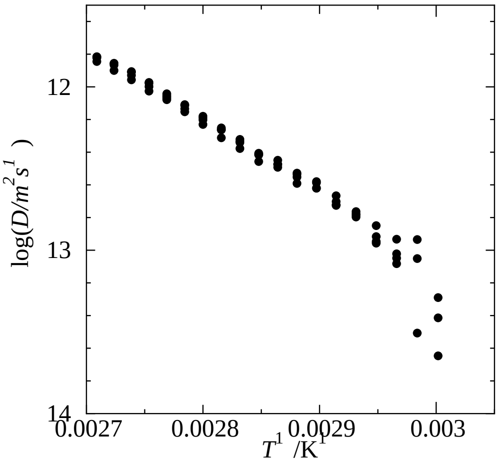

Figure 1. Temperature-dependence of the diffusion coefficient in the plastic crystalline phase of HME.

IV-M Phase Transition Mechanism of Reentrant Liquid Crystal

When conventional liquid loses its isotropic (I) symmetry and assumes uniaxial orientational order, the nematic (N) liquid crystalline state is formed. The smectic A (S_A) state is characterized by its one-dimensional translational order in addition to the nematic order. It is therefor natural that the phase transition sequence be I-N-S_A on lowering the temperature. However, the reentrant liquid crystal exhibits a transition sequence, I-N-S-N-(S)-crystal (doubly reentrance sequence) on lowering the temperature. The second N phase is called reentrant nematic (RN), and the S to RN transition means that 1-D translational lattice melts on lowering the temperature. Due to this peculiarity, the nature of this transition sequence has been one of the interesting topics in recent liquid crystal research.

IV-M-1 Neutron Small-Angle Scattering of Reentrant Liquid Crystal CBOBP

OISHI, Osamu

The reentrant liquid crystal, CBOBP (4-cyanobenzoyloxy-[4-octylbenzoyloxy]-p-phenylene), exhibits a transition sequence, I-510-N-458-S_{Ad}-431-N-415-S_{A1}-398-crystal(The transition temperatures are shown in K.) on lowering the temperature.

We made neutron diffraction study to clarify the structure of the liquid crystalline phases and hence to clarify the microscopic mechanism of this phenomenon. For this purpose a compound with perdeuterated chain, CBOBP-d17 was prepared. SANS-U instrument was used at an wavelength of 7 Å with a velocity selector.

Figure 1 shows the magnitudes of the scattering vectors of the diffraction peaks. The two data points at lowest temperatures correspond to the supercooled S_{A1} phase. It is revealed that two peaks coexist in the RN phase.

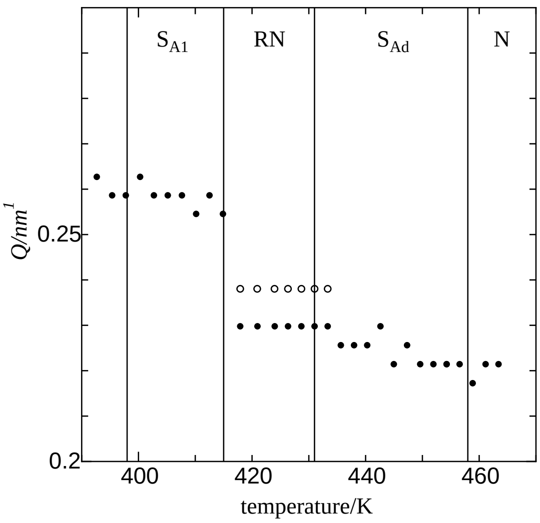

Figure 1. Magnitudes of the scattering vectors in the liquid crystalline phases.

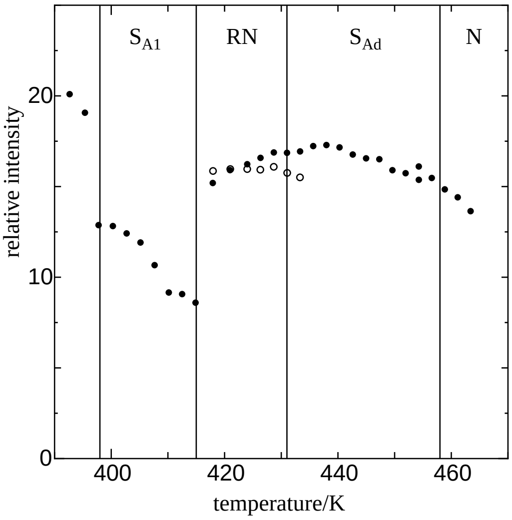

Figure 2. Relative intensities of the diffraction peaks.

IV-N Systematic Study of Organic Conductors

Thanks to the systematic view to structure-property relationship studied particularly in BEDT-TTF-based conductors, recently our understanding of organic conductors has made a great progress. From the concept of "universal phase diagram" in the θ-phase, we can predict metal-insulator transition temperatures of a large number of organic conductors. This kind of concept is generalized to δ-phase salts, that have twisted overlaps. Examining symmetry-property relationship in organic conductors, we can extract a general rule that magnetism of insulator phases is paramagnetic for uniform and dimerized structures, whereas non magnetic for tetramerized or lower-symmetry structures. We have attempted to apply this rule to TTM-TTP compounds, which have metallic one-dimensional half-filled bands. Contrary to the above rule, these compounds, which have been expected to be paramagnetic in view of the uniform columns, show non magnetic ground states owing to their extreme one-dimensionality and the lattice modulation.

IV-N-1 Structural Genealogy of BEDT–TTF–Based Organic Conductors III. Twisted Molecules: δ and α' Phases

MORI, Takehiko
(Tokyo Inst. Tech. and IMS)

[*Bull. Chem. Soc. Jpn.* **72**, 2011 (1999)]

δ-phase (β-PF_6 type) BEDT-TTF (bis(ethylenedithio)tetrathiafulvalene)-based organic conductors are characterized by the twisted overlap mode in the stack. Since the twisted mode has large intermolecular orbital overlap, the δ-phase is regarded as a twisted dimer structure. This type of overlap is, however, insensitive to small changes of the structure. On the contrary, an oblique interaction alters the warping of the open Fermi surface, to control the metal-insulator transition temperature, T_{MI}. Through the change of this oblique interaction, T_{MI} is scaled by the axis ratio for a family of salts with the same stacking pattern. As a general summary of BEDT-TTF salts, an empirical rule is proposed to predict, from the number of crystallographically independent molecules, whether an insulating state of BEDT-TTF salts will be paramagnetic or nonmagnetic. This rule is based on hypothetical pair formation of spins located on each dimer, and universally applies to all BEDT-TTF salts. This rule is extended to metallic salts, and among the potentially nonmagnetic salts, a dimerized dimer structure is the necessary condition of superconductivity. The potentially paramagnetic superconductors have strongly dimerized structures like β and κ phases (Table 1). From this we can make a reasonable prediction as to superconducting phases.

Table 1. Classification of Organic Superconductors.

ET-Based	Other Donors
Potentially paramagnetic	
β-Phase	$(TMTSF)_2X$
κ-Phase	$(DMET)_2X$
	$(DTEDT)_3Au(CN)_2$
Potentially nonmagnetic	
$\beta_{21\times2}$-$(ET)_2ReO_4$	$\beta''_{20\times2}$-$(BO)_2ReO_4H_2O$
$\beta''_{211\times2}$-$(ET)_2SF_5CF_2SO_3$	
β''_{421}-$(ET)_2Pt(CN)_4H_2O$	
β''_{421}-$(ET)_2Pd(CN)_4H_2O$	
$\beta''_{321\times2}$-$(ET)_3Cl_2(H_2O)_2$	
β''_{431}-$(ET)_4H_2O[Fe(ox)_3]PhCN$	
α-$(ET)_2NH_4Hg(SCN)_4$	
θ-$(ET)_2I_3$	

IV-N-2 Raman and Optical Investigations on Charge Localization in the One-Dimensional Organic Conductors (TTM–TTP)$(I_3)_{5/3}$ and (TSM–TTP)$(I_3)_{5/3}$

KAWAMOTO, Tadashi[1]; ASHIZAWA, Minoru[1]; ARAGAKI, Masanobu[1]; MORI, Takehiko[2], YAMAMOTO, Takashi[3]; TAJIMA, Hiroyuki[3]; KITAGAWA, Hiroshi[4]; MITANI, Tadaoki[4]; MISAKI, Yohji[5]; TANAKA, Kazuyoshi[5]
([1]Tokyo Inst. Tech., [2]Tokyo Inst. Tech. and IMS; [3]ISSP; [4]JAIST; [5]Kyoto Univ.)

[*Phys. Rev. B* **60**, 4635 (1999)]

The title compounds, which have polyiodide chains along the donor stacking direction and show characteristic copper luster, exhibit metallic behavior above T_{MI} = 20 K. High pressure resistivity, the Raman spectra, and optical reflectance of these salts have been measured to investigate the origin of the low-temperature insulating state and the iodine species. For (TSM-TTP)$(I_3)_{5/3}$ two kinds of conducting behavior have been observed (Figure 1); below 20 K some low-conducting samples have shown an increase of the resistivity of more than 10^3 times, but other high-conducting samples have shown an increase of less than ten times. The increase of resistivity is almost suppressed under a pressure of 11.5 kbar in the high-conducting phase of (TSM-TTP)$(I_3)_{5/3}$. The Raman spectra provide clear evidence that the polyiodide chain is composed of I_3^- in these compounds. The Raman spectra and the X-ray photographs indicate that the increase of resistivity originates in the disorder. The chain axis optical reflectance spectra show plasma edges appearing in the infrared region and three peaks from the infrared to the visible range; the latter originate from the intramolecular transition and polyiodide ions. Temperature dependence of optical conductivity is metallic even below T_{MI}. From these results, the origin of the low-temperature insulating state is attributed to disorder driven localization.

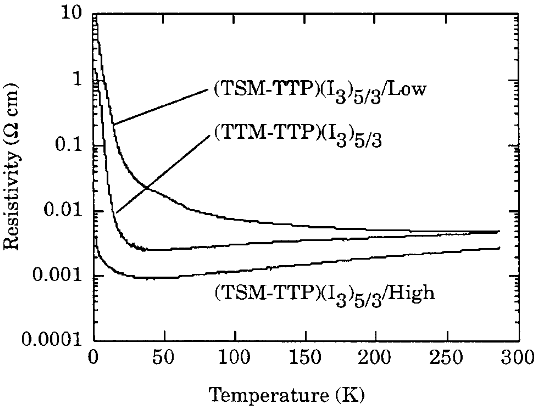

Figure 1. Temperature dependence of electrical resistivity of (TTM-TTP)$(I_3)_{5/3}$ and (TSM-TTP)$(I_3)_{5/3}$.

IV-N-3 Raman Investigation of the One-Dimensional Organic Conductor with a Half-Filled Band, (TTM-TTP)I_3

KAWAMOTO, Tadashi[1]; MORI, Takehiko[2]; KITAGAWA, Hiroshi[3]; MITANI, Tadaoki[3]; MISAKI, Yohji[4]; TANAKA, Kazuyoshi[4]
([1]Tokyo Inst. Tech.; [2]Tokyo Inst. Tech. and IMS; [3]JAIST; [4]Kyoto Univ.)

[*J. Phys. Soc. Jpn.* **68**, 3748 (1999)]

Raman spectra of the title compound, which shows metallic conduction in spite of the 1:1 composition, have been investigated. The Raman line at 112 cm^{-1}, originating from the symmetric stretching of the discrete I_3^- anions, splits in two below 150 K. This corresponds to the lattice modulation coming from the triiodide anions.

IV-N-4 ESR Investigation of Organic Conductors (DTM-TTP)(TCNQ)(TCE) and (TMET-TTP)(TCNQ)

HOSHINO, Hirotada[1]; ARAGAKI, Masanobu[1]; MURATA, Kyoji[1]; KAWAMOTO, Tadashi[1]; MORI, Takehiko[2]; MISAKI, Yohji[3]; TANAKA, Kazuyoshi[3]
([1]Tokyo Inst. Tech.; [2]Tokyo Inst. Tech. and IMS; [3]Kyoto Univ.)

[*J. Phys. Soc. Jpn.* **69**, 1845 (2000)]

Magnetic properties of the title compounds are investigated by ESR measurements, and from the temperature dependence of the *g*-values, the spin susceptibility is separated into donor and TCNQ contributions. For (DTM-TTP)(TCNQ)(TCE), the overall spin susceptibility decreases gradually from room temperature to 200 K, and more rapidly below 200 K, indicating a gradual crossover from a metallic to nonmagnetic insulating state. For (TMET-TTP)$_2$-(TCNQ), the spin susceptibility exhibits a gradual increase from room temperature to 50 K, followed by a rapid Curie-like increase that is attributed to the isolated TCNQ molecules (Figure 1). The donors remain paramagnetic even in the insulating state in accordance with the two-dimensional θ-type arrangement of the donor conducting sheet.

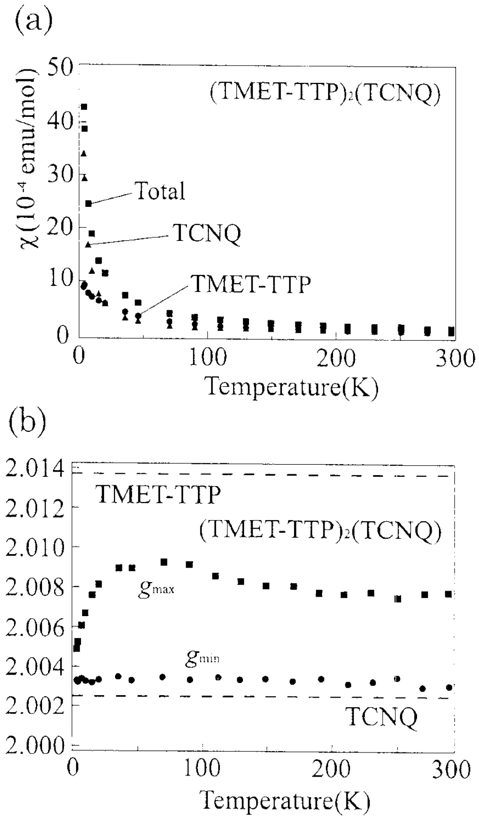

Figure 1. (a) Spin susceptibility and (b) *g*-value of (TMET–TTP)$_2$(TCNQ). The *g*-value are measured in the directions of g_{max} and g_{min} in the ac plane. The broken lines in (b) are *g*-values of TMET–TTP and TCNQ.

IV-N-5 Structural and Magnetic Properties of Cu[C(CN)$_3$]$_2$ and Mn[C(CN)$_3$]$_2$

HOSHINO, Hirotada[1]; IIDA, Kazuki[1]; KAWAMOTO, Tadashi[1]; MORI, Takehiko[2]
([1]Tokyo Inst. Tech.; [2]Tokyo Inst. Tech. and IMS)

[*Inorg. Chem.* **38**, 4229 (1999)]

Single crystal X-ray structure analyses and the measurements of static magnetic susceptibility and ESR have been performed for the title compounds. Crystal data for Cu[C(CN)$_3$]$_2$: space group P_{mna}, a = 7.212(5), b = 5.452(7), c = 10.696(7) Å, and Z = 2, Mn[C(CN)$_3$]$_2$: space group P_{mna}, a = 7.742(5), b = 5.411(6), c = 10.561(6) Å, and Z = 2. Both salts are essentially isostructural (Figure 1). The Cu atoms are bridged by two $[C(CN)_3]^-$ anions to form an infinite double chain structure, in which Cu has a square planar coordination (d_{Cu-N} = 1.986(6) Å). The third CN end of the anion is weakly coordinated to the adjacent Cu chain (d_{Cu-N} = 2.47(1) Å), making a three-dimensional network. The crystal is composed of two such interwoven networks. In the Mn complex, the third Mn-N distance (2.256(6) Å) is as short as the equatorial coordinations (2.236(4) Å), so that Mn is coordinated octahedrally. These compounds exhibit paramagnetic behavior following the Curie-Weiss law with Weiss temperatures, –1.4 K and –9 K, respectively, and the Mn complex undergoes an antiferromagnetic transition at T_N = 5 K.

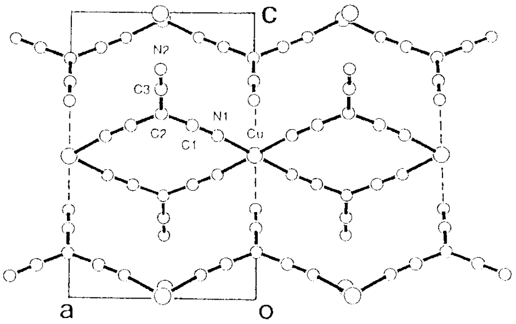

Figure 1. Double chain structure of $Cu[C(CN)_3]_2$.

IV-O Photoelectron Spectroscopy of Organic Solids in Vacuum Ultraviolet Region

The works of ultraviolet photoelectron spectroscopy (UPS) with synchrotron radiation light source (UVSOR-UPS) of advanced organic materials have been proceeded to find their quantitative electronic structures and also to analyze their structures of assemblies.

IV-O-1 Angle-Resolved Photoemission Measurements of ω-(n-pyrrolyl)alkanethiol Self-Assembled Monolayers Using *in-situ* Sample Preparation Apparatus

HASEGAWA, Shinji; HORIGOME, Toshio; YAKUSHI, Kyuya; INOKUCHI, Hiroo; OKUDAIRA-KAMIYA, Koji[1]; UENO, Nobuo[1]; SEKI, Kazuhiko[2]; WILLICUT, J. Robert[3]; McCARLEY, L. Robin[3]; MORIKAWA, Eizi[4]; SAILE, Volker[4]
([1]Chiba Univ.; [2]RCMS, Nagoya Univ.; [3]Louisiana State Univ.; [4]Louisiana State Univ. CAMD)

[*J. Electron Spectrosc. Relat. Phenom.* in press]

An *in-situ* sample preparation apparatus was developed for measuring intrinsic angle-resolved ultraviolet photoemission spectra (ARUPS) from ω-(n-pyrrolyl)alkanethiol self-assembled monolayers (pyrrolyl-SAMs) on an Ag surface. The apparatus enables the preparation of the SAMs directly from the thiol solution and the measurement of ARUPS without exposing the sample to air. The spectral features of the SAMs were analyzed with the aid of *ab-initio* molecular orbital calculations. It was observed that the ARUPS features associated with the π bands originating from the substituent pyrrole are distinct from the features associated with the alkyl chain.

IV-O-2 Photoemission Spectra of $LiNiO_2$ Catalyst for Oxidative Coupling of Methane

MIYAZAKI, Takafumi[1]; AOKI, Masaru; TAKAYASU, Osamu[1]
([1]Toyama Univ.)

[*Jpn. J. Appl. Phys.* **38**, 51 (1999)]

Surface-lattice oxygen species of $LiNiO_2$ with a layered structure were investigated for an oxidative reaction of methane. $LiNiO_2$ resulted in formation of C_2-hydrocarbons without by-products of carbon dioxide at an initial stage reaction which was an oxidative coupling process by surface lattice oxygen. For understanding of the origin of the catalytic activities, photoemission spectra of $Li_xNi_{2-x}O_2$ ($0 < x \leq 1$) were measured. From comparison of the valence band structures, it was suggested that an anisotropic charge distribution and the layered structure contributed to the formation of active lattice oxygen and the catalytic performance of $LiNiO_2$, respectively.

IV-O-3 Intramolecular Energy-Band Dispersion in Oriented Thin Films of n-$CF_3(CF_2)_{22}CF_3$ Observed by Angle-Resolved Photoemission with Synchrotron Radiation

MIYAMAE, Takayuki; HASEGAWA, Shinji; YOSHIMURA, Daisuke[1]; ISHII, Hisao[1]; UENO, Nobuo[2]; SEKI, Kazuhiko[3]
([1]Nagoya Univ.; [2]Chiba Univ.; [3]RCMS, Nagoya Univ.)

[*J. Chem. Phys.* **112**, 3333 (2000)]

Angle-resolved ultraviolet photoelectron spectra were measured for oriented films of perfluorotetracosane, n-$CF_3(CF_2)_{22}CF_3$, as a model compound of poly(tetrafluoroethylene) using synchrotron radiation. The main spectral features showed continuous changes in both peak positions and intensities with photon energy, incident angle, and photoelectron take-off angle. The intramolecular energy-band dispersion of poly(tetrafluoroethylene) was mapped from the photo-energy dependence of the normal emission spectra.

RESEARCH ACTIVITIES V
Department of Applied Molecular Science

V-A Molecular Mechanisms of Oxygen Activation by Heme Enzymes

By sharing a common prosthetic group, the heme enzymes such as cytochrome P450s, peroxidases, and catalases catalyze their own unique biological functions; monooxygenation, hydrogen peroxide dependent oxidation, and dismutation of hydrogen peroxide, respectively. Our efforts have been focused on the elucidation of the structure-biological function relationship of thoses heme enzymes by employing both enzymic systems including mutants and their model systems.

V-A-1 Investigations of the Myoglobin Cavity Mutant H93G with Unnatural Imidazole Proximal Ligands as a Modular Peroxide O-O Bond Cleavage Model System

ROACH, Mark P.; OZAKI, Shin-ichi[1]; WATANABE, Yoshihito
([1]Yamagata Univ.)

[*Biochemistry* **39**, 1446 (2000)]

A general inability to carry out extensive variations in the electronic characteristics of proximal heme iron ligands in heme proteins has hampered efforts to obtain a clear understanding of the role of the proximal heme iron ligand in the activation of oxygen and peroxide. The disadvantage of the frequently applied site directed mutagenesis technique is that it is limited by the range of natural ligands available within the genetic code. The myoglobin cavity mutant H93G has its proximal histidine ligand replaced by glycine, a mutation which leaves an open cavity capable of accommodation of a variety of unnatural potential proximal ligands. We have carried out investigations of the effect of changing the electron donor characteristics of a variety of substituted imidazole proximal ligands on the rate of formation of myoglobin compound II and identified a correlation between the substituted imidazole N-3 pK_a (which provides a measure of the electron donor ability of N-3) and the apparent rate of formation of compound II. A similar rate dependence correlation is not observed upon binding of azide. This finding indicates that O–O bond cleavage and not the preceding peroxide binding step is being influenced by the electron donor characteristics of the substituted imidazole ligands. The proximal ligand effects are clearly visible but their overall magnitude is quite low (1.7 fold increase in O–O bond cleavage rate per pK_a unit). This appears to provide support for recent commentaries that the partial ionization of the proximal histidine ligand in typical heme peroxidases may not be enough of an influence to provide a mechanistically critical push effect. Further attempts were made to define the mechanism of the influence of N-3 pK_a on O–O bond cleavage by using peracetic acid and cumene hydroperoxide as mechanistic probes. The observation of heme destruction in these reactions indicates that displacement of the proximal imidazole ligands by peracetic acid or cumene hydroperoxide has occurred. A combination mutation; H64D/H93G was prepared with the objective of observing compound I of H64D/H93G with substituted imidazoles as proximal ligands upon reaction with H_2O_2. This double mutant was found to simultaneously bind imidazole to both axial positions, an arrangement which prevents a reaction with H_2O_2.

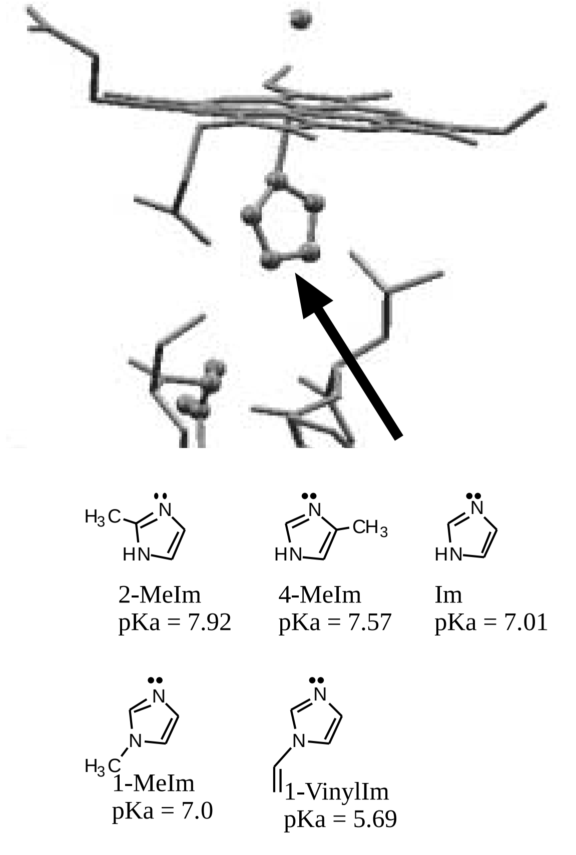

Figure 1. Active site of the ferric imidazole adduct of H93G Mb. Also shown are the five Im-X used as proximal ligands for H93G and their pK_a values

V-A-2 Formation and Catalytic Roles of Compound I in the Hydrogen Peroxide-Dependent Oxidations by His64 Myoglobin Mutants

MATSUI, Toshitaka; OZAKI, Shin-ichi; WATANABE, Yoshihito

[*J. Am. Chem. Soc.* **121**, 9952 (1999)]

A His64 → Asp mutant of sperm whale myoglobin (Mb), H64D Mb, has been prepared to mimic the active site of chloroperoxidase from the marine fungus *Caldariomyces fumago*, in which distal glutamic acid is suggested to enhance the compound I formation by H_2O_2. The H64D mutant allows us to see the accumulation of compound I in the reaction of Mb with H_2O_2 for the first time. The successful observation of compound I is due to at least 50-fold improvement in the formation rate of compound I as well as its stabilization upon the His64 → Asp replacement. Catalytic activity of wild type Mb and a series of His64 Mb mutants (H64A, H64S, H64L, and H64D Mb) are examined for one-electron oxidation and oxygenation by using H_2O_2 as an oxidant. The H64D mutant is the best catalyst among the myoglobins and shows 50~70-fold and 600~800-fold higher activity than the wild type in the one-electron oxidations and peroxygenations, respectively. The origin of the varied activity upon the mutations is discussed on the basis of the formation rate and stability of compound I.

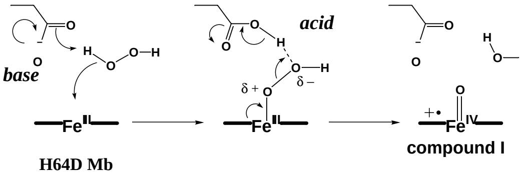

Scheme 1. Roles of distal aspartate of H64D myoglobin in the reaction with H_2O_2.

V-A-3 Proximal Ligand Control of Heme Iron Coordination Structure and Reactivity with Hydrogen Peroxide: Investigations of the Myoglobin Cavity Mutant H93G with Unnatural Oxygen Donor Proximal Ligands

ROACH, Mark P.; PUSPITA, Waheeda J.; WATANABE, Yoshihito

[*J. Inorg. Biochem.* **81**, 173 (2000)]

The role of the proximal heme iron ligand in activation of hydrogen peroxide and control of spin state and coordination number in heme proteins is not yet well understood. Although there are several examples of amino acid sidechains with oxygen atoms which can act as potential heme iron ligands, the occurrence of protein-derived oxygen donor ligation in natural protein systems is quite rare. The sperm whale myoglobin cavity mutant H93G Mb (Barrick, D. *Biochemistry* **33**, 6546 (1994)) has its proximal histidine ligand replaced by glycine, a mutation which leaves an open cavity capable of accommodation of a variety of unnatural potential proximal ligands. This provides a convenient system for studying ligand-protein interactions. Molecular modeling of the proximal cavity in the active site of H93G Mb indicates that the cavity is of a sufficient size to accommodate benzoate and phenolate in conformations that allow their oxygen atoms to come within binding distance of the heme iron. In addition, benzoate may occupy the cavity in an orientation which allows one carboxylate oxygen atom to ligate to the heme iron while the other carboxylate oxygen is within hydrogen bonding distance of serine 92. The ferric phenolate and benzoate complexes have been prepared and characterized by UV-visible and MCD spectroscopies. The benzoate adduct shows characteristics of a six-coordinate high-spin complex. To our knowledge, this is the first known example of a six-coordinate high-spin heme complex with an anionic oxygen donor proximal ligand. The benzoate ligand is displaced at alkaline pH and upon reaction with hydrogen peroxide. The phenolate adduct of H93G Mb is a five-coordinate high-spin complex whose UV-visible and MCD spectra are distinct from those of the histidine 93 to tyrosine (H93Y Mb) mutant of sperm whale myoglobin. The phenolate adduct is stable at alkaline pH and exhibits a reduced reactivity with hydrogen peroxide relative to that of both native ferric myoglobin, and the exogenous ligand free derivative of ferric H93G Mb. These observations indicate that the identity of the proximal oxygen donor ligand has an important influence on both the heme iron coordination number and the reactivity of the complex with hydrogen peroxide.

V-A-4 Mechanisms of Sulfoxidation Catalyzed by High-Valent Intermediates of Heme Enzymes: Electron Transfer *vs.* Oxygen Transfer Mechanism

GOTO, Yoshio; MATSUI, Toshitaka; OZAKI, Shin-ichi[1]; WATANABE, Yoshihito; FUKUZUMI, Shunichi[2]
([1]Yagata Univ.; [2]Osaka Univ)

[*J. Am. Chem. Soc.* **121**, 9497 (1999)]

The mechanism of sulfoxidation catalyzed by high-valent intermediates of heme enzymes has been studied by direct observation of the reduction of compounds I of HRP (horseradish peroxidase) and His64Ser myoglobin (Mb) mutant as well as $O{=}Fe^{IV}TMP^{+\bullet}$ (**1**) (TMP = 5,10,15,20-tetramesitylporphyrin dianion) by sulfides. The reaction of thioanisole and compound I of HRP (10 μM, pH 7.0, 298K) gives the resting state of HRP with accumulation of compound II as an intermediate. The yield of sulfoxide by a stoichiometric reaction of HRP compound I with thioanisole was only 25 ± 5%. On the other hand, the same sulfoxidation by both **1** and His64Ser Mb compound I exclusively exhibited two-electron process resulting in quantitative formation of sulfoxide. When 1,5-dithiacyclooctane (DTCO) is employed as a substrate, the reaction of His64Ser Mb compound I with DTCO exhibits rapid formation of compound II which decays to the ferric state due to the low oxidation potential of DTCO. The observed rate constants (log k) of the reactions of **1** and compounds I of HRP and His64Ser Mb with a series of p-substituted thioanisoles correlate with the one-electron oxidation potentials (E^0) of the sulfides. A comparison of these correlations with the established correlation between log k and E^0 for the corresponding electron transfer reactions of substituted *N*,*N*-dimethylanilines has revealed that the reactions of compound I of HRP with the sulfides proceed via electron transfer while that the sulfoxidation of sulfides by **1** and compound I of His64Ser Mb occurs via direct oxygen transfer rather than electron transfer.

V-B Model Studies of Non-Heme Proteins

Non-heme proteins play important roles in biological redox processes. Many reactions catalyzed by the non-heme enzymes are quite similar to those by hemoproteins. We are interested in the active intermediates responsible for oxidation and oxygenation by non-heme enzyme, especially the similarity and differences.

V-B-1 A Bis(μ-oxo)dicopper(III) Complex with Aromatic Nitrogen Donors: Structural Characterization and Reversible Conversion between Copper(I) and Bis(μ-oxo)dicopper(III) Species

HAYASHI, Hideki[1]; FUJINAMI, Shuhei[1]; NAGATOMO, Shigenori; OGO, Seiji; SUZUKI, Masatatsu[1]; UEHARA, Akira[1]; WATANABE, Yoshihito; KITAGAWA, Teizo
([1]Kanazawa Univ.)

[*J. Am. Chem. Soc.* **122**, 2124 (2000)]

It is important to explore how the nature of donor atoms and the stereochemistry of ligands influence the structures and properties of bis(μ-oxo)dicopper(III) complexes. In this context, we have synthesized a bis(μ-oxo)dicopper(III) complex, $[Cu_2(O)_2(Me_2\text{-tpa})_2tpa](PF_6)_2\cdot 2(CH_3)_2CO$ (**1b**), having a tetradentate tripodal ligand containing aromatic nitrogen donors. The most striking feature of **1b** is the reversible conversion with a precursor copper (I) complex $[Cu(Me_2\text{-tpa})]^+$ (**1a**) in CH_2Cl_2 at –80 °C by bubbling N_2 gas. Such reversible behavior has not been observed for the bis(μ-oxo)-dicopper(III) complexes. Thus reactivity patterns in copper–dioxygen chemistry significantly vary with ligand system. Me_2-tpa has a unique ability to stabilize both copper(I) and copper(III) oxidation states: it can take not only a square planar structure having weak ligation from the axial positions suitable for formation of copper (III) oxidation state but also a pyramidal structure sitable for formation of copper(I) oxidation state.

V-B-2 Characterization of Imidazolate-Bridged Cu(II)-Zn(II) Heterodinuclear and Cu(II)-Cu(II) Homodinuclear Hydroperoxo Complexes as Reaction Intermediate Models of Cu, Zn-SOD

OHTSU, Hideki[1]; ITOH, Shinobu[2]; NAGATOMO, Shigenori; KITAGAWA, Teizo; OGO, Seiji; WATANABE, Yoshihito; FUKUZUMI, Shunichi[1]
([1]Osaka Univ.; [2]Osaka City Univ.)

[*Chem. Commun.* 1051 (2000)]

Copper-zinc superoxide dismutase (Cu, Zn-SOD) contains an imidazolate-bridged Cu(II)-Zn(II) heterodinuclear metal center in its active site. This enzyme catalyses a very rapid two-step dismutation of superoxide to dioxygen and hydrogen peroxide through an alternate reduction and oxidation of the active-site copper ion. An outer-sphere electron transfer from superoxide to Cu(II) center occurs to produce O_2 and Cu(I) center which may be oxidized by another molecule of superoxide in the presence of proton to produce H_2O_2 via a hydroperoxo-Cu(II) species. The hydroperoxo-copper(II) species is a key intermediate in biological oxidations catalyzed by copper enzymes including SOD. We report herein the first characterization of SOD model hydroperoxo-Cu(II) intermediates generated by the reactions of hydrogen peroxide with the imidazolate-bridged Cu(II)-Zn(II) heterodinuclear and Cu(II)-Cu(II) homodinuclear complexes.

V-B-3 Synthesis and X-ray Crystal Structure of a Novel Mn(II)-Semiquinonate Complex $[Mn^{II}(TPA)(DTBSQ)]BPh_4$, and Its Dioxygenase-like Activity: Relevance to Manganese(II)-Dependent Catechol Dioxygenases

FUNABIKI, Takuzo[1]; OGO, Seiji; ITO, Tomoyuki[1]; MATSUI, Hajime[1]; YAMAMOTO, Takashi[1]; TANAKA, Tsunehiro[1]; HOSOKOSHI, Yuko; MAKIHARA, Nobuyuki; WATANABE, Yoshihito
([1]Kyoto Univ.)

Catechol dioxygenases play key roles in the metabolism of various aromatic compounds, converting aromatics to aliphatics with insertion of molecular oxygen between a C–C bond of a benzene ring, and have been studied extensively in recent years from both sides of enzymes and models. We here report synthesis of a novel Mn(II)-semiquinonate complex, $[Mn^{II}(TPA)(DTBSQ)]X$ (**1**, DTBSQ: 3,5-di-tert-butyl-1,2-benzosemiquinonate; TPA: tris(2-pyridylmethyl)amine; X: Cl or BPh_4), that is oxygenated with molecular oxygen in the intradiol cleavage fashion. The complex is a new type of mononuclear mono(3,5-di-tert-butyl-1,2-benzosemiquinonate)manganese(II) complex, and highly peculiar not only for the electronic configuration keeping the Mn(II) state even after coordination of a semiquinonate radical anion, but also for the geometric configuration that is not in the usual octahedral geometry.

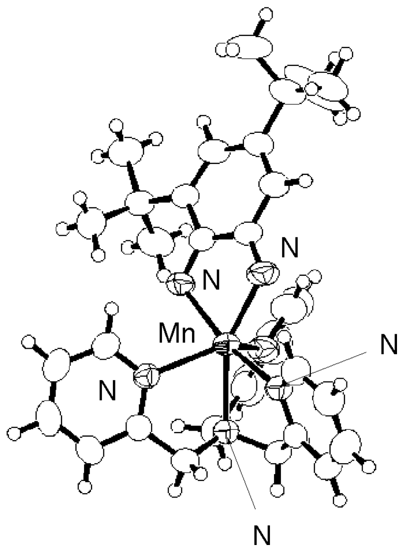

Figure 1. ORTEP drawing of **1**.

V-B-4 Infrared Spectroscopic Features of the Cyclic Hydrogen-Bonded *cis*(Hydroxo)–Fe^{III} –(Carboxylato) Unit of Lipoxygenase Active Site Models

OGO, Seiji; YAMAHARA, Ryo[1]; ROACH, Mark P.; AKI, Michihiko; OGURA, Takashi[2]; KITAGAWA, Teizo; MASUDA, Hideki[1]; WATANABE, Yoshihito
([1]Nagoya Inst. Tech. and IMS; [2]Univ. Tokyo)

[submitted for publication]

Lipoxygenases (LOs) are mononuclear non-heme iron enzyme which are widely distributed among plants and mammals. LOs catalyze the peroxidation of polyunsaturated fatty acids containing the *cis,cis*-1,4-diene moiety to the corresponding 1-hydroperoxy-*trans,cis*-2,4-diene. This paper reports infrared (IR) spectroscopic features of the structurally characteristic *cis*(hydroxo)–Fe^{III}–(carboxylato) unit of lipoxygenase active site model complexes, [Fe^{III}(tnpa)(OH)(RCO$_2$)]-ClO$_4$ (**1a**: R = CH$_3$ and **1b**: R = H). The vibrational modes were unequivocally assigned by isotopic substitution of the hydroxo ($^{18}OH^-$, $^{16}OD^-$, and $^{18}OD^-$ for $^{16}OH^-$) and the carboxylato (**1a**: $^{12}CH_3{}^{12}C^{18}O_2^-$, $^{13}CH_3{}^{12}C^{16}O_2^-$, $^{12}CH_3{}^{13}C^{16}O_2^-$, and $^{13}CH3^{13}C^{16}O_2^-$ for $^{12}CH_3{}^{12}C^{16}O_2^-$ and **1b**: $H^{13}C^{16}O_2^-$ for $H^{12}C^{16}O_2^-$) ligands in the solid state (in mineral oil) and in the liquid state (in acetonitrile). The crystal structure of **1a** was determined by X-ray analysis. It was confirmed by electrospray ionization mass spectrometry (ESI-MS) that the structures of the complexes are preserved in acetonitrile.

V-C Aqueous Organometallic Chemistry

In recent years, aqueous organometallic chemistry has been widely studied because of industrial advantages and environmental concerns. Few organometallic aqua complexes have been, until now, isolated and used as water-soluble reagents in aqueous media. We have investigated a homogeneous hydrogenation in aqueous media using organometallic aqua complexes whose structures and properties drastically change as a function of pH because of deprotonation of the aqua ligands.

V-C-1 pH-Selective Hydrogenation with an Organometallic Aqua Complex as a Catalyst Precursor in Very Acidic Media

MAKIHARA, Nobuyuki; OGO, Seiji; WATANABE, Yoshihito

[*Organometallics* in press]

An organometallic aqua complex [Cp*Ir^{III}(H$_2$O)$_3$]$^{2+}$ (**1**) serves as a catalyst precursor for aqueous hydrogenation of water-soluble compounds with C=O or C=C bonds under very acidic conditions. The hydrogenation shows unique pH-selectivity depending upon substrates. The rates of hydrogenation of carbonyl compounds show a maximum in a pH range of about 2 to 3. The rates of hydrogenation of water-soluble alkenes show a maximum in a pH range of about –1 to 2. Above pH 4, complex **1** is deprotonated to form a catalytically inactive dinuclear complex [(Cp*Ir^{III})$_2$(μ-OH)$_3$]$^+$ (**2**). This is the first example of a pH-selective hydrogenation using an organometallic aqua complex as the catalyst precursor under very acidic conditions.

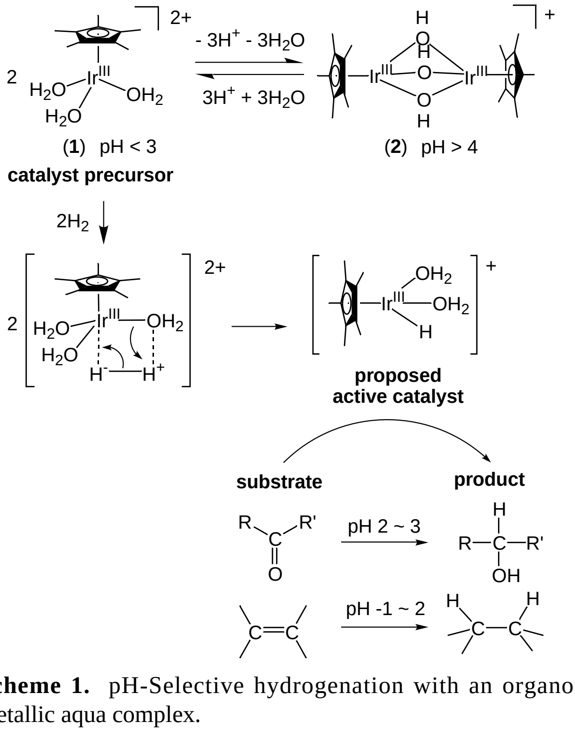

Scheme 1. pH-Selective hydrogenation with an organometallic aqua complex.

V-D Magnetic Structure of Oligo-Nitroxide-Transition Metal Complexes

Since one or two decades, considerable attention has been devoted to stable nitroxide radicals and their metal complexes which are now widely used as building blockes for the design of moleculaer-based magnetic materials. In this field, we have introduced a new strategy of employing π-conjugated polyaminoxyls as ligands in which the 2*p*-spins of the NO groups interact ferromagnetically ($J_1 > 0$). The dimensionality of the complex and the sign and magnitude of the exchange coupling between the neighboring spins may be readily tuned by this strategy. Depending on the nature of the additional interchain or interlayer interaction, the polymers are expected to become an antiferromagnet or ferri/ferromagnet. By modifying and extending this design strategy to bis- and tris(aminoxyl) radicals having triplet and quartet ground states, respectively, we have been able to construct with the aid of magnetic metal ions one-dimensional (1D) chain, two-dimensional (2D) network and three-dimensional (3D) parallel-crosses structures in which both the organic 2p and metallic 3d spins have been ordered in macroscopic scales. Since such a rational approach by self-assembly to the tailored extended systems having relevant physical properties is of great importance in materials synthesis. For these materials, the magnetic structures of the crystals are also interesting.

V-D-1 Influence of the Thermal Excitations of the Ferrimagnetic (–1/2,5/2,–1/2) Linear Trimer on the Paramagnetic Behavior of the Layered Metal-Radical Complex $\{Mn(hfac)_2\}_3(R_X)_2 \cdot n\text{-}C_7H_{16}$

MARKOSYAN, Ashot S.[1]**; HOSOKOSHI, Yuko; INOUE, Katsuya**
([1]IMS and Moscow State Univ., Russia)

[*Phys. Lett. A* **261**, 212 (1999)]

The complex $\{Mn(hfac)_2\}_3(\mathbf{3R}_\Delta)_2 \cdot n\text{-}C_7H_{16}$ forms a two-dimensional honeycomb-like spin network. It is shown that the spins of Mn(II) form with the two 1/2-spins of different adjacent triradicals $\mathbf{3R}_\Delta$ linear $(\bar{1}/2,5/2,\bar{1}/2)$ ferrimagnetic trimers, which determine the paramagnetic properties of the complex. The intratrimer excitations result in the decay of the trimers above 140 K. The experimental data can well be described within this model both at high and low temperatures thus proving the importance of the thermal excitations within the trimers. The best agreement was obtained at J_{TR}/k = –176.4 K and λ' = +0.333 emu/mol. The power series expansion for the 2D honeycomb network gives J_{TR}/k = –175.4 K and J_1/k = +0.226 K.

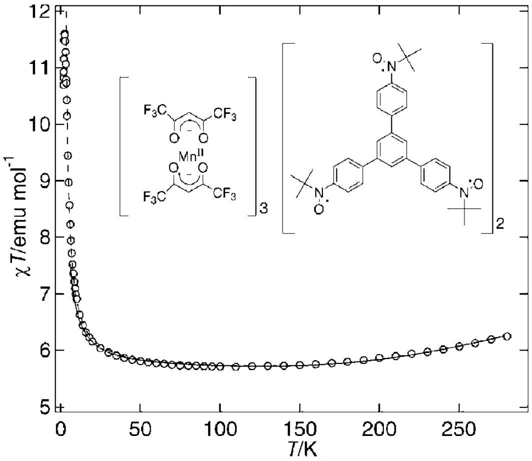

Figure 1. The temperature dependence of $\chi_m T$ for the layered complex $\{Mn(hfac)_2\}_3(\mathbf{3R}_\Delta)_2 \cdot n\text{-}C_7H_{16}$. Open circles are the experimental data, the solid and the dashed lines are the least squares fits for a 2D and 3D lattice, respectively.

V-D-2 Synthesis and Magnetic Properties of Bis(hexafluoroacetylacetonate) Copper(II) Complex with 5-Bromo-1,3-Phenylenebis(*N-tert*-butylaminoxyl) as a Bridging Ligand

IWAHORI, Fumiyasu; INOUE, Katsuya; IWAMURA, Hiizu[1]
([1]Kyushu Univ.)

[*Mol. Cryst. Liq. Cryst.* **334**, 533 (1999)]

Bis(hexafluoroacetylacetonato)copper(II), $Cu(hfac)_2$ (= M) reacts with 5-bromo-1,3-phenylenebis(*N-tert*-butylaminoxyl), $\mathbf{1}_{Br}$ to yield a complex of formula $[M_3 \cdot (\mathbf{1}_{Br})_2]$. The X-ray crystal structure shows that it crystallize in the space group *P*1, with *a* = 12.469(2) Å, *b* = 15.278(2) Å, *c* = 11.602(2) Å, α = 104.59(1)°, β = 111.86(1)°, γ = 88.32(1)°, and *Z* = 1. The crystal contains copper(II) trinuclear structure, M-$\mathbf{1}_{Br}$-M-$\mathbf{1}_{Br}$-M. The magnetic susceptibility measurements revealed a structual transition at *ca.* 48 K accompanied by a temperature hysterisis. (Figure 1)

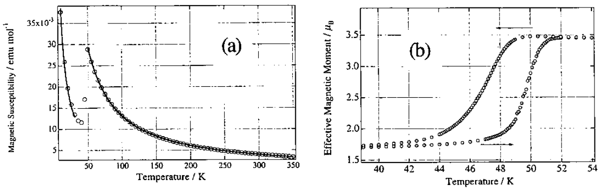

Figure 1. (a) χ_m versus *T* plot for $[Cu(hfac)_2]_3(\mathbf{1}_{Br})_2$ measured at a magnetic field of 50000 Oe; (b) Observed μ_{eff} versus *T* plots in the temperature range 39–45 K. Solid lines are calculated on Curie-Weiss law (15–45 K) and the trinuclear complex model (50–350 K).

V-D-3 Magnetic Behaviour of the Ferrimagnetic (–1/2,5/2,–1/2) Linear Trimer in Complexes of $Mn(hfac)_2$ with Bis- and Trisnitroxide Radicals

MARKOSYAN, Ashot S.[1]**; IWAMURA, Hiizu**[2]**; INOUE, Katsuya**
([1]IMS and Moscow State Univ., Russia; [2]Kyushu Univ.)

[*Mol. Cryst. Liq. Cryst.* **334**, 549 (1999)]

Characterization and magnetic properties of new metal-radical complexes with bivalent Mn having a general formula {[Mn(hfac)$_2$]$_m$(**R**)$_n$} are given. (Figure 1) In these complexes, the aminoxyl radicals have magnetic, triplet or qualtet, ground state and form with Mn^{2+} heterospin structures. They show 1D, 2D, and 3D behaviour depending on the crystal structure, chemical formula and molecular structure of radical. In the ordered state, the complexes form a ferrimagnetic structure due to a strong nagetive coupling between the radical and Mn spins. Magnetic anisotropy in some single crystal was studied. The 3D complex {[Mn(hfac)$_2$]$_3$(**3R**$_T$)$_2$} with a linear triradical can be described within a sublattice model of ferrimagnetism, one sublattice of which os formed by 1D chains, while the other consists of magnetically isolated Mn^{2+} ions. Its comparatively high T_C = 45 K is accounted for the large interchain exchange interaction (3.9 K) through the isolated Mn^{2+}.

Analysis of their paramagnetic properties shows that the hagher energy excitations are related to the desintegration of the ferrimagnetic (–1/2,5/2,–1/2) linear trimer species, which can be isolated in all these compounds.

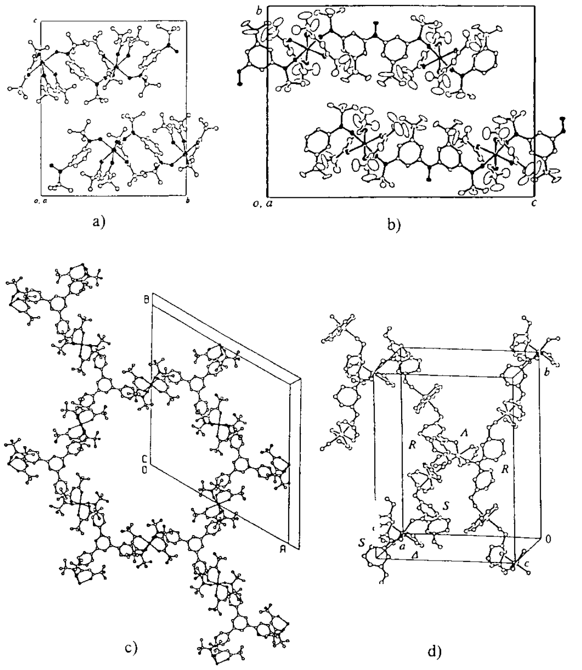

Figure 1. 1D chains of {[Mn(hfac)$_2$](**2R**)} extending along *b*-axis (a); an enatiomeric pair of isotactic 1D chains of {[Mn(hfac)$_2$](**3R**$_T$)·*n*-C$_6$H$_{14}$} (the molecules of *n*-C$_6$H$_{14}$ are disordered and not shown for clarity) (b); 2D hexagonal net of {[Mn(hfac)$_2$]$_3$(**3R**$_\Delta$)$_2$·*n*-C$_7$H$_{16}$} viewed down to the *c*-axis (the *n*-C$_7$H$_{16}$ molecules are not shown) (d); 3D parallel-crossed structure of {[Mn(hfac)$_2$]$_3$(**3R**$_T$)$_2$} (the CF$_3$ and (CH$_3$)$_2$C groups are not shown.

V-D-4 Exchange Coupling Parameters and Energy Levels for Cyclic Metal-Radical Complexes of Bis(hexafluoroacetylacetonato) manganese(II) with 5-*tert*-butyl-1,3-phenylenebis(*N*-*tert*-butyl-aminoxyl) and (4-*N*-*tert*-butyl-*N*-oxyamino)pyridine

RABU, Pierre[1]**; DRILLON, Marc**[1]**; IWAMURA, Hiizu**[2]**; GÖITZ, Gunter**[2]**; ITOH, Tetsuji**[2]**; MATSUDA, Kenji**[2]**; KOGA, Noboru**[2]**; INOUE, Katsuya**
([1]Inst. Phys. Chim. Matér. Strasbourg, France; [2]Kyushu Univ.)

[*Eur. J. Inorg. Chem.* **211**, 216 (2000)]

Temperature-dependant paramagnetic susceptibility data for two cyclic dimer complexes of bis(hexafluoroacetylacetonato)manganese (II) with 5-*tert*-butyl-1,3-phenylenebis(*N*-*tert*-butylaminoxyl) **1** and 4-(*N*-*tert*-butyl-*N*-oxyamino)pyridine have been analyzed to obtain two sets of two intermolecular exchange coupling parameters J_1 and J_2. (Figure 1, Scheme 1) A previous model, based on one of these interractions being much weaker than the other, could not be explicitly correlated to these actual exchange-coupling paramaters. However, the energy levels of the low lying spin states were found to be reproduced reasonably well by the approximate method.

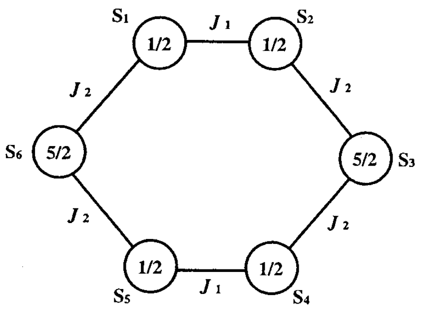

Scheme 1. A cyclic arrangement of the spins in [Mn(hfac)$_2$·**1**]$_2$.

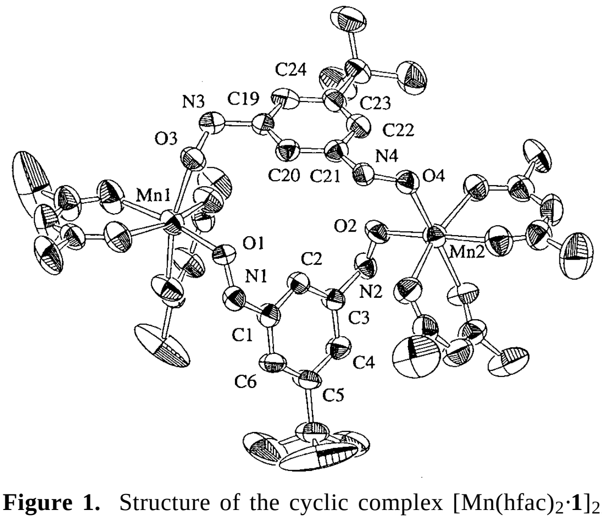

Figure 1. Structure of the cyclic complex [Mn(hfac)$_2$·**1**]$_2$; Fluorine atoms, *N*-*tert*-Butyl groups and hydrogene atoms are omitted for clarity; thermal ellipsoids are drawn at the 50% probability level.

V-D-5 Synthesis and Magnetic Properties of a New Complex Made up of Mn(hfac)$_2$ and a Radical with a Triplet Ground State

KUMAGAI, Hitoshi; HOSOKOSHI, Yuko; MARKOSYAN, Ashot S.[1]**; INOUE, Katsuya**

(*[1]IMS and M.V. Lomonosov Moscow State Univ.)*

[*New J. Chem.* **24**, 537 (2000)]

A new metal-radical complex of Mn(II) made up of Mn(hfac)$_2$ and the radical 4-*N*-*tert*-butylaminoxyl-4'-(1-oxyl-3-oxide-4,4,5,5-tetramethylimidazolin-2-yl)-biphenyl (BIPNNNO) was synthesized. The X-ray single crystal structural analysis revealed that the complex consists of discrete molecules [Mn(hfac)$_2$]·(BIPNNNO)$_2$. The magnetic characteristics of this complex were studied and the Mn–radical and intraradical exchange integrals were evaluated: –135 ± 10 K and 72 ± 5 K, respectively. These values are compared with those of complexes of Mn(hfac)$_2$ with different aminoxyl polyradicals.

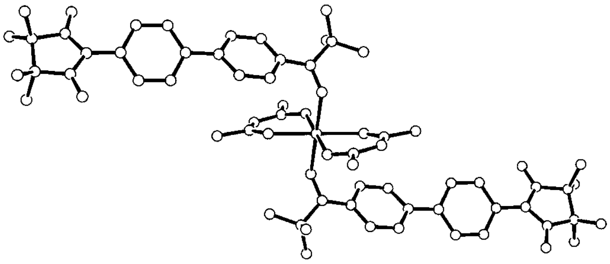

Figure 1. View of the discrete structure of Mn(hfac)$_2$-(BIPNNNO)$_2$.

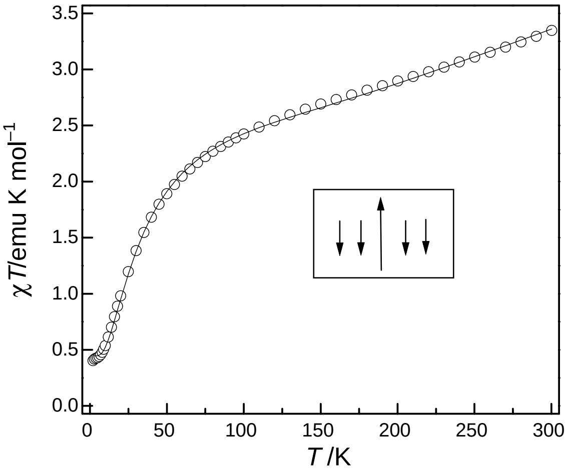

Figure 2. Temperature dependence of $\chi_m T$ of the complex Mn(hfac)$_2$(BIPNNNO)$_2$. The experimental data are shown by symbols and the solid line is the theoretical fit. The spin scheme of the complex is drawn in the frame.

V-D-6 Two-Dimensional Complexes of the General Formula [Mn(hfac)$_2$]$_3$·(R)$_2$ with Variable Metal-Radical Exchange Interactions

TANAKA AKITA, Motoko; HOSOKOSHI, Yuko; MARKOSYAN, Ashot S.[1]; IWAMURA, Hiizu[2]; INOUE, Katsuya

(*[1]IMS and M.V. Lomonosov Moscow State Univ.; [2]Kyushu Univ)*

[*J. Phys. Chem.* submitted]

Magnetic properties of a series of new layered metal-nitroxide polyradical complexes with the general formula [M(hfac)$_2$]$_3$($\mathbf{R}_\Delta$)$_2$, M = Mn(II) or Cu(II), are studied. In these complexes the radicals have a quartet ground state and contribute essentially in magnetism. Several exchange interactions, between M and the NO group of the radical, the intraradical NO–NO interactions, are responsible in forming the magnetic properties of these heterospin systems. Depending on the character of the interlayer chemical bonds, they show either ferro/ferrimagnetic or antiferromagnetic long range order. The hirerachry of the different exchange interactions is established and the Mn–NO and Cu–NO exchange integrals are evaluated from analysis of the temperature dependence of the paramagnetic susceptibility. With increasing intraradical exchange interaction, the complexes exhibit a clear 2D behavior.

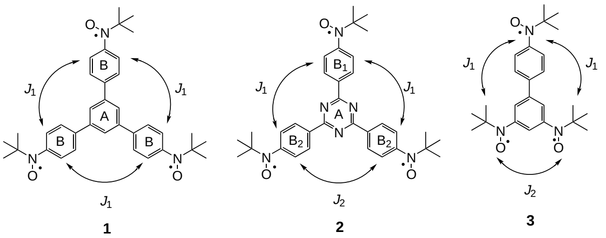

Figure 1. Triangular triradicals **1**, **2** and **3** with three ligating sites. A and B indicate the aromatic rings in different positions.

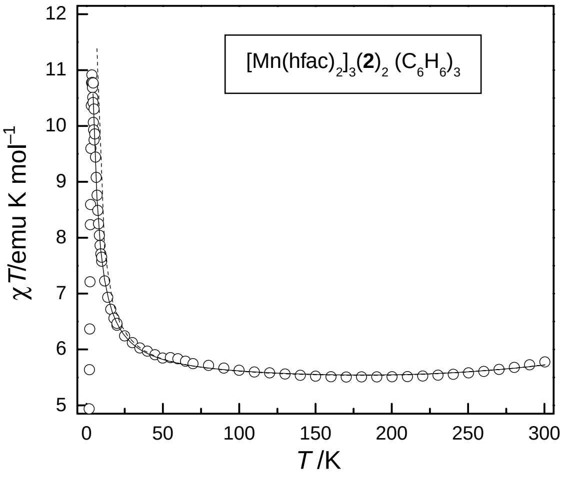

Figure 2. The temperature dependence of the product $\chi_m T$ for the complex [Mn(hfac)$_2$]$_3$(**2**)$_2$·(C$_6$H$_6$)$_3$. Open circles are the experimental data. The solid and the dot lines are the theoretical fits in the 2D and 3D models, respectively.

V-E Synthesis of Chiral Molecule-Based Magnets

The design of molecular materials with interesting magnetic and optical or electrical properties is one of the major challenges in the last few years. The synthesis and study of chiral molecular-based magnetic materials which are transparent for light are of great interest. Novel magneto-optical phenomena have been theoretically predicted and observed in chiral paramagnetic materials in 1997. Although novel properties are expected for such compounds, few examples of chiral molecular-based magnetic materials are still known. To get more insight in their properties it is therefore important to construct such chiral molecule-based magnets in a systematic way. We designed and synthesized a chiral organic radical which was can be employed to construct chiral molecular-based magnets.

V-E-1 Synthesis and Characterization of a Chiral Molecule-Based Metamagnet Made by a Chiral Triplet Organic Radical and Transition Metal Ion

KUMAGAI, Hitoshi; INOUE, Katsuya

[*Mol. Cryst. Liq. Cryst.* **334**, 487 (1999)]

Crystals of {**1**·M(II)(hfac)$_2$}$_n$ (M = Mn, Cu) were obtained by mixing the 1,3-bis(*N*-*tert*-butylamino-*N*-oxyl)-5-{1-methyl-1-((*S*)-2-methylbutoxy)ethyl}-benzene (**1**) and bis(hexafluoroacetylacetonato)M(II) {M(II)·(hfac)$_2$} in diethyl ether/*n*-heptane. A single crystal of {**1**·Mn(II)(hfac)$_2$}$_n$ is triclinic, space group *P*1 (No. 1), with a = 11.0005(3) Å, b = 11.8183(4) Å, c = 17.7135(7) Å, α = 81.607(3)°, β = 84.801(3)°, γ = 63.516(2)°, V = 2038.3(1) Å^3, and D_X = 1.380 g/cm^3 for Z = 1. A single crystal of {**1**·Cu(II)(hfac)$_2$}$_n$ is triclinic, space group *P*1 (No. 1), with a = 11.2831(7) Å, b = 11.5615(7) Å, c = 18.0163(9) Å, α = 82.384(4)°, β = 74.242(4)°, γ = 61.826(5)°, V = 1993.9(2) Å^3, and D_X = 1.43 g/cm^3 for Z = 1. An X-ray crystal structure analysis revealed the formation of a helical one-dimensional polymeric structure. It not only contains a (*S*) chiral carbon center but also (*R*) C2 chiral skeleton of the 1,3-bis(*N*-*tert*-butylamino-*N*-oxyl)benzene moiety. Each of the two aminoxyl radical centers are coupled ferromagnetically within the organic radical molecule and is coupled antiferromagnetically to the d^5 manganese(II) ions. The temperature dependence of the magnetization revealed that the heterospin system behaves as a metamagnet below 5.4 K. (Figure 1)

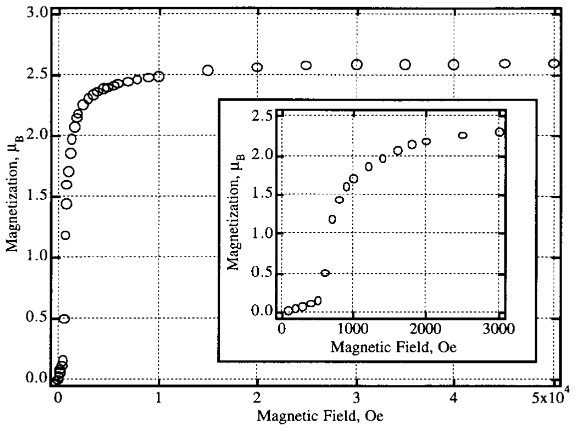

Figure 1. Field dependence of the magnetic moment at 1.8 K. Inset shows magnetic field range of 0 to 3000 Oe.

V-E-2 Synthesis, Structure and Magnetic Properties of a Chiral One-Dimensional Molecule-Based Magnet

KUMAGAI, Hitoshi; MARKOSYAN, Ashot S.[1]; INOUE, Katsuya

([1]IMS and Moscow State Univ., Russia)

[*Mol. Cryst. Liq. Cryst.* **343**, 97 (2000)]

A novel chiral organic radical 2-{4'-((*S*)-2''-methylbutoxy)phenyl}-4,4,5,5-tetramethylimidazoline-1-oxyl-3-oxide (**1**) and its metal complex, [**1**·Mn(II)(hfac)$_2$]$_n$ were synthesized and characterized. The radical **1** crystallizes in the orthorhombic space group $P2_12_12_1$ (No. 19) with a = 11.494(3) Å, b = 25.328(3) Å, c = 6.1281(5) Å, V = 1748.0(4) Å^3. The complex [**1**·Mn(II)-(hfac)$_2$]$_n$ crystallizes in the same space group with a = 14.081(1) Å, b = 15.940(1) Å, c = 16.075(1) Å, V = 3608.1(4) Å^3. X-ray crystal structure analysis of the complex revealed the formation of a helical-chain structure. (Figure 1) The oxygen atoms of the radical **1** are ligated to two different manganese ions in cis position and exhibit the Δ configuration in [**1**·Mn(II)-(hfac)$_2$]$_n$. The magnetic measurements revealed that this chiral complex behaves as a ferrimagnet below T_C = 4.5 K. It is characterized by a strong intrachain exchange correlation, the ratio between the intrachain and interchain exchange interactions being about 10^{-5}.

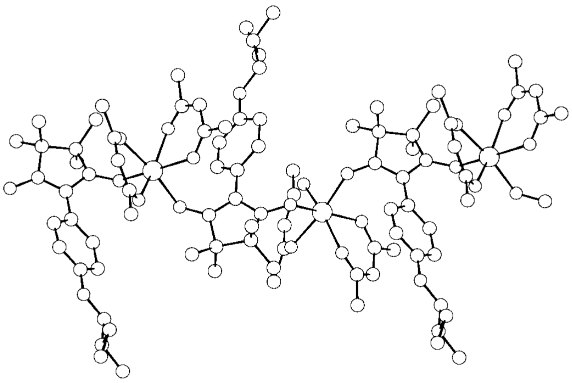

Figure 1. The X-ray crystal structure of the complex of [**1**·Mn(II)(hfac)$_2$]$_n$. Hydrogene atoms and fluorine atoms are omitted for clarity.

V-F Synthesis and Characterization of Quantum-Spin Systems

There has been considerable current interest in the study of a low-dimensional quantum-spin system with an energy gap. Organic radicals suit such study, since they consist only of light elements and form ideal Heisenberg spin systems. By the appropriate design of molecules, we can obtain a variety of Heisenberg spin systems. As S = 1/2 antiferromagnetic lattices, we have synthesized a frustrated double chain system with an energy gap. Moreover, we have developed the study of intermediate state between S = 1/2 and S = 1. We have synthesized novel S = 1 species made of organic biradicals, having strong intramolecular exchange couplings of $2J/k_B$ ~ 200–700 K ($H = -2J\boldsymbol{S}_i \cdot \boldsymbol{S}_j$). Connection of the S = 1 molecules by the intermolecular antiferromagnetic exchange couplings in the crystalline state, leads to the intermediate state between S = 1/2 and S = 1. Adding to these, we focus on the ladder system, which is interesting in terms of Haldane state and the high T_C superconductivity. For the S = 1/2 Heisenberg spin ladder with antiferromagnetic legs and rungs, the ground state of the resonating valence bond (RVB) state or the dimerized state is theoretically expected. Experimentally, the singlet ground state was observed in some ladder systems formed by Cu-based compounds. The study of spin ladder systems has been mainly devoted to that of S = 1/2, but that of S = 1 is also interesting. For the ground state of the S = 1 ladder with antiferromagnetic legs ($J_{\|}$) and rungs ($J_{\perp}$), the Haldane state is expected in the extreme limit of $J_{\perp} \rightarrow 0$, and the dimer state in $J_{\|} \rightarrow 0$. In its ground state phase diagram on the $J_{\|}/J_{\perp}$ versus the energy gap (Δ), the phase transition from the dimer state to the Haldane state through a gapless point can be expected. A similar behavior of an existence of a gapless point between two different phases with their own finite excitation gaps is known for the S = 1 Heisenberg alternating antiferromagnetic chain system.

V-F-1 Construction of a Quantum-Spin System of *S* = 1/2 Antiferromagnetic Chain with the Next-Nearest-Neighbor Interactions

HOSOKOSHI, Yuko; KATOH, Keiichi; INOUE, Katsuya; GOTO, Tsuneaki[1]
([1]ISSP, Univ. Tokyo)

[*J. Phys. Soc. Jpn.* **68**, 2910 (1999)]

We have succeeded in synthesizing a new compound of a railroad trestle model, *i.e.*, a zigzag chain with next-nearest-neighbor interactions, having energy gap above the singlet ground state. We have synthesized novel organic radicals F_2PIMNH and Cl_2PIMNH, where F_2PIMNH = 2-[4'-*N*-*tert*-butylamino-2',6'-difluorophenyl]-4,4,5,5-tetramethyl-4,5-dihydro-1*H*-imidazol-1-oxyl and Cl_2PIMNH = 2-[4'-*N*-*tert*-butylamino-2',6'-dichlorophenyl]-4,4,5,5-tetramethyl-4,5-dihydro-1*H*-imidazol-1-oxyl. Both crystals include zigzag uniform chains made of hydrogen bondings. The magnetism of Cl_2PIMNH is explained by a uniform chain model with $2J_1/k_B = -3.4$ K and gapless ground state is suggested. On the other hand, the temperature dependence of χ_p in F_2PIMNH shows a maximum at around 3.4 K, and the χ_p values decrease rapidly below this temperature and goes exponentially to zero as $T \rightarrow 0$. Singlet ground state of this material is suggested. The magunitude of the energy gap, Δ = 3.1 K, was estimated by fitting the data below 2.4 K with the expression of $\chi \propto \exp(-\Delta/T)$. Comparison of the crystal structure between F_2PIMNH and Cl_2PIMNH, suggests that only F_2PIMNH has significant exchange coupling between the next-nearest-neighbors. The next nearest contact in F_2PIMNH is much shorter than the one in Cl_2PIMNH. There is theoretical expectation for the energy gap in the Heisenberg antiferromagnetic chain with the next-nearest-neighbor interaction. F_2PIMNH studied here is the first example of this model exhibiting an energy gap.

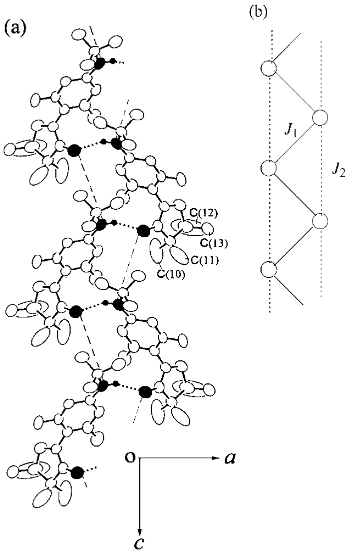

Figure 1. (a) Crystal structure of F_2PIMNH. (b) Scheme of the magnetic interactions in F_2PIMNH.

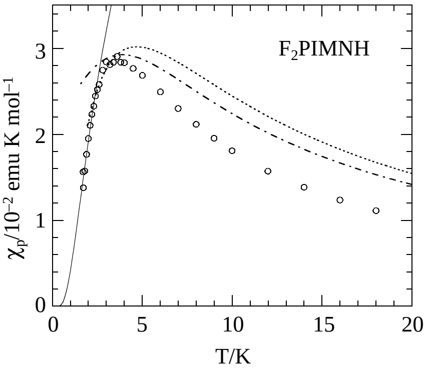

Figure 2. Temperature dependence of χ_p of F_2PIMNH. The solid curve is the fit of $\chi \propto \exp(-\Delta/T)$ with Δ = 3.1 K. The dotted broken curve is the calculation for the uniform chain with $2J/k_B = -6$ K, the interchain interactions by the mean-field treatment of $2zJ'/k_B = -5.2$ K are adopted. The dotted curve represents the calculation for the alternating chain with $2J/k_B = -7.9$ K and $2zJ'/k_B = -6.3$ K.

V-F-2 Magnetic Properties of Low Dimensional Quantum Spin Systems Made of Stable Organic Biradicals PNNNO, F$_2$PNNNO and PIMNO

HOSOKOSHI, Yuko; NAKAZAWA, Yasuhiro; INOUE, Katsuya; TAKIZAWA, Kohichi[1]; NAKANO, Hiroki[1]; TAKAHASHI, Minoru[1]; GOTO, Tsuneaki[1]
([1]ISSP, Univ. Tokyo)

[*Phys. Rev. B* **60**, 12924 (1999)]

Stable organic biradical crystals PNNNO, F$_2$PNNNO and PIMNO of the PNNNO family were synthesized. (PNNNO = 2-[4'-(*N-tert*-butyl-*N*-oxyamino)phenyl]-4,4,5,5-tetramethyl-4,5-dihydro-1*H*-imidazol-1-oxyl 3-oxide, F$_2$PNNNO = 2-[2',6',-difluoro-4'-(*N-tert*-butyl-*N*-oxyamino)phenyl]-4,4,5,5-tetramethyl-4,5-dihydro-1*H*-imidazol-1-oxyl 3-oxide, PIMNO = 2-[4'-(*N-tert*-butyl-*N*-oxyamino)-phenyl]-4,4,5,5-tetramethyl-4,5-dihydro-1*H*-imidazol-1-oxyl.) All the molecules have strong intramolecular ferromagnetic exchange couplings to form $S = 1$ species. Depending on the molecular structure, the magnitude of the exchange coupling varies with $2J/k_B \sim$ 200–700 K. Both crystals of PNNNO and F$_2$PNNNO include similar chain structure formed by the contacts between the nitronyl nitroxide units. However, the magnetic behaviour is quite different from each other. The difference is attributed to the interchain interactions. Only F$_2$PNNNO has short contacts between the *N-tert*-butyl nitroxides as interchain interactions. The different interchain molecular arrangements are related to the difference in the molecular structure. There are noticeable difference in the dihedral angles between the benzene ring and radical planes owing to the electrostatic repulsion between the fluorine atoms and oxygen atoms on radical units. The interchain interactions in F$_2$PNNNO dominate the magnetism of this compound. The temperature dependence of the susceptibility suggests the existence of the energy gap above the singlet ground state. Moreover, the magnetization isotherm at low temperature exhibits a plateau at half the value of the saturation magnetization. These properties are quite rare among higher-dimensional spin systems than one-dimensional ones. Our theoretical calculation gives a qualitatively good explanation for the observed results.

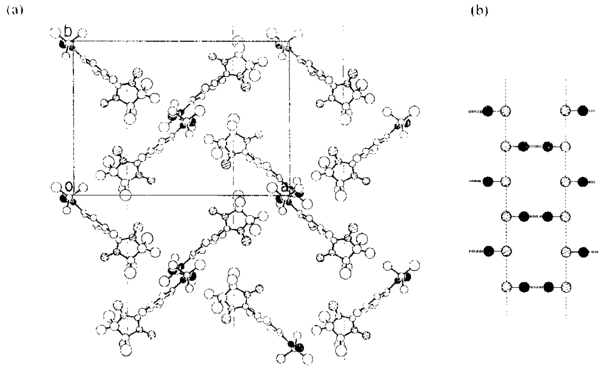

Figure 1. (a) Crystal structure of F$_2$PNNNO projected on the *ab* plane. *Pbca*, $a = 19.857$, $b = 14.010$, $c = 13.481$ Å, $V = 3750.5$ Å^3, $Z = 8$. Black and shaded ellipses represent the *N-tert*-butyl nitroxide and nitronyl nitroxide, respectively. (b) Schematic display of the crystal structure of F$_2$PNNNO. Black and shaded circles are correspond to the *N-tert*-butyl nitroxide and nitronyl nitroxide, respectively. Solid and broken lines represent the exchange path of the intra- and intermolecular interactions, respectively.

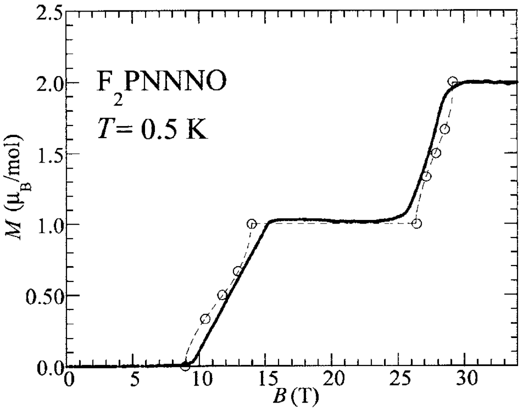

Figure 2. Magnetization process of F$_2$PNNNO at 0.5 K. Circles represent the calculated results.

V-F-3 Singlet Ground States in an Organic S = 1/2 Spin Ladder and a Novel Double Spin Chain of Ferromagnetic Dimers Formed by an Organic Tetraradical

KATOH, Keiichi; HOSOKOSHI, Yuko; INOUE, Katsuya; GOTO, Tsuneaki[1]
([1]ISSP, Univ. Tokyo)

[*J. Phys. Soc. Jpn.* **69**, 1008 (2000)]

We have synthesized novel organic polyradicals BIP-BNO and BIP-TENO, which crystallize to form spin systems with a double spin chain, where BIP-BNO and BIP-TENO denote 3,5'-bis(*N-tert*-butylaminoxyl)-3',5'-dibromobiphenyl and 3,3',5,5'-tetrakis(*N-tert*-butylaminoxyl)biphenyl, respectively. The crystals of BIP–BNO form a two-leg ladder of $S = 1/2$ with antiferromagnetic legs and rungs. The ground state of this material is singlet. The BIP–TENO molecule includes $S = 1/2$ spin pairs (dimers) in which the two spins are coupled ferromagnetically. The BIP-TENO crystals form a double spin chain consisting of dimers. All dimers interact antiferromagnetically with each other. This system can be regarded as an antiferromagnetic two-leg ladder when the dimer is taken as a unit. The ground state of this material is singlet and the existence of excitation gaps is suggested by the temperature dependence of the static magnetic susceptibility.

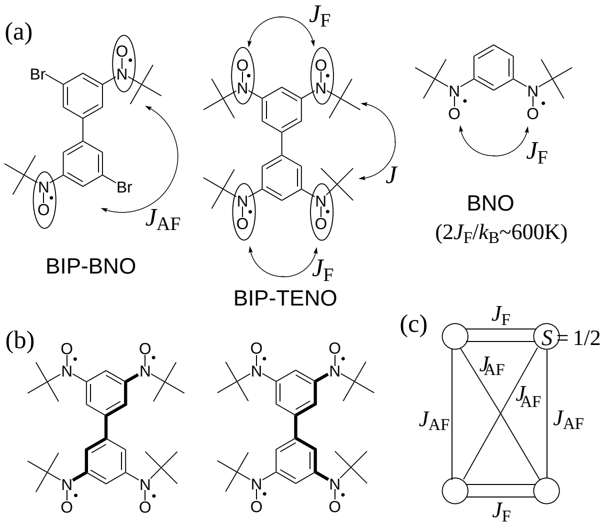

Figure 1. (a) Molecular structures of BIP-BNO, BIP-TENO and a related compound. Ellipses in BIP-BNO and BIP-TENO represent the spin-concentrated parts in a molecule. Each NO group corresponds to an S = 1/2 spin. (b) Path of the throughbond antiferromagnetic exchange interaction in BIP-TENO, which is indicated by bold lines. (c) Schematic diagram of the magnetic model of a BIP-TENO molecule. A circle, a double bond and a single bond represent an S = 1/2 spin, a ferromagnetic exchange coupling, and an antiferromagnetic exchange coupling, respectively.

V-F-4 Observation of Magnetization Plateau of 1/4 in a Novel Double Spin Chain of Ferromagnetic Dimmers Formed by an Organic Tetraradical

GOTO, Tsuneaki[1]; BARTASHEVICH, M. I.[1]; HOSOKOSHI, Yuko; KATOH, Keiichi[2]; INOUE, Katsuya
([1]ISSP, Univ. Tokyo; [2]GUAS)

[*Physica B* in press]

We have measured the susceptibility and low temperature magnetization curve of the novel organic tetraradical crystal BIP-TENO. The susceptibility data indicate that double spin chains of ferromagnetic dimmers are formed in the crystal and the spin system is regarded as an S = 1 antiferromagnetic two-leg ladder. The magnetization is nearly zero up to 10 T and the spin gap is closed at 11.6 T. Above 12 T, the magnetization increases and a plateau corresponding to a quarter of the saturation magnetization appears at 44.8 T.

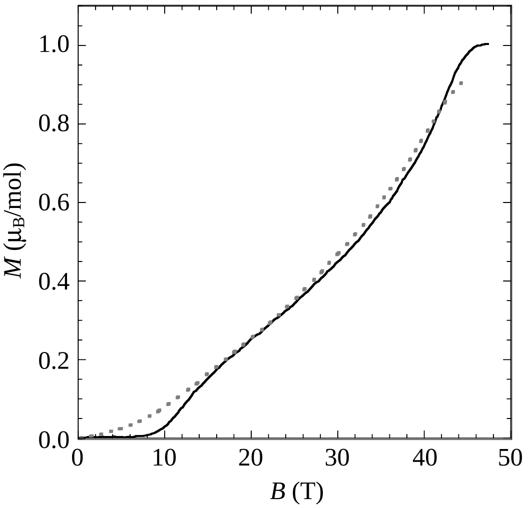

Figure 1. Magnetization curves of BIP–TENO for 1.7 K (solid) and 4.2 K (dotted) in pulsed high magnetic fields up to about 50 T.

V-G Pressure Effects on Molecular Magnetism

'Pressure' is a powerful tool to control the molecular packings and physical properties. The molecule-based materials with small densities are 'soft' and can be expected to exhibit large pressure effects. For the magnetic measurements with high-accuracy, we have developed a small high-pressure clamp cell made of non-magnetic Cu–Ti alloy which can be equipped to a Quantum Design SQUID magnetometer for the dc and ac magnetic measurements. The inner pressure of the clamp cell has been calibrated by the superconducting transition temperature of Pb. We have already discovered that some kind of structural change can be suppressed by pressurization. We are now studying the pressure effects on the molecule-based magnetic materials in wider range. In molecular materials, the spin density are delocalized and distributed in a molecule and the spin-density-distribution plays an important role in the exchange interactions. It is attractive to control the sign of the exchange coupling by pressurization. The pressure effects on the related compounds with similar crystal structures are studied.

V-G-1 Pressure Effect on Mn Complexes of Bisaminoxyl Radicals

HOSOKOSHI, Yuko; SUZUKI, Kentaro[1]; INOUE, Katsuya; IWAMURA, Hiizu[2]
([1]GUAS; [2]Kyushu Univ.)

[*Mol. Cryst. Liq. Cryst.* **334**, 511 (1999)]

The pressure effects on the magnetic properties of one-dimensional Mn(hfac)$_2$ complexes with 1,3-bis(*N*-*tert*-butylaminoxyl)benzene ($\mathbf{1}_H$) and 5-chloro-1,3-bis(*N*-*tert*-butylaminoxyl)benzene ($\mathbf{1}_{Cl}$) have been studied. These complexes have similar chain structures and, due to the weak interchain interactions, undergo three-dimensional magnetic phase transitions at low temperature. At ambient pressure, the former is a metamagnet with T_N = 5.4 K, and the latter is a ferrimagnet with T_C = 4.8 K. The opposite sign of the interchain interactions in these materials is attributed to the different way of packing of the chains. Application of the pressure less than 7 kbar to these materials mainly affects the interchain interactions. The high-temperature behaviour is almost independent of the pressure. In the metamagnetic compound of $[\mathrm{Mn(hfac)_2}]\cdot\mathbf{1}_\mathrm{H}$, enhancement of the antiferromagnetic interchain interactions by pressurization was observed. The transition temperature becomes higher and the critical field becomes larger with applying pressure. The closer spacing of each chains caused by pressurization, yields larger antiferromagnetic interchain interactions in this compound. On the other hand, the response to the pressure of the ferromagnetic compound of $[\mathrm{Mn(hfac)_2}]\cdot\mathbf{1}_\mathrm{Cl}$ is rather complicated. The transition temperature becomes higher and the antiferromagnetic interchain interactions are induced by pressurization. The interchain exchange coupling in this compound should be sensitive to the relative orientation of the chain structure. The decrease of the ferromagnetic contribution and/or the increase of the antiferromagnetic one in the interchain interactions is brought about by pressurization.

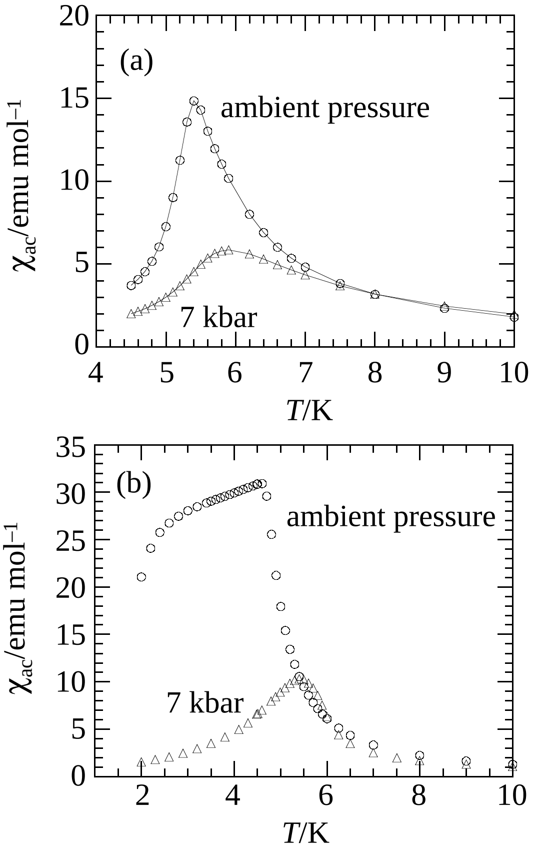

Figure 1. (a) Temperature dependence of the ac susceptibility of $[\mathrm{Mn(hfac)_2}]\cdot\mathbf{1}_\mathrm{H}$ at ambient pressure (○) and under 7 kbar (△). (b) Temperature dependence of the ac susceptibility of $[\mathrm{Mn(hfac)_2}]\cdot\mathbf{1}_\mathrm{Cl}$ at ambient pressure (○) and under 7 kbar (△).

V-G-2 Pressure Effect on Cu(hfac)$_2$ Complex with 5-Bromo-1,3-phenylenebis(*N-tert*-butyl-aminoxyl)—Suppression of the Structural Change under Pressure

HOSOKOSHI, Yuko; IWAHORI, Fumiyasu[1]; SUZUKI, Kentaro[1]; INOUE, Katsuya
([1]GUAS)

5-Bromo-1,3-phenylenebis(*N-tert*-butyl-aminoxyl) (**1**) forms a complex with $\mathrm{Cu(hfac)_2}$ with the formula $[\mathrm{Cu(hfac)_2}]_3\cdot\mathbf{1}_2$. The X-ray crystal structural analysis at room temperature revealed the discrete cluster formation of this unit. The temperature dependence of the susceptibility shows abrupt decrease at around 48 K with thermal hysteresis. The structural change at this temperature is suspected. We studied the magnetic properties under pressure and found that the anomaly at around 48 K disappears under 6 kbar. The susceptibility behaviour under 6 kbar is well understood based on the room-temperature crystal structure. Starting from the non-interacting 3 mol of $S = 1/2$ spin at room temperature, as temperature decreases, ferromagnetic exchange couplings within a cluster dominates the magnetism.

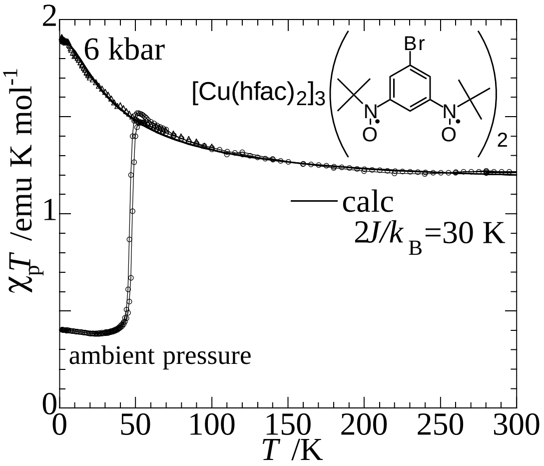

Figure 1. Temperature dependence of $\chi_\mathrm{p}T$ of $[\mathrm{Cu(hfac)_2}]_3\cdot\mathbf{1}_2$ at ambient pressure (○) and under pressure (△). Solid curve is the calclation for the ferromagnetic linear trimer model with $2J/k_\mathrm{B}$ = 30 K.

V-H Desorption Induced by Electronic Transitions at the Surface of Van der Waals Condensates

The electronic excitation on the surface of a van der Waals condensate may lead the desorption of neutral and charged molecules, either in the ground state or in excited ones. The phenomena discussed here are neither thermal desorption nor direct mechanical sputtering but processes through a transformation of an electronic excitation energy into a kinetic energy of a desorbing particle. Close investigation of this DIET (Desorption Induced by Electronic Transitions) phenomena will reveal the dynamical aspect of the electronic excitation and its relaxation process at the surface. In this research project, we have determined the absolute total desorption yield at the surface of solid Ne, Ar, and Kr and have investigated the desorption of the excimer, Ne_2*.

V-H-1 Absolute Measurement of Total Photo Desorption Yield of Solid Ne in Vacuum Ultraviolet Range

ARAKAWA, Ichiro[1]; ADACHI, Takashi[2]; HIRAYAMA, Takato[2]; SAKURAI, Makoto[3]
([1]IMS and Gakushuin Univ.; [2]Gakushuin Univ.; [3]Kobe Univ.)

[*Surf. Sci.* **451**, 136 (2000)]

Absolute yields of photo-induced desorption at the surface of solid Ne have been measured between 25 and 100 nm of wavelength of incident light. There are strong dependence of the total desorption yield of Ne both on the excitation energy and on the thickness of Ne films. On a thick film, the desorption yield is 1–2 atoms/photon by the bulk exciton excitation and 2–10 atoms/photon by the bulk ionization. The main component in the desorbed species is neutral Ne molecules in the ground state; the absolute yield of metastable desorption at the excitonic excitation is the order of 10^{-3} metastable/photon.1) The absolute yield of the order of unity for the total desorption by the bulk exciton excitation can quantitatively be understood by the following internal sputtering model. From optical absorption data, the number of excitons created per photon per layer is estimated at about 0.1. The kinetic energies of the particles desorbed through the cavity ejection mechanism is about 0.2 eV and those by the excimer dissociation one 1 eV. Because the cohesive energy of Ne is 0.019 eV, the desorbing paticle, which is originated from the 2nd or 3rd layer, can blow 10 or more neutral Ne atoms in the overlayer off. The product of these values results in an order of unity of absolute yield of the total desorption. By the surface exciton excitation, the yield is 0.1–0.3 atoms/photon, which value means that the desorption probability of the surface exciton is almost unity.

Reference

1) T. Hirayama, A. Hayama, T. Koike, T. Kuninobu, I. Arakawa, K. Mitsuke, M. Sakurai and E. V. Savchenko, *Surf. Sci.* **390**, 266 (1997).

V-H-2 Desorption of Excimers from the Surface of Solid Ne by Low Energy Electron or Photon Impact

HIRAYAMA, Takato[1]; HAYAMA, Akira[1]; ADACHI, Takashi[1]; ARAKAWA, Ichiro[2]; SAKURAI, Makoto[3]
([1]Gakushuin Univ.; [2]IMS and Gakushuin Univ.; [3]Kobe Univ.)

[*Phys. Rev. B* **63**, in press (2001)]

If solid Ne surface is irradiated by 20–200 eV electrons or by 55–75 nm synchrotron radiation, Ne_2* excimers in $^3\Sigma_u$ state are desorbed to form a luminescent ‘plume’ in front of the sample. The kinetic energy of the desorbed excimers was found to be 0.2 ± 0.1 eV, which indicates that the cavity ejection mechanism1) is valid for the excimer desorption. The decay with time of the plume emission is not of single exponential type, because the emission lifetime of the desorbed excimers, which is of the order of 10^{-6} s, depends on their vibrational level. Most of them are in the highest vibrational level since desorption takes place much faster than vibrational relaxation.

Reference

1) L. F. Chen, G. Q. Huang and K. S. Song, *Nucl. Instrum. Methods Phys. Res., Sect. B* **116**, 61 (1996).

V-I Bioinorganic Studies on Structures and Functions of Non-Heme Metalloenzymes Using Model Complexes

Metal-containing enzymes have been widely distributed in both plants and animals and have been related to metabolic processes such as hydroxylation, oxygen transport, oxidative catalysis, electron transfer, and so on. In this project the structures and functions for the metal complexes are studied as a model of several metallo-enzymes by some physico-chemical methods.

V-I-1 A Novel Diiron Complex as a Functional Model for Hemerythrin

ARII, Hidekazu[1]; NAGATOMO, Shigenori; KITAGAWA, Teizo; MIWA, Tomohiro[1]; JITSUKAWA, Koichiro[1]; EINAGA, Hisahiko[1]; MASUDA, Hideki[2]
([1]Nagoya Inst. Tech.; [2]Nagoya Inst. Tech. and IMS)

[*J. Inorg. Biochem.* in press (2000)]

Diiron(II) complexes with a novel dinucleating polypyridine ligand, *N*,*N*,*N'*,*N'*-tetrakis(6-pivalamido-2-pyridylmethyl)-1,3-diaminopropan-2-ol (HTPPDO), were synthesized as functional models of hemerythrin. Structural characterization of the complexes, $[\mathrm{Fe^{II}}_2\text{-}(\mathrm{Htppdo})(\mathrm{PhCOO})](\mathrm{ClO_4})_3$ (**1**), $[\mathrm{Fe^{II}}_2(\mathrm{Htppdo})(p\text{-}\mathrm{Cl}\text{-}\mathrm{PhCOO})](\mathrm{ClO_4})_3$ (**2**), $[\mathrm{Fe^{II}}_2(\mathrm{Htppdo})(p\text{-}\mathrm{Cl}\text{-}\mathrm{PhCOO})]\text{-}(\mathrm{BF_4})_3$ (**2'**) and $[\mathrm{Fe^{II}}_2(\mathrm{tppdo})(p\text{-}\mathrm{Cl}\text{-}\mathrm{PhCOO})](\mathrm{ClO_4})_2$ (**3**), were accomplished by electronic absorption and IR spectroscopic, electrochemical, and X-ray diffraction methods. The crystal structures of **1** and **2'** revealed that the two iron atoms are asymmetrically coordinated with HTPPDO and bridging benzoate. One of the iron centers (Fe(1)) has a seven-coordinate capped octahedral geometry comprised of an N_3O_4 donor set which includes the propanol oxygen of HTPPDO. The other iron center (Fe(2)) forms an octahedron with an N_3O_3 donor set and one vacant site. The two iron atoms are bridged by benzoate (**1**) or *p*-chlorobenzoate (**2**). On the other hand, both Fe atoms of complex **3** are both symmetrically coordinated with N_3O_4 donors and two bridging ligands, benzoate and the propanolate of TPPDO. Reactions of these complexes with dioxygen were followed by electronic absorption, resonance Raman and ESR spectroscopies. Reversible dioxygen-binding was demonstrated by observation of an intense LMCT band for O_2^{2-} to Fe(III) at 610 (**1**) and 606 nm (**2**) upon exposure of dioxygen to acetone solutions of **1** and **2** prepared under an anaerobic conditions at –50 °C. The resonance Raman spectra of the dioxygen adduct of **1** exhibited two peaks assignable to the ν(O–O) stretching mode at 873 and 887 $\mathrm{cm^{-1}}$, which shifted to 825 and 839 $\mathrm{cm^{-1}}$ upon binding of $^{18}O_2$. ESR spectra of all dioxygen adducts were silent. These findings suggest that dioxygen coordinates to the diiron atoms as a peroxo anion in a μ-1,2 mode. Complex **3** exhibited irreversible dioxygen binding. These results indicate that the reversible binding of dioxygen is governed by the hydrophobicity of the dioxygen-binding environment rather than the iron redox potentials.

V-I-2 Reactivity of Hydroperoxide Bound to a Mononuclear Non-Heme Iron Site

WADA, Akira[1]; OGO, Seiji; NAGATOMO, Shigenori; KITAGAWA, Teizo; WATANABE, Yoshihito; JITSUKAWA, Koichiro[1]; MASUDA, Hideki[2]
([1]Nagoya Inst. Tech.; [2]Nagoya Inst. Tech. and IMS)

The first isolation and spectroscopic characterization of the high-spin mononuclear iron(III) complex with hydroperoxide in an end-on mode, $[\mathrm{Fe(bppa)(OOH)}]^{2+}$, and the stoichiometric oxidation of substrates by the mononuclear iron-oxo intermediate produced by its decomposition have been described. The purple species (**2**) obtained from reaction of $[\mathrm{Fe(bppa)(HCOO)}]\text{-}(\mathrm{ClO_4})_2$ with H_2O_2 in acetone solution at -50 °C gave characteristic UV-vis (λ_{max} = 568 nm, ε = 1200 $\mathrm{M^{-1}cm^{-1}}$), ESR (*g* = 7.54, 5.78 and 4.25, *S* = 5/2), and ESI mass spectra (*m*/*z* = 288.5 corresponding to the ion, $[\mathrm{Fe(bppa)(OOH)}]^{2+}$). The resonance Raman spectrum of **2** in d_6-acetone revealed two intense bands at 621 and 830 $\mathrm{cm^{-1}}$, in which the former band shifted to 599 $\mathrm{cm^{-1}}$ when reacted with ^{18}O-labeled H_2O_2 and the latter band showed a small isotope shift to 813 and 826 $\mathrm{cm^{-1}}$ upon reaction with of $H_2{}^{18}O_2$ and D_2O_2, respectively. Reactions of the isolated $\mathrm{(bppa)Fe^{III}\text{-}OOH}$ (**2**) with various substrates (single turnover oxidations) revealed that the iron-oxo intermediate generated by decomposion of complex **2** is a nucleophilic intermediate formulated as $[\mathrm{(bppa)Fe^{III}–O^{\bullet}}]$.

V-J Synthesis and Physical Properties of Novel Molecular Metals

Development of organic materials which exhibit interesting electrical properties such as metallic conductivity and superconductivity has received considerable attention. A bis-fused TTF, 2,5-bis(1,3-dithiol-2-ylidene)-1,3,4,6-tetrathiapentalene (TTP) is a promising π-electron framework for preparation of stable metals down to low temperatures, because it has a ladder-like array of sulfur atoms indispensable for constructing two-dimensional network of the donors. In fact, we have found that the unsubstituted TTP has a strong tendency to afford highly conducting radical cation salts retaining metallic conductivity down to $\leq$ 1.2 K regardless of shape and size of counter anions. In the present study, we have developed several organic metals by means of comprehensive modification of TTP, namely i) introduction of substituents, ii) exchange of sulfur atoms in the TTP framework with selenium, iii) synthesis of TTP analogs possessing non-TTF donor unit.

V-J-1 Preparation, Structures and Physical Properties of Selenium Analogues of DTEDT as Promising Donors for Organic Metals

FUJIWARA, Hideki[1,2]; MISAKI, Yohji[1,2]; YAMABE, Tokio[1]; MORI, Takehiko[2,3]; MORI, Hatsumi[4]; TANAKA, Shoji[4]
([1]Kyoto Univ.; [2]IMS; [3]Tokyo Inst. Tech.; [4]ISTEC)

[*J. Mater. Chem.* **10**, 1565 (2000)]

Three selenium analogues of DTEDT [2-(1,3-dithiol-2-ylidene)-5-(2-ethanediylidene-1,3-dithiole)-1,3,4,6-tetrathiapentalene] have been synthesized. They showed four pairs of single-electron redox waves. The E_1 values are a little higher by 0.02–0.05 V than that of DTEDT. On the other hand, the E_2–E_1 values are almost equal to that of DTEDT. TCNQ complex and cation radical salts of them show fairly high electrical conductivities and several salts exhibit metallic conductivities. Especially the ReO_4^- and $Au(CN)_2^-$ salts of DTEDS and the SbF_6^-, TaF_6^- and I_3^- salts of DSEDS exhibited stable metallic behaviour down to 1.5–4.2 K. An X-ray crystal structure analysis of the metallic salt $(DSEDS)_3TaF_6$ reveals that this salt has two-dimensional β-type packing motif of donor molecules similar to the superconducting $(DTEDT)_3Au(CN)_2$. The calculated Fermi surface of $(DSEDS)_3TaF_6$ is a two-dimensional closed ellipsoid.

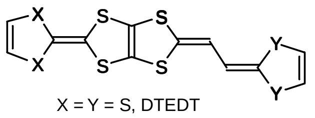

X = Y = S, DTEDT
X = S, Y = Se, DTEDS
X = Se, Y = S, DSEDT
X = Y = Se, DSEDS

(a)

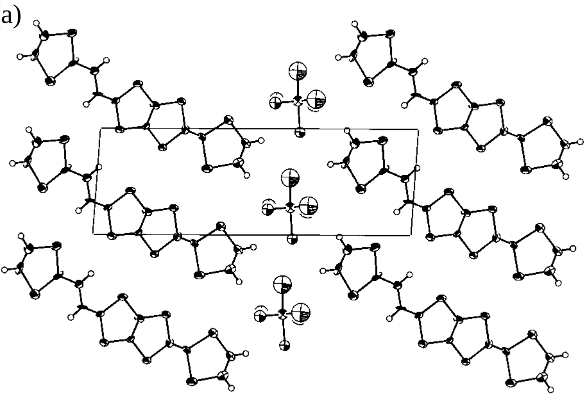

(b)

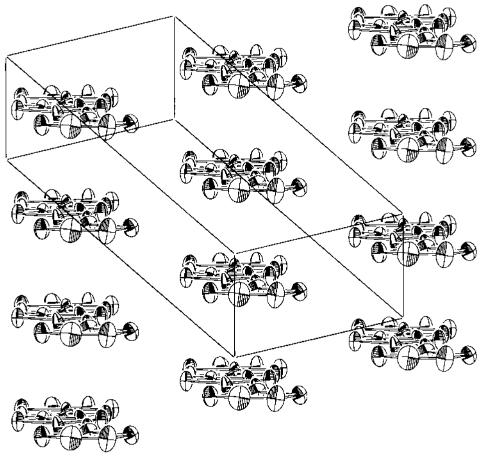

Figure 1. Crystal structures of $(DSEDS)_3TaF_6$ viewed (a) along the *c*-axis and (b) along the molecular long axis.

V-J-2 Preparation and Properties of Gold Complexes with TTF Dithiolato Ligands

MISAKI, Yohji[1,2,3]; TANI, Yoshihiro[1]; TANIGUCHI, Masateru[1]; MAITANI, Tatsuyuki; TANAKA, Kazuyoshi; BECHGAARD, Klaus[3]
([1]Kyoto Univ.; [2]IMS; [3]Risø National Lab.)

[*Mol. Cryst. Liq. Cryst.* **343**, 59 (2000)]

Several gold(III) complexes with TTF dithiolato ligands have been prepared as the tetrahexylammonium salts. The cyclic voltammograms in DMF showed two or three pairs of redox waves. X-Ray structure analysis of $Ph_4P{\cdot}Au(eodt)_2{\cdot}(DMF)_2$ reveals that the $Au(eodt)_2$ anion takes a significantly folded chair conformation. Charge-transfer salts of $Au(dt)_2$ derivatives with TCNQ showed high conductivity (σ_{rt} = 10^0–10^1 S cm^{-1} on a compressed pellet).

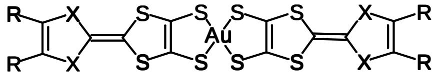

X = S, R = H, $Au(dt)_2$
X = S, R = SMe, $Au(tmdt)_2$
X = S, R = SEt, $Au(tedt)_2$
X = S, 2R = $-(CH_2)_4-$, $Au(chdt)_2$
X = S, 2R = $-O(CH_2)_2O-$, $Au(eodt)_2$
X = Se, R = H, $Au(ds)_2$

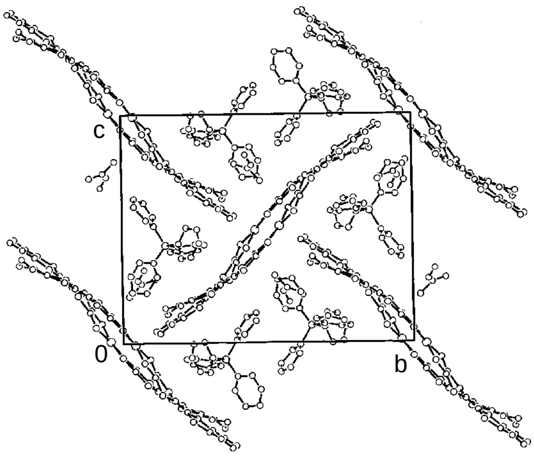

Figure 1. Crystal structure of $Ph_4P{\cdot}Au(eodt)_2{\cdot}(DMF)_2$ viewed onto the *bc* plane.

V-J-3 New TTP Donors Containing Chalcogenopyran-4-ylidene: Preparation, Structures, and Electrical Properties

TAKAHASHI, Kazuyuki[1]; NAKAYASHIKI, Takashi[1]; MISAKI, Yohji[1,2]; TANAKA, Kazuyoshi[1]
([1]Kyoto Univ.; [2]IMS)

Several selenium analogues of TM-PDT-TTP (2-[4,5-bis(methylthio)-1,3-dithiol-2-ylidene]-5-(pyran-4-ylidene)-1,3,4,6-tetrathiapentalene), SM-PDT, SM-TPST, SM-SPDT, and TM-SPDT have been prepared. Among them, SM-PDT affords relatively high conducting 1:1 radical cation salt, $(SM\text{-}PDT)AsF_6{\cdot}H_2O$ (σ_{rt} = 8.3 S cm^{-1}, E_a = 0.045 eV). X-Ray structure analysis of $(SM\text{-}PDT)AsF_6{\cdot}H_2O$ revealed that the side-by-side interactions are inhibited owing to existence of the anions on the side of the donor columns. Instead, the donors form two-dimensional sheets thanks to significant interaction along the donor long axis as well as stacking structure (Figure 1).

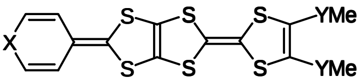

X = O, Y = S, TM-PDT
X = O, Y = Se, SM-PDT
X = S, Y = Se, SM-TPDT
X = Se, Y = Se, SM-SPDT
X = Se, Y = S, TM-SPDT

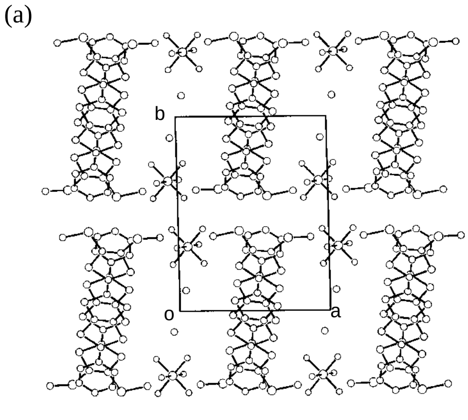

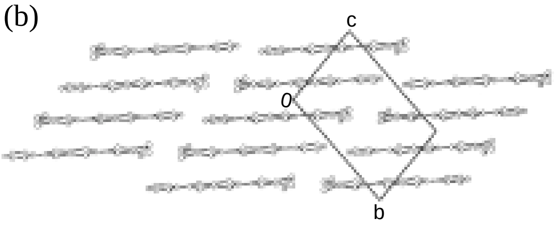

Figure 1. Donor sheet structure of $(SM\text{-}PDT)AsF_6{\cdot}H_2O$.

V-J-4 Structures and Properties of CHEO-TTP Salts

TANIGUCHI, Masateru[1]; MIURA, Takeshi[1]; MISAKI, Yohji[1,2]; TANAKA, Kazuyoshi[1]; YAMABE, Tokio[1]; MORI, Takehiko[2,3]
([1]Kyoto Univ.; [2]IMS; [3]Tokyo Inst. Tech.)

Radical cation salts of CHEO-TTP, where CHEO-TTP is 2-(4,5-cyclohexeno-1,3-dithiol-2-ylidene)-5-(4,5-ethylenedioxy-1,3-dithiol-2-ylidene)-1,3,4,6-tetrathiapentalene showed metallic temperature dependence down to liquid helium temperature. An X-ray crystal structure analysis of $CHEO\text{-}TTP(ReO_4)_{0.35}$ reveals that the arrangement of the donors is the so-called κ-type. The band structure calculated based on a tight-binding approximation suggests the present salt has a two-dimensional Fermi surface similar to those of the superconducting κ-type salts.

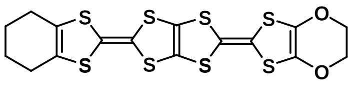

CHEO-TTP

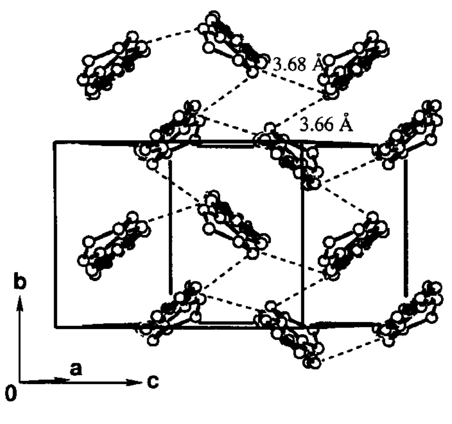

Figure 1. Donor sheet structure of $CHEO\text{-}TTP(ReO_4)_{0.35}$.

V-J-5 Structures and Physical Properties of $(CHTM\text{-}TTP)_2TCNQ$

TANIGUCHI, Masateru[1]; MISAKI, Yohji[1,2]; TANAKA, Kazuyoshi[1]; MORI, Takehiko[2,3]; NAKAMURA, Toshikazu
([1]Kyoto Univ.; [2]IMS; [3]Tokyo Inst. Tech.)

X-Ray structure analysis of the title compound revealed that the donors form a two-dimensional conducting sheets of the so-called β-type, while no significant interaction was observed in the TCNQ sheets. The frequency of CN stretching obtained by IR spectroscopy suggested the degree of charge-transfer in

TCNQ is about –1. A tight binding band calculation indicates the present complex has a quasi one-dimensional Fermi surface closed to the stacking direction. It exhibited metal-like temperature dependence of resistivity down to T_{MI} = 30 K though the resisitvity increased one around 220 K.

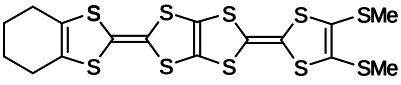

CHTM-TTP

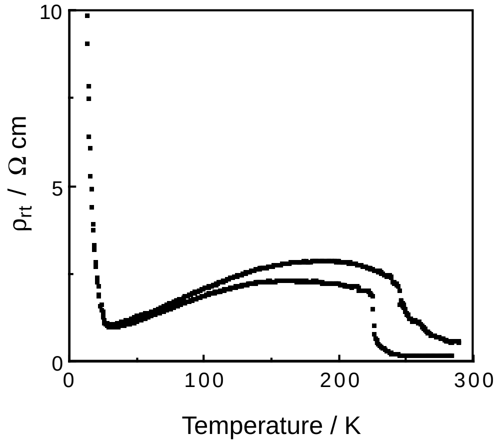

Figure 1. Conducting behaviour of $(\mathrm{CHTM\text{-}TTP})_2\mathrm{TCNQ}$.

V-K Fast Bimolecular Reaction Kinetics in Solution

Since April 2000, we started a new research project for obtaining microscopic pictures of chemical reactions in a solution phase. For this purpose, we construct a new time-resolved spectrometer that can trace reaction kinetics in solution with a time resolution of a few hundreds of femtoseconds. In particular, we try to detect time dependent transient absorption in the near-infrared region accompanying photoexcitation of reactant molecules and following photochemical reactions. A mode-locked Ti:sapphire laser system modified by Prof. Taira's Group, Laser Research Center for Molecular Science, will be used for this study.

V-K-1 Ultrafast Bimolecular Reaction Kinetics between S_1 *trans*-Stilbene and Carbon Tetrachloride Studied by Sub-Picosecond Time-Resolved Visible Absorption Spectroscopy

IWATA, Koichi[1,2]; HAMAGUCHI, Hiro-o[1]
([1]Univ. Tokyo; [2]IMS)

[*Chem. Lett.* 456 (2000)]

Ultrafast bimolecular reaction kinetics between S_1 *trans*-stilbene and carbon tetrachloride is monitored by sub-picosecond time-resolved visible absorption spectroscopy. After the photoexcitation at 270 nm, the S_n–S_1 transition of *trans*-stilbene observed at 580 nm is quenched in a few picoseconds due to a bimolecular photochemical reaction between *trans*-stilbene and carbon tetrachloride. The observed reaction kinetics is well explained by assuming a time dependent bimolecular rate constant derived either from Smoluchowski's theory or from Collins-Kimball's theory of diffusion-controlled reactions. It is not obvious if diffusion is a suitable concept for describing a translational motion of molecules in a time period of a few picoseconds. The model of diffusion should be used for transportation phenomena, such as heat dissipation or molecular motion, in a macroscopic system. However, the experimental result suggests that the molecular motion in solution for a few picosecond time period is well described as a diffusion process for this molecular system.

V-L Development of Model Core Potentials and Post Hartree-Fock Calculations to Atoms and Molecules

We have developed various types of model core potentials for various elements and applied the MCPs to investigate the electronic structures of atoms, molecules, and clusters at levels of post Hartree-Fock calculations. We also investigaed the electronic and vibrational structures of molecules using basis functions for all electrons.

V-L-1 A Theoretical Study on the Ionization of CO_2 and CS_2 with Analysis of the Vibrational Structure of the Photoelectron Spectra

TAKESHITA, Kouichi[1]; SHIDA, Norihiro[2]; MIYOSHI, Eisaku
([1]Tokyo Univ. Agric.; [2]Nagoya Inst. Tech.)

[*J. Chem. Phys.* **112**, 10838 (2000)]

We have studied the vibrational eigenfunctions, the Frank-Condon factors (FCFs), and the theoretical intensity curves of the four ionic states ($^2\Pi_g$, $^2\Pi_u$, $^2\Sigma_u^+$, and $^2\Sigma_g^+$) of CO_2 and CS_2 by explicit vibrational calculations using the global region of the potential energy (PE) surface at the MRSDCI level.

The theoretical intensity curves reproduce well the PE spectra. An assignment of the vibrational structures agrees in most cases with that obtained by Turner *et al.*

For the first ionic state ($^2\Pi_g$) of CO_2, the vibrational excitations of the antisymmetric stretching mode should be observed. This situation is connected with the fact that the difference of the vibrational frequencies of the antisymmetric stretching mode between the final and initial states is large. The difference between the two is 1063 cm^{-1}. The FCFs of the (0 0 2) and (1 0 2) transitions are 0.013 and 0.005, respectively. For the first ionic state ($^2\Pi_g$) of CS_2, the difference of the two is 220 cm^{-1}, which is a fifth of that for CO_2. The FCF of the (0 0 2) transition is 0.002.

The spectra of the second ionic states ($^2\Pi_u$) of CO_2 and CS_2 have broad features compared with the other states. This is attributed to the large change (~0.06 Å) in the bond length upon ionization. The change of the $^2\Pi_u$ state is more than three times as large as that of the other states.

V-L-2 A Theoretical Study on the Ionization of OCS with Analysis of the Vibrational Structure of the Photoelectron Spectrum

TAKESHITA, Kouichi[1]; SHIDA, Norihiro[2]; MIYOSHI, Eisaku
([1]Tokyo Univ. Agri.; [2]Nagoya Inst. Tech.)

[*Theor. Chem. Acc.* submitted]

We have studied the vibrational eigenfunctions, the Frank-Condon factors (FCFs), and the theoretical intensity curves of the four ionic states ($1^2\Pi$, $2^2\Pi$, $1^2\Sigma^+$, and $2^2\Sigma^+$) of OCS by explicit vibrational calculations using the global region of the potential energy (PE) surface at the MRSDCI level.

The theoretical intensity curves reproduce well the PE spectrum except for the spin-orbit splitting. The present calculation supports the assignment of the vibrational structures obtained by Turner *et al.* Delwiche *et al.* have reported the more resolved PE spectrum. An assignment of the vibrational structures is almost consistent with their assignment.

The present calculation proposes the following additional assignment: For the fourth peak of the first ionic state, the (3 0) transition also contributes to intensity in addition to the (0 1) transition. The weak peak at 18.6 eV of the fourth ionic state should be assigned to the (1 2) transition.

V-L-3 Configuration Interaction Study of Differential Correlation Energies in Ca^+, Ca and Ca^-

OSANAI, You[1]; NORO, Takeshi[2]; MIYOSHI, Eisaku
([1]Aomori Univ.; [2]Hokkaido Univ.)

[*Phys. Rev. A* **62**, in press (2000)]

Configuration interaction (CI) calculations have been carried out for Ca^+ (4s ^2S, 3d ^2D and 4p $^2P^o$), Ca ($4s^2$ ^1S and 3d4s ^1D) and Ca^- ($4s^24p$ $^2P^o$) using very large Slate-type orbitals. The effect of Ar-like core was included by allowing the excitation from the most important subshells of the core, 3s and 3p, explicitly. A series of multi-reference single and double excitation CI calculations was performed adding important configurations representing valence correlation to the reference space, and convergence of CI energies and wavefunctions was investigated. Valence correlation can be described adequately only when the reference space is expanded so largely that valence correlation is almost completely described by reference functions alone. The relativistic effects were estimated by carrying out Dirac-Fock calculations. The present calculations gave the ionization potentials to 4s ^2S, 3d ^2D and 4p $^2P^o$ to be 6.079, 7.819 and 9.179 eV, respectively, and the excitation energy to 3d4s ^1D to be 2.805 eV. All these calculated values are in good agreement with the observed values. The electron affinity was obtained to be 17.7 meV, which is in excellent agreement with the recent observed values, 17.5 ~ 21.5 meV.

V-L-4 Spin-Orbit Configuration Interaction Calculations of Low-Lying Electronic States of NaCl Using Model Core Potential

MIYOSHI, Eisaku; SEIJO, Luis; SAKAI, Yoshiko[1]
([1]Kyushu Univ.)

We performed spin-orbit CI calculations for the low-lying $\Omega = 0^+$ states of the NaI molecule in the framework of the model core potentail (MCP) method.

For the I atom, we used scalar relativistic dsp-MCP and (8s/7p/6d) basis set augmented with one diffuse s- and p-type GTFs and two d- and f-type polarization GTFs, resulting in (6111/5111/5111/11). For the Na atom, we used all-electron (533/5) augmented with two p- and d-type polarization GTFs, resulting in (521111/4111/11). The spin-orbit term was calculated in the follwing form:

$$V_{SO,nl}^{mcp}(r) = \lambda \sum_i \frac{B_i \exp\left(-\beta_i r^2\right)}{r^2}$$

where λ is a scaling factor.

The potential energy curve of the $A^1\Sigma^+$ state calculated at spin-free scalar relativistic treatment (quasi-relativistic calculation including only mass-velocity and Dawin terms) is almost the same as those given by previous MO calculations but the potential energy curve of the first excited $A0^+$ state calculated at spin-orbit CI treatment is almost the same as those given from the data of previous experiments. The first excited $A0^+$ state has a weight (80%) of the covalent $^3\Pi$ state and 20% of the covalent $A^1\Sigma^+$ state around the ground state equilibrium distance. Thus, the state can be a dipole-allowed transition state with a large transition probability from the ionic ground $X^1\Sigma^+$ state.

V-M Theoretical Study of the Electronic Structures of Weakly Bound Molecules

The electronic structures of weakly bound molecules such as van der Waals molecules are investigated by using sophisticated methods for electronic states, *i.e.*, multi-reference single and double excitation configuration interaction (MRSDCI) and multi-reference coupled pair approximation (MRCPA) calculations.

V-M-1 *Ab initio* Molecular Orbital Study of $Fe(CO)_n$ (n = 1, 2, and 3)

HONDA, Hiroaki[1]; NORO, Takeshi[1]; MIYOSHI, Eisaku
([1]Hokkaido Univ.)

[*Theor. Chem. Acc.* **104**, 140 (2000)]

Various unsaturated iron carbonyl complexes $Fe(CO)_n$ (n = 1 to 4) have been produced by the UV photolysis of iron pentacarbonyl $Fe(CO)_5$. Among them the spectroscopic studies of the FeCO radical has been extensively performed from both experimental and theoretical points of view and there have been a few experimental spectroscopic constants of $Fe(CO)_2$ and $Fe(CO)_3$.

Although there have been published several theoretical studies for $Fe(CO)_2$ and $Fe(CO)_3$, there are few comprehensive studies for the change of bonding nature in the $Fe(CO)_n$ (n = 1 to 3) radicals. In this study we have carried out MCSCF calculations for the $Fe(CO)_n$ (n = 1 to 3) to investigate the nature of bonding respect to change in the number of CO ligands. The calculated bond lengths of R(Fe–C) are reasonably in agreement with experimental values and more sophisticated theoretical results. From the Mulliken population analysis, the traditional donation and back donation mechanism is valid for FeCO through $Fe(CO)_3$.

V-M-2 *Ab initio* CASSCF and MRSDCI Calculations of the $(C_6H_6)_3^+$ Radical

MIYOSHI, Eisaku; GHOSH, Tapas Kumar

[*Chem. Phys. Lett.* **323**, 434 (2000)]

Ab initio complete active space self-consistent-field (CASSCF), single-reference singly and doubly excited configuration interaction (SRSDCI), and multi-reference SDCI (MRSDCI) calculations were performed for the benzene trimer cation radical, $(C_6H_6)_3^+$, in the ground state. We obtained the equilibrium geometry of the D_{6h} sandwich structure and found that the global minimum of the cation is at the distorted C_{2v} sandwich structures. This minimum is 0.032 eV lower than that of the D_{6h} sandwich structure. The dissociation energy (D_e) relative to $(C_6H_6)_2^+ + C_6H_6$ was calculated to be 0.43 eV, in comparison to the experimental value (D_0) of 0.34 ± 0.02 eV. Our calculations suggest that the bands observed by Nishi and co-workers at 1.02 and 1.29 eV can both be assigned to the split components of the $^2E_{1u}$ state, which are charge resonance states. This is also the case for the benzene dimer cation radical. In the ground state of the trimer cation radical, almost all the charge is localized at the central benzene ring, which has a gross charge of +0.9. This observation contrasts with speculations by experimentalists that the charge is localized in the dimer core or delocalized over all three benzene rings.

V-M-3 Molecular Orbital Study on OH Stretching Frequency of Phenol Dimer and its Cation

GHOSH, Tapas Kumar; MIYOSHI, Eisaku

[*Theor. Chem. Acc.* **105**, in press(2000)]

Ab initio calculations were performed to investigate the structure and bonding of the phenol dimer and its cation, especially, the OH stretching frequencies. Some stable structures of the phenol dimer and its cation were obtained at the Hartree-Fock level and were found in agreement with predictions based on spectroscopic investigations. In these dimers the phenol moieties are bound by a single OH··O hydrogen bond. The hydrogen bond is much stronger in the dimer cation than in the neutral dimer. The calculated binding energy of the phenol dimer in the most stable structure was 6.5 ~ 9.9 kcal/mol at various levels of calculation compared with the experimental value of ≥ 5 kcal/mol. The binding energy of the phenol dimer cation is more than three times (24.1 ~ 30.6 kcal/mol) as large as that of the neutral dimer. For the phenol dimer the OH stretching frequency of the proton accepting phenol (PAP) is 3652 cm^{-1} and that of the proton donating phenol (PDP) is 3516 cm^{-1}; these are in agreement with observed values of 3654 cm^{-1} and 3530 cm^{-1}, respectively. For the phenol dimer cation the OH stretching frequency of the PAP is 3616 ~ 3618 cm^{-1} in comparison with an observed value of 3620 ± 3 cm^{-1}. That of the PDP in the dimer cation is calculated to be 2434 ~ 2447 cm^{-1}, which is 1210 ~ 1223 cm^{-1} smaller than that of the bare phenol. The large reduction of the OH stretching frequency of the PDP in the phenol dimer cation is attributed to the formation of a stronger hydrogen bond in the cation than in the neutral dimer.

V-N Theory for Quantum Liquids and Molecular Dynamics Study Using Potentials by *ab initio* Molecular Orbital Calculations

We derived generalized Ornstein-Zernike equations for quantum liquids. The set of equations can be applicable to homogeneous and isotropic Bose and Fermi liquids such as ^{3}He, ^{4}He, and electron liquids at arbitrary temperature. Using potentials obtained by ab initio molecular orbital calculations, molecular dynamics calculations were also performed to investigate physical properties of liquid mercury.

V-N-1 An Integral Equation Theory for Quantum Liquids: Finite-Temperature Kohn-Sham Debsity-Functional Formulation

SUMI, Tomonari; SATO, Hirofumi; HIRATA, Fumio; MIYOSHI, Eisaku

[*Phys. Rev. E* submitted]

We derived a generalized Ornstein-Zernike equation for quantum liquids, where the uncertainty in particle position is considered by using a self-correlation function for an ideal quantum liquid. To determine a self-consistent solution of the finite-temperature Kohn-Sham equation introduced by Chihara [*Prog. Theor. Phys.* **50**, 1156 (1973)] combined with the generalized Ornstein-Zernike equation for quantum liquids, we present two types of closure relation. One is obtained by extending Percus' method for quantum liquids, and the other is derived from the nonlinear Debye-H_ckel approximation. These sets of equations can be used to determine the pair correlation function and the direct correlation function for homogeneous and isotropic Bose and Fermi liquids.

V-N-2 Structure Change of Supercritical Mercury

SUMI, Tomonari; MIYOSHI, Eisaku

It has been well known that density fluctuations and correlation lengths which are related to the long-range structure of liquids have maxima in the supercritical region. Morita *et al.* found by using small-angle X-ray scattering experiments that the maxima for supercritical water, CO_2, and CF_3H are in a little lower density region than the critial isochore.1) They also estimated the density fluctuations and correlation lengths of Hg by using the equations of state and showed that the maxima are in the lower density region from the critical isochore and the deviations become larger with increasing temperature.

We have performed molecular-dynamics (MD) calculations for liquid mercury in the regions including the metal-nonmetal transition region under pair-potential approximation using the potential energy curve of the dimeric Hg, and showed that the pair-potential approximation gives a good qualitative description of the metallic interatomic force for liquid mercury and MD calculations using this approximation demonstrate the characteristic change of force fields between liqiud metal and liquid semiconductor.2) In the present study, we performed MD calculations for superdritical mercury under fixed pressures and discussed the relationship between fluctuations of the long-range structure and the change of the local structure.

The density dependence of the first peak of the pair distribution function were examined for supercritical mercury under a fixed pressure, showing that the peak shifts to longer distance with decreasing density, while the peak height has minimum at a density. This change is due to a crossover from shorter distance between the nearest neighboring atoms in liquid phase to longer distance in gas phase. It can be easily considered that the fluctuations of local structure become large near the crossover region.

References

1) T. Morita *et al.*, *J. Chem. Phys.* **112**, 4203 (2000).
2) T. Sumi, E. Miyoshi and K. Tanaka, *Phys. Rev. B* **59**, 6153 (1999).

V-O Determination of Structures of Neutral Clusters

The relationship between the structure and dynamics in floppy systems is a subject that has focused much attention recently. Specifically the “geared interconversion” of hydrogen bonded dimers such as $(HCl)_2$, $(DCl)_2$, and $(HF)_2$ have been studied extensively both experimentally and theoretically. Most of the experimental studies focused on the spectroscopy of these species, from which the tunneling splitting could be extracted. We applied a hexapole field to extract the dipole moment of $(HCl)_2$ and we find that interconversion’’ of hydrogen bonded dimers can be directly observed by the hexapole field method. Secondly, the metal-ligand cluster beam serves as a model system for studying metal-ligand interaction, however little is known about interaction between Al and simple molecule as isolated system in the gas phase. We demonstrate again how successfully the hexapole method can be applied to newly synthesized complexes of Al–CH_3CN and Al–NH_3.

V-O-1 Focusing of DCl and HCl Dimers by an Electrostatic Hexapole Field—The Role of the Tunneling Motion

IMURA, Kohei[1]; KASAI, Toshio[2]; OHOYAMA, Hiroshi[1]; NAAMAN, Ron[3]
([1]Osaka Univ.; [2]IMS and Osaka Univ.; [3]Weizmann Inst. Sci.)

[*J. Chem. Phys.* **110**, 355 (1999)]

The focusing of HCl and DCl dimers was observed using a 2-m-long electrostatic hexapole field. The results indicate the existence of two types of species. The first is the homodimers, either the $H^{35}Cl{\cdot}H^{35}Cl$ or the $D^{35}Cl{\cdot}D^{35}Cl$, for which the data indicate a fast tunneling motion. The second is the heterodimers, $H^{35}Cl{\cdot}H^{37}Cl$ or $D^{35}Cl{\cdot}D^{37}Cl$, that do not show evidence for significant tunneling motion on the time scale of the experiment. In the case of HCl dimers, even at relatively high fields, only one species could be focused, the heterodimer. The electric dipole moments for both $(DCl)_2$ isotopomers were determined to be 1.5 ± 0.2 D, which is the same value as observed for $(HCl)_2$.

V-O-2 Tunneling Motion in $(HCl)_2$ Hydrogen-Bonded Dimer Probed by Electrostatic Hexapole and Doppler-Selected TOF Measurement for the Internal Energy Distribution of [ClHCl]

IMURA, Kohei[1]; OHOYAMA, Hiroshi[1]; NAAMAN, Ron[2]; CHE D.-C.[3]; HASHINOKUCHI, Masahiro[3]; KASAI, Toshio[3]
([1]Osaka Univ.; [2]Weizmann Inst. Sci.; [3]IMS and Osaka Univ.)

[*J. Mol. Struct.* **552**, 137 (2000)]

The tunneling motion in $(HCl)_2$ hydrogen bonded dimer and its deuterate was probed by a 2-m long electrostatic hexapole field. The focusing curves of the dimers confirmed existence of homo and hetero dimers in the cluster beam. The homodimer, either $H^{35}Cl{\cdot}H^{35}Cl$ or $H^{37}Cl{\cdot}H^{37}Cl$, undergoes fast tunneling motion for the two hydrogen atoms in the dimer. The heterodimer, namely $H^{35}Cl{\cdot}H^{37}Cl$ on the other hand, does not show such fast tunneling motion on the time scale of experiment. The observed ratio of homo to hetero dimer was estimated to be 20 ± 10, and this value differs largely from the natural abundance for chlorine isotope. An experimental scheme to discern homo and hetero dimers is proposed here. By looking at fragments in $(HCl)_2$ dimer photodissociaiton using a Doppler-selected time-of-flight (TOF) technique, internal energy distribution of [ClHCl] fragment was measured in 121.6-nm photodissociation. The TOF spectrum consists of fast and slow velocity components for dissociated H atoms. It is found that the slow H component arises from the hydrogen escapes after many collisions. The fast H component arises from direct H escape without any collision, thus this component reflects internal and/or electronic state of counter part fragment, *i.e.* [ClHCl]. Vibrational structure of [ClHCl] was observed for the fast H component of the TOF spectrum.

V-P Reaction Dynamics in the Gas Phase and on Surface

The reactions of metastable rare gas atoms with small molecules have provided a long-standing interest, because of the variety of possible involved reaction channels. These include electronic energy transfer, molecular dissociation, excimer formation, Penning ionization, etc. Among them, Penning ionization has been widely studied in recent years. It has been suggested that anisotropy effects influence Penning ionization. We explore the stereodynamical aspect of this reaction using the oriented molecular beam of CH_3Cl.

Surface reactions of hydrogen with atomic and molecular adsorbates on metal and semiconductor surfaces have been paid much attention because of the fundamental interest in the mechanism and dynamics of these reactions. Especially, abstraction of chemisorbed H(D) atoms by the gas-phase H(D) atoms have been extensively studied theoretically and experimentally because of its simplicity and its important roles in the catalytic reactions. We directly identify the desorbed molecules during the reaction and discuss a possible model of H-D exchange reaction.

V-P-1 Evidence for Steric Effect in Methyl Chloride Ionization by Metastable Argon Atoms

OHOYAMA, Hiroshi[1]; KAWAGUCHI, Hiroshi[1]; YAMATO, Masanori[1]; KASAI, Toshio[2]; BRUNETTI, Brunetto G.[3]; VECCHIOCATTIVI, Franco[3]
([1]Osaka Univ.; [2]IMS and Osaka Univ.; [3]Univ. Perugia)

[*Chem. Phys. Lett.* **313**, 484 (1999)]

The orientation dependence of methyl chloride ionization by collision with metastable argon atoms at an average collision energy of 0.09 eV has been investigated, using an electric hexapole field selector followed by an orienting field. The steric opacity function of the process has been determined. The highest reactivity has been found for approaches of the metastable atom towards the Cl-end of the molecule, while the lowest corresponds to the opposite approaches close to the CH_3-end. The stereo-selectivity is discussed in terms of spatial distribution of the highest occupied molecular orbital of CH_3Cl, mainly localized on the chlorine atom.

V-P-2 Direct Observation of Steric Effect in Penning Ionization Reaction of Ar* + $CHCl_3 \rightarrow CHCl_2^+ + Cl + e^- + Ar$

YAMATO, Masanori[1]; OKADA, Seiki[1]; WU, Victor Wei-Keh[1]; OHOYAMA, Hiroshi[1]; KASAI, Toshio[2]
([1]Osaka Univ.; [2]IMS and Osaka Univ.)

[*J. Chem. Phys.* **113**, 6673 (2000)]

Steric effect in the Penning ionization reaction of Ar* ($^3P_{2,0}$) + $CHCl_3 \rightarrow Ar + CHCl_2^+ + Cl + e^-$ was directly observed at an average collision energy of 0.13 eV using the oriented $CHCl_3$ molecular beam. The product $CHCl_2^+$ ions are measured for the H-end, the CCl_3-end, and sideways orientations. The obtained steric opacity function reveals that the CCl_3-end orientation is more favorable than the H-end orientation, and the sideways approach is found to be more favorable than the collinear approaches from both ends of the molecule. Furthermore, we confirm the good correlation between Penning ionization anisotropy and the electron density distribution of $2a_2$ HOMO orbital of $CHCl_3$ molecule, whose electron cloud is mostly localized around the sideways. These results substantiate the electron exchange mechanism which is commonly accepted for Penning ionization reaction, where the overlap of projectile atomic and target molecular orbital plays a key role in Penning ionization efficiency.

V-P-3 Hydrogen Adsorption and Reaction on the Ir{100}-(1×5) Surface

MORITANI, Kousuke[1]; OKADA, Michio[1]; KASAI, Toshio[2]; MURATA, Yoshitada[3]
([1]Osaka Univ.; [2]IMS and Osaka Univ.; [3]Univ. Electro-Commun.)

[*Surf. Sci.* **445**, 315 (2000)]

Adsorption of hydrogen (deuterium) on the Ir{100} surface has been studied with low-energy electron diffraction (LEED) and temperature-programmed desorption (TPD). At least three well-defined peaks can be identified with peak temperatures (T_p) of 125, 240, and 375 K in the TPD spectrum for the surface saturated with H at ~100 K. From the LEED observations, it can be concluded that these three peaks in the TPD spectrum correspond to H_2 desorption from the (1×5), (1×3), and (1×1) restructured phases, respectively. Furthermore, the result suggests that a metastable state of (1×3) exists on the Ir{100} surface in addition to the (1×1) phase. The series of TPD spectra for coadsorption of H_2 and D_2 on the Ir{100} surface show that an energetic D(H) atom produced in the dissociation process of incident $D_2(H_2)$ replaces a preadsorbed H(D) atom via energy transfer and the expelled H(D) atom moves to another adsorption site.

V-P-4 Hot Atom Mechanism in Hydrogen Exchange Reaction on the Ir{100} Surface

OKADA, Michio[1]; MORITANI, Kousuke[1]; NAKAMURA, Mamiko[1]; KASAI, Toshio[2]; MURATA, Yoshitada[3]
([1]Osaka Univ.; [2]IMS and Osaka Univ.; [3]Univ. Electro-Commun.)

[*Chem. Phys. Lett.* **323**, 586 (2000)]

H_2 exposure was found to induce the desorption of HD and D_2 molecules from the D-precovered Ir{100} surface. This result suggests that energetic H atoms (hot H atoms) produced in the dissociation process of incident H_s molecules react with preadsorbed D atoms and desorb as HD molecules or produce secondary energetic D atoms via energy transfer. Secondary energetic D atoms (secondary hot D atoms) also induce the associative reactions with preadsorbed D atoms and desorb as D_2 molecules.

V-Q Millimeter-Wave Spectroscopy Combined with Pulsed-Jet Expansion Technique for the Detection of the Novel Unstable Species and the van der Waals Mode Transitions of Molecular Clusters

Molecular clusters have inherently low-frequency vibrations, so called van der Waals (vdW) vibrational modes, which are characteristic of the weakly bound complexes. The frequency of the vdW mode usually falls in the far-infrared region (30–300 cm^{-1}). However, if a cluster is extremely floppy, it sometimes falls in the submillimeter-wave (SMMW) region below 30 cm^{-1}.

In this project, a millimeter-wave absorption spectrometer combined with pulsed-jet expansion technique has been devised and applied to the direct observation of the rovibrational transitions of the vdW bending band of molecular clusters. We have applied this technique to observe the vdW bending bands of the Ar–HCN (j = 1–0 and 2–1) and Ar–DCN (j = 1–0) clusters as well as the Ar–HBr (Σ_1–Σ_0) and OCO–HF (1^1–0^0 ($\nu_b{}^1$)) clusters. In this year, we have extended our measurements to the clusters as He–HCN, Ne–HCN, H_2–HCN, and H_2–H_2O. To increase the detection sensitivity, we employed a White-type multi-reflection optical system in the millimeter-wave region. The radiation was focused 20 times on the jet beam, and the improved sensitivity (of about one order of magnitude) was attained than the previous single path measurement.

The He–HCN cluster, for example, is a very weakly bound cluster with a binding energy of only 9 cm^{-1}. We have observed a number of j = 1–0 vdW transitions in 95–125 GHz and several observed levels are very close to the dissociation limit. The HCN part behave almost like a free rotor and dissociate with the excitation of vdW bending mode. The anisotropic intermolecular potential was determined by the least square fitting of the observed transitions.

The H_2–HCN, and H_2–H_2O clusters have rather complicated energy levels, because they have two internal rotors in the cluster, although the H_2 part behaves as a free rotor. Due to the spin statistics, the clusters have different internal rotation states between *para* and *ortho*-H_2 species, thus different dissociation energies, structures and vdW bending frequencies. The observed vdW transitions were analyzed to discuss the potential energy surface around HCN and H_2O.

In the supersonic jet expansions short lived species can survive thanks to the collision-less environment and ultra low rotational as well as vibrational temperature. The millimeter-wave spectrometer combined with supersonic jet nozzle and glow discharge electrodes, as well as the UV excimer laser photolysis devices, also have been set up for the detection of novel unstable species, such as radicals, molecular ions, and ionic and radical clusters.

V-Q-1 Millimeter-Wave Spectroscopy of the van der Waals Bending Band of He–HCN

HARADA, Kensuke; WHITHAM, Christopher J.; TANAKA, Keiichi[1]
([1]*IMS and Kyushu Univ.)*

The He–HCN cluster is a quite weakly bound cluster with the binding energy D_0 of 9 cm^{-1}.1,2) The HCN part is almost freely rotating in the cluster. Recently two vdW bending transitions have been reported by molecular beam electric resonance technique.1) The observation of the vdW transitions up to the dissociation limit is quite important for the determination of the potential energy surface and the theoretical analysis of the potential energy surface and intermolecular dynamics. In the present work, we observed the vdW bending transitions of the He–HCN cluster up to the dissociation limit and determined the empirical intermolecular potential function.

The multi-reflection millimeter wave jet cell was used for the experiment. The 14 atm mixed gas of 0.3% HCN and 99.7% He was injected to the vacuum chamber from a pulsed nozzle with a repetition rate of 60 Hz. The vacuum chamber was evacuated by a 10 inch diffusion pump. The millimeter wave radiation from a backward wave oscillator was passed twenty times through the jet expansion using a White type optical path and detected by InSb detector.

The energy level of He–HCN is labeled by the quantum numbers of j, l, and J where j is the internal rotation quantum number of HCN part, l is the rotational quantum number of the pseudo-diatomic complex and J is the total rotational quantum number. The stick diagram of the observed vdW transitions of He–HCN is shown in Figure 1. The 13 vdW bending transitions with $\Delta l = 0$ and l = 0~4 have been assigned in the frequency region of 95–125 GHz. The Q branch transitions and part of the R branch transitions are split to the hyperfine components due to the nuclear quadrupole interaction of the nitrogen nucleus. The highest observed energy level is the j = 1, l = 4, J = 5 level which is predicted to locate 0.5 cm^{-1} below the dissociation limit from the semi-empirical potential analysis.2)

We used the one dimensional internal rotation Hamiltonian with the anisotropic intermolecular potential for the analysis. The potential function determined is shown in Figure 2. The angle between the HCN axis and the cluster axis is denoted by θ. The intermolecular potential $V(\theta)$ has a global minimum at $\theta = 0°$ (the linear structure of He–HCN) and the energy difference between $\theta = 0°$ and $\theta = 180°$ (the linear structure of He–NCH) is 6 cm^{-1}. The center of mass distance R of He and HCN is 4.3 Å at $\theta = 0°$, while it is 0.8 Å shorter at $\theta = 70°$ than that at $\theta = 0°$.

References

1) S. Drucker, F. Tao and W. Klemperer, *J. Phys. Chem.* **99**, 2646 (1995).
2) K. M. Atkins and J. M. Hutson, *J. Chem. Phys.* **105**, 440 (1996).

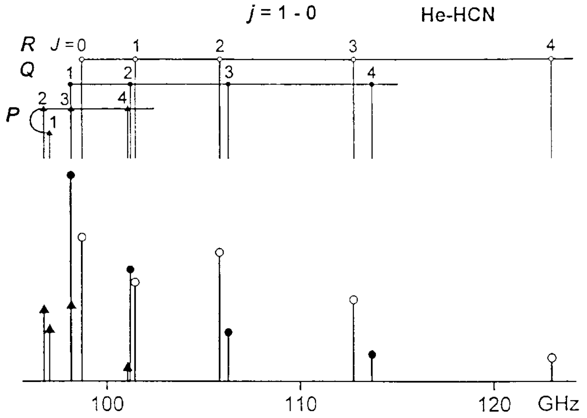

Figure 1. The stick diagram of the observed vdW bending transitions of He–HCN.

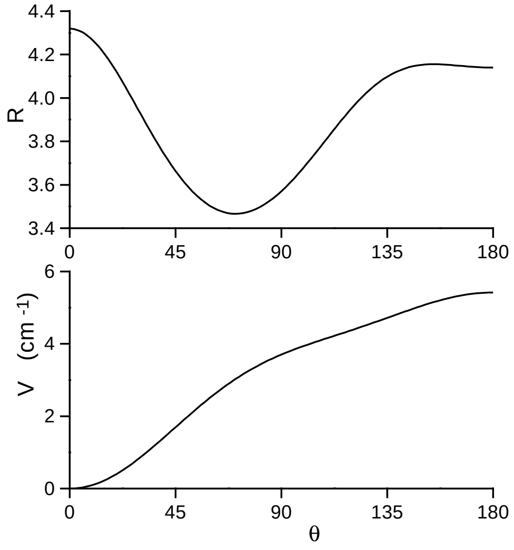

Figure 2. The R-θ and V-θ dependence curve of He–HCN.

V-Q-2 Millimeter Wave Spectroscopy of the HCN–H_2 Cluster

ISHIGURO, Masazumi[1]; WHITHAM, Christopher J.; HARADA, Kensuke; TANAKA, Takehiko[1]; TANAKA, Keiichi[2]
([1]Kyushu Univ.; [2]IMS and Kyushu Univ.)

Hydrogen H_2 containing molecular clusters are very weakly bound having large amplitude motion of both H_2 and its partner and they could have different configurations of between *para* (j = 0) and *ortho* (j = 1) hydrogen species. Recently, vibrational spectrum in the superfluid He droplets and ro-vibrational spectrum in the gas phase for the HCN–H_2 clusters have been observed. Vibrational spectrum in the He droplets suggests that o-H_2 binds to the N site of HCN molecule. Contrastedly, p-H_2 binds to the H site of HCN.1) In the gas phase, only HCN-(o-H_2) was detected.2) In this work, millimeter-wave absorption spectroscopy combined with a pulsed-jet expansion technique was applied to the measurement of the pure rotational and rovibrational transitions of the van der Waals (vdW) bending band of the HCN–H_2 cluster in the 75–150 GHz region.

So far, four rotational lines (J = 3–2 to 6–5) for the ground Σ_0 state of the HCN–(o-H_2) cluster split into hyperfine structure due to the nitrogen nucleus were observed. Rotational constant B_0 = 12899.718(20) MHz and centrifugal distortion constant D_0 = 12.2470(16) MHz were derived together with its higher order constants. The hyperfine constants determined eqQ = –2.830(33) MHz which is smaller than that of HCN molecule means a large amplitude motion of HCN <θ> = 31.1° in the ground linear form. The bond length between HCN and H_2 parts is derived to be 3.90 Å. This value strongly suggests that o-H_2 is bonding to the N site of the HCN molecule in the gas phase.

Some lines belonging to the Σ_1–Σ_0 vdW bending band of HCN–(o-H_2) were also observed. The Σ_1–Σ_0 vdW bending frequency 136.831 GHz of HCN–(o-H_2) is larger than that of He–HCN 96.8 GHz, but much smaller than that of Ar–HCN 164.89 GHz. The hyperfine constant in the Σ_1 state indicate the cluster has T-shape in the excited state of the vdW bending mode.

References

1) M. Ishiguro and R. E. Miller, *55th International Symposium on Molecular Spectroscopy* MF02, Ohio, 2000.
2) M. Ishiguro and R. E. Miller, *55th International Symposium on Molecular Spectroscopy* MF03, Ohio, 2000.

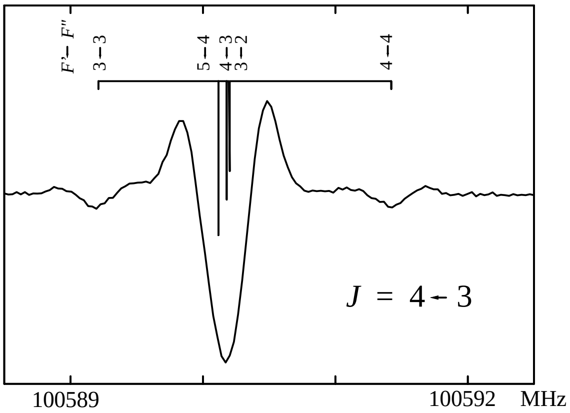

Figure 1. The J = 3–4 rotational line of the HCN–(o-H_2) in the ground Σ_0 state.

V-Q-3 Millimeter Wave Spectra of the H_2–H_2O van der Waals Complex

WHITHAM, Christopher J.; HARADA, Kensuke; TANAKA, Keiichi[1]
([1]IMS and Kyushu Univ.)

The hydrogen-water system is of interest due to the lightness (ie large rotational constants) of both parts which means that quantum dynamics effects are very important. High resolution spectra of such systems is helpful in developing models of the dynamics which include internal rotations of both partners.1) In addition, hydrogen–water collisions are believed to be important in the astronomical observations of intense water maser radiation.2) A recent infrared study of H_2–H_2O provided the motivation for this study.3)

We have observed pure rotational transitions of the weakly bound H_2–H_2O and H_2–D_2O complexes using a direct absorption millimeter wave spectrometer in the range 70–300 GHz. Internal rotation states involving ortho:H_2 (j = 1) Σ, ortho:H_2O $\Pi(1_{01})$ and para:H_2O $\Sigma(0_{00})$ were observed. The *e*/*f* parity splitting in the Π state provides important information on the intermolecular bending potential. Further work includes observation of the more weakly bound para:H_2–H_2O complex and direct excitation of the H_2O $\Sigma(1_{01})$–$\Pi(1_{01})$ transition which is predicted to lie in the 350 GHz region.

References

1) D. C. Clary and P. J. Knowles, *J. Chem. Phys.* **93**, 6334 (1990).
2) T. R. Phillips, S. Maluendes, A. D. McLean and S. Green, *J. Chem. Phys.* **101**, 5824 (1994).
3) M. J. Weida and D. J. Nesbitt, *J. Chem. Phys.* **110**, 156 (1999).

Table 1. Table of observed rotational transitions (MHz).

		H_2–H_2O	
J_{upper}–J_{lower}	$\Pi_e(1_{01})$	$\Pi_f(1_{01})$	$\Sigma(0_{00})$
2–1	71683.66	84983.56	85793.39
3–2	108760.57	126875.70	128002.72
4–3	146471.39	168017.75	169333.54
5–4	184341.19	208103.49	209391.38
		H_2–D_2O	
2–1	70684.54	82151.76	84412.97
3–2	106026.81	122766.98	126060.49
4–3	143955.50	162801.07	167009.37
5–4		202008.61	206976.05

V-Q-4 Millimeter Wave Spectroscopy of the van der Waals Bending Band of OCO-DF Generated in a Supersonic Jet Expansion

WHITHAM, Christopher J.; HARADA, Kensuke; ISHIGURO, Masazumi[1]; TANAKA, Takehiko[1]; TANAKA, Keiichi[2]
([1]Kyushu Univ.; [2]IMS and Kyushu Univ.)

The OCO–HF is a hydrogen-bonded quasi-linear cluster with a dissociation energy of 672 cm^{-1}.1) The inter molecular potential has minima at a bend structure of the COH angle of 22° and ~10 cm^{-1} potential barrier is expected at the linear structure of OCO-HF.2) In the preceding work, we have measured the van der Waals (vdW) bending band of OCO–HF directly by the millimeter wave jet spectroscopy. As a result, the vibrational frequency of vdW bending mode of OCO–HF has been determined precisely to be 272548.8017(49) MHz. To determine the complicated two dimensional inter molecular potential function with the COH bending and the OHF bending vibrations, it is important to observe vdW bending mode of OCO–DF as well as OCO–HF. In the present work, we have measured the vdW bending band of OCO–DF by the millimeter wave jet spectroscopy.

The 10 atm mixed gas of 1% DF, 5% CO_2, 31% Ar, and 63% Ne was injected to the vacuum chamber by the pulsed nozzle. We have measured 235–315 GHz region. The 31 rovibrational transitions of $P(2)$–$P(4)$, $Q(1)$–$Q(15)$, and $R(0)$–$R(12)$ were assigned to the 1^1–0^0 ($\nu_b{}^l$) fundamental band of the lowest vdW bending mode. The spectral pattern for OCO–DF was almost same as OCO–HF. The band has intense *Q* and *R* branch lines, while the *P* branch lines were rather weak. Figure 1 shows the fast scan spectrum of the band head of *Q* branch.

The usual linear molecule Hamiltonian with the rotational energy and the (2,2) interaction energy was used for the analysis. The band origin of the 1^1–0^0 ($\nu_b{}^l$) band has been determined to be 255815.6639(31) MHz, which is 6.1% smaller than that of OCO–HF. Furthermore, the rotational constant, centrifugal distortion constant, *l*-type doubling constant, and its higher order term were determined precisely. The analysis of the intermolecular potential function is now underway. In order to determine the precise two dimensional intermolecular bending potential surface, the measurement of the van der Waals hot band will be important.

References

1) L. Oudejans and R. E. Miller, *J. Chem. Phys.* **109**, 3474 (1998).
2) D. J. Nesbit and C. M. Lovejoy, *J. Chem. Phys.* **96**, 5712 (1992).

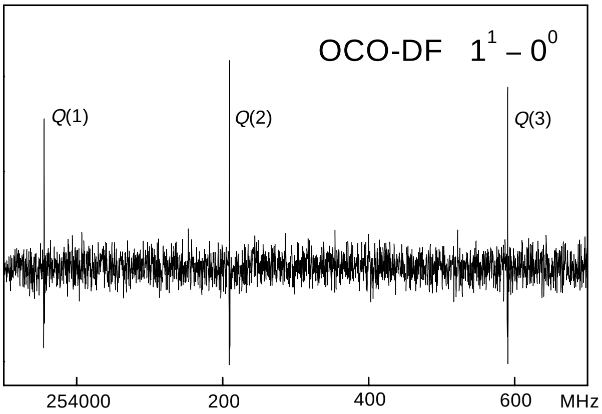

Figure 1. Fast scan spectrum of the head of *Q* branch for the OCO–DF.

V-R Ion-Molecule Reactions in the Troposphere

Ion chemistry in the troposphere is the most complicated among all level of earth's atmosphere because of the presence of a variety of trace compounds. We have studied ion-molecule reactions in the troposphere by investigating ion mobility distribution and its dependence on reaction time, pressure and temperature using an ion mobility spectrometer.[1,2] In order to confirm the ion-molecule reactions occurring in the troposphere, we have developed a high-resolution ion mobility/mass spectrometer which is capable of chemical identification of ion species forming ion peaks in mobility spectra. Using this spectrometer, we have been investigating the ion processes in conditioned laboratory air as well as in natural air. Experiments have been extended to the study on the role of ion-induced nucleation in the troposphere.

References

1) K. Nagato and T. Ogawa, *J. Geophys. Res.* **103**, 13917 (1998).
2) K. Nagato, D. J. Tanner, H. R. Friedli and F. L. Eisele, *J. Geophys. Res.* **104**, 3471 (1999).

V-R-1 Measurements of Mobility and Mass Spectra of Tropospheric Ions

NAGATO, Kenkichi

[*J. Aerosol Res. Jpn.* **15**, 110 (2000)]

An ion mobility/mass spectrometer (Figure 1) has been developed for the purpose of investigating the ion evolution in the lower troposphere. Total ion mobility spectra, mass spectra, and mass-resolved mobility spectra were obtained for positive and negative ions produced and aged for 0.02–0.5 s in the ambient air. In this range of aging time, positive ions were observed to evolve from $NH_4^+(H_2O)_n$ to the ions of pyridines and amines that have higher proton affinities. It is also demonstrated that mass-resolved mobility spectra could be useful to analyze the detailed pathway of the evolution. Four series of hydrated cluster ions were observed in the negative ion mass spectra, which are believed to be ions of formic acid ($HCOO^-(H_2O)_n$) and oxalic acid ($COOHCOO^-(H_2O)_n$) along with NO_2^--$(H_2O)_n$ and $NO_3^-(H_2O)_n$. This suggests that organic acids play important roles in the negative ion evolution in the lower troposphere.

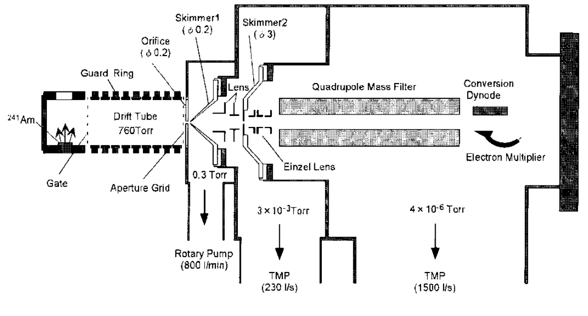

Figure 1. Schematic view of the ion mobility/mass spectrometer.

V-R-2 Experimental Study of Ion-Induced Nucleation in the Troposphere

NAGATO, Kenkichi; KIM, Chan Soo[1]; ADACHI, Motoaki[2]; OKUYAMA, Kikuo[1]
([1]Hiroshima Univ.; [2]Osaka Pref. Univ.)

There is a growing interest in the ion-induced nucleation in the troposphere.[1)] In order to investigate the role of tropospheric ions in the aerosol formation, measurements of mass spectra for positive and negative ions generated by α-ray radiolysis in the $NH_3/SO_2/H_2O$/Air mixture were made by using an ion mobility/mass spectrometer. In the negative ion mass spectra at low SO_2 and H_2O concentrations (Figure 1a), SO_2^-, SO_3^-, SO_4^-, and SO_5^- were observed as major SO_2-originated ions, which indicates that SO_2 were directly ionized by ion-molecule reactions. With increasing the concentrations of SO_2 and H_2O (Figure 1c), HSO_4^- and $HSO_4^-{\cdot}H_2SO_4$ ions became dominant, suggesting that SO_2 were primarily converted into H_2SO_4. This result agrees with our previous experiments that charged particle fraction decreased with increasing the concentrations of SO_2 and H_2O.[2,3)] It was also observed that the addition of NH_3 led the decrease in H_2SO_4.

References

1) F. Yu and R. P. Turco, *Geophys. Res. Lett.* **27**, 883 (2000).
2) T. O. Kim, *et al., Aerosol Sci. Tech.* **26**, 527 (1997).
3) T. O. Kim, *et al., Aerosol Sci. Tech.* **29**, 111 (1998).

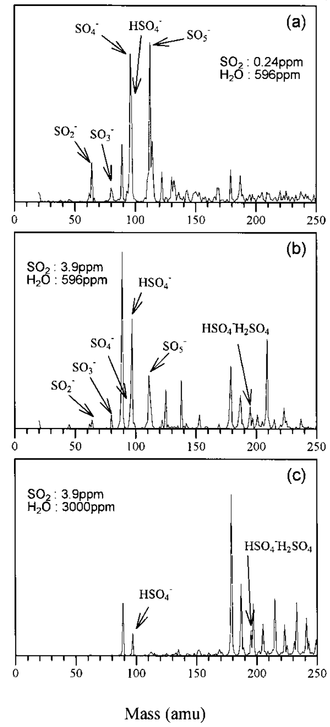

Figure 1. Mass spectra of negative ions generated by α-ray radiolysis in the SO_2/H_2O/Air mixture.

V-S Monte Carlo Simulation of Molecular Clusters

Physical properties of clusters have attracted much attention. Using Monte Carlo simulation methods, we investigate the properties of clusters and gels, helium in random potential, and other systems.

V-S-1 Boson Localization on the Superfluid-Insulator Transition by Quantum Loop Algorithm

HASHIMOTO, Masahito; TAKASU, Masako

[*Prog. Theor. Phys. Suppl.* **138** 529 (2000)]

For some systems in critical phenomena, Monte Carlo simulations using conventional algorithm is inefficient, because of strong correlation between successive MC configurations. Our system of helium in random potential suffers from this difficulty in critical region between superfluid phase and glass insulator phase. The loop algorithm overcomes this difficulty. We apply this algorithm to soft core boson system, and carry out calculations with random boson Hubbard model. This method is potentially useful for studying molecular clusters.

V-S-2 Monte Carlo Simulation of the Formation of Chemical Gel and Clusters

NOSAKA, Makoto; TAKASU, Masako

Gel is an important material used in everyday life. We focus our attention to the formation process of chemical gel and clusters. By changing the number of monomers, linkers and radicals, we obtain the phase diagram of gel. We also discuss efficient algorithm for determining the percolation of polymers.

V-S-3 Linear-shaped Motion of DNA in Concentrated Polymer Solutions Under a Steady Field

NOGUCHI, Hiroshi; TAKASU, Masako

[*J. Phys. Soc. Jpn.* submitted]

We studied the electrophoretic behavior of DNA chains in linear-polymer solutions using Brownian dynamics with an anisotropic friction tensor. We simulated the linear-shaped motion of DNA observed in highly concentrated solutions using a model with a chain segment equal to 1/4 of the persistence length. A linear conformation is seen for a chain with high segment-density regions, which remain at the same positions in space, with a high anisotropy of friction, while a U-shaped conformation is seen for a chain with a low anisotropy of friction.

V-T Development of Shaped Pulse Solid-State NMR Spectroscopy

Shaped radio frequency (rf) pulses are commonly employed in a solution high-resolution nuclear magnetic resonance (NMR) spectroscopy. They are used for selective excitation in multidimensional NMR experiments and broadband spin decoupling for resolution enhancements. However, they are less applied to solid state NMR experiments where the samples usually have much larger spectral widths than those of solution-state samples. In metallic or magnetic materials, the spin-echo method is still employed and only shifts and relaxation data are analyzed. Modern NMR techniques as a multiple quantum NMR provides a correlation of spin interactions between two nuclei, which seems to be very important even in these solid materials. We are currently developing a waveform generator and a transmission line probe, which enable excitations and detections of nuclear spins over a large spectral range.

V-T-1 Shaped Pulse Solid-State NMR Experiment

TAKAOKA, Kazuma[1]; ITOH, Toshiki[1]; KUBO, Atsushi; IMASHIRO, Fumio[1]; TERAO, Takehiko[1]
([1]Kyoto Univ.)

Shaped radio frequency (rf) pulses are commonly employed in a solution high-resolution nuclear magnetic resonance (NMR) spectroscopy. However, they are less applied to solid state NMR experiments where the samples usually show much larger spectral widths than those of solution-state samples. We have developed a fast wave form generator which could be employed for solid state shaped pulse experiments. Although the circuit was wired by cables on universal printed circuit boards, it worked stable to a clock frequency of 30 MHz. The waveform generator can be controlled by TTL signals from a spectrometer, and it can generate four different shaped pulses. We would like to publish our design elsewhere. We are also currently developing a transmission line probe,[1)] which may enables the broadband excitation of heavily broadened solid-state NMR spectra such as ^{195}Pt NMR of Pt nanoparticles. However, here we will demonstrate that the waveform generator is also useful in the experiments with an ordinary commercial NMR probe. Figure 1 (a) shows a ^{2}H solid-state magic-angle spinning NMR spectrum of a rigid deuterium sample with a quadrupole coupling of 160 kHz. An adiabatic inversion pulse WURST20[2)] was applied before the conventional observation pulse sequence and the result is shown in (b). The magnetization was inverted almost completely compared with (a), although the rf pulse amplitude was only 56 kHz. When a rectangular pulse with the same rf strength was used, only 40% of the magnetization were inverted. We conclude that adiabatic pulses may be promising, if it is difficult to obtain enough rf field strength, especially in triple-resonance experiments.

References
1) Conradi, M. S., *Concepts Magn. Reson.* **5**, 243 (1993).
2) Kupce, E.; Freeman, R., *J. Magn. Reson. A* **118**, 299 (1996).

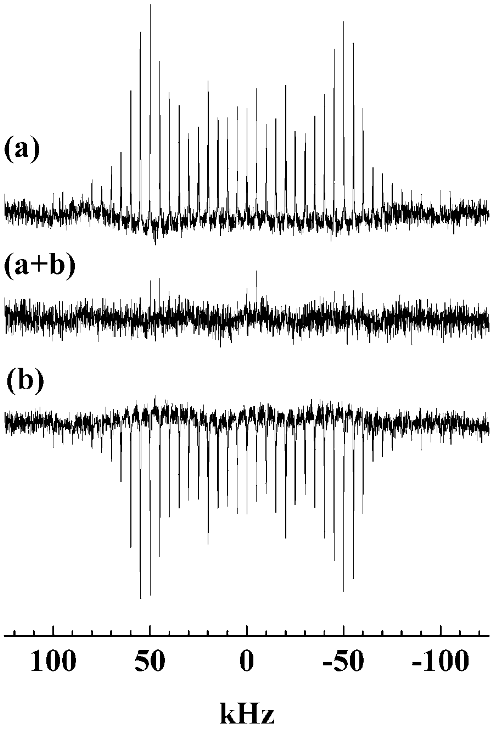

Figure 1. The inversion efficiencies of a ^{2}H magnetization by an adiabatic pulse, WURST20. (a) ^{2}H MAS NMR spectra of 2,2'-thiobis[5,5'-dimethyl-3-hydroxy-2-cyclohexen-1-one]-d_2. In (b), the magnetization was inverted by a WURST20 with length of 64 μs and a rf amplitude of 56 kHz. The rf frequency was swept during the pulse from –200 kHz to +200 kHz.

V-U Development of ^{13}C High-Resolution NMR Spectroscopy for Nematic and Cholesteric Liquid Crystals

When nematic and cholesteric liquid crystals are spun around a certain axis inclined from a static magnetic field, the directors of liquid crystals can be oriented in a perpendicular direction to the spinning axis. We have reported previously that ^{13}C NMR spectra recorded under this condition can be employed to determine a molecular diffusion rate along a pitch axis of a cholesteric liquid crystal (Y. Nishiyama, *et al., Mol. Phys.* **96**, 1569 (1999)). In the course of the study, we fortunately found a high-resolution two-dimensional NMR experiment, which correlates an isotropic chemical shift and a chemical shift anisotropy of nematic liquid crystals. This technique might be also applicable to determine structures of oriented biomacromolecules in a membrane.

V-U-1 Direct Determination of ^{13}C Chemical Shift Anisotropies of Liquid Crystals by Combining OMAS NMR and Rotor-Synchronous Pulses with Hankel Transformation

NISHIYAMA, Yusuke[1]; KUBO, Atsushi; TERAO, Takehiko[1]
([1]Kyoto Univ.)

The chemical shift anisotropies of liquid crystals are directly determined by a rotor-synchronous π pulse train under off-magic-angle spinning (OMAS). Using chemical shift anisotropies, we can determine the ^{13}C NMR peak correlations between a liquid crystalline phase and an isotropic phase. These peak correlations directly enable us to assign the spectrum of a liquid crystalline phase from the assignments for an isotropic phase. When a liquid crystal with a positive (negative) magnetic susceptibility anisotropy is spun around the axis inclined from the static magnetic filed by the angle ε larger (smaller) than the magic angle, the directors are randomly distributed in a plane perpendicular to the spinning axis. The orientation dependence of NMR resonance frequency vanishes by the spinning averaging over a half-rotor cycle. A rotor-synchronous π pulse re-introduces the orientation dependence, and the resulting free induction decay (FID) is expressed by the 0th Bessel function of the first kind $J_0(2C_2t/\pi)$, where C_2 is a coefficient related to the chemical shift anisotropy. The value of $|C_2|$ is determined by the Hankel transformation of the FID. The sign of C_2 is determined from a tilted 2D spectrum or from slices of 2D spectra recorded at two different angles ε. The property of the Hankel transformation is discussed. These theoretical results were verified by ^{13}C OMAS experiments with a π pulse train on a nematic liquid crystal of *p*-methoxy-benzilidene-*p*-n-butylaniline (MBBA).

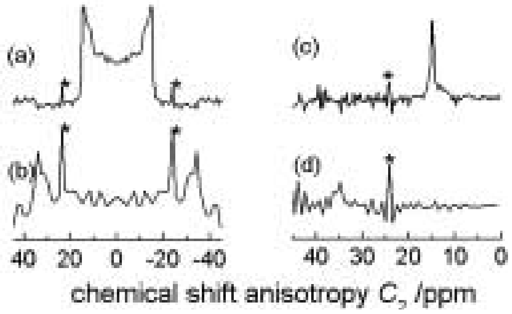

Figure 1. Comparisons between (a, b) Fourier transformed and (c, d) Hankel transformed spectra of MBBA at 302 K. The upper spectra (a, c) represent carbon-1 at 120.3 ppm and The lower spectra (b, d) represent carbon-9 at 175.1 ppm. The asterisks indicate the cycling sidebands due to the XY-8 phase cycling.

RESEARCH ACTIVITIES VI
Department of Vacuum UV Photoscience

VI-A Electronic Structure and Decay Mechanism of Inner-Shell Excited Molecules

This project is being carried out in collaboration with UVSOR, Photon Factory (KEK-PF), Shizuoka University, Osnabrück University, Brazilian Synchrotron Radiation Facility (LNLS), Uppsala University, and Lund University. We are interested in ionic fragmentations and electron emissions via inner-shell excitation of molecules and in their polarization dependence. Last year in high-resolution C1s photoabsorption spectra of acetylene, C_2H_2, we found that the lowest σ_u* state is embedded in the 3sσ_g Rydberg state and is dissociative through interaction with the lowest π* state with bent geometry due to the Renner-Teller effect, that the 3pσ_u and 3pπ_u Rydberg states are clearly resolved and show different vibrational structures, and that the C1s σ_g and σ_u ionization channels show different ionization thresholds, to which the Rydberg series are converging. [For preliminary results, see J. Adachi, N. Kosugi, E. Shigemasa and A. Yagishita, *Chem. Phys. Lett.* **309**, 427 (1999)]. Dr. Jun-ichi Adachi, technical associate, left the Kosugi group for KEK-PF as a research associate in October 1999. Now Dr. Takaki Hatsui has joined the Kosugi group as a new research associate in this field in August 2000. Next year we will extend our experimental and theoretical approaches to several open-shell and unstable molecules.

VI-A-1 Exchange Interaction in the 1s-σ* Resonance of the Triplet Ground State of S_2 in Comparison with O_2

RÜHL, Eckart[1]; FLESCH, Roman[1]; TAPPE, Werner[1]; NOVIKOV, Dimitri[2]; KOSUGI, Nobuhiro
([1]Osnabrück Univ.; [2]HASYLAB)

It is interesting to compare the 1s-σ* resonance of S_2 with that of O_2. The experimental exchange splitting is observed to be ~1 eV in the S 1s-σ* excited states of $^3\Sigma^-$ as shown in Figure 1. It should be noticed that the higher σ* resonance is stronger than the lower σ* resonance in O_2, but in S_2 the lower state is stronger than the higher one. The exchange splitting in the ionized states ΔE_{exch}(ion) is given by $3K_{\mathrm{cx}}$[1)] (~1.1 eV for O_2, ~0.2 eV for S_2), where K_{cx} is an exchange integral between the core electron and the π_x* (or π_y*) electron. The exchange splitting in the excited states $\Delta E_{\mathrm{exch}}(\sigma^*)$ is given as follows:[1)]

$$\begin{aligned}\Delta E_{\mathrm{exch}}(\sigma^*) &= E\{\sigma^*(^2\Sigma^- \text{ ion core})\} - E\{\sigma^*(^4\Sigma^- \text{ ion core})\}\\ &= 3K_{\mathrm{cx}} - 7/3K_{\mathrm{vx}} - 2/3K_{\mathrm{cv}},\end{aligned}$$

where v denotes the σ* electron. In O_2, K_{cv} and K_{vx} are 1.1~1.2 eV and then $\Delta E_{\mathrm{exch}}(\sigma^*)$ ~ –2.75 eV < 0; that is, the σ* state related to the $^4\Sigma^-$ ion core is higher than that related to $^2\Sigma^-$. (Note that this discussion is based on a single electron and frozen orbital picture and if electron correlation is taken into account, $\Delta E_{\mathrm{exch}}(\sigma^*)$ is changed to –1.75 eV from –2.75 eV.[2)]) In S_2, K_{cx} is much smaller than in O_2. If so, $\Delta E_{\mathrm{exch}}(\sigma^*) < 0$ and the higher σ* state could be stronger than the lower σ* state. However, this is inconsistent with the present result. This indicates that the picture of the $^4\Sigma^-$ and $^2\Sigma^-$ ion cores and an additional σ* electron does not hold any longer in the S1s-σ* excited states, but the picture of the $^4\Sigma^-$ and $^2\Sigma^-$ valence states and an additional core electron is a good approximation. In this case, the exchange spilitting is give as follows:

$$\Delta E_{\mathrm{exch}}(\sigma^*) = E(^3\Phi_2) - E(^3\Phi_1) = 3K_{\mathrm{vx}} - 7/3K_{\mathrm{cx}} - 2/3K_{\mathrm{cv}} > 0,$$

where the exchange interaction within the valence electrons K_{vx} is much larger than the exchange interaction involving the deep S 1s core, K_{cx} and K_{cv}. The experimental and calculated $\Delta E_{\mathrm{exch}}(\sigma^*)$ are ~ +0.67 eV and ~ +1.15 eV. The experimental and calculated intensity ratios are ~ 1.26 and ~ 1.72.

References

1) N. Kosugi, E. Shigemasa and A. Yagishita, *Chem. Phys. Lett.* **190**, 481 (1992).
2) A. Yagishita, E. Shigemasa and N. Kosugi, *Phys. Rev. Lett.* **72**, 3961 (1994).

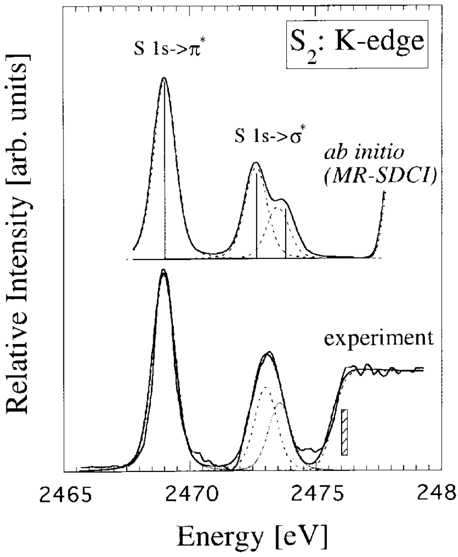

Figure 1. S 1s photoabsorption spectra of S_2 in comparison with theoretical prediction.

VI-A-2 Polarization Dependence of O^+/O_2^+ Fragmentations at the Terminal O1s-to-σ* Excitation of Ozone: A Memory Effect of Core-Hole Localization During the Auger Decay

NAVES de BRITO, Arnaldo[1]; SORENSEN, Stacey[2]; BJÖRNEHOLM, Olle[3]; GEJO, Tatsuo; KOSUGI, Nobuhiro

([1]LNLS, Brazil; [2]Lund Univ.; [3]Uppsala Univ.)

[*Chem. Phys. Lett.* in press]

The photoelectron-photoion-photoion coincidence (PEPIPICO) spectra of ozone, O_3 have been measured at the O1s edge for the first time. When an ozone molecule is dissociated after the Auger decay, several different combinations of fragments can be produced. Out of these possibilities, we have chosen to concentrate on the O^+/O_2^+ PEPIPICO spectra. By observing the O^+/O_2^+ ion pair coincidences, we discriminate against possible ultra-fast neutral dissociation before the Auger decay: $O^*–O–O \rightarrow O^* + O–O$. This process cannot produce the fragments $O^+ + O_2^+$, but rather $O^{2+} + O_2$. Due to the local character of the terminal O1s (O 1s) core excitations in O_3, the excitations are considered to take place in the local O–O bond environment, with the unoccupied valence orbitals locally having π or σ character. The $O_T1s \rightarrow 7a_1(\sigma^*)$ transition dipole is theoretically estimated to be 7° from the $O_T^*–O$ bond, being nearly parallel to the $O_T–O$ bond containing an excited terminal atom (O_T). Therefore, we can evaluate preferential fragmentation from $O_T^*–O–O$ to $O_T^+ + O–O^+$ or $O_T–O^+ + O^+$ via $(O_T–O–O)^{2+}$ at the $O_T1s \rightarrow 7a_1(\sigma^*)$ excitation by relating the asymmetry parameter β of the PEPIPICO spectra to the angle between the transition dipole and the bond to be broken. The present analysis shows that photo-induced breaking of the bond closest to the core-excited terminal atom, $O_T^+ + O–O^+$, occurs in high probability of 70 ± 10%. This result is interpreted as a "memory" effect of the initially localized core hole in dicationic states $(O_T–O–O)^{2+}$ after or during the Auger decay.

VI-A-3 Molecular Field and Spin-Orbit Splittings in the 2p Ionization of Second-Row Elements: A Breit-Pauli Approximation Applied to OCS, SO_2, and PF_3

KOSUGI, Nobuhiro; ISHIDA, Toshimasa[1]
([1]Shizuoka Univ.)

[*Chem. Phys. Lett.* in press]

Angular distribution of photoelectrons is one of fundamental properties in the inner-shell photoionization process in addition to the photon energy dependence of the photoionization cross sections. The angular distribution of 1s electrons has been investigated for fixed-in-space molecules by utilizing linear polarization of synchrotron radiation. We expect this technique will also be applicable to the photoionization dynamics study in the 2p electron of second-row elements, by combining with theoretically predicted wavefunctions of the spin-orbit split 2p ionized states, $^2P_{3/2}$ and $^2P_{1/2}$. The most accurate approach to take into account the spin-orbit interaction is a four-component method based on the Dirac-Fock configuration interaction calculations, but this is very complicated and is not generally used. In the present work, an ab initio Breit-Pauli (BP) approach as a two-component spin-orbit Hamiltonian is newly developed to analyze the molecular field splitting (MFS) in the $^2P_{3/2}$ state and the spin-orbit splitting ($\Delta_{3/2,1/2}$), and to get $2p^{-1}$ wavefunctions for three typical molecules, OCS, SO_2 and PF_3. The BP Hamiltonian is diagonalized by using a minimum number of the $2p^{-1}$ configurations. The diagonal elements in the 6×6 BP matrix are corrected by the 2p hole-state energies calculated with the non-relativistic $(2p)^5$-SDCI calculations, resulting in good agreement with the experimental energy separations due to MFS. The $(2p)^5$-SDCI is configuration interaction with single and double substitutions from reference states with five electrons in the 2p manifold. On the other hand, to reproduce $\Delta_{3/2,1/2}$ the relaxation in the 2p orbital itself is essential. The bond angle effect is important to determine MFS due to σ and π character in the 2p orbital and to determine the spin-orbit wavefunction. A similar BP Hamiltonian calculation to interpret "linearly polarized" 2p photoabsorption spectra of molecules containing second-raw elements such as HCl is now under way.

VI-B Soft X-ray Photoelectron-Photoabsorption Spectroscopy and Electronic Structure of Transition Metal Compounds

This project is being carried out in collaboration with UVSOR, Photon Factory (KEK-PF), and Uppsala University. We are measuring Ni 2p photoabsorption, and resonantly emitted photoelectron and soft X-ray spectra of molecular Ni complexes with planar geometry. Dr. Yasutaka Takata, who was a research associate in charge of this project in the Kosugi group, left for Spring-8 as a research associate of RIKEN (IPCR) in May 2000. Now Dr. Hiroshi Oji has joined the Kosugi group as a postdoctoral IMS fellow in this field in April 2000.

VI-B-1 Ni 2p Photoabsorption and Resonant Photoelectron Spectroscopy of High-Spin Ni Complex, Ni(*N*,*N*'-dimethylethylenediamine)$_2$Cl$_2$

OJI, Hiroshi; TAKATA, Yasutaka; HATSUI, Takaki; KOSUGI, Nobuhiro

In our previous studies, we found the planar Ni complexes with a $3d^8$ low-spin ground state show characteristic resonant behavior in the Ni 3p and 3s resonant photoelectron spectra, which form a contrast to these of Ni metal and Ni oxide.1) The kinetic energy of Ni 3p satellite peaks decrease as the photon energy increases, indicating the one electron, or excitonic, feature of the excited states in the planar Ni complexes. In the present work, we measured soft X-ray Ni 2p absorption and resonant Ni 3s and 3p photoelectron spectra of a 3d^8 high-spin Ni complex, Ni(N,N'-dimethylethylenediamine)$_2$Cl$_2$ (Ni(DED)$_2$Cl$_2$) to clarify the effect of the spin state on the core-excited states of the system. Figure 1 shows the kinetic energy of the Ni 3p main and satellite photoelectron peaks (a, b, c) as a function of the photon energy. Figure shows a nearly linear relationship between the kinetic energy of the these satellite peaks and the photon energy with the slope ($\Delta KE/\Delta h\nu$) of +1. This dependence of satellite peaks on the photon energy is different from that of the low-spin complexes where the slope becomes negative (*e.g.* $\Delta KE/\Delta h\nu = -0.55 \pm 0.05$ for K$_2$[Ni(CN)$_4$]$^{1)}$), but is similar to that of NiO, where the correlation and multiplet interaction are important.

Reference

1) Y. Takata, T. Hatsui and N. Kosugi, *J. Electron Spectrosc. Relat. Phenom.* **88**, 235 (1998).

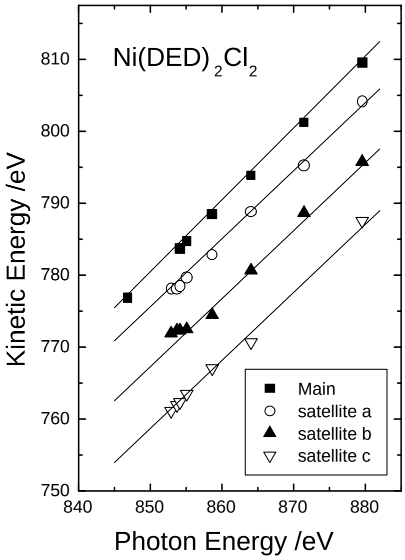

Figure 1. Photon energy dependence of the kinetic energy of Ni 3p main and satellite photoelectron peaks.

VI-B-2 Mg and Al K-edge XAFS Measurements with a KTP Crystal Monochromator

TAKATA, Yasutaka; SHIGEMASA, Eiji; KOSUGI, Nobuhiro

[*J. Synchrotron Radiat.* in press]

There has been a strong demand for monochromator crystals with a larger lattice spacing than the Si, Ge and InSb crystals widely used in the soft X-ray region, especially in order to get a wide energy range covering the Mg (1305 eV) and Al (1560 eV) K-edges and their EXAFS region. As crystal monochromators to get these near-edge spectra, beryl (1010) [2d = 15.965 Å] and quartz (1010) [2d = 8.512 Å] have been used, respectively; however, the energy range (k range) is limited because beryl and quartz contain Al and Si, respectively. Recently, a YB$_{66}$ (400) [2d = 11.72 Å] crystal monochromator has been introduced to measure EXAFS for the Mg, Al and Si K-edges. There is no absorption edge originating from the elements contained in the YB$_{66}$ crystal from 1200 eV up to the Y L$_{III}$ edge of 2080 eV. However, this crystal has a serious problem; two positive glitches at 1386 and 1438 eV are caused by sharp increase in reflectivity of the (600) reflection at the Y L$_{II,III}$ edges. Although to solve such a problem, a cut-off mirror is employed, it is still hard to completely exclude these glitches.

The KTP (011), KTiOPO$_4$, [2d = 10.95 Å] crystal can be used in the crystal monochromator. The KTP (011) crystal has a little shorter lattice spacing than YB$_{66}$ (400), but it can cover the Mg and Al K-edges and has no absorption edge from 1200 eV up to the P K-edge of 2145 eV. We have introduced the KTP (Crystal Laser Co., France) crystal at the soft X-ray double crystal beamline BL1A of the UVSOR facility and examined its performance and applicability to the EXAFS measurement in the energy range between 1200 and 2000 eV. The KTP crystal monochromator at the BL1A proves to supply stable photon beams and the energy resolution is estimated to be about 0.5–0.8 eV. The KTP has two excellent advantages in comparison with YB$_{66}$. First, there is no absorption structure originating in the elements contained in KTP in the energy range to be measured. Secondly, a higher throughput is available. By use of the KTP monochromator, reliable EXAFS spectra for the Mg and Al K-edges have been observed for a wide k range. The UVSOR storage ring is being operated at a rather low energy (750 MeV), and the BL1A utilizes radiation from a bending magnet, whose critical energy is 424 eV. The radiation damage proves to be less serious for beryl and quartz crystals; therefore, we can expect a small radiation damage to the KTP crystal.

VI-C Observation of Vibrational Coherence (Wavepacket Motion) in Solution-Phase Molecules Using Ultrashort Pulses

With recent remarkable improvements of ultrashort-pulse lasers, we are now able to generate an optical pulse shorter than a few tens of femtoseconds. Owing to its ultrashort duration and broad frequency bandwidth, the ultrashort pulse can excite a molecule ‘impulsively’ to generate a coherence superposition of a number of vibrational state either in the excited state or in the ground state. This vibrationally coherent state evolves in time, which is called wavepacket motion. The observation and control of the wavepacket motion is one of the most interesting topics in modern spectroscopy. In past years, we have generated ultrashort optical pulses whose duration is ten ~ a few tens of femtoseconds by utilizing several nonlinear optical methods. In this year, we constructed experimental setups using these ultrashort pulses, and performed time-resolved measurements to observe vibrational coherence (wavepacket motion) in the excited state and the ground state.

VI-C-1 Observation of Vibrational Coherence of S$_1$ *trans*-Stilbene in Solution by 40-fs-Resolved Absorption Spectroscopy

TAKEUCHI, Satoshi; TAHARA, Tahei

[*Chem. Phys. Lett.* **326**, 430 (2000)]

Recent remarkable advance in laser technology has made it possible to generate an optical pulse shorter than a few tens of femtoseconds. Owing to its ultrashort duration and broad energy bandwidth, the ultrashort pulse can excite a molecule into a coherent superposition of a number of vibrational states. The coherent properties of the prepared state and its time evolution have been receiving much attention in relation to the exploration of a possible role of the vibrational coherence in photochemical processes.

In this project trying to examine the mechanism for the excited-state vibrational coherence, we carried out time-resolved absorption measurements for trans-stilbene in solution with use of a setup based on 10-fs pulses (Figure 1). We measured a temporal behavior of the S$_n$ ← S$_1$ absorption signal around 640 nm following the 320-nm excitation with a time-resolution as good as 40 fs (Figure 2). In the obtained data, an underdumped oscillation due to the S$_1$ vibrational coherence was observed in the early times. The Fourier-transform analysis showed that the S$_1$ in-plane deformation mode (ν_{25}, 200 cm^{-1}) predominantly gives rise to the oscillatory signal. We considered the mechanism for this mode-specificity, and found that the amplitude of the vibrational coherence signal can be related to the S$_n$ ← S$_1$ resonance-Raman activities of the S$_1$ vibronic levels and their Franck-Condon activities in the S$_1$ ← S$_0$ excitation process. With reference to the reported S$_1$ vibrational spectra, we evaluated the relative amplitude of the ν_{25} component against that of the ν_{24} mode (285 cm^{-1}) that appears strongly in the S$_1$ Raman spectra, and obtained the ratio consistent with the experimental data. It was concluded that the substantial contribution of the ν_{25} mode in the pump-probe data results from significant displacements among the S$_0$, S$_1$, and S$_n$ potentials along the corresponding vibrational coordinate.

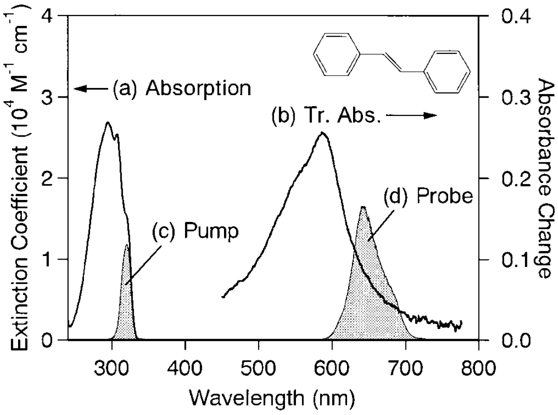

Figure 1. Spectral properties of *trans*-stilbene in the S$_0$ and S$_1$ states. (a) Steady-state absorption spectrum of *trans*-stilbene in heptane. (b) S$_n$ ← S$_1$ transient absorption spectrum of *trans*-stilbene in heptane measured at 1 ps after 267-nm photoexcitation. Spectra of the pump (c) and the probe (d) pulses used in the 40-fs-resolved absorption measurements are also shown.

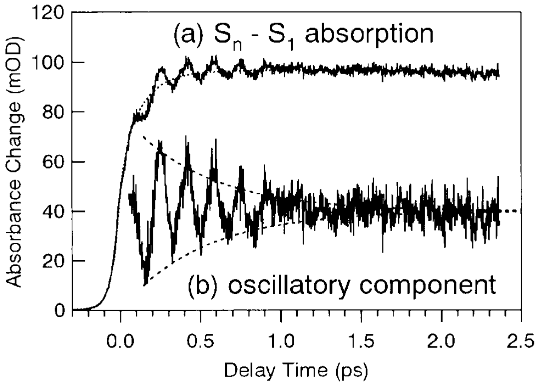

Figure 2. Time-resolved absorption signal of *trans*-stilbene in heptane (10^{-2} M). (a) Temporal behavior of the S$_n$ ← S$_1$ absorption (640 nm) measured with excitation at the reddest edge of the ground-state absorption (320 nm). (b) Oscillatory component depicted in a magnified scale.

VI-C-2 Generation of Two Independently-Tunable Pulses for Extremely-Fast Pump-Probe Absorption Spectroscopy

TAKEUCHI, Satoshi; TAHARA, Tahei

Time-resolved absorption spectroscopy using ultrashort pump and probe pulses has been widely employed for the studies of the dynamical properties of photoexcited molecules. With increasing progresses in laser technology, the time-resolution of these measurements has also been improved drastically, which gives us a chance to even observe new phenomena occurring within a few tens of femtoseconds. In order to achieve such a good time-resolution in molecular spectroscopy, we previously reported the construction of a time-resolved absorption spectrometer utilizing 10-fs pulses generated from a high-power optical parametric amplifier (OPA). In this setup, the second harmonic of the 10-fs pulse was used as a pump pulse in the uv region, while the 10-fs fundamental pulse in the visible region was used as a probe pulse. Consequently, the pump wavelength changed with the tuning of the probe wavelength. This restriction placed on the combination of the pump and probe wavelengths has so far limited the applicability of this spectrometer. Although we successfully applied the spectrometer to the observation of the vibrational coherence of S_1 *trans*-stilbene,1) it is apparently highly desirable that the pump and probe wavelengths can be tuned *independently* in the pump-probe measurements. For this purpose, we modified the previous apparatus by adding another low-power OPA with a single-pass amplification scheme (Figure 1). In this modified setup, the entire output of the high-power OPA (10–20 fs, 10 μJ, 1 kHz) is frequency-doubled to generate the pump pulse (≈ 0.3 μJ) tunable in the range of 250–375 nm. On the other hand, the output of the low-power OPA in the visible region (500–750 nm) is used as a probe and a reference pulse that are tunable independently of the pump wavelength. The time-resolution of this apparatus is typically *ca.* 40 fs, as evaluated by the FWHM of a cross-correlation trace between the two pulses. The independent tunability as well as the good time-resolution achieved in this spectrometer is highly suitable to extremely-fast molecular spectroscopy. Making the most use of these advantages, we are now investigating the coherent properties of molecules during ultrafast chemical reactions.

Reference

1) S. Takeuchi and T. Tahara, *Chem. Phys. Lett.* **326**, 430 (2000).

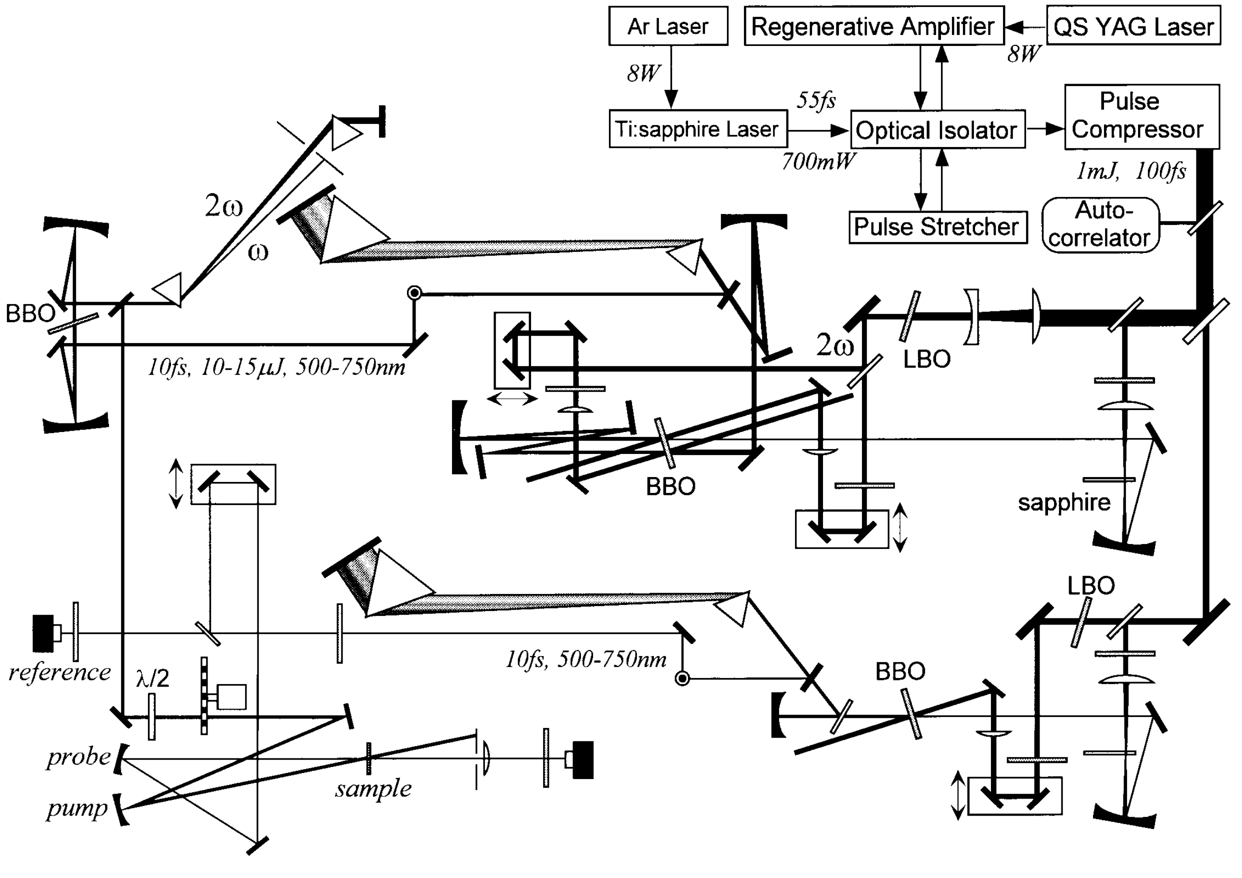

Figure 1. Experimental apparatus of the extremely-fast time-resolved absorption spectrometer using independently-tunable pump and probe pulses.

VI-C-3 Measurement of Impulsive Stimulated Raman Scattering Using Ultra-Short Pulses Generated by a Krypton Gas-Filled Hollow Fiber

FUJIYOSHI, Satoru[1]**; TAKEUCHI, Satoshi; TAHARA, Tahei**
([1]GUAS)

Impulsive stimulated Raman scattering (ISRS) spectroscopy is one of the third-order nonlinear spectroscopy suitable to the study of the low-frequency molecular vibrations. The frequency region to which this technique is sensitive depends on the duration of the pulse used in the measurements. Therefore, we need to use short pulses in order to obtain the information about the molecular vibrations in the wide frequency region.

We generated ultra-short pulses (τ ~ 35 fs, 800 nm) by using a Kr gas-filled hollow fiber (the autocorrelation is shown in inset of Figure 1) and applied it to the ISRS measurement. The homodyne ISRS signal obtained from liquid CS_2 is shown in figure 1. In addition to the electric response (sharp peak around 0 ps) and nuclear response (collective motion, broad peak around 0.2 ps), a beating signal with a period of 51 fs can be recognized. This beating signal corresponds to the intramolecular vibration at 655 cm^{-1}, which becomes observable with use of optical pulses as short as 35 fs.

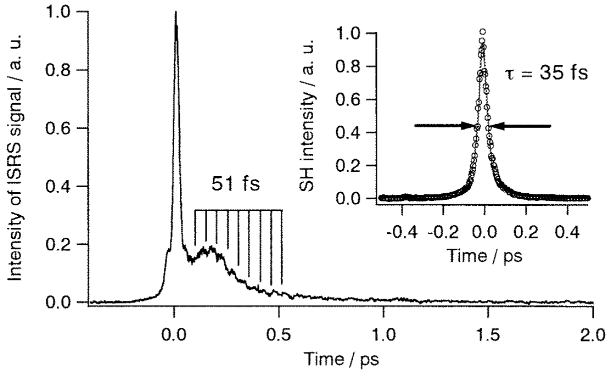

Figure 1. Impulsive stimulated Raman scattering signal of liquid CS_2. Inset: The autocorrelation of ultra short pulses that are used in this measurement.

VI-C-4 Construction of an Apparatus for Optical Heterodyne Detected Impulsive Stimulated Raman Scattering Measurement Using a Phase Mask

FUJIYOSHI, Satoru[1]; TAKEUCHI, Satoshi; TAHARA, Tahei
([1]GUAS)

Femtosecond optical heterodyne detected impulsive stimulated Raman scattering (OHD-ISRS) spectroscopy is one of the time-domain spectroscopies that can afford information about the low-frequency molecular vibrations. In order to achieve stable heterodyne detection, the relative optical phase between the signal light and the local oscillator (LO) light needs to be accurately controlled. We previously reported OHD-ISRS measurements, in which the phase control was attained by active adjustment of the optical path length.1) Recently, a diffractive optics (phase mask) was reported to be applicable in this spectroscopy, which does not require active path-length stabilization2,3) and hence facilitate heterodyne detection. We constructed an apparatus with use of the phase mask and the diagram is shown in Figure 1a.

In this apparatus, the visible femtosecond pulse is first divided into two pluses. Each pulse is diffracted into two first-order pulses. The first pair is used as pump pulses and the second pair is used as probe and LO pulses. Figure 1b shows OHD-ISRS signal obtained from liquid carbon tetrachloride with this setup using 75-fs femtosecond pulses (700 nm). The relative phase between the signal light and the LO light was kept stable over a span of one hour even without any active feed back.

References

1) S. Matsuo and T. Tahara; *Chem. Phys. Lett.* **264**, 636 (1997).
2) G. D. Goodno, *et al., J. Opt. Soc. Am. B* **15**, 1791 (1998).
3) A. A. Maznez, *et al., Opt. Lett.* **23**, 1319 (1998).

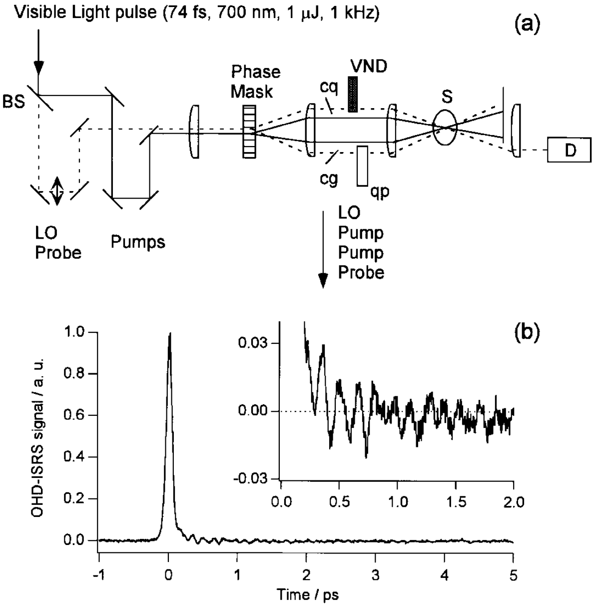

Figure 1. (a) Constructed apparatus of an OHD-ISRS measurement. (b) Optical heterodyne detected impulsive stimulated Raman scattering signal of liquid carbon tetrachloride measured using a phase mask. Inset: The signal in the early time region is depicted in a magnified scale.

VI-D Studies of Primary Photochemical/physical Processes Using Femtosecond Electronic Spectroscopy

Ultrafast spectroscopy is playing an essential role in elucidation of photochemical reactions. Thanks to the recent advance in laser technology, we are now able to examine the dynamics of chemical reactions taking place in the femtosecond time region. In this project, we study primary photochemical/physical processes in the condensed phase by time-resolved fluorescence and absorption spectroscopy with a few hundreds femtoseconds time-resolution. Time-resolved fluorescence and absorption spectroscopy are complimentary to each other. The advantage of fluorescence spectroscopy lies in the fact that fluorescence originates from the transition between the “well-known” ground state and the excited state in question. Thus time-resolved fluorescence spectroscopy can afford unique information not only about the dynamics but also other properties of the excited singlet states such as their energies and oscillator strengths. On the other hand, however, time-resolved absorption spectroscopy is considered to be more versatile because it can detect not only fluorescent excited singlet states but also other "dark" transients. In this year, we investigated the ultrafast dynamics of excited-state proton transfer of anthaquinone derivatives, isomerization of azobenzene, and relaxation of the S_2 state of zinc(II) porphyrins, with use of these time-resolved electronic spectroscopy. In addition, we started construction of a new setup for femtosecond time-resolved infrared spectroscopy.

VI-D-1 Ultrafast Excited-State Proton Transfer Dynamics of 1,8-dihydroxyanthraquinone (chrysazin) Studied by Femtosecond Time-Resolved Fluorescence Spectroscopy

ARZHANTSEV, Sergei; TAHARA, Tahei

[*Chem. Phys. Lett.* **330**, 83 (2000)]

The steady-state fluorescence spectrum of 1,8-dihydroxyanthraquinone (crysazin) shows very large Stokes shift and dual bands emission. This fluorescence feature indicates that a marked geometry change takes places in the excited state. The steady-state fluorescence has been considered as an evidence of the proton transfer reaction across the intramolecular hydrogen bond in the excited state. Femtosecond time-resolved fluorescence intensities of crysazin in hexane have been measured at room temperature for a wide visible wavelength region (470–670 nm) using up-conversion method. Time-resolved fluorescence spectra were reconstructed after deconvolution taking account of the finite instrumental response. The time-resolved fluorescence spectra are presented in Figure 1. The following three points can be noted from these spectra: (1) Both parts in a dual fluorescence (the blue part and the red part) exist even at the time origin. The relative intensity of the blue part is high immediately after photoexcitation, compared with that in the steady-state fluorescence. (2) The fluorescence intensity of the blue part decreases and that of the red part increases in a few picoseconds. (3) After 5 ps, the fluorescence does not show any significant spectral change and it is very similar to the steady-state fluorescence spectrum. The fluorescence intensity decreases monotonously at all the observed wavelengths.

Almost instantaneously appearance of both of the "normal-form type" fluorescence and the "tautomeric-form type" fluorescence indicates that a barrierless excited-state proton transfer occurs in the time scale of several tens of femtoseconds, reflecting delocalization of the excited-state wavefunction. We assign the fluorescence dynamics in a few picosecond time scale to an additional proton translocation reflecting the intramolecular vibrational relaxation.

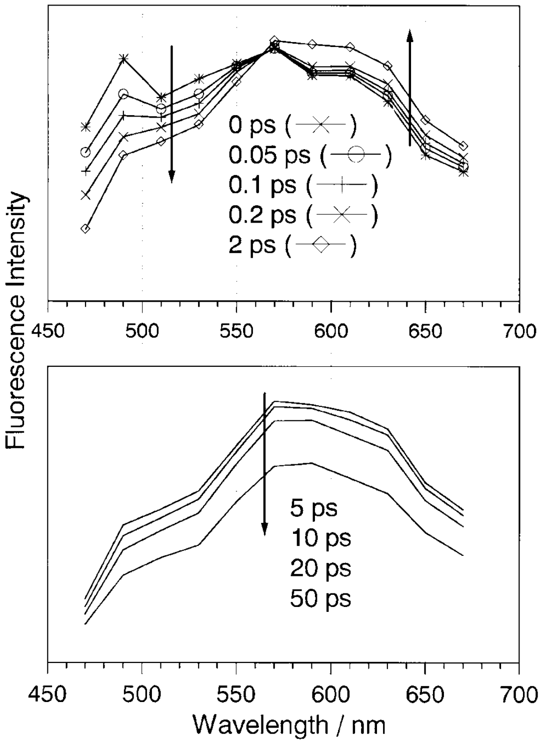

Figure 1. Reconstructed time-resolved fluorescence spectra of chrysazin. The spectra in the early time region are presented in the top panel. The spectra after 5 ps are presented in the bottom panel.

VI-D-2 Femtosecond Dynamics of Photoexcited *trans*-Azobenzene Observed by Time-Resolved Fluorescence Up-Conversion Spectroscopy

FUJINO, Tatsuya; ARZHANTSEV, Sergei; TAHARA, Tahei

The femtosecond time-resolved fluorescence spectroscopy was applied to study the photochemistry of *trans*-azobenzene. The excitation wavelength (280 nm, third harmonic pulses of a Ti:saphhire oscillator) in the present experiments corresponds to the blue side of the $S_2(\pi\pi^*) \leftarrow S_0$ absorption ($\varepsilon_{280} \approx 10000$ mol^{-1} dm^3 cm^{-1}), and the molecules were initially photoexcited to the $S_2(\pi\pi^*)$ state. The femtosecond time-resolved fluorescence signals were measured in the wavelength region from 340 to 680 nm using the up-conversion method. The fluorescence decays obtained from a hexane solution (5.0×10^{-3} mol dm^{-3}) at four different wavelengths are shown in Figure 1. These data clearly shows that the temporal behavior of the fluorescence signals varies with the change of fluorescence wavelength. The fluorescence decay at 440 nm looks quite similar to the cross-correlation trace, indicating that the lifetime of the major portion of the fluorescence is shorter than the time resolution. This rapid decay was also dominant in the near-ultraviolet region (340~420 nm). The second fluorescence component becomes noticeable in the fluorescence decay at longer wavelength. In the signals at 560 and 620 nm, the intensity of the second component becomes comparable to that of the first rapid component. A global fitting was performed for the quantitative analysis of the observed decays, and it was clarified that the fluorescence consists of two decay components having lifetimes of ~ 110 and ~ 500 fs. The spectral analysis referring to the steady state fluorescence spectrum clarified that the two fluorescence components exhibit spectra with intensity maxima at ~ 400 and ~ 650 nm. Since these spectra are good mirror images of the $S_2 \leftarrow S_0$, and the $S_1 \leftarrow S_0$ bands in the absorption, they were assignable to the fluorescence from the S_2 and S_1 states, which have planar structure around the central NN bond.

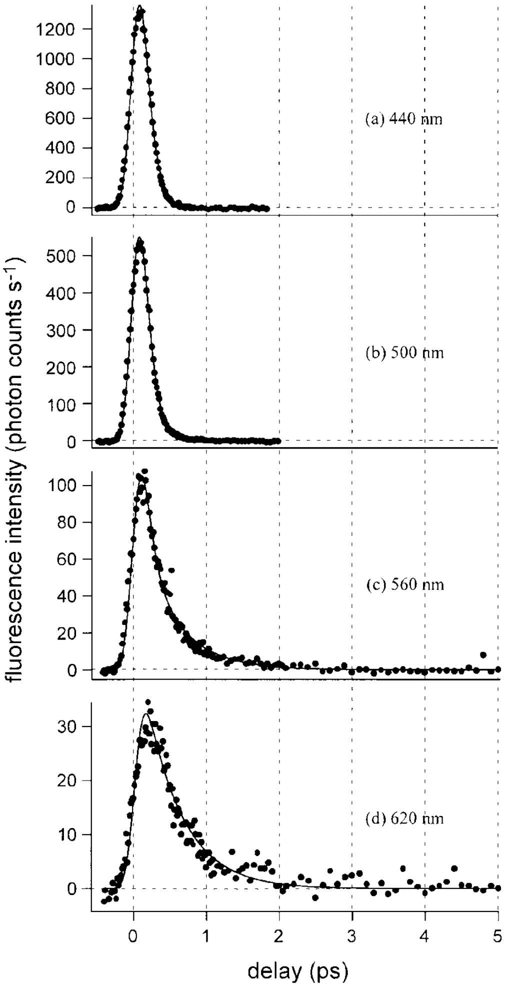

Figure 1. Time-resolved fluorescence of trans-azobenzene in hexane solution (5.0×10^{-3} mol dm^{-3}) at 440 nm (a), 500 nm (b), 560 nm (c), and 620 nm (d). The dots are experimental data and the solid curves are the results of fitting analysis.

VI-D-3 S_2 Emission of a Series of Zinc(II) Porphyrins Studied by Femtosecond Fluorescence Spectroscopy

ASANO-SOMEDA, Motoko[1]; ARZHANTSEV, Sergei; TAHARA, Tahei
([1]Tokyo Inst. Tech.)

Fluorescence from the second electronically excited singlet state (S_2 emission) has been observed for various metalloporphyrins even under the steady-state condition. Zinc(II) porphyrin is one of the typical metalloporphyrins and exhibits S_2 emission. However, quantum yields of S_2 emission largely depend on the porphyrin peripheral substituents, and in some of zinc(II) porphyrins, no steady-state S_2-emission could have been detected. To elucidate what controls the S_2 emission intensity and the radiationless transitions from the S_2 state, we have performed time-resolved fluorescence study for a series of zinc(II) porphyrins, which involves "non-S_2-emissive" porphyrins. For all six compounds, S_2 emission was successfully detected by using up-conversion method. The decay rates of the S_2 emission were coincident with the rise rates of the S_1 emission, and the observed S_2 lifetimes vary from 2 ps to 70 fs depending upon the peripheral substituents. There is no clear correlation between the S_2 lifetimes and S_2–S_1 energy gaps or transition dipole moments of the S_2 state. However, the S_2 lifetime strongly correlates with the intensity ratio of the Q(0,0) and Q(1,0) absorption bands. This leads to a suggestion that a substle difference in the electronic structure of the porphyrin π-system, which is sensitive to the peripheal substituents, remarkably affects the $S_2 \rightarrow S_1$ internal conversion rate.

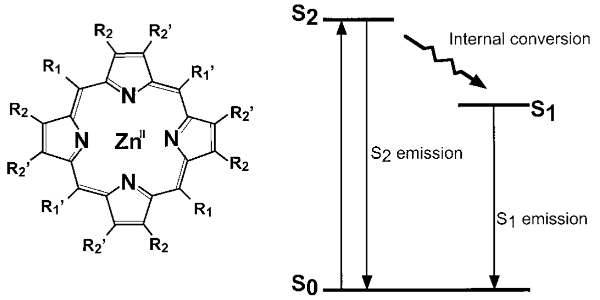

Figure 1. Molecular structure and schematic diagram of the relaxation processes of zinc(II) porphyrin.

VI-D-4 Construction of Femtosecond IR-IR Pump-Probe Spectrometer

FUJINO, Tatsuya; TAHARA, Tahei

An apparatus for femtosecond IR-IR pump-probe measurements was constructed. The setup is based on a regeneratively amplified output of a Ti:sapphire laser that delivers 100 fs pulses of ~ 0.7 mJ at a repetition rate of 1 kHz. These pulses are used to pump a commercial optical parametric generation and amplification (OPG/OPA) system operating with a BBO crystal. The differential frequency between the signal and idler pulses was generated by a $AgGaS_2$ crystal, and it is used as a frequency-tunable infrared source (3~12 µm, ~ 3 µJ). A long-wave pass (> 2500 nm) filter and a Ge filter are used to separate the mid-infrared pulses from the signal and idler. A beam splitter divides the infrared pulse into two parts. The intense pulse was used to excite the fraction of molecules, and the weak one was utilized to probe the induced transmission change. Both pulses are focused on a sample by a CaF_2 lens (focal length 150 mm), and the sample-transmitted probe (signal) energy as well as the pulse-to-pulse fluctuation (reference) of the probe are measured with the two HgCdTe detectors. The data from the signal and reference detectors are used to determine the IR transmission with (T) and without the pump (T_0) pulse. The normalized pump-induced transmission change, $\Delta T/T_0 = T/T_0 - 1$, is determined as a function of delay time between the pump and probe pulse.

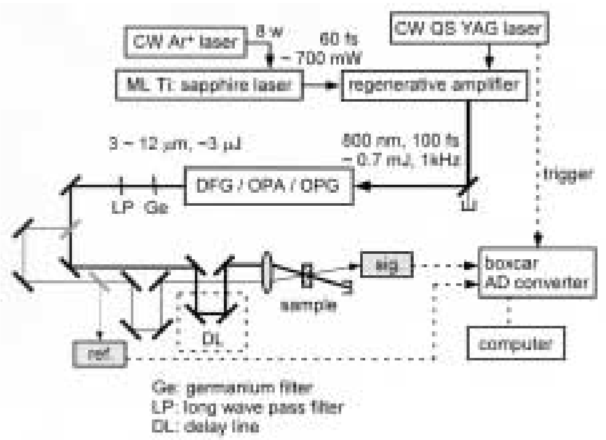

Figure 1. Apparatus for the femtosecond IR-IR pump-probe measurements.

VI-E Studies of Photochemical Reactions Using Picosecond Time-Resolved Vibrational Spectroscopy

Time-resolved vibrational spectroscopy is a very powerful tool for the study of chemical reactions. It often affords detailed information about the molecular structure of short-lived intermediates, which is not obtainable with time-resolved electronic spectroscopy. However, for molecules in the condensed phase, we need energy resolution as high as 10 cm^{-1} in order to obtain well-resolved vibrational spectra. This energy resolution is compatible only with time-resolution lower than one picosecond because of the limitation of the uncertainty principle. In this sense, picosecond measurements are the best compromise between the energy resolution and time resolution for time-resolved frequency-domain vibrational spectroscopy. In this project, we study photochemical processes and short-lived transient species by using picosecond time-resolved Raman spectroscopy. In this year, we studied the picosecond dynamics of the excited state of several fundamental aromatic compounds. In addition, we found that strong hyper-Raman scattering was observed from *all-trans* retinal when amplified picosecond pulses were used for excitation. We obtained information about the low-lying excited singlet states of this molecule from the data of the hyper Raman excitation profile.

VI-E-1 Observation of Picosecond Time-Resolved Raman Spectra of *p*-Nitroaniline

FUJINO, Tatsuya; TAHARA, Tahei

P-nitroaniline is a prototypical molecule that shows intramolecular charge-transfer (CT) with photo-excitation. Because of its simple structure with an electron donor group (–NH_2) and an acceptor group (–NO_2), *p*-nitroaniline has a variety of photochemical properties associated with the CT excited state. Time-resolved Raman spectroscopy was performed to study the picosecond dynamics of this CT state in solutions. In this experiment, the excitation pulse (390 nm) was the second harmonics of the regeneratively amplified output of a Ti:sapphire laser. The first Stokes pulse (465 nm, for the water solutions) of H_2 Raman shifter or second Stokes pulse (509 nm, for the toluene solution) of D_2 Raman shifter excited by 390-nm pulse was used as probe. Transient Raman spectra of *p*-nitroaniline in toluene solution are shown in Figure1. The Raman bands assignable to the T_1 state appeared with the time constant of several tens picosecond after the excitation whereas the S_1 Raman band was not observed. The lifetime of T_1 state was estimated at ~ 5 ns by measuring the decay of the transient Raman bands. In water solution, on the other hand, transient Raman bands assignable to the S_1 state were observed with its lifetime of ~ 10 ps whereas T_1 Raman band was not observed. These results indicated that the lifetime of S_1 (CT) state and the intersystem crossing rate to the T_1 (CT) state are strongly affected by the change of the solvent polarity.

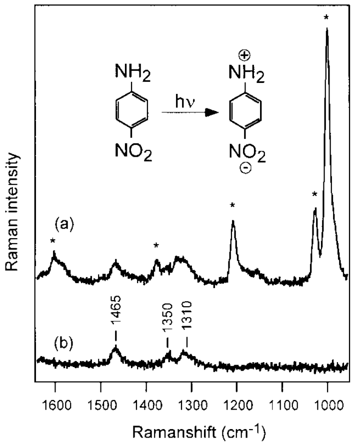

Figure 1. Picosecond time-resolved Raman spectra of *p*-nitroaniline in toluene solution (1.5×10^{-2} mol dm^{-3}) at the delay time of 50 ps. Transient spectra (b) was obtained after the subtraction of the solvent (*) and the ground state signals from (a).

VI-E-2 Femtosecond and Picosecond Time-Resolved Spectra of 5-Dibenzosuberenone

UEDA, Atsuhiro[1]; FUJINO, Tatsuya; MIZUNO, Misao; TAHARA, Tahei; TAKAHASHI, Hiroaki[1]
([1]Waseda Univ.)

Femtosecond time-resolved absorption and picosecond time-resolved resonance Raman spectra of 5-dibenzosuberenone were measured. It was observed in the time-resolved absorption spectra that the S_1 state decayed in a few picoseconds after excitation, while the T_1 state became prominent with time changing in band shape. In the picosecond time-resolved Raman spectra, a Raman band at 1490 cm^{-1} was observed immediately after excitation, which was assigned to the S_1 state. Several Raman bands assignable to the T_1 state were also observed to increase in intensity with time. In addition, a T_1 Raman band exhibited a frequency upshift from 1498 to 1517 cm^{-1}. The observed frequency shift was considered to be caused by the vibrational cooling process in the T_1 state, and it was detectable thanks to the very rapid intersystem crossing.

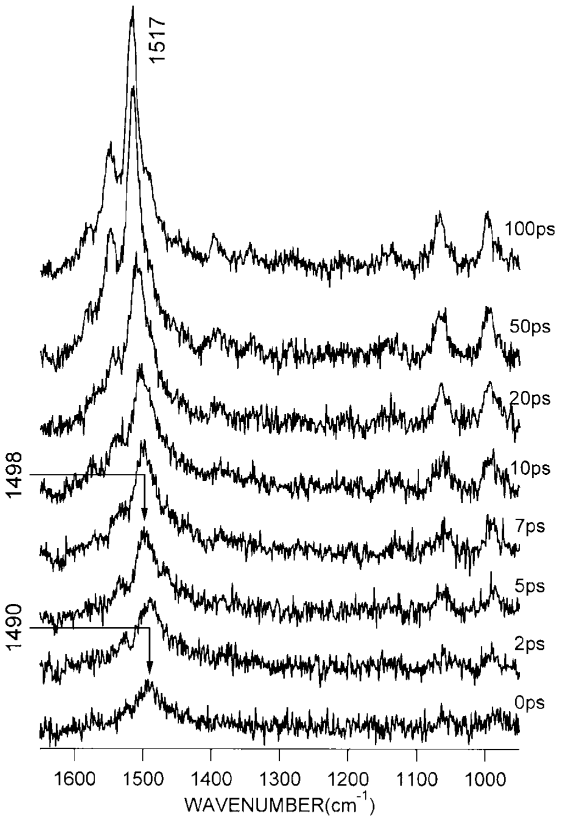

Figure 1. Picosecond time-resolved resonance Raman spectra of 5-dibenzosuberenone in acetonitrile.

VI-E-3 Resonance Hyper-Raman Scattering of *all-trans* Retinal from a Diluted Solution: Excitation Profile and Energy Levels of the Low-Lying Excited Singlet States

MIZUNO, Misao; HAMAGUCHI, Hiro-o[1]; TAHARA, Tahei
([1]Univ. Tokyo)

Strong hyper-Raman scattering of *all-trans* retinal was observed from a diluted solution under the resonance condition by using picosecond amplified Ti:sapphire laser pulses for excitation. Figure 1a shows resonance hyper-Raman (RHR) spectra of *all-trans* retinal in cyclohexane excited at every 10 nm from 770 nm to 840 nm. The concentration of the sample solution is only 1 × 10^{-3} mol dm^{-3}, which is much lower than the concentration in typical RHR measurements (~ 1 mol dm^{-3}).[1)] This implies that the intensity of RHR scattering from *all-trans* retinal is very high. The RHR intensity increases with shortening of the excitation wavelength whereas the spectral pattern does not change significantly. In *all-trans* retinal, there exist three low-lying excited singlet states, that is, the ^1B_u, ^1A_g and $^1n\pi^*$ states. The hyper-Raman resonance enhancement is considered to predominantly arise from two-photon resonance with the ^1A_g state, and hence, RHR intensity is expected to be the maximum when double the excitation photon energy matches the energy of the ^1A_g state. Figure 2 shows the RHR excitation profile of the intensity of the 1575 cm^{-1} band. The slope of the RHR excitation profile is close to that of the one-photon $^1B_u \leftarrow S_0$ absorption band (broken line in Figure 2), which indicates that the energy separation between the ^1A_g state and the ^1B_u state is small. In addition, the spectral pattern of the RHR spectrum is very similar to that of resonance Raman spectrum that is observed with half wavelength of RHR excitation (Figure 1b). It suggests that the resonance mechanism of RHR scattering of *all-trans* retinal is attributed to the A-term of the vibronic theory[2)] and that Franck-Condon factor between the S_0 state and the ^1A_g state resembles that between the S_0 state and the ^1B_u state.

References

1) C. C. Bonang and S. M. Cameron, *Chem. Phys. Lett.* **187**, 619 (1991).
2) Y. C. Chung and L. D. Ziegler, *J. Chem. Phys.* **88**, 7287 (1988).

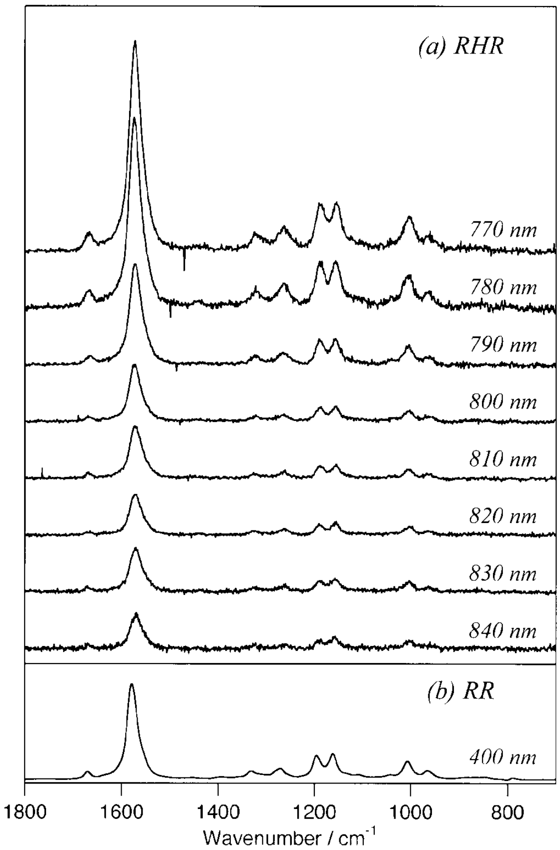

Figure 1. (a) Resonance hyper-Raman (RHR) and (b) resonance Raman (RR) spectra of *all-trans* retinal in cyclohexane (1 × 10^{-3} mol dm^{-3}).

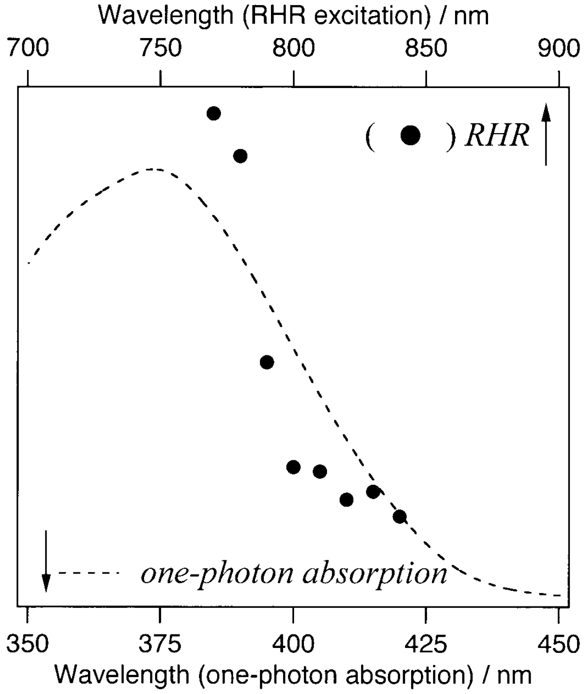

Figure 2. Excitation profile of the 1575 cm^{-1} of the RHR band. The black circles indicate RHR band intensities. Broken line shows absorption spectrum of *all-trans* retinal in cyclohexane.

VI-F Synchrotron Radiation Stimulated Surface Reaction and Application to Nanoscience

Study of synchrotron radiation (SR) stimulated surface reaction is a promising topic both in fundamental and applied science. Dynamical process induced by the photostimulated coreelectron excitations on surfaces is attracting considerable attention in the surface science field. Semiconductor nano-structure fabrication by SR stimulated etching and thin film growth is considered to find an important application in the future devices such as molecular devices and molecular bioelectronics

VI-F-1 SR-Stimulated Etching and OMVPE Growth for Semiconductor Nanostructure Fabrication

NONOGAKI, Youichi; HATATE, Hitoshi[1]; OGA, Ryo[1]; YAMAMOTO, Shunnsuke[1]; FUJIWARA, Yasufumi[1]; TAKEDA, Yoshikazu[1]; NODA, Hideyuki; URISU, Tsuneo
(*[1]Nagoya Univ.)*

[*Mater. Sci. Eng. B* **74**, 7 (2000)]

Synchrotron radiation- (SR-) stimulated etching and selective area growth by organometallic vapor phase epitaxy were performed to form ordered array of InP crystals on SiO_2-patterned InP (001) substrate. The SR-stimulated etching was used to pattern the SiO_2 film, because photochemical reaction using SR was expected to provide smooth surfaces, vertical side walls and fine patterning. In the first place, we investigated basic properties of the SR-stimulated etching by using mm-size pattern of SiO_2 mask. The etched depth was observed to increase linearly with the irradiation dose. It was found that the etching depth was controlled very accurately. Next, we used μm-size patterns of SiO_2 masks for fabricating the ordered array of InP crystals. In a atomic force microscope image of the sample after the etching, a steep side wall was observed. However, the etched surface was not smooth, against our expectation. Moreover, some dusts were observed on the surface. By these dusts, it was found that the SR-stimulated etching had a resolution of ≤ 100 nm at most.

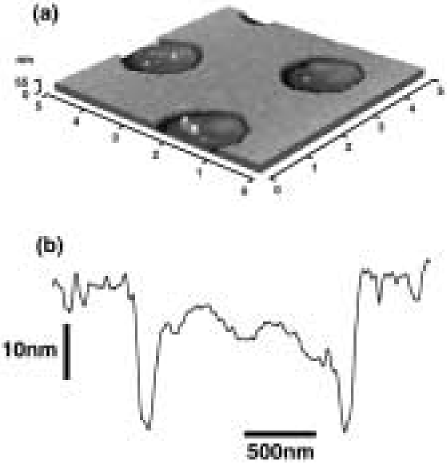

Figure 1. AFM observation of SiO_2 mask prepared by SR-stimulated etching. In (a) it is shown as a bird view image, and in (b) line profile near circular opening. Steep side wall is observed. However, surface is not smooth, against our expectation.

VI-F-2 Aligned Island Formation Using Step-Band Networks on Si(111)

HOMMA, Yoshikazu[1]; FINNIE, Paul[1]; OGINO, Toshio[1]; NODA, Hideyuki; URISU, Tsuneo
(*[1]NTT Basic Res. Lab.)*

[*J. Appl. Phys.* **86**, 3083 (1999)]

We have achieved control of island formation using a patterned Si(111) surface with a periodic array of atomic-step bands and holes. Liquid metals, Au-Si or Ga, migrate on the patterned surface by annealing and form an island at a particular position in each pattern unit. The islands show highly uniform positions and narrow size distributions. To obtain such good uniformity, the diffusion length of surface atoms should be comparable with the pattern period. High mobility on step bands is also necessary factor. Periodic arrays of Au islands are used as seeds for selective growth using a vapor-liquid-solid reaction (VLS). Figure 1 shows VLS Si pillars grown on a Au-island arranged substrate using disilane gas. All Si pillars grow at the positions where Au islands were located.

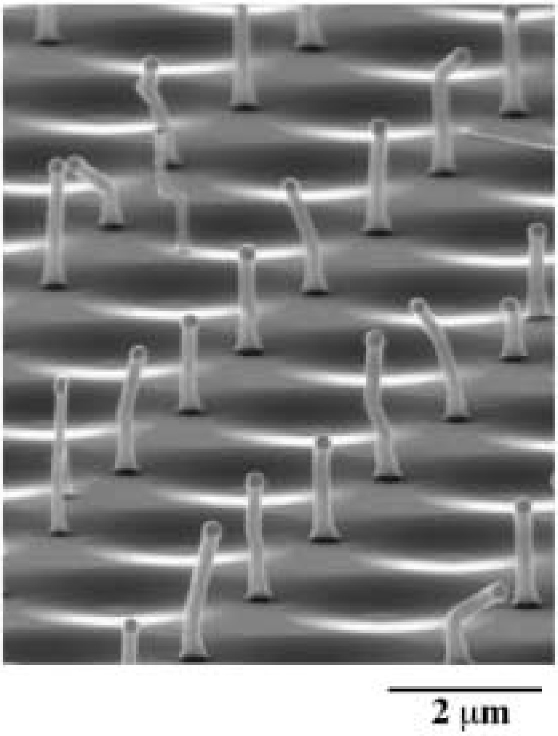

Figure 1. SEM image of Si pillars grown on Au-island arranged Si(111) substrates. The substrate was exposed to disilane gas of 1×10^{-2} Torr for 5 min at 620 °C. The angle of the electron beam incidence was 75°.

VI-F-3 Scanning Tunneling Microscopy Study of Surface Morphology of Si(111) after Synchrotron Radiation Stimulated Desorption of SiO_2

GAO, Yongli[1]**; MEKARU, Harutaka; MIYAMAE, Takayuki**[2]**; URISU, Tsuneo**
([1]Univ. Rochester; [2]Natl. Inst. Mater. Chem. Res.)

[*J. Vac. Sci. Technol., A* **18**, 1153 (2000)]

The surface morphology of Si(111) was investigated using scanning tunneling microscopy after desorption of surface SiO_2 by synchrotron radiation (SR) illumination. The surface shows large regions of atomically flat Si(111)-7×7 structure, and is characterized by the formation of single bilayer steps nicely registered to the crystal structure. This is in sharp contrast to Si(111) surfaces after thermal desorption of SiO_2 at temperatures 880 °C and above, where the surface steps are much more irregular. X-ray photoemission spectroscopy is also applied to investigate the process of the synchrotron radiation stimulated desorption.

VI-F-4 Assignments of Bending and Stretching Vibrational Spectra and Mechanisms of Thermal Decomposition of SiH_2 on Si(100) Surfaces

NODA, Hideyuki; URISU, Tsuneo

[*Chem. Phys. Lett.* **326**, 163 (2000)]

Vibrations of hydrogen-chemisorbed Si(100) surfaces with 3×1 and 1×1 structures were studied by buried metal layer-infrared reflection absorption spectroscopy. The SiH_2 bend scissors mode was found to split into two distinct peaks at 902 and 913 cm^{-1}; they were assigned to isolated dihydride (ID) and adjacent dihydride (AD), respectively. The observed differences in the dependence on annealing temperature showed that the small peak near 2090 cm^{-1} and the 2107 cm^{-1} peak were assignable to the symmetric stretching mode of ID and less stable AD, respectively. These observations have enabled discussion on the mechanisms of the thermal decomposition of dihydride species. It has been found that AD is slightly less stable than ID and that both AD and ID produce coupled monohydride by thermal decomposition.

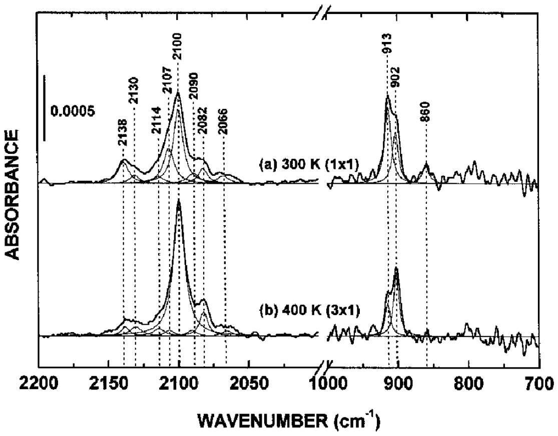

Figure 1. p-Polarized BML-IRRAS spectra associated with H/Si(100) surfaces with (a) 1×1 (b) 3×1. Narrow lines show peak-resolved spectra calculated assuming that the shape of each peak is Lorentzian.

VI-F-5 Control of Surface Composition on Ge/Si(001) by Atomic Hydrogen Irradiation

KOBAYASHI, Yoshihiro[1]**; SUMITOMO, Koji**[1]**; SHIRAISHI, Kenji**[1]**; URISU, Tsuneo; OGINO, Toshio**[1]
([1]NTT Basic Res. Lab.)

[*Surf. Sci.* **436**, 9 (1999)]

The surface composition of Ge/Si(001)2×1 surfaces after atomic hydrogen (H) irradiation was investigated using IR reflection spectroscopy in ultrahigh-vacuum. It was confirmed that an extremely high dose of H at room temperature causes an etching reaction of the surface Ge layer. However, when H is irradiated at a temperature higher than 150 °C, the etching reaction dose not occur; instead, Ge segregated at the surface is observed to move into a subsurface and Si tends to exist on the topmost surface as a hydride in mixed Ge–Si and pure Si–Si dimers. This is in remarkable contrast to the Ge/Si(001) surface in the absence of hydrogen, where Ge is segregated at the surface and forms Ge–Ge pure dimers. The phenomenon of ‘reverse segregation’ by H irradiation may be understood by the thermochemical consideration that Si–H bonds are much more stable than Ge–H bonds. The result of first-principles total energy calculations in which the presence of hydrogen changes the stable composition at the surface from Ge to Si is also consistent with the phenomenon.

VI-F-6 Reconstruction of BL4A Beam Line and Infrared Reflection Absorption Spectroscopy System

WANG, Zhihong; NODA, Hideyuki; NONOGAKI, Youichi; URISU, Tsuneo

Re-arrangement of the beam line at BL4A has already started this year. Now it is still under construction. The IRRAS (Infrared Reflection Absorption Spectroscopy) system has been moved from BL4B to BL4A2. The reaction gas lines have been reconstructed connecting with new interlock system. The reaction chamber for IRRAS measurement was also reconstructed. The new system only use one chamber instead of formal two for the sample transfer to the measurement chamber to make the transfer more easy and efficient. The interlock system connecting these chambers and turbo molecular pumps also has been changed to the more simple and practical one.

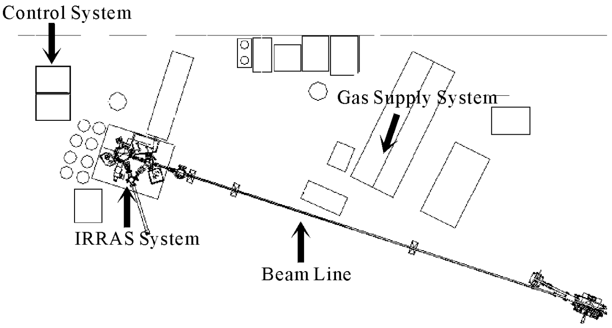

Figure 1. Schematic drawing of the BL4A2 beam line with the IRRAS system.

VI-G Photoionization Dynamics Studied by Electron Spectroscopy Combined with a Continuous Synchrotron Radiation Source

Molecular photoionization is a major phenomenon in vacuum UV excitation and provides a large amount of information on fundamental electron-core interactions in molecules. Especially, neutral resonance states become of main interest, since they often dominate photoabsorption cross sections and lead to various vibronic states which are inaccessible in direct ionization. We have developed a versatile machine for photoelectron spectroscopy in order to elucidate dynamical aspects of superexcited states such as autoionization, resonance Auger decay, predissociation, vibronic couplings, and internal conversion. Introduction of a new methodology, two-dimensional photoelectron spectroscopy, allows us to investigate superexcited states in the valence excitation region of acetylene, nitric oxide, carbonyl sulfide, sulfur dioxide and so on. In this method, the photoelectron yield is measured as a function of both photon energy and electron kinetic energy (binding energy). The spectrum, usually represented as a contour plot, contains rich information on photoionization dynamics.

VI-G-1 Superexcitation and Subsequent Decay of Triatomic Molecules Studied by Two-Dimensional Photoelectron Spectroscopy

MITSUKE, Koichiro; HATTORI, Hideo[1]; HIKOSAKA, Yasumasa[2]
([1]Nitto Tech. Inf. Cent. Co.; [2]Inst. Mater. Struct. Sci.)

[*J. Electron Spectrosc. Relat. Phenom.* in press]

Photoionization and photodissociation processes of SO_2 and CS_2 in the vacuum UV are studied by using two-dimensional photoelectron spectroscopy with a monochromatized synchrotron radiation source. The principal focus is on the mechanisms of autoionization and neutral dissociation of superexcited states. Photoelectron spectra of SO_2 exhibit characteristic peaks at the electron kinetic energy below 1.8 eV which are assigned as resulting from autoionizing transitions of excited atomic sulfur, S*, into the ground $S^+(^4S^o)$ state. These S* atoms are in the singlet Rydberg states converging to $S^+(^2D^o)$. The precursor molecular states, SO_2^*, are considered to be multiple-electron excited Rydberg states lying at the photon energy above ~ 22 eV. The onset of the photoelectron yield due to the atomic autoionization accords with that expected from the thermochemical threshold for the formation of S* through three-body dissociation $SO_2^* \rightarrow S^* + O + O$. The two-dimensional photoelectron spectrum of CS_2 provides tangible evidence for the formation of a dipole-forbidden Rydberg state $(6\sigma_g)^{-1}(3d\sigma_g)^1\ ^1\Sigma_g^+$ at the photon energy of 14.88 eV which autoionizes into the $\nu_3 = 1$ vibrational state of the antisymmetric stretch ν_3 mode of CS_2^+ ($X\ ^2\Pi_{g,\Omega}$, Ω = 1/2 and 3/2). This Rydberg state is expected to borrow substantial oscillator strength from the $(6\sigma_g)^{-1}(5p\sigma_u)^1\ ^1\Sigma_u^+$ state through vibronic coupling involving the ν_3 vibration.

VI-G-2 Photoelectron Spectroscopy of Atomic and Molecular Radicals Prepared by RF Atom Source

MITSUKE, Koichiro; IWASAKI, Kota

There is very little knowledge on the electronic structures of atomic or molecular radicals, though these transient species often play important roles in the elementary reactions in the stratosphere and various plasmas for industrial purposes. Furthermore, studies of superexcited states of such radicals have not yet evolved mainly owing to their low density, short lifetime with respect to fluorescence emission and collisional quenching, and interference with photoelectron bands of other stable or unstable species. To overcome these serious problems we have employed an intense RF radical source that can operate compatibly with our photoelectron spectrometer installed at the beam line BL3B of the UVSOR facility.

Atomic and molecular radicals are produced by an electrical discharge in the resonant cavity (source) which has been tuned so that its load becomes purely resistive. Radicals escape from the source into a vacuum environment through an aperture of 0.5 mm diameter. Under optimal operating conditions, 90% of the molecular H_2, O_2, or N_2 leaves the source in dissociated form. The maximum flux of the radical beam is calculated from a gas flow of 0.5 sccm to be *ca.* 10^{16} radicals $cm^{-2}s^{-1}$ at the ionization region of an electron energy analyzer which is about 30 cm distant from the aperture of the source. As a result, the maximum density at the analyzer position is estimated to be about 10^{10} radicals cm^{-2} by assuming the mean translational energy of the radical beam of < 1 eV.

VI-H Development of a Laser-Synchrotron Radiation Combination Technique to Study Photoionization of Polarized Atoms

In conventional photoionization experiments, the most standard method has generally been taken to be measurement of energy and angular distributions of photoelectrons from randomly oriented (unpolarized) atoms or molecules. However, information obtained from these experiments is insufficient, since the initial state constituted of atoms and photons is not selected and the internal properties of final photoions and electrons are not analyzed. In this project, we have performed photoelectron spectroscopy of polarized atoms using linearly-polarized laser light, aiming at complete quantum-mechanical photoionization experiments. Initial excitation with a linearly polarized synchrotron radiation permits ensemble of atoms to be aligned along the electric vector of the light. From an angular distribution of photoelectrons from polarized atoms, we are able to gain insight into the magnitude and phase shift difference of transition dipole matrix elements of all final channels which are allowed by selection rules.

VI-H-1 Laser Photoionization of Polarized Ar Atoms Produced by Excitation with Synchrotron Radiation

MITSUKE, Koichiro; HIKOSAKA, Yasumasa[1]; IWASAKI, Kota
([1]Inst. Mater. Struct. Sci.)

[*J. Phys. B* **33**, 391 (2000)]

The combination technique is incorporated into an apparatus for two-dimensional photoelectron spectroscopy of atoms and molecules in order to investigate photoionization dynamics of polarized atoms. Ground state Ar atoms are excited with linearly polarized synchrotron radiation to Rydberg states lying below the first ionization potential. Aligned atoms thus formed are ionized by irradiation of laser which is also linearly polarized. Photoelectrons emitted in the direction of the electric vector of synchrotron radiation are sampled and energy-analyzed. Photoelectron angular distribution is measured with respect to the electric vector of the laser (see Figure 1). Derivation is made on the expressions which correlate asymmetric coefficients for the angular distribution with theoretical dynamic parameters involving transition dipole matrix elements. The anisotropy of the present angular distribution can be reasonably explained, assuming that the matrix elements and phase shift differences are essentially independent of the total angular momentum quantum number of the final state and that the spin-orbit interaction in the continuous spectrum is small. In the case of the photoionization of the Ar*(3d[1/2]$_1$) state the ratio of the reduced dipole matrix elements between those for the εp and εf parial waves is evaluated from the observed asymmetry parameter to be 0.60 on the presumption that the phase shift difference of the two waves is equal to π/2.

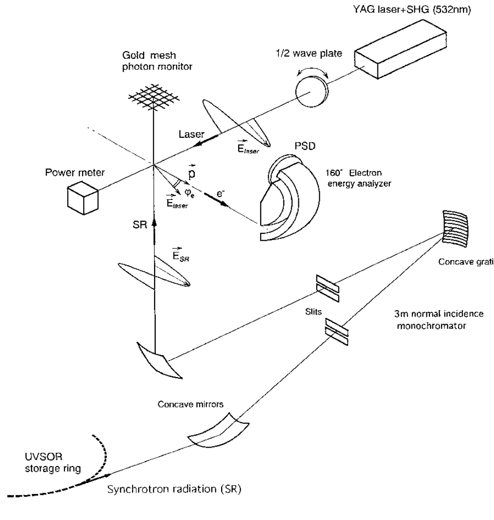

Figure 1. Geometry of the laser-synchrotron radiation combination experiment for investigating photoionization dynamics of polarized atoms. The electric vector $\vec{E}_{\mathrm{SR}}$ of the monochromatized synchrotron radiation is fixed and parallel to the electron sampling direction $\vec{p}$. In contrast, the electric vector $\vec{E}_{\mathrm{laser}}$ of the laser can be rotated around its propagation direction. Photoelectron angular distribution is measured as a function of the angle φ_e between $\vec{E}_{\mathrm{laser}}$ and $\vec{E}_{\mathrm{SR}}$.

VI-H-2 Development of a New Angle-Resolved Energy Analyzer for Photoelectron Spectroscopy of Polarized Atoms

IWASAKI, Kota; MITSUKE, Koichiro

A conical electron energy analyzer has been developed to measure the angular distribution of photoelectrons from polarized rare gas atoms excited with synchrotron radiation. Since the photoelectron yield of this type of experiment is quite small, we intend to achieve high angular resolution and wide angular acceptance simultaneously.

Our analyzer consists of a set of an inner and outer conical deflector electrodes, cylindrical lenses, a gas cell and a position sensitive detector (PSD) as shown in Figure 1. Photoelectrons emitted in the gas cell are accelerated between the cell and an extractor electrode, and then focused on an entrance slit by the cylindrical lenses. The electron trajectories between the inner and outer conical electrodes are similar to those expected for a conventional parallel-plate analyzer. However, our conical analyzer has rather larger energy dispersion and larger angular aberration than the parallel-plate analyzer. Energy selected electrons exiting from the conical deflector electrodes are detected with the PSD

$$\frac{\Delta E}{E} = \frac{\Delta R}{1.11R} + k_1\alpha + k_2\alpha^2 \approx \frac{1}{30},$$

mounted behind the analyzer. The energy resolution is expressed as

where R denotes the distance between the entrance and exit slits, α the angular deviation of electrons with respect to the mean trajectory of the incident electrons in the dispersion plane, and k_1 and k_2 angular aberration coefficients. On the other hand, the conical analyzer is incapable of focussing the electron trajectories in the azimuth direction. The azimuth angular resolution is thus estimated to be 1.5° from the diameter of the sample volume (ϕ 1 mm) and the position sensitivity of the PSD. At a PSD particular position, the angular distribution can be measured in the range of 0°–25° at the same time. By rotating the PSD about the synchrotron radiation propagation axis, we can obtain the photoelectron angular distribution from –5° to 95° with respect to the electric vector of synchrotron radiation.

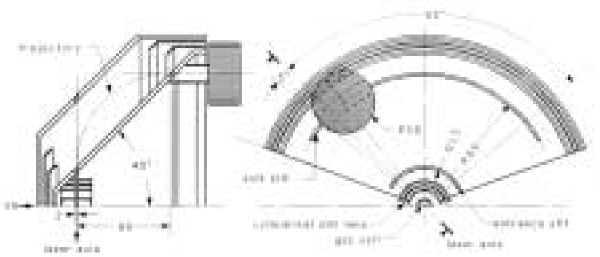

Figure 1. Schematic diagram of the conical analyzer. Principal electrodes of the analyzer are depicted by taking two different views. Left: a cross sectional view on the plane which includes the propagation vectors of the laser and synchrotron radiation. Right: a top view.

VI-I Vacuum UV Spectroscopy Making Use of a Combination of Synchrotron Radiation and a Mode-Locked or Pulsed UV Laser

An ultraviolet laser system has been developed which synchronizes precisely with the synchrotron radiation (SR) from the storage ring of the UVSOR facility. A mode-locked Ti:sapphire laser is made to oscillate at the frequency of the ring in a multibunch operation mode. The delay timing between SR and laser pulses can be changed from 0 to 11 ns. We have developed another system, a pulsed dye laser pumped by an excimer laser, for SR-laser combination experiments. The second harmonic of the dye laser is tunable at 265–280 nm with a pulse energy of *ca.* 2 mJ pulse^{-1} at a repetition rate of 10–100 Hz. This laser system is mainly devoted to observing neutral species produced by neutral or ionic photofragmentation induced by SR excitation of molecules. The following three combination studies have been performed: (1) two-photon ionization of helium atoms studied as the prototype of the time-resolved experiment, (2) laser induced fluorescence (LIF) excitation spectroscopy of $N_2^+(X\ ^2\Sigma_g^+)$ ions produced by synchrotron radiation photoionization of N_2 or N_2O, and (3) resonance enhanced multiphoton ionization (REMPI) spectroscopy of $S(3s^23p^4\ ^3P_{J''}, J'' = 0, 2)$ dissociated from Rydberg states of OCS. Among these topics LIF spectroscopy of ions is making marked progress in improvements of spectral resolution and fluorescence counts. These improvements are brought about by introducing an RF ion trap and by narrowing the laser band-width. As a consequence, we can obtain reliable rotational distribution curves of $N_2^+(X\ ^2\Sigma_g^+)$.

VI-I-1 Rotational State Distribution of N_2^+ Produced from N_2 or N_2O Observed by a Laser-Synchrotron Radiation Combination Technique

NIIKURA, Hiromichi[1]; MIZUTANI, Masakazu; MITSUKE, Koichiro
([1]GUAS)

[*Chem. Phys. Lett.* **317**, 45 (2000)]

Pump-probe spectroscopy making use of a combination of laser and synchrotron radiation has been performed at the beam line BL3A2 in UVSOR to study ionization and dissociation dynamics of N_2 and N_2O in the vacuum UV energy region. The fundamental light emitted from the planar-type undulator was dispersed by a 2.2 m grazing incidence constant deviation monochromator in the photon energy range 15.5–19 eV. The second harmonic of a mode-locked Ti:sapphire laser was used for laser-induced fluorescence (LIF) spectroscopy of $N_2^+(X\ ^2\Sigma_g^+, v, N)$ cations produced by synchrotron radiation photoionization. Fluorescence was collected in the perpendicular direction to the two light beams, dispersed by another monochromator, and detected with a photomultiplier tube. To increase the number density of ions, we employed a cylindrical ion trap. The collisional quenching of the rotational distribution of ions can be disregarded in the ion trap. We can clearly resolve the rotational structure of the R-branch resulting from the transition $(B\ ^2\Sigma_u^+, v' = 0, N + 1) \leftarrow (X\ ^2\Sigma_g^+, v'' = 0, N)$ of N_2^+ produced from N_2. The yield curves for N_2^+ $(X\ ^2\Sigma_g^+, v'' = 0, 1)$ are also measured as a function of the photon energy of the synchrotron radiation. The rotational temperature of N_2^+ $(X\ ^2\Sigma_g^+, v'' = 0)$ produced from N_2O^+ $(B\ ^2\Pi)$ is determined from an LIF spectrum to be in the range of 200–230 K. The analysis based on the impulsive model indicates that the equilibrium bond angle of $N_2O^+(B\ ^2\Pi)$ in the vibrational ground state is much larger than 130°.

VI-J Monochromator Newly Developed on the Beam Line BL2B2 in UVSOR

A grazing incidence monochromator has been constructed which supplies photons in the energy region from 20 to 200 eV. This monochromator will bridge the energy gap between the beam lines BL3A2 and BL8B1, thus providing for an accelerating demand for the high-resolution and high-flux photon beam from the research field of photoexcitation of inner-valence electrons or *L*-shell electrons in the third-row atom.

VI-J-1 Performance of the Dragon-Type Monochromator at UVSOR

ONO, Masaki; YOSHIDA, Hiroaki[1]; HATTORI, Hideo; MITSUKE, Koichiro
([1]Hiroshima Univ.)

[*Nucl. Instrum. Methods Phys. Res., Sect. A* in press]

A Dragon-type monochromator has been newly constructed at the bending-magnet beamline BL2B2 of the UVSOR facility. The monochromator has been designed to cover the energy range 20–200 eV with three gratings (G1: 80–200 eV, G2: 40–100 eV, G3: 20–50 eV). A resolving power, $E/\Delta E$, of 5000 and a photon flux more than 1×10^{10} photons s^{-1} at a 100-mA ring current are expected. The optical alignment and performance test have been finished.

The resolving power is evaluated from the ion yield spectra of the rare gas atoms: the $3d_{5/2}{}^{-1}5p$ line of Kr (91.2 eV, exploited for G1 and G2), $2snp + 2pns$ series of He (60–65 eV, for G2) and $3s^{-1}np$ series of Ar (25–30 eV, for G3). Moreover, the photon flux is estimated by measuring the photocurrent of a gold mesh which is put in the path of the photon beam. Figure 1 summarizes the resolving power and photon flux at a 100-mA ring current when both the entrance and exit slits are set to 100 μm wide. The solid line in Figure 1(b) shows the expected values derived theoretically.[1] By adjusting the slit widths, we can attain the resolving power of 2000–8000 and the photon flux of 1×10^{10} photons s^{-1} simultaneously at a 100-mA ring current.

The second-order contribution is inspected on the basis of the ion yield spectrum of Kr around 45.6 eV. The peak of the $3d_{5/2}{}^{-1}5p$ line at 91.2 eV appears due to the contaminating second-order light. The percentage of the second-order light at 45.6 eV is estimated to be 7% from the ratio between the absorption cross sections at 45.6 and 91.2 eV.

Reference

1) H. Yoshida and K. Mitsuke, *J. Synchrotron Radiat.* **5**, 774 (1998).

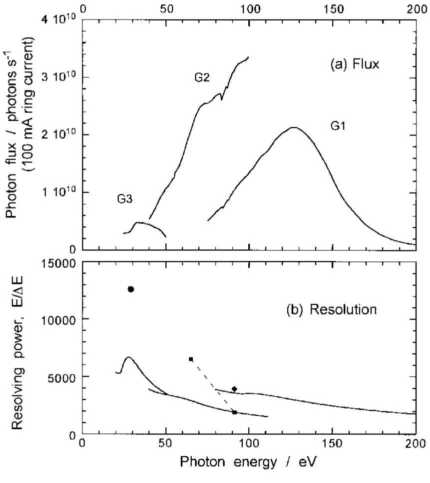

Figure 1. (a) The photon flux at a 100-mA ring current and (b) resolving power when the entrance and exit slit widths are set to 100 μm. The solid lines in panel (b) indicate the expected values.

VI-J-2 Anisotropy of the Fragment Ions from Small Molecules Excited with Synchrotron Radiation

ONO, Masaki; MIZUTANI, Masakazu; MITSUKE, Koichiro

In order to make assignments of core-electron excited states and study their decay dynamics, an apparatus for symmetry-separated absorption spectroscopy has been developed at the end-station of the beam line BL2B2. The spectrometer contains two ion detectors each of which comprises a grid made of copper mesh followed by a ceratron electron multiplier. Two ion detectors are placed in the parallel and perpendicular direction to the electric vector of synchrotron radiation. Retarding voltages were applied to the grids so that only fragment ions with high kinetic energy were allowed to reach the entrance of the ceratron multiplier. The difference in the collection efficiency and sensitivity of the ceratron multiplier between the two ion detectors were corrected by measuring the spectrum of SF_6. From the O_h symmetry it is predicted that the fragment ion yield via core excited states of SF_6 should be isotropic.

Figure 1 shows preliminary results of ion yield spectra of the fragment ions from SF_6 and the calculated asymmetry parameter β, when the retarding voltage is set to 5 V. In the ion yield spectra the prominent peaks in the region of > 170 eV are due to the resonance excitation of a sulfur $2p$ electron. The β parameter is almost 2 at low photon energies below 30 eV, which manifests that fragmentation occurs faster than the molecular rotation. There exist several features around 20–60 eV and a broad peak centered at ~ 100 eV in the yield spectra. The interpretation of these features is now in progress. The artificial structures around 110 eV arise from an imperfect photon-flux normalization process involving photocurrent measurements at the gold mesh (see the preceding theme VI-J-1).

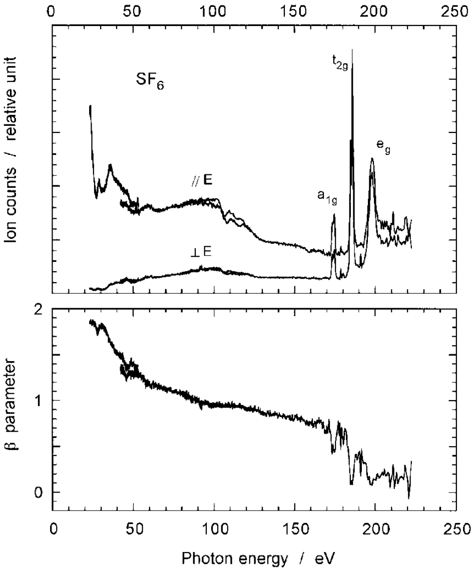

Figure 1. Ion yield spectra and the asymmetry parameter of the fragment ions from SF_6. A retarding voltage of 5 V is applied to the two copper grids.

VI-K Thin Film Preparation with Chemical Vapor Deposition Using Vacuum Ultraviolet Radiation

Thin-film deposition at temperatures as low as possible and without damages is one of the key technologies for fabrication of ultra-large scale integrated circuit (ULSI). Photon-assisted chemical vapor deposition is a promising way to prepare particularly dielectric thin-films. Silicon dioxide films have been prepared from tetraethoxyorthosilicate ($Si\text{-}(OC_2H_5)_4$) with chemical vapor deposition using vacuum ultraviolet radiation. The growth rate increases with decreasing the substrate temperature.

VI-K-1 Silica Film Preparation by Chemical Vapor Deposition Using Vacuum Ultraviolet Excimer Lamps

KUROSAWA, Kou; YANAGIDA, Hideaki[1]; TAKEZOE, Noritaka; KAWASAKI, Yasuhiro[1]; FUJITA, Masashi[2]; YOKOTANI, Atsushi[2]
([1]IMS and Univ. Miyazaki; [2]Univ. Miyazaki)

[*CLEO-2000* CMX4]

New scheme for silica film fabrication by a photo-chemical vapor deposition was developed by using excimer lamps in vacuum ultraviolet to ultraviolet spectral region. Smooth and uniform silica films were deposited at room temperature at a deposition rate of 1 nm/min.

VI-K-2 Silica Film Preparation by Chemical Vapor Deposition Using Vacuum Ultraviolet Excimer Lamps

KUROSAWA, Kou; YAKEZOE, Noritaka; YANAGIDA, Hideaki[1]; MIYANO, Jyunichi[2]; MOTOYAMA, Yoshikazu[2]; TOSHIKAWA, Kiyohiko[2]; KAWASAKI, Yasuhiro[1]; YOKOTANI, Atsushi[3]
([1]IMS and Univ. Miyazaki; [2]Miyazaki OKI Electric; [3]Univ. Miyazaki)

[European Materials Research Society Spring Meeting 2000, D-II-4]

We have prepared SiO_2 thin films on silicon wafers from tetraethoxyorthosilicate (TEOS; $Si(OC_2H_5)_4$) by photo-chemical vapor deposition with the use of various excimer lamps which emit incoherent light at 302 (XeCl), 222 (KrCl), 172 (Xe_2), 146 (Kr_2) and 126 nm (Ar_2). The film deposition is observed at wavelengths shorter than 172 nm. With 10-mW/cm^2 172-nm radiation, the growth rate is 8 nm/min on the room temperature substrate. The deposition efficiency depends on the wavelength and shows the maximum value for 146-nm radiation. Addition of O_2 to TEOS induces inhibition of C and H impurity inclusion in the films.

VI-L Ultraviolet, Visible and Infrared Spectroscopy of Solids

Work of ultraviolet (UV), visible (VIS) and Infrared (IR) spectroscopy of solids have been proceeded. These are mainly performed using synchrotron radiation (beamlines BL7B and BL1B at UVSOR), owing to the wide wavelength continuity of synchrotron radiation with no structure.

VI-L-1 Performance of IR-VUV Normal Incidence Monochromator Beamline at UVSOR

FUKUI, Kazutoshi; MIURA, Hiroshi[1]; NAKAGAWA, Hideyuki[1]; SHIMOYAMA, Iwao[2]; NAKAGAWA, Kazumichi[3]; OKAMURA, Hidekazu[3]; NANBA, Takao[3]; HASUMOTO, Masami; KINOSHITA, Toyohiko[4]
([1]Fukui Univ.; [2]Jpn. Atom. Res. Inst.; [3]Kobe Univ.; [4]Univ. Tokyo)

The beamline BL7B at the UVSOR facility for solid-state spectroscopy has been reconstructed and opening for users. This beamline consists of a 3 m normal incidence monochromator and covers from vacuum ultraviolet to infrared region. The optical configuration and the performance, such as photon number, purity and resolving power, have been investigated. The resolving power is over 8000 at around 180 nm and enough for solid-state spectroscopy over whole wavelength range. High purity and low stray of the monochromated light is almost fulfilled over whole range. The wavelength accuracy is less than 0.1 nm.

VI-L-2 Pseudogap Formation in the Intermetallic Compounds $(Fe_{1-x}V_x)_3Al$

OKAMURA, Hidekazu[1]; KAWAHARA, Jun[1]; NANBA, Takao[1]; KIMURA, Shin-ich[1]; SODA, Kazuo[2]; MIZUTANI, Uichiro[2]; NISHINO, Yoichi[3]; KATO, Masaaki[3]; SHIMOYAMA, Iwao[1]; MIURA, Hiroshi[4]; FUKUI, Kazutoshi; NAKAGAWA, Kazumichi[1]; NAKAGAWA, Hideyuki[4]; KINOSHITA, Toyohiko[5]
([1]Kobe Univ.; [2]Nagoya Univ.; [3]Nagoya Inst. Tech.; [4]Fukui Univ.; [5]Univ. Tokyo)

[*Phys. Rev. Lett.* **84**, 3674 (2000)]

Optical conductivity data of the intermetallic compounds $(Fe_{1-x}V_x)_3Al$ ($0 \le x \le 0.33$) reveal that their density of states around the Fermi energy (E_F) is strongly reduced as x is increased. In particular, Fe_2VAl ($x = 0.33$) has a deep, well-developed pseudogap of 0.1–0.2 eV at E_F and a small density ($\sim 5 \times 10^{20}$ cm^{-3}) of carriers, which is highly unusual for intermetallic compounds. It is shown that the pseudogap results from the band structures of Fe_2VAl, rather than from temperature-dependent correlation effects. Based on the present results, we propose a simple model that consistently explains both the semiconductorlike transport and the metallic photoemission results previously observed from Fe_2VAl.

VI-M Dynamics and Relaxation of Atoms and Molecules Following Core-Level Excitation

Monochromatized X-ray from synchrotron radiation excites a core electron of an atom or molecule, and the core hole thereby created is usually filled by an outer-orbital electron through an Auger process. In molecules, the core electrons are localized near the atom of origin, in contrast to valence electrons, which are often delocalized over the entire molecule. Although core electrons do not participate in chemical bonding, the energy of an atomic core-level in the molecule depends on the chemical environment of the atom. Site-specific excitation and fragmentation are thus of considerable interest. To elucidate the dynamics and relaxation of atoms and molecules following core-level excitation, we have used photoelectron spectroscopy and the energy-selected-photoemission photoion coincidence method.

VI-M-1 Site-Specific Phenomena in Si:2p Core-Level Photoionization of $X_3Si(CH_2)_nSi(CH_3)_3$ (X = F or Cl, n = 0–2) Condensed on a Si(111) Surface

NAGAOKA, Shin-ichi; MASE, Kazuhiko[1]; NAGASONO, Mitsuru[2]; TANAKA, Shin-ichiro[3]; URISU, Tsuneo; OHSHITA, Joji[4]; NAGASHIMA, Umpei[5]
([1]KEK-PF; [2]MAX-lab; [3]Nagoya Univ.; [4]Hiroshima Univ.; [5]Natl. Inst. Adv. Interdisciplinary)

[*Chem. Phys.* **249**, 15 (1999)]

We used photoelectron spectroscopy and the energy-selected-photoelectron photoion coincidence (ESPEPICO) method to study site-specific phenomena in the Si:2p photoionization of $X_3Si(CH_2)_nSi(CH_3)_3$ (X = F or Cl, n = 0–2) condensed on a Si(111) surface. The site-specific excitation and the occurrence of different chemical shifts at two Si sites were revealed in the total electron-yield spectra and the photoelectron spectra of $F_3Si(CH_2)_nSi(CH_3)_3$ (n = 1, 2), although they were not clearly revealed in those of $Cl_3SiSi(CH_3)_3$. We conclude that these site-specific phenomena are easily observed in molecules in which the two Si sites are located far apart and in which electron migration between the two Si-containing groups does not occur. This was supported by our ab initio calculation. Site-specific fragmentation was revealed in the ESPEPICO spectrum of F_3SiCH_2-$CH_2Si(CH_3)_3$, although it was negligible for Cl_3SiSi-$(CH_3)_3$ and was less remarkable in $F_3SiCH_2Si(CH_3)_3$ than in $F_3SiCH_2CH_2Si(CH_3)_3$. Site-specific fragmentation also occurred when the two Si sites were located far apart.

VI-M-2 Site-Specific Fragmentation Following C:1s Core-Level Photoionization of 1,1,1-Trifluoroethane Condensed on a Au Surface and of a 2,2,2-Trifluoroethanol Monolayer Chemisorbed on a Si(100) Surface

NAGAOKA, Shin-ichi; TANAKA, Shin-ichiro[1]; MASE, Kazuhiko[2]
([1]Nagoya Univ.; [2]KEK-PF)

We used photoelectron spectroscopy, the energy-selected-photoelectron photoion coincidence (ESPEPICO) method, the Auger-electron photoion coincidence (AEPICO) method, and the ab initio method to study site-specific phenomena in the C:1s photoionization of 1,1,1-trifluoroethane (CF_3CH_3, TFEt) condensed on a Au surface. Site-specific excitation and occurrence of different chemical shifts at two carbon sites were evident in the total electron-yield spectrum and the photoelectron spectrum, and site-specific fragmentation was evident in the ESPEPICO spectrum. The fragmentation processes inferred from the ESPEPICO and AEPICO results were very different from those occurring in the vapor phase. We also studied the effect of the surface on the site-specific phenomena observed in a 2,2,2-trifluoroethanol (TFEtOH) monolayer chemisorbed on a Si(100) surface (CF_3CH_2OSi\{substrate\}). The molecular structure of TFEtOH is the same as that of TFEt except that it has a hydroxyl group substituted for one of the hydrogen atoms. Although site-specific phenomena were also observed in TFEtOH, the fragmentation process was very different from that of TFEt because of the chemisorption structure of TFEtOH on Si(100).

VI-M-3 Ion Desorption Induced by Core-Electron Transitions Studied with Electron–Ion Coincidence Spectroscopy

MASE, Kazuhiko[1]; TANAKA, Shin-ichiro[2]; NAGAOKA, Shin-ichi; URISU, Tsuneo
([1]KEK-PF; [2]Nagoya Univ.)

[*Surf. Sci.* **451**, 143 (2000)]

The recent investigations of ion desorption induced by core-electron transitions using electron–ion coincidence (EICO) spectroscopy are described. In a study of $CF_3CH(OH)CH_3$ chemisorbed on a Si(100) surface using photoelectron photoion coincidence (PEPICO) spectroscopy, site-specific ion desorption is directly verified, that is, F^+ desorption is predominant for C 1s photoionization at the $–CF_3$ site, while H^+ desorption is predominantly induced by C 1s photoionization at the $–CH_3$ site. A study of condensed H_2O using Auger electron photoion coincidence (AEPICO) spectroscopy showed that H^+ desorption is stimulated by O KVV Auger processes leaving two-hole states. The H^+ desorption probability is found to depend on the bonding character of the orbitals where holes are created and on the effective hole–hole Coulomb repulsion. AEPICO investigations of H^+ desorption induced by resonant core-electron excitations of condensed H_2O clearly showed that one-electron–one-core hole or one-electron–two-valence hole states are responsible for the H^+ desorption mechanism. These investigations demonstrate that EICO spectroscopy combined with synchrotron radiation is a novel and powerful tool for the study of ion desorption induced by core-electron excitations. Furthermore, a comparison of PEPICO and photoelectron spectra showed that the surface core-level shift of condensed H_2O is 0.7 eV. This study shows that PEPICO spectroscopy is also promising as a method to investigate the electronic structure of the specific sites responsible for ion desorption.

VI-M-4 Electron–Ion Coincidence Study for the TiO_2(110) Surface

TANAKA, Shin-ichiro[1]; MASE, Kazuhiko[2]; NAGASONO, Mitsuru[3]; NAGAOKA, Shin-ichi; KAMADA, Masao
([1]Nagoya Univ.; [2]KEK-PF; [3]MAX-lab)

[*Surf. Sci.* **451**, 182 (2000)]

Photo-stimulated desorption from the TiO_2(110) surface was investigated by using electron–ion coincidence spectroscopy and synchrotron radiation. The desorption of O^+ ions was observed to be coincident with the emission of photoelectrons from the O1s, Ti2s, Ti2p, Ti3s and Ti3p levels, and their satellite peaks due to the shake-up excitation. However, no ion desorption was observed in coincidence with the O2s or valence photoelectrons. The O^+ peak intensities in the coincidence spectra are analyzed, and the result is unexpected from a simple expansion of the Knotek-Feibelman model. The shake-up excitation of O1s levels yields O^+ desorption more efficiently than does the O1s single-electron excitation.

VI-M-5 Development of Electron-Ion Coincidence Spectroscopy for Study of Vapor-Phase Dynamics

MASE, Kazuhiko[1]; NAGAOKA, Shin-ichi
([1]KEK-PF)

An electron-ion coincidence spectrometer for vapor-phase dynamics study is being built now. The equipment consists of an electron gun, a cylindrical mirror analyzer (CMA) and a reflectron-type time-of-flight ion mass analyzer. Sample gas is excited with the electron beam and the CMA analyzes energy of emitted or scattered electrons. Mass spectra of produced ions are measured with a multichannel scalar taking the energy-analyzed electron signal as the starting trigger.

VI-M-6 High-Resolution Angle-Resolved Ion-Yield Measurements of H_2O and D_2O in the Region of O 1s to Rydberg Transitions

OKADA, Kazumasa[1]; UEDA, Kiyoshi[2]; TOKUSHIMA, Takashi[1]; SENBA, Yasunori[1]; YOSHIDA, Hiroaki[1]; SHIMIZU, Yuuichiro[2]; SIMON, Mare[3]; CHIBA, Hisashi[2]; OKUMURA, Hiroki[4]; TAMENORI, Yuusuke[5]; OHASHI, Haruhiko[5]; SAITO, Norio[6]; NAGAOKA, Shin-ichi; SUZUKI, Isao H.[6]; ISHIGURO, Eiji[7]; KOYANO, Inosuke[4]; IBUKI, Toshio[8]; HIRAYA, Atsunari[1]
([1]Hiroshima Univ.; [2]Tohoku Univ.; [3]LURE; [4]Himeji Inst. Tech.; [5]JASRI; [6]Electrotech. Lab.; [7]Univ. Ryukyus; [8]Kyoto Univ. Edu.)

[*Chem. Phys. Lett.* **326**, 314 (2000)]

Angle-resolved energetic-ion yield spectra have been observed in the O 1s excitation region of H_2O and D_2O with the incident photon-energy resolution better than 14000. Vibrational structures appear in most of the Rydberg members and are ascribed to the bending vibrations. The assignments of the electronic states are established on the basis of the angular distribution data for the energetic ions.

VI-M-7 Molecular Deformation in the O $1s^{-1}2\pi_u$ Excited States of CO_2 Probed by the Triple-Differential Measurement of Fragment Ions

SAITO, Norio[1]; UEDA, Kiyoshi[2]; SIMON, Mare[3]; OKADA, Kazumasa[4]; SHIMIZU, Yuuichiro[2]; CHIBA, Hisashi[2]; SENBA, Yasunori[4]; OKUMURA, Hiroki[5]; OHASHI, Haruhiko[6]; TAMENORI, Yuusuke[6]; NAGAOKA, Shin-ichi; HIRAYA, Atsunari[4]; YOSHIDA, Hiroaki[4]; ISHIGURO, Eiji[7]; IBUKI, Toshio[8]; SUZUKI, Isao H.[1]; KOYANO, Inosuke[5]
([1]Electrotech. Lab.; [2]Tohoku Univ.; [3]LURE; [4]Hiroshima Univ.; [5]Himeji Inst. Tech.; [6]JASRI; [7]Univ. Ryukyus; [8]Kyoto Univ. Edu.)

[*Phys. Rev. A* in press]

Measurement of mass-, energy-, and angle-resolved fragment ions revealed that the β value for C^+ with kinetic energy $\geq$ 3 eV is ~ 0.9 in the region of the O 1s $\rightarrow 2\pi_u$ excitation and that β value for O^+ with kinetic energy $\geq$ 4 eV varies from –0.23 to –0.57 across the O 1s $\rightarrow 2\pi_u$ resonance. These findings postulate that the CO_2 molecule excited to the lower branch of the vibronically split O $1s^{-1}2\pi_u$ excited states deforms into a bent geometry while the molecule excited to the higher branch remains in a linear geometry.

VI-M-8 Resonant Auger Spectrum Following Kr:2p → 5s Photoexcitation

NAGAOKA, Shin-ichi; IBUKI, Toshio[1]; SAITO, Norio[2]; SHIMIZU, Yuuichiro[3]; SENBA, Yasunori[4]; KAMIMORI, Katsuya[4]; TAMENORI, Yuusuke[3]; OHASHI, Haruhiko[3]; SUZUKI, Isao H.[2]
([1]Kyoto Univ. Edu.; [2]Electrotech. Lab.; [3]JASRI; [4]Hiroshima Univ.)

[*J. Phys. B* in press]

Resonant Auger electron spectra following Kr:2p → 5s photoexcitation have been measured for the first time using monochromatized undulator radiation and a cylindrical-mirror electron-energy analyzer. It is found that the kinetic energy of the resonant Auger electron is higher than that of the corresponding normal Auger electron. The angular distribution of the resonant Auger electrons is nearly isotropic relative to the polarization direction of the incident light.

VI-M-9 Angle-Resolved Electron and Ion Spectroscopy Apparatus on the Soft X-Ray Photochemistry Beamline BL27SU at SPring-8

UEDA, Kiyoshi; YOSHIDA, Hiroaki[2]; SENBA, Yasunori[2]; OKADA, Kazumasa[2]; SHIMIZU, Yuuichiro[3]; CHIBA, Hisashi[1]; OHASHI, Haruhiko[3]; TAMENORI, Yuusuke[3]; OKUMURA, Hiroki[4]; SAITO, Norio[5]; NAGAOKA, Shin-ichi; HIRAYA, Atsunari[2]; ISHIGURO, Eiji[6]; IBUKI, Toshio[7]; SUZUKI, Isao H.[5]; KOYANO, Inosuke[4]

([1]Tohoku Univ.; [2]Hiroshima Univ.; [3]JASRI; [4]Himeji Inst. Tech.; [5]Electrotech. Lab.; [6]Univ. Ryukyus; [7]Kyoto Univ. Edu.)

We have designed and constructed the apparatus for the angular distribution measurements of photoejected electrons and ions from free molecules, as a part of the endstation of a c-branch of the beamline 27SU, a soft X-ray photochemistry beamline at SPring-8. The experimental procedures are described in combination with the use of a capability to switch the horizontal and vertical directions of the linear polarization of the light produced by the figure-8 undulator. As typical examples of the experimental results, we present angle-resolved energetic ion yield spectra of the O 1s excitation region of CO_2 and the angle-resolved resonant Auger emission of Ne following the 1s → 3p excitation.

VI-M-10 Monochromator for a Soft X-Ray Photochemistry Beamline BL27SU of SPring-8

OHASHI, Haruhiko[1]; ISHIGURO, Eiji[2]; TAMENORI, Yuusuke[1]; OKUMURA, Hiroki[3]; HIRAYA, Atsunari[4]; YOSHIDA, Hiroaki[4]; SENBA, Yasunori[4]; OKADA, Kazumasa[4]; SAITO, Norio[5]; SUZUKI, Isao H.[5]; UEDA, Kiyoshi[6]; IBUKI, Toshio[7]; NAGAOKA, Shin-ichi; KOYANO, Inosuke[3]

([1]JASRI; [2]Univ. Ryukyus; [3]Himeji Inst. Tech.; [4]Hiroshima Univ.; [5]Electrotech. Lab.; [6]Tohoku Univ.; [7]Kyoto Univ. Edu.)

A high-resolution monochromator using varied line space plane gratings (VLSG) and spherical focusing mirrors was installed in one of three branches of BL27SU. The performance of the monochromator was evaluated from the photoabsorption spectrum of nitrogen molecule. The resolving power over 10^4 was confirmed.

VI-N Study on RF-Photocathode for Compact X-Ray Sources

Electron storage rings are useful and practical devices as x-ray sources because which produce a number of photons owing to high electron current and various insertion devices. However, these synchrotron radiation facilities usually occupy large area and cost much. So that there have been many works to investigate more compact x-ray sources such as x-ray lasers and free electron lasers. It is also useful to use laser undulator radiation or backward Compton scattering caused by the interactions of electron beams with laser photons, if we provide enough electrons to produce practical intensity of x-rays. RF-photocathode would produce dense electron beam so that it is a useful candidate of a electron source. It is necessary to search good materials as the photocathode for construction of a practical compact x-ray source. Cesium telluride has reported to have a good quantum efficiency, so that we have been studied about it.

VI-N-1 Preliminary Study on Photoemission from Cesium Telluride Irradiated by Polarized Photon

TAKASHIMA, Yoshifumi; KOBAYAKAWA, Hisashi[1]; TAKAGI, Masahiro[1]; KIMURA, Kenichi[1]; SUGIYAMA, Harue[1]; FURUTA, Fumio[1]; NAKANISHI, Tsutomu[1]
([1]Nagoya Univ.)

Cesium telluride is a good candidate for a material to be used as a photocathode for RF-gun because of its high quantum efficiency and long life. The quantum efficiency of the photocathode for polarized photon measured with changing the incident angle of the light gives us important information about the optical constants of the materials of the photocathode.

We preliminary measured the quantum efficiency of cesium telluride by using linear polarized photon. Figure 1 shows a sketch of our experimental set up. A Xe lamp was used as a light source. The light from the Xe lamp passed through a monochrometer and a polarizer then enter a vacuum chamber in which cesium telluride was evaporated on molybdenum block as a photocathode. The incident angle of the light was 60°. We rotated the polarizer in order to change the direction of polarization. Figure 2 shows the quantum efficiency for the incident light of 250nm wavelength with changing the direction of polarization. The quantum efficiency has peaks at 90° and 270°. The direction of polarization was parallel to the reflection plane at these angles.

For the further study, we should change the incident angle of the light and measure the quantum efficiency in order to obtain the information of optical constant of cesium telluride.

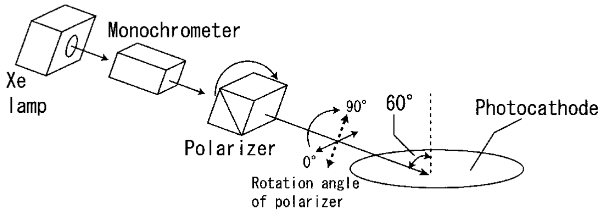

Figure 1. Sketch of experimental set up.

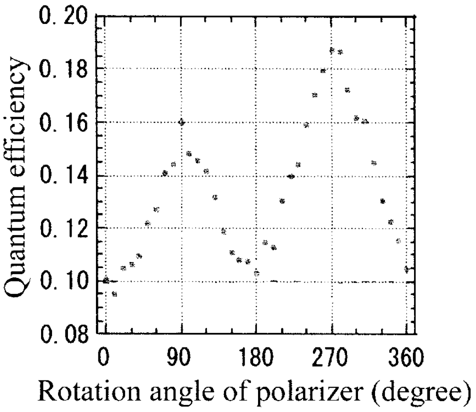

Figure 2. Quantum efficiency of cesium telluride with rotation angle of polarizer for incident light of 250 nm.

RESEARCH ACTIVITIES VII
Coordination Chemistry Laboratories

Professor Yasuhiro Uozumi and Associate Professor Hiroyuki Kawaguchi joined to laboratories of Synthetic Coordination Chemistry and Functional Coordination Chemistry. Prof. Isao Nishida, Prof. Yasutaka Tanaka took the position of Synthetic Coordination Chemistry from April 1998. Prof. Hiromu Sakurai (Kyoto Pharmacy Univ.) and Assoc. Prof. Yasushi Mizobe (Univ. Tokyo) finished their term as Adjunct Prof. in March 2000 in the Laboratory of Coordination Bond. Their effort during their term is gratefully appreciated. Prof. Takuzo Aida (Univ. Tokyo) and Assoc. Prof. Itaru Hamachi (Kyushu Univ.) continue the position of the laboratory of Coordination Bond.

VII-A New Insight into Mechanism of Oxygen Activation in Biological Oxygenases

One of the remaining frontiers in organic chemistry is the direct functionalization of saturated hydrocarbons. The catalytic cycle that oxidizes a hydrocarbon R–H to an alcohol R–OH employing cytochrome P-450 and methane monooxygenase is a well-established process, however no reasonable mechanism for oxygen activation and for formation of the R-OH is available at present. Recently the present author has proposed a new idea that elucidates many biological oxygenation reactions including monooxygenases and dioxygenases comprehensively. In this new concept, the importance of electrophilic nature of a metal-peroxide adduct and the role of the substrate as an electron donor to the peroxide adduct were emphasized (Y. Nishida, *Trends Inorg. Chem.* **5**, 89 (1998)). This idea has been supported by many experimental facts, especially by the work of Sligar *et al.* (*Science* **287**, 1615 (2000)). We are now continuing the study on the reactivity of the metal-peroxide adducts in order to ascertain that my idea is applicable to other reactions, such as degradation of DNA and proteins by the metal-peroxide adducts.

VII-A-1 Interaction between a Copper(II) Compound and Protein Investigated in terms of the Capillary Electrophoresis Method

NISHINO, Satoshi; ISHIKAWA, Yoshihiro; NISHIDA, Yuzo

[*Inorg. Chem. Commun.* **2**, 438 (1999)]

Recently there have been a number of reports on peptides which aggregate in ways that may be relevant to their biological activity. The formation of amyloid deposits in Alzheimer’s disease and the conversion of PrP^C (the normal cellular prion protein) into PrP^{Sc} and its truncated form PrP 27–30, the abnormal disease-causing isoform) in certain human and animal neurodegenerative diseases are typical examples. Very recently we have postulated that a copper(II)-peroxide adduct plays an important role in the formation of PrP^{Sc} protein and its truncated form PrP 27-30. However the mechanism of conversion from PrP^C into PrP^{Sc} is unknown at present. In order to elucidate the above problems it seems necessary to obtain detailed information on the interaction between the metal chelaltes and protein, but at present there are few suitable ways to study the interaction between the protein and a small metal chelate. In this paper, we have shown that the capillary electrophoresis method is very useful for studying the interaction in question.

VII-A-2 Contribution of a Metal-Peroxide Adduct to Neurodegeneration is due to its Oxidase Activity

NISHIDA, Yuzo; NISHINO, Satoshi

[*J. Bioscience* **54C**, 1107 (1999)]

Many hypothesis have been developed to explain aging and age-related neurodegenerative diseases, one of he most compelling is the role of oxidative stress to induce changes in protease activity in brains of patients of Alzheimer’s disease and prion diseases. At the moment, however, there is no clear answer how protein degradation may be achieved in the brain. We have observed that several metal compounds can degrade proteins in the presence of hydrogen peroxide, and elucidated the reaction scheme based on the new theoretical point for the reactivity of a metal-peroxide adduct with η^1-coordination mode. In this article we have pointed out the importance of a copper(II)-peroxide adduct to promote neurodegenerative diseases such as prion disease and amyotrophic lateral sclerosis through its oxidative protease activity.

VII-A-3 DNA Promotes the Activation of Oxygen Molecule by Binuclear Cobalt(II) Compounds

NISHIDA, Yuzo; NISHINO, Satoshi; GUO, Li Li; KUNITA, Mami; MATSUSHIMA, Hideaki; TOKII, Tadashi

[*Inorg. Chem. Commun.* **2**, 609 (1999)]

During the past decades there has been an explosion in the research effort directed towards the isolation and evaluation of naturally occurring DNA cleaving agents and towards the design and synthesis of model compounds that can specifically recognize and cut DNA. The potential scope of the utility of these compounds ranges from the creation of synthetic restriction enzymes for use of biologists to the development of chemotherapeutic agents that may be effective against a variety of neoplastic diseases. The bleomycins (BLM) are family of glycopeptide-derived antibiotics, discovered by Umezawa and co-workers, which have been used clinically against certain malignant lymphomas and squamous cell carcinomas. The therapeutic activity of BLM is generally believed to correlate with the ability of an “active-BLM,” which is derived from either Fe(II)-BLM/O_2 or Fe(III)-BLM/H_2O_2 system, to bind to and degrade DNA. This means that Fe-BLM is a dangerous species for the human beings, because it always contains an active oxygen species, although the active bleomycin is quickly bleached when this drug is activated outside of this target(DNA). The most desirable agent for clinical use, should be that the agent cleaves DNA oxidatively through production of an active oxygen species only when it reacts with DNA. In this report we have showed that some binuclear cobalt(II) compounds with H(HPTP)(see below) belong to this type of compounds.

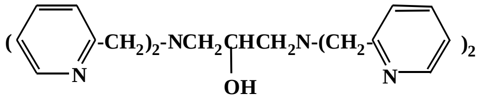

H(HPTP)

VII-A-4 Structure and Function of “Free Iron Ion” in Biological System and Their Model Compounds

NISHIDA, Yuzo

[*Recent Res. Dev. Pure Appl. Chem.* **3**, 103 (1999)]

Iron is as essential participant in many human metabolic processes, but recent studies on neurodegenerative diseases have revealed that free ion, *i.e.*, excess iron ion in the cell, is potentially dangerous, and abnormalities in rain iron metabolism have been described for several neurodegenerative diseases, including Alzheimer’s disease and Parkinson’s disease. In this study we have prepared several model compounds for the “free iron(II) ion” in the cell, and discussed origin of the free iron ion formation, and the mechanism of oxygen activation, the cell damage, and cancer process by the free iron ion in biology. We have pointed out that hydrogen peroxide and free iron(III) ion which is captured by a chelate containing peptide-group should be a serious origin for the iron ion toxicity in cells.

VII-A-5 New Insight into Oxidative DNA Cleavage Reaction Catalyzed by Metal Chelates

NISHIDA, Yuzo

[*Recent Res. Dev. Pure Appl. Chem.* **3**, 123 (1999)]

Mechanism of oxidative DNA cleavage reactions catalyzed by a metal compound was re-considered based on the new concept on the chemical reactivity of the metal-peroxide adduct. The fact that chemically inert Co(III)-bleomycin-OOH mediate DNA strand scission only when irradiated at 366 nm light, and the recent results on the steric interaction between the Co(III)-bleomycin-OOH and oligomer investigated by NMR technique has lead to the conclusion that photoirradiation at 366 nm on the Co(III)-bleomycin-OOH induces d-d transition (from t_{2g} orbital to d_{z^2}-orbital) and charge transfer transition (from the ligand orbital to d_{z^2}-orbital), leading to facile O-O heterolysis of the peroxide ion; after this terminal oxygen atom is transferred directly into C(4’-position)-H bond of the sugar moiety, to give the corresponding hydroxylated derivative, leading to strand scission. The results obtained from the model compounds including Fe(III) and Cu(II) all support the above conclusion, and new mechanism for DNA cleavage reaction, which excludes the possible formation of 4’-carbon radical as an intermediate, was proposed for DNA cleavage by the Fe(III)-bleomycin.

VII-A-6 Cleavage of C–N bond of Peptide Group by Copper(II)-peroxide Adduct with η^1-Coordination Mode

NISHINO, Satoshi; KUNITA, Mami; KANI, Yoshiyuki; OHBA, Shigeru; MATSUSHIMA, Hideaki; TOKII, Tadashi; NISHIDA, Yuzo

[*Inorg. Chem. Commun.* **3**, 145 (2000)]

The bioactivation of many peptide hormones and neuropeptides involves oxidative cleavage of carboxy-terminal glycine-extended precursors. The process is catalyzed by the enzyme peptidylglycine α-amidating monooxygenase (PAM), which comprises two subunits. One of these, requires copper ion, ascorbate and molecular oxygen, and facilitates α-hydroxylation of glycine residues. A range of chemical models of PAM has been developed, however the detailed reaction mechanism of cleavage of C-N bond is not clear at present.

Very recently we have reported that some copper(II) compounds exhibit high activity for degrading albumin in the presence of hydrogen peroxide, and postulated that a copper(II)-peroxide adduct may play an important role in the formation of PrP 27-30 and PrP^{Sc}, which are believed to be an abnormal disease-causing isoform of prion protein, and also in conformational change in mutated SOD enzyme observed for ALS patients. In this study we have obtained a clear evidence to support that a copper(II)-peroxide adduct with η^1-Coordination mode can cleave the C-N bond of peptide group and hydroxylate the alkyl group nearby; this may give a new idea to elucidate the reaction mechanism of PAM enzyme.

VII-A-7 Important role of Proton in Activation of Oxygen Molecule in Heme-Containing Oxygenases

NISHIDA, Yuzo

[*Inorg. Chem. Commun.* **3**, 310 (2000)]

Peroxoiron(III) complexes are increasingly being considered as potential intermediates in oxidation reactions catalyzed by both non-heme and heme-centers. In cytochrome P-450 and heme-oxygenase, a hydroperoxide adduct of Fe(III) with η^1-coordination mode has been considered to be an important intermediate but detailed electronic property and reactivity of the peroxide adduct are less known at present. In recent years, Density Functional Theory (DFT) has emerged as an accurate alternative first-principles approach to quantum mechanical molecular investigations. DFT currently accounts for approximately 90% of all quantum chemical calculations being performed, not only because of its proven chemical accuracy, but also of its relatively cheap computational expense. In this study we have investigated the electronic property of the peroxide adduct of the heme compounds in terms of DFT.

DFT (density-functional theory) calculations have revealed that the position of proton of a hydroperoxide adduct of Fe(III)-porphyrin compound influences greatly the electron density on the oxygen atoms of the peroxide ion, suggesting that the position of proton in the hydroperoxo-iron(III) compound plays an important role in controlling the electronic interaction between the hydroperoxide adduct and porphyrin system (OOH-π interaction). These are very useful to consider the reaction mechanism of the both cytochrome P450 and heme-oxygenase.

VII-B Electronic Structure and Reactivity of Metal Cluster Complexes

Dimetal complexes with metal-metal bond have been a subject of wide interest in these three decades. Meta-metal single- or mulltiple bonds show different reactivitties and properties from those in organic compounds. The reported dimetal complexes were mainly 4d metal complexes. Enhanced metal-metal and metal-ligand interactions are expected for 5d metal cluster compounds. However, rather fewer examples of 5d metal complexes, especially dimetal complexes of iridium(II), have been explored. We have been interested in development of chemistry of Ir_2^{4+} and Ir_2^{5+} complexes.

VII-B-1 A One-Step Synthesis of an Ir(II) Dinuclear Complex. Preparation, Structures and Properties of Bis(μ-acetato)dichlorodicarbonyldiiridium(II) Complexes

EBIHARA, Masahiro; KANEMATSU, Naohiro[1]; KAWAMURA, Takashi[1]
([1]Gifu Univ.)

[*J. Chem. Soc., Dalton Trans.* 4413 (1999)]

A bis(μ-acetato)dicarbonyldichlorodiiridium(II) complex, $[Ir_2(\mu\text{-}O_2CMe)_2Cl_2(CO)_2]$ **1**, was prepared by the one-step reaction of H_2IrCl_6 with $MeCO_2Li$ under O_2 in a mixture of acetic acid and acetic anhydride. Dissolution of **1** into various ligating solvents gave $[Ir_2(\mu\text{-}O_2CMe)_2Cl_2(CO)_2L_2]$ (L = MeCN: **2**, dmso: **3**, py: **4**, 4-isopropylpyridine: **5**). X-ray structure determinations of **2**, **3** and **4** gave the Ir–Ir distances of 2.569(1), 2.5980(5) and 2.5918(5) Å, respectively, which are in the range of the reported Ir(II)–Ir(II) single-bond distances. CV of **2**, **4** and **5** exhibited a one-electron quasi-reversible oxidation wave at $E_{1/2}$ of 1.30, 0.97 and 0.94 V vs Fc^+/Fc, respectively. Complex **3** gave no CV response in the potential window of dmso.

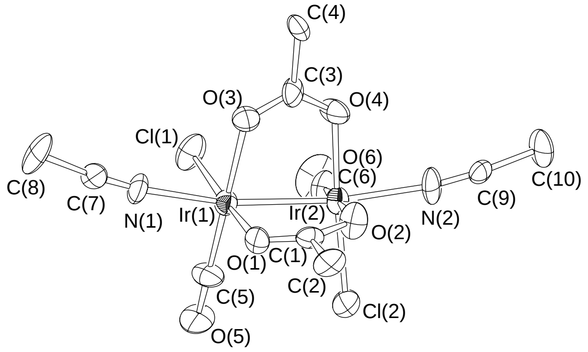

Figure 1. Structure of $[Ir_2(\mu\text{-}O_2CMe)_2Cl_2(CO)_2(CH_3CN)_2]$.

VII-B-2 Preparation and Structure of Bis(μ-acetato)dichlorodicarbonyldiiridium(II) Complexes with group 15 ligands, $[Ir_2(\mu\text{-}O_2CMe)_2Cl_2(CO)_2L_2]$ (L = PPh_3, PCy_3, $P(OPh)_3$, $AsPh_3$, $SbPh_3$), and ESR and DFT Studies of Electronic Structure of Their Cationic Radicals

EBIHARA, Masahiro; KANEMATSU, Naohiro[1]; KAWAMURA, Takashi[1]
([1]Gifu Univ.)

Bis(μ-acetato)dichlorodicarbonyldiiridium(II) complex with group 15 compounds as the axial ligands, $[Ir_2(\mu\text{-}O_2CMe)_2Cl_2(CO)_2L_2]$ (L = PPh_3 **6**, PCy_3 **7**, $P(OPh)_3$ **8**, $AsPh_3$ **9**, $SbPh_3$ **10**) were synthesized. The Ir–Ir distances (2.6936(7) Å of **7**, 2.6458(8) Å of **8**, 2.6207(9) Å of **9** and 2.6200(9) Å of **10**) were longer than those of the complexes with axial MeCN, py or dmso. The complexes had a chemically reversible one-electron oxidation wave of which $E_{1/2}$ (*vs.* Fc^+–Fc) values were between 0.22 of **7** and 0.75 V of **8** depending on their axial ligands. Electrolytic or radiolytic oxidation of **6, 7** and **9** gave their cationic radicals. The ESR spectra of **6**$^{+\bullet}$, **7**$^{+\bullet}$ and **9**$^{+\bullet}$ at 77 K were pseudo-axially symmetric with g tensors of $g_\perp$ = 2.15 and $g_{||}$ = 1.96, 2.18 and 1.95, and 2.20 and 1.96, respectively. Their hyperfine coupling splitting indicates that their odd electron is delocalized equivalently onto the two axial phosphorous or arsenic atoms. The odd electron densities were estimated form the hyperfine coupling tensors as $\rho \approx 0.1$ on the P atom of **6**$^{+\bullet}$ and **7**$^{+\bullet}$ and $\rho \approx 0.15$ on the As atom of **9**$^{+\bullet}$. These ESR results indicate that their SOMO is the σ_{IrIr} orbital with the $\sigma_{IrP}^*/\sigma_{IrAs}^*$ character. DFT calculations for the model complexes, $[Ir_2(\mu\text{-}O_2CH)_2Cl_2(CO)_2(PH_3)_2]^{+\bullet}$ and $[Ir_2(\mu\text{-}O_2CH)_2Cl_2(CO)_2(AsH_3)_2]^{+\bullet}$, gave an electronic structure consistent with the ESR results. A similar DFT calculation of $[Ir_2(\mu\text{-}O_2CH)_2Cl_2(CO)_2(py)_2]^{+\bullet}$ gave a result that its odd electron is accommodated in the orbital with σ_{IrIr}, σ^*_{IrN} and π_{IrCr}^* character. This calculated result, however, is not consistent with the previously reported results of the ESR study of $[Ir_2(\mu\text{-}O_2CMe)_2Cl_2(CO)_2(py)_2]^{+\bullet}$ showing that the odd electron occupies the δ_{IrIr}^* orbital.

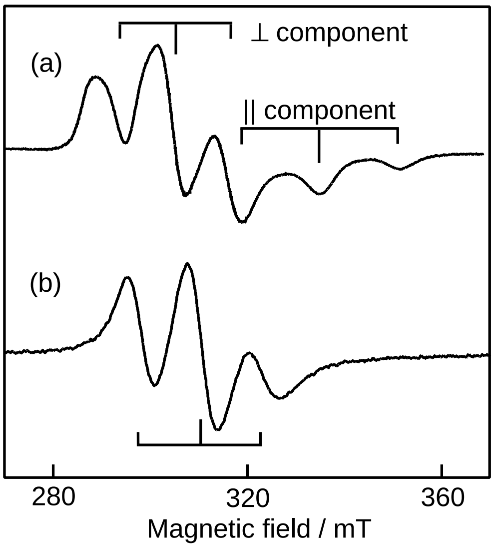

Figure 1. X-Band ESR spectrum of complex **6**$^{+\bullet}$ (a) in frozen solution at 77 K and (b) in fluid solution at 273 K.

VII-C Research on the Relationship between Structure of Vanadyl Complex and Insulin-Mimetic Activity

The number of people suffering from diabetes mellitus (DM), one of the life-style related disease, has risen to approximately 14 million, including the figure of potential patients in Japan. DM is classified mainly into two types; insulin-dependent DM (IDDM: type 1) is associated with absolute insulin deficiency and non-insulin dependent DM (NIDDM: type 2) is with relative insulin deficiency. Although NIDDM is treated with several types of synthetic medicines, IDDM is given daily insulin injections to normalize the high blood glucose levels. Vanadium ions and complexes have been found to be active to normalize the high blood glucose level in not only experimental animals but the patients with both type of DM. Then we have developed several types of vanadyl complexes in VO^{2+} state and evaluated their in vitro and in vivo insulinomimetic activities to know the relationship between structure of vanadyl complexes and their insulinomimetic activities.

VII-C-1 Stereospecific and Structure-Dependent Insulin-Mimetic Oxovanadium(IV) Complexes with N,N’-Ethylene-bis-amino Acids

KAWABE, Kenji[1]; TADOKORO, Makoto[1]; ICHIMURA, Akio[1]; KOJIMA, Yoshitane[1]; TAKINO, Toshikazu[2]; SAKURAI, Hiromu[3]
([1]Osaka City Univ.; [2]Kyoto Pharm. Univ.; [3]IMS and Kyoto Pharm. Univ.)

[*J. Am. Chem. Soc.* **121**, 7937 (1999)]

The structure-insulinomimetic activity relationship of the tetradentate oxovanadium(IV) complexes with N,N’-ethylene-bis-amino acid (XeX) was examined. The complexes $[VO(XeX)(H_2O)]$, where X = G (Gly), mG or Gm (N-methylglycine), L- and D-A (Ala), L- and D-V (Val), L- and D-M (Met), and L- and D-P (Pro), were prepared and structurally characterized by X-ray analysis and CD spectra. The insulin-mimetic activity of the complexes was evaluated in an *in vitro* system in terms of IC_{50} value due to FFA release from isolated rat adipocytes. The *in vitro* insulin-like activities of the complexes were found to depend on the absolute configuration of the complexes and the complexes which contain achiral amino acids or D-amino acids were found to have higher insulin-mimetic activities than the corresponding L-isomers. In addition, the insulin-like activities of the complexes were found to depend on the acid dissociation constants of the amino acids as the ligands, partition coefficients and redox potentials of them.

VII-C-2 A New Type of Orally Active Insulin-Mimetic Vanadyl Complex: Bis(1-oxy-2-pyridinethiolate)oxovanadium(IV) with VO-(S_2O_2) Coordination Mode

SAKURAI, Hiromu[1]; SANO, Hiromi[2]; TAKINO, Toshikazu[2]; YASUI, Hiroyuki[2]
([1]IMS and Kyoto Pharm. Univ.; [2]Kyoto Pharm. Univ.)

[*Chem. Lett.* 913 (1999)]

A new purple vanadyl complex, bis(1-oxy-2-pyridinethiolato)oxovanadium(IV), VO(OPT), with $VO(S_2O_2)$ coordination mode, was prepared by mixing 2-mercaptopyridine-N-oxide or 1-hydroxy-2-pyridinethione and $VOSO_4$, and characterized by UV, IR and EPR spectra, magnetic susceptibility and partition coefficient. Based on the higher *in vitro* insulin-mimetic activity of VO(OPT) (IC_{50} = 0.19 mM) than that of $VOSO_4$ (IC_{50} = 0.9 mM), the complex was found to be a potent agent for treating insulin-dependent diabetes mellitus in rats when given by daily intravenous injection or oral administration.

VII-C-3 Evidence for the Improvement of Noninsulin-Dependent Diabetes Mellitus in KKA^y Mice with Daily Oral Administration of Bis(6-methylpicolinato)oxovanadium(IV) Complex

FUJISAWA, Yae[1]; SAKURAI, Hiromu[2]
([1]Kyoto Pharm. Univ., [2]IMS and Kyoto Pharm. Univ.)

[*Chem. Pharm. Bull.* **47**, 1668 (1999)]

A vanadyl complex, bis(6-methylpicolinato)oxovanadium(IV), VO(6MPA), with $VO(N_2O_2)$ coordination mode, was found to exhibit a normoglycemic effect on KKA^y mice with hereditary noninsulin-dependent diabetes mellitus with daily oral administration.

VII-C-4 In vivo Coordination Structural Changes of a Potent Insulin-Mimetic Agent, Bis(picolinato)oxovanadium(IV), Studied by Electron Spin-Echo Envelope Modulation Spectroscopy

FUKUI, Koichi[1]; FUJISAWA, Yae[2]; OHYA-NISHIGUCHI, Hiroaki[1]; KAMADA, Hitoshi[1]; SAKURAI, Hiromu[3]
([1]Inst. Life Support Techn., Yamagata Technopolis Found.; [2]Kyoto Pharm. Univ.; [3]IMS and Kyoto Pharm. Univ.)

[*J. Inorg. Biochem.* **77**, 215 (1999)]

Bis(picolinato)oxovanadium(IV) $[VO(pic)_2]$ is one of the most potent insulin-mimetic vanadium complexes. To probe coordination structural changes of this complex in vivo and provide insights into the origin of its high potency, an electron spin-echo envelope modulation (ESEEM) study was performed on organs (kidney, liver and bone) of $VO(pic)_2$- and $VOSO_4$-treated rats. Kidney and liver samples from both types of rats exhibited a ^{14}N ESEEM signal that could be attributed to equatorially coordinating amine nitrogen.

The relative intensity of the amine signal was larger for the organs of the rat treated with the less potent $VOSO_4$, suggesting that this amine coordination inhibits the insulin-mimetic activity. The spectra of kidney and liver from the $VO(pic)_2$-treated rat contained a weak signal due to the picolinato imine nitrogen. This suggests that some picolinato species (including both the bis-picolinato and a partially decomposed monopicolinato species) still exist in the organs as a minor species, where the proportions of the picolinato species to the total amount of the EPR-detectable $V^{IV}O$ species are estimated as 8–16% in the kidney and 12–24% in the liver. The picolinato ligand presumably serves to prevent VO^{2+} from being converted into the inactive amine-coordinated species. Bone samples from both types of rats exhibited an ESEEM signal due to ^{31}P nuclei. The VO^{2+} in bone is therefore most likely incorporated into the hydroxyapatite $Ca_{10}(PO_4)_6(OH)$ matrix, which is consistent with the hypothesis that the bone-accumulated VO^{2+} is gradually released and transported to other organs as is Ca^{2+}. No ^{14}N signals were observed, even in the bone samples of the $VO(pic)_2$-treated rats, indicating that vanadium uptake by bone requieres complete decomposition of the complex.

VII-C-5 Role of Vanadium in Treating Diabetes

SAKURAI, Hiromu[1]; FUJISAWA, Yae[2]; FUJIMOTO, Seiki[2]; YASUI, Hiroyuki[2]; TAKINO, Toshikazu[2]
([1]IMS and Kyoto Pharm. Univ.; [2]Kyoto Pharm. Univ.)

[*J. Trace Elem. Exp. Med.* **12**, 393 (1999)]

Since insulin-dependent diabetes mellitus (IDDM), which causes many severe secondary complications, is characterized by hyperglyceria due to absolute deficiency of insulin, the diseases is controlled by daily injection of insulin. Therefore, the development of insulin replacements or mimetics upon oral administration is an important investigation. Recent studies indicate that vanadium, which is proposed to be one of essential trace elements in animals and humans, relates to both glucose and lipid metabolisms, and the metal in turn shows insulin-mimetic effect. Thus several types of vanadium complex have been proposed to be insulin mimetics. In 1990, we proposed first vanadyl-cysteinate complex, which normalized the blood glucose level of IDDM rats on oral administration. On the other hand, simple vanadium compounds such as vanadyl sulfate and sodium vanadate have been reported to be useful to treat human non-insulin-dependent diabetes mellitus (NIDDM). Based on the observations, we have developed several types of vanadyl complexes with different coordination modes such as $VO(O_4)$, $VO(N_4)$, $VO(S_4)$, $VO(O_2N_2)$, $VO(S_2N_2)$ and $VO(O_2S_2)$, and found that vanadyle-methylpicolinate complex with long acting character and low toxicity is the most effective to treat IDDM as well as NIDDM rats, when administered orally. The mechanism was also studied with respect to the pharmacokinetic analysis and vanadium distribution in animals.

VII-C-6 Ternary Complex Formation between VO(IV)-picolinic Acid or VO(IV)-6-Methylpicolinic Acid and Small Blood Serum Bioligands

KISS, Erzsébet[1]; GARRIBBA, Eugenio[2]; MICERA, Giovanni[2]; KISS, Tamás[3]; SAKURAI, Hiromu[4]
([1]Kossuth Univ.; [2]Univ. Sassari.; [3]Jozsef Attila Univ.; [4]IMS and Kyoto Pharm. Univ.)

[*J. Inorg. Chem.* **78**, 97 (2000)]

In order to assess the role of the low molecular mass bioligands of blood serum in vanadium binding, a study was made of the interactions of the complexes formed in the VO(IV)-picolinic acid and VO(IV)-6-methylpicolinic acid systems with various low molecular mass constituents of blood serum, such as oxalate, lactate, citrate and phosphate. The speciation of VO(IV) in these ternary systems and also in the binary VO(IV)-picolinic acid and VO(IV)-6-methylpicolinic acid systems was studied by pH-potentiometry at 25 °C and at an ionic strength $I = 0.2$ M (KCl). The binding modes of the complexes formed were determined by spectral (electronic absorption and EPR) methods. Picolinic acid and 6-methylpicokinic acid were found to form mono and bis complexes through the pyridine nitrogen and carboxylate oxygen, but the presence of the methyl group in 6-methylpicolinic acid surprisingly decreases the stability of its complexes significantly. The results obtained on the ternary systems reveal that mixed ligand complex formation is favoured in these systems, especially with citrate, and must therefore be taken into account in the speciation description of VO(IV) in blood serum.

VII-D-7 An Orally Active Antidiabetic Vanadyl Complex, Bis(1-oxy-2-pyridinethiolato)oxovanadium (IV), with $VO(S_2O_2)$ Coordination Mode; *In vitro* and *In vivo* Evaluation in Rats

SAKURAI, Hiromu[1]; SANO, Hiromi[2]; TAKINO, Toshikazu[2]; YASUI, Hiroyuki[2]
([1]IMS and Kyoto Pharm. Univ.; [2]Kyoto Pharm. Univ.)

[*J. Inorg. Biochem.* **80**, 99 (2000)]

According to Pearson’s HSAB (hard and soft acids and bases) rule, the vanadyl ion is classified as a hard acid. However, vanadyl-cysteine methyl ester and dithiocarbamate complexes with $VO(S_2O_2)$ and $VO(S_4)$ coordination modes, respectively, that contain bonds with a combination of hard acid (VO^{2+}) and soft base (sulfur) have been found to form stable complexes and exhibit insulin-mimetic activities in *in vitro* and *in vivo* evalutions. Based on such observations, a purple bis(1-oxy-2-pyridinethiolato)oxovanadium(IV) (VO(OPT)) complex with $VO(S_2O_2)$ coordination mode was prepared and found to have a strong insulin-mimetic activity in *in vitro* evalution, which followed *in vivo* effectiveness on intraperitoneal injection and oral administration. Then, we examined the real-time ESR analysis of vanadyl species in the blood of live rats given VO(OPT) by use of the blood circulation monitoring-ESR method. The clearance of vanadyl species from the blood in terms of half-life ($t_{i/2}$) was determined as 15 min in VO(OPT)-treated rats, while $t_{i/2}$ of $VOSO_4$-treated rats was 5 min, indicating the long-term acting character of VO(OPT). On the basis of the results, VO(OPT) with $VO(S_2O_2)$ coordination mode is proposed to be a potent orally active insulin-mimetic complex in treating insulin-dependent diabetes mellitus in experimental animals.

VII-C-8 Interaction of Vanadyl Complexes with Biological Systems: Structure-Insulinomimetic Activity Relationship of Vanadyl-Picolinate Complexes

SAKURAI, Hiromu[1]; TAMURA, Asuka[2]; TAKINO, Toshikazu[2]; OZUTSUMI, Kazuhiko[3]; KAWABE, Kenji[4]; KOJIMA, Yoshitane[4]
([1]IMS and Kyoto Pharm. Univ.; [2]Kyoto Pharm. Univ.; [3]Ritsumeikan Univ.; [4]Osaka City Univ.)

[*Inorg. React. Mechan.* **2**, 69 (2000)]

Since bis(picolinato)oxovanadium(IV), ($VO(PA)_2$), complex was found in 1995 to have good insulino-mimetic activities, the structure-activity relationship was examined to develop more active complexes. By introducing an electron-donating group such as methyl group into the picolinate ligand, bis(3- and 6-methylpicolinate)oxovanadium(IV) ($VO(3MPA)_2$ and $VO(6MPA)_2$) were prepared. By introducing an electron-withdrawing group such as a halogen atom into the ligand, bis(5-iodo- and 4-choloro-picolinato)oxovanadium(IV) ($VO(5IPA)_2$ and $VO(4ClPA)_2$) were prepared. The structure of the complexes was characterized by EXAFS, ESR, IR and absorption spectra.

In vitro insulionmimetic activity of the complexes were in the order of $VO(5IPA)_2 > VO(6MPA)_2 > VO(PA)_2 > VO(3MPA)_2 > VO(4ClPA)_2$. Among four best complexes, both $VO(5IPA)_2$ and $VO(3MPA)_2$ were found to be potent agents to treat the hyperglycemia of streptozotocin (STZ)-induced diabetic rats. On the basis of the results, introduction of halogen atom or methyl group into the picolinate ligand was indicated to be a useful method to design more active insulinomimetic complexes.

VII-C-9 Synthesis of New Vanadyl Complexes of Hydroxyazine-Type Heterocycles and Their Insulin-Mimetic Activities

KATOH, Akira[1]; TAGUCHI, Kazutoshi[1]; OKADA, Hiroko[1]; HARATA, Manabu[1]; FUJISAWA, Yae[2]; TAKINO, Toshikazu[2]; SAKURAI, Hiromu[3]
([1]Seikei Univ.; [2]Kyoto Pharm Univ.; [3]IMS and Kyoto Pharm. Univ.)

[*Chem. Lett.* 866 (2000)]

Four kinds of vanadyl complexes of hydroxyazine-type heterocycles were synthesized. Bis(1,2-dihydro-4,6-dimethyl-2-oxo-1-pyrimidinolato)-and bis(1,2-dihydro-2-oxo-3,5,6-trimethyl-1-pyrimidinolato)-oxovanadium(IV) complexes showed higher insulin-mimetic activity than vanadyl sulfate as a positive control.

VII-C-10 Speciation of Insulin-Mimetic VO(IV)-Containing Drugs in Blood Serum

KISS, Tamás[1]; KISS, Erzsébet[2]; GARRIBBA, Eugenio[3]; SAKURAI, Hiromu[4]
([1]Jozsef Attila Univ.; [2]Kossuth Univ.; [3]Univ. Sassari.; [4]IMS and Kyoto Pharm. Univ.)

[*J. Inorg. Biochem.* **80**, 65 (2000)]

The biospeciations of three potential insulin-mimetic VO(IV) compounds, $VO(maltolate)_2$, $VO(picolinate)_2$ and $VO(6\text{-}Me\text{-}picolinate)_2$, in blood serum were assessed via modelling calculations, using the stability constants reported in the literature for the binary insulin-mimetic complexes and their ternary complexes formed with the most important low molecular mass binders in the serum: oxalic acid, citric acid and phosphate. The binding capabilities of two high molecular mass serum proteins, albumin and transferrin, were also taken into account.

VII-D Syntheses of Transition Metal-Sulfur Clusters and Development of Their Catalysis

This project focuses on the development of the new, relilable synthetic pathways affording the transition metal-sulfur clusters with the tailored core structures in high yield, and also on the determination of the detailed structures of the novel clusters prepared in this study by the X-ray crystallography. Activation of the small molecules will be attempted by the use of polynuclear homo- or hetero-metallic site in these clusters to exploit the new catalytic reactions that are inaccessible by the mononuclear complex catalyst.

VII-D-1 Syntheses of a Dinuclear Ir Complex Containing Bridging Tetraselenide Ligands $[(C_5Me_5)Ir(\mu\text{–}Se_4)_2Ir(C_5Me_5)]$ and its Conversion into $Ir_2Pd_2Se_3$ and $Ir_2Pd_3Se_5$ Clusters

NAGAO, Shoken[1]; SEINO, Hidetake[1]; MIZOBE, Yasushi[2]; HIDAI, Masanobu[1]
([1]Univ. Tokyo; [2]Univ. Tokyo and IMS)

[*Chem. Commun.* 207 (2000)]

Treatment of $[Cp^*IrCl(\mu\text{–}Cl)_2IrCp^*Cl]$ ($Cp^* = \eta^5\text{–}C_5Me_5$) with Li_2Se_4 gave a tetraselenide-bridged diiridium complex $[Cp^*Ir(\mu\text{–}Se_4)_2IrCp^*]$, which reacted further with two equivalents of $[Pd(PPh_3)_4]$ to afford a mixture of bimetallic tetra- and penta-nuclear selenido clusters $[(Cp^*Ir)_2\{Pd(PPh_3)\}_2(\mu_3\text{–}Se)_2(\mu_2\text{–}Se)]$ and $[(Cp^*Ir)_2\{Pd(PPh_3)\}_3(\mu_3\text{–}Se)_3(\mu_3\text{–}Se_2)]$.

VII-D-2 Preparation of Sulfido-Bridged Di- or Trinuclear Pyrrolylimido and Diazoalkane Complexes Derived from a Tungsten Dinitrogen Complex

SEINO, Hidetake[1]; MIZOBE, Yasushi[2]; HIDAI, Masanobu[1]
([1]Univ. Tokyo; [2]Univ. Tokyo and IMS)

[*Bull. Chem. Soc. Jpn.* **s**, 631 (2000)]

Tungsten pyrrolylimido and diazoalkane complexes, *cis*,*mer*-$[WCl_2(NNC_4H_4)(PMe_2Ph)_3]$ and *cis*,*mer*-$[WCl_2(NN{=}CRR')(PMe_2Ph)_3]$, which are readily derived from the dinitrogen complex *cis*-$[W(N_2)_2(PMe_2Ph)_4]$, reacted with $[PPh_4][WS_4]$ to give the sulfide-bridged di- or trinuclear pyrrolylimido and diazoalkane complexes, $[PPh_4][WCl(NNC_4H_4)(PMe_2Ph)_2(\mu\text{–}S)_2WS_2]$ (**1**) and $[PPh_4][WCl(NN{=}CRR')(PMe_2Ph)_2(\mu\text{–}S)_2WS_2]$ (**2**; R = R' = Me (**2a**); R = Me, R' = Ph), or $[\{WCl(NNC_4H_4)(PMe_2Ph)_2(\mu\text{–}S)_2\}_2W]$ (**3**) and $[\{WCl(NN{=}CMePh)(PMe_2Ph)_2(\mu\text{–}S)_2\}_2W]$. Treatment of **1** or **2a** with tetraalkylthiuram disulfide resulted in the formation of sulfide-dithiocarbamate complexes: $[W(NNC_4H_4)(PMe_2Ph)(S_2CNR_2)(\mu\text{–}S)_2WS(S_2CNR_2)]$ (R = Et, Pr) and $[W(NN{=}CMe_2)(PMe_2Ph)(S_2CNEt_2)(\mu\text{–}S)_2WS(S_2CNEt_2)]$. On the other hand, replacement of two PMe_2Ph ligands in **1** and **2** by $Ph_2PCH_2CH_2PPh_2$ (dppe) afforded $[PPh_4][WCl(NNC_4H_4)(dppe)(\mu\text{–}S)_2WS_2]$ and $[PPh_4][WCl(NN{=}CRR')(dppe)(\mu\text{–}S)_2WS_2]$ (R = R' = Me; R = Me, R' = Ph (**3**)), where **3** has been shown to react further with $[RhCl(cod)]_2$ (cod = 1,5-cyclooctadiene) to give a bimetallic trinuclear complex $[WCl(NN{=}CMePh)(dppe)(\mu\text{–}S)_2W(\mu\text{–}S)_2Rh(cod)]$.

VII-E Reductive Activation of Carbon Monoxide derived from Carbon Dioxide and Oxidative Activation of Hydroxy- and Oxo-Groups Derived from Water

An electrophilic attack of CO_2 to coordinatively unsaturated low valent metal complexes affords M-η^1-CO_2 complexes, which are easily converted to M-CO ones in both protic and aprotic media. Accordingly, organic synthesis through M-CO complexes derived from CO_2 is highly desired from the development of a new C1 resources. A major problem of the reduction of CO_2 using homogeneous catalysis is reductive cleavages of M-CO bonds under reductive conditions. Because of accumulation of too many electrons in the central metals. Ligand localized redox reactions rather than metal centered ones as electron sources would avoid unfavorable CO evolution in the reduction of CO_2. A flexible ligand which has an ability to change the bonding modes among monodentate, bidentate and bridging form to connect metals and carbonyl carbon of M-CO bonds would meet the requirements of smooth M-η^1-CO_2 formation and depression of reductive cleavage of M-CO bond under reduictive conditions.

Acids or bases generated in industrial process are not utilized as resources and just wasted after neutralization. Proton gradient (Δp) between inside and outside of a cell is depicted as the sum of electric activity ($\Delta\psi$) and chemical activity (ΔpH) components. $\Delta p = \Delta\psi - Z\Delta pH$ ($Z = 2.303RT/F$) Proton gradient is equivalent to the neutralization energy because the neutralization reaction takes place to form water if the separating membrane is removed. Thus, neutralization energy results from the formation of water. Biological system effectively creates and consumes neutralization energy in various reactions. Acids and bases, therefore, have potential energy sources, which are provided by chemical bondings (chemical energy). Along this line, we tried to convert the neutral energy to electronic energy by using ruthenium-aqua complexes.

VII-E-1 Oxidation of Hydrocarbon by Mono- and Dinuclear Ruthenium Quinone Complexes via Hydrogen Atom Abstraction

WADA, Tohru; TSUGE, Kiyoshi; TANAKA, Koji

[*Chem. Lett.* 910 (2000)]

Deprotonation and two-electron oxidation of dinuclear $[Ru^{II}_2(OH)_2(3,6\text{-}Bu^t_2Q)_2(btpyan)]^{2+}$ (Bu^t_2Q = 3,6-di(*tert*-butyl)-1,2-quinone, btpyan = 1,8-bis-(2,2':6',2''-terpyridyl)anthracene, $[\mathbf{1}]^{2+}$) was converted to bis(ruthenium-oxo) complex $[Ru^{II}_2(O)_2(3,6\text{-}Bu^t_2Q)_2(btpyan)]^{2+}$, which oxidized 1,3-cychrohexadiene, 1,2-dihydronaphtalene to corresponding aromatics in higher yields (90%, 94%) in the presence of $AgClO_4$ and Bu^tOK. An analogous mononuclear $[Ru^{II}(OH_2)(3,6\text{-}Bu^t_2Q)(Ph\text{-}terpy)]^{2+}$ (Ph-terpy = 4'-phenyl-2,2':6',2''-terpyridine, $[\mathbf{2}]^{2+}$) was converted to the ruthenium-hydroxo complex $[Ru^{II}(OH)(3,6\text{-}Bu^t_2Q)(Ph\text{-}terpy)]^{2+}$ under similar condoitions, but displayed the low activity for the oxidation compared with the dinuclear complex $[\mathbf{1}]^{2+}$. On the other hand, 9,10-dihydroanthracene was converted to anthracene by $[\mathbf{2}]^{2+}$ in 42% yield, while it was not oxidized by $[\mathbf{1}]^2$ due to the steric hindrance.

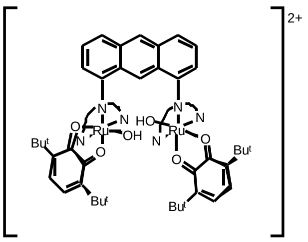

$[\mathbf{1}]^{2+}$

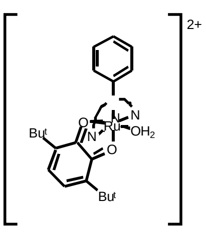

$[\mathbf{2}]^{2+}$

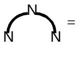

= 2,2':6',2''-terpyridine

VII-E-2 Electrochemical Water-Oxidation to Dioxygen Catalyzed by Oxidized Form of Bis(ruthenium-hydroxo) Complex in H_2O

WADA, Tohru; TSUGE, Kiyoshi; TANAKA, Koji

[*Angew. Chem., Int. Ed. Engl.* **39**, 1479 (2000)]

Much attention has been paid to oxidation of water to dioxygen by homogeneous catalysts. Of particular interest are di- and tetranuclear complex derived from transition metals, since extended X-ray absorption fine structure studies indicated that the O_2-evolving center (OEC) in Photosystem II is composed of a tetranuclear Mn cluster with di-μ-oxo dimeric Mn units. The cyclic voltammetry of $[Ru(OH)(Q)Ru(OH)(Q)]^{2+}$ showed two redox couples at $E_{1/2}$ = 0.43 V and 0.35 V in MeOH. After $[Ru(OH)(Q)Ru(OH)(Q)]^{2+}$ was converted to $[Ru(O)(SQ)Ru(O)(SQ)]^0$ by an addition of 2.0 equiv of *t*BuOK to the MeOH solution, the redox process of the resultant oxo complex displayed also two nearly reversible redox couples at $E_{1/2}$ = 0.40 V and 0.30 V (eq. 1).

$$
\begin{aligned}
&[Ru(Q)(O)Ru(Q)(O)]^{2+}\\
&\quad \underset{0.40\ V}{\overset{e^-}{\rightleftharpoons}} [Ru(Q)(O)Ru(SQ)(O)]^{+}\\
&\quad \underset{0.30\ V}{\overset{e^-}{\rightleftharpoons}} [Ru(SQ)(O)Ru(SQ)(O)]^{0} \qquad (1)
\end{aligned}
$$

The complex on ITO electrode exhibited a broad redox couple centered at +0.40 V (*vs.* Ag/AgCl), and an irreversible anodic wave at +1.20 V, which is associated with two-electron oxidations of $[Ru(OH)(Q)Ru(OH)(Q)]^{2+}$ and $[Ru(O)(Q)Ru(O)(Q)]^{2+}$ affording $[Ru(OH)(Q)Ru(OH)(Q)]^{4+}$ and $[Ru(O)(Q)Ru(O)(Q)]^{4+}$, respectively. A strong anodic current at potential more positive than +1.5 V is apparently caused by the oxidation of water to dioxygen. Indeed, when controlled-potential electrolysis of the bis(ruthenium-hydroxo) complex modified on ITO electrode at 1.70 V (*vs.* Ag/AgCl) in water (pH 4.0), 1.1 ml of O_2 was evolved after 20.2 C passed in the electrolysis. The current efficiency for O_2 evolution was 95% and the turnover number was 500 based on the complex. The current density of the electrode was 0.12 mA/cm^2 in the initial stage. The current gradually decreased with decrement of pH in the aqueous phase and almost stopped at pH 1.2. The current density of the electrode for the oxidation of water recovered, when the pH of water was readjusted to 4.0 by an addition of aqueous KOH to the aqueous phase. The oxidation of water by the bis(ruthenium-hydroxo) complex modified ITO finally evolved 15.0 ml of O_2 (turnover 6730), before the evolution completely stopped in 40 h.

VII-E-3 Selective Production of Acetone in Electrochemical Reduction of CO₂ Catalyzed by Ru-naphthyridine Complex

MIZUKAWA, Tetsunori; TSUGE, Kiyoshi; NAKAJIMA, Hiroshi; TANAKA, Koji

[*Angew. Chem., Int. Ed. Engl.* **111**, 373 (1999)]

Carbon dioxide is smoothly converted to CO on metals by oxide transfer from M–CO_2 to CO_2, while reductive cleavage of the resultant metal–CO bond (eq. 1) is the major problem in utilization of CO_2 as a C1 resource. Acylation of the metal–CO complexes

$$[\mathrm{M{-}\eta^1{-}CO_2}]^0 \xrightarrow[-\mathrm{CO_3^{2-}}]{\mathrm{CO_2}} [\mathrm{M{-}CO}]^{2+} \xrightarrow{2e^-} [\mathrm{M}]^0 + \mathrm{CO} \qquad (1)$$

derived from CO_2 under reductive conditions, therefore, would provide new methodologies for utilization of CO_2 as a staring material in organic synthesis. One and two-electron reductions of $[\mathrm{Ru(bpy)_2(napy)(CO)}](\mathrm{PF_6})_2$ (napy = 1,8-naphthyridine-κ*N*) take place in napy localized orbitals, which induce nucleophilic attack of the free nitrogen of κ^1-napy to the carbonyl carbon (eq. 2). Electron transfer from the reduced form of napy to the CO group in the metallacycle enables reductive activation of the CO group without the metal–CO bond cleavage and gives rise to electrophilic attack of $(CH_3)_4N^+$ to the carbonyl carbon. As a result, $CH_3C(O)CH_3$ and CO_3^{2-} were catalytically produced in the electrochemical reduction of $[\mathrm{Ru(bpy)(napy{-}\kappa}N)_2\mathrm{(CO)_2}](\mathrm{PF_6})_2$ in the presence of in CO_2-saturated DMSO when $(CH_3)_4NBF_4$ was used as an electrolyte (eq. 3).

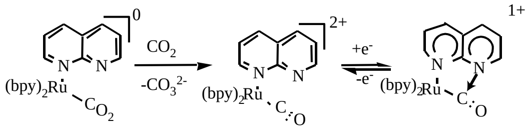

(2)

$$2\mathrm{CO_2} + 4e^- + 2(\mathrm{CH_3})_4\mathrm{N}^+ \rightarrow \mathrm{CH_3C(O)CH_3} + \mathrm{CO_3^{2-}} + 2(\mathrm{CH_3})_3\mathrm{N} \qquad (3)$$

VII-E-4 Energy Conversion from Proton Gradient to Electricity Based on Characteristic Redox Behavior of an Aqua Ruthenium Complex

TSUGE, Kiyoshi; KURIHARA, M.; TANAKA, Koji

[*Bull. Chem. Soc. Jpn.* **73**, 607 (2000)]

A ruthenium aqua complex with a quinone ligand $[\mathrm{Ru(trpy)(dbq)(H_2O)}]^{2+}$ (trpy = 2,2’:6,2”-terpyridine, dbq = 3,5-di-*t*-butyl-1,2-benzoquinone) $[\mathrm{Ru(q)(H_2O)}]^{2+}$) was prepared. Its electrochemical properties and electronic absorption spectra were measured in the presence of a base in acetone. The detailed analysis of those measurements revealed that the addition of base caused not only the deprotonation but also the reduction of $[\mathrm{Ru(q)(H_2O)}]^{2+}$. The redox reactions coupled with acid-base reactions were demonstrated from the large difference in redox properties of aqua and hydroxo complexes. Taking advantage of unique redox reactions induced by the acid-base equilibrium between aqua and hydroxo complexes, we have succeeded in construction of the first energy transducer which converts the proton gradient to electricity. A similar ruthenium aqua complex with a bipyridine ligand, $[\mathrm{Ru(trpy)(bpy)(H_2O)}]^{2+}$, also reversibly dissociates a proton of the aqua ligand. However, it has no ability to convert the proton gradient to electricity due to the lack of a suitable molecular orbital, which can accommodate electrons on the electron-rich hydroxo ligand.

$$[\mathrm{M(Q)(H_2O)}]^{2+} + \mathrm{OH^-} \rightleftharpoons [\mathrm{M(S)(OH)}]^+ + \mathrm{H_2O} \quad (1)$$

VII-E-5 Double Addition of CO₂ and CH₃OH to Ruthenium Carbonyl Complex with Novel Mono-dentate Dithiolene

SUGIMOTO, Hideki; TSUGE, Kiyoshi; TANAKA, Koji

[*Chem. Lett.* 1007 (1999)]

The reaction of $[\mathrm{Ru(CO)_2Cl(terpy)}]\mathrm{PF_6}$ and Na_2mnt in CH_3OH gave a yellow complex (**1a**) with mono-dentate mnt [Ru(CO)$_2$(terpy-κ^3*N*,*N*’,*N*”)(mnt-κ*S*)] and with bidentate mnt [Ru(CO)$_2$(terpy-κ^2*N*,*N*’)(mnt-κ^2*S*,*S*’)]. On the other hand, the reaction between $[\mathrm{Ru(CO)_2Cl(terpy)}]^+$ and $Cs_2S_2C_2Ph_2$ in CH_3OH under aerobic conditions gave a complex (**2**) with thio-carboxylic acid and methoxy carbonyl groups rather than the expected [Ru(CO)$_2$(SSC$_2$Ph$_2$-κ^1*S*)(terpy-κ^3*N*,*N*’,*N*”)] (**1**). The most characteristic feature of **2** is that the carbonyl and the uncoordinate thiolate of **1** are changed to methoxy carbonyl and thio-carboxylato units, respectively. Although it is not clear that the carboxylato moiety of **2** exists as protonated or deprotonated form by X-ray analysis, the former is deduced from the elemental analysis and the charge balance of **2**. Unprecedented double addition of CO_2 and methanol to thiolate and carbonyl ligands located far from each other is apparently caused by the long-range π–π interaction between basic $Ph_2C_2SS^{2-}$ and acidic carbonyl units through d-orbitals of the ruthenium atom.

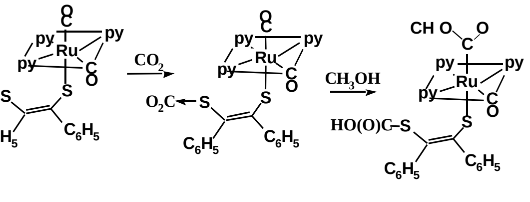

VII-E-6 Structural and Spectroscopic Characterization of Ruthenium(II) Complexes with Methyl, Formyl and Acetyl Groups as Model Species in Multi-Step CO_2 Reduction

OOYAMA, Dai; TOMON, Takashi; TSUGE, Kiyoshi; TANAKA, Koji

The molecular structures of Ru(II) complexes with methyl, formyl and acetyl groups $[Ru(bpy)_2(CO)L]^+$ (L = CH_3, C(O)H and $C(O)CH_3$) were examined from the view point of active species in multi-step reduction of CO_2 on Ru. The methyl complex was prepared by the reaction of $[Ru(bpy)_2(OH_2)_2]^{2+}$ with trimethylsilyl acetylene and fully characterized by infrared, Raman, ^{13}C NMR and single-crystal X-ray crystallography. Disorder of the Ru–CO and Ru–C(O)H bonds in the crystal structure of the formyl complex made it difficult to determine the bond parameters of the two groups accurately, but the molecular structure of the analogous acetyl complex, which was obtained by the reaction of $[Ru(bpy)_2(CO_3)]$ with propiolic acid, was determined by X-ray analysis. The ruthenium-carbonyl (Ru–C–O) bond angles of the methyl and acetyl complex with 174(1) and 175.5(5)°, respectively, are in the ranges of those of previously characterized $[Ru(bpy)_2(CO)L]^{n+}$ (L = CO_2, C(O)OH, CO and CH_2OH). On the other hand, the Ru–CH_3 and Ru–$C(O)CH_3$ bond distances showed unusual relationship against the stretching frequency in the raman spectra.

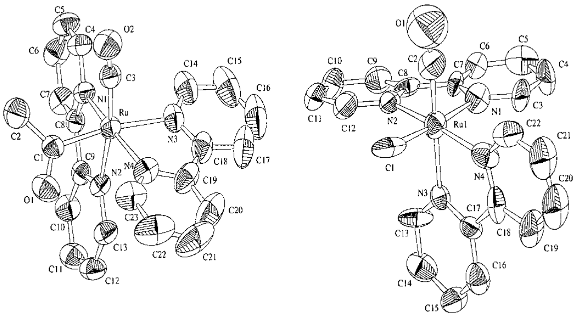

Figure 1. Molecular Structures of $[Ru(bpy)_2(CO)(C(O)CH_3)]^+$ and $[Ru(bpy)_2(CO)(CH_3)]^+$.

VII-F Synthesis of Transition-Metal Chalcogenido Complexes and Their Cluster-Forming Reactions

Transition-metal chalcogenido aggregates are of well-documented importance in biological systems and industrial processes such as hydrodesulfurization. A wide variety of metal chalcogenido clusters have been synthesized, in which the tetrathiometalato anions have been widely used as a building block. In this project, we are focusing on preparation of chalcogenido/chalcogenolato complexes as a precursor for cluster syntheses and their cluster-forming reactions.

VII-F-1 Synthesis of Bis{(2-dimthylphenylphosphino)ethane-1-thiolato}bis(tert-butylthiolato)molybdenum(IV) and Its Cluster-Forming Reactions with $FeCl_2$ and CuBr

ARIKAWA, Yasuhiro[1]; KAWAGUCHI, Hiroyuki; KASHIWABARA, Kazuo[1]; TATSUMI, Kazuyuki[1]
([1]Nagoya Univ.)

[*Inorg. Chem.* **38**, 4549 (1999)]

The Mo(IV) complex $Mo(dmsp)(S^tBu)_2$ (**1**) was readily prepared by the reaction of $Mo(S^tBu)_4$ with 2 equiv of $HSCH_2CH_2PMe_2$ (Hdmsp). The X-ray analysis of **1** reveals a distorted octahedral geometry with a *cis*-disposition of two ^{t}BuS ligands. Treatment of **1** with $FeCl_2$ and CuBr led to the formation of heterometallic clusters, $[Mo(O)(dmsp)_2]_2FeCl_2$ (**2**) and $[MoBr(dmsp)_2(\mu_3\text{-}S)Cu_2]_2(\mu_2\text{-}S^tBu)_2$ (**3**), respectively. The oxo ligand in **2** is most probably derived from adventitious H_2O contained in hygroscopic $FeCl_2$. In the structure of **2**, an $FeCl_2$ unit bridges two square-pyramidal $Mo(O)(dmsp)_2$ fragments through interactions between iron and sulfur atoms of dmsp. The formation of **3** involves C–S bond cleavage of one ^{t}BuS ligand of **1** and rearrangement of ligands between the Mo and Cu sites, resulting in the structure consisting of two $MoCu_2BrS(dmsp)_2$ units and two ^{t}BuS bridges.

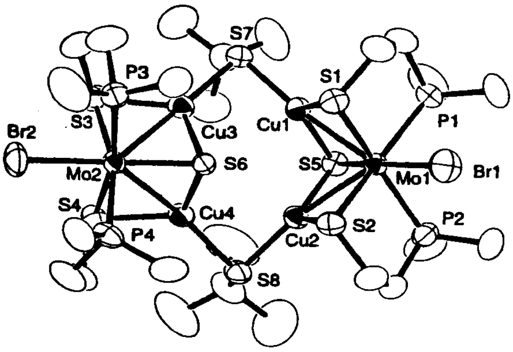

Figure 1. Structure of **3**.

VII-F-2 Synthesis and Structure of a Triply-Fused Incomplete-Cubane Cluster $[\{(\eta^5\text{-}C_5Me_5)WS_3\}_3Cu_7(MeCN)_9](PF_6)_4$ and a 2D Polymer $[(\eta^5\text{-}C_5Me_5)WS_3Cu_3(MeCN)(pz)]PF_6$ (pz = pyrazine)

LANG, Jian-Ping[1]; KAWAGUCHI, Hiroyuki; TATSUMI, Kazuyuki[1]
([1]Nagoya Univ.)

[*Chem. Commun.* 2315 (1999)]

The reaction of $(PPh_4)[Cp^*W(S)_3]$ with 3 equiv of $[Cu(MeCN)_4](PF_6)$ in MeCN yielded a triply-fused incomplete-cubane cluster $[\{(\eta^5\text{-}C_5Me_5)WS_3\}_3Cu_7(MeCN)_9](PF_6)_4$ (**1**). Furthermore, we constructed a 2D polymeric structure $[(\eta^5\text{-}C_5Me_5)WS_3Cu_3(MeCN)(pz)]PF_6$ (**2**) by treating **1** with pyrazine in the presence of LiCl. The $W_3S_9Cu_7$ framework of **1** is broken during the reaction with LiCl and pyrazine, providing a WS_3Cu_3 incomplete-cubane cluster as a building block of the stacked sheet structure of **2**.

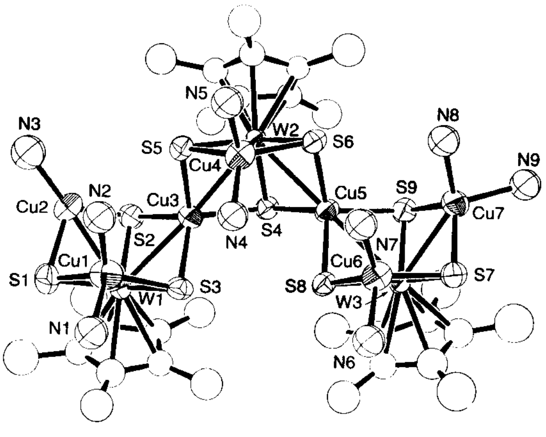

Figure 1. Structure of **1**.

VII-F-3 Synthesis and Structures of the Halfsandwich W(VI) Triselenido and W(II) Selenolato Complexes

KAWAGUCHI, Hiroyuki; TATSUMI, Kazuyuki[1]
([1]Nagoya Univ.)

[*Chem. Commun.* 1299 (2000)]

The reaction of Cp^*WCl_4 with $LiSe^tBu$ at room temperature gave rise to a mixture of *syn*- and *anti*-$Cp^*_2W_2(\mu\text{-}Se)_2(Se)_2$ (**1**), in which C–Se bond cleavage took place. When the similar reaction was carried out in the presence of ^{t}BuNC, the W(II) selenolato complex $Cp^*W(Se^tBu)(CN^tBu)_3$ (**2**) was formed. The structure of **2** was confirmed by X-ray analysis. While two of the isocyanides are nearly linear [C–N–C = 175.8(8)°, 164.3(7)°], the other contains essentially an sp^2-type nitrogen atom [N–C–N, 128.7(6)°] amongst the smallest of the known bent isocyanides (122–156°). In another experiment, a freshly prepared $Cp^*WCl_4/LiSe^tBu$ mixture was quickly transferred into Li_2Se_2 in THF. Cation exchange with PPh_4Br in CH_3CN provided $(PPh_4)[Cp^*W(Se)_3]$ (**3**) concomitant with a mixture of *syn*- and *anti*-**1**. The anion part of **3** has a three-legged piano-stool structure. The average W–Se distance

(2.322 Å) of **3** is similar to that of $(PPh_4)_2[WSe_4]$.

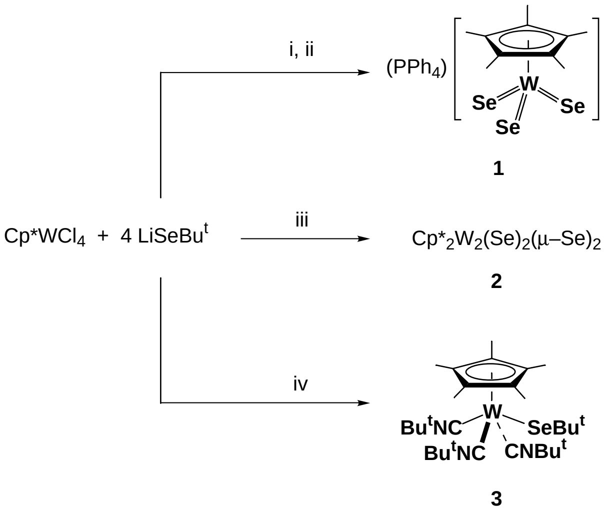

Scheme 1. *Reagents and condititons*: i, Li_2Se_2, THF; ii, PPh_4Br, CH_3CN; iii, 30 min, –78 °C, THF; iv, Bu^tNC, THF.

VII-G Artificial Photoreaction systems on a Protein Surface

New methodologies are developed which one can construct an artificial photoreaction systems on a protein matrix. Using the protein-based photosystems, we aim to investigate characteristics for electron transfer phenomena in a protein matrix. Furthermore, based on these results, we would like to design and semisynthesize an efficient photoreaction system such as an artificial photoreaction center.

VII-G-1 Direct Observation of the Ferric-Porphyrin Cation Radical as an Intermediate in the Photo-Triggered Oxidation of Ferric- to Ferryl-Heme Tethered to Ru(bpy)$_3$ in Reconstituted Myoglobin

HAMACHI, Itaru[1,2]; TSUKIJI, Shinya[1]; SHINKAI, Seiji[1]; OISHI, Shigero[3]
([1]Kyushu Univ.; [2]IMS; [3]Kitasato Univ.)

[*J. Am. Chem. Soc.* **121**, 5500 (1999)]

Using semisynthetic myoglobins (Ru(bpy)$_3$–Mbs) with covalently-appended Ru(bpy)$_3$ (bpy = 2,2’-bipyridine), an oxidized-Mb is photo-produced through intramolecular electron abstraction reaction as a key step. UV-visible spectra, electron paramagnetic resonance measurements and reactivity tests identify the photo-oxidized Mb as a ferryl-species (*i.e.* Fe^{4+}–heme). By circular dichroism (CD) spectroscopy, high performance liquid chromatography (HPLC) and SDS polyacrylamide gel electrophoresis (SDS-PAGE), the photo-oxidation proceeds without the damage of the protein structure. Significantly, we report the first direct observation of ferryl-Mb photogeneration via the intermediate porphyrin cation radical. As a consequence of this observation and proposed mechanism, the rate constants for each step can be clearly determined. The photo-excited Ru^{2+}(bpy)$_3$ is oxidatively quenched by [Co(NH$_3$)$_5$Cl]$^{2+}$, a sacrificial acceptor, to produce Ru^{3+}(bpy)$_3$ which then proceeds to abstract an electron from the porphyrin ring with a first order rate constant of 7.1×10^5 s^{-1}, in the first step. The electron transfer is followed by iron(III) oxidation by the porphyrin radical with concurrent deprotonation (a first order rate constant of 4.0×10^4 s^{-1} at pH 7.5, and 2.0×10^5 s^{-1} at pH 9.0) in the second step. Consistent with this mechanism, it is demonstrated that the rate of the fast step of the porphyrin radical generation is independent of pH, whereas the slower step of ferryl-heme formation is dependent on pH. Simulation of the detailed pH dependence of the kinetics clearly shows that the deprotonation-protonation equilibrium of the protein matrix can control the ferryl-heme generation in a heme pocket of Mb.

VII-G-2 Construction of Artificial Photosynthetic Reaction Centers on a Protein Surface: Vectorial, Multistep, and Proton-Coupled Electron Transfer for Long-Lived Charge Separation

HU, Yi-Zhen[1]; TSUKIJI, Shinya[1]; SHINKAI, Seiji[1]; OISHI, Shigero[3]; HAMACHI, Itaru[1,2]
([1]Kyushu Univ.; [2]IMS; [3]Kitasato Univ.)

[*J. Am. Chem. Soc.* **122**, 241 (2000)]

Artificial photosynthetic reaction centers have been constructed on a protein surface by cofactor reconstitution, which mimic the function of photosynthetic organisms to convert light energy to chemical potential in the form of long-lived charge-separated states. They feature a ruthenium tris(2,2’-bipyridine) moiety as the sensitizer, which is mechanically linked (*i.e.* in catenane-type) with a cyclobis(paraquat-*p*-phenylene) unit (BXV^{4+}, acceptor) and covalently linked with a protoheme or Zn-protoporphyrin (donor) located in the myoglobin pocket. Reconstitution of apo-myoglobin (Mb) with **1** and **2** affords the two Mb-based artificial triads, Mb-(Fe^{III}OH$_2$)–Ru^{2+}–BXV^{4+} and Mb(Zn)–Ru^{2+}–BXV^{4+}. Laser flash photolysis of the Ru(bpy)$_3$ moiety of Mb(Fe^{III}OH$_2$)–Ru^{2+}–BXV^{4+} in an aqueous solution yields an initial charge-separated state, Mb(Fe^{III}-OH$_2$)–Ru^{3+}–BXV$^{3+\bullet}$, via noncovalent electron transfer, followed by dark electron transfer to generate an intermediate consisting of porphyrin cation radical, Mb-(Fe$^{III\bullet}$(OH$_2$)–Ru^{2+}–BXV$^{3+\bullet}$. Mb(Fe$^{III\bullet}$(OH$_2$)–Ru^{2+}–BXV$^{3+\bullet}$ thus generated is subsequently converted, via a proton-coupled process and with a quantum yield of 0.005, into the final charge-separated state, Mb(Fe^{IV}=O)–Ru^{2+}–BXV$^{3+\bullet}$, which bears an energy more than 1 eV above the ground state and a lifetime (τ > 2 ms) comparable to that of natural photosynthetic reaction center. By analogy with a related system reported previously, it was considered that back ET from BXV$^{3+\bullet}$ to Mb(Fe^{IV}=O) might be coupled to the protonation of Mb(Fe^{IV}=O) and governed by the slow interconversion between the metal-oxo form and the proton-activated species, rendering the CS state Mb(Fe^{IV}=O)–Ru^{2+}–BXV$^{3+\bullet}$ specially long-lived. Control experiments clearly demonstrated that partial incorporation of the triads into the protein matrix plays a crucial role in regulating the electron transfer pathway and stabilizing the charge separation state.

VII-G-3 Direct Comparison of Electron Transfer Properties of Two Distinct Semisynthetic Triads with Non-Protein Based Triad: Unambiguous Experimental Evidences on Protein Matrix Effects

HU, Yi-Zhen[1]; TAKASHIMA, Hiroshi[1]; TSUKIJI, Shinya[1]; SHINKAI, Seiji[1]; NAGAMUNE, Teruyuki[3]; OISHI, Shigero[4]; HAMACHI, Itaru[1,2]
([1]Kyushu Univ.; [2]IMS; [3]Univ. Tokyo; [4]Kitasato Univ.)

[*Chem. Eur. J.* **6**, 1907(2000)]

In order to understand the roles of protein matrix in electron transfer (ET) within biological systems, a heme-based donor (Zn-heme: ZnPP)-sensitizer (Ru^{2+}(bpy)$_3$)-acceptor (cyclic viologen: BXV^{4+}) triad **1** was used as a probe molecule. Two semisynthetic systems, Cyt-b_{562}(**1**) and Mb(**1**), in which the triad is incorporated into cytochrome b_{562} (Cyt-b_{562}) or into myoglobin (Mb), were constructed by cofactor reconstitution. These two semisynthetic proteins were compared with the triad itself (*i.e.* without protein matrix) using absorption spectroscopy, steady state emission and excitation studies, laser flash photolysis experiments, and molecular modelling. Photoexcitation of the ZnPP moiety of Cyt-b_{562}(**1**) or Mb(**1**) leads to a direct ET from the triplet state of ZnPP state (^{3}ZnPP) to BXV^{4+} to generate a final charge separated (CS) state, Cyt-b_{562}(Zn^+)–Ru^{2+}–$BXV^{3+\bullet}$ or Mb(Zn^+)–Ru^{2+}–$BXV^{3+\bullet}$. On the other hand, direct ET from the excited ZnPP moiety to the BXV^{4+} moiety is also involved in **1** in the absence of the protein matrix, but the excited state of ZnPP involved is not ^{3}ZnPP, but the singlet excited state (^{1}ZnPP) in this pathway. When the $Ru^{2+}(bpy)_3$ moiety of Cyt-b_{562}(**1**) or Mb(**1**) is excited, a stepwise ET relay occurs with the ion-pair, Cyt-b_{562}(Zn)–Ru^{3+}–$BXV^{3+\bullet}$ or Mb(Zn)–Ru^{3+}–$BXV^{3+\bullet}$, as an intermediate, leading to the same final CS state as that generated in the direct ET pathway. The lifetimes of the corresponding final CS states were determined to be 300 ns for **1** in the absence of the protein matrix, 600–900 ns for Cyt-b_{562}(**1**) and 1.1–18 μs for Mb(**1**), the values of which are greatly affected by the protein matrix. Molecular modeling study of the three systems consistently explained the differences of their photophysical behavior.

VII-G-4 Cyclodextrin-Appended Myoglobin as a Tool for Construction of a Donor-Sensitizer-Acceptor Triad on a Protein Surface

HAMACHI, Itaru[1,2]; TAKASHIMA, Hiroshi[1]; HU, Yi-Zhen[1]; OISHI, Shigero[3]; SHINKAI, Seiji[1]
([1]Kyushu Univ.; [2]IMS; [3]Kitasato Univ.)

[*Chem. Commun.* 1127 (2000)]

A protein-based and noncovalently-linked donor-sensitizer-acceptor triad has been prepared by self-assembly via mechanical linkage and hydrophobic interaction, and its photoinduced electron transfer properties has been studied. Cyclodextrin(CD)-appended hemes are successfully reconstituted with apo-myoglobin to yield CD-appended myoglobins. Upon addition of viologen-connected ruthenium tris(bipyridine) bearing adamantane unit, a donor-sensitizer-acceptor triad is formed on a protein surface, which shows a stepwise, vectrial electron transfer reaction by visible light irradiation. Clearly, this is a novel type of supramolecular photoreaction system.

RESEARCH ACTIVITIES VIII
Laser Research Center for Molecular Science

VIII-A Developments and Researches of New Laser Materials

Although development of lasers is remarkable, there are no lasers which lase in ultraviolet and far infrared regions. However, it is expected that these kinds of lasers break out a great revolution in not only the molecular science but also in the industrial world.

In this project we research characters of new materials for ultraviolet and far infrared lasers, and develop new lasers by using these laser materials.

VIII-A-1 Intense THz Radiation from Femtosecond Laser Pulses Irradiated InAs in a Strong Magnetic Field

OHTAKE, Hideyuki; ONO, Shingo[1]; KAWAHATA, Eiji; LIU, Zhenlin; SARUKURA, Nobuhiko
([1]Sci. Univ. Tokyo)

Since the first observation of THz radiation from InAs surface irradiated with femtosecond laser pulses, considerable effort have been made to design an intense THz-radiation source and to understand the mechanism for generating THz radiation. However, the problem has not been solved. In this paper, we have investigated the intense THz radiation from InAs by applying a strong magnetic field up to 5 T. We compared several different geometries. Besides quadratic magnetic field dependence, we found saturation of the THz-radiation intensity around 3 T. Furthermore, the intensity decreased dramatically above 3 T. It represented that the most suitable magnetic field was 3 T to design an intense THz-radiation source. We also took spectra by a Polarizing Michelson interferometer. The spectral shapes for the different magnetic field directions were significantly different. The center frequency of these spectra shifted to lower frequency with increasing magnetic field. Through these experiments, we found the best configuration and the most suitable magnetic field to obtain an intense THz radiation for various applications such as imaging, sensing, and spectroscopy. This configuration dependence of the spectral shape and the center frequency is attributed to be the initial carrier acceleration processes modulated by a strong magnetic field.

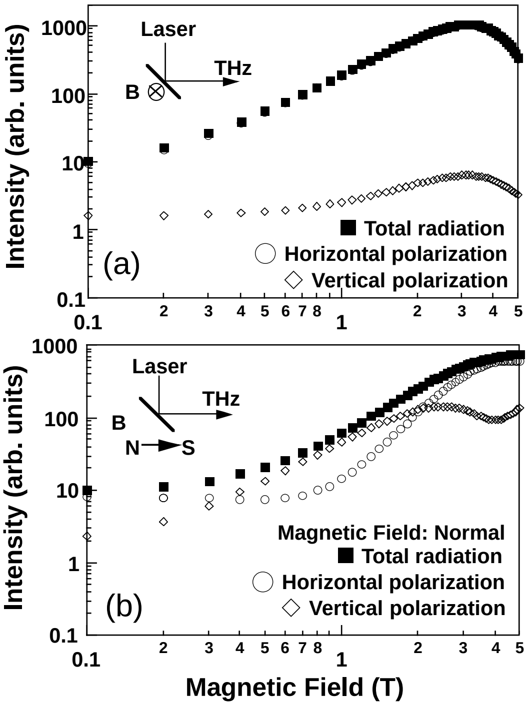

Figure 1. Magnetic field dependence of THz-radiation intensity. Inset indicates the experimental geometry. Closed squares, open circle and diamonds show total radiation, horizontal and vertical polarization, respectively. (a) The saturation of THz radiation intensity is clearly observed. (b) The saturation is not observed.

VIII-A-2 High-Repetition-Rate, High-Average-Power Mode-Locked Ti:Sapphire Laser with an Intracavity cw-Amplification Scheme

LIU, Zhenlin; ONO, Shingo[1]; KOZEKI, Toshimasa; OHTAKE, Hideyuki; SARUKURA, Nobuhiko
([1]Sci. Univ. Tokyo)

We have demonstrated a high-average-power, mode-locked Ti:sapphire laser with an intracavity cw-amplification scheme. The laser generated 150-fs pulses with 3.4-W average power at a repetition rate of 79 MHz. This simple amplification scheme can be applied for the power scaling of other lasers.

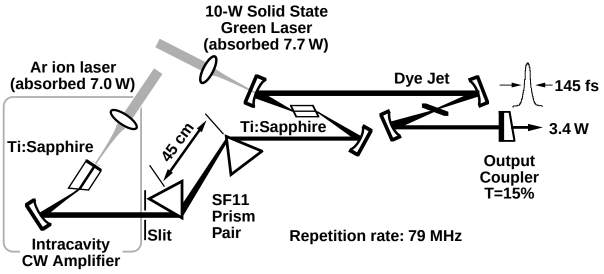

Figure 1. Configuration of high-repetition-rate high-average-power (3.4 W) femtosecond Ti:sapphire laser with an intracavity cw amplifier. The half-cut Brewster Ti:sapphire crystal composed the intracavity cw amplifier.

VIII-A-3 Compact THz-radiation Source Consisting of a Bulk Semiconductor, a Mode-Locked Fiber Laser, and a 2-T Permanent Magnet

ONO, Shingo[1]; TSUKAMOTO, Takeyo[1]; KAWAHATA, Eiji; LIU, Zhenlin; OHTAKE, Hideyuki; SARUKURA, Nobuhiko; NISHIZAWA, Seizi[2]; NAKANISHI, Akio[3]; YOSHIDA, Makoto[4]
([1]Sci. Univ. Tokyo; [2]JASCO Corporation; [3]Sumitomo Special Metals co., Ltd; [4]IMRA AMERICA, INC. JLO)

Various THz-radiation sources have been intensively studied including photo conductive switches irradiated with ultrashort optical pulses. An intense, compact, and simple light source is required for applications in sensing or imaging. We have demonstrated the strong enhancement of THz-radiation power with a magnetic field by using an InAs semiconductor. In this paper, we report on a compact THz-radiation source consisting of a fiber femtosecond laser and a newly designed 2-T permanent magnet shown in Figure 1. A mode-locked frequency doubled Er-doped fiber laser delivered 170-fsec pulses at 780 nm with a 48.5-MHz repetition rate (IMRA model FA7850/10SA) with 30-mW average power and 4.1-kW peak power. The mode-locked fiber laser is a completely turn-key system. It is much smaller than a mode-locked Ti:sapphire laser that requires daily alignment. The used semiconductor sample was undoped bulk InAs with a (100) surface. The 2-T permanent magnet unit consisted of 8 Nd-Fe-B magnet pieces. The remanence magnetic field of the Nd-Fe-B material itself was 1.3 T (NEOMAX-44H). Owing to the new magnetic circuit design, the magnetic field in the center exceeded the remanence magnetic field of the material. The permanent magnet only weighs about 5 kg. The 2-T permanent magnet unit is smaller and much lighter than an electromagnet. At present the average power is estimated to sub-micro watt level. The spectra of the THz radiation were obtained by a Polarizing Michelson interferometer. Many water vapor absorption lines were clearly observed. Therefore, the THz-radiation source is already usable for spectroscopy. Such a simple and compact source will open up new application for THz-radiation.

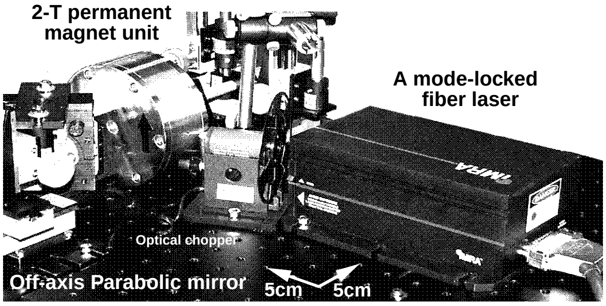

Figure 1. Photograph of a compact THz-radiation source with a bulk semiconductor, a fiber femtosecond laser, and a 2-T permanent magnet. Including the laser, the size is less than 40 × 30 × 15 cm.

VIII-A-4 Spectrum Control of THz Radiation from InAs in a Magnetic Field by Duration and Frequency Chirp of the Excitation Pulses

SUZUKI, Yuji; ONO, Shingo[1]; LIU, Zhenlin; OHTAKE, Hideyuki; SARUKURA, Nobuhiko
([1]Sci. Univ. Tokyo)

The THz-radiation spectrum from InAs in a magnetic field irradiated with femtosecond pulses can be controlled by varying the excitation pulse width and chirp direction of the excitation pulse. A longer excitation pulse width produces lower frequency THz radiation. Also, positively chirped pulse excitation will generate higher power and higher frequency THz radiation, due to the corruption of the impulse response of the semiconductor in the longer pulse width region. The spectral shape of the radiation strongly depends on the chirp direction. This unexpected difference with the same excitation peak power and the same pulse duration with different chirp direction is rather surprising. This difference of THz-radiation for the chirping of the excitation pulses might be attributed to the difference of the photo-carrier relaxation process in the conduction band with oppositely chirped-pulse excitation.

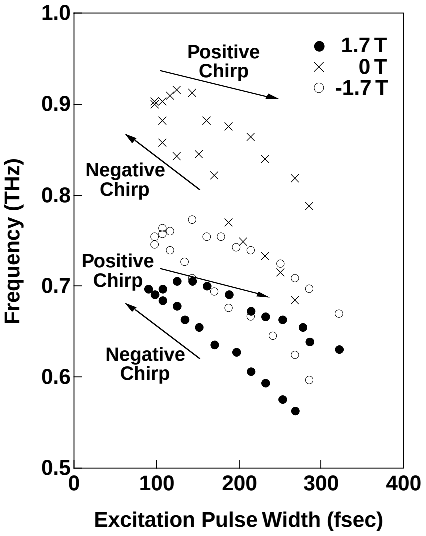

Figure 1. Center frequency spectrum dependence of THz radiation with different excitation chirp, pulse duration and magnetic field. Close circle, open circle and cross show 1.7 T, –1.7 T and 0 T, respectively.

VIII-A-5 LiCAF Crystal as a New Vacuum Ultraviolet Optical Material with Transmission Down to 112 nm

KOZEKI, Toshimasa; SAKAI, Masahiro; LIU, Zhenlin; OHTAKE, Hideyuki; SARUKURA, Nobuhiko; SEGAWA, Yusaburo[1]; OBA, Tomoru[2]; SHIMAMURA, Kiyoshi[3]; BALDOCHI, Sonia L.[3]; NAKANO, Kenji[3]; MUJILATU, Na[3]; FUKUDA, Tsuguo[3]
([1]RIKEN; [2]Optron Inc.; [3]Tohoku Univ.)

$LiCaAlF_6$ (LiCAF) was found to be an ideal optical material for the vacuum ultraviolet region due to its superior transmission characteristic of down to 112 nm, its non hydroscopic nature, and its better mechanical properties compared with LiF.

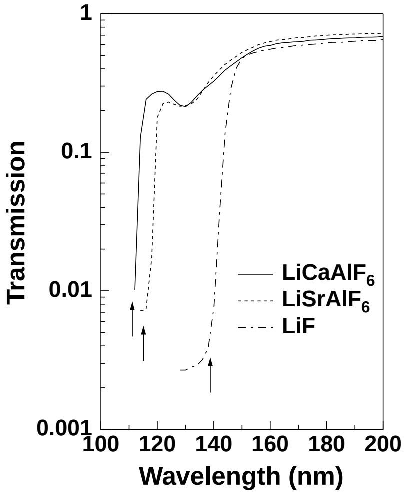

Figure 1. Transmission characteristics of LiCAF, LiSAF, LiF.

VIII-A-6 High Average Power Mode Locked Ti:Sapphire Laser with Intracavity Continuous-Wave Amplifier and Strained Saturable Bragg Reflector

LIU, Tze-An; HUANG, Kai-Fung; PAN, Ci-Ling; LIU, Zhenlin; OHTAKE, Hideyuki; SARUKURA, Nobuhiko

We demonstrate a new scheme for the generation of high average power femtosecond pulses by incorporating an intracavity amplifier and a strained saturable Bragg reflector with low saturation fluence for self-starting mode locking. When the Ti:sapphire oscillator and intracavity amplifier are pumped at 10 W and 15 W, respectively, the average output power is as high as 1.62 W. The pulse duration is about 145 fs, and the peak power reaches 160 kW at a 68 MHz repetition rate. The pulse-formation time of 400 µs is sufficiently short to sustain stable mode locking.

VIII-A-7 THz Radiation from Intracavity Saturable Bragg Reflector in Magnetic Field with Self-Started Mode-Locking by Strained Saturable Bragg Reflector

LIU, Tze-An; HUANG, Kai-Fung; PAN, Ci-Ling; LIU, Zhenlin; ONO, Shingo; OHTAKE, Hideyuki; SARUKURA, Nobuhiko

We demonstrate a new configuration for intracavity generation of THz radiation. A magnetic-field-biased saturable Bragg reflector (SBR) located inside the femtosecond laser cavity is the emitter, while a strained saturable Bragg reflector (SSBR) achieves self-started mode-locking without focusing. The calibrated power of the emitted THz radiation is estimated to be approximately 45 nW with a peak frequency at 0.72 THz and width of approximately 0.7 THz under a 0.88 T magnetic field. The quadratic dependence of THz-radiation power by the SBR on the magnetic field is also observed for the first time.

VIII-A-8 High-Gain, Reflection-Double Pass, Ti:Sapphire Continuous-Wave Amplifier Delivering 5.77 W Average Power, 82 MHz Repetition Rate, Femtosecond Pulses

LIU, Zhenlin; MURAKAMI, Hidetoshi; KOZEKI, Toshimasa; OHTAKE, Hideyuki; SARUKURA, Nobuhiko

A confocal, reflection-double-pass, Ti:sapphire continuous-wave ~cw! amplifier with a small signal gain of 4.2 has been invented. Femtosecond pulses with an 82 MHz repetition rate from a mode-locked Ti:sapphire laser are amplified to 5.77 W average power with a slightly saturated gain of 3.7 through an amplifier pumped by three cw green lasers, and the extraction efficiency reaches 10.6%.

VIII-B Development and Research of Advanced Tunable Solid State Lasers

Diode-pumped solid-state lasers can provide excellent spatial mode quality and narrow linewidths. The high spectral power brightness of these lasers has allowed high efficiency frequency extension by nonlinear frequency conversion. Moreover, the availability of new and improved nonlinear optical crystals makes these techniques more practical. Additionally, quasi phase matching (QPM) is a new technique instead of conventional birefringent phase matching for compensating phase velocity dispersion in frequency conversion. These kinds of advanced tunable solid-state light sources, so to speak “Chroma Chip Lasers,” will assist the research of molecular science.

In this projects we are developing Chroma Chip Lasers based on diode-pumped-microchip-solid-sate lasers and advanced nonlinear frequency conversion technique.

VIII-B-1 Performance of Widely Tunable Yb:YAG Microchip Lasers

SAIKAWA, Jiro; KURIMURA, Sunao; PAVEL, Nicolaie; SHOJI, Ichiro; TAIRA, Takunori

[*OSA TOPS on ASSL 2000* **34**, 106 (2000)]

The properties of the trivalent ytterbium ion doped YAG, such as a smaller quantum defect, longer upper state lifetime, simple energy structure (no excited state absorption) and so on, would promise to achieve a high power and high stability laser operation in microchip configurations. In addition, the wide emission bandwidth of the material around 1 µm allows tunable and/or mode-locked operation. In this work, we have developed a tunable intracavity frequency-doubled Yb:YAG microchip laser that outputs a maximum green power of 520mW with single frequency around the Ar^{3+} laser wavelength of 515 nm by using a 400-µm thick Yb:YAG. By using LBO crystal a wide tuning range from 515.3 to 537.7 nm ($\Delta\lambda$ = 22.4 nm, $\Delta\nu$ = 24.4 THz) was obtained (Figure 1). Then, we applied this tunable green laser to a wavelength-multiplexing holographic memory. We recorded 3 discrete images at 3 different wavelengths in the same position of a 600 ppm Fe-doped $LiNbO_3$ crystal and each image was reconstructed at each wavelength. The laser was proven to have a narrow linewidth and a wide tunability, in order to satisfy wavelength-multiplexing in the holographic storage system as shown in Figure 2. Next, in order to evaluate the potential of Yb:YAG tunability, the wide-bandwidth reflectivity dielectric mirror was deposited directly onto the Yb:YAG microchip. The output coupling mirror had a radius of curvature of 30 mm, and the cavity length was 25 mm. Experimental result of the tunability of the Yb:YAG microchip laser for different output couplers. With a reflectivity of 99.9% around 1010~1100 nm, the widest tunability of 84.5 nm, from 1024.1 to 1108.6 nm was obtained. The output beam was coupled as partially reflected beam at the birefringent filter. The oscillation range that extends beyond the Yb:YAG gain bandwidth, 9.5 nm, was realized since it has a simple energy- level manifolds. If it possible to keep wide band ($\Delta\nu$ ~ 22.4 THz) laser oscillation under mode-locking operation, transform-limited pulsewidth of approximately 50 fs should be feasible. The tuning bandwidth increased by using the high-reflectivity output coupler and peak wavelength shifted to longer wavelength. The shorter band-edge was limited by increase of reabsorption loss in the Yb:YAG, and longer band-edge by coating bandwidth in our experiment. The bandwidth of 22.4 THz indicates the potential of mode-locked operation of the Yb:YAG laser.

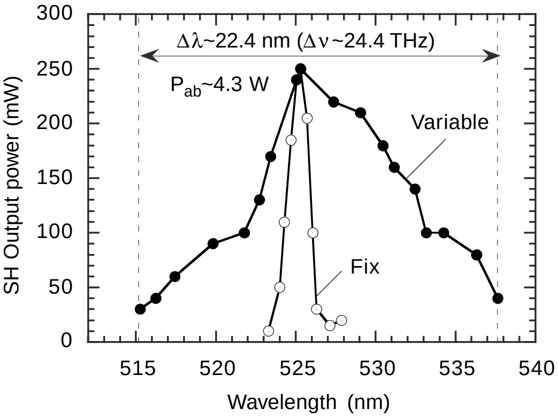

Figure 1. Tuning curve of the intracavity frequency-doubled Yb:YAG microchip laser.

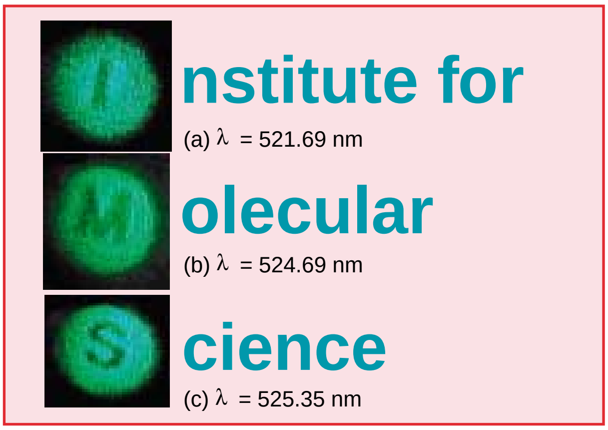

Figure 2. Reconstructed images from wavelength-multiplexed holograms by the tunable intracavity frequency-doubled Yb:YAG laser.

VIII-B-2 High Average Power Diode-Pumped Composite Nd:YAG Laser with Cr^{4+}:YAG Saturable Absorber for Passive Q-Switching

PAVEL, Nicolaie; KURIMURA, Sunao; SHOJI, Ichiro; SAIKAWA, Jiro; TAIRA, Takunori

[*CLEO/Europe* CWB 0006 (2000)]

Passive Q-switching technique is attractive for scientific and industrial applications that do not require accurate repetition rates. This technique can significantly simplify the operation, improve the efficiency, the reliability and the compactness, and reduce the laser costs. In a composite rod both the peak temperature rise and the thermal stress induced by optical pumping are reduced compared to a nonbonded crystal. In this work we show that these improvements, which reduce the thermal lensing effect, made a composite medium a good solution for improving output performances of high average power passively Q-switched lasers.

In experiments we used a composite Nd:YAG rod fabricated by diffusion bonding of a Nd:YAG (5-mm length, 1.1-at.% Nd doping) to an undoped YAG piece (1-mm length). The medium was end-pumped by a 1.55-mm diameter, 0.11-NA OPC fiber-bundles diode. With a plane-plane resonator of 80-mm length and an output mirror of 95% reflectivity at 1064nm, this configuration delivers a cw maximum output power of 7.7 W with an optical efficiency of 36.9%. The slope efficiency is 39.4%, and the laser beam M^2 factor varies among 1.1 and 2.3 on the pump power range. With a Nd:YAG medium (10-mm length, 1.3-at.% Nd doping), the maximum cw power was 8.2-W at 21.8-W absorbed power, the slope efficiency was 41.6%, and the laser beam M^2 factor varies between 1.2 and 3.3 on the pump power range. Cr^{4+}:YAG crystals with varying low-signal transmission T_0 have been used, as well as resonators of various length and output couplings. As an example, Figure 1 shows the average output power for the composite medium and Cr:YAG absorbers of T_0 = 89%, 85%, and 80%. A plane-plane resonator of 80-mm length with an R = 90% output coupler was considered. A maximum average power of 4.21-W in a laser beam of M^2 = 1.3 resulted for the Cr:YAG absorber of T_0 = 89%. The laser generated pulses of 48-ns duration at 24-kHz (~3.65 kW peak power). With the Nd:YAG medium a maximum average power of 3.9-W in a beam of M^2 = 1.9 resulted. When the resonator length was of 40-mm and a Cr:YAG crystal of T_0 = 80% was used, the composite Nd:YAG laser outputs a maximum average power of 2.6-W in a beam of M^2 = 1.45. The pulse width was 17.5-ns, the pulse energy is 0.285-mJ, and the peak power is 16.3-kW. Using the Nd:YAG medium, the maximum average power and beam M^2 factor decreases to 1.8-W and 1.9, respectively. Shorter resonators in spite of reducing the average output power will increases the Q-switched pulse peak power. This way a simple and compact-pumping source for parametric conversion into mid-IR region could be obtained.

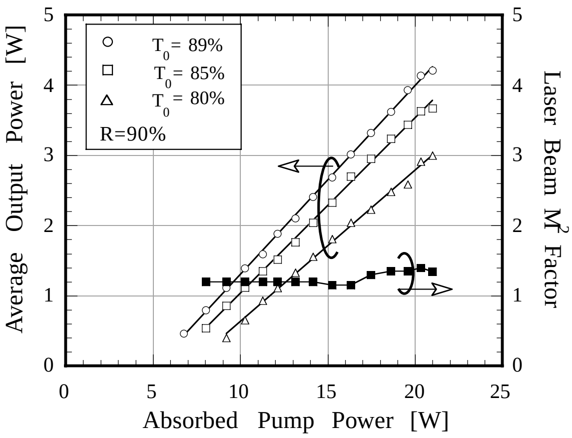

Figure 1. Average output power and beam M^2 factor as a function of absorbed pump power for the composite Nd:YAG, Cr:YAG absorbers.

VIII-B-3 Optical Properties and Laser Characteristics of Highly Nd^{3+}-Doped $Y_3Al_5O_{12}$ Ceramics

SHOJI, Ichiro; KURIMURA, Sunao; SATO, Yoichi; TAIRA, Takunori; IKESUE, Akio[1]; YOSHIDA, Kunio[2]
([1]JFCC; [2]Osaka Inst. Tech.)

[*Appl. Phys. Lett.* **77**, 939 (2000)]

Diode-pumped microchip solid-state lasers have such advantages as compactness, high efficiency, high power, and low numbers of longitudinal and transverse modes. A wide variety of materials have been investigated to develop more efficient and higher power microchip lasers. Although $Nd:YVO_4$ is a suitable material for highly efficient microchip laser owing to its large absorption cross section, high power operation is difficult because its thermo-mechanical properties are poor. On the other hand, while Nd:YAG has good thermal properties, highly efficient microchip laser has never been reported since high doping (> 1 at. %) of neodymium into the YAG crystal is impossible, limiting pump absorption. Recently developed transparent Nd:YAG ceramics are attractive materials because high doping of neodymium is possible without degrading the thermal conductivity. In this work we report measurements of the absorption spectra and the fluorescence lifetime of ceramic Nd:YAG in order to show that it is a promising material as a highly efficient and high power microchip laser. Moreover, we characterized its laser performance. Figure 1 shows the absorption spectra of 2.2 and 4.8 at. % Nd:YAG ceramics and 1.1 at. % single crystal. The 4.8 at. % Nd:YAG ceramic has an absorption coefficient (30.4 cm^{-1}) as large as that of $Nd:YVO_4$.

The input-output power characteristics of 2.4 and 4.8 at. % ceramics and a 0.9 at. % single crystal with microchip structures (the thickness of laser medium < 1mm) are shown in Figure 2. For the 4.8 at. % ceramic, 2.3 times higher output was achieved than that for the single crystal, which indicates the advantage of Nd:YAG ceramics as highly efficient miniature or microchip lasers. We estimated the round-trip cavity losses by obtaining the slope efficiencies with different output-couplers. From this, we found that the loss of the 2.4 at. % ceramic is as low as that of the single crystal. It is concluded that highly Nd^{3+}-doped YAG ceramics are promising as a highly efficient, high-power microchip laser material.

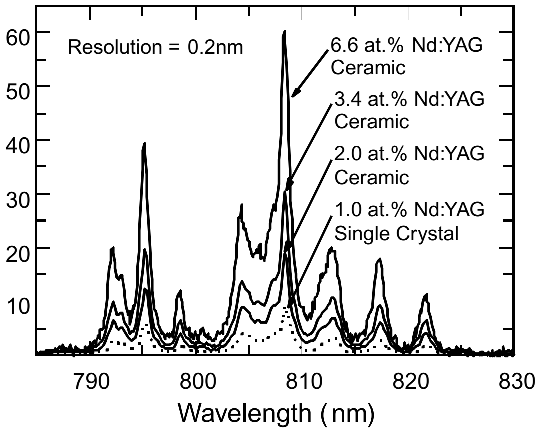

Figure 1. Absorption spectra of Nd:YAG ceramics (solid curves) and Nd:YAG single crystal (dashed curve).

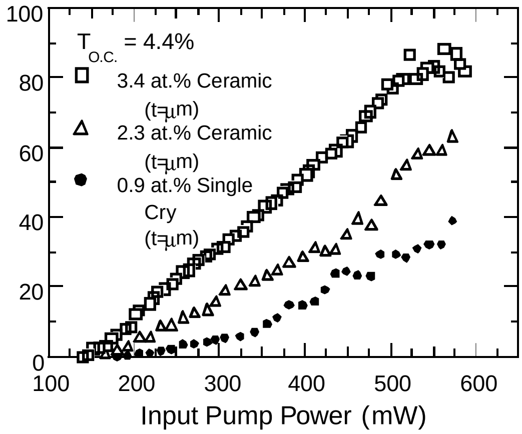

Figure 2. Dependence of the output power on the input pump power for the Nd:YAG ceramics and the single crystal.

VIII-B-4 Development of Multifunction Nonlinear Optical Wavelength Converter

KURIMURA, Sunao; PAVEL, Nicolaie; SHOJI, Ichiro; TAIRA, Takunori

[*Autumn Meeting of Japan Applied Physics Society* 3a-Q-22 (2000)]

Wavelength conversion based on nonlinear optics yields high efficiency without any sacrifice in coherency. Recently developed *Quasi-Phase Matching (QPM)* technique has produced designability of phase matching wavelength and efficiency, together with artificial characteristics of converters in space, frequency, and time domains by using digital patterns defined by photolithography. QPM giving new degree of freedom thus brought about stronger impact than growth of new crystals in the nonlinear optics. We here proposed efficient wide-band infrared generation with cascaded QPM crystals for optical parametric oscillation (OPO) and difference frequency generation (DFG) around 6 μm region, where double bond structures of molecules have characteristic absorption lines. Figure 1 illustrates the geometry, measured emission wavelengths in OPO and required QPM period in DFG in efficient nonlinear crystal, lithium niobate (LN). Since LN has moderate absorption at 6 μm, direct access to 6 μm induces thermal fluctuation enhanced in OPO cavity. Our approach is to use OPO in the transparent region of LN and access to 6 μm by single-pass DFG, which is less sensitive to thermal disturbance. We devised first OPO stage and obtained IR emission plotted in Figure 1(b) with closed circles. The 0.5mm-thick QPM device with a period of 30.9 μm was fabricated by electric field poling in liquid electrodes as shown in Figure 1(d).

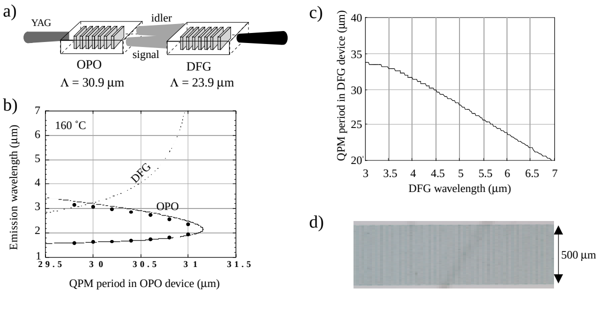

Figure 1. QPM OPO-DFG light source for widely tunable IR light: a) geometry, b) wavelength tunability depending on QPM period, c) calculated DFG period, d) periodical domains in a QPM LN device.

VIII-B-5 Periodical Twinning in Crystal Quartz for Ultraviolet Nonlinear Optics

KURIMURA, Sunao; FEJER, Martin[1]; SHOJI, Ichiro; TAIRA, Takunori; UESU, Yoshiaki[2]; NAKAJIMA, Hirochika[2]
([1]Stanford Univ., U. S. A.; [2]Waseda Univ.)

[*Oyobuturi* **69**, 548 (2000)]

Crystal quartz is attractive for operation in ultraviolet nonlinear optics, which has low absorption from 150 nm, high chemical stability, and low thermooptic coefficients compared with conventional ultraviolet nonlinear crystals. Growth techniques are well established because of widespread in surface-acoustic-wave and timing applications, but unfortunately, it doesn't meet the birefringent phase matching condition due to small birefringence, and electric field poling condition due to lack of ferroelectricity. We devised a new poling technique in crystal quartz using mechanical twinning and demonstrated periodical polarity reversal by using thermal stress. Figure 1 shows an observed twin structure with a period of 80 μm, obtained by thermally induced stress between patterned Cr films and a quartz. The Cr patterned substrate was heated to just below Curie temperature in order to attain reasonable film stress and reduce coercive stress. Twins tend to generate from the edge of Cr pattern and the required duty ratio of Cr to the period was more than 0.5. The depth of twins, however, were several microns, indicating not suitable for bulk nonlinear optics. New technique is under development to improve the depth profile of the twins for a practical UV generator.

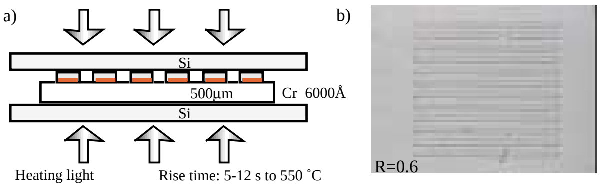

Figure 1. Twin patterning in crystal quartz: a) patterning method by the thermally induced in-plane stress, b) observed periodical twins with a period of 80 µm period, *R*: duty ratio of the Cr film to the period.

Research Center for Molecular Materials

VIII-C Development of Novel Heterocyclic Compounds and Their Molecular Assemblies for Advanced Materials

Heterocycles containing sulfur and/or nitrogen atoms are useful as components of functional materials since heteroatoms in their rings are helpful to stabilize ions or ion-radical species, and extended π-conjugation decreases Coulombic repulsion. In addition intermolecular interactions caused by heteroatom contacts can be expected to form novel molecular assemblies. In this project new electron acceptors, donors, and donor-acceptor compounds based on heterocycles such as 1,2,5-thiadiazole and 1,3-dithiole were synthesized and their properties including those of the charge-transfer complexes or ion-radical salts were investigated. Unique crystal structures were constructed by using weak intermolecular interactions such as hydrogen bonding or heteroatom contacts. Heterocyclic oligomers with rigid structures were also synthesized for molecular wires.

VIII-C-1 Preparation of New TTF Vinylogues Containing Substituents at the Vinyl Positions

YAMASHITA, Yoshiro; TOMURA, Masaaki

TTF vinylogues **1** have a stronger electron-donating ability and reduced on-site Coulomb repulsion owing to the extended π-delocalized system. The physical properties and structures can be tuned by the substituents at the vinyl positions. For example the ortho-substituted phenyl groups can keep the TTF vinylogue skeleton plane by taking twisting conformations, leading to the stable cation radical states.[1)] We have now prepared the new derivatives **1** and **2**, and investigated their properties. New compounds **1a–d** possess cyano or bromo substituents which can induce intermolecular interactions. The synthesis is based on oxidative coupling reaction of the corresponding 1,4-dithiafulvenes. **1e** with 2-pyridyl substituents and **1f** with phenylethynyl groups were also synthesized. **1f** has no steric hindrance caused by substituents. Furthermore, we have obtained cyclophane-type molecules **2** which have a bridge between the phenyl substituents. The following oxidation potentials of new molecules were observed. **1a**; 0.61, 0.84, **1b**; 0.64 (2e), **1c**; 0.51, 0.75, **1d**; 0.68 (2e), **1e**; 0.91 (irrev.), **1f**; 0.57, 0.76, **2a**; 0.48, 0.64, **2b**; 0.52, 0.65; **2c**; 0.40, 0.63V *vs.* SCE.

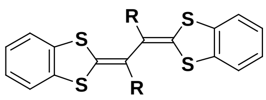

1a; R = *o*-CNC_6H_4
1b; R = *p*-CNC_6H_4
1c; R = *o*-BrC_6H_4
1d; R = *p*-BrC_6H_4
1e; R = 2-Pyridyl
1f; R = PhC≡C-

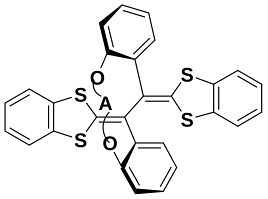

2a; A =CH_2CH_2
2b; A = CH_2SCH_2
2c; A = $(CH_2)_4$

Reference
1) Y. Yamashita, M. Tomura, M. B. Zaman and K. Imaeda, *Chem. Commun.* 1657 (1998).

VIII-C-2 Preparation, Structure, and Properties of 1,3-Bis(1,4-dithiafulven-6-yl)azulenes

OHTA, Akira[1]; YAMAGUCHI, Kyoko[1]; FUJISAWA, Naoki[1]; YAMASHITA, Yoshiro; FUJIMORI, Kunihide[1]
([1]Shinshu Univ.)

Novel bis(1,3-dithiole) electron donors **1** containing an azulene spacer unit were prepared from 1,3-diformylazulene using a Wittig-Horner reaction in 20-85% yields. The first oxidation potentials of **1** are lower than that of TTF, indicating that they are stronger donors than TTF as predicted by the PM3 calculations. In addition to the oxidation waves, they show an irreversible reduction peak at *ca.* –1.4 V. This amphoteric nature is consistent with the absorption data where the longest absorption maxima are observed at 733–762 nm in dichloromethane. The structure features of a benzo-fused derivative were investigated by X-ray analysis. One of the 1,4-dithiafulvenyl groups and the azulene moiety are in almost coplanar, while the other one twists with a torsion angle of 20.8°. The spectroelectrochemical studies on the methylthio derivative reveals that the cation radical and dication state have the longest absorption maxima at 612 and 721 nm, respectively.

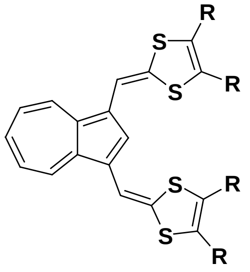

R = H, SMe, SCH_2CH_2S, $(CH=CH)_2$

1

VIII-C-3 Synthesis and Characterization of Novel Strong Electron Acceptors: Bithiazole Analogues of Tetracyanodiphenoquinodimethane (TCNDQ)

SUZUKI, Kazuharu; TOMURA, Masaaki; TANAKA, Shoji; YAMASHITA, Yoshiro

Pyridine analogues of TCNQ are unstable due to the much stronger electron accepting ability. On the other hand, thiophene-TCNQs are generally weak electron acceptors due to the electron donating effect of the thiophene ring. Therefore, we have designed a new electron acceptor **1**, a TCNDQ analogue containing Nitrogen and Sulfur atoms in the skeleton. **1** was prepared by using Pd-catalyzed coupling reaction of dicyanomethanide to a dibromo precursor **4**. The new acceptor shows a strong electron accepting ability and small on-site Coulomb repulsion. The methoxy derivatives **2** and **3** were also obtained by substitution reaction of **1** with methanol. The reduction potentials of **2** and **3** are lower than that of **1** due to the electron donating methoxy substituents. The X-ray analysis of **1** and **2** has revealed the planar structures containing a double bond with *E*-configuration. The acceptors **1**–**3** have characteristic strong absorptions around 550 nm. **1** afforded several charge transfer complexes with electron donors such as TTF.

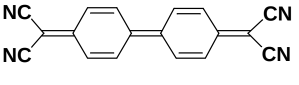

TCNDQ

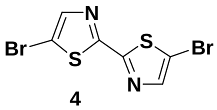

4

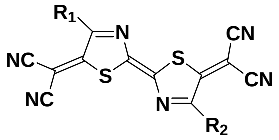

1; $R_1 = R_2 = H$
2; $R_1 = H$, $R_2 = OMe$
3; $R_1 = R_2 = OMe$

VIII-C-4 Heterocyclic TCNQ Analogues Containing Thiophene and Benzothiadiazole Units

SUZUKI, Kazuharu; TOMURA, Masaaki; YAMASHITA, Yoshiro

Sulfur containing TCNQ analogues are highly polarized and are expected to have strong intermolecular interactions by heteroatom contacts. We have recently prepared a TCNDQ derivative **1** containing fused thiadiazole rings. As an extension of this work, we have now prepared new π-extended electron acceptors **2** and **3** composed of benzothiadiazole and thiophene units. They were synthesized using the Pd catalyzed reaction of the corresponding dibromides **4** and **5** with malononitrile anion. The absorption maxima of **2** and **3** were observed at 524 and 635 nm in dichloromethane, respectively. **2** shows stepwise one-electron reduction waves at +0.07 and –0.17 V *vs.* SCE, while **3** shows a one-step two-electron reduction wave at +0.08 V *vs.* SCE. The values of the first reduction potentials are lower than that of TCNQ, indicating that they are not so strong acceptors. However, they are still stronger acceptors than the corresponding thiophene-TCNQ analogues. The X-ray analysis revealed that **2** has a planar geometry and the central double bond takes a Z-configuration. **2** gave various charge transfer complexes and anion radical salts. The Me_4P^+ salt exhibits a high conductivity of 8.4 Scm^{-1}.

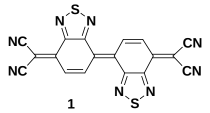

1

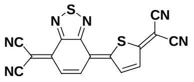

2

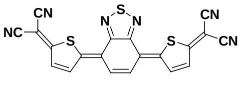

3

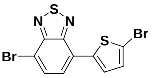

4

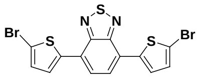

5

VIII-C-5 Crystal Engineering in π-Overlapping Stacks: Unusual One- and/or Two-Dimensional Stacking of π-System in the Crystal Structure of the Cation Radical Salts of Tetrathiafulvalene Vinylogues

TOMURA, Masaaki; YAMASHITA, Yoshiro

[*CrystEngComm* 14 (2000)]

One- and/or two-dimensional π-overlapping stacks have been found in the crystals of the cation radical salts of the tetrathiafulvalene vinylogues **1** and **2** having *o*-substituted phenyl groups at the vinyl positions. The packing mode in the two-dimensional π-stacks could be modified depending on the counter anions. We have observed the pseudo two-dimensional stacking and the zigzag two-dimensional stacking with an angle of nearly 90° in the crystal structure of **1**–$FeCl_4$ and **1**–ReO_4 salts, respectively. In the case of **2**–PF_6–$(H_2O)_8$ salt, we have observed not the two-dimensional π–π overlapping stack found in the cation radical salts of **1**, but the one-dimensional stacking of π-system. The one-dimensional overlapping mode of **2** has brought a square grid-like structure (Figure 1) with a void in which eight water molecules are occupied. The 1,3-dithiole rings in **2** are unfavorable for π-π intermolecular interactions due to the less π-delocalization and steric interactions of the ethylenedithio parts compared to those in **1**. This seems to lead to the novel one-dimensional structure, not the two-dimensional one.

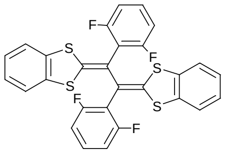

1

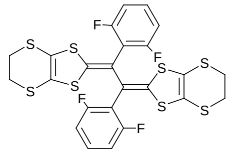

2

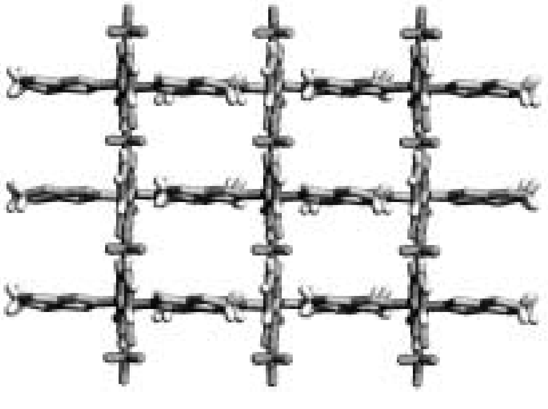

Figure 1. Crystal structure of **2**–PF_6–$(H_2O)_8$ salt viewed along the *c* axis. The water molecules are omitted for clarity.

VIII-C-6 One-Dimensional Supramolecular Tapes in the Co-Crystals of 2,5-Dibromo-3,6-dihydroxy-1,4-benzoquinone (Bromanilic Acid) with Heterocyclic Compounds Containing a Pyrazine Ring Unit

TOMURA, Masaaki; YAMASHITA, Yoshiro

[*CrystEngComm* 16 (2000)]

The design of new molecular architectures for crystal engineering has generated great interest in recent years. We have carried out co-crystallization of 2,5-dibromo-3,6-dihydroxy-1,4-benzoquinone (bromanilic acid) with heterocyclic aromatic compounds, phenazine, quinoxaline and pyrazine. The X-ray crystallographic analyses of the co-crystals suggest the supramolecular synthon formed with bromanilic acid and the heterocyclic compounds can yield the robust one-dimensional supramolecular tapes (Figure 1) and realize preserved interesting crystal structures.

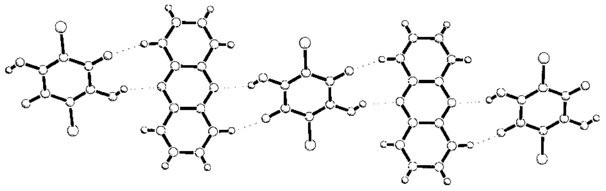

Figure 1. One-dimensional tape in the co-crystal of bromanilic acid with phenazine.

VIII-C-7 A Decamethylferrocene [$Fe(C_5Me_5)_2$] and Chloranilic Acid (CA) Complex with Hydrogen Bonded Supramolecular Structure between CA and H_2O

ZAMAN, Md. Badruz; TOMURA, Masaaki; YAMASHITA, Yoshiro; SAYADUZZAMAN, Md.[1]; CHOWDHURY, A. M. Sarwaruddin[1]
([1]Dhaka Univ.)

[*CrystEngComm* 9 (1999)]

The chloranilic acid as acceptor (A) has been used to prepare crystalline materials with organometallic decamethylferrocene as donor (D). The structure was obtained by single crystal X-ray analysis and the stoichiometric ratio [$D:A:H_2O$ = 1:1:1] was confirmed by elemental analysis. These analyses reveal the molecular complex as $[Fe(C_5Me_5)_2]^+[CA]^-[H_2O]$. The water molecules in this crystal act as cohesive elements by connecting the anions through O–H··O hydrogen bonds to form an infinite one-dimensional supramolecular structure along the b axis (Figure 1). This solid-state structural aspects of DA solids has interesting, highly charged ground states, which are not commonly observed in $Fe(C_5Me_5)_2$ complexes due to the paucity of stability and highly charged species.

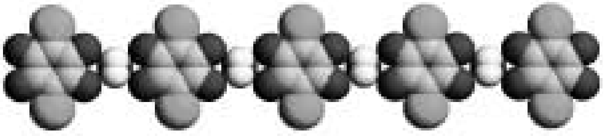

Figure 1. View of the hydrogen bonded network with CA and H_2O molecule.

VIII-C-8 New Hydrogen Bond Donor-Acceptor Pairs between Dipyridylacetylenes and 2,5-Dichloro-3,6-dihydroxy-1,4-benzoquinone

ZAMAN, Md. Badruz; TOMURA, Masaaki; YAMASHITA, Yoshiro

[*Org. Lett.* **2**, 273 (2000)]

The crystalline donor-acceptor hydrogen bonding complexes between 2,5-chloro-3,6-dihydroxy-1,4-benzoquinone (chloranilic acid, H_2CA) and dipyridylacetylenes (DPA) [2,2’-DPA, 3,3’-DPA and 4,4’-DPA] were prepared and crystal structures were revealed by X-ray analysis. The structures of the complexes are formed by intermolecular hydrogen bonding interactions and demonstrate three beautiful supramolecular architectures based on a new common supramolecular synthon (Figure 1), which allows controlling the crystal structures, ionicity and stacking arrangements.

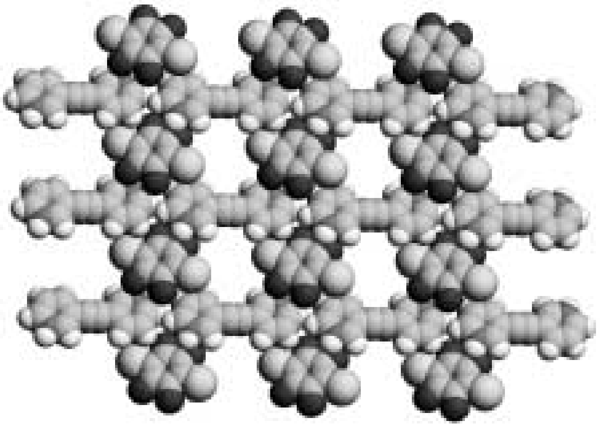

Figure 1. Square grids structure of $[CA]^{2-}[3,3'\text{-}H_2DPA]^{2+}\text{-}(H_2O)_{3.3}$ complex. The water molecules are omitted for clarity.

VIII-C-9 Novel Synthetic Approach to 5–10 nm Long Functionalized Oligothiophenes

TANAKA, Shoji ; YAMASHITA, Yoshiro

The development of precisely-defined oligomers with extended π-conjugation length comparable to the inter-electrode gap currently made by nano-patterning techniques (5~10 nm gap) has generated a great deal of interest. The reason for this is that highly oligomers of this class will become an important tool for providing specific information on the parameters controlling the long-distance electron-tunneling through a single molecular wire. Here we will report a new synthetic approach to a series of precisely defined 5–10 nm long oligothiophenes, using N-silyl-protected 3,4-

diaminothiophene as a key building unit. Scheme 1 shows the synthetic pathways for α-14T (**3**: $l \sim 5$ nm) and α-28T (**5**: $l \sim 10$ nm) derivatives. Purification of all oligomers (**1**–**5**) was achieved by preparative gel permeation chromatography, and the purity was clearly revealed by MALDI-TOF mass spectrometry in the positive ion and linear detection mode using dithranol as matrix. The desilylation and further chemical modifications of the N-silyl-protected 3,4-diaminothiophene moieties of the obtained oligomers will afford various types of 5–10 nm long functionalized oligomers.

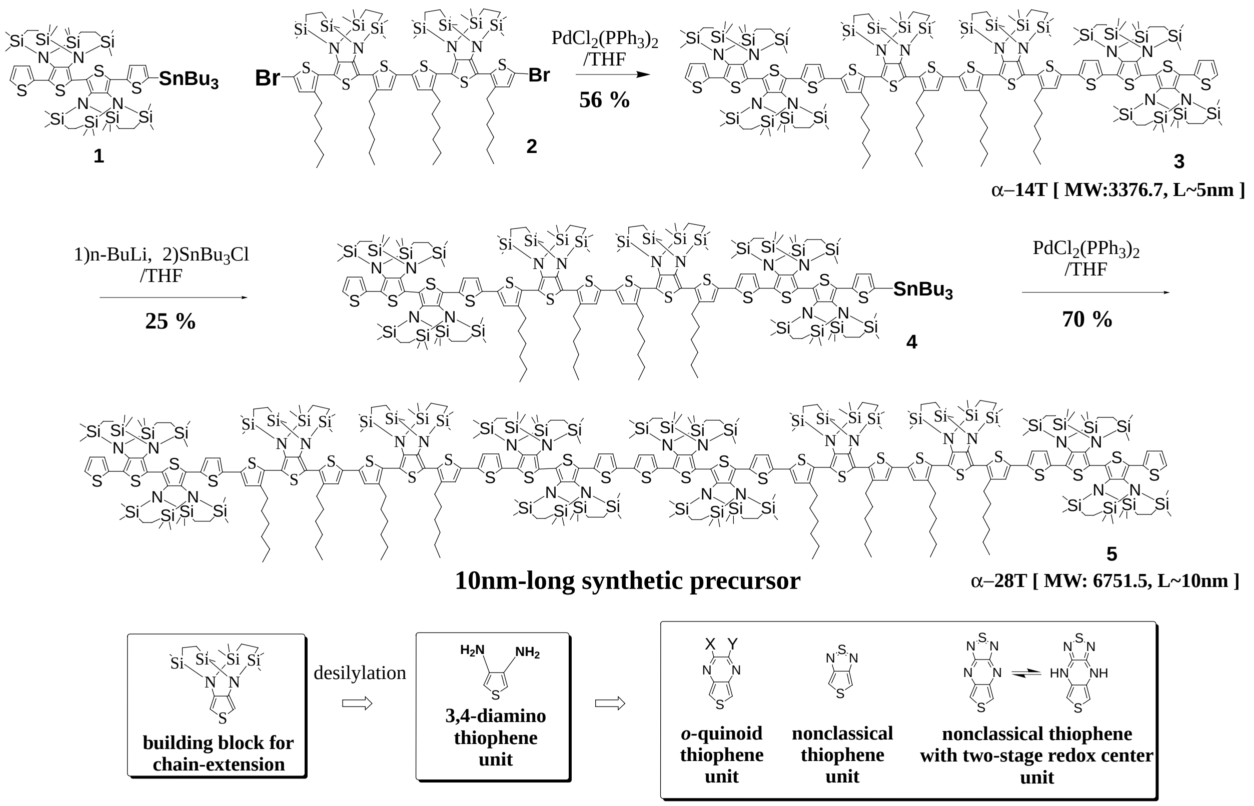

Scheme 1.

VIII-D Elecrtonic Structures and Rectivities of Active Sites of Metalloproteins

Metalloproteins are a class of biologically important macromolecules which have various functions such as oxygen transport, electron transfer, oxidation, and oxygenation. These diverse functions of metalloproteins have been thought to depend on the ligands from amino acid, coordination structures, and protein structures in immediate vicinity of metal ions. In this project, we are studying the relationship between the structures of the metal active sites and functions of metalloproteins.

VIII-D-1 Resonance Raman Spectra of Legitimate Models for the Ubiquitous Compound I Intermediates of Oxidative heme Enzymes

CZARNECKI, Kazimierz[1]; KINCAID, James R.[1]; FUJII, Hiroshi
([1]Marquette Univ.)

[*J. Am. Chem. Soc.* **121**, 7953 (1999)]

Resonance Raman (RR) spectra are reported for two models of the compound I intermediates of oxidative heme proteins; namely, the imidazole (Im) and 2-methyl-imidazole (2-MeIm) complexes of the ferryl π-cation radical derivative of iron-(5,10,15,20-tetra-mesitylporphyrin), $[O{=}Fe(TMP^{+\bullet})(Im)]^+$ and $[O{=}Fe(TMP^{+\bullet})]^+$, which are stablized in dichloromethane solution at –80 °C. The present study yields high quality RR spectra of these complexes and provides the forst opportunity to compare the ν(Fe=O) stretching modes and the structure-sensitive core maker modes for a ferrylporphyrin π-cation radical with the corresponding modes of the neutral parent bearing the same trans-axial ligand. While the observed shifts in the frequencies of the core modes are in agreement with those expected upon formation of the π-cation radical, the results suggest that the isolated effect of macrocycle oxidation on the Fe=O stretching frequency is rather small; the observed shift being only about 4 cm^{-1} to lower frequency.

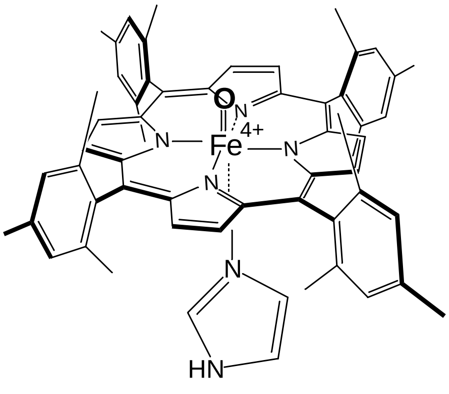

Figure 1. Structure of model complexes of the compounds I of oxidative heme proteins.

VIII-D-2 Spin Distribution in Low-Spin (meso-Tetraalkylporphyrinato)iron(III) Complexes with (dxz,dyz)^4 (dxy)^1 Configuration. Studies by ^{1}H-NMR, ^{13}C-NMR, and EPR Spectroscopies

IKEUE, Takahisa[1]; OHGO, Yoshiki[1]; SAITOH, Takashi[1]; NAKAMURA, Mikio[1]; FUJII, Hiroshi; YOKOYAMA, Masataka[2]
([1]Toho Univ. Sch. Med.; [2]Chiba Univ.)

[*J. Am. Chem. Soc.* **122**, 4068 (2000)]

^{1}H-NMR, ^{13}C-NMR, and EPR studies of a series of low-spin (meso-tetraalkylporphyrinato)iron(III) complexes, $[Fe(TRP)(L)_2]X$ where R = n-Pr, c-Pr, and i-Pr and L represents axial ligands such as imidazoles, pyridines, and cyanide, have revealed that the ground-state electron configuration of $[Fe(TnPrP)(L)_2]X$ and $[Fe(TcPrP)(L)_2]X$ is presented either as the common $(dxy)^2$ $(dxz,dyz)^3$ or as the less common $(dxz,dyz)^4$ $(dxy)^1$ depending on the axial ligands. The ground-state electron configuration of the isopropyl complexes $[Fe(Ti\text{-}PrP)(L)_2]X$ is, however, presented as $(dxz,dyz)^4$ $(dxy)^1$ regardless of the kind of axial ligands. In every case, the contribution of the $(dxz,dyz)^4$ $(dxy)^1$ state to the electronic ground state increases in the following order: HIm < 4-Me_2NPy < 2-MeIm < CN^- < 3-MePy < Py < 4-CNPy. Combined analysis of the ^{13}C and ^{1}H NMR isotropic shifts together with the EPR g values have yielded the spin densities at the porphyrin carbon and nitrogen atoms. Estimated spin densities in $[Fe(TiPrP)(4\text{-}CNPy)_2]^+$, which has the purest $(dxz,dyz)^4$ $(dxy)^1$ ground state among the complexes examined in this study, are as follows: meso-carbon, +0.045; β-pyrrole carbon, +0.0088; α-pyrrole carbon, –0.00026; and pyrrole nitrogen, +0.057. Thus, the relatively large spin densities are on the pyrrole nitrogen and meso-carbon atoms. The result is in sharp contrast to the spin distribution in the $(dxy)^2$ $(dxz,dyz)^3$ type complexes; the largest spin density is at the α-pyrrole carbon atoms in bis(1-methylimidazole)(meso-tetraphenylporphyrinato)-iron(III), $[Fe(TPP)(1\text{-}MeIm)_2]^+$, as determined by Goff. The large downfield shift of the meso-carbon signal, ä +917.5 ppm at –50 °C in $[Fe(TiPrP)(4\text{-}CNPy)_2]^+$, is ascribed to the large spin densities at these carbon atoms. In contrast, the large upfield shift of the β-pyrrole carbon signal, –293.5 ppm at the same temperature, is caused by the spin polarization from the adjacent meso-carbon and pyrrole nitrogen atoms.

VIII-D-3 Post-Assembly Insertion of Metal Ions into Thiol-Derivatized Porphyrin Monolayers on gold

NISHIMURA, Noboru[1]; OOI, Masanori[1]; SHIMATZU, Katsuaki[1]; FUJII, Hiroshi; UOSAKI, Kohei[1]
([1]Hokkaido Univ.)

[*J. Electro. Chem.* **473**, 75 (1999)]

The insertion of metal ions into thiol-derivatized free base porphyrin monolayers pre-assembled on gold has been conducted by refluxing the metal ion solution in which the monolayer-coated gold electrode was immersed. The extend of the metal insertion was estimated from the decrease in the N1s peaks in X-ray photoelectron spectra (XP spectra) assigned to the pyrrole nitrogen which binds a hydrogen atoms. The insertion of Co(II) was completed by refluxing for 3 hr. Although the extent of the metal insertion for the same reflux time depends on the metal ion used, the insertion of several ions including Mn(II), Fe(II), Ni(II), Cu(II) and Zn(II) was possible. Besides XP spectra, the metal insertion was confirmed by the electrocatalytic activity of the monolayers for the reduction of molecular oxygen. The structural characterization has proved that the monolayer is stable during the reflux: neither desorption nor change in the orientation of the porphyrin molecules took place. Compared to the commonly used self-assembly of the pre-metalated porphyrin, this post-assembly metal insertion method has an advantage because neither intra nor intermolecular coordinations of the thiol functionality to the central metal ion take place, thus avoiding the unexpected disorder in the monolayer such as the formation of a multilayer, the blocking of the electrocatalytically active metal ion and loss of the anchoring functionality or thiol.

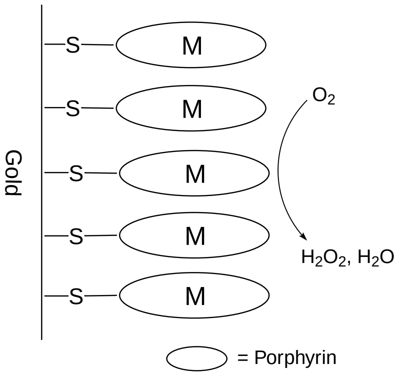

Figure 1. Porphyrin monolayer formed by the self-assemble on gold surface.

VIII-D-4 Electron Spin-Echo Envelope Modulation Spectral properties of Amidate Nitrogen Coordinated to Oxovanadium(IV) Ion

FUKUI, Koichi[1]; FUJII, Hiroshi; OHYA-NISHIGUCHI, Hiroaki[1]; KAMADA, Hitoshi[1]
([1]Inst. Life. Supp. Tech.)

[*Chem. Lett.* 198 (2000)]

Increse evidence shows that vanadium palys a variety of roles in biological systems. For instance, a class of haloperoxidase requires vanadium for their enzymatic activities. Vanadium is also know to have beneficial insulin-mimetic activities, and some vanadium complexes are studied as a candidate for an orally-active anti-diabetic agent. These findings have stimulated interests in the interactions of vanadium with biological substances such as an amnio acids, peptides, and proteins. In the stduies on this subject, interests are often focused on carboxylate, imidazole and amino groups for vanadium-coordinating groups. However, recent studies have shown that amido group can undergo reprotonation/coordination reaction even at physiological conditions when an anchoring group is present. Therefore, it is possible that vanadium-amidate bonding actually ocuurs and plays some roles in biological systems. For characterization of vanadium(IV) cooridnation environments, electron spin-echo envelope modulation (ESEEM) spectroscopy is suited. It has been demonstrated that ESEEM results not only reveal the presence or absence of nitrogen nuclei coordinated to VO^{2+} ion (and possibly the number of the coordinating nitrogen atoms), but allow identification of equatorial nitrogens based on the emprirical correlation between the type of the nitrogen and the ^{14}N hyperfine coupling (HFC) parameter. However, neither the HFC parameters nor the nuclear quadropole coupling (NQC) pararmeters are known for vanadium-coordinated amidataed nitrogens. Here we report the first ESEEM results for a structurally-characterized VO^{2+}-amidate complex.

VIII-D-5 Newly Designed Iron-Schiff Base Complexes as Models of Mononuclear Non-Heme Iron Active Sites

FUNAHASHI, Yasuhiro; FUJII, Hiroshi

High valent iron-oxo species have been suggested as the active intermediates for catalytic oxygenation reactions by iron-containing oxygenases. In the reaction mechanisms of heme and binuclear non-heme iron enzymes, an Fe^{IV}=O porphyrin radical species (Compound I) and a $Fe^{IV}_2(m\text{-}O)_2$ species (Intermediate Q) have been found to be responsible oxidant for alkane hydroxylation and alkene epoxidation. Such the high valent iron-oxo species are inferred to involve in hydroxylation of aromatic compounds by mononuclear non-heme iron oxygenases, the reaction processes of which, however, still remains to be established. In order to gain insight into the active intermediates, we try to synthesize iron complexes with bulky schiff-base ligands as biomimetic models of mononuclear non-heme iron active sites. The active oxygen adduct of these complexes, which would be kinetically stabilized by their steric hindrance, might provide a basis for understanding the oxygenation by mononuclear iron sites.

VIII-D-6 Synthesis and Characterization of High Valent Iron Porphyrin Complexes as Models for Reaction Intermediates of Cytochrome *c* Oxidase

IKEUE, Takahisa; FUMOTO, Yumiko[1]; ONO, Noboru[1]; FUJII, Hiroshi
([1]Ehime Univ.)

Cytochrome c oxidase is the terminal oxidase which reduces molecular oxygen (O_2) to water (H_2O), coupling with proton pumping across the mitochondrial inner membrane. Since discovery of this enzyme, many structural and functional studies have been done to understand its reaction mechanism. Recent X-ray analyses reveal that this enzyme contains a binuclear center, heme-a_3-Cu_B site, as a reaction site in the catalytic core, and Cu_A and Heme-a as electron transfer sites in the backbone structure, respectively. The binuclear center of the resting enzyme is ferric/cupric form. The binuclear active site is reduced to a ferrous/cuprous form by two electrons from cytochrome c through the Cu_A and heme a site. The ferrous/cuprous form of active site reacts with O_2 to yield an internal dioxygen adduct, intermediate A state, which is further converted to intermediate P and F by the aid of the electrons and protons. Although the intermediates P and F have been studied by resonance Raman and flash-flow absorption spectroscopies, the electronic states of these intermediates are not still clear. To reveal the electronic states of these intermediates and to understand the reaction mechanism of cytochrome c oxidase, we have synthesized model complexes of the heme-a_3 site of cytochrome *c* oxidase. The model complex contains a formyl group at pyrrole-β position to mimic the heme a_3 and mesityl groups to stabilize high valent oxo iron species. We have succeeded in the preparation of a high valent oxo iron porphyrin complex as a model for the intermediate P by the oxidation of the ferric model complex with mCPBA or ozone.

VIII-E Molecular Mechanism of Heme Degradation and Oxygen Activation by Heme Oxygenase

Heme oxygenase (HO), an amphipathic microsomal proteins, catalyzes the regiospecific oxidative degradation of iron protoporphyrin IX (heme) to biliverdinIXα, carbon monoxide, and iron in the presence of NADPH-cytochrome P-450 reductase, which functions as an electron donor. Heme oxygenase reaction is the biosynthesis processes of bile pigments and CO which is a possible physiological messenger. Recent development in the bacterial expression of a soluble form of heme oxygenase has made it possible to prepare in the large quantities for structural studies. In this project, we are studying the molecular mechanism of heme degradation and the oxygen activation by heme oxygenase using various spectroscopic methods.

VIII-E-1 Participation of Carboxylate Amino Acid Side Chain in Regiospecific Oxidation of Heme by Heme Oxygenase

ZHOU, Hong[1]; MIGITA, Taiko Catharine[2]; SATO, Michihiko[1]; SUN, Donghu[1]; ZHANG, Xuhong[1]; IKEDA-SAITO, Masao[2]; FUJII, Hiroshi; YOSHIDA, Tadashi[1]

([1]Yamagata Univ. Sch. Med.; [2]Yamaguchi Univ.; [3]Case West. Res. Univ. Sch. Med.)

[*J. Am. Chem. Soc.* **122**, 8311 (2000)]

The regioselective oxidation of the α-meso position by HO is quite unique, in contrast to the non-enzymatic heme degradation that forms a mixture of four possible α, β, γ, δ-biliverdin isomers. The present study shows the first evidence of the formation of biliverdin isomers other than biliverdinIXα by HO mutants. The replacement of the highly conserved arginine 183(R183) of HO-1 with glutamic acid (E) or aspartic acid (D) forms biliverdinIXδ isomer along with normal biliverdinIXα. The absorption and EPR spectra and HO catalytic activity of R183E mutant are similar to those of the wild type heme-HO complex, indicating no significant change in the active site structure with mutation. To investigate the effects of the carboxylate functionalities introduced at the position 183, we prepared R183Q, R183N, R183A, R183T, and R183Y. The HO reactions of these mutants do not produce biliverdin isomers other than the normal biliverdinIXα. These results indicate that the carboxylate group introduced at position 183 is involved in the formation of δ-biliverdin isomer. The formation of δ-biliverdin isomer is expected to result in heme rotation through electronic repulsion between the carboxylate of E183 and heme propionate and/or change in distal side protein structure through a formation of new long-range hydrogen bond interaction network. All of the present results show the importance of the hydrogen bonding interaction between the arginine at position 183 and the carboxylates of the heme propionate group, as well as steric effect of the distal helix, for the α-regioselectivity.

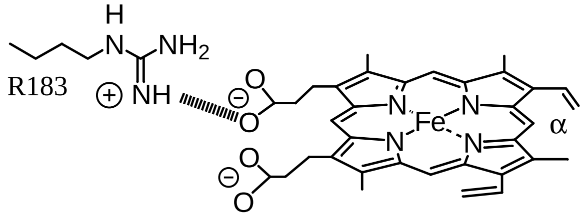

Figure 1. The hydrogen bonding interaction between R183 residue and the carboxylate of heme orients the heme to oxidize the α-meso position.

VIII-F Designing Artificial Photosynthesis at Molecular Dimensions

Photosynthesis is one of the finest piece of molecular machinery that Nature has ever created. Its ultrafast electron transfer and following well-organized sequence of chemical transformation have been, and will continue to be, challenging goals for molecular scientists. We are trying to mimic the function of photosynthesis by assembling molecular units that perform individual physical/chemical action. The molecular units include porphyrins, redox active organic molecules, and transition metal complexes.

Last year we focused our attention on developing organic reactions that utilize photoinduced electron transfer processes and are useful for synthetic organic chemistry. This is an important step toward our ultimate goal, which is to design artificial molecular systems that effect multiple chemical reactions triggered by light on the basis of molecular rationale.

VIII-F-1 Porphyrin Catalyzed Reductive Silylation and Acylation of Quinones under Irradiation of Visible Light

ITO, Hajime; NAGATA, Toshi

Considerable studies were reported for inter- or intramolecular photoinduced electron transfer from porphyrins to quinones, however, the synthetic application of a porphyrin as a photocatalyst for the reduction of quinones is thought to be still difficult. For example, when attempts to obtain the reduced products of a quinone was carried out using a porphyrin catalyst under irradiation of visible light in the presence of a proton source, no reduced products were detected. The reason for this unsuccessful result would be mainly attributed to the reverse electron transfer from a semiquinone anion radical to the porphyrin cation radical generated by the photoinduced electron transfer. If the semiquinone anion radical is chemically trapped by a silyl reagent and the successive silylation occurs, the reductive silylation product of the quinone is obtained. On the basis of this idea, we found both phenylthiotrimethylsilane (PhSTMS) and chlorotrimethylsilane (TMSCl) are a good trapping reagent for the reduced intermediate formed by photoinduced electron transfer from photo-excited porphyrins. In addition, the electrophilic substitution of a silyl sulfide with a phenoxy group releases a thiolate anion which would act as an electron donor. In the presence of a catalytic amount of porphyrin **1** (0.5 mol %), the reductive silylation of duroquinone was proceded under the irradiation of yellow light ($\lambda > 500$ nm) using PhSTMS to give 1,4-bis(trimethylsiloxy)-2,3,5,6-tetramethylbenzene (99%) and diphenyl disulfide (97%) in good yields. We also found that chlorotrimethylsilane (TMSCl), a more easily available silyl reagent, was also useful for the porphyrin-catalyzed reductive silylation.

Despite the reductive silylation and acylation of quinones with chlorotrimethylsilane and metal (K, Mg, Zn) were well known procedure, these methods require a stoichiometric amount of metals as a reductant and generate waste metal salt. Our method exhibit the practical advantage in view of this points. Further work on the precise mechanism for these reactions is underway.

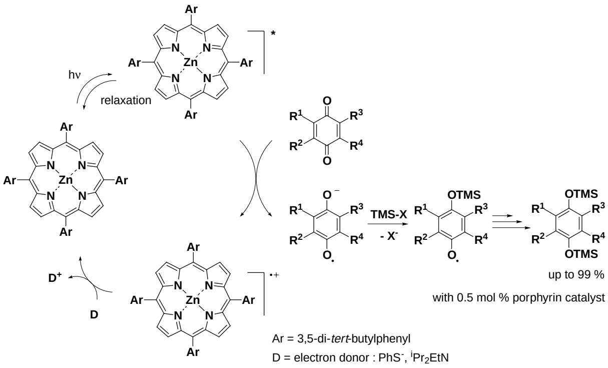

Figure 1. Porphyrin-catalyzed silylation of quinones under visible light.

VIII-G Development of New Metal Complexes as Redox Catalysts

Redox catalysis is an important field of chemistry which translates a flow of electron into chemical transformation. It is also one of the requisites for artificial photosynthesis. This project of ours aims at developing new metal complexes that perform redox catalysis at low overpotential. Our approach is to develop a series of "binary" ligands, which consist of two different types of ligands that are linked together to form metal chelates. Such ligands are particularly useful for utilizing first-row transition metal elements, because fast ligand exchange (which is often a major obstacle in studying first-row transition metal complexes in solution) is suppressed by chelate effects.

VIII-G-1 Synthesis of Terpyridine-Based Binary Ligands and Their Metal Complexes

NAGATA, Toshi; TANAKA, Koji

[*Inorg. Chem.* **39**, 3515 (2000)]

2,2':6',2"-Terpyridine is a promising ligand for application in redox catalysis, thanks to its structural rigidity and chemical stability. Unfortunately, with first-row transition metals it easily forms homoleptic bis(terpyridine) complexes that are too stable to serve as redox catalysts. Such difficulty can be overcome by connecting a bidentate ligand to a terpyridine molecule. The “binary” ligand thus formed is potentially pentadentate and binds an octahedral metal ion leaving one vacant site for catalytic reactions. We already reported synthesis of terpyridine-catechol linked ligands and their cobalt(III) complexes (Figure 1a). Here we report synthesis of a terpyridine-salicylaldehyde linked ligand (Figure 1b) and their metal complexes.

The ligand (tpyC5NHCOsalH) was prepared by condensation of 4-(2-(5-aminopentyloxy)phenyl)-terpyridine and 2-allyloxy-3-diethoxymethyl-5-methylbenzoic acid potassium salt (prepared by 6 steps and 4 steps from commercially avaiable material, respectively), followed by removing the allyl and diethyl acetal protecting groups (60% yield). The metal complexes ($M^{2+} = Mn^{2+}$, Fe^{2+}, Co^{2+}) were prepared by the reaction of the ligand with $[M(CH_3CN)_x](ClO_4)_2$ and 2,6-lutidine (1:1:2 in molar ratio) in CH_3CN. The ESI-MS spectra suggested 5-coordinate complexes, $[M(tpyC5NHCOsal)]^+$, were present in solutions.

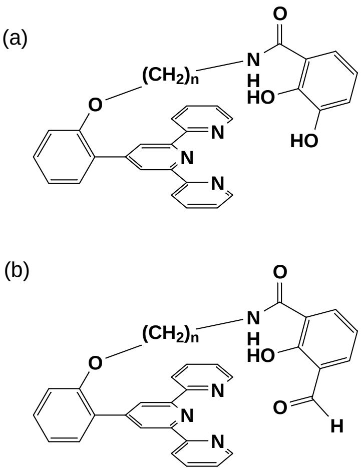

Figure 1. Terpyridine-based binary ligands.

VIII-H Development of Organic n-Type Semiconductors for Molecular Thin-Film Devices

Organic light-emitting diodes (OLEDs) and field-effect transistors (FETs) based on π-conjugated oligomers have been extensively studied as molecular thin-film devices. Organic n-type semiconductors (electron-transport materials) with low electron-injection barriers and high electron mobilities are required for highly efficient OLEDs and n-type FETs. Radical anions of an n-type semiconductor have to be generated easily at the interface with a metal electrode (electron injection), and electrons must move fast in the layer (electron mobility). Compared with organic p-type semiconductors (hole-transport materials), organic n-type semiconductors for practical use are few and rather difficult to develop. Recently, we found that perfluorinated phenylene dendrimers and oligomers are efficient electron-transport materials for OLEDs.

VIII-H-1 Synthesis, Characterization, and Electron-Transport Property of Perfluorinated Phenylene Dendrimers

SAKAMOTO, Youichi; SUZUKI, Toshiyasu; MIURA, Atsushi[1]; FUJIKAWA, Hisayoshi[1]; TOKITO, Shizuo[1]; TAGA, Yasunori[1]
([1]Toyota Central R&D Labs.)

[*J. Am. Chem. Soc.* **122**, 1832 (2000)]

Two perfluorinated phenylene dendrimers, $C_{60}F_{42}$ (MW = 1518) and $C_{132}F_{90}$ (MW = 3295), have been synthesized via a sequence of brominations and cross-couplings using organocopper chemistry. Two other $C_{60}F_{42}$ isomers containing *p*-terphenyl and *p*-quaterphenyl groups were also prepared to see structure-property relationships. Three $C_{60}F_{42}$s showed glass transitions at 125–135 °C. Dendrimer $C_{132}F_{90}$ melts at 426 °C and did not show a glass transition. Organic light-emitting diodes have been fabricated on indium-tin-oxide coated glass substrates by high-vacuum thermal evaporation of TPTE (a tetramer of triphenylamine) as the hole-transport layer, tris(8-quinolinolato)-aluminum as the emission layer, perfluorinated phenylenes as the electron-transport layer, LiF, and Aluminum. The maximum luminance of the device is 2860 cd/m^2 at 24.4 V. The electrochemical measurements indicated that the performance of the devices is improved with increasing electron affinities of the compounds. This is probably because the electron-injection barriers between the metal layers and the electron-transport layers are reduced by increased electron affinities.

VIII-H-2 Perfluorinated Oligo(*p*-Phenylene)s: Efficient n-Type Semiconductors for Organic Light-Emitting Diodes

HEIDENHAIN, Sophie; SAKAMOTO, Youichi; SUZUKI, Toshiyasu; MIURA, Atsushi[1]; FUJIKAWA, Hisayoshi[1]; MORI, Tomohiko[1]; TOKITO, Shizuo[1]; TAGA, Yasunori[1]
([1]Toyota Central R&D Labs.)

[*J. Am. Chem. Soc.* in press]

Perfluorinated oligo(*p*-phenylene)s including perfluoro-*p*-quinquephenyl to -octiphenyl (**PF–5P** to **–8P**) have been synthesized by the organocopper cross-coupling method. Two **PF–6P** derivatives containing trifluoromethyl and perfluoro-2-naphtyl groups were also prepared. All compounds are colorless solids and insoluble in common organic solvents. The differential scanning calorimetry measurements indicated that they are highly crystalline solids without glass transitions. Organic light-emitting diodes have been fabricated on indium-tin-oxide coated glass substrates by high-vacuum thermal evaporation of TPTE (a tetramer of triphenylamine) as the hole-transport layer, tris(8-quinolinolato)aluminum as the emission layer, a perfluorinated oligomer as the electron-transport layer, LiF, and aluminum. The electron-transport capabilities of perfluorinated oligo(*p*-phenylene)s are excellent compared with perfluorinated phenylene dendrimers. The maximum luminance of the naphtyl derivative is 19970 cd/m^2 at 10.0 V. The luminance-voltage and current-voltage characteristics of **PF–7P** and **–8P** are almost identical to those of **PF–6P**. We speculate that the electron mobility in the layer rather than the electron injection at the interface is responsible for determining the current density of **PF–6P** to **–8P**.

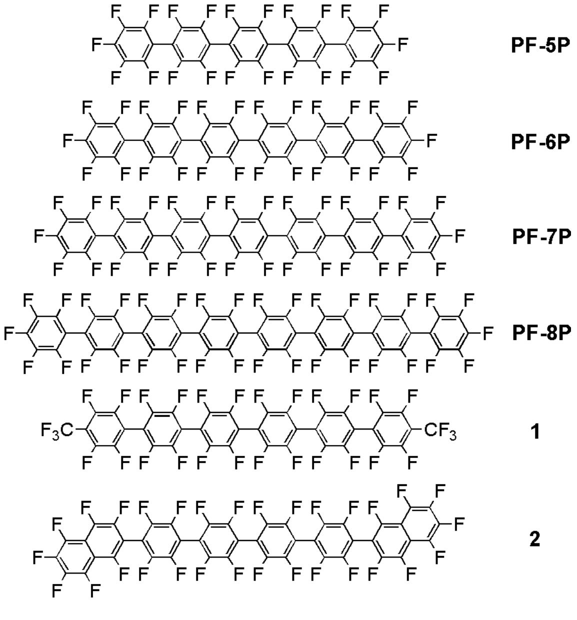

Figure 1. Perfluorinated phenylene oligomers.

VIII-I The Effects of the 2D Spin-Echo NMR Experiment on a Solid-State Homonuclear Sipn-1/2 Pair

The dipolar interaction for a solid-state homonuclear sipn-1/2 pair is averaged out by magic-angle sample spinning (MAS). The 2D spin-echo NMR experiment can reintroduce the influence of the homonuclear dipolar interaction into MAS powder signals.

VIII-I-1 Real Figure of Two-Dimensional Spin-Echo NMR Spectra for a Homonuclear Two-Spin System in Rotating Solids

KUWAHARA, Daisuke; NAKAI, Toshihito[1]; ASHIDA, Jun[2]; MIYAJIMA, Seiichi
([1]Tokyo Univ. Agric. Tech.; [2]Kyoto Univ.)

The 2D spin-echo NMR experiments were recently carried out on polycrystalline [2, 3-$^{13}C_2$] L-alanine under magic-angle sample spinning (MAS) conditions, so that two unusual resonance lines emerged along the F_1 axis (*Chem. Phys. Lett.* **305**, 35 (1999)). To examine a spectral structure observed in the F_1 direction more closely, we executed the 2D NMR experiment using a sufficiently small t_1 increment. As a result, we found many more resonance lines on a spectrum sliced off along the F_1 axis. The line distribution had a very unique and interesting structure. To elucidate the line positions theoretically, we calculated analytically the signals for the 2D spin-echo experiment performed with any t_1 increment on a homonuclear spin-1/2 pair undergoing MAS. We discovered that virtually six resonance lines (exactly twelve resonance lines) occurred on a spectrum sliced off along the F_1 axis. In addition, it was proved that the intensities of some resonance lines were largely dependent on the dipolar interaction.

VIII-J The Applications of Double-Rotation NMR Method

Double-Rotation NMR method (DOR) was applied to rare spins surrounded by abundant homonuclear spins. The application of the method to solid-state quadrupolar nuclei having $I = 1$ was investigated.

VIII-J-1 The Observation of REDOR Phenomenon for CH$_x$ ($x \geq 2$) Spin Systems under DOR

KUWAHARA, Daisuke

Double-Rotation NMR method (DOR) was developed originally to remove second-order line broadenings for solid-state quadrupolar nuclei having half-integer spins. We applied the method to rare spins surrounded by abundant homonuclear spins (*i.e.* protons). DOR averaged out the homonuclear dipolar interactions, so that a CH$_x$ system could be taken as an ensemble of independent CH systems. We could, therefore, detect heteronuclear dipolar interactions for CH$_x$ ($x \geq 2$) spin systems without homonuclear decoupling techniques. In addition, we showed that DOR is also applicable to a solid-state ^{13}C-^{14}N spin pair in order to recover the heteronuclear dipolar interaction that was removed by sample spinning.

Equipment Development Center

VIII-K Development of "IMS Machines"

The technical staff of the Equipment Development Center is partly engaged in planning, researching, designing and constructing "IMS machines." This machine, crowned with the acronym of the Institute for Molecular Science, is a high-tech experimental instrument, with emphasis on new technical idea and co-operative work with members inside and outside the Institute including those in industries. We collect suggestions of new instruments once every year from all of the members of IMS.

In this fiscal year, 1999, three project themes (1 thorough 3) were adopted as IMS machines. IMS machine projects 4 (IMS machine 1998) was completed, and project 5 (IMS machine 1998) is under way.

1. **Sorption-pump-type Large-scale Dilution Refrigerator**
   (proposed by Hideo SHIBAYAMA and Takuhiko KONDOH)
2. **Vacuum-chamber-based High Voltage Application Apparatus to Fabricate Wide-range Nonlinear Optical Wavelength Converters**
   (proposed by Sunao KURIMURA, Takunori TAIRA, Kazuhiro KOBAYASHI and Mitukazu SUZUI)
3. **High-speed Array Detector**
   (proposed by Kazuo WATANABE and Hisashi YOSHIDA)
4. **Thin Shaped Cryostat for Opt-magnetic Measurement**
   (proposed by Shinji IZUMIDA and Takuhiko KONDOH)
5. **Preparation and Transfer System for Ice-embedding Sample**
   (proposed by Shinji HASEGAWA, Kazuhiro KOBAYASHI and Mitukazu SUZUI)

VIII-K-1 Vacuum-Chamber-Based High Voltage Application Apparatus to Fabricate Wide-Range Nonlinear Optical Wavelength Converters

KURIMURA, Sunao; TAIRA, Takunori; KOBAYASHI, Kazuhiro; SUZUI, Mitsukazu

This project aims at development of a vacuum-chamber-based high voltage application apparatus, which allows precise fabrication of a ferroelectric domain pattern in nonlinear optical materials. The reversal of ferroelectric spontaneous polarization is accompanied by the change of the sign of nonlinear optical coefficient, which enables quasi-phase matching (QPM) in wavelength conversion of laser light. QPM, where the period of the domain pattern corresponds to the generated wavelength in optical parametric oscillator, is an universal method to realize phase matching artificially at arbitrary wavelength (Figure 1). Periodic electrodes defined by photolithography are transferred to the domain pattern if the fidelity, affected by the atmosphere such as insulator, electrode materials, and temperature of a crystal, is reasonable (Figure 2). A widely-spread conventional technique using liquid electrodes is simple and easy, but it greatly increases the conductivity between electrodes, leading to the poor fidelity with expanded domains. While our experimental results on poling indicated the atmosphere of insulating oil and photoresist were not appropriate for high fidelity, vacuum atmosphere is an ultimate candidate to suppress surface conductivity. Temperature of the material, another important parameter, affects the domain-nucleation density and the domain wall velocity; temperature control is essential in the system. *Vacuum-based poling apparatus covering wide temperature range*, is a challenging and promising project in fabrication of QPM devices.

We so far designed the apparatus and mainly built the vacuum-related section. Requirements for this system are summarized in Table 1. The poling system consists of three parts: a vacuum chamber, a high voltage supplier, and a temperature controlling unit. The vacuum chamber with 35 cm diameter and 32 cm height was built and high-speed vacuum pumps, a rotary pump and a diffusion pump were equipped into the system. The custom-made flanges were installed to fit the pumps with high exhaust velocity to the chamber. The carefully-checked vacuum system achieved 1×10^{-7} Torr and met our vacuum requirement in such a large chamber. It is now in the final stage of other mechanical parts assembly and will be completed at the end of this August. Another checking point was the ability of high voltage application. Since the required voltage for poling is 22000 V, which is not a low hurdle, we carefully chose shielding electric parts to meet our specification. Specially-designed flanges were provided for electric connection to fit the system. The final difficulty that we are now facing with, is in a crystal mount in a copper setting with heater and cooling pipes to stabilize the temperature. We are planning to place designed cooling pipes to obtain temperature uniformity and a sheathe-shaped heater to meet the short response time as shown in Figure 4. We expect that the assembly will be finished at the end of August and total system will get ready as early as the end of September. We appreciate kind cooperation and meaningful suggestions from all related persons.

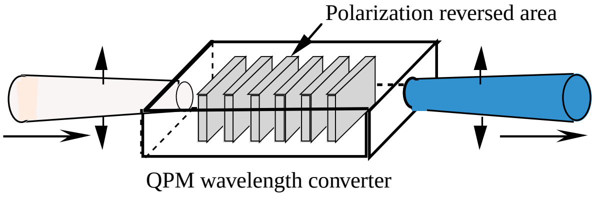

Figure 1. QPM wavelength converter to be fabricated by the vacuum-chamber-based high voltage application apparatus.

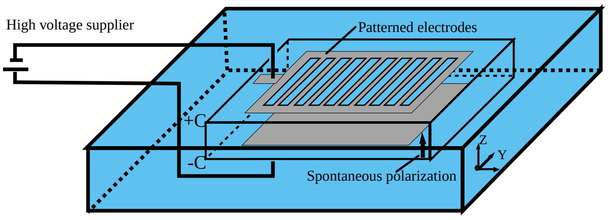

Figure 2. Fabrication method of a periodically poled QPM device.

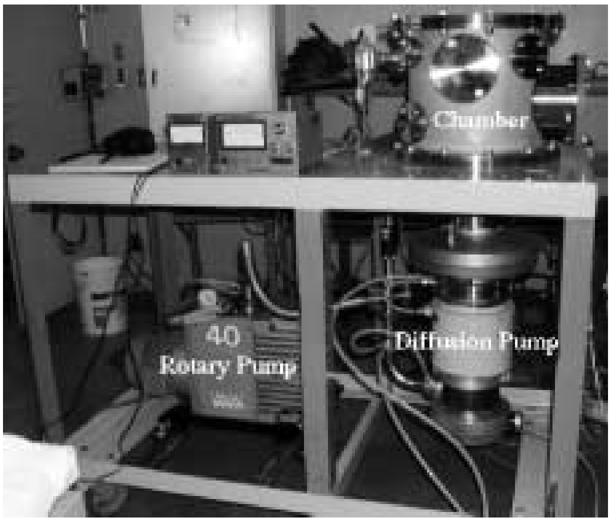

Figure 3. Overall picture of the vacuum system.

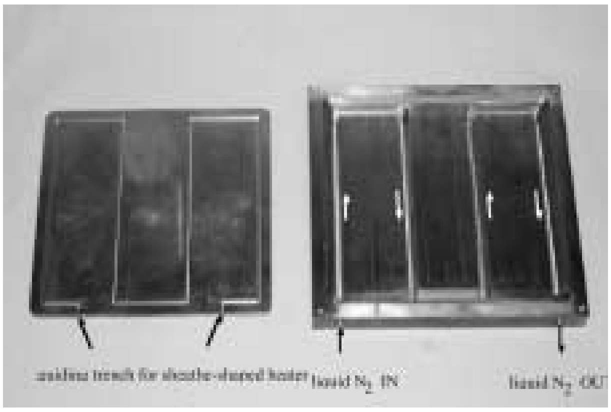

Figure 4. Crystal mount with the cooling pipes and the sheathe-shaped heater. The geometry is designed to have uniform temperature distribution and short response time.

Table 1. Requirements for the apparatus.

Voltage (V)	Vacuum (Torr)	Temperature (°C)	Crystal size
24000	10^{-3} ~ 10^{-7}	–180 ~ 150	3 inch Φ

VIII-L Development of New Laser Materials

VIII-L-1 Deep-Ultraviolet Uight Amplification within a Nanometer-Sized Layer

ASAKA, Shuji; ITOH, Minoru[1]; KAMADA, Masao
([1]Shinshu Univ.)

Light amplification in the deep-ultraviolet region within a nanometer-sized layer is confirmed in mixed rubidium-cesium chloride crystals at room temperature. The probe laser light, which falls on the 275-nm band of Auger-free luminescence arising from radiative transition of the Cl 3p valence electrons into the Cs 5p core holes, is enhanced in intensity when the deep-lying Rb 4p core electrons are pumped into the conduction band by undulator radiation from UVSOR electron storage ring. The obtained enhancement factor roughly corresponds to an amplification coefficient of 7×10^3 /cm, which is much higher than those of typical solid-state lasers. It is emphasized that the amplification occurs in a surface layer as thin as about 20 nm, and that the inverted population between the valence and core bands is realized with any pump power. The present observation may open a new way for nanolaser fabrication.

Ultraviolet Synchrotron Orbital Radiation Facility

VIII-M Development of the UVSOR Light Source

VIII-M-1 New Lattice for UVSOR

KATOH, Masahiro; HAYASHI, Kenji; HONDA, Toru[1]; HORI, Yoichiro[1]; HOSAKA, Masahito; KINOSHITA, Toshio; KOUDA, Shigeru; TAKASHIMA, Yoshifumi; YAMAZAKI, Jun-Ichiro
([1]KEK-PF)

New magnetic lattice has been designed for UVSOR. It can be realized without changing the circumference and the overall shape of the ring. An emittance of 27 nm-rad can be achieved, which is smaller by a factor of 6 than the present value. The number of straight sections will be doubled. Six straight sections will be available for insertion devices. All of them have small betatron function in vertical and are suitable for short period and narrow gap undulators, which are able to produce high brilliance soft X-rays. The new lattice has a dynamic aperture sufficiently large for injection and storage. An improvement on the main RF cavity as well as the use of the existing third harmonic RF cavity for bunch lengthening will make beam lifetime sufficiently long against strong Touschek effect.

VIII-M-2 Development of Longitudinal Feedback System for a Storage Ring Free Electron Laser

KODA, Sigeru; HOSAKA, Masahito; YAMAZAKI, Jun-Ichiro; KATOH, Masahiro; HAMA, Hiroyuki[1]
([1]Tohoku Univ.)

A longitudinal feedback system for a storage ring free electron laser has been developed at the UVSOR. Instantaneous temporal deviation of the FEL optical pulse with respect to the electron bunch is measured in the frequency domain by detecting a phase between higher harmonic components of respective revolution frequencies. The phase deviation is fed back to control the storage ring rf frequency so as to readjust effective length of the optical cavity. Compensating temporal drift with the feedback system, synchronism between the FEL micropulse and the electron bunches was successfully maintained for reasonably long time.

VIII-N Researches by the USE of UVSOR

VIII-N-1 Photoelectron Spectroscopic Study on Photo-Induced Phase Transition in a Spin Crossover Complex [Fe(2-pic)$_3$]Cl$_2$EtOH

KAMADA, Masao; DOI, Yoichiro[1]; FUKUI, Kazutoshi; HARUYAMA, Yuichi[2]; ASAKA, Shuji; TAYAGAKI, Takeshi[3]; YONEMURA, Naoki[3]; TANAKA, Kouichiro[3]
([1]Fukui Univ.; [2]Himeji Inst. Tech.; [3]Kyoto Univ.)

The purpose of the present study is to investigate the photo-induced phase transition using photoelectron spectroscopy. A single crystal of [Fe(2-pic)$_3$]Cl$_2$EtOH was grown at Kyoto university and was filed in a preparation chamber. It was found that the N-1s spectra are shifted to lower binding-energy side with cooling the sample and laser excitation causes the shift of N-1s to higher binding-energy side. The present experimental results indicate that the photo-induced phase transition of [Fe(2-pic)$_3$]Cl$_2$EtOH is closely related to both Fe and N ions and is more complicate and interesting co-operative phenomenon.

VIII-N-2 Photo-Induced Change in Semiconductor-Vacuum Interface of p-GaAs(100) Studied by Photoelectron Spectroscopy

KAMADA, Masao; MURAKAMI, Junichi[1]; TANAKA, Senku[2]; MORÉ, Sam Dylan; ITOH, Minoru[1]; FUJII, Yasuo[2]
([1]Shinshu Univ.; [2]Osaka City Univ.)

The photo-induced change in the semiconductor-vacuum interface on GaAs (100) and Cs/GaAs(100) has been investigated with core-level photoelectron spectroscopy using synchrotron radiation and a mode-locked Nd:YAG laser. Both Ga-3d and As-3d photoelectron peaks showed transient energy shifts under the laser irradiation without any spectral change. The amounts of the energy shifts were strongly dependent on the sample temperature and the laser photon flux. It is shown that the experimental results can be fitted to a theoretical curve which was derived from the photo-induced band bending scheme in the surface layer of the semiconductor.

VIII-N-3 Excitation Spectra of a Long-Persistent Phosphor SrAl$_2$O$_4$:Eu,Dy in Vacuum Ultraviolet Region

KAMADA, Masao; MURAKAMI, Junichi[1]; OHNO, Nobuhito[2]
([1]Shinshu Univ.; [2]Osaka Electro-Commun. Univ.)

This work has been carried out to know the phosphorescence mechanism of the new-type long-persistent phosphor SrAl$_2$O$_4$:Eu,Dy. Luminescence and excitation spectra were obtained by using vacuum ultraviolet (vuv) light as excitation source. It is suggested that the 450-nm and 520-nm luminescence bands in $SrAl_2O_4$:Eu,Dy excited with the vuv light may be produced by a kind of host-sensitization mechanism. Creation spectrum of the long-persistent phosphorescence in the vuv region was firstly measured by observing the after-glow luminescence. A prominent peak was observed around 200 nm, namely in the low-energy tail of the fundamental absorption edge of $SrAl_2O_4$. Therefore, it is suggested that the phosphorescence mechanism in $SrAl_2O_4$:Eu,Dy may be closely related to the defect formation.

VIII-N-4 Two-Dimensional Imaging Technique for Measuring Translational Energy and Angular Distribution of Ionic Photofragments

GEJO, Tatsuo; NAKAMURA, Eiken; SHIGEMASA, Eiji; SAITO, Norio[1]
([1]ETL)

During the last decade, the dynamics of molecules in the valence energy regime has been investigated by preparing excited state at well-defined energy, and analyzing photoelectron energy and angular distribution of ionic photofragments involved. Two-dimensional (2D) imaging technique is one of the most powerful tools for obtaining this information because 2D data and its simple calculation on the basis of momentum conservation law, provide Newton diagram of photofragments, which leads to dynamical process involved immediately.

The system mainly consists of an accelerator lens, a position sensitive detector (PSD) (Roendek) and an electronic system for data analysis and a computer. After the gas passes synchrotron radiation (SR) region, less than one molecule per one photon beam on the average undergoes ionization and/or dissociation. The direction of polarization of SR is parallel to the axis of TOF tube (10 cm). After the acceleration by the ion lens, ionic fragments fly through the TOF tube and hit the PSD. The determination of the impact position on the detector is based on the time delay between the two signals from each end of the wire behind the MCP. The position is obtained by the subtraction of time when both two signals arrive, providing us its velocity and direction in the center-of-mass frame. The 2D images of N_2^+ after the excitation of the valence electrons were successfully obtained. With this technique, we will try to perform the triple coincidence in the ionic fragmentation following inner-shell excitation.

VIII-N-5 Angular Distribution Measurement of Auger Electrons from Fixed in Space Molecules

GUILLEMIN, Renaud[1]; SHIGEMASA, Eiji; LE GUEN, Karine[1]; CEOLINE, Denis[1]; MIRON, Cataline[1]; LECLERCQ, Nicola[1]; UEDA, Kiyoshi[2]; MORIN, Paul[1]; SIMON, Marc[1]
([1]LURE; [2]Tohoku Univ.)

[*Rev. Sci. Instrum.* in press]

A new experimental setup for the measurement of the angular distribution of energetically selected Auger electrons emitted from fixed in space molecules is presented. The system is based on two identical ion detectors with a small angular acceptance placed respectively at 0° and 90° of the polarization axis of the incident radiation, and a large acceptance double-toroidal electron analyzer combined with a position sensitive detection. It allows to select the molecular alignment for s and p ionization channels in parallel and provides an energy and angle measurement of the outgoing electron. The energy and angular performances as well as the calibration procedure are discussed. Samples of results obtained on the carbon monoxide ionized above the C 1s threshold are presented.

VIII-N-6 Construction of a Varied-Line-Spacing Plane Grating Monochromator at BL-4B

SHIGEMASA, Eiji; GEJO, Tatsuo

In order to realize various spectroscopic investigations in the soft X-ray region (100~1000 eV) with high resolution at UVSOR, a new Varied-line-spacing Plane Grating Monochromator (VPGM) at BL-4B was designed in 1999. The beamline is composed of two pre-focusing cylindrical mirrors (M_0 and M_1), the monochromator (M_2 and G), and a post-focusing toroidal mirror (M_3). The schematic drawing of the whole beamline is presented in Figure 1. Synchrotron radiation is deflected horizontally and focused vertically onto the entrance slit S_1 by M_0. M_1 deflects the radiation vertically and focuses it horizontally. The radiation passing through S_1 is converged by the spherical mirror M_2 on a virtual source at a 4-m distance away from the grating center. Two varied-line-spacing plane gratings G with different groove densities (800 and 267 lines/mm) are interchangeable by a linear-translation mechanism without breaking the vacuum. The grating rotation for scanning wavelength is performed with a sine-bar mechanism. The monochromatized radiation passing through the exit slit S_2 is focused onto the sample position by toroidal mirror M_3. The fabrication of all the optical elements and beamline components has been successfully completed and the practical construction is just beginning to be carried out.

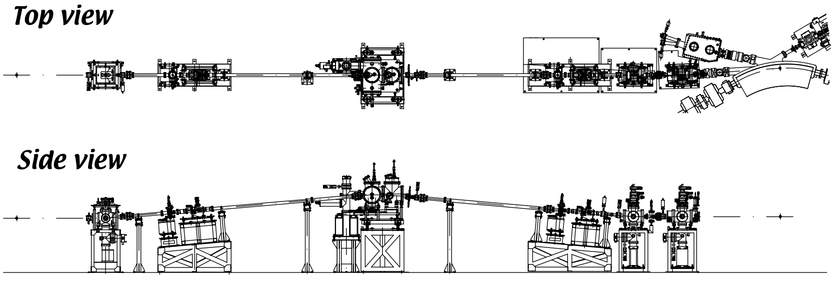

Figure 1. Schematical drawing of the VPGM on BL4B at UVSOR.

Computer Center

VIII-O Theoretical Studies on Electronic Structure and Dynamics of Electronically Excited States in Polyatomic Molecules

VIII-O-1 Theoretical Study of the Potential Energy Surfaces and Bound States of HCP

NANBU, Shinkoh; GRAY, Stephen K.[1]**; KINOSHITA, Tomoko; AOYAGI, Mutsumi**
([1]Argonne Natl. Lab.)

[*J. Chem. Phys.* **112**, 5866 (2000)]

Global, ab initio potential energy surfaces for HCP in its ground 1 $^1\Sigma^+$ (1^1A') and low-lying excited 1^1A", 2^1A', and $1^1\Delta$ (2^1A") electronic states are determined. The multireference configuration interaction method at the double zeta with polarization basis set level is used, although some calculations augmented with diffuse functions are also discussed. Numerous quantum mechanical rovibrational states are then obtained for these surfaces, with emphasis on those corresponding to excited electronic state levels which have not been studied theoretically before. The results agree reasonably well with available experimental data for the 1^1A" state. Futhermore, the presence of certain local minima on the 1^1A" and 2^1A' surfaces leads to one new series of levels on the 1^1A" surface, and two new series on the 2^1A' surface.

VIII-O-2 A Comparative Study of the Quantum Dynamics and Rate Constants of the O(^{3}P) + HCl Reaction Described by Two Potential Surfaces

SKOKOV, Sergei[1]**; TSUCHIDA, Tomoki**[1]**; NANBU, Shinkoh; BOWMAN, Joel M.**[1]**; GRAY, Stephen K.**[2]
([1]Emory Univ.; [2]Argonne Natl. Lab.)

[*J. Chem. Phys.* **113**, 227 (2000)]

Wave packet calculations, using direct and damped-L^2 real propagation methods, of initial state-resolved and cumulative reaction probabilities for the O(^{3}P) + HCl ($^1\Sigma^+$) $\rightarrow$ OH($^2\Pi$) + Cl(^{2}P) reaction are reported. Results are obtained using the recently developed "S4" potential surface of Ramahandran co-workers and, for comparison, the earlier, Koizumi, Schatz and Gordon (KSG) potential energy surface. Most calculations are for total angular momentum $J = 0$, although some $J > 0$ centrifugal sudden results are also obtained. The thermal rate constant and the rate constant for HCl ($v = 1$) are obtained from the $J = 0$ cumulative reaction probability and J-K-shifting, using standard transition-state rotation constants. This type of shifting is justified by examining limited centrifugal sudden calculations. The S4 surface is shown to yield some surprising results. For example, despite a significantly higher ground state adiabatic barrier than the KSG surface, the thermal rate constant is not significantly different from one obtained with the KSG surface, although the one for the vibrationally excited HCl is.

VIII-O-3 Determination of the Global Potential Energy Surfaces for Polyatomic Systems

NANBU, Shinkoh; ISHIDA, Toshimasa[1]**; GRAY, Stephen K.**[2]**; AOYAGI, Mutsumi**
([1]Shizuoka Univ.; [2]Argonne Natl. Lab.)

Computational algorithm of the determination of the global potential energy surfaces for polyatomic systems are developed with using the interpolant moving least squares scheme, which was proposed by Ishida and Schatz [*Chem. Phys. Lett.* **314**, 369 (1999)]. In this scheme, any derivatives in quantum-chemical calculations are not required to construct the surface and in contrast with previously developed schemes based on Shepard interpolation alone. In our new algorithm, the molecular conformations are generated with the Monte Carlo sampling, and then the ab initio calculations for all of the conformations are performed by the parallel computing at the same time. Therefore, we have good advantage for computational time for the normal calculations. Application is made to the tetra-atomic systems, the 2OH $\longleftrightarrow$ H_2O + O reaction.

VIII-O-4 Semiclassical Study of Nonintegrable Systems

TAKAMI, Toshiya

We study nonadiabatic processes in classically nonintegrable systems such as 2D billiards and kicked rotators to reveal essence of the dynamical characters in highly excited states of molecules. Theoretical treatment of the nonadiabatic transition between adjacent levels through an avoided crossing was studied first in pioneering works by Landau, Zener, *etc*. In the nonintegrable systems, however, the Landau-Zener formula cannot be applied because those systems contain essentially many levels, *i.e.* nonadiabatic couplings between adiabatic states cannot be ignored everywhere.

On numerical experiments in nonintegrable systems, we found non-Landau-Zener behavior, and we pointed that the phenomenon arises from nonadiabatic couplings between eigenstates on the endpoints. In order to describe the extra-transition theoretically, we introduce "boundary expansion" to get higher order terms of the nonadiabatic couplings. By the use of the expansion, we construct a new base which can describe nonadiabatic transition locally even in nonintegrable systems. This base is shown to be the same as superadiabatic base by M.V. Berry.

VIII-O-5 Development of *ab initio* MD Method Based on the Direct Evaluation of CAS-SCF Energy Derivatives

KINOSHITA, Tomoko; NANBU, Shinkoh; AOYAGI, Mutsumi

We have been developing an *ab initio* molecular dynamics program to investigate the reaction dynamics of large scale problems, *i.e.*, surface reactions, and biological systems. Since we employed parallelized version of McMurchie-Davidson’s algorithm to evaluate both AO integrals and derivatives of AO integrals, the most time consuming step of electronic structure calculations has been carried out in a tractable way. At each time steps of MD calculations, we obtain analytical energy derivatives of complete active space (CAS) wavefunctions. We continue to develop the codes for non adiabatic and spin-orbit coupling matrix elements. Our direct method can easily extend to apply a number of interesting problems including non adiabatic reactions and spin forbidden processes. For the benchmark test purposes of this program system, the low-lying singlet and triplet surfaces of $CH^+ + H_2 \longleftrightarrow C + H_3^+$ is investigated by using direct *ab initio* molecular dynamics.

RESEARCH FACILITIES

The Institute for Molecular Science includes five research facilities. This section describes their latest equipment and activities. For further information please refer to older IMS Annual Review issues (1978–1999).

Laser Research Center for Molecular Science

This Center was established in 1997 by reorganization of a part of the Instrument Center. The new Center is composed of three research groups which are asked to develop new lasers suitable for pioneering researches in the new field of molecular science. The three groups are

1. Advanced Lasers for Chemical Reaction Studies,
2. Advanced Lasers for Synchrotron Radiation Applications

and

3. Advanced UV and IR Tunable Lasers.

The Laser Research Center are equipped with profitable all-solid-state light sources in various temporaland spectral regions, including femtosecond and nanosecond Optical Parametric Oscillators (OPO). The synchronously femtosecond OPO (OPAL; SPECTRA PHYSICS) is tunable from 1.1 µm up to 1.6 µm. The nanosecond OPO has extraordinarily wide tuning range form 420 nm down to 2.2 mm. The Laser Center also has a fluorescence analyzer (FLUOROLOG2; SPEX) which is composed of a xenon lamp house, and double and single monochromators for spectroscopy. The detector is changeable by rotating a mirror (CCD and PM). Using these instruments, one can carry out various experiments not only in the ultrafast temporal region but also in the steady-state photon-counting region.

Research Center for Molecular Materials

The center was established by reorganization of Chemical Materials Center, Low-Temperature Center, and a part of Instrument Center in 1997. This center plays important roles in the preparation of novel chemical materials, management of chemicals in the institute, and support of liq. N_2 and He. Four research groups in the center cover the following four general research fields. 1) Preparation of Novel Heterocyclic Compounds and their Molecular Assemblies. 2) Electronic Structures and Reactivities of Metalloproteins. 3) Molecular Design of Artificial Photosynthesis System. 4) Organic Molecular Materials with Novel Electronic Properties. In addition to the research activities, the center supports the instruments including high filed NMR, EPR and MALDI-TOF mass spectrometers, SQUID, X-ray diffractometers. The center accepts the elemental analyses and mass spectrometric measurements.

Equipment Development Center

A number of research instruments have been designed and constructed at the mechanical, electronic and glass work sections in this Facility. Examples of our works in this fiscal year are listed below.

Pulsed discharge nozzle attachment
Clamp-type diamond anvil high pressure cell
NMR probe for anisotropic measurements
New scaler system for sine bar mechanisms of UVSOR BL7B beamline
Polyethylene lens for millimeter wave spectroscopy
Data processing program for thermoelectric power measurement
TE module temperature controller
High speed valve controller for molecular beam source
Multichannel microampere constant current source
The surface profiler for optical elements
Thin cell for X-ray
Vacuum line apparatus
Quartz cell

Development of IMS Machines

Equipment Development Center is also engaged in developing IMS Machines. This activity is described in detail in section “RESEARCH ACTIVITIES.”

Ultraviolet Synchrotron Orbital Radiation Facility

The UVSOR accelerator complex consists of a 15 MeV injector linac, a 600 MeV booster synchrotron, and a 750 MeV storage ring. The magnet lattice of the storage ring is the so-called double-bend achromat. A harmonic cavity was commissioned in spring 1993 to suppress longitudinal coupled-bunch instability by Landau damping. The double RF system is routinely operated for user beam time, and the lifetime of the beam has been improved to about 5 hours at 200 mA. The storage ring was divided into four sections by gate valves in spring 1995 in order to make a scheduled shutdown easier. The baking system was also replaced by new one including a controllable indirect heating. The RF power amplifier systems of the booster synchrotron and the storage ring were renewed to solid-state systems in 1996 in order to have more stable operation and easier maintenance. The storage ring is normally operated under multi-bunch mode with partial filling. The single bunch operation is also conducted about three weeks in a year to provide pulsive SR for time-resolved experiments. A resonance transverse kicker was installed in spring 1997 to keep the bunch purity and to study phase dynamics. Typical beam currents under multi-bunch and single-bunch modes are 200 mA and 50 mA, respectively.

The UVSOR storage ring consists of eight bending magnets and three insertion devices. The bending magnet having 2.2 m in radius provides the synchrotron radiation, the critical energy of which is 425 eV. The superconducting wiggler is a wavelength shifter type. The 4T magnetic field can provide soft x-rays up to 6 KeV. A planar undulator consists of 24 pairs of permanent magnets, a period of which is 84 mm. The fundamentals from the undulator provide quasi-monochromatic intense radiation in the range from 8 to 52 eV. A helical undulator was installed to one of the four straight sections of the storage ring in 1996. An optional version of the helical undulator is a helical optical klystron, which is powerful for a free electron laser experiment. The helical undulator consists of two sets of permanent magnets producing a vertical magnetic field and four sets of permanent magnets making a horizontal magnetic field. The four sets of magnets can move in the transverse direction to switch the helicity of the circular polarization. The helical undulator can provide the perfectly circular polarization in the range of 2–45 eV, and the elliptic polarization up to 200 eV. Unfortunately, the superconducting wiggler was shutdown at the beginning of June in 1999 due to the serious problem of the cryogenic system.

Initially 15 beam lines were constructed giving priority for the study of the four fields; “Spectroscopy,” “Photoelectron spectroscopy,” “Photochemical reaction,” and “Elementary process of chemical reaction.” Several years later, 4 beam lines were added to expand the research to the fields, “Solid and surface photochemical reaction” and “Photochemical material processing.” In recent years, “Combination of synchrotron radiation with laser beam” was proposed to add in the important research fields.

The UVSOR have discussed the improvements and upgrades of the beam lines with users. The workshops concerning on VUV beam lines for solid-state research, beam lines for soft x-ray, chemical reaction, and gaseous phases, beam lines for infrared and far infrared regions, grazing incidence monochromators, temporal structure of SR and its application, and gaseous phase experiments, were held in 1994, 1995, 1996, 1997, 1998, and 2000, respectively. About one third of beam lines have been upgraded in recent years. A Seya-Namioka monochromator at beam line 7B has been replaced by a normal-incidence monochromator to improve a resolving power and spectral range for solid-state spectroscopy. Another Seya-Namioka monochromator at beam line 2B2 has been also replaced by a Dragon-type monochromator for gaseous experiments in VUV and EUV ranges. A multi-layer monochromator installed to the beam line 4A has provided good spectral distribution for photochemical reaction experiments. A 15-m SGM monochromator, which took back of a glancing-incidence monochromator at BL8B1 has been used for solid and gaseous phase experiments with high resolving power in EUV range. A Bruker FT-IR interferometer has been installed to beam line 6A1 besides the old FT-FIR of a Martin-Puplett type, and then the improved system can cover the wide wavelength range from 1 µm to 3 mm. A new monochromator (SGM-TRAIN) constructed at beam line 5A has been used for the experiments on solid and surface with high resolving power. The beam line 2A, which has provided VUV photons for gaseous experiment for a long time, is renewed for the use of the bio-specimens. The beam line 6B, which has been constructed for IR experiments, is under renewal for nano-scale photochemical reaction experiments. The rearrangement of the beam lines 4A and 4B has started to construct high-resolution beam line for gaseous phase at BL4B. The UVSOR has now two soft-x-ray stations equipped with a double-crystal monochromator, eight extreme ultraviolet stations with a glancing incidence or a plane-grating monochromator, four vacuum-ultraviolet stations with a Seya-Namioka-type or a normal incidence-type monochromator, a (far) infrared stations equipped with FT interferometers, a multi-layer monochromator, and four white-light stations without monochromator.

The photoelectron spectroscopy combined with SR is one of the powerful techniques to investigate electronic structures. Several kinds of photoelectron spectrometers are working or ready to work in UVSOR: High-performance electron analyzer at soft x-ray beam line 1A, Two-dimensional spectrometer at VUV beam line 3B, Angle-resolved spectrometer at EUV beam line 8B2, and Spin- and angle-resolved photoelectron spectrometer at helical undulator beam line 5A besides a high-resolution type. Photoelectron microscopy system is under construction at BL6A2, where the optical system is modified to have a good demagnified spot.

In Spring 2000, we had one-month shutdown to replace the first manual valve at BL4A, 4B, 5B, and 6B. The purpose is to install new pre-chamber systems for photochemical reaction and gaseous experiments at BL4A, 4B, and 6B. On this occasion, the vacuum system for FEL experiment was also improved, with the break of the vacuum in the third long straight section.

The examination of the radiation protection system in IMS has been conducted in autumn 1999 by the Ministry of Science and Technology. Since the accident happened at a nuclear-fuel company in 1999, the examination was very strict even for our facility. According to their advice, we had confirmed our radiation protection system. The radiation monitor system was also improved in Spring 2000. The gaseous, dust, and area monitors were renewed since the initial installation in 1983.

There were lots of troubles, as usual, but they did not affect the beam times fortunately. Our interlock valve system could succeed in protecting the storage-ring from the air-leakage at BL3B, and from the accidental electric leakage at BL5B. The alarm/emergency call system and also the education/safety system for beginner users work well. New version of the UVSOR guidebook was published for this purpose. The UVSOR facility strongly asks all users to conduct their experimental procedures according to the beam line manuals and the guidebook.

The persons who want to use the open- and the in-house beam lines are recommended to contact with the stationmaster or supervisor and the representative, respectively. The persons who want to know updated information of the UVSOR facility are requested to open http://www.uvsor.ims.ac.jp/.

Computer Center

Since April 1 of 2000, Computer Center of IMS has been reorganized as Research Center for Computational Science in Okazaki National Research Institute. The main super-computers at the Center has been replaced from NEC SX-3/34R to combined vector and scalar parallel system of Fujitsu VPP5000 and SGI 2800. VPP5000 system consists of 30 vector CPU-nodes, and has 256 GB of main memory. SGI 2800 has 256 CPU and 256 GB of memory. With the general purpose computer system NEC SX-5 and IBM SP2 installed last year, these vector and parallel computers are actively utilized mainly for the large scale molecular science simulations. The computers are linked to international networks through Science Information Network(SINET). About 28% of the computer time is used by the research staff at IMS, and the remaining 72% is given out as research grants to scientists outside the institute in molecular science and related field. As of March 1999, the number of project group was 169, consisting of 659 users.

The library programs of the Center amount to 805. Among them, more than 200 programs can be executed immediately. Information on the library program can be found on our center’s home-page (http://ccinfo.ims.ac.jp/). The Quantum Chemistry Literature Database (QCLDB) has also been developed by the QCLDB group in collaboration with the staff member of computer center, and this database can be accessible through our home page.

SPECIAL RESEARCH PROJECTS

IMS has special research projects supported by national funds. Three projects in progress are:
(a) Chemical Reaction Dynamics
(b) Molecular Photophysics and Science
(c) Novel Material Science

These three projects are being carried out with close collaboration between research divisions and facilities. Collaborations from outside also make important contributions. Research fellows join these projects.

(a) Chemical Reaction Dynamics

Folding Mechanism of Protein Molecules Studied by Generalized-Ensemble Algorithms

OKAMOTO, Yuko; SUGITA, Yuji; NAGASHIMA, Takehiro; NISHIKAWA, Takeshi; MITSUTAKE, Ayori; YODA, Takao

Proteins are the most complicated molecules that exist in nature. Since protein structures are closely related to their biological functions, the understanding of their folding mechanism from the first principles is not only very challenging but also very important a problem in theoretical molecular science. To be more specific, it is widely believed that three-dimensional structure of proteins is determined by their amino-acid sequences. However, nobody has succeeded in predicting it solely from the amino-acid-sequence information (prediction from the first principles).

There are two reasons for the difficulty. One reason is that the inclusion of accurate solvent effects is non-trivial because the number of solvent molecules that have to be considered is very large. The other reason for the difficulty is that there exist huge number of local minima in the energy function, and conventional simulation techniques will necessarily get trapped in one of the local minima without ever finding the energy global minimum. Generalized-ensemble algorithms are new simulation algorithms that can alleviate this difficulty (or reviews, see References 1 and 2).

The goal of the present project is to further develop and test the effectiveness of generalize-ensemble algorithms in the protein folding problem and to succeed eventually in the prediction of tertiary structures of proteins from the first principles. We have been developing new generalited-ensemble algorithms. We found that the replica-exchange method and its extension are particularly promising.

References

1) Y. Okamoto, *Recent Res. Devel. Pure & Appl. Chem.* **2**, 1 (1998).
2) U. H. E. Hansmann and Y. Okamoto, *Ann. Rev. Comput. Phys. VI*, D. Stauffer, Ed., World Scientific, pp. 129–157 (1999).

Development and Applications of Basic Theories for Chemical Reaction Dynamics and Their Control

NAKAMURA, Hiroki; ZHU, Chaoyuan; NOBUSADA, Katsuyuki[1]; TERANISHI, Yoshiaki[2]; MISHIMA, Kenji; NAGAYA, Kuninobu[3]; KAMISAKA, Hideyuki[3]; MIL'NIKOV, Gennady V.[4]

([1]Hokkaido Univ.; [2]Inst. Phys. Chem. Res.; [3]GUAS; [4]IMS and Inst. Struct. Macrokinetics, Russia)

Reaction dynamics studies have now been extended to electronically nonadiabatic reactions. It is desirable to formulate accurate semiclassical theories by incorporating the Zhu-Nakamura theory of nonadiabatic transition due to potential curve crossing. Such theories should be able to deal with large reaction systems of chemical interest. In order to develop such theories, we have to investigate their validity first by applying to small systems which can be treated quantum mechanically accurately. As a such prototypical system, we have chosen the DH_2^+ reaction system in which two potential energy surfaces are involved. The quantum mechanical accurate numerical studies have been almost finished. As for the semiclassical treatment, we have first implemented the trajectory surface hopping method with use of the Zhu-Nakamura theory. The preliminary results are very promising, since the Zhu-Nakamura theory can deal with classically forbidden transitions properly. We further plan to incorporate the Zhu-Nakamura theory fully with all phases taken into account into semiclassical propagation methods.

In attempt to formulate hopefully a sort of unified theory of nonadiabatic transition which can cover both crossing and non-crossing cases, we have been working on exponential potential models. We have formulated a general framework for the case that the diabatic potentials and coupling are given by the same exponential function.

Control of molecular processes by manipulating time-dependent external fields would be one of the most important subjects in the coming new century. Using the intriguing phenomenon of complete reflection and our new idea of periodical sweeping of an external field to control nonadiabatic transitions, we have been working on controlling molecular processes such as photodissociation by lasers. The idea of periodic sweeping can also be applied to NMR such as cross polarization and may develop a methodology more effective than the conventional one.

The Energy Landscape for Solvent Dynamics in Electron Transfer Reactions: A Minimalist Model

TANIMURA, Yoshitaka; LEITE, Vitor[1];

ONUCHIC, Jose[2]
([1]Univ. Estadual Paulista; [2]Univ. California, San Diego)

We employ the minimalist models for the solvent, *i.e.*, simpler models that include includes the basic features of a rough-energy landscape: multidimensional degrees of freedom, with each solvent molecule being treated independently; a disordered energy landscape with multiple minima; and a polarizable medium around a charged cavity.

Above the thermodynamic glass transition, it recovers the continuum dielectric limit, where the Marcus theory can be applied. At low temperatures, a polarization-dependent glassy phase appears and a slow non-self-averaging dynamics plays a role. Further investigation is made to address the validity of a collective reaction coordinate representation. Its connection to the study of energy landscapes opens a new theoretical framework to study the questions above.

Constructing Molecular Theory of Chemical Processes in Solution

HIRATA, Fumio; SATO, Hirofumi; KOVALENKO, Andriy; AKIYAMA, Ryo; SETHIA, Ashok; SUMI, Tomonari; IMAI, Takashi; HARANO, Yuichi; IMAMURA, Chikara[1]**; NISHIYAMA, Katsura**[2]
([1]Yamaguchi Pref. Univ.; [2]Osaka Univ.))

Our current research interests and activities are concentrated upon four important chemical processes in solution, in each of which solvent plays essential role: A. the electronic structure of a molecule in solution, B. solvation thermodynamics of protein and related molecules, C. characterization of spatial and temporal density fluctuation in molecular liquids, D. molecular theory of electrode-solution interface. The RISM theory, an integral equation theory of molecular liquids, is our main machinery to attack the problems, which is coupled with other theoretical methodologies including the ab initio molecular oribital method, moelcular simulations, the generalized Langevin equation, and the density functional theory (DFT). Problems on which we have been wroking along the four lines are as follows:

1. Solvent effect on keto-enol tautomers of acetyl-acetone in aqueous solution.
2. Diels-Alder reactions in ambient and supercritical water.
3. Excited state dynamics of a molecule in polar solvent.
4. Solvent effect on NMR chemical shift in polar and non-polar solvents.
5. Partial molar volume of biomolecules in aqueous solution.
6. Salt effect on stability of a dipeptide in water.
7. Stability and folding of peptide and protein in aqueous solution.
8. Solvation dynamics and thermodynamics of ions.
9. Non-equlibrium free energy surface related to electron transfer reactions.
10. Dynamical coupling between intra- and inter molecular motions in liquids.
11. Description of collective excitation in liquds by interaction site model.
12. Time correlation function described by the interaction-site model of molecular liquids.
13. Dynamics of an ion in water.
14. Microscopic characterization of metal-liquid interface.
15. Path integral theory of a hydrated electron.

Imaging of Chemical Dynamics

SUZUKI, Toshinori; KOHGUCHI, Hiroshi; KATAYANAGI, Hideki

Femtosecond time-resolved photoelectron imaging method has been developed, for the first time. The scattering distributions of photoelectrons in [1+1'] REMPI of NO and [1+2'] REMPI of Pyrazine have been observed. Ultrafast decay of optically-prepared S_1 character and corresponding build-up of triplet character were visualized. Rotational coherence effect has been clearly observed in photoelectron intensity and angular distribution. Crossed beam ion imaging method has been applied to inelastic scattering of NO with Ar at the collision energy of 63 meV, and the differential cross sections were compared with scattering calculations by Millard Alexander using the newest *ab initio* surface.

Electronic Structure and Decay Mechanism of Inner-Shell Excited Molecules

KOSUGI, Nobuhiro; HATSUI, Takaki

This project is being carried out in collaboration with UVSOR and Photon Factory (KEK-PF). We are interested in ionic fragmentations and electron emissions via inner-shell excitation of molecules and in their polarization dependence. In high-resolution C1s photoabsorption spectra of acetylene, C_2H_2, we have found that the lowest σ_u* state is embedded in the $3s\sigma_g$ Rydberg state and is dissociative through interaction with the lowest π* state with bent geometry due to the Renner-Teller effect, that the $3p\sigma_u$ and $3p\pi_u$ Rydberg states are clearly resolved and show different vibrational structures, and that the C1s σ_g and σ_u ionization channels show different ionization thresholds, to which the Rydberg series are converging. We will extend our experimental and theoretical approaches to several open-shell and unstable molecules.

Time-Resolved Spectroscopic Study of Photochemical Dynamics in Condensed Phase

TAHARA, Tahei; TAKEUCHI, Satoshi; FUJINO, Tatsuya; ARZHANTSEV, Sergei; MIZUNO, Misao; FUJIYOSHI, Satoru

Time-resolved spectroscopy is one of the most powerful tools for the studies of chemical reactions. It enables us to directly observe the temporal changes occurring in the course of chemical reactions. Recent progress of time-resolved spectroscopy relies on the drastic advance of the laser technology, and we are now able to examine ultrafast dynamics of the primary chemical processes with pico/femtosecond time-resolution. The aims of this project are (1) development of new technique and method in time-resolved spectroscopy, and (2) application of pico/femtosecond spectroscopy to the study of dynamics of molecules in condensed phase. Our research activities of this year can be summarized as follows, in the order of time-resolution of the experiments. First, we constructed experimental setups utilizing 'extremely-short' optical pulses (Δt ~ ten – a few tens of femtoseconds) and carried out time-resolved measurements to observe vibrational coherence (wavepacket motion) of the molecules in the excited state and the ground state. Especially, the vibrational coherence in the S_1 state of *trans*-stilbene is examined and discussed in detail. Secondly, with use of time-resolved fluorescence spectroscopy having a few hundreds femtoseconds time-resolution, we studied excited-state proton transfer of anthraquinone derivatives, isomerization of azobenzene, and relaxation process of the S_2 state of zinc(II) prophyrins. Thirdly, we applied picosecond time-resolved Raman spectroscopy to the study of photochemical dynamics of several fundamental aromatic molecules including p-nitroaniline. In addition, we examine the excitation profile of resonance hyper-Raman scattering of *all*-trans retinal by using picosecond amplified laser pulses. Finally, we started construction of a new apparatus for femtosecond infrared spectroscopy.

Production of Optical Knife—Site-Specific Fragmentation Following Core-Level Photoexcitation

NAGAOKA, Shin-ichi

Monochromatized synchrotron radiation can excite core electrons of an atom in a specific chemical environment selectively, discriminating the core electrons from those of like atoms having different chemical environments. This site-specific excitation often results in site-specific fragmentation, which is of importance in understanding localization phenomena in chemical reactions and which is potentially useful for synthesizing materials through selective bond breaking. Synchrotron radiation can indeed play the part of an optical knife for molecules. When bond dissociation around an atomic site is required in the synthesis, one can use the optical knife that has the photon energy corresponding to the specific excitation of that site. These site-specific phenomena have been of considerable interest to many researchers. To elucidate the site-specific fragmentation, we have used photoemission spectroscopy, the energy-selected-photoemission photoion coincidence method, and *ab initio* molecular-orbital calculations, and have studied site-specific phenomena in the C:1s and Si:2p photoexcitation of organic and organosilicon molecules condensed on a Si surface and in the vapor phase [$X_3Si-(CH_2)_nSi(CH_3)_3$ (X = F or Cl, n = 0–3), *trans*-F_3-$SiCH=CHSi(CH_3)_3$, $F_3SiC\equiv CSi(CH_3)_3$, CF_3CH_3, CF_3-$CH(OH)CH_3$ and $CF_3CD(OH)CH_3$]. An electron-ion coincidence spectrometer for vapor-phase site-specific-dynamics study is also being built now. The equipment consists of an electron gun, a cylindrical mirror analyzer (CMA) and a reflectron-type time-of-flight ion mass analyzer.

Theoretical Study on the Unimolecular Reaction Dynamics of Acetyl Radical $CH_3CO \rightarrow CH_3 + CO$

ITO, Masakatsu; NANBU, Shinkoh; AOYAGI, Mutsumi

We investigate the dissociation dynamics of acetyl radical with the classical trajectory method using the electronic model hamiltonian based on our ab initio calculations. At each time step in our classical trajectory calculations, the electronic hamiltonian is diagonalized to obtain the instantaneous adiabatic states and then the Hellmann-Feynmann forces are evaluated to drive the nuclear coordinates. Our hamitonian is based on the valence bond (VB) description of the electronic wavefunctions. Since acetyl radical and its dissociative products have different bonding characters, the wavefunctions along the dissociation process are approximately expanded by two correponding VB bases states. We found that the energy of the CCO bending excitation does not efficiently transfer into the dissociation coordinate (C–C) over the time period of 30 ps. It is suggested that this slow transfer or redistribution of internal energy could be one of the important sources for the discrepancy between the RRKM rate constants and the experimental results.

(b) Molecular Photophysics and Science

(1) Laser Cooling and Trapping of Metastable Helium Atoms
(2) Laser Spectroscopic Studies of Atoms and Ions in Liquid Helium

MORITA, Norio; MORIWAKI, Yoshiki; KUMAKURA, Mitsutaka

In studies on "laser cooling and trapping of metastable helium atoms," the design and construction of a new laser cooling and trapping apparatus are now in progress. With this new apparatus we can expect to confine a much larger number of metastable He atoms at much lower temperature. On the other hand, in "laser spectroscopic studies of atoms and ions in liquid helium," we have successfully measured some excitation and emission spectra of Yb^+ ions in liquid helium, and have well understood their spectral properties through our theoretical analyses (see II-B-1). Moreover, motivated by one of the results of this experiment, we have also measured fine structure changing cross sections of Ca^+ and Sr^+ ions in collisions with He atoms (see II-B-2).

Structures of Reaction Intermediates of Bovine Cytochrome c Oxidase Probed by Time-Resolved Vibrational Spectroscopy

KITAGAWA, Teizo

Structures of reaction intermediates of bovine cytochrome c oxidase (CcO) in its reactions of the fully reduced form with O_2 and the fully oxidized form with H_2O_2 were investigated with time-resolved resonance Raman (RR) and infrared spectroscopy. Six oxygen-associated RR bands were observed for the reaction of CcO with O_2. The isotope shifts for an asymmetrically labeled dioxygen, $^{16}O^{18}O$, have established that the primary intermediate of heme a_3 is an end-on type O_2 adduct, and the subsequent intermediate (P) has an oxoiron heme with Fe=O stretch ($\nu_{Fe=O}$) at 804/764 cm^{-1} for $^{16}O_2/^{18}O_2$ derivatives, although so far a peroxy structure has been postulated for it. The P intermediate is converted to the F intermediate having $\nu_{Fe=O}$ at 785/751 cm^{-1} and then to the ferric hydroxy species with $\nu_{Fe–OH}$ at 450/425 cm^{-1} (443/417 cm^{-1} in D_2O). The conversion rate from P to F intermediates is significantly slower in D_2O than in H_2O. The P intermediate was also generated by incubation of fully oxidized CcO with CO and O_2 but the F was not. The reaction of oxidized CcO with H_2O_2 yielded the same oxygen isotope-sensitive bands as those of P and F, indicating the identity of intermediates. Infrared spectra revealed the occurrence of deprotonation of one carboxylic acid side chain and protonation of the other upon deligation of a ligand from heme a_3. The protonation was not seen with a mixed valence enzyme. UVRR spectrum excited at 244 nm indicated deprotonation of Tyr244 at weakly alkaline pH and gave a prominent band assignable to the linoleoyl-type cis C=C stretch of phospholipids which must be tightly bound to purified CcO. The intensity titration with phosphatidylcholines indicated that twenty-one fatty acids chains are attached to one CcO molecule.

Laser Raman Beat Detection of Magnetic Resonance

KATO, Tatsuhisa; MATSUSHITA, Michio

Laser Raman beat detection is a coherent optical-RF double resonance technique where the optical and RF field induce coherence within a three level system and a resultant Raman beat signal is detected using heterodyne detection. This technique can be applied to the study of electron paramagnetic resonance and nuclear magnetic resonance not only in the ground state of a molecule but also in the electronic excited state.

There are some causes to hide the Raman beat signal, that is, the inhomogeneity of the circumstance of the molecule, the fluctuation of the applied field, and the interference by the crystal phonon. It is the key to success in the Raman beat detection to eliminate these cause of the incoherence. Then it is needed to prepare the sophisticated single crystal sample, the highly stabilized magnetic field, and a cryostat of liquid helium. It has been completed to set up the apparatus, and the Raman beat detection was applied to the study on the delocalized excitation in molecular crystals of 1,4-dibromonaphthalene. The result was published in *Phys. Rev. Lett.* **83(10)**, 2018 (1999).

Structure, Relaxation and Control of Reactive Cluster Studied by Two-Color Laser Spectroscopy

FUJII, Masaaki

A molecular cluster is a microscopic system of solution and / or crystal, and is thought to provide detailed information on relaxation and reaction dynamics in condensed phase. However the molecular clusters which have been studied are mainly static system which has no reaction pathway after photo-excitation, and consequently spectroscopic information which concerns the reaction mechanism has not been obtained sufficiently. In this research project started from 2000, we will apply various laser spectroscopy to the reactive clusters to reveal detailed mechanism of intracluster reaction.

For the ground state, the structure of the cluster can be determined by the combination of the IR dip spectroscopy and ab initio MO calculations.$^{1)}$ The IR dip spectroscopy is a kind of IR-UV double resonance spectroscopy which provides the spectrum which corresponds to the infrared absorption spectrum of the cluster (see Figure 1). Briefly, a tunable IR laser is introduced to the clusters and is scanned its frequency over the fundamental vibrational region (typically 2400~4000 cm^{-1}). Then a tunable UV laser, of which the frequency is fixed to the S_1 origin of a specific cluster, is introduced and resonant enhanced multiphoton ionization signal via S_1 is monitored. When the IR laser is resonant to a vibrational level of the cluster, the ion signal decreases much because of loss of the population in the vibrational ground state. Thus, the IR absorption spectrum of the cluster can be measured by this depletion spectroscopy. The same spectrum can be obtained when the fluorescence intensity from S_1 is monitored instead of the ion current.

The IR spectrum in the excited state S_1 can also be measured by the depletion spectroscopy, when the UV laser is introduced before the IR laser shot (the UV-IR fluorescence dip spectroscopy; see Figure 2). The molecule is excited to S_1 by the UV laser, and the fluorescence intensity is monitored as well as the IR dip spectroscopy for S_0. Then the S_1 molecules are further excited to the vibrationally excited level in S_1 by the IR laser. In general, the fluorescence quantum yield decreases in the higher vibronic level. Thus, the total fluorescence intensity decreases when the IR laser frequency resonant to the vibrational level in S_1.

Similarly, the IR spectrum of the ionic cluster can be measured by the depletion spectroscopy (mass-selected ion dip spectroscopy; see Figure 3). The ionic cluster can be prepared by the multiphoton ionization via S_1, and the ion current due to the cation cluster of the specific size can be measured through a mass-filter. When the ionic cluster is vibrationally excited by the IR laser, the cluster is dissociated by the vibrational predissociation. Therefore, the IR transition can be measured by the decrease of the parent cluster. The same spectrum can be obtained by monitoring the enhancement of fragments (mass-selected multiphoton dissociation spectroscopy). In addition to these “dip” spectroscopies, the PFI-ZEKE photoelectron spectroscopy2) and the nonresonant ionization detected IR spectroscopy3) are also important method to obtain the spectral information in the cation and the overtone states.

Here, we have obtained an example of the spectroscopy of the reactive cluster phenol/ammonia system.4) Recently, it has been pointed that the hydrogen transfer from phenol to ammonia occurs in the photoexcited phenol/ammonia cluster in addition to proton transfer. The application of the IR dip spectroscopy clearly proofs that the hydrogen transfer occurs in the photoexcited phenol $(NH_3)_{3,4}$ clusters. Figure 4 shows the transition scheme of the IR dip spectroscopy, which was employed in this work. The pump UV laser (ν_1) was tuned to the S_1–S_0 transition of PhOH–$(NH_3)_n$ (n = 3, 4). After a long delay time (180 ns), the IR laser (ν_{IR}) was irradiated and scanned in the energy region from 2700 cm^{-1} to 3700 cm^{-1}. Then, just after ν_{IR}, the ionization laser (ν_2) was irradiated. If ν_{IR} is resonant to a certain vibrational transition, the cluster is dissociated through the vibrational predissociation process, thus, the ion signal $(NH_3)_nH^+$ due to ν_2 decreases. Therefore, the vibrational transition of the reaction product which gives $(NH_3)_nH^+$ can be observed as a dip of the ion signal.

Figure 5a shows an IR dip spectrum which was obtained by fixing ν_1 to 35498 cm^{-1}, which corresponds to a lower vibronic band in the S_1 state of PhOH–$(NH_3)_3$. This frequency was chosen according to the work by Pino *et al.*4) The spectrum was measured by monitoring $(NH_3)_3H^+$. To measure the vibrational transition of the reaction product via S_1, ν_{IR} was introduced at the delay time of 180 ns from ν_1 (see Figure 4). The spectrum drawn by the solid curve was measured at a moderate intensity of ν_{IR} (0.2 mJ), while that shown by the dotted curve was obtained by using an intense ν_{IR} (0.4 mJ). As can be seen in the figure, two bands with comparable intensities were observed at 3180 and 3250 cm^{-1}, and a broad band was also found in the region of 2700~3100 cm^{-1}. In the energy region higher than 3300 cm^{-1}, we could not observe any bands, even when intense ν_{IR} was used.

In order to confirm that the IR dip spectrum shows the vibrational structure of the reaction product via S_1, we also observed the IR dip spectrum of PhOH–$(NH_3)_3$ in the ground state S_0. Figure 5b shows the IR dip spectrum of PhOH–$(NH_3)_3$ in S_0, which was obtained by introducing ν_{IR} earlier than ν_1 and ν_2. As can be seen in the figure, sharp bands at around 3400 cm^{-1}, and a broad band at ~3200 cm^{-1} can be observed on the very broad background signal. This spectral feature is very close to the IR dip spectrum of the 2-naphthol–$(NH_3)_3$ cluster in S_0.5) From an analogy of 2-naphthol–$(NH_3)_3$, we tentatively assigned the sharp bands at ~3400 cm^{-1}, the broad bands at ~3200 cm^{-1} and the broad background to ν_3 in NH_3, ν_1 in NH_3 and ν_{OH} in phenol, respectively. Though the vibrational assignment has not yet been confirmed, it is clear that the IR dip spectrum drastically changes before (Figure 5b) and after (Figure 5a) the electronic excitation to S_1 by the UV laser ν_1. It is concluded that the IR dip spectrum with a long delay (Figure 5a) shows the IR transitions of the reaction product. The possible reaction products from PhOH–$(NH_3)_3$ in S_1 are PhOH(T_1)–$(NH_3)_3$, PhO$^-$(T_1)–$(NH_3)_3H^+$ or $(NH_3)_3H$. The vibrational spectrum of PhOH(T_1)–$(NH_3)_3$ is thought to maintain some similarity to that of the cluster in S_0. It is thus natural to exclude the possibility of PhOH(T_1)–$(NH_3)_3$, because of the drastic change of the vibrational structure in comparison to the IR dip spectrum of the cluster in S_0 (Figure 5b). If the ion pair PhO$^-$(T_1)–$(NH_3)_3H^+$ is formed, the vibrational spectrum is expected to be similar to that of $NH_4^+(NH_3)_2$. The IR dip spectrum of $NH_4^+(NH_3)_2$ has been reported by Y. T. Lee’s group.6) According to their assignments, the $NH_4^+(NH_3)_2$ cluster shows the NH stretch vibration of the NH_3 moiety at 3413.7 cm^{-1}, and the NH stretch vibration of NH_4^+ at 3395.4 cm^{-1}. In the IR dip spectrum of the reaction product, no bands are observed in the region higher than 3300 cm^{-1}. Such a large difference does not support the generation of the ion pair. Therefore, we concluded that the neutral radical $NH_4(NH_3)_2$ is formed via PhOH–$(NH_3)_3$ in S_1. This supports the hydrogen transfer of photo-excited PhOH-$(NH_3)_3$, as proposed by Pino *et al.*4)

References

1) R. Yoshino *et al.*, *J. Phys. Chem. A* **102**, 6227 (1998).

2) T. Omi *et al.*, *Chem. Phys. Lett.* **252**, 287 (1996); S. Ishiuchi *et al.*, *Chem. Phys. Lett.* **283**, 243 (1998).

3) K. Takazawa *et al.*, *Chem. Phys. Lett.* **189**, 592 (1992); K. Müller-Dethlefs *et al.*, *Z. Naturforsch., A: Phys. Sci.* **39**, 1089 (1984); *Chem. Phys. Lett.* **112**, 291 (1984); K. Müller-Dethlefs and M. C. R. Cockett, “*Zero Kinetic Energy (ZEKE) Photoelectron Spectroscopy*,” Chapter 7, “Nonlinear Spectroscopy for Molecular Structure Determination”, R. W. Field *et al.*, Eds. (Blackwell Science,

Oxford, 1998), and references therein.; E. W. Schlag, "*ZEKE Spectroscopy*" (Cambridge University Press, Cambridge, 1998) , and references therein.
4) G. A. Pino *et al.*, *J. Chem. Phys.* **111**, 10747 (1999).
5) Y. Matsumoto *et al.*, *J. Mol. Struct.* (in press).
6) J. M. Price *et al.*, *J. Phys. Chem.* **95**, 2182 (1991).

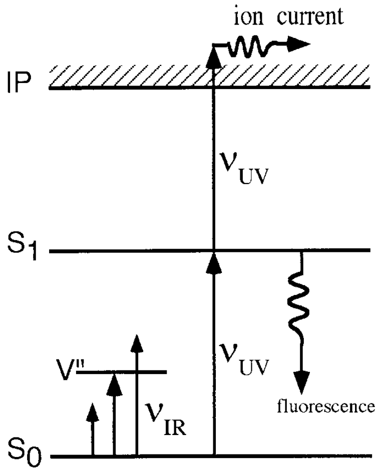

Figure 1. Principle of the IR Dip Spectroscopy. The IR transition in the ground state cluster can be measured.

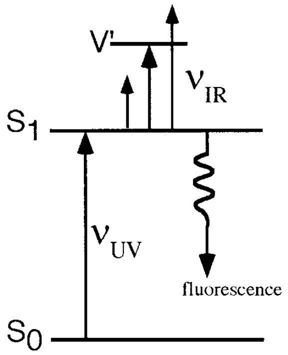

Figure 2. Principle of the UV-IR Fluorescence Dip Spectroscopy. The IR transition of the cluster in the S1 state can be obtained.

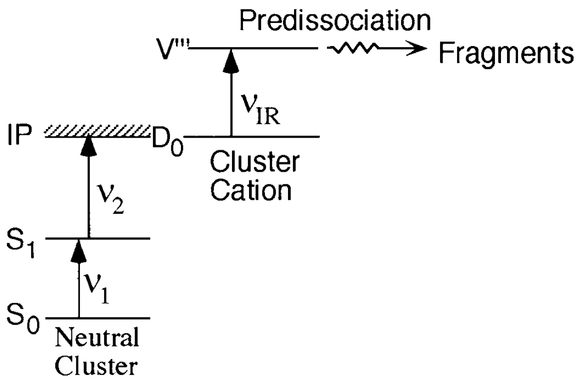

Figure 3. Principle of the mass-selected IR Ion Dip Spectroscopy. The IR transition of the cluster cation can be measured by the depletion of the parent cluster cation. The same spectrum can be measure by monitoring the enhancement of the fragments produced by the IR predissociation.

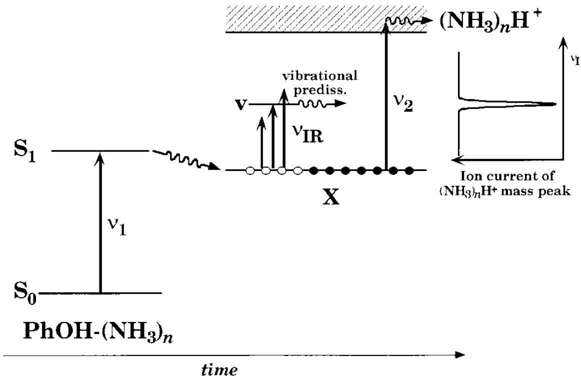

Figure 4. Schematic diagram showing the principle of IR dip spectroscopy which was employed in this work.

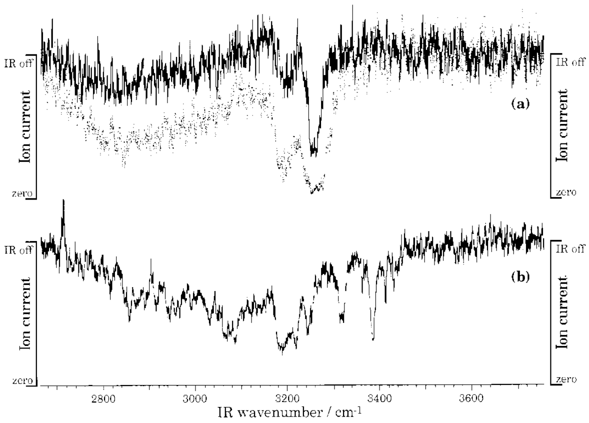

Figure 5. (a) IR dip spectrum of the reaction product which was observed by fixing ν_1 to the lower vibronic band in the S_1 state of PhOH–$(NH_3)_3$ (35498 cm^{-1}) and monitoring $(NH_3)_3H^+$. The third harmonics of the YAG laser was used as the ionization laser ν_2. The IR laser ν_{IR} was irradiated after 180 ns from the excitation to S_1 due to ν_1. The solid curves and the dotted curves show the spectra obtained by adjusting the laser power of ν_{IR} to 0.2 mJ and 0.4 mJ, respectively. (b) IR dip spectrum of PhOH–$(NH_3)_3$ in S_0. The IR laser ν_{IR} was irradiated before 20 ns from the excitation to S_1 due to ν_1.

SR-Pump and Laser-Probe Experiments for the Photofragmentation Dynamics of Molecules

MITSUKE, Koichiro; MIZUTANI, Masakazu; IWASAKI, Kota

Synchrotron radiation-laser combination techniques developed at UVSOR in Okazaki were employed for probing ionic and neutral photofragments produced in the vacuum ultraviolet. First, N_2^+ ($X\ ^2\Sigma_g^+$, v_X = 0 and 1) fragments resulting from direct ionization or autoionization of N_2 or N_2O were detected by laser induced fluorescence (LIF) excitation spectroscopy in the wavelength region of the $B\ ^2\Sigma_u^+ \leftarrow X\ ^2\Sigma_g^+$ transition. The partitioning of the excess energy impulsively released in dissociation was found to mainly determine the rotational distribution of N_2^+ from N_2O. Second, CN neutral fragments were dissociated from CH_3CN by excitation with synchrotron radiation of 15–20 eV. They were probed by LIF excitation spectroscopy utilizing the transition of $B\ ^2\Sigma^+\ v_B = 0 \leftarrow$

$X\ ^2\Sigma^+\ v_X = 0$. Either the dissociative ionization leading to CN + CH_3^+ or predissociation of superexcited states into CN + CH_3* may give rise to the CN fragments. We constructed a novel optics containing spheroidal and spherical mirrors and an optical fiber in order to improve the collection efficiency of the fluorescence. Third, the combination technique was incorporated into an apparatus for two-dimensional photoelectron spectroscopy to investigate photoionization dynamics of polarized atoms. Aligned Ar atoms formed by excitation with synchrotron radiation were ionized by irradiation of laser and the photoelectron angular distribution was measured with respect to the laser polarization. Derivation was made on the expressions which correlate asymmetry coefficients for the angular distribution with theoretical dynamic parameters including transition dipole matrix elements. The observed anisotropic angular distributions were reasonably explained, assuming that the matrix elements and phase shift differences are essentially independent of the total angular momentum quantum number of the final state and that the spin-orbit interaction in the continuous spectrum is small.

Electronic Structure and Optical Properties of III-V Nitrides

FUKUI, Kazutoshi; YAMAMOTO, Akio[1]; TANAKA, Satoru[2]; AOYAGI, Yoshinobu[3]; YAMAGUCHI, Shigeo[4]; AMANO, Hiroshi[4]; AKASAKI, Isamu[4]
([1]Fukui Univ.; [2]Hokkaido Univ.; [3]Inst. Phys. Chem. Res.; [4]Meijo Univ.)

The soft X-ray absorption (SXA) around nitrogen *K*-edge (N-*K*) have been measured to investigate the electronic structure of the wurtzite III-V nitrides, especially the structure of the unoccupied states. The N-*K* absorption spectra of III-V nitrides near the N *K*-edge in principle represent the partial density of the final states with *p* symmetry according to the selection rule. Since the core levels are strictly localized in space, the N-*K* absorption spectrum gives us the site-specific information. The N-*K* absorption spectrum also gives us the information about the final states symmetry p_{xy} and p_z, because the incidence soft X-ray light is linearly polarized. Under this project, the first results of N-*K* SXA spectra of wurtzite $Al_{1-x}In_xN$ (x = 0, 0.53, 0.78, 1) have been measured. The results of x = 0.53 and 0.78 reflect on their unstable crystallinity. The SXA spectra show the structure-less features and the incidence angle dependence of the SXA spectra is also unclear compared with that of wurtzite $Al_{1-x}Ga_xN$ and $In_{1-x}Ga_x$-N. However, the successional change of the spectral shape as the function of x can be seen.

Decay and Dissociation Dynamics of Core Excited Molecules

SHIGEMASA, Eiji; GEJO, Tatsuo

Recently the influence of nuclear motion within the core-hole lifetime to the dissociation dynamics becomes an extraordinarily intriguing subject in the research field of molecular core-level spectroscopy. The dynamics of molecular inner-shell excitation and relaxation processes is complex even for simple molecules, and thus it is advantageous to use various experimental techniques together with high performance monochromators in the soft x-ray region. At the UVSOR, there is only one monochromator available for high-resolution spectroscopy in the photon energy region of interest (100–550 eV), where the core edges of chemically important elements lie. In 1999 design study for a new monochromator at BL4B was started in order to improve the situation. A Varied-line-spacing Plane Grating Monochromator (VPGM) has been chosen for this work. Thanks to the availability for high quality gratings and simple scanning mechanism, VPGM seems to be one of the most promising monochromators to realizing high resolution in the soft x-ray range.

All the optical elements needed for the present (four mirrors and one grating) have been successfully fabricated. The vacuum chambers for the mirrors and grating and other beamline components were also manufactured in good condition and conveyed to the experimental hall of the UVSOR. It is expected that the first light through the new monochromator will be available in near future and the performance tests for it to be terminated in 2000.

(c) Novel Material Science

Theory of Electronic Phases in Molecular Conductors and Insulators: Electron Correlations and Dimensional Crossovers

YONEMITSU, Kenji; KISHINE, Jun-ichiro; MORI, Michiyasu; KUWABARA, Makoto; MIYASHITA, Naoyuki[1]
([1]GUAS)

Electron correlations in low-dimensional molecular materials are essential for the understanding of novel electronic phases and their dynamical properties. i) In quasi-one-dimensional organic conductors (TMTCF)$_2$X, various changes in electronic properties can be interpreted from the viewpoint of dimensional crossovers. For weak interchain hopping, one-particle motion is effectively confined into the chains by electron correlation. The three-dimensionally ordered, antiferromagnetic phase is achieved from a charge-localized phase. For weak dimerization, electron correlation is so weak that three-dimensionality is first achieved in one-particle motion to produce a Fermi liquid, and then the nesting of the Fermi surface induces the magnetically ordered phase. Even in the latter case, the optical conductivity spectra with different polarization vectors and excitation energies show that quantum-mechanical motion of electrons is confined into the chains as the energy scale increases. Local excitation spectra for infinitely long, one-dimensional systems are studied by the thermodynamic density-matrix renormalization-group method. ii) In one-dimensional halogen-bridged binuclear metal complexes, M$_2$L$_4$X, competition between electron-lattice and electron-electron interactions brings about variety of charge and lattice ordering phases. The stability of each electronic phase is studied from the strong-coupling limit. The dependence of the electronic phase on the ligand, the halogen ion and the counter ion is qualitatively understood in a model with strong on-site repulsion and electron-lattice couplings. However, a long-range part of the electron-electron interaction is needed to reproduce the optical conductivity by the exact-diagonalization method. iii) The charge-ordering and magnetic-coupling patterns of two-dimensional organic conductors θ-(BEDT-TTF)$_2$X are understood on the basis of the anisotropy in Coulomb repulsion strengths and transfer integrals. Some of the optical properties may indicate importance of electron-phonon interaction as well, so that both static and dynamical properties are consistently studied with unconstrained Hartree-Fock and random-phase approximations.

Size-Controlled Synthesis of Colloidal Metal Clusters

NEGISHI, Yuichi; TSUKUDA, Tatsuya

Colloidal metal clusters have gained much attention because of their noble catalystic reactivities. Because the reactivity of the cluster depends on their size and shape, the synthesis of clusters while controlling these parameters is critical especially from the viewpoint of applications. Most of the preparative methods reported so far involve the reduction of the relevant metal ions in the presence of a ligand reagent, which stabilizes the resultant clusters and prevents further coalescence. Under these conditions, the cluster size and shape can be controlled by adjusting the relative concentration of the ligands over the metal ions. We have been exploiting a method to prepare the clusters having a well-defined size and shape by taking advantage of hollow structures of various host molecules. The transmission electron microscopy observations have revealed that the Pd clusters stabilized by cyclodextrins have diameters in the range of 2–5 nm. The experimental conditions will be further optimized so as to narrow the width of the cluster size distributions with a help of mass spectrometry.

Spectroscopic and Physico-Chemical Studies of Organic Conductors

YAKUSHI, Kyuya; YAMAMOTO, Kaoru; URUICHI, Mikio; NAKANO, Chikako; OUYANG, Jianyong; DING, Yuqin; MAKSIMUK, Mikhail; DROZDOVA, Olga; SIMONYAN, Mkhital

The reflectivity of an organic conductor provides us with a wealth of information on the electronic structure. For instance, the anisotropy of a band structure, band width, effect of electron-electron correlation, and electron-molecular vibration (*e-mv*) coupling parameters can be extracted from the analysis of the reflectivity or optical conductivity curve. Raman spectroscopy is a complementary method to reflection spectroscopy for investigating molecular vibrations (local phonons). For the past year, we have obtained the following results. (1) The reflectivity of (EO-TTP)$_2$AsF$_6$ can be almost perfectly fitted down to 600 cm^{-1} by Drude model. The complete fitting by Drude model is rather exceptional for organic metals. From the analysis of the reflectivity, we determined the temperature dependence of the intra-chain and inter-chain transfer integrals. (2) The reflectivity of (BEDT-ATD)$_2$X(solvent) (X = PF$_6$, AsF$_6$, BF$_4$; solvent = THF, DHF, DO) shows a remarkable deviation from Drude model. This strongly correlated system shows a Peierls-Hubbard type of $4k_F$ phase transition. The fluctuation of the lattice distortion is observed above the phase transition temperature. (3) We investigated the C=C stretching modes in the Raman and infrared spectra of κ-(BEDT-TTF)$_2$Cu[N(CN)$_2$]Br. We found a large factor group splitting, which was attributed to the inter-dimer interaction inside the conducting layer.

Recently, a charge-ordered ground state has been found in several organic conductors. We are investigating the charge ordering (CO) or charge disproportionation phenomena in organic conductors using the technique of vibrational spectroscopy. We have obtained the following results. (1) The C=C stretching modes of θ-(BEDT-TTF)$_2$RbZn(SCN)$_4$ show noticeable variations in the Raman spectrum below the phase transition temperature. The low-temperature vibrational spectrum was successfully explained in terms of the charge ordering. (2) The interpretation was confirmed by investigating the isotopic compound, in which the two carbon atoms at the central C=C bond of BEDT-TTF was replaced by ^{13}C. (3) In θ-(BDT-TTP)$_2$-Cu(NCS)$_2$, we found a second-order phase transition at 250 K, which was proved to be accompanied by a charge disproportionation by the use of Raman spectrum. (4) We found a magnetic phase transition at 5 K in θ-(BDT-TTP)$_2$Cu(NCS)$_2$. The ground state is a non-magnetic state.

In some charge-transfer salts of phthalocyanine, localized unpaired d-electrons coexist with itinerant π-electrons. We are investigating these π-d electron systems from the viewpoint that it is analogous to an f-electron system, in which a narrow f-band coexists with a wide s-band. We have obtained the following results. (1) The magnitude of the π-d exchange interaction was determined from the analysis of the temperature dependence of the *g* value and linewidth of the ESR signal in the dilute alloy system $Co_{0.01}Ni_{0.99}Pc(AsF_6)_{0.5}$. The estimated Kondo temperature was 10^{-5} K. (2) We measured the pressure dependence of the resistivity of $CoPc(AsF_6)_{0.5}$ down to 50 K. In contrast to NiPc-$(AsF_6)_{0.5}$, the temperature of the resistivity minimum decreases down to 100 K at 0.9 GPa. (3) We found an antiferromagnetic (AF) phase transition at 12 K in newly prepared π-d system, (DMTSA)FeCl$_4$. The heat capacity experiment suggested that the magnetic moment of Fe^{2+} ($S = 5/2$) took in part in the AF state and the AF interaction has a low-dimensional character.

Broad-Line Solid State NMR Investigation of Electronic States in Molecular-Based Conductors

NAKAMURA, Toshikazu; TSUKADA, Hiroshi

Competition of the electronic phases in molecular based conductors has attracted much attention. The aims of this project are to clarify these electronic phases stabilized at low temperatures and to explore novel electronic phases in molecular-based conductors by microscopic investigation. It is worth noting that spin-Peierls (spin-singlet), commensurate spin density wave (C-SDW), incommensurate spin density wave (IC-SDW), and superconducting phases can be realized by applying appropriate pressures even in the same system. Investigation of such electronic phases in molecular based conductors is important to understand the unsolved fundamental problems in the field of solid state physics.

Broad-line solid state NMR is a powerful measurement to clarify the fundamental electronic properties. In this project, we are preparing the second NMR system to study more detailed electronic structure from microscopic points of view. We also try to carry out experiments with new devices under unconventional circumstance.

The following topics are in progress.

[1] Successive SDW transition in (EDT-TTF)$_2$AuBr$_2$.
[2] Magnetic properties of organic spin-ladder systems, (BDTFP)$_2$X.
[3] NMR and ESR investigation of organic conductors based on TTP derivatives.
[4] Magnetic structures of the antiferromagnetic states in Pd(dmit)$_2$ families.
[5] Competition between local and itinerant electrons in charge-transfer salts: (CPDT-STF)-TCNQ.

Development of New Organic Conductors and Their Physical Properties

KOBAYASHI, Hayao; FUJIWARA, Hideki; FUJIWARA, Emiko; ADACHI, Takafumi; NARYMBETOV, Bakhyt Zh.; TANAKA, Hisashi; TAMURA, Itaru; KOBAYASHI, Akiko[1]
([1]Univ. Tokyo)

In order to contribute for further development of solid state physics and chemistry of molecular materials, we have tried to develop new types of molecular conductors and to improve the conventional methods of X-ray structure analysis and resistivity measurements at high pressure. The main results obtained in the last one year are as follows: (1) we have recently found the first single-component molecular metal. Since the discoveries of the semiconducting properties of phtalocyanines and aromatic hydrocarbones around 1950, many chemists have dreamed to develop metallic crystal composed of simgle molecules. Our fingings will open a way to develop molecular metals or even superconductors soluble in organic solvents. (2) Following after the first discovery of antiferromagnetic organic superconductor κ-BETS$_2$FeBr$_4$, the second antiferromagnetic organic superconductor κ-BETS$_2$-FeCl$_4$ was discovered. Neel temperature ($T_N = 0.45$ K) and the superconducting transition temperature ($T_c = 0.1$ K) are much lower than those of κ-BETS$_2$FeBr$_4$ ($T_N =$ 2.4 K, $T_c = 1.1$ K). In these systems, the π-d interaction between π conduction electrons in BETS layers and magnetic d electrons in the anion sites is considered to be mediated by halogen atoms of FeX_4^- anions. The microscopic mechanism of magnetic interaction between Fe^{3+} ions below T_c will be of special interest because π conduction electrons are in the superconducting state. (3) We have succeeded to obtain the accurate resistivity data of organic single crystal up to 15 GPa by adopting diamond-anvile four-probe technique. In the course of these studies, we have examined the possiblity of the superconducting transition of (TMTTF)$_2$PF$_6$, the sulfur-analog of the first organic superconductor (TMTSF)$_2$PF$_6$ and found the superconducting transition above 52 kbar. Bechgaars salt with PF$_6$ anion is the first “TM system” whose superconductivity was found in both Se- ans S-analogs. (4) The development of “pure organic magnetic conductor” based on stable organic radicals is one of the next important targets of the chemists in the fields of molecular conductors and molecular magnets. We are now trying to prepare candidate molecules suitable to construct such systems.

Constraction of a Catalase Active Site by Site Directed Mutagenesis of Myoglobin

HARA, Isao; MATSUI, Toshitaka; OZAKI, Shin-ichi; WATANABE, Yoshihito

A double mutant protein of myoglobin (Mb) that exhibits altered axial ligation has been prepared by site-directed mutagenesis. The original axial ligand residue, histidine 93(F8), was replaced with glycine, and also histidine 64(E7) was replaced with tyrosine as an axial ligand, resulting in H64Y/H93G Mb. Tyrosine coordination to the ferric heme iron is verified by optical absorption, EPR and resonance Raman spectroscopy. The optical absorption spectrum of a ferric form of H64Y/H93G Mb is characteristic of high spin heme and similar to those observed in bovine liver catalase and natural occurring mutants of hemoglobin having a tyrosinate ligand. In contrast, wild-type and H64Y/H93G Mb exhibit almost the same spectra in ferrous and carbon monoxy forms, suggesting coordination of a histidine residue, possibly histidine 97(FG3), in the reduced forms of the mutant. The tyrosinate ligation in the ferric H64Y/H93G Mb is confirmed by the observation of $\nu_{\text{Fe-O}}$ band at 597 cm^{-1} in a resonance Raman spectrum. Although EPR spectrum of ferric H64Y/H93G Mb consists of at least two sets of rhombic high spin signals, the major component is similar to bovine liver catalase in the g-values. These results indicate successful conversion of Mb into a catalase-like protein in terms of coordination structure and electronic properties of the heme iron.

Construction and Characterization of Chiral Molecule-Based Magnets in a Systematic Way

INOUE, Katsuya; KUMAGAI, Hitoshi; IMAI, Hiroyuki

The design of multi-functional molecular materials is one of the current interests. Especially the molecular magnetic materials with conducting and/or optical properties are one of the challenging target in the last few years. The synthesis and study of optical properties on molecular-based magnetic materials being transparent for light, are of great interest. Novel magneto-optical phenomena, MChD effect, have been theoretically predicted and observed in chiral paramagnetic materials in 1997. Although novel properties are expected for such compounds, few examples of chiral molecular-based magnetic materials are still known. To get more insight in their properties it is therefore important to construct such chiral molecule-based magnets in a systematic way. We designed and synthesized a chiral organic radical which was can be employed to construct chiral molecular-based magnets. We have introduced a strategy of using π-conjugated high-spin oligonitroxide radicals which can be used as bridging ligands for paramagnetic transition metal ions in order to assemble and align the electron spins on a macroscopic scale. By this strategy, we have made a chiral metamagnet with a $T_N = 5.5$ K and a ferrimagnet with a $T_C = 4.5$ K. (see V-E). The observation of MChD effect of this complex is now underway.

STM Study on Synchrotron-Radiation Stimulated SiO_2 Desorption on Si (111) Surface

NONOGAKI, Youichi; URISU, Tsuneo

We have been developing UHV-STM systems with special process chambers for synchrotron radiation (SR) irradiation. Using the UHV-STM systems, we have investigated SR-stimulated SiO_2 desorption on Si (111) surface which is one of most interesting topics not only for surface science but for nano-fabrication in the Si-based device engineering. We expect that SR-stimulated SiO_2 desorption become most significant etching techniques for the fine pattern fabrication on the Si surfaces. Since the SiO_2 desorption was induced by surface photochemical reaction without physical sputtering, the etching is expected to be very low damage and high precision processes.

It was found that an atomically flat surface was obtained after two hours SR irradiation even at a low temperature of ~700 °C. The surface has bilayer atomic steps and 7×7 reconstruction on the terrace. The bilayer steps tend to pass along crystallographic axis. This is in sharp contrast to Si surfaces after thermal desorption of SiO_2 at temperatures of 880 °C, where the steps are much more irregular. It indicates that the bilayer atomic steps reach thermodynamic equilibrium under synchrotron radiation at temperatures much lower than those necessaries for thermal desorption.

We conclude that SR-stimulated SiO_2 desorption occurs and shows different characteristics from thermal desorption. However, we still do not know the mechanisms how the SiO_2 desorb from the surface and how the steps rearrange. To consider these mechanisms, time dependence of STM images observed at the same area would be good help. Now, we plan to use Si wafer with marks for position detection, which is made by conventional lithography and wet chemical etching.

Design and Construction of UVSOR-BL4A2 Beam Line for Nano-Structure Processing

TAKEZOE, Noritaka; YANAGIDA, Hideaki[1]; KUROSAWA, Kou; NONOGAKI, Youichi; NODA, Hideyuki; MEKARU, Harutaka[2]; URISU, Tsuneo
([1]IMS and Univ. Miyazaki; [2]Himeji Inst. Tech.)

[7th International Conference on Synchrotron Radiation Instrumentation]

We have designed and constructed a new beam line BL4A2 at UVSOR mainly for nano-structure fabrication based on synchrotron radiation stimulated surface photochemical reactions. In order to obtain high-photon flux, we use white ray beam focused with only one mirror. The beam line is connected with ultra-high vacuum scanning tunneling microscope for in-situ atomic scale pbservations, low energy electron diffraction and Auger electron spectroscope for surface crystal structure characterization, and photo-stimulated surface reaction chamber. In order to monitor the optical properties with atomic scale, a near field optical microscope is planned to be installed.

Study on RF-Photocathode for Compact X-Ray Sources

TAKASHIMA, Yoshifumi; KOBAYAKAWA, Hisashi[1]; KIMURA, Kenichi[1]; SUGIYAMA, Harue[1];

FURUTA, Fumio[1]; NAKANISHI, Tsutomu[1]
([1]Nagoya Univ.)

When a charged particle is passing through a object with a relativistic velocity, atoms in the object feel a pulse of electromagnetic field which causes electromagnetic radiations from the objects. Cherenkov radiation is one of this kind of radiation. If a object has a periodical structure, a coherent x-ray called "Parametric x-ray Radiation(PXR)"[1,2] is generated. PXR has good monochromaticity and is radiated in a conical direction away from a direction of incident charged particles. Thus PXR is a good candidate of a hard x-ray source. However, in spite of optimizing the thickness of the target radiator of crystal, the highest intensity of PXR achieved up to now is about 10^{-5} photons/e^- and is not enough to use in practical applications unless we use a very high current electron beam.

RF-photocathode would produce high peak current of electron beam so that it is useful as a electron source. Figure 1 shows a plan of our system. Now we are studying the photocathode made of cesium telluride and constructing the RF system.

References

1) M. I. Ter-Mikaelian, *High-Energy Electromagnetic Processes in Condensed Media*, Wiley, New York (1972).
2) S. A. Vorob'ev, B. N. Kalinin, S. Pak and A. P. Potylitsin, *JETP Lett.* **41**, 1 (1985).

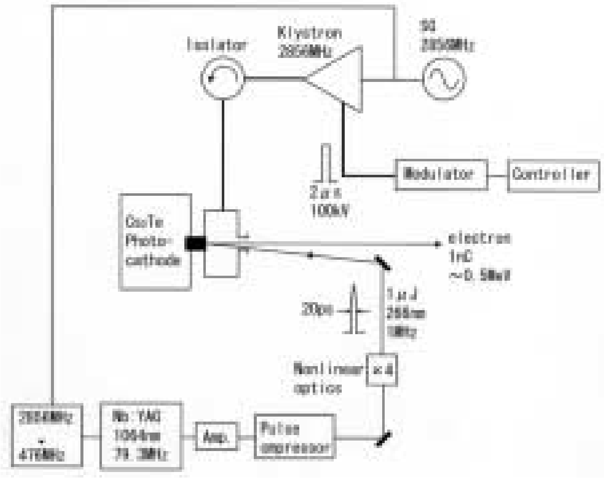

Figure 1. System of RF-gun.

Reductive Activation of Metal-Carbonyl Complexes Derived from Carbon Dioxide and Oxidative Activation of Metal-Hydroxy and -Oxo Complexes Derived from Water

TANAKA, Koji: WADA, Tohru: MIZUKAWA, Tetsunori; SHIREN, Kazushi; WADA, Hiroaki[1]; KOBAYASHI, Katsuaki; TOMON, Takashi
([1]RIKEN)

Some of metal-carbonyl complexes are obtained through metal-CO_2 adducts which are produced by an attack of CO_2 to the reduced form of those metal-complexes and subsequent oxide transfer from the CO_2 group to free CO_2. Accordingly, organic synthesis through M-CO_2 and M-CO complexes is highly desired in the view point of the development of a new C1 resources. A major problem of the reduction of CO_2 using homogeneous catalysis is reductive cleavages of M-CO bonds under reductive conditions. Accumulation of too much electrons in the central metals in the reduction of CO_2 can be avoided by using ligand localized redox reactions rather than metal centered ones. Ligands which can flexibly change the coordination modes among monodentate, bidentate and bridging form which connects metals and carbonyl carbon of M-CO bonds would meet the requirements of smooth M-η^1-CO_2 formation and depression of reductive cleavage of M-CO bond under reductive conditions.

Acids or bases generated in industrial process are just wasted after neutralization. Proton gradient (Δp) between inside and outside of a cell is represented as the sum of electric activity ($\Delta\Psi$) and chemical activity (ΔpH) components. $\Delta p = \Delta\Psi - Z\Delta\text{pH}$ ($Z = 2.303RT/F$) Proton gradient is equivalent to the neutralization energy because the neutralization reaction takes place to form water if the separating membrane is removed. Thus, neutralization energy results from the formation of water. Biological system effectively creates and consumes neutralization energy in various reactions. Acids and bases, therefore, have potential energy sources provided by chemical bondings (chemical energy). Along this line, we tried to convert the neutral energy to electronic energy by using ruthenium-aqua complexes.

Developments and Researches of New Laser Materials

SARUKURA, Nobuhiko; OHTAKE, Hideyuki; LIU, Zhenlin; KAWAHATA, Eiji; KOZEKI, Toshimasa; ONO, Shingo[1]
([1]Sci. Univ. Tokyo)

Although development of lasers is remarkable, there are no lasers which lase in ultraviolet and far infrared regions. However, it is expected that these kinds of lasers break out a great revolution in not only the molecular science but also in the industrial world.

In this project we research characters of new materials for ultraviolet and far infrared lasers, and develop new lasers by using these laser materials.

New Advanced Organic Materials Based on Novel Heterocyclic Compounds

YAMASHITA, Yoshiro; TANAKA, Shoji; TOMURA, Masaaki

We have succeeded in preparing new electron donors and acceptors with extended π-conjugation. For example, TTF vinylogues bearing various substituents at the vinyl positions have been prepared using an oxidative dimerization reaction of 1,4-dithiafulvenes. We have prepared derivatives bearing cyano or bromo substituents which can induce intermolecular interactions. Novel bis(1,3-dithiole) electron donors containing an azulene spacer unit were also synthesized.

They have small HOMO-LUMO gaps and show the longest absorption maxima at 733–762 nm. As electron acceptors, bithiazole analogues of tetracyanodiphenoquinodimethane (TCNDQ) were prepared using Pd-catalyzed coupling reaction of dicyanomethanide to the corresponding dibromide precursors. Heterocyclic TCNQ analogues containing thiophene and benzothiadiazole units were also prepared using the similar Pd-catalyzed reaction. They are polarized molecules and show strong absorptions at longer wavelengths than 500 nm. They gave charge transfer complexes with various electron donors. Decamethylferrocenium salts of anilate anions were obtained as single crystals. The unique crystal structures involving intermolecular interactions such as hydrogen bonding were revealed by X-ray analysis. A new type of hydrogen-bonding system has also been developed by using dipyridylacetylenes as proton acceptor and chloranilic acid as proton donor. The component molecules are combined via three-center hydrogen bonded interactions. Furthermore, we have prepared thiophene oligomers as promising molecular-scale electronic wire which have small energy gaps with a rigid and coplanar main chain. Details of these works are described in VIII-C section.

Molecular Mechanism of Oxygen Activation by Metalloenzymes

FUJII, Hiroshi; FUNAHASHI, Yasuhiro; MIZUTANI, Mamoru; IKEUE, Takahisa

Metalloenzymes are a class of biologically important macromolecules which have various functions such as oxygen transport, electron transfer, oxidation, and oxygenation. These diverse functions of metalloenzymes have been thought to depend on the coordination structure of the active site in the protein matrices; the ligand donors, the geometry, and the coordination mode of reactant and substrate. Furthermore, it has been thought that protein structures in immediate vicinity of active metal ion are related to enzymatic function, regio-selectivity, and stereo-selectivity. In this project, we are studying the molecular mechanism of activation of molecular oxygen mediated by metalloenzymes.

(1) Resonance Raman(RR) spectra are reported for two models of the compound I intermediates of oxidative heme proteins; namely, the imidazole (Im) and 2-methyl-imidazole (2-MeIm) complexes of the ferryl π-cation radical derivative of iron-(5,10,15,20-tetramesitylporphyrin). While the observed shifts in the frequencies of the core modes are in agreement with those expected upon formation of the π-cation radical, the results suggest that the isolated effect of macrocycle oxidation on the Fe=O stretching frequency is rather small.

(2) To reveal the electronic states of these intermediates and to understand the reaction mechanism of cytochrome c oxidase, we have synthesized model complexes of the heme-a_3 site of cytochrome c oxidase. We have succeeded in the preparation of a high valent oxo iron porphyrin complex as a model for the intermediate P by the oxidation of the ferric model complex with mCPBA or ozone.

(3) Heme oxygenase catalyzes the regiospecific oxidative degradation of iron protoporphyrin IX (heme) to biliverdin, CO and Fe, utilizing molecular oxygen and electrons donated from the NADPH-cytochrome P450 reductase. The regioselective oxidation of the α-meso position by HO is quite unique, in contrast to the non-enzymatic heme degradation. We have shown the first evidence of the formation of biliverdin isomers other than biliverdinIXα by HO mutants.

Generation of Reactive Species via Electron Transfer on Metal Complexes, as Basis of Chemical Energy Conversion Systems

NAGATA, Toshi; ITO, Hajime; ITO, Kaname

This project aims at developing redox catalysis reactions suitable for chemical energy conversion. Our current interest focuses on modeling photosynthesis, that is, driving endothermic chemical transformation by using light energy via photoinduced electron transfer. Progress has been made in the following topics during the last year:

A. Application of photoinduced electron transfer as a synthetic tool, where photoexcited organic molecules (like porphyrins) are considered from a synthetic point of view as short-lived reducing/oxidizing reagents. Two reaction systems, reductive silylation of quinones and diketones and oxidation of alcohols, have been discovered.

B. Development of binary ligands that allow control over the metal coordination environment. A new class of binary ligands, terpyridine-salicylaldehyde, were prepared and studies on the redox properties of the metal complexes are currently under way.

Design and Synthesis of New Tellurium-Containing Donors

KOBAYASHI, Hayao; SUZUKI, Toshiyasu; FUJIWARA, Hideki; OJIMA, Emiko

In the field of molecular conductors, systems based on tellurium-containing donor molecules have not received as much attention as systems based on sulfur- or selenium-containing donors. By incorporating heavy chalcogen atoms such as tellurium into donor molecules, a new metallic system with a wider bandwidth and a higher dimensionality is expected to appear. We have synthesized two TTeF derivatives of 1-Benzyl-2,5-dihydropyrrole and 1-Methyl-2,5-dihydropyrrole. The X-ray structure analyses showed that the intermolecular Te-Te distances are shorter than the sum of the van der Waals radii (3.95 and 3.96 Å, respectively).

Ball on Disk Tribometer

WATANABE, Michio; KONDOH, Takuhiko; MIYASHITA, Harumi

This year we have newly built a Ball on Disk Tribometer (Figure 1) to clear frictional phenomena of metals,ceramics,macromolecular materials and surface modificated materials.

Now we are evaluating the performance both in antigalling and in coefficient of friction regard to some samples.

Figure 1. Ball on Disk Tribometer.

Investigation of Dynamics on Photo-Excited Solids and Surfaces by Using the Combination of Synchrotron Radiation and Laser

KAMADA, Masao; TAKAHASHI, Kazutoshi

Dynamics on solids and surfaces excited by photons has attracted much interest from both of basic and application sides. We have been investigating the photo-induced phenomena using the combination of synchrotron radiation and laser. Photo-induced core-level shifts observed on GaAs (100) can be interpreted in terms of surface photo-voltage effects. To understand the non-equilibrium dynamics of the negative-electron affinity on GaAs surfaces is an interesting subject and is useful for producing a practical spin-polarized electron emitter. We have investigated the time-response on the negative-electron affinity GaAs surfaces using photoelectron spectroscopy.

It is also important subject to investigate photo-induced phase transition using photoelectron spectroscopy based on the combination of synchrotron radiation and laser. Core-level and valence-band photoelectron spectra showed clearly the characteristics of the photo-induced phase.

We have been also investigating the two-photon excitation experiments using synchrotron radiation and laser in recent years, since simultaneous excitation with two photons (SR and laser) is interesting and promising field to understand the symmetry-forbidden states and excited-state dynamics. The experiments are in progress on BaF_2 and ZnSe.

OKAZAKI CONFERENCES

The Sixty-Fourth Okazaki Conference

Molecular Orbital Theory for the New Millennium (January 21–23, 2000)

Organizers: **TEN-NO, Seiichiro** *(Nagoya Univ.)*
NAKANO, Haruyuki *(Univ. Tokyo)*
HADA, Masahiko *(Univ. Kyoto)*

Invited Overseas Speakers:
LINDH, Roland *(Univ. Lund, Sweden)*
HARRISON, Robert J. *(Pacific Northwest Natl. Lab., U. S. A.)*
MUKHERJEE, Debashis *(Indian Assoc. Cult. Sci., India)*
HEAD-GORDON, Marin *(Univ. California, Berkeley, U. S. A.)*
NOGA, Jozef *(Slovak Acad. Sci., Slovakia)*
KOCH, Henrik *(Univ. Southern Denmark, Odense, Denmark)*
JENSEN, Jan H. *(Univ. Iowa, USA)*
LEE, Yoon S. *(KAIST, South Korea)*
HESS, Bernd A. *(Univ. Erlangen, Germany)*

Owing to the recent algorithmic and theoretical progresses according to the development of high-speed super computers, theoretical chemistry is entering a new dimension. For the past decade, remarkable progresses have been put forward in the molecular orbital theory especially in the following topics: 1) Scalable molecular orbital theory for large molecular systems, 2) A new molecular orbital theory using reduced density matrices as variational parameters, 3) Multireferece many electron theories for accurate calculations of quasi-degenerated systems, which may include chemical reactions and excited states, 4) Many electron theories including the complete basis set effects for calculations with spectroscopic accuracies, 5) Treatment of solvents and inert fragments as effective potentials, 6) Relativistic molecular orbital theory accurately approximating the 4-component equations. On entering the new millennium, the 64th Okazaki conference explored new dimensions and directions in the molecular orbital theory, mainly focusing on scalable quantum chemical methods and multireference many electron theories and inviting leading quantum chemists having devoted contributions for modern strategies in the molecular orbital theory.

The Sixty-Fifth Okazaki Conference

Advantages of Utilization of SR in Nano-Structure Creation (January 27–29, 2000)

Organizers: **URISU, Tsuneo** *(IMS)*
KUROSAWA, Kou *(IMS)*

Invited Oversea Speakers:
BACHER, W. *(Forschungszentrum Karlsruhe)*
BERMUDEZ, V. M. *(Naval Res. Lab.)*
GRAY, S. M. *(Lund Univ.)*
JO, S.K. *(Kyung Won Univ.)*
SCHWENTNER, N. *(Freie Univ. Berlin)*
URQUART, S. G. *(Univ. Saskatoon)*
WEAVER, J. H. *(Univ. Illinois Urbana-Campain)*

Nanostructures, which is expected to realize a new functional devices using quantum effects, has lately attracted considerable attention. However, techniques of fabricating the nanostructures by controlling sizes and orientations with sufficient precision are not yet sufficiently developed, and this hinders nanostructures to realize its expected excellent performances. To create ideal nanostructures, atom-molecule-level evaluation and controls of the surface reactions are essentially important, and the technological developments based on the new sciences such as synchrotron radiation science is necessary. In this conference, scientists in many different field such as surface science, solid sate physics, semiconductor materials and processes, who are interested in the creation of nanostructures with controlled structures and orientations by the atom and molecule-level preciseness have gathered and discussed about the subjects of photo-excited surface reactions, method of nanostructure fabrication and its evaluation technologies. Especially, the discussions were made emphasizing the role of synchrotron radiation in the nanostructure fabrication and evaluations, and the future prospects.

JOINT STUDIES PROGRAMS

As one of the important functions of an inter-university research institution, IMS undertakes joint studies programs for which funds are available to cover research expenses as well as travel and living expenses of individuals. The proposals from domestic scientists are reviewed and controlled by an inter-university committee. The programs are carried out under one of five categories:

(1) Joint Studies on Special Projects (a special project of significant relevance to the advancement of molecular science can be carried out by a team of several groups of scientists).
(2) Research Symposia (a symposium on timely topics organized by collaboration between outside and IMS scientists).
(3) Cooperative Research (a research program carried out by outside scientists with collaboration from an IMS scientist).
(4) Use of Facility (a research program carried out by outside scientists at the research facilities of IMS except the UVSOR facility).
(5) Joint Studies Programs Using beam lines at the UVSOR Facility.
A. Special Projects, B. Cooperative Research Projects, C. Invited Research Projects, D. Use-of-UVSOR Projects.

In the fiscal year 1999, the numbers of joint studies programs accepted for categories (1)–(4) were 1, 10, 115, and 216, respectively, and those accepted for subcategories 5(A)–5(D) were 1, 8, 2, and 150, respectively.

(1) Special Projects

A. Molecular Theory of Chemical Reactions in Solution

HIRATA, Fumio; KINOSHITA, Masahiro[1]; SATO, Hirofumi; YOSHIMORI, Akira[2]; MATSUBAYASHI, Nobuyuki[1]; NISHIYAMA, Katsura[3]; CHONG, Song-Ho[4]; ISHIDA, Tateki[5]
([1]Kyoto Univ.; [2]Kyushu Univ.; [3]Osaka Univ.; [4]München Tech.; [5]Univ. Texas)

Outline of the project:

There are two aspects in chemical reactions: the reactivity or chemical equilibrium and the reaction dynamics. The reactivity of molecules is a synonym of the free energy difference between reactant and product. Two important factors determining the reactivity in solution are the changes in the electronic structure and the solvation free energy. Those quantities can be evaluated by the coupled quantum and the extended RISM equations, or the **RISM-SCF** theory. Formulating the reaction dynamics is much more demanding. The reaction dynamics in solutions involves two elements to be considered. One of those is the determination of reaction paths, the other the time evolution along the reaction path. The reaction path can be determined most naively by calculating the free energy map of reacting species. The RISM-SCF procedure can be employed for such calculations. If the rate-determining step of the reaction is an equilibrium between the reactant and the transition state, the reaction rate can be determined from the free energy difference of the two states based on the transition state theory. On the other hand, for such a reaction in which dynamics of solvent reorganization determines the reaction rate, the time evolution along the reaction path may be described by a coupled RISM and the generalized Langevin equation (GLE) with the same spirit as the Kramers theory: the time evolution along a reaction path can be viewed as a stochastic barrier crossing driven by thermal fluctuations and damped by friction. Our treatment features microscopic description of solvent structure in the level of the density pair correlation functions, which distinguishes the theory from the earlier attempts using phenomenological solvent models.

In the joint study proposed here, we challenge two important problems in chemical reactions in solution. The first is photochemical reactions which involve a quantum-chemical treatment of excited states of a molecule and solvent effects. The other problem is related to the reaction rate, especially, the relation between dynamic properties of liquids such as the viscosity and the reaction rate. Such study requires an element of the non-equilibrium statistical mechanics in order to describe solvent dynamics. In the recent study, we have proposed a new theory based on the interaction-site model of liquids, which describes the solvent response to changes of solute (electronic structure , position, *etc.*) in terms of the collective excitation in liquids.

Summary:

It is the electronic structure of molecules that primarily governs a chemical reaction. However, for a reaction in solution, it is also well regarded that solvent plays an essential role to determine both direction (equilibrium) and rate of the reaction. Formulation of such a problem requires two theoretical elements: the electronic structure theory (quantum chemistry) and the statistical mechanics of liquids. Few years ago, we have proposed a theory referred to as RISM-SCF which combines the two theoretical elements, and have clarified a variety of chemical reactions in solution, including the problem related to the proton affinity. These problems were concerned basically with the stability of a chemical species in solution.

Problem studied along this line during the last two and a half year are summarized in the following.

(1) Keto-enole isomerization reaction of form-amide in aprotic polar solvents.
(2) Water structure and auto-ionization (pKw) in a wide range of temperature and density including the super-critical region.

(3) Syn-anti equilibrium of acetic-acid in water.
(4) Reaction free energy surface of a Menshutkin reaction.
(5) Solvent effect on keto-enole isomerization reaction of acetyle-acetone.
(6) Acid-base equilibrium in of hydrogen-halide in water.
(7) Diels-Alder reaction in ambient and super-critical water.

The other aspect in chemical reactions requires development in non-equilibrium statistical mechanics of molecular liquids. The progress made along this lines are summarized as follows.

(1) Development of a new theory for dynamics of molecular liquids based on the interaction-site model and the mode-coupling theory.
(2) Calculation of the time correlation functions based on the new theory.
(3) Ion dynamics in polar solvent.
(4) Theory for dynamics of water.
(5) Ion dynamics of water.
(6) Excited state dynamics of a molecule in a variety of solvent.

In what follows, we provide a brief outline of the progress made in the project for few selected topics.

A-1 Acid-Base Equilibrium in Aqueous Solutions of Hydrogen Halides

Among the hydrogen halides in aqueous solutions, the hydrogen fluoride (HF) exhibits weak acidity, while all the other halides (HCl, HBr, HI) are classified as strong acids. Considering the fact that the electronegativity of the fluorine atom (F) is the largest among the halogen atoms, the behavior contradicts apparently with our intuition. The problem has attracted a lot of attentions by theoretical chemists from the earliest stage in development of the quantum chemistry. In fact, L. Pauling discussed the problem in his famous text book “Nature of Chemical Bonds.” The key to solve this puzzle is to take account for “solvent effects.” Pauling has shown based on the experimental data of the solvation free energy that the non-dissociated state of HF in aqueous solution has lower free energy than its dissociated state. Unfortunately, Pauling could not explain in molecular level why the non-dissociated state is more stable than the dissociated state, because his analysis was entirely phenomenological.

We have revisited the classical problem with our new theoretical tool, the **RISM-SCF** method, and have clarified in molecular detail the reason why FH shows weak acidity. In that study, we first have shown qualitatively that HF in fact is a weak acid, and have provided the following answer to the question why the non-dissociated state is more stable. The hydrogen fluoride can form two types of hydrogen-bonds with water molecules, (H_2O–––H–F and HF–––H–O–H), while the other hydrogen halide can make only one hydrogen-bond (H_2O–––H–X).

The thermodynamic cycle for the reaction is illustrated in Figure 1. The process VI in the cycle corresponds to the acid-base equilibrium in solution, and the free energy (ΔG(VI)) associated with the process determines the strength of the acid. The processes, I, II, V are reactions in gas phase, and the free energy change associated with the reactions can be obtained from the electronic-state calculation for isolated molecules involved in the reactions. The free energy change for the processes III and IV, which are associated with dissolving of the molecules into water, or the solvation free energies, can be calculated based on the RISM-SCF method. The RISM-SCF results for ΔG(VI) are shown by the solid lines in Figure 2, along with the results by Pualing and McCoubrey, which have been separately obtained based on the experimental estimates of the solvation free energy. In the figure, the data plotted by the filled circles represent those obtained from the RHF level of the electronic state calculation, while those by the filled triangles depict the results from the calculation with electron correlation in the MP2 level. As can be clearly seen, the RISM-SCF calculations, both with and without electron correlation, reproduce the empirical estimates due to Pauling and McCoubrey, which of course agree qualitatively with experiments stated above: namely, the non-dissociated state of HF is more stable than its dissociated state, while the other hydrogen halides show opposite trend. The physical reason why such inversion of stability occurs can be clarified by examining the radial distribution functions (RDF) of water molecules around the dissociated and non-dissociated hydrogen-halides, which are shown in Figures 3a and 3b. Exhibited in Figure 3a is the RDF between the oxygen atoms of water and the hydrogen atoms in HX. The results indicate that those atom pairs form strong hydrogen-bond for all the hydrogen halides studied. On the other hand, the RDF between water hydrogen and the halogen atom of solute (Figure 3b) shows a conspicuous peak at around 1.7 A only for HF, which is indicative of a hydrogen-bond. These are illustrated schematically in Figure 4. The results strongly indicate that HF gains the excess stability in its non-dissociated form by making two types of hydrogen-bonds.

The problem studied above is what has been taught in the high school chemistry, and it has been discussed by Pauling in his text book in order to demonstrate the victory of quantum mechanics in the field of molecular science. The present study is the first to clarify the essential physics of the problem in molecular details.

$$\begin{tikzcd}
& \frac{1}{2}X_{2(vac.)}+\frac{1}{2}H_{2(vac.)}+H_2O_{(vac.)} \arrow[dl, "I"'] \arrow[dr, "II"] & \\
HX_{(vac.)}+H_2O_{(vac.)} \arrow[rr, "V"] \arrow[d, "III"'] & & H_3O^{+}_{(vac.)}+X^{-}_{(vac.)} \arrow[d, "IV"] \\
HX_{(aq.)}+H_2O_{(aq.)} \arrow[rr, "VI"] & & H_3O^{+}_{(aq.)}+X^{-}_{(aq.)}
\end{tikzcd}$$

Figure 1. Thermodynamic Cycles for Chemical Processes of Hydrogen Halides.

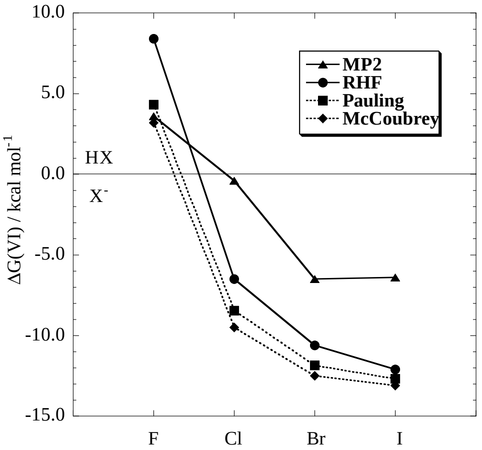

Figure 2. Free energy differences between hydrogen halides (HX) and its dissociated anion (X^-).

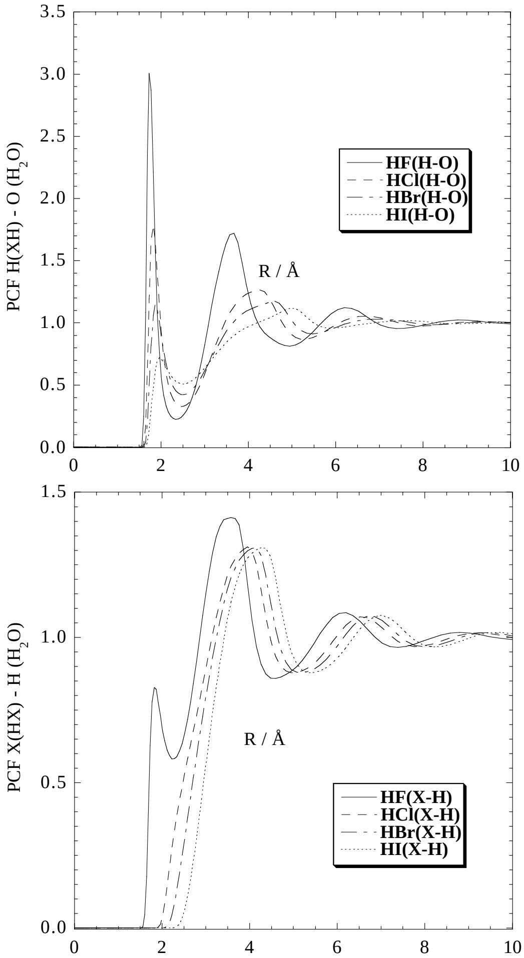

Figure 3. Pair correlation Functions of hydrogen halides; (a) H-water(O), (b) X-water(H)

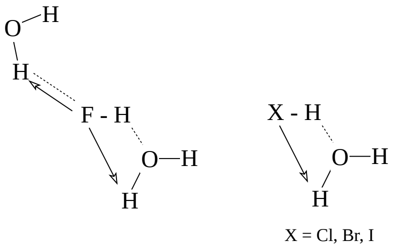

Figure 4. Illustration of hydrogen-bond structure of HF and other hydrogen halides.

A-2 Diels-Alder Reactions in Ambient and Supercritical Water

Organic reactions utilizing the supercritical water have been attracting much attention from the industrial chemistry, since it provides a great possibility of minimizing the effect on environment. The Diels-Alder reaction is a cyclo-addition reaction, which is reported to be greatly accelerated by aqueous solvent. Recent experiments indicate that the rate and yield of the reaction increase dramatically by bringing the solvent to supercritical conditions. In the study, we have investigated the Diels-Alder reaction concerning methyl-vinyl-ketone and cyclopentadiene in ambient and supercritical water based on the RISM-SCF method. (Figure 1) In the study, we have intended to answer the following questions.

(a) Why and how the reaction is accelerated when the system is transferred into aqueous environment from gas phase?

(b) Is the physical cause of the increase in reaction rate in the super-critical condition same as that in ambient water?

(c) Why the reaction yield increases in the supercritical conditions?

(d) How the stereo-selectivity is influenced by solvent?

In Figure 2, shown is the free energy diagram concerning the reaction obtained from the RISM-SCF calculation. (All the results are relative to the free energy of the reactant.) It is obvious from the results that the reaction proceeds favorably in aqueous environment compared to in gas phase at normal conditions, and that the reaction rate dramatically increases. The solvent effect can be decomposed into the electrostatic and hydrophobic contributions. Such decomposition indicates that the hydrophobic effect contributes dominantly to increase the reactivity as well as the reaction rate. The electrostatic effect becomes rather small because the stabilization due to the hydrogen-bond is largely canceled out by the destabilization caused by electronic distortion. The reason why the reactivity and the reaction rate increase in aqueous environment is because the probability of the two non-polar solutes being in contact is enhanced by the hydrophobic interaction. Unlike the case of the ambient condition, the solvent effect in supercritical water is not so large with respect to both the reactivity and reaction rate. In this case, the reactivity and reaction rate are governed by the thermal motion due to temperature increase, not by the solvent effects.

Figure 2 indicates that the equilibrium of the reaction in the supercritical condition favors the reactant. This apparently contradicts with the experimental results which exhibit dramatic increase of the reaction yield upon transferring the system from the ambient to supercritical environments. However, the apparent contradiction can be resolved if one considers that the yield is determined not only by the equilibrium constant but also by other factors, especially, by the solubility of the reactant species. Let us define the apparent yield by $K_{\mathrm{eff}} = K_{\mathrm{H}}K$, where K_{H} and K are the solubility and the equilibrium constant, respectively. The equilibrium constant K in the supercritical condition is $1/10^7$ of that in the ambient water, while K_{H}

is about 10^{11} times greater in the supercritical water. Consequently, the yield as a product of those constants exhibits marked increase.

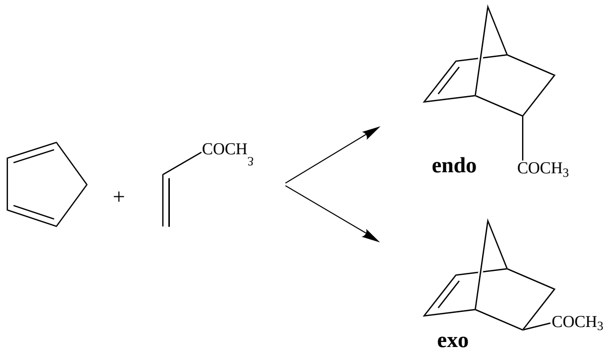

Figure 1. Scheme of the reaction.

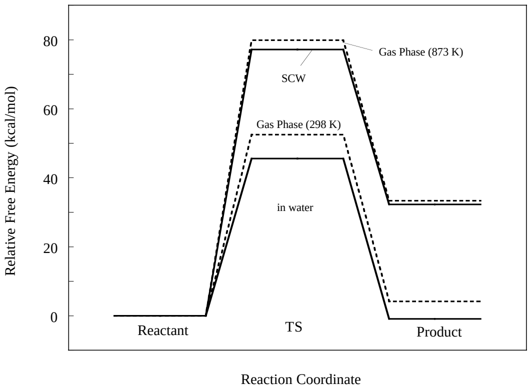

Figure 2. The total free energies of TS and the products relative to those of the reactants for the end-trans reaction.

A-3 Excited States Dynamics of Benzonitrile in Water, Alcohol, and Acetonitrile

When a molecule in polar liquids is photo-excited, a relaxation process of solvent molecules around the solute is induced, because the solvent configuration is not in equilibrium with the electronic state of solute right after the vertical excitation. The process is called "solvation dynamics." Conversely, the solvent dynamics induces time dependent change in the excited state of solute. Such processes can be observed experimentally by means of the time resolved Stokes shift, providing detailed information with respect to the dynamics of solvent and solute excited states. In the present study, we have investigated such a problem based on the RISM-SCF method coupled with the theory of solvation dynamics which we have proposed few years ago.

In order to formulate the problem, we generalize the expression for the reaction field in solvated Fock operator such that the time dependent solvent dynamics can be taken account,

$$V_u(t) = \rho \sum_{j \in u} \int_0^{\infty} \frac{q_j}{r} g_{uj}(r,t) 4\pi r^2 dr,$$

where $g(r;t)$ is the space-time correlation function, which describes time evolution of the solvent distribution around solute. Given $g(r;t)$, one can realize the time evolution of the solute excited state in solution by solving the Schrodinger equation at each step of discretised time course after the vertical excitation. It is therefore crucial to be able to calculate $g(r;t)$. Here, we employ the most primitive method, the site-site Smolchowski-Vlasov (SSSV) theory, to obtain $g(r;t)$ [F. Hirata, *J. Chem. Phys.* **96**, 4619 (1992)].

In the present study, we examine the excited state dynamics of benzonitrile (BN) in three different solvents; water, alcohol, and acetonitrile. Shown in Figure 1 is the structure (bond lengths, bond angles) of BN in ground state along with the corresponding experimental data, which are in parenthesis. In Figure 2, we have shown a typical example of $g(r;t)$ between solute and water at $t = 0$ and $t = \infty$ calculated by means of SSSV. One can see how the hydrogen-bond between solute-N_8 and water-H strengthens as time elapses. In Figure 3, shown is the dipole moment of BN as a function of time. In all cases, the behavior can not described by a single exponential, but requires more than two time constants. It can also be understood that the behavior is very sensitive to solvent.

The most interesting results obtained in the study is the time correlation function ($C^u{}_q(t)$) of the partial charges of solute atoms, which is defined by;

$$C_q^u(t) = \frac{q_u(t) - q_u(\infty)}{q_u(0) - q_u(\infty)}$$

where $q_u(t)$ is the partial charge of the atom u of BN at time t after the vertical transition (t = 0). Therefore, $C^u{}_q(t)$ describes how the partial charges of solute atoms increased (or decreased) after the vertical transition. It is readily seen from the Figure 4 that the time dependence of the partial charges is different qualitatively from atom to atom. For example, in water and methanol, the partial charges on C_6 (dashed lines) and N_8 (dense dotted lines) exhibit monotonic decrease, while those on C_1 (solid lines) and C_7 (coarse dotted lines) decreases rapidly short time after the transition, but turn into increase. Even more interesting is the qualitative difference in behaviors observed in the hydrogen-bonded solvent (water and methanol) and the non-hydrogen-bonded polar liquid (acetonitrile). Such difference is conspicuous in the behavior of the charge on C_1. Considering the sign of the charges, it can be concluded that global flow of electrons takes place from C_6 to N_8 as time elapses: it is the reason why the partial charges of those atoms change monotonically. However, the story is not that simple for the atoms located in between C_6 to N_8. In the case of water and methanol, the electron population on C_1 overshoots that of the final (equilibrium) state in the initial period, while that on C_7 is too short. Then, the electron transfers from C_1 to C_7 to settle down in equilibrium states. Although we have not carried out further study with respect to the electronic structure, such study will reveal detailed dynamics of the excited states of solvated molecules.

To our knowledge, this is the first attempt to realize time evolution of electronic charge on atoms in solution after the vertical transition. There is no experimental data available at the moment, which corresponds to our theoretical results. It should be deferred to future study to verify if the theoretical prediction is correct or not. The essential contribution of the new treatment is to have proposed a new methodology which describes the excited state dynamics of a molecule in solution in atomic detail without making use of empirical parameters.

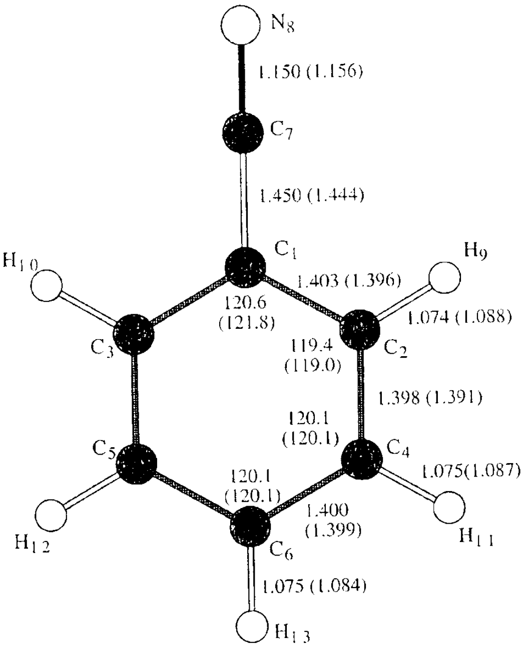

Figure 1. Optimized geometry for benzonitrile in the gas phase with site numbering. Values in parentheses are the experimental values.

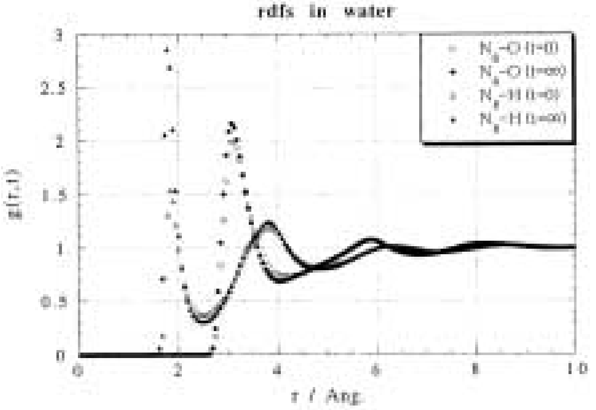

Figure 2. Time dependent radial distribution functions between the solute and solvent sites in water. Those before and after the solvent relaxation are denoted by *t* = 0 and *t* = infinity.

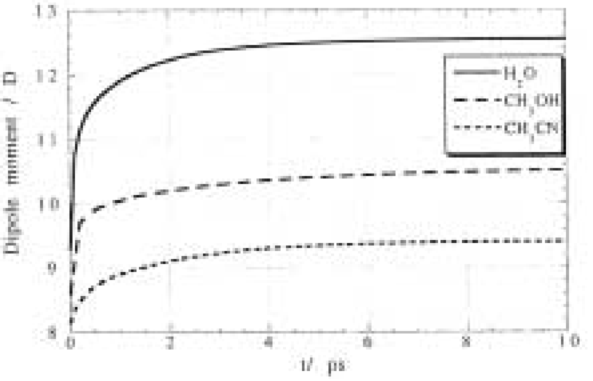

Figure 3. Time dependent variations of solute dipole moment after the vertical excitation.

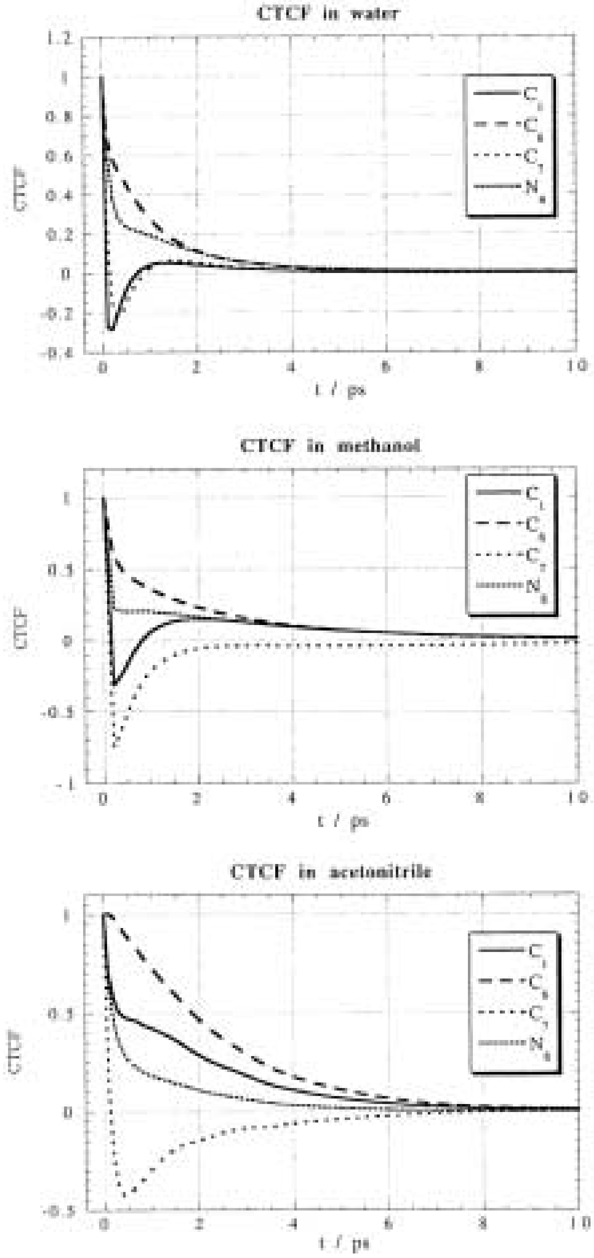

Figure 4. Solute charge time correlation functions for C_1, C_6, C_7, and N_8 sites in benzonitrile: (a) in H_2O, (b) in CH_3OH, (c) CH_3CN.

References

1) T. ISHIDA, F. HIRATA and S. KATO, "Thermodynamics analysis of the solvent effect on tautomerization of acetylacetone: An ab initio approach," *J. Phys. Chem.* **110**, 3938 (1999).
2) K. Naka, H. Sato, A. Morita, F. Hirata and S. Kato, "RISM-SCF study for the free energy profile of Menshutkin type reaction $NH_3 + CH_3Cl \rightarrow NH_3CH_3^+ + Cl^-$ in aqueous solution," *Theor. Chem. Acc. (Fukui issue)* **102**, 1, 165, (1999).
3) H. Sato and F. Hirata, "The syn- / anti- conformational equilibrium of acetic acid in water studied by the RISM-SCF/MCSCF method," *THEOCHEM (Morokuma issue)*, **461-462**, 113 (1999).
4) H. SATO and F. HIRATA, "Revisiting the acid-base equilibrium in aqueous solutions of hydrogen halides: study

by the ab initio electronic structure theory combined with the statistical mechanics of molecular liquids," *J. Am. Chem. Soc.* **121**, 2460 (1999).
5) S. Chong and F. Hirata, "Dynamics of Ions in Liquid Water: An Interaction-Site-Model Description," *J. Chem. Phys.* **111**, 3654 (1999).
6) S. Chong and F. Hirata, "Interaction-Site-Model Description of Collective Excitations in Liquid Water I: Theoretical Study," *J. Chem. Phys.* **111**, 3083 (1999).
7) S. Chong and F. Hirata, "Interaction-Site-Model Description of Collective Excitations in Liquid Water II: Comparison with Simulation Results," *J. Chem. Phys.* **111**, 3095 (1999).
8) H. Sato and F. Hirata, "Ab initio Study on Molecular Properties and Thermodynamics of Water: A Theoretical Prediction of pKw over a Wide Range of Temperature and Density," *J. Phys. Chem. B* **103**, 6596 (1999).
9) T. Ishida, F. Hirata, and S. Kato, "Solvation dynamics of benzonitrile excited state in polar solvents: A time-dependent reference interaction site model self-consistent field approach," *J. Chem. Phys.* **110**, 11423 (1999).
10) H. Sato and F. Hirata, "ab initio study of water (II): liquid structure, electronic and thermodynamic properties over a wide range of temperature and density," *J. Chem. Phys.* **111**, 8545 (1999).
11) Y. Harano, H. Sato, and F. Hirata, "Solvent Effects on a Diels-Alder Reaction in Supercritical Water: RISM-SCF study," *J. Am. Chem. Soc.* **122**, 2289 (2000).
12) Y. Harano, H. Sato, and F. Hirata, "Theoretical Study on Diels-Alder Reaction in Ambient and Supercritical Water: Viewing Solvent Effect through the Frontier Orbitals," *Chem. Phys.* **258**, 151 (2000).
13) K. Nishiyama, F. Hirata, and T. Okada, "Average Energy Relaxation and Rearrangement of Solute-Solvent Radial Distribution Function in Solvation Dynamics: A Connection between Spectroscopic Results and RISM Theory," *J. Mol. Liq.* in press.

(2) Research Symposia

(from September 1999 to August 2000)

1. Design and Synthesis of Novel π Electron Systems
   (November 28–30, 1999)
   Chair: **MISAKI, Yoji**

2. New aspects in nonlinear optical materials and devices
   (November 29, 1999)
   Chair: **TAIRA, Takunori; KURIMURA, Sunao**

3. Current Status and Future Prospect of Physical Chemistry II
   (December 6, 1999)
   Chair: **YOSHIHARA, Keitaro** *(JAIST)*

4. Core-Level Excited State and its Dynamics—Current Status and Future Prospect—
   (January 6–7, 2000)
   Chair: **NAGAOKA, Shinichi**

5. Chemistry and Physics of Microparticles and Clusters composed of Transition Metal Atoms
   (March 8–9, 2000)
   Chair: **KONDO, Tamotsu** *(Toyota Inst. Tech.)*

6. Molecular Science of Condensed-Phase Dynamics: Now and Future
   (May 25–27, 2000)
   Chair: **TAHARA, Tahei**

7. Symposium on Physical Chemistry for Young Researchers of Molecular Science
   (June 9, 2000)
   Chair: **MIKAMI, Naohiko** *(Tohoku Univ.)*

8. Vibrational Spectroscopy of Proteins
   (June 22–24, 2000)
   Chair: **OGURA, Takashi** *(Univ. Tokyo)*

9. New aspects of Stereodynamics in Chemical Reactions
   (July 18–19, 2000)
   Chair: **OHNO, Koichi** *(Tohoku Univ.)*

10. Current Aspects and Future Prospects of Spin Chemistry—Possibility of High Frequency Electron Spin Resonance—
    (July 18–19, 2000)
    Chair: **KATO, Tatsuhisa**

(3) Cooperative Research

This is one of the most important categories that IMS undertakes for conducting its own research of the common interest to both outside and IMS scientists by using the facilities at IMS. During the first half of the fiscal year of 1999 ending on September 30, 48 outside scientists joined Cooperative Research programs and during the second half, 67 outside scientists did. The names and affiliations of those collaborators are found in Research Activities.

(4) Use of Facility

The number of projects accepted for the Use-of-Facility Program of the Computer Center during the fiscal year of 1999 amounted 166 (664 users) and computer time spent for these projects is 70, 251 hours (converted to the IBM SP2 time), and amounted to 93% of the total annual CPU time used. The numbers of projects accepted for the Use-of-Facility program during the fiscal year of 1999 amounted to 14 for the Laser Research Center for Molecular Science and 47 for the Research Center for Molecular Materials.

(5) UVSOR

In the UVSOR Facility with the 750 MeV electron storage ring, there are twenty beam lines available for synchrotron radiation research (see *UVSOR ACTIVITY REPORT 1999*). The Experimental Facility of each beam line is described also in this report. Under the following programs, a number of SR studies have been carried out by many users outside and inside IMS: A. the UVSOR Special Projects, B. the UVSOR Cooperative Research Projects, C. the UVSOR Invited Research Projects, and D. the Use-of-UVSOR Projects.

A. UVSOR Special Project

In fiscal year of 1999, following UVSOR special projects have been carried out.

1. Title: Construction of angle-resolved photoelectron spectrometer for organic thin films
   Beam Line: 8B2
   Representative of project: **UENO, Nobuo**

B. UVSOR Cooperative Research Projects

Under this joint-study program, many synchrotron radiation experiments have been carried out with the beam lines of in-house staff in cooperation with scientists who were invited from other institutions. The total number of the projects in this category was 8 in the fiscal year of 1999.

C. The UVSOR Invited Research Projects

Under this joint-study program, several scientists were invited from other institutions of help for construction of new beam lines and improvement of the UVSOR storage ring and others. The total number of the projects in this category was 2 in the fiscal year of 1999.

D. The Use-of-UVSOR Projects

Tne out of the total of nineteen UVSOR beam lines are available for general users outside and inside IMS for their synchrotron radiation studies in the field of molecular science. The total number of the projects in this category was 147 in the fiscal year of 1999.

FOREIGN SCHOLARS

Visitors from abroad are always welcome at IMS and they have always played an important role in the research activities of the Institute. The foreign scientists who visited IMS during the past year (September 1999–August 2000) are listed below.

[*1] indicates attendance at an Okazaki Conference; [*2] a MONBUSHO (the Ministry of Education, Science, Sports and Culture, Japan) or JSPS (the Japan Society for the Promotion of Science) Invited Fellow; [*3] an IMS councillor; [*4] an IMS visiting professor or associate professor from abroad (period of stay from 6 to 12 months); [*5] a JSPS Post-Doctoral or Ronpaku Fellow; [*6] an IMS visiting scientist and [*7] a visitor to IMS.

Scientists who would like to visit IMS under programs [*2] and [*4] are invited to make contact with IMS staff in their relevant field.

Dr. Hu Ying[*5]	Fudan University	(China)	Nov. ’98–
Dr. Sergei Y. Arzhantsev[*5]	Moscow State University	(Russia)	Nov. ’98–
Dr. Nicolaie Pavel[*2][*4]	Atomic Physics National Institute	(Romania)	Mar. ’99–
Dr. Franz Xaver Bronold	Otto-von-Guericke-University	(Germany)	–Sep. ’99
Prof. Anthony Siegman[*6]	Stanford University	(U. S. A.)	Sep. ’99
Prof. Poh-Kun Tseng [*7]	Synchrotron Radiation Research Center	(China)	Sep. ’99
Dr. Olga Drozdova[*7]	Russian Academy of Sciences	(Russia)	Sep. ’99
Dr. Tamar Seideman[*7]	The Steacie Institute for Molecular Science	(Canada)	Sep. ’99
Dr. Christopher Whitham[*6]	Oxford University EPSRC	(U. K.)	Sep.–Dec. ’99
Prof. Lubomir Pavlov[*2][*4]	Bulgarian Academy	(Bulgaria)	Sep. ’99–Mar. ’00
Prof. Xian-He Bu[*2][*5]	Nankai University	(China)	–Oct. ’99
Prof. Klaus Müller-Dethlefs[*2]	The University of York	(U. K.)	–Oct. ’99
Prof. Anders Irbäck[*7]	Lund University	(Sweden)	Oct. ’99
Prof. Angel E. Garcia[*7]	Los Alamos National Laboratory	(U. S. A.)	Oct. ’99
Prof. Marian Kryszewski[*6]	Polish Academy of Sciences	(Poland)	Oct. ’99
Prof. Stanislaw Kryszewski[*6]	University of Gdanisk	(Poland)	Oct. ’99
Dr. John S. Tse[*7]	Steacie Institute for Molecular Science	(Canada)	Oct. ’99
Prof. Martin Fejer[*6]	Stanford University	(U. S. A.)	Oct.–Nov. ’99
Prof. Jiri Horacek[*7]	Charles University	(Czech)	Oct.–Nov. ’99
Dr. Salai Cheettu Ammal[*7]	Tohoku University	(Japan)	Oct. ’99–Mar. ’00
Dr. Mark P. Roach[*5]	University of South Carolina	(Canada)	–Nov. ’99
Prof. Ingolf Lindau[*6]	Lund University	(Sweden)	Nov. ’99
Dr. Marc Simon[*7]	LURE	(France)	Nov. ’99
Dr. Gennady Mil’nikov[*5]	Inst. of Chemical Phys.	(Russia)	–Dec. ’99
Prof. Luis Seijo[*2]	Universidad Autonoma de Madrid	(Spain)	–Dec. ’99
Prof. Vladimir I. Osherov[*2]	Russian Academy of Sciences	(Russia)	–Dec. ’99
Prof. Denis Salahub[*6]	University of Montreal	(Canada)	Dec. ’99
Dr. Olga Drozdova[*7]	Russian Academy of Sciences	(Russia)	Dec. ’99
Prof. Hans Ågren[*6]	Royal Institute of Technology	(Sweden)	Dec. ’99
Prof. Klaus Müller-Dethlefs[*7]	The University of York	(U. K.)	Dec. ’99
Dr. Hrusak Jan[*7]	Heyrovsky Inst. of Phys. Chem.	(Czech)	Dec. ’99
Dr. Petr Nachtgall[*7]	Heyrovsky Inst. of Phys. Chem.	(Czech)	Dec. ’99
Prof. Sotiris Xantheas[*7]	Pacific Northwest Laboratories	(U. S. A.)	Dec. ’99
Prof. Rainer Weinkauf[*7]	Heinrich Heine Universität	(Germany)	Dec. ’99
Prof. Michael Schmitt[*7]	Heinrich Heine Universität	(Germany)	Dec. ’99
Prof. Mike Duncan[*7]	University of Georgia	(U. S. A.)	Dec. ’99
Prof. Aolamowicz Ludwik[*7]	Arizona State University	(U. S. A.)	Dec. ’99
Prof. Michio Okumura[*6][*7]	California Institute of Technology	(U. S. A.)	Dec. ’99
Prof. Kyoung-koo Baeck[*7]	Kang-Nung National University	(Korea)	Dec. ’99
Prof. Peter Hackett[*6][*7]	National Research Council of Canada	(Canada)	Dec. ’99
Prof. Seong Keun Kim[*6][*7]	Seoul National University	(Korea)	Dec. ’99
Prof. James Lisy[*6][*7]	University of Illinois	(U. S. A.)	Dec. ’99
Prof. G. N.-Schatteburg[*7]	Technichen Universität München	(Germany)	Dec. ’99
Prof. Elis Kochanski[*7]	Universitë Louis Pasteur	(France)	Dec. ’99
Prof. Ori Cheshnovsky[*7]	Tel Aviv University	(Israel)	Dec. ’99
Prof. Richard Zare[*3]	Stanford University	(U. S. A.)	Dec. ’99
Prof. Kwang S. Kim[*7]	Pohang University	(Korea)	Dec. ’99
Prof. Kyoung-Koo Baeck[*7]	Kang-Nung National University	(Korea)	Dec. ’99
Prof. Jim Muckerman[*7]	Brookhaven National Laboratory	(U. S. A.)	Dec. ’99
Prof. Leonard Proniewics[*7]	Jagellonian University	(Poland)	Dec. ’99–Jan. ’00
Prof. Jong-Ho Choi[*2]	Korea University	(Korea)	Dec. ’99–Feb. ’00
Prof. Sang Yeon Lee[*2]	Kyungpook National University	(Korea)	Dec. ’99–Feb. ’00

Prof. Gyusung Chung[*2]	Konyang University	(Korea)	Dec. ’99–Feb. ’00
Dr. Olga Drozdova[*7]	Russian Academy of Sciences	(Russia)	Jan. ’00
Prof. Kit H. Bowen[*6]	Johns Hopkins University	(U. S. A.)	Jan. ’00
Prof. Nicholas C. Handy[*7]	University of Cambridge	(U. K.)	Jan. ’00
Prof. David Baker[*7]	University of Washington	(U. S. A.)	Jan. ’00
Dr. Zhengtin Gan[*1]	North West University	(China)	Jan. ’00
Prof. K. Baeck Kyoung[*1]	Kang-Nung National University	(Korea)	Jan. ’00
Prof. B. A. Hess[*1]	Universitaet Erlangen	(Germany)	Jan. ’00
Prof. Yeon Sang Lee[*1]	Kyungpook National University	(Korea)	Jan. ’00
Prof. H. Jan Jensen[*1]	University of Iowa	(U. S. A.)	Jan. ’00
Prof. Henrik Koch[*1]	University of Southern Denmark	(Denmark)	Jan. ’00
Prof. Debashis Mukherjiee[*1]	Indian Association for the Cultivation of Science	(India)	Jan. ’00
Prof. Martin Hend-Gordon[*1]	University of California	(U. S. A.)	Jan. ’00
Prof. J. Robert Harrison[*1]	Pacific Nothwest National Laboratory	(U. S. A.)	Jan. ’00
Prof. Roland Lindh[*1]	University of Lund	(Sweden)	Jan. ’00
Prof. Debashis Mukherjee[*1]	Indean Association for Cultivation of Science	(India)	Jan. ’00
Prof. Jozef Noga[*1]	Slovakia Academy of Sciences	(Slovakia)	Jan. ’00
Prof. John H. Weaver[*1]	University of Illinois	(U. S. A.)	Jan. ’00
Prof. Stephen G. Urquhart[*1]	University of Saskatoon	(Canada)	Jan. ’00
Prof. Nikolaus Schwentner[*1]	Freie Universitaet	(Germany)	Jan. ’00
Dr. Victor Bermudez[*1]	Naval Research Laboratory	(U. S. A.)	Jan. ’00
Prof. Struan M. Gray[*1]	Lund University	(Sweden)	Jan. ’00
Prof. Sam K. Jo[*1]	Kyung Won University	(Korea)	Jan. ’00
Prof. Walter Bacher[*1]	Karlsruhe GMBH	(Germany)	Jan.–Feb. ’00
Dr. Maiti C. Nakul[*5]	Tata Institute for Funfamental Research	(India)	–Feb. ’00
Dr. Gennady Mil’nikov[*7]	Institute of Structural Macrokinetics	(Russia)	Feb.–Mar. ’00
Prof. Marcel Bogey[*5]	Universite des Sci. & Technologies de Lille	(France)	Feb.–Mar. ’00
Prof. Hyun Ahn Kwang[*2*4]	Kyung Hee University	(Korea)	Feb.–Jul. ’00
Prof. Wensheng Bian[*5]	Shandong University	(China)	Feb. ’00–
Dr. Bailleux Stephane[*5]	Universite des Sci. & Technologoe de Lille	(France)	–Mar. ’00
Dr. Puspita Waheeda Jahan[*6]	Nagoya University	(Japan)	–Mar. ’00
Prof. Ashot Markosyan[*7]	Moscow State University	(Russia)	–Mar. ’00
Mr. Prasanna Ghulsasi[*6]	BhaBha Atomic Research Center	(India)	–Mar. ’00
Prof. Shaul Mukamel[*7]	University of Rochester	(U. S. A.)	Mar. ’00
Dr. Richard Rosenberg[*7]	Advanced Photon Source	(U. S. A.)	Mar. ’00
Prof. Karl Freed[*2]	University of Chicago	(U. S. A.)	Mar. ’00
Prof. Stanislav Nespurek[*7]	Academy of Sciences of the Czech Republic	(Czech)	Mar. ’00
Dr. Dave Teehan[*6]	Daresbury Laboratory	(U. K.)	Mar. ’00
Prof. Bruce Hamilton[*6]	UMIST	(U. K.)	Mar. ’00
Prof. Bernhard Brutschy[*7]	Johann Wolfgang Goeth-Universität	(Germany)	Mar. ’00
Dr. David Rayner[*6]	National Research Council of Canada	(Canada)	Mar. ’00
Prof. Jiri Horacek[*7]	Charles University	(Czech)	Mar.–Apr. ’00
Prof. Vladimil Osherov[*7]	Russian Academy of Sciences	(Russia)	Mar.–Apr. ’00
Dr. Andriy Kovalenko[*7]	University of Utah	(U. S. A.)	Mar.–Apr. ’00
Prof. Josef Stepanek[*7]	Charles University	(Czech)	Apr.–May’00
Dr. Olga Drozdova[*2*4]	Russian Academy of Sciences	(Russia)	Apr. ’00–
Dr. Nakul Maiti[*5]	Tata Institute	(India)	Apr.–Jun. ’00
Prof. Coucouvanis Dimitri[*5]	University of Michigan	(U. S. A.)	May’00
Prof. Yasuyuki Ishikawa[*2]	University of Puerto Rico	(U. S. A.)	May.–Aug. ’00
Dr. Mkhitar Simonyan[*6]	Armenian Academy of Sciences	(Armenia)	May. ’00–
Prof. Yu-Jun Mo[*2*4]		(China)	May. ’00–
Prof. Zhengqiang Li[*2*4]		(China)	May. ’00–
Prof. Goswami Sreebrata[*7]	Indian Association for the Cultivation of Sci.	(India)	Jun. ’00
Prof. Hans Ågren[*6]	Royal Institute of Technology	(Sweden)	Jun. ’00
Prof. Hertel Ingolf[*6]	Max-Born Institute	(Germany)	Jun. ’00
Dr. Cheal Kim[*2]	Seoul National Polytechnic University	(Korea)	Jun.–Aug. ’00
Prof. Younkyoo Kim[*6]	Hankuk University of Foreign Studies	(Korea)	Jun.–Aug. ’00
Prof. Myoungsik Cha[*2]	Pusan National University	(Korea)	Jun. ’00–
Prof. Benjamin Whitaker[*2]	University of Leeds	(U. K.)	Jun. ’00–
Dr. Viktor Gritsenko[*2*4]	Russian Academy of Sciences	(Russia)	Jun. ’00–
Prof. Leigh Canham[*6]	Dera Malvern	(U. K.)	Jul. ’00
Prof. Bruce Hamilton[*6]	UMIST	(U. K.)	Jul. ’00
Prof. M.P. Halsall[*6]	UMIST	(U. K.)	Jul. ’00
Prof. Hywel Price[*6]	Daresbury Laboratory	(U. K.)	Jul. ’00

Dr. Jung Hoon Ro[*7]	Pusan National University	(Korea)	Jul. ’00
Prof. Lars Pettersson[*6]	Stockholm University	(Sweden)	Jul. ’00
Prof. Josef Hormes[*7]	Louisiana State University	(U. S. A.)	Jul. ’00
Prof. Jiri Hudecek[*6]	Charles University	(Czech)	Jul. ’00–
Prof. Alan Verma[*7]	North Eastern Hill University	(India)	Jul. ’00–
Prof. Jong-In Choe[*7]	Chung-Ang University	(Korea)	Aug. ’00–
Dr. Olga Gritsenko[*6]	Russian Academy of Science	(Russia)	Aug. ’00–

AWARDS

Professor Nakamura

Professor Hiroki Nakamura of Department of Theoretical Studies won the “Chunichi Culture Prize” in 2000 for his establishment of the fundamental theory of nonadiabatic transition due to curve crossing. Nonadiabatic transitions are well known to play crucial roles in various fields of physics, chemistry, and biology as one of the most important mechanisms of state and/or phase changes. Since the pioneering works done by Landau, Zener, and Stueckelberg in 1932, many investigators challenged to complete the theory with no full success. Professor Nakamura has also been working on the subject over twenty years, and recently he finally succeeded in obtaining the complete solutions of the Landau-Zener-Stueckelberg curve crossing problems in collaboration with his graduate student, C. Zhu. This theory provides the accurate compact formula for nonadiabatic transition probability, which replaces the celebrated Landau-Zener formula completely. Besides, it furnishes a complete set of accurate compact expressions for probabilities and phases to treat not only the Landau-Zener type but also the nonadiabatic tunneling type curve crossing problems. His research is thus evaluated as creating the fundamentally important aspects of nonadiabatic transitions, and it is expected that the theory would open up useful applications to a wide range of physical and chemical problems.

Professor Iwata’s Scientific Achievements

Professor Suehiro Iwata of Theoretical Division received the Chemical Society of Japan Award in 1999 for his contribution to “Developments of Molecular Orbital Theory and Applications to Molecular Science.” His scientific achievements relevant to the award are summarized as following.

1. Developments of effective Hamiltonian theory. He has developed new method of effective Hamiltonian in Fock-space representation, and proved that the semi-empirical formalism can be derived from his method.
2. Theoretical studies on electronic excited states and ionized states. He has developed “Valence vacant orbital method” to describe electronic excited states and ionized states. He applied his method to the assignments of photoelectron spectra and characterization of highly excited electronic states.
3. Theoretical contribution to Cluster Science. He has applied the Quantum Chemistry methods to the analysis of structure, reactivity and spectroscopy of molecular clusters, i.e., metal cluster, phenol-water system, and anionic states of water cluster. Especially, he has discovered that electronic structure of water cluster anion can be characterized as “electron-hydrogen bonding,” where a diffuse anionic orbital has new type of hydrogen bonding nature with surrounding H–O group.

Professor Watanabe’s Scientific Achievements

Professor Yoshihito Watanabe, Department of Applied Molecular Science, received the Scientific Award of the Chemical Society of Japan in 1999 for his contribution to “Elucidation of Molecular Mechanism for the Formation of High Valent Oxidative Intermediates in Heme Enzymes.” Proteins containing the heme prosthetic group catalyze various kinds of oxidation and oxygenation reactions. Prof. Watanabe’s studies aim to elucidate structure-function relationship of the protein moiety in activation of the O–O bond of peroxides. He focused his attention on the formation and decay mechanism of so called compound I intermediate, which should have an oxidized heme including $\mathrm{O{=}Fe^{V}}$ Por, $\mathrm{O{=}Fe^{IV}}$ $\mathrm{Por^{+\bullet}}$, $\mathrm{Fe^{III}Pro^{++}}$, $\mathrm{O{=}Fe^{IV}}$ Por + amino acid cation radical, $\mathrm{ROO{-}Fe^{III}}$ Por, or $\mathrm{Fe^{III}}$ Por N-oxide. He chemically synthesized each of them and characterized individually. According to his idea, for an enzyme to generate such high-valent species, a proton donor and acceptor should be located at a specified position. He introduced such residues to an appropriate position using site-directed mutagenesis technique and succeeded in converting myoglobin, an oxygen carrier protein, to a peroxidase. Thus his idea on the acid/base catalysis in the formation of high valent intermediates was proved.

Professor Fujita

Associate Professor Makoto Fujita of Coordination Chemistry Laboratories (1997–1999; currently, Professor of Graduate School of Engineering, Nagoya University) received the Divisional Award of the Chemical Society of Japan in Organic Chemistry in 1999 for his contribution to “Precise Construction and Function of Molecular Complexes through Self-Assembly”

His scientific achievements relevant to the award are summarized as follows.

1. Development of cis-endcapped transition metals (in particular, palladium(II)) as versatile units for metal-directed self-assembly of nano-sized, discrete organic frameworks such as square molecules, linked-ring molecules (catenane), cages, tubes, and capsules.
2. Development of new functions of self-assembled hollow cage frameworks exploiting the large cavity within the cage: *e.g.*, labile (or stable) molecules are stabilized (or activated).
3. Extension of the self-assembled discrete structures into infinite systems (coordination polymers), in particular, porous coordination networks that show zeolite-like functions.

Associate Professor Tahara's Scientific Achievements

Associate professor Tahei Tahara of Department of Vacuum UV Photoscience received the Morino Science Award in 2000 for his contribution to "Ultrafast Spectroscopic Study of the Dynamics of Condensed-Phase Molecules." Throughout his careers, he has been continuously working at the frontier of the time-resolved spectroscopic studies of photochemical processes in condensed phase. Starting from the nanosecond experiments, he has extended his research fields to even faster phenomena occurring in the picosecond and femtosecond time regions. Making the most use of vibrational and electronic spectroscopies, he has successfully clarified the dynamical properties of important elementary processes such as *cis-trans* isomerization and charge / proton transfer, which is essential for the full understanding of the chemical reactions. It is also highly noteworthy that he has been making enormous efforts to design and develop novel methods in time-resolved molecular spectroscopy. Thus, his scientific contributions have covered a broad range of subjects, and the parts of his achievements relevant to the award are summarized as follows. (1) nanosecond transient Raman study of aromatic carbonyls and charge-transfer complexes in the excited state, (2) picosecond transient Raman study of the *cis-trans* photoisomerization dynamics, and development of a picosecond two-dimensional CARS spectrometer, (3) development of a phase-stabilized femtosecond time-domain Raman spectrometer and its application to the observation of the vibrational coherence of molecular liquids, and (4) femtosecond fluorescence/absorption studies of the relaxation processes from higher excited states as well as the dynamics of photoinduced proton-transfer reactions. Recently, he has made further steps forward to extremely-fast molecular spectroscopy utilizing 10-fs pulses, and succeeded in observing the excited-state vibrational coherence.

Associate Professor Taira's Scientific Achievements

Associate professor Takunori Taira of Laser Research Center for Molecular Science received the first research promotion award from the Miyagi Science and Technology Foundation in 2000 for his contributions to "Diode-laser-pumped microchip solid-state lasers."

Pumping of solid state active media by diodes has opened up new horizons in the solid state lasers. The professor is leading the laser society, while demonstrating new concepts such as a Nd:YVO_4-based microchip laser, a Q-switch-integrated frequency doubler, a Yb:YAG-based tunable green laser, and a ceramic Nd:YAG laser. All of these achievements were pioneering works and paved the way for practical compact lasers. The Nd:YVO_4-based microchip laser has already been launched into the market. All lasers were developed through the design rule he devised, in which he first introduced M^2 factor to optimize a laser cavity. The success in a Yb:YAG laser was brought about by this design rule, although the material is difficult to oscillate due to its energy structure.

He is currently expanding his research area into new laser materials such as Nd:Y_2O_3 and Nd:BSO, and new laser geometries like edge pumping and $\chi^{(2)}$-cascaded mode locking. His innovative ideas strongly attract researchers outside of Institute for Molecular Science, resulting in many collaborative works.

LIST OF PUBLICATIONS

Department of Theoretical Studies

J. HRUSAK, Z. HERMAN and S. IWATA, "The Heat of Formation of the SiF_2^{++} Dication: A Theoretical Prediction," *Int. J. Mass Spectrom.* **192**, 165 (1999).
W.-N. WANG, H.-R. TANG, K.-N. FAN and S. IWATA, "Theoretical Studies of $[Si_4NO]^-$ with Ab Initio MO and DFT Methods," *Chem. Phys. Lett.* **310**, 313 (1999).
M. SAEKI, T. TSUKUDA, S. IWATA and T. NAGATA, "Electronic Isomers in $[(CO_2)_nROH]^-$ Cluster Anions. II. Ab Initio Calculations," *J. Chem. Phys.* **111**, 6333 (1999).
K. SATOH and S. IWATA, "Theoretical Study of Vibrational Spectra for $Cl^-(H_2O)$: Temperature Dependence and the Infulenced of Ar_n (n = 1–3)," *Chem. Phys. Lett.* **312**, 522 (1999).
K. OKADA and S. IWATA, "Accurate Potential Energy and Transition Dipole Moment Curves of Several Electronic States of CO^+," *J. Chem. Phys.* **112**, 1804 (2000).
T. TSURUSAWA and S. IWATA, "Theoretical Studies of the Water Cluster Anions Containing the OH{e}HO Structure: Energies and Harmonic Frequencies," *Chem. Phys. Lett.* **315**, 433 (2000).
T. TSURUSAWA and S. IWATA, "The Electron-Hydrogen Bonds and the OH Harmonic Frequency Shifts in Water Cluster Complexes with a Group 1 Metal Atom, $M(H_2O)_n$ (M = Li and Na)," *J. Chem. Phys.* **315**, 433 (2000).
M. J. WOJCIK, H. NAKAMURA, S. IWATA, and W. TATARA, "Theoretical Study of Multidimensional Proton Tunneling in the Excited State of Tropolone," *J. Phys. Chem.* **112**, 6322 (2000).

A. MITSUTAKE, U. H. E. HANSMANN and Y. OKAMOTO, "Temperature Dependence of Distributions of Conformations of a Small Peptide," *J. Mol. Graphics Modell.* **16**, 226 (1998).
Y. SUGITA and Y. OKAMOTO, "Replica-Exchange Molecular Dynamics Method for Protein Folding," *Chem. Phys. Lett.* **314**, 141 (1999).
Y. OKAMOTO, "Tackling the Multiple-Minima Problem in Protein Folding by Monte Carlo Simulated Annealing and Generalized-Ensemble Algorithms," *Int. J. Mod. Phys. C* **10**, 1571 (1999).
M. KINOSHITA, Y. OKAMOTO and F. HIRATA "Peptide Conformations in Alcohol and Water: Analyses by the Reference Interaction Site Model Theory," *J. Am. Chem. Soc.* **122**, 2773 (2000).
A. MITSUTAKE and Y. OKAMOTO, "Helix-Coil Transitions of Amino-Acid Homo-Oligomers in Aqueous Solution Studied by Multicanonical Simulations," *J. Chem. Phys.* **112**, 10638 (2000).
Y. OKAMOTO, "First-Principles Protein Folding Simulations," *Mol. Sim.* **24**, 351 (2000).
T. NISHIKAWA, H. OHTSUKA, Y. SUGITA, M. MIKAMI and Y. OKAMOTO, "Replica-Exchange Monte Carlo Method for Ar Fluid," *Prog. Theor. Phys. Suppl.* **138**, 270 (2000).
Y. OKAMOTO, "Protein Folding Simulations by Monte Carlo Simulated Annealing and Generalized-Ensemble Algorithms," *Prog. Theor. Phys. Suppl.* **138**, 301 (2000).
Y. SUGITA and Y. OKAMOTO, "An Analysis on Protein Folding Problem by Replica-Exchange Method," *Prog. Theor. Phys. Suppl.* **138**, 402 (2000).

L. PICHL, H. NAKAMURA and J. HORACEK, "Analytical Treatment of Singular Equations in Dissociative Recombination," *Comput. Phys. Commun.* **124**, 1 (2000).
C. ZHU, H. NAKAMURA and K. NOBUSADA, "Electronically Adiabatic Chemical Reactions Analyzed by the Semiclassical Theory of Nonadiabatic Transition," *Phys. Chem. Chem. Phys.* **2**, 557 (2000).
M. WOJCIK, H. NAKAMURA, S. IWATA and W. TATARA, "Theoretical Study of Multidimensional Proton Tunneling in the Excited State of Tropolone," *J. Chem. Phys.* **112**, 6322 (2000).
L. PICHL, V. I. OSHEROV and H. NAKAMURA, "Nonadiabatic Transitions in a Two-State Exponential Potential Model," *J. Phys. A: Math. Gen.* **33**, 3361 (2000).
K. NOBUSADA, H. NAKAMURA, Y. LIN and B. RAMACHANDRAN, "Quantum Reaction Dynamics of $O(^3P)$ + HCl on a New ab initio Potential Energy Surface," *J. Chem. Phys.* **113**, 1018 (2000).
L. PICHL, H. NAKAMURA and J. HORACEK, "Complete Rreflection in Two-State Crossing and Non-Crossing Potential Models," *J. Chem. Phys.* **113**, 906 (2000).

Y. IMAMURA, S. TEN-NO, K. YONEMITSU and Y. TANIMURA, "Ab initio MO Studies on Electronic States of BEDT-TTF Molecules," *J. Chem. Phys.* **111**, 266 (1999).
K. OKUMURA, A. TOKMAKOFF and Y. TANIMURA, "Two-Dimensional Line Shape Analysis of Photon Echo Signal," *Chem. Phys. Lett.* **314**, 488 (1999).
K. OKUMURA, B. BAGCHI and Y. TANIMURA, "Cage Dynamics in the Third-Order Off-Resonant Response of Liquid Molecules: A Theoretical Realization," *Bull. Chem. Soc. Jpn.* **73**, 873 (2000).
T. STEFFEN and Y. TANIMURA, "The Fifth and Seventh Order 2D Raman Spectroscopy for Harmonic System with Nonlinear System-Bath Interactions: Gaussian-White Case," *J. Phys. Soc. Jpn.* **69**, 3115 (2000).
P. G. DE GENNES and K.OKUMURA, "On the Toughness of Biocomposites," *R. Acad. Sci. Paris* **IV**, 257 (2000).
P. G. DE GENNES, K. OKUMURA, M. SHAHINPOOR and K. J. KIM, "Mechanoelectric Effects in Ionic Gels," *Europhys. Lett.* **50**, 513 (2000).

H. TANAKA, R. YAMAMOTO, K. KOGA and X. C. ZENG, "Can Thin Disk-Like Clusters be More Stable than Compact Droplet-Like Clusters?" *Chem. Phys. Lett.* **304**, 378 (1999).
J. SLOVAK, K. KOGA, H. TANAKA and X. C. ZENG, "Confined Water in Hydrophobic Nanopores: Dynamics of Freezing into Bilayer Ice," *Phys. Rev. E* **60**, 5833 (1999).
G. T. GAO, X. C. ZENG and H. TANAKA, "The Melting Temperature of Proton-Disordered Hexagonal Ice: A Computer Simulation of TIP4P Model of Water," *J. Chem. Phys.* **112**, 8534 (2000).
H. TANAKA, "A Molecular Dynamics Study of the Connectivity of Water Molecules in Supercooled States," *Phys. Chem. Chem. Phys.* **2**, 1595 (2000).

T. KIKUCHI, "Kinetics of a Finite One-Dimensional Spin System as a Model for Protein Folding," *Biophys. Chem.* **85**, 93 (2000).
K. GOHDA, I. MORI, D. OHTA and T. KIKUCHI, "A CoMFA Analysis with Conformational Propensity: An Attempt to Analyze the SAR of a Set of Moleculas with Different Conformational Flexibility Using a 3D-QSAR Method," *J. Comput. Aided Mol. Des.* **14**, 265 (2000).
H. KURA, H. OKA, J.-L. BIRBAUM and T. KIKUCHI, "Study on Photobase Generation from α-Aminoketones: Photocrosslinking of Epoxides with Carboxlic Acids," *J. Photopolym. Sci. Technol.* **13**, 145 (2000).

R. TAKASU, H. ITO, K. NISHIKAWA, K. HASHIMOTO, R. OKUDA and K. FUKE, "Solvation Process of Na_m in Small Ammonia Clusters: Photoelectron Spectroscopy of $Na_m^-(NH_3)_n$ ($m \leq 3$)," *J. Electron Spectros. Relat. Phenom.* **106**, 127 (2000).
K. HASHIMOTO, T. KAMIMOTO and K. DAIGOKU, "Theoretical Study of $[Na(H_2O)_n]^-$ (n = 1–4) Clusters: Geometries, Vertical Detachment Energies and IR Spectra," *J. Phys. Chem. A* **104**, 3299 (2000).

M. KINOSHITA, Y. OKAMOTO and F. HIRATA, "Peptide Conformations in Alcohol and Water: Analyses by the Reference Interaction Site Model Theory," *J. Am. Chem. Soc.* **122**, 2773 (2000).
M. KINOSHITA, "Binary Fluid Mixture Confined between Macroparticles: Surface-Induced Phase Transition and Long-Range Surface Forces," *Chem. Phys. Lett.* **325**, 281 (2000).

H. SATO and F. HIRATA, "Ab initio Study of Water: Liquid Structure, Electronic and Thermodynamic Properties over a Wide Range of Temperature and Density," *J. Chem. Phys.* **111**, 8545 (1999).
Y. HARANO, H. SATO and F. HIRATA, "Solvent Effects on a Diels-Alder Reaction in Supercritical Water: RISM-SCF Study," *J. Am. Chem. Soc.* **122**, 2289 (2000).
Y. HARANO, H. SATO and F. HIRATA, "A Theoretical Study on a Diels-Alder Reaction in Ambient and Supercritical Water: Viewing Solvent Effects through Frontier Orbitals," *Chem. Phys.* **258**, 151 (2000).
H. SATO, A. KOVALENKO and F. HIRATA, "Self-Consistent Field, *Ab initio* Molecular Orbital and Three-Dimensional Reference Interaction Site Model Study for Solvation Effect on Carbon Monoxide in Aqueous Solution," *J. Chem. Phys.* **112**, 9463 (2000).
H. SATO, N. MATUBAYASI, M. NAKAHARA and F. HIRATA, "Which Carbon Oxide is More Soluble? Ab initio Study on Carbon Monoxide and Dioxide in Aqueous Solution," *Chem. Phys. Lett.* **323**, 257 (2000).
T. YAMAZAKI, H. SATO and F. HIRATA, "NMR Chemical Shifts in Solution: A RISM-SCF Approach," *Chem. Phys. Lett.* **325**, 668 (2000).
J. P. SNYDER, N. S. CHANDRAKUMAR, H. SATO and D. C. LANKIN, "The Unexpected Diaxial Orientation of cis-3,5-Difluoropiperidine in Water: A Potent CF-NH Charge Dipole Effect," *J. Am. Chem. Soc. (Commun.)* **122**, 544 (2000).
A. SETHIA, Y. SINGH and F. HIRATA, "ElectronL Self-Trapping in Two Dimensional Fluid," *Chem. Phys. Lett.* **326**, 199 (2000).
T. IMAI, M. KINOSHITA and F. HIRATA, "Salt Effect on Stability and Solvation Structure of Peptide: An Integral Equation Study," *Bull. Chem. Soc. Jpn.* **73**, 1113 (2000).
T. IMAI, M. KINOSHITA and F. HIRATA, "Theoretical Study for Partial Molar Volume of Amino Acids in Aqueous Solution: Implication of Ideal Fluctuation Volume," *J. Chem. Phys.* **112**, 9469 (2000).
A. KOVALENKO and F. HIRATA, "Potentials of Mean Force of Simple Ions in Ambient Aqueous Solution. I. Three-Dimensional Reference Interaction Site Model Approach," *J. Chem. Phys.* **112**, 10391 (2000).
A. KOVALENKO and F. HIRATA, "Potentials of Mean Force of Simple Ions in Ambient Aqueous Solution. II. Solvation Structure from the Three-Dimensional Reference Interaction Site Model Approach, and Comparison with Simulations," *J. Chem. Phys.* **112**, 10403 (2000).
A. KOVALENKO and F. HIRATA, "Hydration Free Energy of Hydrophobic Solutes Studied by a Reference Interaction Site Model with a Repulsive Bridge Correction and a Thermodynamic Perturbation Method," *J. Chem. Phys.* **113**, 2793 (2000).
V. SHAPOVALOV, T. N. TRUONG, A. KOVALENKO and F. HIRATA, "Liquid Structure at Metal Oxide-Water Interface: Accuracy of a Three-Dimensional RISM Methodology," *Chem. Phys. Lett.* **320**, 186 (2000).

L. LI, R. L. FU, X. SUN and K. YONEMITSU, "Electric-Field Response of Exciton in Electroluminescent Polymer," *Phys. Status Solidi B* **214**, 337 (1999).

Y. IMAMURA, S. TEN-NO, K. YONEMITSU and Y. TANIMURA, "Structures and Electronic Phases of the Bis(ethylenedithio)tetrathiafulvalene (BEDT–TTF) Clusters and κ-(BEDT-TTF) Salts: A Theoretical Study Based on Ab Initio Molecular Orbital Methods," *J. Chem. Phys.* **111**, 5986 (1999).

H. JIANG, X. H. XU, X. SUN and K. YONEMITSU, "Localized Vibrational Modes of Excitation in Electroluminescent Polymers," *Chin. Phys. Lett.* **16**, 836 (1999).

M. MORI, K. YONEMITSU and H. KINO, "Quasi-One-Dimensional Natures in (Et$_n$Me$_{4-n}$Z)[Pd(dmit)$_2$]$_2$," *J. Low Temp. Phys.* **117**, 1723 (1999).

J. KISHINE and K. YONEMITSU, "Phase Transitions from Incoherent and from Coherent Metal Phases in Quasi-One-Dimensional Organic Conductors," *J. Low Temp. Phys.* **117**, 1741 (1999).

K. YONEMITSU, "Magnetic and Pairing Correlation Functions and Interchain Coherence in Quasi-One-Dimensional Dimerized Organic Conductors," *J. Low Temp. Phys.* **117**, 1765 (1999).

M. KUWABARA and K. YONEMITSU, "Numerical Studies of Ground State Phase Diagrams for the MMX Chains," *Mol. Cryst. Liq. Cryst.* **341**, 533 (2000).

K. YONEMITSU, "Charge Gap and Interchain Correlation in Quasi-One-Dimensional Dimerized Organic Conductors," *Mol. Cryst. Liq. Cryst.* **341**, 543 (2000).

M. MORI, K. YONEMITSU and H. KINO, "Role of Dimensionality in Dimerized Two-Band Systems," *Mol. Cryst. Liq. Cryst.* **341**, 549 (2000).

J. KISHINE and K. YONEMITSU, "Interplay of Correlation, Randomness and Dimensionality Effects in Weakly-Coupled Half-Filled Random Hubbard Models," *Mol. Cryst. Liq. Cryst.* **341**, 555 (2000).

K. YONEMITSU, "Effects of Dimerization on Spin, Charge and Hopping Correlation Functions in Quasi-One-Dimensional Organic Conductors," *Physica B* **284-288**, 515 (2000).

M. MORI, K. YONEMITSU and H. KINO, "Possible Ground State Phases of Pd(dmit)$_2$ Salts," *Physica B* **284-288**, 1495 (2000).

M. KUWABARA and K. YONEMITSU, "Magnetic Property of MMX Chains as Dimerized Quarter-Filled Systems," *Physica B* **284-288**, 1545 (2000).

J. KISHINE and K. YONEMITSU, "Dimensionality Effects in Half-Filled Random Hubbard Chains," *Physica B* **284-288**, 1946 (2000).

M. KUWABARA and K. YONEMITSU, "Charge Ordering and Lattice Modulation in Quasi-One-Dimensional Halogen-Bridged Binuclear Metal Complexes," *Mol. Cryst. Liq. Cryst.* **343**, 47 (2000).

M. MORI and K. YONEMITSU, "Collective Excitations around Charge Ordered States and Coexistent States with Different Orders," *Mol. Cryst. Liq. Cryst.* **343**, 221 (2000).

X. SUN, R. L. FU, K. YONEMITSU and K. NASU, "Photoinduced Polarization Inversion in a Polymeric Molecule," *Phys. Rev. Lett.* **84**, 2830 (2000).

K. YONEMITSU and J. KISHINE, "Dimensionality Effects on the Charge Gap in the Dimerized Hubbard Model at Quarter Filling: the Density-Matrix and Perturbative Renormalization-Group Approaches," *J. Phys. Soc. Jpn.* **69**, 2107 (2000).

J. KISHINE, "Quantum Phase Transitions and Collapse of the Mott Gap in the $d = 1 + \varepsilon$ Dimensional Hubbard Model with $2k_F$ Umklapp Scattering," *Phys. Rev. B* **62**, 2377 (2000).

N. MIYASHITA, S. WATANABE, M. MATSUZAWA and J. H. MACEK, "Influence of Short-Range Interference on Ionization Threshold Law," *Phys. Rev. A* **61**, 14901 (2000).

Department of Molecular Structure

M. KUMAKURA and N. MORITA, "Magneto-Optical Trap of Metastable Helium-3 Atoms," *Appl. Phys. B: Lasers Opt.* **70**, 555 (2000).

Y. MORIWAKI and N. MORITA, "Spectroscopic Studies on Yb$^+$ Ions in Liquid Helium," *Eur. Phys. J. D* **13**, 11 (2001).

T. AKASAKA, M. T. H. Liu, Y. NIINO, Y. MAEDA, T. WAKAHARA, M. OKAMURA, K. KOBAYASHI and S. NAGASE, "Photolysis of Diazirines in the Presence of C$_{60}$: A Chemical Probe for Carbene/Diazomethane Partitioning," *J. Am. Chem. Soc.* **122**, 7134 (2000).

T. AKASAKA, S. OKUBO, M. KONDO, Y. MAEDA, T. WAKAHARA, T. KATO, T. SUZUKI, K. YAMAMOTO, K. KOBAYASHI and S. NAGASE, "Isolation and Characterization of Two Pr@C$_{82}$ Isomers," *Chem. Phys. Lett.* **319**, 153 (2000).

M. FUJITSUKA, O. ITO, K. KOBAYASHI, S. NAGASE, K. YAMAMOTO, T. KATO, T. WAKAHARA and T. AKASAKA, "Transient Spectroscopic Properties of Endohedral Metallofullerenes, La@C$_{82}$ and La$_2$@C$_{80}$," *Chem. Lett.* 902 (2000).

M. MORIYAMA, T. SATO, A. YABE, K. YAMAMOTO, K. KOBAYASHI, S. NAGASE, T. WAKAHARA and T. AKASAKA, "Vibrational Spectrocopy of Endohedral Dimetallofullerene La$_2$@C$_{80}$," *Chem. Lett.* 524 (2000).

Y. MAEDA, S. TAKAHASHI, T. WAKAHARA, T. AKASAKA, Y. SASAKI, M. FUJITSUKA, O. ITO, K. KOBAYASHI, S. NAGASE, M. KAKO and Y. NAKADAIRA, "Metal-Free Bis-Germylation: C$_{60}$-Sensitized Reaction of Digermirane with Benzonitrile," *ITE Letters on Batteries, New Technologies & Medicine* **1**, 408 (2000).

T. AKASAKA, Y. MAEDA, T. WAKAHARA, M. OKAMURA, M. FUJITSUKA, O. ITO, K. KOBAYASHI,

S. NAGASE, M. KAKO, Y. NAKADAIRA and E. HORN, "Novel Metal-Free Bis-Silylation: C_{60}-Sensitized Reaction of Disilirane with Benzonitrile," *Org. Lett.* **1**, 1509 (1999).
T. AKASAKA, S. OKUBO, T. WAKAHARA, K. KOBAYASHI, S. NAGASE, M. KAKO, Y. NAKADAIRA, T. KATO, K. YAMAMOTO, H. FUNASAKA, Y. KITAYAMA anf K. MATSUURA, "Endohedrally Metal-Doped Heterofullerenes: $La_2@C_{79}N$ and $La@C_{81}N$," *Chem. Lett.* 945 (1999).

M. TSUBAKI, K. KOBAYASHI, T. ICHISE, F. TAKEUCHI and S. TAGAWA, "Diethylpyrocarbonate-Modification Abolishes Fast electron Accepting Ability of Cytochrome b_{561} from Ascorbate but does not Influence on Electron Donation to Monodehydroascorbate Radical: Identification of the Modification Sites by Mass Spectrometric Analyses," *Biochemistry* **39**, 3276 (2000).

S. G. KRUGLIK, A. G. SHVEDKO and T. KITAGAWA, "Saturation Raman Spectroscopy as a Tool for Studying the Excited States of Complex Organic Molecules: Application to Nickel Octaethylporphyrin," *Asian J. Phys.* **7**, 365 (1998).
T. TOMITA, S. HIROTA, T. OGURA, J. S. OLSON and T. KITAGAWA, "Resonance Raman Investigation of Fe–N–O Structure of Nitrosylheme in Myoglobin and Its Mutants," *J. Phys. Chem. B* **103**, 7044 (1999).
S. ITOH, M. TAKI, H. KUMEI, S. TAKAYAMA, S. NAGATOMO, T. KITAGAWA, N. SAKURADA, R. ARAKAWA and S. FUKUZUMI, "Model Complexes of the Active Form of Galactose Oxidase. Physicochemical Properties and Reactivity of Cu(II)– and Zn(II)–Phenoxyl Radical Complexes of the Novel Organic Cofactor," *Angew. Chem., Int. Ed. Engl.* **38**, 2775 (1999).
S. ITOH, H. BANDOH, S. NAGATOMO, T. KITAGAWA and S. FUKUZUMI, "Aliphatic Hydroxylation by a Bis(μ-oxo)dinickel(III) Complex," *J. Am. Chem. Soc.* **121**, 8945 (1999).
Y. MIZUTANI, Y. UESUGI and T. KITAGAWA, "Intramolecular Vibrational Energy Redistribution and Intermolecular Energy Transfer in the (d,d) Excited State of Nickel Octaethylporphyrin," *J. Chem. Phys.* **111**, 8950 (1999).
S. NAKASHIMA, S. TANIGUCHI, T. OKADA, A. OSUKA, Y. MIZUTANI and T. KITAGAWA, "Evidence for π–π Interactions in the S_1 State of Zinc Porphyrin Dimers Revealed by Picosecond Time-Resolved Resonance Raman Spectroscopy," *J. Phys. Chem. A* **103**, 9184 (1999).
N. SUZUKI, T. HIGUCHI, Y. URANO, K. KIKUCHI, H. UEKUSA, Y. OHASHI, T. UCHIDA, T. KITAGAWA and T. NAGANO, "Novel Iron Porphyrin-Alkanethiolate Complex with Intramolecular NH···S Hydrogen Bond: Synthesis, Spectroscopy, and Reactivity," *J. Am. Chem. Soc.* **121**, 11571 (1999).
M. SUGA, J. OKU, H. MASUDA, M. TAKAKI, M. MUKAI and T. KITAGAWA, "Mechanism of the Anionic Cyclopolymerization of Bis(dimethylvinylsilyl)methane," *Macromolecules* **32**, 1362 (1999).
A. WADA, S. OGO, Y. WATANABE, M. MUKAI, T. KITAGAWA, K. JITSUKAWA, H. MASUDA and H. EINAGA, "Synthesis and Characterization of Novel Alkylperoxo Mononuclear Iron(III) Complexes with a Tripodal Pyridylamine Ligand: A Model for Peroxo Intermediates in Reactions Catalyzed by Non-Heme Iron Enzymes," *Inorg. Chem.* **38**, 3592 (1999).
Y. UESUGI, Y. MIZUTANI, S. G. KRUGLIK, A. G. SHVEDKO, V. A. ORLOVICH and T. KITAGAWA, "Characterization of Stimulated Raman Scattering of Hydrogen and Mathane Gases as a Light Source of Picosecond Time-Resolved Raman Spectroscopy," *J. Raman Spectrosc.* **31**, 339 (2000).
H. HAYASHI, S. FUJINAMI, S. NAGATOMO, S. OGO, M. SUZUKI, A. UEHARA, Y. WATANABE and T. KITAGAWA, "A Bis(μ-oxo)dicopper(III) Complex with Aromatic Nitrogen Donors: Structural Characterization and Reversible Conversion between Copper (I) and Bis(μ-oxo)dicopper(III) Species," *J. Am. Chem. Soc.* **122**, 2124 (2000).
N. OKISHIO, R. FUKUDA, M. NAGAI, S. NAGATOMO and T. KITAGAWA, "Interactions of Phosphatidylinositol 3-kinase SH3 Domain with Its Ligand Peptide Studied by Absorption, Circular Dichroism, and UV Resonance Raman," *Biopolymers (Biospectroscopy)* **57**, 208 (2000).
K. YAMAMOTO, Y. MIZUTANI and T. KITAGAWA, "Nanosecond Temperature Jump and Time-Resolved Raman Study of Thermal Unfolding of Ribonuclease A," *Biophys. J.* **79**, 485 (2000).
T. UCHIDA, T. MOGI and T. KITAGAWA, "Resonance Raman Studies of Oxo Intermediates in the Reaction of Pulsed Cytochrome *bo* with Hydrogen Peroxide," *Biochemistry* **39**, 6669 (2000).
T. OGIHARA, S. HIKICHI, M. AKITA, T. UCHIDA, T. KITAGAWA and Y. MOROOKA, "An Approach to the O_2 Activating Mononuclear Non-Heme Fe Enzymes: Structural Characterization of Fe(II)–Acetato Complex and Formation of Alkylperoxoiron(III) Species with the Highly Hindered Hydrotris(3-tert-butyl-5-isopropyl-1-pyrazolyl)borate," *Inorg. Chim. Acta* **297**, 162 (2000).

M. MATSUSHITA and T. KATO, "NQR by Coherent Raman Scattering of a Triplet Exciton in a Molecular Crystal," *Phys. Rev. Lett.* **83**, 2018 (1999).
T. AKASAKA, S. OKUBO, T. WAKAHARA, K. YAMAMOTO, K. KOBAYASHI, S. NAGASE, T. KATO, M. KAKO, Y. NAKADAIRA, Y. KITAYAMA and K. MATSUURA, "Endohedrally Metal-Doped Heterofullerenes: $La@C_{81}N$ and $La_2@C_{79}N$," *Chem. Lett.* 945 (1999).
M. KUMAGAI, H. KANAMORI, M. MATSUSHITA and T. KATO, "Development of Phase-Lock System between Two Single-Mode Lasers for Optical-Optical Double Resonance Spectroscopy," *Jpn. J. Appl. Phys.* **38**, 6102 (1999).

T. AKASAKA, S. OKUBO, M. KONDO, Y. MAEDA, T. WAKAHARA, T. KATO, T. SUZUKI, K. YAMAMOTO, K. KOBAYASHI and S. NAGASE, “Isolation and Characterization of a $Pr@C_{82}$ Isomer,” *Chem. Phys. Lett.* **319**, 153 (2000).

M. FUJITSUKA, O. ITO, K. KOBAYASHI, S. NAGASE, K. YAMAMOTO, T. KATO, T. WAKAHARA and T. AKASAKA, “Transient Spectroscopic Properties of Endohedral Metallofullerenes, $La@C_{82}$ and $La_2@C_{80}$,” *Chem. Lett.* 902 (2000).

Department of Electronic Structure

T. NAKABAYASHI, K. KOSUGI and N. NISHI, “Liquid Structure of Acetic Acid Studied by Raman Spectroscopy and Ab Initio Molecular Orbital Calculations,” *J. Phys. Chem. A* **103**, 8595 (1999).

T. TAKAMUKU, A. YAMAGUCHI, M. TABATA, N. NISHI, K. YOSHIDA, H. WAKITA and T. YAMAGUCHI, “Structure and Dynamics of 1,4-Dioxane-Water Binary Solutions Studied by X-ray Diffraction, Mass Spectrometry, and NMR Relaxation,” *J. Mol. Liq.* **83**, 163 (1999).

N. NISHI, T. NAKABAYASHI and K. KOSUGI, “Raman Spectroscopic Study on Acetic Acid Clusters in Aqueous Solutions:Dominance of Acid-Acid Association Producing Microphases,” *J. Phys. Chem. A* **103**, 10851 (1999).

T. TAKAMUKU, T. YAMAGUCHI, M. ASATO, M. MATSUMOTO and N. NISHI, “Structure of Clusters in Methanol-Water Binary Solutions Studied by Mass Spectrometry and X-ray Diffraction,” *Z. Naturforsch., A: Phys. Sci.* **55**, 513 (2000).

K. OHASHI, H. IZUTSU, Y. INOKUCHI, K. HINO, N. NISHI and H. SEKIYA, “Vibrational and Electronic Spectra of (Benzene–Benzyl Alcohol)$^+$: Predominance of Charge Resonance Interaction over Hydrogen-Binding Interaction,” *Chem. Phys. Lett.* **321**, 406 (2000).

K. OHASHI, Y. INOKUCHI, H. IZUTSU, K. HINO, N. YAMAMOTO, N. NISHI and H. SEKIYA, “Electronic and Vibrational Spectra of Aniline-Benzene Hetero-Dimer and Aniline Homo-Dimer Ions,” *Chem. Phys. Lett.* **323**, 43 (2000).

S. ISHIUCHI, M. SAEKI, M. SAKAI and M. FUJII, “IR Dip Spectra of Photochemical Reaction Products in a Phenol/Ammonia Cluster—Examination of Intracluster Hydrogen Transfer,” *Chem. Phys. Lett.* **322**, 27 (2000).

M. MITSUI, Y. OHSHIMA, S. ISHIUCHI, M. SAKAI and M. FUJII, “Structural Characterization of the Acridine–$(H_2O)_n$ (n = 1–3) Clusters by Fluorescence Dip Infrared Spectroscopy,” *Chem. Phys. Lett.* **317**, 211 (2000).

L. WANG, H. KOHGUCHI and T. SUZUKI, “Femtosecond Time-Resolved Photoelectron Imaging,” *Faraday Discuss. Chem. Soc.* **113**, 37 (1999).

Y. MO and T. SUZUKI, “Vector Correlation in Molecular Photodissociation: Quantum Mechanical Expression and Comparison with the Formal Expansion Formula,” *J. Chem. Phys.* **112**, 3463 (2000).

H. KATO, J. LEE, K. SAWABE and Y. MATSUMOTO, “Photochemistry of N_2O on Si(100): Surface Photo-Oxidation,” *Surf. Sci.* **445**, 209 (2000).

K. WATANABE, H. KATO and Y. MATSUMOTO, “Photo-Stimulated Desorption of Rare Gas Atoms Induced by UV-NIR Photons at a Semiconductor Surface,” *Surf. Sci. Lett.* **446**, L134 (2000).

K. WATANABE and Y. MATSUMOTO, “Photochemistry of Methane on Cu(111),” *Surf. Sci.* **454-456**, 262 (2000).

T. YAMASE and H. NARUKE, “Luminescence and Energy Transfer Phenomena in Tb^{3+}/Eu^{3+}-mixed Polyoxometallolanthanoates $K_{15}H_3[Tb_{1.4}Eu_{1.6}(H_2O)_3(SbW_9O_{33})(W_5O_{18})_3]\cdot 25.5H_2O$ and $Na_7H_{19}[Tb_{4.3}Eu_{1.7}O_2\text{-}(OH)_6(H_2O)_6Al_2(Nb_6O_{19})_5]\cdot 47H_2O$,” *J. Phys. Chem. B* **103**, 8850 (1999).

H. NARUKE and T. YAMASE, “Mixed-Valence Ammonium Trivanadate with a Tunnel Structure Prepared by Pyrolysis of Polyoxovanadate,” *Bull. Chem. Soc. Jpn.* **72**, 2699 (1999).

C. HU, B. YUE and T. YAMASE, “Photoassisted Dehalogenation of Organo-Chlorine Compounds by Paratungstate A in Aqueous Solutions,” *Appl. Catal., A* **194-195**, 99 (2000).

H. NARUKE and T. YAMASE, “A Novel-Type Mixed-ligand Polyoxotungstolanthanoate, $[Ln(W_5O_{18})\text{-}(BW_{11}O_{39})]^{12-}$ (Ln = Ce^{3+} and Eu^{3+}),” *Bull. Chem. Soc. Jpn.* **73**, 375 (2000).

E. ISHIKAWA and T. YAMASE, “Photoreduction Processes of a-Dodecamolybdophospahate, $\alpha\text{-}[PMo_{12}O_{40}]^{3-}$: ^{31}P-NMR, Electrical Conductivitiy, and Crystallographic Studies,” *Bull. Chem. Soc. Jpn.* **73**, 641 (2000).

H. NARUKE, N. FUKAYA and T. YAMASE, “$Na_{10}(glycine)_2[H_2W_{12}O_{42}]\cdot 28H_2O$,” *Acta Crystallogr., Sect. C: Cryst. Struct. Commun.* **56**, 177 (2000).

T. YAMASE and H. MAKINO, “Crystal and Electronic Structure and Magnetic Susceptibility of the Photochemically Prepared Layered Vanadyl Phosphate, $Na(VO)_2(PO_4)_2\cdot 4H_2O$,” *J. Chem. Soc., Dalton Trans.* 1143 (2000).

Department of Molecular Assemblies

L. MARTIN, S. TURNER, P. DAY, P. GUIONNEA, J. A. K. HOWARD, M. URUICHI and K. YAKUSHI, “Synthesis, Crystal Structure and Properties of the Semiconducting Molecular Charge-Transfer Salt $(\text{bedt-ttf})_2\text{Ge}(\text{C}_2\text{O}_4)_3\cdot\text{PhCN}$ [bedt-ttf = bis(ethylenedithio)tetrathia-fulvalene],” *J. Mater. Chem.* **9**, 2731 (1999).

J. OUYANG, J. DONG, K. YAKUSHI , K. TAKIMIYA and T. OTSUBO, “Spectroscopic Study of Isostructural Charge-Transfer Salts: Non-metallic DMTTA–BF_4 and Metallic DMTSA–BF_4,” *J. Phys. Soc. Jpn.* **68**, 3708 (1999).

K. YAKUSHI, M. URUICHI and Y. YAMASHITA, “Phase Transition in Narrow-band Organic Metals $(\text{BEDT-ATD})_2X(\text{solvent})$ ($X = \text{PF}_6$, AsF_6, BF_4; solvent = THF, DHF, DO),” *Synth. Met.* **109**, 33 (2000).

C. NAKANO, K. YAKUSHI, M. KOHAMA, K. UEDA and T. SUGIMOTO, “Estimation of the Site-Energy difference In the crystal of $\text{Et}_4\text{N}(\text{DMTCNQ})_2$,” *Solid State Commun.* **113**, 677 (2000).

K. YAKUSHI, J. ULANSKI, H. YAMOCHI and G. SAITO, “Observation of Plasmons by Normal-Incidence Reflectivity in Two-Dimensional Organic Metals,” *Phys. Rev. B* **61**, 9891 (2000).

X. CHEN, C. YANG, J. QIN, K. YAKUSHI, Y. NAKAZAWA and K. ICHIMURA, “The Intercalation Reaction of 1,10-Phenanthroline with Layered Compound FePS_3,” *J. Solid State Chem.* **150**, 258 (2000).

O. DROZDOVA, H. YAMOCHI, K. YAKUSHI, M. URUICHI, S. HORIUCHI and G. SAITO, “Determination of the Charge on BEDO-TTF in its Complexes by Raman Spectroscopy,” *J. Am. Chem. Soc.* **112**, 4436 (2000).

K. TAKEDA, I. SHIROTANI and K. YAKUSHI, “Pressure-Induced Insulator-to-Metal-to-Insulator Transitions in One-Dimensional Bis(dimethylglyoximato)platinum(II), $\text{Pt}(\text{dmg})_2$,” *Chem. Mater.* **12**, 912 (2000).

C. YANG, X. CHEN, J. QIN, K. YAKUSHI, Y. NAKAZAWA and K. ICHIMURA, “Synthesis, Characterization, and Magnetic Properties of Intercalation Compound of 1,10-Phenanthroline with Layered MnPS_3,” *J. Solid State Chem.* **150**, 281 (2000).

D. ZHANG, J. QIN, K. YAKUSHI, Y. NAKAZAWA and K. ICHIMURA, “Preparation of a New Nanocomposite of Conducting Polyaniline into Layered MnP_3,” *Mater. Sci. Eng. A* **286**, 183 (2000).

T. NAKAMURA, W. MINAGAWA, R. KINAMI and T. TAKAHASHI, “Possible Charge Disproportionation and New Type Charge Localization in θ-$(\text{BEDT-TTF})_2\text{CsZn}(\text{SCN})_4$,” *J. Phys. Soc. Jpn.* **69**, 504 (2000).

T. NAKAMURA, H. TSUKADA, T. TAKAHASHI, S. AONUMA and R. KATO, “Low Temperature Electronic States of β’-type $\text{Pd}(\text{dmit})_2$ Compounds,” *Mol. Cryst. Liq. Cryst.* **343**, 187 (2000).

H. HOBAYASHI, A. SATO, H. TANAKA , A. KOBAYASHI and P. CASSOUX, “A Novel Superconductor with Insulating Magnetic Ground State,” *Coord. Chem. Rev.* **190-192**, 921 (1999).

A. SATO, E. OJIMA, H. KOBAYASHI, Y. HOSOKOSHI, K. INOUE, A. KOBAYASHI and P. CASSOUX, “Coexistence of Antiferromagnetically Ordered Fe^{3+} Spins and Metal π-Electrons in λ-$\text{BETS}_2\text{FeCl}_4$,” *Adv. Mater.* **11**, 1192 (1999).

H. TANAKA, T. ADACHI, E. OJIMA, H. FUJIWARA, K. KATO, H. KOBAYASHI, A. KOBAYASHI and P. CASSOUX, “Pressure-Induced Superconducting Transition of λ-$(\text{BETS})_2\text{FeCl}_4$ with π-d Coupled Antiferromagnetic Insulating Ground State at Ambient Pressure,” *J. Am. Chem. Soc.* **121**, 11243 (1999).

A. SATO, H. KOBAYASHI and A. KOBAYASHI, “Structural Electrical and Magnetic Properties of low Dimensional Conductors Based on Unsymmetrical π Donor EDT-TTF and Analogous Selenium-Substituted Molecules,” *J. Mater. Chem.* **9**, 2365 (1999).

H. FUJIWARA and H. KOBAYASHI, “New π-Extended Organic Donor Containing a Stable TEMPO Radical as a Candidate for Conducting-Magnetic Multifunctional Materials,” *Chem. Commun.* 2417 (1999).

E. OJIMA, H. FUJIWARA and H. KOBAYASHI, “Synthesis, Structure, and Properties of New Organic Conductors Based on Tellurocycle-Fused TTF Donor Molecules,” *Adv. Mater.* **11**, 1527 (1999).

E. OJIMA, H. FUJIWARA, H. KOBAYASHI and A. KOBAYASHI, “Synthesis, Structures and Properties of New Organic Conductors Based on Tellurocycle-Fused TTF Donor Molecules,” *Adv. Mater.* **11**, 1527 (1999).

L. V. ZORINA, B. Zh. NARYMBETOV, S. S. KHASANOV, R. P. SHIBAEVA, N. D. KUSHCH, E. B. YAGUBSKII, A. KOBAYASHI and H. KOBAYASHI, “Crystal Structures of the New BETS-Based Organic Metal: α-$(\text{BETS})_2\text{TlHg}(\text{SeCN})_4$ and κ-$(\text{BETS})_2\text{C}(\text{CN})$,” *Synth. Met.* **102**, 1735 (1999).

T. COURCET, I. MALFANT, H. GORNITZKA, P. CASSOUX and H. KOBAYASHI, “Preparation, X-ray Crystal Structure, Electrical and Optical Properties of a New BETS Charge Transfer Salt: θ-$(\text{BETS})_4\text{Cu}_2\text{Cl}_6$,” *Synth. Met.* **102**, 1761 (1999).

H. KOBAYASHI, H. AKUTSU, H. TANAKA, A. KOBAYASHI, M. TOKUMOTO, L. BROSSARD and P. CASSOUX, “On the Low-Temperature State of Highly Correlated BETS Conductors,” *Synth. Met.* **102**, 1654 (1999).

K. KODAMA, T. NAKAMURA, T. TAKAHASHI, E. OJIMA and H. KOBAYASHI, “Metal-Insulator Transition in α-$(\text{BEDT-TSeF})_2\text{I}_3$ and α-$(\text{BEDT-TTF})_2\text{I}_3$,” *Synth. Met.* **103**, 1963 (1999).

H. KOBAYSASHI, H. AKUTSU, E. OJIMA, A. SATO, H. TANAKA, A. KOBAYASHI and P. CASSOUX, “Superconductor-to-Insulator Transition of λ-$(\text{BETS})_2\text{GaBr}_x\text{Cl}_{4-x}$,” *Synth. Met.* **103**, 1837 (1999).

H. MORIYAMA, M. ABE, S. HANAZATO, H. MOTOKI, T. WATANABE and H. KOBAYASHI, “Synthesis and Characterization of C_{60} Anion Radical Crystals Stabilized by Organic Dye Cations,” *Synth. Met.* **103**, 2374 (1999).

Y. MISAKI, H. FUJIWARA, T. MARUYAMA, M. TANIGUCHI, T. YAMABE, T. MORI, H. MORI and S. TANAKA, “Novel Oxygen Containing π-Electron Donors for Organic Metals: 2-(1,3-Dithiol-2-ylidene)-5-(pyran-

4-ylidene)-1,3,4,6-tetrathiapentalenes," *Chem. Mater.* **11**, 2360 (1999).
A. SATO, E. OJIMA, H. AKUTSU, Y. NAKAZAWA, H. KOBAYASHI, H. TANAKA, A. KOBAYASHI and P. CASSOUX, "Magnetic Properties of λ-BETS$_2$(Fe$_x$Ga$_{1-x}$)Cl$_4$ Exhibiting a Superconductor-to-Insulator Transition ($0.35 < x < 0.5$)," *Phys. Rev. B* **61**, 111 (2000).
H. TANAKA, E. OJIMA, H. FUJIWARA, Y. NAKAZAWA, H. KOBAYASHI and A. KOBAYASHI, "A New κ-type Organic Superconductor Based on BETS Molecules, κ-(BETS)$_2$GaBr$_4$," *J. Mater. Chem.* **10**, 245 (2000).
T. ADACHI, E. OJIMA, B. Zh. NARYMBETOV, H. KOBAYASHI, T. MIYAZAKI and M. TOKUMOTO, "Electric Properties of Organic Conductor, β'-(BEDT-TTF)$_2$ICl$_2$ up to 10 GPa," *Chem. Lett.* 406 (2000).
T. ADACHI, E. OJIMA, K. KATO, H. KOBAYASHI, T. MIYAZAKI, M. TOKUMOTO and A. KOBAYASHI, "Superconducting Transition of (TMTTF)$_2$PF$_6$ above 50 kbar [TMTTF = tetramethyltetrathiafulvalene]," *J. Am. Chem. Soc.* **122**, 3238 (2000).
M. MASUDA, T. NAITO, T. INABE, N. HANASAKI, H. TAJIMA, T. OTSUKA, K. AWAGA, B. NARYMBETOV and H. KOBAYASHI, "A One-Dimensional Macrocyclic π-Ligand Conductor Carrying a Magnetic Center, Structure and Electrical, Optical and Magnetic Properties of TPP[Fe(Pc)(CN)$_2$]$_2$ (TPP = tetraphenylphosphonium and [Fe(Pc)(CN)$_2$] = dicyano(phthalocyaninato) iron(III))," *J. Mater. Chem.* **10**, 631 (2000).
T. ADACHI, E. OKJIMA, B. Zh. NARYMBETOV, H. KOBAYASHI, T. MIYAZAKI, and M. TOKUMOTO, "Electrical Properties of an Organic Conductors, β'-(BEDT-TTF)$_2$ICl$_2$ up to 10 GPa," *Chem. Lett.* 406 (2000).
Y. NISHIO, M. TAMURA, K. KAJITA, S. AONUMA, H. SAWA, R. KATO and H. KOBAYASHI, "Thermodynamical Study of (DMe-DCNQI)$_2$Cu System—Mechanism of Reentrant Metal-Insulator Transition—," *J. Phys. Soc. Jpn.* **69**, 1414 (2000).
T. OTSUKA, A. KOBAYASHI, Y. MIYAMOTO, J. KIUCHI, N. WADA, E. OJIMA, H. FUJIWARA and H. KOBAYASHI, "Successive Antiferromagnetic and Superconducting Transitions in an Organic Metal, κ-(BETS)$_2$-FeCl$_4$," *Chem. Lett.* 732 (2000).
H. FUJIWARA, Y. MISAKI, T. YAMABE, T. MORI, H. MORI and S. TANAKA, "Preparation, Structures and Physical Properties of Selenium Analogues of DTEDT as Promising Donors for Organic Metals," *J. Mater. Chem.* **10**, 1565 (2000).

H. TADA, H. TOUDA, M. TAKADA and K. MATSUSHIGE, "Quasi-Intrinsic Semiconducting State of Titanyl-Phtahlocyanine Films Obtained under Ultrahigh Vacuum Conditions," *Appl. Phys. Lett.* **76**, 873 (2000).
D. SCHLETTWEIN, K. HESSE, H. TADA, S. MASHIKO, U. STORM and J. BINDER, "Ordered Growth of Substituted Phthalocyanine Thin Films—Hexadecafluorophthalocyaninatozinc on Alkali Halide (110) and Microstructured Si Surfaces," *Chem. Mater.* **12**, 989 (2000).
D. SCHLETTWEIN, H. TADA and S. MASHIKO, "Substrate-Induced Order and Multilayer Epitaxial Growth of Substituted Phthalocyanine Thin Films," *Langmuir* **16**, 2872 (2000).

S. FUJIKI, Y. KUBOZONO, S. EMURA, Y. TAKABAYASHI, S. KASHINO, A. FUJIWARA, K. ISHII, H. SUEMATSU, Y. MURAKAMI, Y. IWASA, T. MITANI and H. OGATA, "Structure and Raman Scatterings of Cs$_3$C$_{60}$ under High Pressure," *Phys. Rev. B* **62**, 5366 (2000).
Y. MARUYAMA, S. MOTOHASHI, K. SUZUKI, S. TAKAGI and H. OGATA, "Structures and Magnetic Properties of High-Temperature Reaction Products of Cerium Metal and C$_{60}$ Solid," *Solid State Commun.* **115**, 463 (2000).

M. ARAGAKI, T. MORI, Y. MISAKI, S. TANAKA and T. YAMABE, "Facile Preparation of TTP Series Donors by Using Cyanoethyl Groups," *Synth. Met.* **103**, 1601 (1999).
M. ASHIZAWA, M. ARAGAKI, T. MORI, Y. MISAKI and K. TANAKA, "Preparation and Properties of Cyclohexylenedithio Substituted TTP Donors," *Synth. Met.* **103**, 1603 (1999).
T. MORI, "Systematizing Structural Modifications of BEDT-TTF-Based Organic Conductors," *Synth. Met.* **103**, 1683 (1999).
S, HANAZATO, T. MORI, H. MORI and S. TANAKA, "Pressure-Induced Insulating State in (BO)$_2$Cl(H$_2$O)$_x$," *Synth. Met.* **103**, 1770 (1999).
T. KAWAMOTO, T. MORI Y. MISAKI, K. TANAKA, H. MORI and S. TANAKA, "Metal-Insulator Transition in (TTM-TTP)(I$_3$)$_{5/3}$ with High Oxidation State," *Synth. Met.* **103**, 1829 (1999).
H. MORI, S. TANAKA and T. MORI, "Universal Phase Diagram of θ-Type Salts—Controlling the Electronic States by U/W or Dihedral Angle," *Synth. Met.* **103**, 1880 (1999).
H. MORI, N. SAKURAI, S. TANAKA, H. MORIYAMA, T. MORI, H. KOBAYASHI and A. KOBAYASHI, "Electronic Structure of θ-Type BETS Salts," *Synth. Met.* **103**, 1882 (1999).
T. MORI, T. KAWAMOTO, K. IIDA, J. YAMAURA, T. ENOKI, Y. MISAKI, T. YAMABE, H. MORI and S. TANAKA, "TTM-TTP-Based Metallic Conductor with a Half-Filled Band," *Synth. Met.* **103**, 1885 (1999).
T. KAWAMOTO, M. ASHIZAWA, M. ARAGAKI, T. MORI, T. YAMAMOTO, H. TAJIMA, H. KITAGAWA, T. MITANI, Y. MISAKI and K. TANAKA, "Raman and Optical Investigations on Charge Localization in the One-Dimensional Organic Conductors (TTM-TTP)(I$_3$)$_{5/3}$ and (TSM-TTP)(I$_3$)$_{5/3}$," *Phys. Rev. B* **60**, 4635 (1999).
T. MORI, "Structural Genealogy of BEDT-TTF-Based Organic Conductors III. Twisted Molecules: δ and α'

Phases," *Bull. Chem. Soc. Jpn.* **72**, 2011 (1999).

H. HOSHINO, K. IIDA, T. KAWAMOTO and T. MORI, "Structural and Magnetic Properties of $Cu[C(CN)_3]_2$ and $Mn[C(CN)_3]_2$," *Inorg. Chem.* **38**, 4229 (1999).

T. KAWAMOTO, T. MORI, H. KITAGAWA, T. MITANI, Y. MISAKI and K. TANAKA, "Raman Investigation of the One-Dimensional Organic Conductor with a Half-Filled Band, $(TTM\text{-}TTP)I_3$," *J. Phys. Soc. Jpn.* **68**, 3748 (1999).

H. HOSHINO, M. ARAGAKI, K. MURATA, T. KAWAMOTO, T. MORI, Y. MISAKI and K. TANAKA, "ESR Investigation of Organic Conductors (DTM-TTP)(TCNQ)(TCE) and (TMET-TTP)(TCNQ)," *J. Phys. Soc. Jpn.* **69**, 1845 (2000).

H. MORI, T. OKANO, S. TANAKA, M. TAMURA, Y. NISHIO, K. KAJITA and T. MORI, "Discontinuous Change of Metal-Insulator Transition in the Alloyed θ-System: $\theta\text{-}(BEDT\text{-}TTF)_2(Rb_{1-x}Cs_x)Zn(SCN)_4$," *J. Phys. Soc. Jpn.* **69**, 1751 (2000).

T. MIYAZAKI, M. AOKI and O. TAKAYASU, "Photoemission Spectra of $LiNiO_2$ Catalyst for Oxidative Coupling of Methane," *Jpn. J. Appl. Phys.* **38**, 51 (1999).

T. MIYAMAE, S. HASEGAWA, D. YOSHIMURA, H. ISHII, N. UENO and K. SEKI, "Intramolecular Energy-Band Dispersion in Oriented Thin Films of $n\text{-}CF_3(CF_2)_{22}CF_3$ Observed by Angle-Resolved Photoemission with Synchrotron Radiation," *J. Chem. Phys.* **112**, 3333 (2000).

Department of Applied Molecular Science

Y. GOTO, T. MATSUI, S. OZAKI, Y. WATANABE and S. FUKUZUMI, "Mechanisms of Sulfoxidation Catalyzed by High-Valent Intermediates of Heme Enzymes: Electron Transfer *vs.* Oxygen Transfer Mechanism," *J. Am. Chem. Soc.* **121**, 9497 (1999).

S. TAKARA, S. OGO, Y. WATANABE, K. NISHIKAWA, I. KINOSHITA and K. ISOBE, "Direct Observation by Electrospray Ionization Mass Spectrometry of a Key Intermediate $[Cp^*RhMo_3O_8(OMe)_5]^-$ ($Cp^* = \eta^5\text{-}C_5Me_5$) in the Formation of a Double Bookshelf-Type Oxide Cluster $[(Cp^*Rh)_2Mo_6O_{20}(OMe)_2]^{2-}$," *Angew. Chem., Int. Ed. Engl.* **38**, 3051 (1999).

A. WADA, S. OGO, Y. WATANABE, M. MUKAI, T. KITAGAWA, K. JITSUKAWA, H. MASUDA and H. EINAGA, "Synthesis and Characterization of Novel Alkylperoxo Mononuclear Iron(III) Complexes with a Tripodal Pyridylamine Ligand: A Model for Peroxo Intermediates in Reactions Catalyzez by Non-Heme Iron Enzymes," *Inorg. Chem.* **38**, 3592 (1999).

S. OGO, N. MAKIHARA and Y. WATANABE, "pH-Dependent Transfer Hydrogenation of Water-Soluble Carbonyl Compounds with $[Cp^*Ir^{III}(H_2O)_3]^{2+}$ ($Cp^* = \eta^5\text{-}C_5Me_5$) as a Catalyst Precursor and HCOONa as a Hydrogen Donor in Water," *Organometallics* **18**, 5470 (1999).

S. OGO, O. BURIEZ, J. B. KERR and R. H. FISH, "Bioorganometallic Chemistry 12. Reaction of $[Cp^*Rh\text{-}(H_2O)_3(OTf)_2$ with Nicotinamide Adenine Dinucleotide in Water: Synthesis, Structure, and a pH Dependent ^1H NMR and Voltammetric Study of the Cyclic Trimer Product, $[Cp^*Rh(\mu\text{-}\eta^1(N_1){:}\eta^2(N6,N7)$-5'-Adenosine Pyrophosphate-5'-Ribose-Nicotinamide$)]_3(OTf)_3$," *J. Organomet. Chem.* **589**, 66 (1999).

K. SHIREN, S. OGO, S. FUJINAMI, H. HAYASHI, M. SUZUKI, A. UEHARA, Y. WATANABE and Y. MORO-OKA, "Synthesis, Structures, and Properties of Bis(μ-oxo)nickel(III) and Bis(μ-superoxo)nickel(II) Complexes: An Unusual Conversion of a $Ni(III)_2(\mu\text{-}O)_2$ Core into a $Ni(II)_2(\mu\text{-}OO)_2$ Core by H_2O_2," *J. Am. Chem. Soc.* **122**, 254 (1999).

M. P. ROACH, S. OZAKI and Y. WATANABE, "Investigations of the Myoglobin Cavity Mutant H93G with Unnatural Imidazole Proximal Ligands as a Modular Peroxide O–O Bond Cleavage Model System," *Biochemistry* **39**, 1446 (2000).

H. HAYASHI, S. FUJINAMI, S. NAGATOMO, S. OGO, M. SUZUKI, A. UEHARA, Y. WATANABE and T. KITAGAWA, "A Bis(μ-oxo)dicopper(III) Complex with Sterically Hindered Aromatic Nitrogen Donors: Structural Characterization and Reversible Conversion between Copper(I) and Bis(μ-oxo)dicopper(III) Species," *J. Am. Chem. Soc.* **122**, 2124 (2000).

R. YAMAHARA, S. OGO, Y. WATANABE, T. FUNABIKI, K. JITSUKAWA, H. MASUDA and H. EINAGA, "(Catecholato)iron(III) Complexes with Tetradentate Tripodal Ligands Containing Substituted Phenol and Pyridine Units as Structural and Functional Model Complexes for the Catechol-Bound Intermediate of Intradiol-Cleaving Catechol Dioxygenases," *Inorg. Chim. Acta* **300-302**, 587 (2000).

H. OHTSU, S. ITOH, S. NAGATOMO, T. KITAGAWA, S. OGO, Y. WATANABE and S. FUKUZUMI, "Characterization of Imidazolate-Bridged Cu(II)-Zn(II) Heterodinuclear and Cu(II)-Cu(II) Homodinuclear Hydroperoxo Complexes as Reaction Intermediate Models of Cu, Zn-SOD," *Chem. Commun.* 1051 (2000)

S. HAYAMI, K. INOUE and Y. MAEDA, "Structures and Magnetic Properties of Binuclear Iron(III) Spin-Crossover Complexes," *Mol. Cryst. Liq. Cryst.* **335**, 1285 (1999).

M. MANAGO, S. HAYAMI, Y. YANO, K. INOUE, R. NAKATA, A. ISHIDA and Y. MAEDA, "Valence Delocalization and Crystal Structure of $[Fe_3O(pazo)_6(py)_3]apy$: An Example of the Mixed Valence Delocalization between Two Iron Atoms," *Bull. Chem. Soc. Jpn.* **72**, 2229 (1999).

T. KAWASHIMA, T. MANABE, M. YAMASHITA, K. TORIUMI, H. KITAGAWA, T. MITANI, H.

OKAMOTO, K. INOUE, Y. HOSOKOSHI and M. SHIRO, “Synthesis and Physical Properties of Quasi-One-Dimensional Halogen-Bridged Cu^{II}-Pt^{IV} Mixed-Metal MX-Chain Compounds,” *Synth. Met.* **103**, 2648 (1999).

Y. HOSOKOSHI, K. KATOH, K. INOUE and T. GOTO, “Construction of a Quantum-Spin System of $S = 1/2$ Antiferromagnetic Chain with the Next-Nearest-Neighbor Interactions,” *J. Phys. Soc. Jpn.* **68**, 2910 (1999).

Y. HOSOKOSHI, Y. NAKAZAWA, K. INOUE, K.TAKIZAWA, H. NAKANO, M. TAKAHASHI and T. GOTO, “Magnetic Properties of Low Dimensional Quantum Spin Systems Made of Stable Organic Biradicals PNNNO, F$_2$PNNNO and PIMNO,” *Phys. Rev. B* **60**, 12924 (1999).

A. S. MARKOSYAN, Y. HOSOKOSHI and K. INOUE, “Influence of the Thermal Excitations of the Ferrimagnetic (–1/2,5/2,–1/2) Linear Trimer on the Paramagnetic Behavior of the Layered Metal-Radical Complex $\{\mathrm{Mn(hfac)_2}\}_3(\mathrm{R}_X)_2\cdot n\text{-}\mathrm{C_7H_{16}}$,” *Phys. Lett. A* **261**, 212 (1999).

K. MUKAI, M. YANAGIMOTO, Y. SHIMOBE, K. INOUE and Y.HOSOKOSHI, “Doping Effect of Magnetic Properties on the Spin-Peierls Compound *p*-CyDOV,” *Chem. Phys. Lett.* **311**, 446 (1999).

H. KUMAGAI and K. INOUE, “Synthesis and Characterization of a Chiral Molecule-Based Metamagnet Made by a Chiral Triplet Organic Radical and Transition Metal Ion,” *Mol. Cryst. Liq. Cryst.* **334**, 487 (1999).

Y. HOSOKOSHI, K. SUZUKI, K. INOUE and H. IWAMURA, “Pressure Effect on Mn Complexes of Bisaminoxyl Radicals,” *Mol. Cryst. Liq. Cryst.* **334**, 511 (1999).

F. IWAHORI, K. INOUE and H. IWAMURA, “Synthesis and Magnetic Properties of Bis(hexafluoroacetyl-acetonate) Copper(II) Complex with 5-Bromo-1,3-Phenylenebis(*N-tert*-butylaminoxyl) as a Bridging Ligand,” *Mol. Cryst. Liq. Cryst.* **334**, 533 (1999).

A. S. MARKOSYAN, H. IWAMURA and K. INOUE, “Magnetic Behaviour of the Ferrimagnetic (–1/2,5/2,–1/2) Linear Trimer in Complexes of Mn(hfac)$_2$ with Bis- and Trisnitroxide Radicals,” *Mol. Cryst. Liq. Cryst.* **334**, 549 (1999).

A. SATO, E. OJIMA, H. KOBAYASHI, Y. HOSOKOSHI, K.INOUE and P. CASSOUX, “Coexistence of Antiferromagnetically Ordered Fe^{3+} Spins and Metal π-electrons in λ-BETS$_2$FeCl$_4$ [BETS = bis(ethylenedithio)-tetraselenafulvalene],” *Adv. Mater.* **11**, 1192 (1999).

P. RABU, M. DRILLON, H. IWAMURA, G. GÖLITZ, T. ITOH, K. MATSUDA, N.U KOGA and K. INOUE, “Exchange Coupling Parameters and Energy Levels for Cyclic Metal-Radical Complexes of Bis(hexafluoroacetylacetonato)manganese(II) with 5-*tert*-butyl-1,3-phenylenebis(*N-tert*-butylaminoxyl) and (4-*N-tert*-butyl-*N*-oxyamino)pyridine,” *Eur. J. Inorg. Chem.* **211**, 216 (2000).

H. KUMAGAI, A. S. MARKOSYAN and K. INOUE, “Synthesis, Structure and Magnetic Properties of a Chiral One-Dimensional Molecule-Based Magnet,” *Mol. Cryst. Liq. Cryst.* **343**, 97 (2000).

K. KATOH, Y. HOSOKOSHI, K. INOUE and T. GOTO, “Singlet Ground States in an Organic $S = 1/2$ Spin Ladder and a Novel Double Spin Chain of Ferromagnetic Dimers Formed by an Organic Tetraradical,” *J. Phys. Soc. Jpn.* **69**, 1008 (2000).

H. KUMAGAI, Y. HOSOKOSHI, A. S. MARKOSYAN and K. INOUE, “Synthesis and Magnetic Properties of a New Complex Made up of Mn(hfac)$_2$ and a Radical with a Triplet Ground State,” *New J. Chem.* **24**, 537 (2000).

I. ARAKAWA, T. ADACHI, T. HIRAYAMA and M. SAKURAI, ‘‘Absolute Measurement of Total Photo Desorption Yield of Solid Ne in Vacuum Ultraviolet Range,” *Surf. Sci.* **451**, 136 (2000).

H. NISHIKAWA, Y. MISAKI, T. YAMABE and M. SHIRO, “Synthesis and Properties of Dimethoxy-Substituted Unsymmetrical TTF Derivatives,” *Synth. Met.* **102**, 1693 (1999).

H. FUJIWARA, T. NISHIKAWA, Y. MISAKI and T. YAMABE, “Synthesis and Properties of Tris-Fused Donor Containing Thiopyran Ring,” *Synth. Met.* **102**, 1737 (1999).

Y. MISAKI, M. TANIGUCHI, K. TANAKA, K. TAKIMIYA, A. MORIKAMI, T. OTSUBO and T. MORI, “Structures and Properties of (TMEO-ST-TTP)$_2$AsF$_6$,” *Chem. Lett.* 859 (1999).

Y. MISAKI, H. FUJIWARA, T. MARUYAMA, M. TANIGUCHI, T. YAMABE, T. MORI, H. MORI and S. TANAKA, “Novel Oxygen Containing π-Electron Donors for Organic Metals: 2-(1,3-Dithiol-2-ylidene)-5-(pyran-4-ylidene)-1,3,4,6-tetrathiapentalenes,” *Chem. Mater.* **11**, 2360 (1999).

Y. MISAKI, K. TANAKA, M. TANIGUCHI, T. YAMABE, T. KAWAMOTO and T. MORI, “Structures and Electrical Properties of (EO-TTP)$_2$AsF$_6$,” *Chem. Lett.* 1249 (1999).

A. DELUZET, P. BATAIL, Y. MISAKI, P. AUBAN-SENZIER and E. CANADELL, “Donor Slabs Robustness and Band Filling Variations in BDT-TTP-based Molecular Conductors: β-(BDT-TTP)$_6$[Re$_6$S$_6$Cl$_8$]$\cdot$(CH$_2$Cl–CHCl$_2$)$_2$ and β-(BDT-TTP)$_6$[Mo$_6$Cl$_{14}$]$\cdot$(CH$_2$Cl–CHCl$_2$)$_2$,” *Adv. Mater.* **12**, 436 (2000).

M. TANIGUCHI, Y. MISAKI and K. TANAKA, “Theoretical Estimation of the Electron-Molecular Vibration (EMV) Coupling in Several Oragnic Donor Molecules,” *Solid State Commun.* **114**, 75 (2000).

Y. MISAKI, Y. TANI, M. TANIGUCHI, T. MAITANI, K. TANAKA and K. BECHGAARD, “Preparation and Properties of Gold Complexes with TTF Dithiolato Ligands,” *Mol. Cryst. Liq. Cryst.* **343**, 59 (2000).

H. FUJIWARA, Y. MISAKI, T. YAMABE, T. MORI, H. MORI and S. TANAKA, “Preparation, Structures and Physical Properties of Selenium Analogues of DTEDT as Promising Donors for Organic Metals,” *J. Mater. Chem.* **10**, 1565 (2000).

H. HONDA, T. NORO and E. MIYOSHI, “*Ab initio* Molecular Orbital Study of Fe(CO)$_n$ (n = 1, 2, and 3),” *Theor. Chem. Acc.* **104**, 140 (2000).

K. TAKESHITA, N. SHIDA and E. MIYOSHI, “A Theoretical Study on the Ionization of CO_2 and CS_2 with Analysis of Vibrational Structure of the Photoelectron Spectra,” *J. Chem. Phys.* **112**, 10838 (2000).
E. MIYOSHI and T. K. GHOSH, “*Ab initio* CASSCF and MRSDCI Calculations of the $(C_6H_6)_3^+$ Radical,” *Chem. Phys. Lett.* **323**, 434 (2000).

K. IMURA, T. KASAI, H. OHOYAMA and R. NAAMAN, “Focusing of DCl and HCl Dimers by an Electrostatic Hexapole Field—The Role of the Tunneling Motion,” *J. Chem. Phys.* **110**, 355 (1999).
H. OHOYAMA, H. KAWAGUCHI, M. YAMATO, T. KASAI, B. G. BRUNETTI and F. VECCHIOCATTIVI, “Evidence for Steric Effect in Methyl Chloride Ionization by Metastable Argon Atoms,” *Chem. Phys. Lett.* **313**, 484 (1999).
K. IMURA, M. VENEZIANI, T. KASAI and R. NAAMAN, “The Reaction of $O(^1D)$ with H_2O, D_2O Monomers and Clusters and the Intracomplex Reaction in $N_2O–X_2O$ (X = H, D) Photo-Initiated at 193 nm and 212.8 nm,” *J. Chem. Phys.* **111**, 4025 (1999).
K. MOIRTANI, M. OKADA, T. KASAI and Y. MURATA, “Hydrogen Adsorption and Reaction on the Ir{100}-(1×5) Surface,” *Surf. Sci.* **445**, 315 (2000).
M. OKADA, K. MOIRTANI, M. NAKAMURA, T. KASAI and Y. MURATA, “Hot Atom Mechanism in Hydrogen Exchange Reaction on Ir{100} Surface,” *Chem. Phys. Lett.* **323**, 586 (2000).

T. BABA, T. TANAKA, I. MORINO, K. M. T. YAMADA and K. TANAKA “Detection of the Tunneling-Rotation Transitions of Malonaldehyde in the Submillimeter-Wave Region,” *J. Chem. Phys.* **110**, 4131 (1999).
K. TANAKA, Y. TACHIKAWA, K. SAKAGUCHI, T. HIKIDA and T. TANAKA, “Time-Resolved Infrared Diode Laser Spectroscopy of the ν_3 Band of the Jet-Cooled $Fe(CO)_2$ Radical Produced by Ultraviolet Photolysis of $Fe(CO)_5$,” *J. Chem. Phys.* **111**, 3970 (1999).
K. TANAKA, S. BAILLEUX, A. MIZOGUCHI, K. HARADA, T. BABA, I. OGAWA and M. SHIRASAKA, “van der Waals Bending Bands of the ArDCN Cluster Observed by Millimeter-Wave Spectroscopy Combined with a Pulsed Supersonic Jet Technique,” *J. Chem. Phys.* **113**, 1524 (2000).

K. NAGATO, “Development of an Ion Mobility/Mass Spectrometer,” *J. Aerosol Res. Jpn. (in Japanese)* **15**, 110 (2000).

M. HASHIMOTO and M. TAKASU, “Boson Localization on the Superfluid-Insulator Transition by Quantum Loop Algorithm,” *Prog. Theor. Phys. Suppl.* **138**, 529 (2000).
N. URAKAMI, M. IMAI, Y. SANO and M. TAKASU, “The Effects of Chondroitin Sulfate on the Tobacco Mosaic Virus Configuration,” *Prog. Theor. Phys. Suppl.* **138**, 390 (2000).

Department of Vacuum UV Photoscience

M. NEEB, A. KIVIMÄKI, B. KEMPGENS, H. M. KÖPPE, K. MAIER, A. M. BRADSHAW and N. KOSUGI, “Partial Electron Yield Spectrum of N_2: Doubly Excited States at the K-Shell Threshold,” *Chem. Phys. Lett.* **320**, 217 (2000).
L. G. M. PETTERSSON, T. HATSUI and N. KOSUGI, “Ni 2p-3d Photoabsorption and Strong Charge Transfer Satellites in Divalent Ni Complexes with Molecular Ligands. Evaluation of π-Back Donation Based on the Density Functional Theory Approach,” *Chem. Phys. Lett.* **311**, 299 (1999).
A. JÜRGENSEN, N. KOSUGI and R. G. CAVELL, “The Sulphur 2p Photoabsorption Spectrum of NSF_3,” *Chem. Phys.* **247**, 445 (1999).
J. ADACHI, N. KOSUGI, E. SHIGEMASA and A. YAGISHITA, “Vibronic Coupling and Valence Mixing in the 1s-Rydberg Excited States of C_2H_2 in Comparison with N_2 and CO,” *Chem. Phys. Lett.* **309**, 427 (1999).

T. FUJINO and T. TAHARA, “Picosecond Time-Resolved Raman Study of *trans*-Azobenzene,” *J. Phys. Chem. A* **104**, 4203 (2000).
S. TAKEUCHI and T. TAHARA, “Vibrational Coherence of S_1 *trans*-Stilbene in Solution Observed by 40-fs-resolved Absorption Spectroscopy: Comparison of the Low-Frequency Vibration Appearing in the Frequency-Domain and Time-Domain Spectroscopies,” *Chem. Phys. Lett.* **326**, 430 (2000).
T. TAHARA and S. MATSUO, “Femtosecond Material Response Probed by Phase-Stabilized Optical Heterodyne Detected Impulsive Stimulated Raman Scattering,” *Laser Chem.* **19**, 149 (1999).

Y. HOMMA, P. FINNIE, T. OGINO, H. NODA and T. URISU, “Aligned Island Formation Using Step-Band Networks on Si(111),” *J. Appl. Phys.* **86**, 3083 (1999).
Y. NONOGAKI, H. HATATE, R. OGA, S. YAMAMOTO, Y. FUJIWARA, Y. TAKEDA, H. NODA and T. URISU, “SR-Stimulated Etching and OMVPE Growth for Semiconductor Nanostructure Fabrication,” *Mater. Sci. Eng. B* **74**, 7 (2000).
H. NODA and T. URISU, “Assignments of Bending and Stretching Vibrational Spectra and Mechanisms of Thermal Decomposition of SiH_2 on Si(100) Surfaces,” *Chem. Phys. Lett.* **326**, 163 (2000).
Y. KOBAYASHI, K. SUMITOMO, K. SHIRAISHI, T. URISU and T. OGINO, “Control of Surface

Composition on Ge/Si(001) by Atomic Hydrogen Irradiation," *Surf. Sci.* **436**, 9 (1999).

S. FUCHI, Y. NONOGAKI, H. MORIYA, Y. FUJIWARA and Y. TAKEDA, "Effects of GaP Cap Layer Growth on Self-Assembled InAs-Islands Grown on GaP (001) by Organometallic Vapor Phase Epitaxy," *Jpn. J. Appl. Phys.* **39**, 3290 (2000).

Y. FUJIWARA, T. KAWAMOTO, S. FUCHI, M. ICHIDA, Y. NONOGAKI, A. NAKAMURA and Y. TAKEDA, "Er-Related Luminescence from Self-Assembled InAs Quantum Dots Doped with Er by Organometallic Vapor-Phase Epitaxy," *J. Lumin.* **87-89**, 326 (2000).

Y. GAO, H. MEKARU, T. MIYAMAE and T. URISU, "Scanning Tunneling Microscopy Study of Si(111) Surface Morphology after Removal of SiO_2 by Synchrotron Radiation Illumination," *Appl. Phys. Lett.* **76**, 1392 (2000).

Y. GAO, H. MEKARU, T. MIYAMAE and T. URISU, "Scanning Tunneling Microscopy Study of Surface Morphology of Si(111) after Synchrotron Radiation Stimulated Desorption of SiO_2," *J. Vac. Sci. Technol., A* **18**, 1153 (2000).

K. MASE, S. TANAKA, S. NAGAOKA and T. URISU, "Ion Desorption Induced by Core-Electron Transitions Studied with Electron-Ion Coincidence Spectroscopy," *Surf. Sci.* **451**, 143 (2000).

K. MITSUKE, Y. HIKOSAKA and K. IWASAKI, "Laser Photoionization of Polarized Ar Atoms Produced by Excitation with Synchrotron Radiation," *J. Phys. B: At.; Mol. Opt. Phys.* **33**, 391 (2000).

H. NIIKURA, M. MIZUTANI and K. MITSUKE, "Rotational State Distribution of N_2^+ Produced from N_2 and N_2O Observed by a Laser-Synchrotron Radiation Combination Technique," *Chem. Phys. Lett.* **317**, 45 (2000).

K. KUROSAWA, H.YANAGIDA, N. TAKEZOE, Y. KAWASAKI, M. FUJITA, J. MIYANO and A. YOKOTANI, "Silica Films Preparation by Chemical Vapor Deposition Using Vacuum Ultraviolet Excimer Lamps," *Summary of Papers of CLEO 2000* CMX4 (2000).

M. KATTO, Y. TAKIGAWA, K. KUROSAWA, K. TAKAHASHI and T. YAMANAKA, "Detection of Vacuum Ultraviolet Radiation with Optical Storage Film, Imaging Plate," *Summary of Papers of CLEO 2000* CtuA1 (2000).

Y. MOTOYAMA, J. MIYANO, K. TOSHIKAWA, Y. YAGI, H. MUTOU, K. KUROSAWA, A. YOKOTANI and W. SASAKI, "Quality Improvement of SiO_2 Films by Adding Foreign Gases in Photo-Chemical Vapor Deposition," *197th Meeting of Electrochemical Society* **2000-1**, 909 (2000).

J. MIYANO, Y. MOTOYAMA, K. TOSHIKAWA, T. YOKOYAMA, H. MUTOU, K. KUROSAWA, A. YOKOTANI and W. SASAKI, "SiO_2 Deposition Mechanism in Photo-CVD Using VUV Excimer Lamp," *197th Meeting of Electrochemical Society* **2000-1**, 910 (2000).

K. KUROSAWA, N. TAKEZOE, H. YANAGIDA, J. MIYANO, Y. MOTOYAMA, K. TOSHIKAWA, Y. KAWASAKI and A. YOKOTANI, "Silica Film Preparation by Chemical Vapor Deposition Using Vacuum Ultraviolet Excimer Lamps," *International Conference on Electronic Materials & European Materials Research Society Spring Meeting* D-II-3 (2000).

T. SAKAKIBARA, Y. TAKIGAWA and K. KUROSAWA, "Texture and Thermoelectric Properties of $(AgBiTe_2)_{0.5}(Ag_2Te)_{0.5}$ Composite," *XIX International Conference on Thermoelectrics* PI-10 (2000).

N. TAKEZOE, H. YANAGIDA, K. KUROSAWA, T. URISU, H. NODA and H. MEKARU, "Design and Construction of UVSOR-BL4A2 Beam Line for Nano-Structure Processing," *7th International Cpnference on Syncrotron Radiation Instrumentation* POS2-188 (2000).

H. OKAMURA, J. KAWAHARA, T. NANBA, S. KIMURA, K. SODA, U. MIZUTANI, Y. NISHINO, M. KATO, I. SHIMOYAMA, H. MIURA, K. FUKUI, K. NAKAGAWA, H. NAKAGAWA and T. KINOSHITA, "Pseudogap Formation in the Intermetallic Compounds $(Fe_{1-x}V_x)_3Al$," *Phys. Rev. Lett.* **84**, 3674 (2000).

S. NAGAOKA, K. MASE, M. NAGASONO, S. TANAKA, T. URISU, J. OHSHITA and U. NAGASHIMA, "Site-Specific Phenomena in Si:2p Core-Level Photoionization of $X_3Si(CH_2)_nSi(CH_3)_3$ (X = F or Cl, $n = 0–2$) Condensed on a Si(111) Surface," *Chem. Phys.* **249**, 15 (1999).

K. OHARA, S. NAGAOKA and K. MUKAI, "A CIDEP Study on the Photosensitized Reaction of Maleimide with Xanthone: Addition Effect of Hydrochloric Acid," *Bull. Chem. Soc. Jpn.* **73**, 37 (2000).

S. NAGAOKA, M. INOUE, C. NISHIOKA, Y. NISHIOKU, S. TSUNODA, C. OHGUCHI, K. OHARA, K. MUKAI and U. NAGASHIMA, "Tunneling Effect in Antioxidant, Prooxidant, and Regeneration Reactions of Vitamin E," *J. Phys. Chem. B* **104**, 856 (2000).

H. UNO, K. KASAHARA, N. NIBU, S. NAGAOKA and N. ONO, "Thermal and Photochemical Isomerization of Tetraaryl Tetrakis(trifluoromethyl)[4]radialenes," *J. Org. Chem.* **65**, 1615 (2000).

K. MASE, S. TANAKA, S. NAGAOKA and T. URISU, "Ion Desorption Induced by Core-Electron Transitions Studied with Electron-Ion Coincidence Spectroscopy," *Surf. Sci.* **451**, 143 (2000).

S. TANAKA, K. MASE, M. NAGASONO, S. NAGAOKA and M. KAMADA, "Electron-Ion Coincidence Study for the TiO_2(110) Surface," *Surf. Sci.* **451**, 182 (2000).

K. OKADA, K. UEDA, T. TOKUSHIMA, Y. SENBA, H. YOSHIDA, Y. SHIMIZU, M. SIMON, H. CHIBA, H. OKUMURA, Y. TAMENORI, H. OHASHI, N. SAITO, S. NAGAOKA, I. H. SUZUKI, E. ISHIGURO, I. KOYANO, T. IBUKI and A. HIRAYA, "High-Resolution Angle-Resolved Ion-Yield Measurements of H_2O and

D_2O in the Region of O 1s to Rydberg Transitions," *Chem. Phys. Lett.* **326**, 314 (2000).

Coordination Chemistry Laboratories

Y. NISHIDA, "Structure and Function of 'Free Iron Ion' in Biological System and Their Model Compounds," *Recent Res. Devel. Pure & Appl. Chem.* **3**, 103 (1999).

Y. NISHIDA, "New Insight into Oxidative DNA Cleavage Reaction Catalyzed by Metal Chelates," *Recent Res. Devel. Pure & Appl. Chem.* **3**, 123 (1999).

S. NISHINO, Y. ISHIKAWA and Y. NISHIDA, "Interaction between a Copper(II) Compound and Protein Investigated in Terms of the Capillary Electrophoresis Method," *Inorg. Chem. Commun.* **2**, 438 (1999).

Y. NISHIDA and S. NISHINO, "Contribution of a Metal-Peroxide Adduct to Neurodegeneration is due to Its Oxidase Activity," *J. Bioscience* **54C**, 1107 (1999).

Y. NISHIDA, S. NISHINO, L.L. GUO, M. KUNITA, H. MATSUSHIMA and T. TOKII, "DNA Promotes the Activation of Oxygen Molecule by Binuclear Cobalt(II) Compounds," *Inorg. Chem. Commun.* **2**, 609 (1999).

S. NISHINO, M. KUNITA, Y. KANI, S. OHBA, H. MATSUSHIMA, T. TOKII and Y. NISHIDA, "Cleavage of C–N Bond of Peptide Group by Copper(II)-Peroxide Adduct with η^1-Coordination Mode," *Inorg. Chem. Commun.* **3**, 145 (2000).

Y. NISHIDA, "Important role of Proton in Activation of Oxygen Molecule in Heme-Containing Oxygenases," *Inorg. Chem. Commun.* **3**, 310 (2000).

N. KANEMATSU, M. EBIHARA and T. KAWAMURA, "A One-Step Synthesis of an Ir(II) Dinuclear Complex. Preparation, Structures and Properties of Bis(μ-acetato)dichlorodicarbonyldiiridium(II) Complexes," *J. Chem. Soc., Dalton Trans.* 4413 (1999).

T. KAWAMURA, H. KACHI, H. FUJII, C. KACHI-TERAJIMA, Y. KAWAMURA, N. KANEMATSU, M. EBIHARA, K. SUGIMOTO, T. KURODA-SOWA and M. MUNAKATA, "δ_{MM}*-π_L Odd Electron Delocalization onto Aromatic Bridging Ligands in a Paramagnetic Dirhodium Complex and Intermolecular π-Stack Interaction in Crystal," *Bull. Chem. Soc. Jpn.* **73**, 657 (2000).

S. NAGAO, H. SEINO, Y. MIZOBE and M. HIDAI, "Syntheses of a Dinuclear Ir Complex Containing Bridging Tetraselenide Ligands $[(C_5Me_5)Ir(\mu\text{-}Se_4)_2Ir(C_5Me_5)]$ and Its Conversion into $Ir_2Pd_2Se_3$ and $Ir_2Pd_3Se_5$ Clusters," *Chem. Commun.* 207 (2000).

H. SEINO, D. NONOKAWA, G. NAKAMURA, Y. MIZOBE and M. HIDAI, "Protonation and Methylation of Zerovalent Molybdenum Complexes of the Types *trans*-$[Mo(CNR)(L)(Ph_2PCH_2CH_2PPh_2)_2]$ (R = Ph or Bu; L = N_2, CO, or Nitrile) and *trans*-$[Mo(CO)(L')(Ph_2PCH_2CH_2PPh_2)_2]$ (L' = N_2 or Nitrile) to Give Carbyne or Hydrido Complexes," *Organometallics* **19**, 2002 (2000).

H. SEINO, C. ARITA, D. NONOKAWA, G. NAKAMURA, Y. HARADA, Y. MIZOBE and M. HIDAI, "Conversion of Benzaldehyde Imines into Isocyanides at a Low-Valent Molybdenum Center. Preparation and Reactivities of Isocyanide-Dinitrogen Complexes *trans*-$[Mo(RNC)(N_2)(Ph_2PCH_2CH_2PPh_2)_2]$ (R = Aryl, Alkyl)," *Organometallics* **18**, 4165 (1999).

H. SUGIMOTO, K. TSUGE and K. TANAKA, "Double Addition of CO_2 and CH_3OH to Ruthenium Carbonyl Complex with Novel Monodentate Dithiolene," *Chem. Lett.* 1007 (1999).

T. MIZUKAWA, K. TSUGE, H. NAKAJIMA and K. TANAKA, "Selective Production of Acetone in Electrochemical Reduction of CO_2 Catalyzed by Ru–Naphthyridine Complex," *Angew. Chem., Int. Ed. Engl.* **38**, 362 (1999).

K. TSUGE, M. KURIHARA and K. TANAKA, "Energy Conversion from Proton Gradient to Electricity Based on Characteristic Redox Behavior of ab Aqua Ruthenium Complex," *Bull. Chem. Soc. Jpn.* **73**, 607 (2000).

T. WADA, T. TSUGE and K. TANAKA, "Electrochemicl Oxiadrition Iof Water to Dioxugen Catalyzedby the Oxidized Form of the Bis(ruthenium-hydroxo) Complex in H_2O," *Angew. Chem., Int. Ed. Engl.* **39**, 1479 (2000).

T. NAGATA and K. TANAKA, "Pentadentate Terpyridine-Catechol Linked Ligands and Their Cobalt(III) Complexes," *Inorg. Chem.* **39**, 3515 (2000).

N. TAGUCHI, K. KASHIWABARA, K. NAKAJIMA, H. KAWAGUCHI and K. TATSUMI, "Syntheses and Structures of Ruthenium(II) Complexes Bearing Hybrid Phosphine-Thioehter Ligands, $Me_2PCH_2CH_2SR$," *J. Organomet. Chem.* **587**, 290 (1999).

T. NAGASAWA, H. KAWAGUCHI and K. TATSUMI, "Isolation of Pentamethylcyclopentadienyl Tris(tert-Butylthiolato) Complexes of Tungsten(IV) and Carbon-Sulfur Bond Activation," *J. Organomet. Chem.* **592**, 46 (1999).

Y. ARIKAWA, H. KAWAGUCHI, K. KASHIWABARA and K. TATSUMI, "Synthesis of Bis{(2-dimethylphosphino)ethane-1-thiolato}bis(t-butylthiolato)Molybdenum(IV) and Its Cluster Forming Reactions with $FeCl_2$ and CuBr," *Inorg. Chem.* **38**, 4549 (1999).

J. LANG, H. KAWAGUCHI and K. TATSUMI, "Synthesis and Structures of a Triply-Fused Incomplete Cluster $[\{(\eta^5\text{-}C_5Me_5)WS_3\}_3Cu_7(MeCN)_9](PF_6)_4$ and a 2D Polymer $[(\eta^5\text{-}C_5Me_5)WS_3Cu_3Cl(MeCN)(pz)]PF_6$ (pz = pyrazine)," *Chem. Commun.* 2315 (1999).

Y. YAMAMOTO, H. KITAHARA, R. OGAWA, H. KAWAGUCHI, K. TATSUMI and K. ITOH, "Ru(II)-Catalyzed Cycloadditions of 1,6-Heptadiynes with Alkenes: New Synthetic Potential of Ruthenacyclopentatrienes as Biscarbenoids in Tandem Cyclopropanation of Bicycloalkenes and Heteroatom-Assisted Cyclocotrimerization of 1,6-Heptadiynes with Heterocyclic Alkynes," *J. Am. Chem. Soc.* **122**, 4310 (2000).
H. KAWAGUCHI and K. TATSUMI, "Synthesis and Structures of Half-Sandwich W(VI) Tri(selenido) and W(II) Selenolato Complexes," *Chem. Commun.* 1299 (2000).

I. HAMACHI, S. TSUKIJI, S. SHINKAI and S. OISHI, "Direct Observation of the Ferric-Porphyrin Cation Radical as an Intermediate in the Photo-Triggered Oxidation of Ferric- to Ferryl-heme Tethered to Ru(bpy)$_3$ in Reconstituted Myoglobin," *J. Am. Chem. Soc.* **121**, 5500 (1999).
Y-Z. HU, S. TSUKIJI, S. SHINKAI, S. OISHI and I. HAMACHI, "Construction of Artificial Photosynthetic Reaction Centers on a Protein Surface: Vectorial, Multistep, and Proton-Coupled Electron Transfer for Long-Lived Charge Separation," *J. Am. Chem. Soc.* **122**, 241 (2000).
Y-Z. HU, H. TAKASHIMA, S. TSUKIJI, S. SHINKAI, T. NAGAMUNE, S. OISHI and I. HAMACHI, "Direct Comparison of Electron Transfer Properties of Two Distinct Semisynthetic Triads with Non-Protein Based Triad: Unambiguous Experimental Evidences on Protein Matrix Effects," *Chem. Eur. J.* **6**, 1907 (2000).
I. HAMACHI, H. TAKASHIMA, Y-Z. HU, S. OISHI and S. SHINKAI, "Cyclodextrin-Appended Myoglobin as a Tool for Construction of a Donor-Sensitizer-Acceptor Triad on a Protein Surface," *Chem. Commun.* 1127 (2000).

Laser Research Center for Molecular Science

K. SHIMAMURA, N. MUJILATU, K. NAKANO, S. L. BALDOCHI, Z. LIU, H. OHTAKE, N. SARUKURA and T. FUKUDA, "Growth and Characterization of Ce-Doped LiCaAlF$_6$ Single Crystals," *J. Cryst. Growth* **197**, 896 (1999).
S. IZUMIDA, S ONO, Z. LIU, H. OHTAKE and N. SARUKURA, "Intense THz-Radiation Sources Using Semiconductors Irradiated with Femtosecond Laser Pulses in a Magnetic Field," *J. Nonlinear Opt. Phys. Mater.* **8**, 71 (1999).
Z. LIU, S. IZUMIDA, S. ONO, H. OHTAKE and N. SARUKURA, "High-Repetition-Rate, High-Average-Power, Mode-Locked Ti:Sapphire Laser with an Intracavity Continuous Wave-Amplification Scheme," *Appl. Phys. Lett.* **74**, 3622 (1999).
S. IZUMIDA, S. ONO, Z. LIU, H OHTAKE and N. SARUKURA, "Spectrum Control of THz Radiation from InAs in a Magneric Field by Duration and Frequency Chirp of the Excitation Pulses," *Appl. Phys. Lett.* **75**, 451 (1999).
H. OHTAKE, S. ONO, Z. LIU, N. SARUKURA, M. OHTA, K. WATANABE and Y. MATSUMOTO, "Enhanced THz Radiation from Femtosecond Laser Pulse Irradiated InAs Clean Surface," *Jpn. J. Appl. Phys.* **38**, L1186 (1999).
T. A. LIU, K. F. HUANG, C. L. PAN, Z. LIU, S. ONO, H. OHTAKE and N. SARUKURA, "THz Radiation from Intracavity Saturable Bragg Reflector in Magnetic Field with Self-Started Mode-Locking by Strained Saturable Bragg Reflector," *Jpn. J. Appl. Phys.* **38**, L1333 (1999).
T. A. LIU, K. F. HUANG, C. L. PAN, Z. LIU, S. ONO, H. OHTAKE and N. SARUKURA, "High Average Power Mode Locked Ti:Sapphire Laser with Intracavity Continuous-Wave Amplifire and Straind Saturable Bragg Reflector," *Jpn. J. Appl. Phys.* **38**, L1109 (1999).
S. ONO, T. TSUKAMOTO, M. SAKAI, Z. LIU, H. OHTAKE, N. SARUKURA, S. NISHIZAWA, A. NAKANISHI and M. YOSHIDA, "Compact THz-Radiation Source Consisting of a Bulk Semiconductor, a Mode-Locked Fiber Laser a, and a 2-T Permanent Magnet," *Rev. Sci. Instrum.* **71**, 554 (2000).
H. OHTAKE, S. ONO, M. SAKAI, Z. LIU, T. TSUKAMOTO and N. SARUKURA, "Saturation of THz-Radiation Power from Femtosecond-Laser Irradiated InAs in a High Magnetic Field," *Appl. Phys. Lett.* **76**, 1398 (2000).
H. OHTAKE, S. ONO, M. SAKAI, Z. LIU, T. TSUKAMOTO and N. SARUKURA, "Intense THz Radiation from Femtosecond Laser Pulses Irradiated InAs in a Strong Magnetic Field," *J. Lumin.* **87–89**, 902 (2000).
H. OHTAKE, S. ONO, E. KAWAHATA, T. KOZEKI, H. MURAKAMI, Z. LIU and N. SARUKURA, "Development of Intense and Compact THz-Radiation Source Using Femtosecond-Laser Irradiated InAs Emitter in a High Magnetic Field," *J. Chin. Chem. Soc.* **47**, 609 (2000).
Z. LIU, H. MURAKAMI, T. KOZEKI, H. OHTAKE and N. SARUKURA, "High-Gain, Reflection-Double Pass, Ti:Sapphire Continuous-Wave Amplifier Delivering 5.77 W Average Power, 82 MHz Repetition Rate, Femtosecond Pulses," *Appl. Phys. Lett.* **76**, 3182 (2000).

Research Center for Molecular Materials

M. B. ZAMAN, M. TOMURA, Y. YAMASHITA, M. SAYADUZZAMAN and A. M. CHOWDHURY, "A Decamethylferrocene [Fe(C$_5$Me$_5$)$_2$] and Chloranilic acid (CA) Complex with Hydrogen Bonded Supramolecular Structure between CA and H$_2$O Molecules," *CrystEngComm* 9 (1999).
M. B. ZAMAN, M. TOMURA and Y. YAMASHITA, "New Hydrogen Bonded Donor-Acceptor Pairs between Dipyridylacetylenes and 2,5-Dichloro-3,6-dihydroxy-1,4-benzoquinone," *Org. Lett.* **2**, 273 (2000).

M. TOMURA and Y. YAMASHITA, “Crystal Engineering in π-overlapping Stacks: Unusual One-and Two Dimensional Stacking of the π-System in the Crystal Structure of the Cation Radical Salts of Tetrathiafulvalene Vinylogues,” *CrystEngComm* 14 (2000).

M. TOMURA and Y. YAMASHITA, “One-Dimensional Supramolecular Tapes in the Co-Crystals of 2,5-Dibromo-3,6-dihydroxy-1,4-benzoquinone (bromanilic acid) with Heterocyclic Compounds Containing a Pyrazine Ring Unit,” *CrystEngComm* 16 (2000).

E. HASEGAWA, K. IWAYA, T. IRIYAMA, T. KITAZUME, M. TOMURA and Y. YAMASHITA, “Reaction of Ethyl 2-haloethyl-1-tetralone-2-carboxylate and Samarium Diiodide: First Example of Intramolecular O-Alkylation of Samarium Ketyl Radical by Carbon-halogen Bond,” *Tetrahedron Lett.* **41**, 6447 (2000).

K. CZARNECKI, J. R. KINCAID and H. FUJII, “Resonance Raman Spectra of Legitimate Models for the Ubiquitous Compound I Intermediates of Oxidative heme Enzymes,” *J. Am. Chem. Soc.* **121**, 7953 (1999).

N. NISHIMURA, M. OOI, K. SHIMATZU, H. FUJII and K. UOSAKI, “Post-Assembly Insertion of Metal Ions into Thiol-Derivatized Porphyrin Monolayers on Gold,” *J. Electro. Chem.* **473**, 75 (1999).

K. FUKUI, H. FUJII, H. OHYA-NISHIGUCHI and H. KAMADA, “Electron Spin-Echo Envelope Modulation Spectral properties of Amidate Nitrogen Coordinated to Oxovanadium(IV) Ion,” *Chem. Lett.* 198 (2000).

T. IKEUE, Y. OHGO, T. SAITOH, M. NAKAMURA, H. FUJII and M. YOKOYAMA, “Spin Distribution in Low-Spin (meso-Tetraalkylporphyrinato)iron(III) Complexes with $(dxz,dyz)^4$ $(dxy)^1$ Configuration. Studies by ^{1}H-NMR, ^{13}C-NMR, and EPR Spectroscopies,” *J. Am. Chem. Soc.* **122**, 4068 (2000).

H. ZHOU, C. T. MIGITA, M. SATO, D. SUN, X. ZHANG, M. IKEDA-SAITO, H. FUJII and T. YOSHIDA, “Participation of Carboxylate Amino Acid Side Chain in Regiospecific Oxidation of Heme by Heme Oxygenase,” *J. Am. Chem. Soc.* **122**, 8311 (2000).

K. AIKAWA and T. NAGATA, “Synthesis of a Dinucleating Ligand Xanthene-bis(tris(2-pyridylmethyl)amine) and Its Manganese Complex,” *Inorg. Chim. Acta* **306**, 223 (2000).

T. NAGATA and K. TANAKA, “Pentadentate Terpyridine-Catechol Linked Ligands and Their Cobalt(III) Complexes,” *Inorg. Chem.* **39**, 3515 (2000).

Y. SAKAMOTO, T. SUZUKI, A. MIURA, H. FUJIKAWA, S. TOKITO and Y. TAGA, “Synthesis, Characterization, and Electron-Transport Property of Perfluorinated Phenylene Dendrimers,” *J. Am. Chem. Soc.* **122**, 1832 (2000).

Equipment Development Center

T. TSUJIBAYASHI, M. WATANABE, O. ARIMOTO, M. ITOH, S. NAKANISHI, H. ITOH, S. ASAKA and M. KAMADA, “Resonance Enhancement Effect on Two-Photon Absorption due to Excitons in Alkalin-Earth Fluorides Excited with Synchrotron Radiation and Laser Light,” *Phys. Rev. B* **60**, R8442 (1999).

V. B. MIKHAILIK, M. ITOH, S. ASAKA, Y. BOKUMOTO, J. MURAKAMI and M. KAMADA, “Amplification of Impurity-Associated Auger-Free Luminescence in Mixed Rubidium-Caesium Chloride Crystals under Core-Level Excitation with Undulator Radiation,” *Opt. Commun.* **171**, 71 (1999).

Ultraviolet Synchrotron Orbital Radiation Facility

T. TSUJIBAYASHI, M. WATANABE, O. ARIMOTO, M. ITOH, S. NAKANISHI, H. ITOH, S. ASAKA and M. KAMADA, “Resonant Enhancement Effect on Two-Photon Absorption due to Excitons in Alkaline-Earth Fluorides Excited with Synchrotron Radiation and Laser Light,” *Phys. Rev. B* **60**, 8442 (1999).

N. KIDA, N. OHNO, K. DEDUCHI and M. KAMADA, “VUV Optical Spectra of Hydrogen-Bonded Ferroelectrics $PbHPO_4$ and $PbHAsO_4$,” *J. Electron Spectrosc. Relat. Phenom.* **101/103**, 603 (1999).

V. B. MIKAHAILIK, M. ITOH. S. ASAKA, Y. BOKUMOTO, J. MURAKAMI and M. KAMADA, “Amplification of Impurity-Associated Auger-Free Luminescence in Mixed Rubidium-Caesium Chloride Crystals under Core-Level Excitation with Undulator Radiation,” *Opt. Commun.* **171**, 71 (1999).

M. KAMADA, J. MURAKAMI and N. OHNO, “Excitation Spectra of a Long-Persistent Phosphor $SrAl_2O_4$:Eu,Dy in Vacuum Ultraviolet Region,” *J. Lumin.* **87/89**, 1042 (2000).

T. TSUJIBAYASHI, M. WATANABE, O. ARIMOTO, M. ITOH, S. NAKANISHI, H. ITOH, S. ASAKA and M. KAMADA, “Two-Photon Excitation Spectra of Exciton Luminescence in BaF_2 Obtained by Using Synchrotron Radiation and Laser,” *J. Lumin.* **87/89**, 254 (2000).

M. KAMADA, J. MURAKAMI, S. TANAKA, S. D. MORÉ, M. ITOH and Y. FUJII, “Photo-Induced Change in Semiconductor-Vacuum Interface of p-GaAs(100) Studied by Photoelectron Spectroscopy,” *Surf. Sci.* **454/456**, 525 (2000).

S. MORÉ, S. TANAKA, S. TANAKA, Y. FUJII and M. KAMADA, “Coadsorption of Cs and O on GaAs: Formation of Negative Electron Affinity Surfaces at Different Temperatures,” *Surf. Sci.* **454/456**, 161 (2000).

M. HOSAKA, S. KODA, J. YAMAZAKI and H. HAMA, “Temporal Stability of the UVSOR-FEL Micropulse,” *Nucl. Instrum. Methods Phys. Res., Sect. A* **445**, 208 (2000).

E. MURAKAMI, T. HAYAISHI, Y. LU, Y. MORIOKA, F. KOIKE, E. SHIGEMASA and A. YAGISHITA, "Post-Collision Interaction Effects Induced by Auger Cascades Following Xe L_1-Shell Photoionization," *J. Electron Spectrosc.* **101-103**, 167 (1999).
T. HAYAISHI, Y. FUJITA, M. IZUMISAWA, T. TANAKA, E. MURAKAMI, E. SHIGEMASA, A. YAGISHITA and Y. MORIOKA, "Multi-Step Post-Collision Interaction Effects in K-Shell Photoionization of Kr," *J. Phys. B: At.; Mol. Opt. Phys.* **33**, 37 (2000).
A. EHRESMANN, S. MACHIDA, M. KITAJIMA, M. UKAI, K. KAMETA, N. KOUCHI, Y. HATANO, E. SHIGEMASA and T. HAYAISHI, "Dissociative Single and Double Photoionization with Excitation between 37 and 69 eV in N_2," *J. Phys. B: At.; Mol. Opt. Phys.* **33**, 473 (2000).
T. IBUKI , K. OKADA, T. GEJO and K. SAITO, "K Shell Excitation of Some Organic Molecules," *J. Electron Spectrosc. Relat. Phenom.* **101/103**, 149 (1999).
T. IBUKI , K. OKADA, K. SAITO and T. GEJO, "Molecular Size Effect on the Site-Specific Fragmentation of N and O K Shell Excited CH_3OCOCN and CH_3OCOCH_2CN Molecules," *J. Electron Spectrosc. Relat. Phenom.* **107**, 39 (2000).

S. KIMURA, H. KITAZAWA, G. KIDO and T. SUZUKI, "Optical and Magneto-Optical Studies on Magnetic Phase Transition of CeSb and CeBi," *Physica B* **281-282**, 449 (2000).
H. OKAMURA, T. INAOKA, S. KIMURA, T. NANBA, F. IGA, S. HIURA and T. TAKABATAKE, "Energy Gap Evolution in the Optical Spectra of Kondo Alloy System $Yb_{1-x}Lu_xB_{12}$," *Physica B* **281-282**, 280 (2000).
H. OKAMURA, J. KAWAHARA, T. NANBA, S. KIMURA, I. SHIMOYAMA, K. NAKAGAWA, K. SODA, U. MIZUTANI, Y. NISHINO, M. KATO, K. FUKUI, H. MIURA and H. NAKAGAWA, "Pseudogap Formation in the Intermetallic Compounds $(Fe_{1-x}V_x)_3Al$," *Phys. Rev. Lett.* **84**, 3674 (2000).
S. KIMURA, H. KITAZAWA, G. KIDO and T. SUZUKI, "Electronic Structure in the Magnetically Ordered States of CeSb Studied by Magneto-Optical Spectroscopy in the Infrared Region," *J. Phys. Soc. Jpn.* **69**, 647 (2000).

Computer Center

S. KONDO, K. TOKUHASHI, M. SUGIE and M. AOYAGI, "Ab Initio Study of $PH_2 + O_2$ Reaction by Gaussian-2 Theory," *J. Phys. Chem.* **103**, 8082 (1999).
S. NANBU, S. K. GRAY, T. KINOSHITA and M. AOYAGI, "Theoretical Study of the Potential Energy Surfaces and Bound States of HCP," *J. Chem. Phys.* **112**, 5866 (2000).
S. SKOKOV, T. TSUCHIDA, S. NANBU, J. M. BOWMAN and S. K. GRAY, "A Comparative Study of the Quantum Dynamics and Rate Constants of the $O(^3P)$ + HCl Reaction Described by Two Potential Surfaces," *J. Chem. Phys.* **113**, 227 (2000).

REVIEW ARTICLES AND TEXTBOOKS

Department of Theoretical Studies

K. FUKE, K. HASHIMOTO and S. IWATA, "Structures, Spectroscopies and Reactions of Atomic Ions with Water Clusters," *Adv. Chem. Phys.* **110**, 431 (1999).

Y. OKAMOTO, "Protein Folding Simulations by Monte Carlo Simulated Annealing and Multicanonical Algorithm" in *Optimization in Computational Chemistry and Molecular Biology: Local and Global Approaches*, C. A. Floudas and P. M. Pardalos, Eds., Kluwer Academic Publishers, pp. 73–90 (2000).

H. NAKAMURA, "Complete Solutions of the Landau-Zener-Stueckelberg Curve Crossing Problems, and Their Generalizations and Applications," *XXI-ICPEAC Invited Papers*, Y. Itikawa *et al.*, Eds., American Institute of Physics, pp. 495–509 (2000).

Y. TANIMURA, "The 5th- and 7th-Order 2D Raman Spectroscopy for Intramolecular Vibrational Modes" in *Proc. of Two-Dimensional Correlation Spectroscopy,* Y. Ozaki and I. Noda, Eds., American Institute of Physics, pp. 144–153 (2000).
Y. TANIMURA, "Two-Dimensional Spectroscopy of Liquids," *J. Electrochem. Soc. Jpn. (in Japanese)* **68**, 125–129 (2000).
Y. TANIMURA, "Chemical Reaction Dynamics and Ultrafast Nonlinear Spectroscopy," *Kagaku (in Japanese)* **44**, 103–112 (2000).
K. OKUMURA, Y. TANIMURA and A. TOKMAKOFF, "Information in the Two-Dimensional Fifth-Order Raman Spectroscopy—Anharmonicity, Nonlinearity, Mode Coupling, and Molecular Structure—" in *Proc. of Two-Dimensional Correlation Spectroscopy,* Y. Ozaki and I. Noda, Eds., American Institute of Physics; New York, pp. 321–324 (2000).
Y. SUZUKI and Y. TANIMURA, "Dynamical Stokes Shift Observed by Two-Dimensional Raman Spectroscopy" in *Proc. of Two-Dimensional Correlation Spectroscopy,* Y. Ozaki and I. Noda, Eds., American Institute of Physics; New York, pp. 329–332 (2000).

H. SATO and F. HIRATA, "An Interplay between Quantum and Statistical Mechanics Manifested in Properties of Liquid Water (in Japanese)," *BUTSURI (monthly membership journal of the Physical Society of Japan)* **54**, 696 (1999).

Department of Molecular Structure

S. NAGASE, K. KOBAYASHI, T. AKASAKA and T. WAKAHARA, "Endohedral Metallofullerenes—Theory, Electrochemistry, and Chemical Reactions" in *Fullerenes: Chemistry, Physics and Technology,* K. M. Kadish and R. S. Ruoff, Eds., Wiley; New York, pp. 395–436 (2000).
T. AKASAKA, S. OKUBO, T. WAKAHARA, K. KOBAYASHI, S. NAGASE, T. KATO, K. YAMAMOTO, M. KAKO and Y. NAKADAIRA, "Isolation and Characterization of a Pr@C82 Isomer" in *Recent Advances in the Chemistry and Physics of Fullerenes,* K. Kadish and R. Ruoff, Eds., The Electrochemical Society; Pennington, NJ, pp. 771–778 (1999).

M. TSUBAKI, "Heme-Steroid Interaction in Cytochrome P450c21 Studied by EPR and FTIR Spectroscopies" in *Molecular Steroidogenesis,* M. Okamaoto, Y. Ishimura and H. Nawata, Eds., Universal Academy Press, Inc.; Tokyo, pp. 69–72, (2000).

T. KITAGAWA and Y. MIZUTANI, "Ultrafast Dynamics of Hemeproteins" in *Ultrafast Chemical Dynamics (in Japanese),* KIKAN KAGAKU SOSETSU **44**, 162–175 (2000).
T. KITAGAWA, "Progress Report on Molecular Biometallics (1996–2000), A Project of the Priority Areas for Research under the Auspices of the Japanese Government," *J. Biol. Inorg. Chem.* **5**, 410–415 (2000).

T. KATO, K. YAMAMOTO, S. OKUBO and T. AKASAKA, "Spin Chemistry of Metallofullerenes," *Proceedings of the Symposium on Recent Advances in the Chemistry and Physics of Fullerenes and Related Materials* **7**, K. M. Kadish *et al.* Eds., The Electrochemical Society, Inc.; Pennington (1999).
N. HAYASHI and T. KATO, "State Correlated Raman Spectroscopy," *Proceedings of the International Conference of the Two-Dimensional Correlation Spectroscopy*, Y. Ozaki and I. Noda, Eds., American Institute of Physics; New York, 127–133 (2000).

Department of Electronic Structure

M. FUJII, "Observation of Highly Vibrationally Excited Molecules and Possibility of Application to Reaction Control," *Rev. Laser Eng.* **27**, 404 (1999).

T. YAMASE, "Chapter 8, Spectra of Rare-Earth Ions" in *Science of Rare-Earths (in Japanese)*, G. Adachi Ed., Kagaku Dohjin; Kyoto, pp. 127–163 (1999).
T. YAMASE, "Molecular Design of Rare-earth Phosphors," *Kagaku Kogyo (in Japanese)* **51**, 682–689 (2000).

Department of Applied Molecular Science

Y. WATANABE, "High-Valent Intermediates" in *The Porphyrin Handbook*, K. M. Kadish, K. M. Smith and R. Guilard, Eds., Vol. 4, Academic Press; San Diego, pp. 97–118 (1999).
Y. WATANABE and H. FUJII, "Characterization of High-Valent Oxo-Metalloporphyrins" in *Structure and Bonding*, B. Meunier Ed., Springer Verlag; Berlin, Vol. 97, pp. 62–89 (2000).
S. OZAKI, T. MATSUI, M.P. ROACH and Y. WATANABE, "Rational Molecular Design of a Catalytic Site: Engineering of Catalytic Function to the Myoglobin Active Site Framework," *Coord. Chem. Rev.* **198**, 39–59 (2000).

K. INOUE, F. IWAHORI, A. S. MARKOSYAN and H. IWAMURA, "One-Dimensional Ferro- and Ferrimagnetic Chains Made up of an Alternating Array of 1,3-Bis(*N*-*tert*-butyl-*N*-oxy-amino)benzene Derivatives and Mn(II)(hfac)$_2$," *Coord. Chem. Rev.* **198**, 219 (2000).

Department of Vacuum UV Photoscience

Y. NONOGAKI, Y. FUJIWARA and Y. TAKEDA, "Organometallic Vapor Phase and Droplet Heteroepitaxy of Quantum Structures" in *InP and Related Compounds—Materials, Applications and Devices*, M. O. Manasreh Ed., Optoelectronic Properties of Semiconductors and Surperlattices, Gordon and Breach Science Publishers, **9**, pp. 570–602 (2000).

K. MITSUKE, "SR-Pump and Laser-Probe Experiments for the Photofragmentation Dynamics of Atoms and Molecules" in *The Physics of Electronic and Atomic Collisions*, Y. Itikawa *et al.* Eds., American Institute of Physics; New York, Conference Proceedings **500**, 172 (2000).
K. MITSUKE and H. NAKAMURA, "Conference Report—Photo-Dynamics and Reaction Dynamics of Molecules," *Comments Modern Phys. D* **2**, 75 (2000).

K. MUKAI, Y. KANESAKI, Y. EGAWA and S. NAGAOKA, "Free-Radical-Scavenging Action of Catechin and Related Compounds in Homogeneous and Micellar Solutions" in *Phytochemical and Phytopharmacenticals*, F. Shahide and C.-T. Ho, Eds., AOCS Press; Champaign, Illinois, 222 (2000).

Laser Research Center for Molecular Science

N. SARUKURA, "Special Issues on New Materials in Ultraviolet Region," *Rev. Laser Eng. (in Japanese)* **27**, 518 (1999).

Research Center for Molecular Materials

Y. WATANABE and H. FUJII, "Characterization of High-Valent Oxo-Metalloporphyrins" in *Mtal-Oxo and Mtal-Peroxo Species in Catalytic Oxidations*, B. Meunier Ed., Structure & Bonding **97**, Springer; Berlin 61 (2000).

Ultraviolet Synchrotron Orbital Radiation Facility

S. KIMURA, "Application of Circularly Polarized Infrared Synchrotron Radiation—Infrared Magnetic Circular Dichroism—," *Housyakou (in Japanese)* **13**, 62 (2000).

AUTHOR INDEX

to “Research Activities” and “Special Research Projects”